

Proceedings of the U.S. Nuclear Regulatory Commission

Sixteenth Water Reactor Safety Information Meeting

Volume 3

- Nuclear Plant Aging
- Structural and Seismic Engineering
- Mechanical Research
- Environmental Effects in Primary Systems

Held at
National Institute of Standards and Technology
Gaithersburg, Maryland
October 24-27, 1988

Date Published: March 1989

Compiled by: Allen J. Weiss

**Office of Nuclear Regulatory Research
U.S. Nuclear Regulatory Commission
Washington, DC 20555**

Proceedings prepared by
Brookhaven National Laboratory



ABSTRACT

This five-volume report contains 141 papers out of the 175 that were presented at the Sixteenth Water Reactor Safety Information Meeting held at the National Institute of Standards and Technology, Gaithersburg, Maryland, during the week of October 24-27, 1988. The papers are printed in the order of their presentation in each session and describe progress and results of programs in nuclear safety research conducted in this country and abroad. Foreign participation in the meeting included twenty different papers presented by researchers from Germany, Italy, Japan, Sweden, Switzerland, Taiwan and the United Kingdom. The titles of the papers and the names of the authors have been updated and may differ from those that appeared in the final program of the meeting.

PROCEEDINGS OF THE
16th WATER REACTOR SAFETY INFORMATION MEETING

October 24-27, 1988

Published in Five Volumes

GENERAL INDEX

VOLUME 1

- Plenary Session
- Decontamination and Decommissioning
- License Renewal
- Human Factors
- Generic Issues
- Risk Analysis/PRA Applications
- Innovative Concepts for Increased Safety of Advanced Power Reactors

VOLUME 2

- Industry Safety Research
- Non-Destructive Evaluation
- Materials Engineering
 - Pressure Vessel Research
 - Radiation Effects
 - Degraded Piping

VOLUME 3

- Nuclear Plant Aging
- Structural and Seismic Engineering
- Mechanical Research
- Environmental Effects in Primary Systems

VOLUME 4

- Code Uncertainty for ECCS Rule
- International Code Assessment Program
- Thermal Hydraulics
- 2D/3D Data Applications

VOLUME 5

- NUREG-1150
- Accident Management
- Recent Advances in Severe Accident Research
- TMI-2
- BWR Mark I Shell Failure

REGISTERED ATTENDEES (NON-NRC)
16th WATER REACTOR SAFETY INFORMATION MEETING

J. A. ADAM
STONE & WEBSTER
245 SUMMER ST
BOSTON MA 02107
USA

S. L. ADDITON
TENERA
2011 EYE STREET N.W., SUITE 300
WASHINGTON DC 20006
USA

M. J. ADES
SAVANNAH RIVER LABORATORY
BLDG. 773-43A
AIKEN SC 29808
USA

D. W. AKERS
EG&G IDAHO INC.
P.O. BOX 1625
IDAHO FALLS ID 83415
USA

H. AKIMOTO
JAPAN ATOMIC RESEARCH INST.
TOKAI-MURA, NAKA-GUN
IBARAKI-KEN 319-11
JAPAN

N. S. AKSAN
PAUL SCHERRER INSTITUTE
WUERENLINGEN CH5303
SWITZERLAND

R. P. ALLEN
PACIFIC NORTHWEST LABORATORY
P.O. BOX 999
RICHLAND WA 99352
USA

R. A. ALLEN
SAVANNAH RIVER LABORATORY
AIKEN SC 29808
USA

K. ALMENAS
UNIVERSITY OF MARYLAND
COLLEGE PARK MD 20742
USA

A. ALONSO
MADRID POLYTECHNIC UNIVERSITY
JOSE GUTIERREZ ABASCAL 2
MADRID 28006
SPAIN

H. ALSMEYER
KERNFORSCHUNGSZENTRUM, IRB/PRS
POSTFACH 3640
7500 KARLSRUHE
FRG

J. G. ANDERSEN
GENERAL ELECTRIC CO.
175 CURTNER AVE
SAN JOSE CA 95125
USA

J. M. ANDERSON
BECHTEL POWER CORP.
15740 SHADY GROVE ROAD
GAITHERSBURG MD 20874
USA

K. B. ANDERSSON
SWEDISH NUCLEAR POWER INSPECTORATE
BOX 27016
STOCKHOLM SW S-10252
SWEDEN

C. E. APPERSON
SAVANNAH RIVER LABORATORY
1635 ALPINE DR.
AIKEN SC 29801
USA

K. J. ARAJ
BDM
7915 JONES BRIDGE DRIVE
MCLEAN VA 22102
USA

W. C. ARCIERI
ENSA
15825 SHADY GROVE ROAD
ROCKVILLE MD 20850
USA

W. W. ASCROFT-HUTTON
HINI
BAYNARDS HOUSE/WESTBOURNE GROVE
LONDON ENGLAND W2 4TF
UK

B. ATEFI
SCIENCE APPLICATIONS INT'L CORP.
1710 GOODRIDGE DR.
MCLEAN VA 22102
USA

N. I. AVDOSHKIN
USSR EMBASSY
1125 16TH ST NW
WASHINGTON DC 20036

S. M. BAJOREK
WESTINGHOUSE POWER SYSTEMS DIVISION
P.O. BOX 355
PITTSBURGH PA 15230-2728
USA

K. K. BANDYOPADHYAY
BROOKHAVEN NATIONAL LABORATORY
BLDG 129
UPTON NY 11973
USA

R. A. BARI
BROOKHAVEN NATIONAL LABORATORY
BLDG. 197C
UPTON NY 11973
USA

G. P. BAROIS
FRAMATOME
TOUR FIAT - CEDEX 16
PARIS LA DEFENSE FR 92084
FRANCE

J. H. BARON
MADRID POLYTECHNIC UNIVERSITY
JOSE GUTIERREZ ABASCAL 2
MADRID 28006
SPAIN

B. R. BASS
OAK RIDGE NATIONAL LABORATORY
PO BOX 2003
OAK RIDGE TN 37831
USA

J. A. BAST
GENERAL ELECTRIC CO.
P.O. BOX 1072, BLDG. F3-8
SCHENECTADY NY 12301
USA

P. D. BAYLESS
EG&G IDAHO INC.
P.O. BOX 1625
IDAHO FALLS ID 83415
USA

P. BEDNARIK
SCIENCE & TECHNOLOGY
3900 LINNEAN AVE., NW
WASHINGTON DC 20008
CZECHOSLOVAKIA

K. D. BERGERON
SANDIA NATIONAL LABS.
P.O. BOX 5800
ALBUQUERQUE NM 87185
USA

R. F. BEYER
WESTINGHOUSE
206 NAVAJO RD.
PITTSBURGH PA 15241
USA

V. M. BHARGAVA
VIRGINIA POWER
5000 DOMINION BLVD.
GLEN ALLEN VA 23060
USA

W. BINNER
AUSTRIAN RESEARCH CENTER
SEIBERSDORF A-2444
AUSTRIA

D. P. BIRMINGHAM
BABCOCK & WILCOX CO.
1562 BEESON STREET
ALLIANCE OH 44601
USA

D. BIZZAK
CARNEGIE-MELLON UNIVERSITY
386 HUNTINGDON AVENUE
N. HUNTINGDON PA 15642
USA

R. J. BOHL
LOS ALAMOS NATIONAL LABORATORY
P.O. BOX 1663, MS K560
LOS ALAMOS NM 87545
USA

T. C. BORDINE
CONSUMERS POWER COMPANY
1945 WEST PARNALL RD.
JACKSON MI 49201
USA

R. B. BORSUM
BABCOCK & WILCOX CO.
1700 ROCKVILLE PIKE, #525
ROCKVILLE MD 20852
USA

B. E. BOYACK
LOS ALAMOS NATIONAL LAB
PO BOX 1663
LOS ALAMOS NM 87545
USA

D. R. BRADLEY
SANDIA NATIONAL LABS.
P.O. BOX 5800
ALBUQUERQUE NM 87185
USA

R. J. BRANDON
GE NUCLEAR CORP
6728 LOOKOUT BEND
SAN JOSE CA 95120
USA

P. A. BRATBY
NATIONAL NUCLEAR CORP.
BOOTHS HALL, CHELFORD ROAD
KNUTSFORD
UK

R. J. BREEDING
SANDIA NATIONAL LABS., DIV. 6410
P.O. BOX 5800
ALBUQUERQUE NM 87185
USA

S. J. BRETT
CEGB, GENERATION DEV. & CONSTRUCTION
GEN. DEV. & CONST. DIV. BARNWOOD
GLOUCESTER GL47RS
UK

I. BRITTAIN
UKAEA/AEE WINFRITH
DOERCHESTER
DORSET DT28DH
UK

J. M. BROUGHTON
EG&G IDAHO INC.
P.O. BOX 1625
IDAHO FALLS ID 83415
USA

S. BRYANT
CENTRAL ELECTRICITY GENERATING BD.
BOOTHS HALL, CHELFORD RD
KNUTSFORD, CHESHIRE WA1680G
UK

C. E. BUCHHOLZ
GENERAL ELECTRIC CO.
175 CURTNER AVE
SAN JOSE CA 95125
USA

B. BUESCHER
EG&G IDAHO INC.
P.O. BOX 1625
IDAHO FALLS ID 83415
USA

L. C. BUFFARDI
GEORGE MASON UNIVERSITY
4400 UNIVERSITY DRIVE
FAIRFAX VA 22030
USA

J. D. BYRON
ELECTRIC POWER RESEARCH INSTITUTE
3412 HILLVIEW AVE.
PALO ALTO CA 94303
USA

J. I. CALVO
CONSEJO SEGURIDAD NUCLEAR
SOR ANGELA DE LA CRUZ 3
MADRID 28020
SPAIN

A. L. CAMP
SANDIA NATIONAL LABS. DIV. 6412
P.O. BOX 5800
ALBUQUERQUE NM 87185
USA

D. D. CARLSON
SANDIA NATIONAL LABS., DIV. 6513
P.O. BOX 5800
ALBUQUERQUE NM 87185
USA

R. CARO
CONSEJO DE SEGURIDAD NUCLEAR
C/SOR ANGELA DE LA CRUZ, 3
MADRID 28020
SPAIN

D. E. CARROLL
SANDIA NATIONAL LABS.
P.O. BOX 5800
ALBUQUERQUE NM 87185
USA

R. CARUSO
NUCLEAR ENERGY AGENCY
38 BLYVD. SUCHET
PARIS 75016
FRANCE

D. A. CASADA
OAK RIDGE NATIONAL LABORATORY
PO BOX 2009, BLDG. 9104-1
OAK RIDGE TN 37831
USA

J. H. CHA
KOREA ADVANCED ENERGY RESEARCH INST.
PO BOX 7, DAEDUK-DANJI
TAEJON CHUNG-NAM
KOREA

S. CHAKRABORTY
PAUL SCHERRER INSTITUTE
WUERENLINGEN CH5303
SWITZERLAND

R. CHAMBERS EG&G IDAHO INC. P.O. BOX 1625 IDAHO FALLS ID 83415 USA	D. CROUCH BROOKHAVEN NATIONAL LABORATORY BLDG. 130 UPTON NY 11973 USA	M. DIMARZO UNIVERSITY OF MARYLAND MECHANICAL ENGINEERING DEPT. COLLEGE PARK MD 20016 USA	F. A. ELIA STONE AND WEBSTER PO BOX 2325 BOSTON MA 02014 USA
Y. I. CHANG ARGONNE NATIONAL LABORATORY 9700 S. CASS AVE. ARGONNE IL 60439 USA	W. H. CULLEN MATERIALS ENGINEERING ASSOCIATES 9700-B M. L. KING HIGHWAY LANHAM MD 20706 USA	M. R. DINSEL BECHTEL POWER CORP. 15740 SHADY GROVE ROAD GAITHERSBURG MD 20874 USA	G. T. EMBLEY GENERAL ELECTRIC BOX 1092 SCHENECTADY NY 12301 USA
D. CHAPIN MPR ASSOCIATES, INC. 1050 CONNECTICUT AVENUE, N.W. WASHINGTON DC 20036 USA	G. E. CUMMINGS LAWRENCE LIVERMORE NATIONAL LAB P.O. BOX 808, L-198 LIVERMORE CA 94526 USA	S. R. DOCTOR PACIFIC NORTHWEST LABORATORY P.O. BOX 999 RICHLAND WA 99352 USA	T. C. ENG DEPARTMENT OF ENERGY EH-35, MAIL STOP F-137 WASHINGTON DC 20545 USA
S. C. CHENG TAIWAN POWER COMPANY TAIPEI ROC	H. D. CURET ADVANCED NUCLEAR FUELS 2101 HORN ROAD RICHLAND WA 99352 USA	C. V. DODD OAK RIDGE NATIONAL LABORATORY PO BOX 2008 OAK RIDGE TN 37831 USA	R. G. ESPEFALT SWEDISH STATE POWER BD. VATTENFALL VALLINGBY S-16287 SWEDEN
L. Y. CHENG BROOKHAVEN NATIONAL LABORATORY BLDG 703 UPTON NY 11973 USA	B. D. CURRY PHILADELPHIA ELECTRIC CO. PO BOX A SARATOGA BR. POTTSTOWN PA 19464 USA	T. F. DORIAN DOUB. MUNTZING & GLASGOW, CHARTERED 808 17TH STREET, N. W., SUITE 400 WASHINGTON DC 20006 USA	C. R. FARRAR LOS ALAMOS NATIONAL LAB. MS J576 LOS ALAMOS NM 87545 USA
R. D. CHEVERTON OAK RIDGE NATIONAL LABORATORY PO BOX 2009 OAK RIDGE TN 37831 USA	R. A. CUSHMAN NIAGRA MOHAWK POWER CORP. 301 PLAINHELD ROAD SYRACUSE NY 13212 USA	J. DRCEC NPP KRSKO PO VRBINA 12 KRSKO 68270 YUGOSLAVIA	H. E. FILACCHIONE SCIENTECH 11821 PARKLAWN DR. ROCKVILLE MD 20878 USA
W. G. CHOE TU ELECTRIC 400 N. OLIVE STREET DALLAS TX 75201 USA	D. A. DAHLGREN SANDIA NATIONAL LABS., ORG. 6440 P.O. BOX 5800 ALBUQUERQUE NM 87123 USA	S. S. DUA GENERAL ELECTRIC M/C BOX 769, 175 CURTNER AVE. SAN JOSE CA 95125 USA	S. R. FISCHER MIDDLE SOUTH UTILITIES 188 E. CAPITOL STREET, SUITE 600 JACKSON MS 39201 USA
O. K. CHOPRA ARGONNE NATIONAL LABORATORY 9700 S. CASS AVE., BLDG 335 ARGONNE IL 60439 USA	J. DALLMAN EG&G IDAHO INC. P.O. BOX 1625 IDAHO FALLS ID 83415 USA	S. W. DUCE EG&G IDAHO INC P.O. BOX 1625 IDAHO FALLS ID 83415 USA	R. G. FITZPATRICK BROOKHAVEN NATIONAL LABORATORY BLDG 130 UPTON NY 11973 USA
B. CHUNG KOREA ADVANCED ENERGY RESEARCH INST. NSC, DAE DUK DAN-JI, BOX 7 CHOONG-NAM KOREA	R. DAMERON ANATECH 10975 TORREYANA RD., SUITE 301 SAN DIEGO CA 92121 USA	J. J. DUCCO CEA FRENCH ATOMIC ENERGY COMMISSION DAS/SASC.CEN/FAR, BP NO. 6 FONTENAY-AUX-ROSES 92265 FRANCE	C. W. FORSBERG OAK RIDGE NATIONAL LABORATORY P.O. BOX 2008, BLDG 4500N OAK RIDGE TN 37831 USA
D. T. CHUNG SCIENTECH 11821 PARKLAWN DR. ROCKVILLE MD 20878 USA	J. DARLSTON CENTRAL ELECTRICITY GENERATING BD. BERKLEY NUCLEAR LABS GLOUCESTER GL139PB UK	R. B. DUFFEY EG&G IDAHO INC. P.O. BOX 1625 IDAHO FALLS ID 83415 USA	E. FOX OAK RIDGE NATIONAL LABORATORY P.O. BOX 2009 OAK RIDGE TN 37831-8063 USA
H. CHUNG ARGONNE NATIONAL LABORATORY 9700 S. CASS AVE. ARGONNE IL 60439 USA	W. L. DAUGHERTY SAVANNAH RIVER LABORATORY PO BOX A AIKEN SC 29808 USA	K. K. DWIVEDI VIRGINIA POWER 5000 DOMINION BLVD. GLEN ALLEN VA 23060 USA	G. FREI SIEMENS HAMMERBACHERSTR. 12 ERLANGEN 852 FRG
J. P. CHURCH SAVANNAH RIVER LABORATORY BLDG. 773-41A AIKEN SC 29808 USA	N. W. DAVIES UKAEA, RISLEY LABORATORY WARRINGTON CHESHIRE WA3 6AT UK	J. L. EDSON EG&G IDAHO INC. P.O. BOX 1625 IDAHO FALLS ID 83415 USA	B. C. FRYER ADVANCED NUCLEAR FUELS 1930 CYPRESS RICHLAND WA 99352 USA
D. B. CLAUSS SANDIA NATIONAL LABS. DIV. 6442 P.O. BOX 5800 ALBUQUERQUE NM 87122 USA	M. A. DAYE BECHTEL POWER CORP. 15740 SHADY GROVE RD. GAITHERSBURG MD 20877 USA	G. R. EIDAM BECHTEL/GPUN P.O. BOX 72 MIDDLETOWN PA 17057 USA	H. FUJIMOTO COMPUTER SOFTWARE DEVELOPMENT CO. 4-1, SHIBAKOEN 2-CHOME, MINATO-KU TOKYO 105 JAPAN
M. COLAGRÖSSI ENEA/DISP VIA VITALIANO BRANCATI, 48 ROME 00144 ITALY	J. A. DE MASTRY FLORIDA POWER AND LIGHT CO. BOX 14000 JUNO BEACH FL 33408 USA	D. M. EISSENBERG OAK RIDGE NATIONAL LABORATORY PO BOX 2009, BLDG. 9104-1 OAK RIDGE TN 37831 USA	P. J. FULFORD NUS CORPORATION 910 CLOPPER ROAD GAITHERSBURG MD 20878 USA
M. W. CONEY CENTRAL ELECTRICITY GENERATING BD. C.E.R.L., KELVIN AVENUE LEATHERHEAD SURREY KT227SE UK	L. O. DeGEORGE COMMONWEALTH EDISON P.O. BOX 767 CHICAGO IL 60690 USA	Z. J. ELAWAR ARIZONA NUCLEAR POWER PROJECT, 7202 P.O. BOX 52034 PHOENIX AZ 85072 USA	R. R. FULLWOOD BROOKHAVEN NATIONAL LABORATORY BLDG 130 UPTON NY 11973 USA
W. R. CORWIN OAK RIDGE NATIONAL LABORATORY PO BOX 2009 OAK RIDGE TN 37831 USA	L. V. DeWITT SAVANNAH RIVER LABORATORY 1313 WILLIAMS DR. AIKEN SC 29801 USA	G. ELETTI ENEA/DISP VIA VITALIANO BRANCATI, 48 ROME 00144 ITALY	F. M. GANTENBEIN CEA FRENCH ATOMIC ENERGY COMMISSION CEN-SACLAY DEMT/SMTS/EMSI GIF-SUR-YVETTE 91191 FRANCE

F. GELBARD
SANDIA NATIONAL LABS.
P.O. BOX 5800
ALBUQUERQUE NM 87185
USA

D. I. GERTMAN
EG&G IDAHO INC.
P.O. BOX 1625
IDAHO FALLS ID 83415
USA

T. GINSBERG
BROOKHAVEN NATIONAL LABORATORY
BLDG 820
UPTON NY 11973
USA

T. GINZBURG
APPLIED BIOMATHEMATICS INC.
100 NORTH COUNTRY ROAD
SETAUKET NY 11733
USA

B. GITNICK
ENSA, INC.
15825 SHADY GROVE RD., STE. 120
ROCKVILLE MD 20850
USA

H. G. GLAESER
GESELLSCHAFT FÜR REAKTORSICHERHEIT
FORSCHUNGSGELANDE
D-8046 GARCHING
FRG

J. GLEASON
WYLE LABORATORY
7800 GOVERNORS DRIVE WEST
HUNTSVILLE AL 35807
USA

D. W. GOLDEN
EG&G IDAHO INC.
P.O. BOX 1625
IDAHO FALLS ID 83415
USA

M. GOMOLINSKI
CEA FRENCH ATOMIC ENERGY COMMISSION
CEN/FAR, BP NO. 6
FONTENAT-AUX-ROSES 92265
FRANCE

C. GONZALEZ
MADRID POLYTECHNICAL UNIVERSITY
JOSE GUTIERREZ ABASCAL, 2
MADRID 28006
SPAIN

E. D. GORHAM-BERGERON
SANDIA NATIONAL LABS.
P.O. BOX 5800
ALBUQUERQUE NM 87185
USA

T. C. GORRELL
SAVANNAH RIVER LABORATORY
RX TECH, DU PONT (SRP)
AIKEN SC 29808
USA

G. A. GREENE
BROOKHAVEN NATIONAL LABORATORY
BLDG. 820M
UPTON, NY 11973
USA

P. GRIFFITH
MIT
ROOM 7-044
CAMBRIDGE MA 02139
USA

F. GRIMM
SIEMENS
HAMMERBACHERSTR. 12
ERLANGEN 852
FRG

C. GRIMSHAW
BROOKHAVEN NATIONAL LABORATORY
BLDG. 130
UPTON NY 11973
USA

W. W. GUNTHER
BROOKHAVEN NATIONAL LABORATORY
BLDG 130
UPTON NY 11973
USA

S. HABER
BROOKHAVEN NATIONAL LABORATORY
BLDG. 130
UPTON NY 11973
USA

D. R. HAFFNER
WESTINGHOUSE HANFORD CO.
P.O. BOX 1970 A3-30
RICHLAND WA 99352
USA

F. M. HAGGAG
OAK RIDGE NATIONAL LABORATORY
P.O. BOX 2008, BLDG 4500-S
OAK RIDGE TN 37831-6151
USA

A. N. HALL
HM NUCLEAR INSTALLATIONS INSPECTORATE
ST PETER'S HOUSE, BALLIOL RD
BOOTLE, MERSEYSIDED L203LZ
UK

R. J. HAMMERSLEY
FAUSKE & ASSOCIATES
16W070 WEST 83RD STREET
BURR RIDGE IL 60521
USA

A. M. HASHIMOTO
JAPAN INST. OF NUCLEAR SAFETY
3-17-1 TOYANOMON
MINATOKU, TOKYO 105
JAPAN

Y. A. HASSAN
DEPT OF NUCL ENERGY, TEXAS A & M
COLLEGE STATION TX 77843
USA

J. R. HAWTHORNE
MATERIALS ENGINEERING ASSOCIATES
9700-B M. L. KING HIGHWAY
LANHAM MD 20706
USA

H. D. HAYNES
OAK RIDGE NATIONAL LABORATORY
PO BOX 2009, BLDG. 9201-3
OAK RIDGE TN 37831
USA

J. HAZELTINE
WYLE LABORATORY
7800 GOVERNORS DRIVE WEST
HUNTSVILLE AL 35807
USA

R. E. HENRY
FAI
16W070 WEST 83RD STREET
BURR RIDGE IL 60521
USA

G. F. HEWITT
UKAEA/HARWELL LABORATORY
THERMAL HYDRAULICS DIV, BLDG 392
OXON OX110RA
UK

J. HIBBARD
MPR ASSOCIATES, INC.
1050 CONNECTICUT AVENUE, N.W.
WASHINGTON DC 20036
USA

D. E. HIDINGER
GENERAL ELECTRIC
14 CORONET CT.
SCHENECTADY NY 12309
USA

J. C. HIGGINS
BROOKHAVEN NATIONAL LABORATORY
BLDG 130
UPTON NY 11973
USA

C. J. HIGGINS
APPLIED RESEARCH ASSOCIATES, INC.
4300 SAN MATEO NE, STE B 380
ALBUQUERQUE NM 87111
USA

P. R. HILL
PENNSYLVANIA POWER & LIGHT CO.
2 N. NINTH STREET
ALLENTOWN PA 18101
USA

J. E. HINTON
DU PONT DE NEMOURS
SRP 707-C, RM. 329
AIKEN SC 29808
USA

T. J. HIRONS
LOS ALAMOS NATIONAL LABORATORY
P.O. BOX 1663, MS E561
LOS ALAMOS NM 87545
USA

M. HIROSE
NUCLEAR POWER ENG'G TEST CTR
FUJITA KMKO BLDG., TORANOMON, MINATO-
TOKYO 105
JAPAN

S. A. HODGE
OAK RIDGE NATIONAL LABORATORY
PO BOX 2009, BLDG. 9104-1
OAK RIDGE TN 37831
USA

P. G. HOFMANN
KERNFORSCHUNGSZENTRUM, IMF
POSTFACH 3640
7500 KARLSRUHE
FRG

C. H. HOFMAYER
BROOKHAVEN NATIONAL LABORATORY
BLDG 129
UPTON NY 11973
USA

G. S. HOLMAN
LAWRENCE LIVERMORE NATIONAL LAB
P.O. BOX 808, L-197
LIVERMORE CA 94550
USA

K. R. HOOPINGARNER
PACIFIC NORTHWEST LABORATORY
P.O. BOX 999
RICHLAND WA 99352
USA

R. G. HOPPE
WESTINGHOUSE ELECTRIC CORP.
P.O. BOX 79
W. MIFFLIN PA 15122
USA

K. G. HORNBERGER
OAK RIDGE NATIONAL LABORATORY
P.O. BOX 2009
OAK RIDGE TN 37831-8056
USA

P. J. HOSEMANN
PAUL SCHERRER INSTITUTE
WUERENLINGEN CHS303
SWITZERLAND

B. J. HSEIH
ARGONNE NATIONAL LABORATORY
9700 SO CASS AVE.
ARGONNE IL 60439
USA

A. H. HSIA
URA
240 MONROE STREET
ROCKVILLE MD 20854
USA

H-N HSIAU
TAIWAN POWER COMPANY
TAIPEI TAIWAN
ROC

K. HU
BROOKHAVEN NATIONAL LABORATORY
BLDG. 475B
UPTON NY 11973
USA

D. S. HUMPHRIES
SCIENTECH
11821 PARKLAWN DR.
ROCKVILLE MD 20852
USA

M. L. HYDEP
SAVANNAH RIVER LABORATORY
AIKEN SC 29808
USA

C. R. HYMAN
OAK RIDGE NATIONAL LABORATORY
PO BOX 2009, BLDG. 9104-1
OAK RIDGE TN 37831
USA

T. IGUCHI
JAPAN ATOMIC RESEARCH INST.
TOKAI-MURA, NAKA-GUN
IBARAKI-KEN 319-11
JAPAN

R. L. IMAN
SANDIA NATIONAL LABS. DIV 6415
P.O. BOX 5800
ALBUQUERQUE NM 87185
USA

J. R. IRELAND
LOS ALAMOS NATIONAL LAB
PO BOX 1663, MSK 551
LOS ALAMOS NM 87544
USA

M. ISHII
PURDUE UNIVERSITY
WEST LAFAYETTE ID
USA

S. K. ISKANDER
OAK RIDGE NATIONAL LABORATORY
P.O. BOX 2008
OAK RIDGE TN 37831-6151
USA

R. IVANY
COMBUSTION ENGINEERING, INC.
1000 PROSPECT HILL RD.
WINDSOR CT 06095
USA

J. M. IZQUIERDO
CONSEJO SEGURIDAD NUCLEAR
SOR ANGELA DE LA CRUZ 3
MADRID 28020
SPAIN

M. J. JACOBUS
SANDIA NATIONAL LABS., DIV. 6447
P.O. BOX 5800
ALBUQUERQUE NM 87185
USA

J. F. JANSKY
BTB-LEONBERG
RIEKSTRASSE 5
LEONBERG D-7250
FRG

D. B. JARRELL
PACIFIC NORTHWEST LABORATORY
P.O. BOX 999
RICHLAND WA 99352
USA

G. W. JOHNSEN
EG&G IDAHO INC.
P.O. BOX 1625
IDAHO FALLS ID 83415
USA

A. B. JOHNSON
PACIFIC NORTHWEST LABORATORY
P.O. BOX 999
RICHLAND WA 99352
USA

E. R. JOHNSON
WESTINGHOUSE ELECTRIC CORP.
P.O. BOX 2728
PITTSBURGH PA 15230-2728
USA

H. V. JULIAN
VOLIAN ENTERPRISES, INC.
PO BOX 410
MURRYSVILLE PA 15668
USA

J. E. KALINOWSKI
SAVANNAH RIVER LABORATORY
AIKEN SC 29808
USA

P. S. KALRA
ELECTRIC POWER RESEARCH INSTITUTE
3412 HILLYVIEW AVE.
PALO ALTO CA 94303
USA

F. B. KAM
OAK RIDGE NATIONAL LABORATORY
PO BOX 2008
OAK RIDGE TN 37831
USA

H. KAMATA
JAPAN ATOMIC RESEARCH INST.
TOKAI-MURA, NAKA-GUN
IBARAKI-KEN 319-11
JAPAN

D. D. KANA
SOUTHWEST RESEARCH INSTITUTE
6220 CULEBRA ROAD
SAN ANTONIO TX 78284
USA

L. D. KANNBERG
PACIFIC NORTHWEST LABORATORY
P.O. BOX 999
RICHLAND WA 99352
USA

S. KARIMIAN
BROOKHAVEN NATIONAL LABORATORY
BLDG. 130
UPTON NY 11973
USA

W. Y. KATO
BROOKHAVEN NATIONAL LABORATORY
BLDG 197C
UPTON NY 11973
USA

K. R. KATSMA
EG&G IDAHO INC.
P.O. BOX 1625
IDAHO FALLS ID 83415
USA

G. KATZENMEIER
KERNFORSCHUNGSZENTRUM, PHDR
POSTFACH 3640
7500 KARLSRUHE 1
FRG

W. R. KEANEY
GENERAL ASSOCIATES CORP
1314 OAKVIEW DR.
WORTHINGTON OH 43085
USA

J. E. KELLY
SANDIA NATIONAL LABS. DIV. 6418
P.O. BOX 5800
ALBUQUERQUE NM 87185
USA

C. R. KEMPF
BROOKHAVEN NATIONAL LABORATORY
BLDG. 197-C
UPTON NY 11973
USA

W. L. KIRK
LOS ALAMOS NATIONAL LABORATORY
P.O. BOX 1663, N-DO, MS E561
LOS ALAMOS NM 87545
USA

E. KNOGLINGER
PAUL SCHERRER INSTITUTE
WUERENLINGEN CH5303
SWITZERLAND

A. KOHSAKA
JAPAN ATOMIC RESEARCH INST.
TOKAI-MURA, NAKA-GUN
IBARAKI-KEN 319-11
JAPAN

M. J. KOMSI
IMATRAN VOIMA OY
P.O. BOX 112
VANTAA 01601
FINLAND

C. A. KOT
ARGONNE NATIONAL LABORATORY
9700 S. CASS AVE., BLDG 335
ARGONNE IL 60439
USA

G. S. KRAMER
BATTELLE COLUMBUS
505 KING AVE.
COLUMBUS OH 43201
USA

T. S. KRESS
OAK RIDGE NATIONAL LABORATORY
P.O. BOX 2009
OAK RIDGE TN 37831-8063
USA

C. A. KROPP
ENEA/DISP
VIA ANGUILLARESE K 1+300
ROME 00060
ITALY

G. A. KRUEGER
PHILADELPHIA ELECTRIC
2301 MARKET ST., N2-1
PHILADELPHIA PA 19101
USA

R. C. KRYTER
OAK RIDGE NATIONAL LABORATORY
P.O. BOX 2008
OAK RIDGE TN 37831-6010
USA

R. KUBOTA
HITACHI
SAIWAICHO 3-1-1
IBARAKI-KEN 317
JAPAN

C. A. KUKIELKA
PENNSYLVANIA POWER & LIGHT CO.
2 N. NINTH STREET
ALLENTOWN PA 18101
USA

D. S. KUPPERMAN
ARGONNE NATIONAL LABORATORY
9700 S. CASS AVE.
ARGONNE IL 60439
USA

K. F. KUSSMAUL
UNIVERSITY OF STUTTGART
PFAFFENWALDRING 32
STUTTGART 80 7000
FRG

P. S. LACY
URA
51 MONROE STREET
ROCKVILLE MD 20854
USA

T. K. LARSON
EG&G IDAHO INC.
P.O. BOX 1625
IDAHO FALLS ID 83415
USA

D. LEAVER
TANERA
1340 SARATOGA-SUNNYSIDE ROAD, SUITE 2
SAN JOSE CA 95129
USA

R. E. LECKENBY
UKAEA, RISLEY LABORATORY
WARRINGTON
CHESHIRE WA36AT
UK

M. LEE
BROOKHAVEN NATIONAL LABORATORY
BLDG. 130
UPTON NY 11973
USA

N. E. LEE
COMBUSTION ENGINEERING
1000 PROSPECT HILL RD
WINDSOR CT 06095
USA

J. R. LEHNER
BROOKHAVEN NATIONAL LABORATORY
BLDG. 130
UPTON NY 11973
USA

K. M. LEIGH
UKAEA/SRD
WIGSHAW LANE, CULCHETH
WARRINGTON WA34NE
UK

S. J. LEVINSON
BABCOCK & WILCOX CO.
3315 OLD FOREST RD
LYNCHBURG VA 24506
USA

P. M. LEWIS
PACIFIC NORTHWEST LABORATORY
P.O. BOX 999
RICHLAND WA 99352
USA

K. LIESCH
GESELLSCHAFT FUR REAKTORSICHERHEIT
FORSCHUNGSGELANDE
D-8046 GARCHING
FRG

J. N. LILLINGTON
UKAEA/AEE WINFRITH
DOERCHESTER
DORSET DT28DH
UK

C. L. LIN
ELECTRIC POWER RESEARCH INSTITUTE
3412 HILLYVIEW AVE.
PALO ALTO CA 94303
USA

L. LINDSTROM
SWEDISH NUCLEAR POWER INSPECTORATE
BOX 27016
STOCKHOLM SW S-10252
SWEDEN

Y. Y. LIU
ARGONNE NATIONAL LABORATORY
9700 S. CASS AVE.
ARGONNE IL 60439
USA

R. LOFARO
BROOKHAVEN NATIONAL LABORATORY
BLDG. 130
UPTON NY 11973
USA

J. P. LONGWORTH
CENTRAL ELECTRICITY GENERATING BD.
COURTNEY HSE., WARWICK LA
LONDON
UK

F. J. LOSS
MATERIALS ENGINEERING ASSOCIATES
9700-B M. L. KING HIGHWAY
LANHAM MD 20706
USA

A. L. LOWE, JR.
BABCOCK & WILCOX CO.
PO BOX 10935
LYNCHBURG VA 24506
USA

T. S. LUBNOW
MPR ASSOCIATES
1050 CONNECTICUT AVE., NW
WASHINGTON DC 20036
USA

W. J. LUCKAS, JR.
BROOKHAVEN NATIONAL LABORATORY
BLDG. 130
UPTON NY 11973
USA

H. L. MAGLEBY
EG&G IDAHO INC.
P.O. BOX 1625
IDAHO FALLS ID 83415
USA

A. P. MALINAUSKAS
OAK RIDGE NATIONAL LABORATORY
P.O. BOX 2008
OAK RIDGE TN 37831-6135
USA

R. M. MANDL
SIEMENS
HAMMERBACHERSTR. 12
ERLANGEN 852
FRG

C. F. MARKUS
WESTINGHOUSE ELECTRIC CORP.
P.O. BOX 79
W. MIFFLIN PA 15122-0079
USA

C. W. MARSCHALL
BATTELLE COLUMBUS
505 KING AVE.
COLUMBUS OH 43201
USA

P. MARSILI
ENEA/DISP
VIA VITALIANO BRANCATI, 48
ROME 00144
ITALY

B. MAVKO
J. STEFAN INSTITUTE
JAMOVA 39
LJUBLJANA 61000
YUGOSLAVIA

D. E. McCABE
MATERIALS ENGINEERING ASSOCIATES
9700-B M. L. KING HIGHWAY
LANHAM MD 20706
USA

L. D. McCANN
WESTINGHOUSE ELECTRIC CORP.
P.O. BOX 79
W. MIFFLIN PA 15122-0079
USA

R. K. McCARDELL
EG&G IDAHO INC.
P.O. BOX 1625
IDAHO FALLS ID 83415
USA

D. J. McCLOSKEY
SANDIA NATIONAL LABS.
P.O. BOX 5800
ALBUQUERQUE NM 87122
USA

K. P. McKay
WESTINGHOUSE ELECTRIC CORP.
P.O. BOX 79
W. MIFFLIN PA 15228
USA

N. R.H. McMillan
UKAEA/SRD
WIGSHAW LANE, CULCHETH
WARRINGTON WA34NE
UK

C. MEDICH
SIET
VIA NINO BIXIO 27
PIACENZA ITALY 29100
ITALY

H. B. MEIERAN
H B MEIERAN ASSOCIATES
458 SOUTH DALLAS AVENUE
PITTSBURGH PA 15208
USA

M. MERILO
ELECTRIC POWER RESEARCH INSTITUTE
3412 HILLVIEW AVE.
PALO ALTO CA 94303
USA

J. G. MERKLE
OAK RIDGE NATIONAL LABORATORY
P.O. BOX 2009
OAK RIDGE TN 37831-8049
USA

J. F. MEYER
SCIENTECH
11821 PARKLAWN DRIVE
ROCKVILLE MD 20852
USA

A. MEYER-HEINE
CEA FRENCH ATOMIC ENERGY COMMISSION
CEN CADARACHE-DERS/SEMAR BP NO. 1
SAINT PAUL LEZ DURANCE 13108
FRANCE

S. M. MIHAIU
YANKEE ATOMIC ELECT. CO.
508 MAIN ST.
BOLTON MA 01740
USA

J. S. MILLER
GULF STATES UTILITIES
P.O. BOX 220
ST. FRANCISVILLE LA 70775
USA

A. MINATO
ENERGY RESEARCH LAB., HITACHI LTD.
1168 MORIYAMA-CHO
HITACHI-SHI IBARAKI-KEN 316
JAPAN

S. M. MODRO
F25-AUSTRIA C/O EG&G
P.O. BOX 1625
IDAHO FALLS ID 83415
USA

T. MOMMA
JAERI C/O GENERAL ELECTRIC SAPS
RT. 168 S.
BEAVER PA 15077
USA

F. J. MOODY
GE NUCLEAR ENERGY
175 CURTNER AVE. MAIL CODE-769
SAN JOSE CA 95125
USA

R. J. MOORE
SAVANNAH RIVER LABORATORY
BLDG. 707C
AIKEN SC 29808
USA

F. I. MOPSIK
NAT'L INST. OF STDS. & TECH.
GAITHERSBURG MD 20899
USA

M.J. MOREAU
GENERAL ELECTRIC
P.O. BOX 1072
SCHENECTADY NY 12301
USA

V. MUBAYI
BROOKHAVEN NATIONAL LABORATORY
BLDG. 130
UPTON NY 11973
USA

Y. MURAO
JAPAN ATOMIC RESEARCH INST.
TOKAI-MURA, NAKA-GUN
IBARAKI-KEN 319-11
JAPAN

S. A. NAFF
SIEMENS AG,UB.KWU.UBS
POSTFACH 3220
ERLANGEN 8520
FRG

C. NAKAMURA
JAPAN ATOMIC RESEARCH INST.
TOKAI-MURA, NAKA-GUN
IBARAKI-KEN 319-11
JAPAN

R. K. NANSTAD
OAK RIDGE NATIONAL LABORATORY
PO BOX 2008, MS 6151
OAK RIDGE TN 37831
USA

A. NATLIZIO
ATOMIC ENERGY OF CANADA
SHERIDAN PARK RSCH. COMPT.
MISSISSAUGA ONTARIO L5K1B2
CANADA

D. J. NAUS
OAK RIDGE NATIONAL LABORATORY
P.O. BOX 2009, BLDG 9204-1
OAK RIDGE TN 37831-8056
USA

E. NEGRENTI
ENEA/DISP
V. ANGUILLARESE, 301
ROME 00060
ITALY

D. B. NEWLAND
NATIONAL NUCLEAR CORP.
BOOTH'S HALL, CHELFORD ROAD
KNUTSFORD ENGLAND
UK

L. Y. NEYMOTIN
BROOKHAVEN NATIONAL LABORATORY
BLDG 475B
UPTON NY 11973
USA

Y. NOGUCHI
CHUBU ELECTRIC POWER CO. INC
900 17TH ST. N.W., SUITE 714
WASHINGTON DC 20006
USA

P. NORTH
EG&G IDAHO INC.
P.O. BOX 1625
IDAHO FALLS ID 83415
USA

H. NOURBAKHSH
BROOKHAVEN NATIONAL LABORATORY
BLDG. 130
UPTON NY 11973
USA

S. P. NOWLEN
SANDIA NATIONAL LABS.
PO BOX 5800, DIV. 6447
ALBUQUERQUE NM 87185
USA

E. I. NOWSTRUP
CONSULTANT
17605 PARK MILL DR
ROCKVILLE MD 20855
USA

A. NUHM
TECHNICATOME
CEN CADARACHE
CADARACHE 13115
FRANCE

J. O'HARA
BROOKHAVEN NATIONAL LABORATORY
BLDG. 130
UPTON NY 11973
USA

K. R. O'KULA
SAVANNAH RIVER LABORATORY
BLDG. 773-41A
AIKEN SC 29808
USA

C. F. OBENCHAIN
EG&G IDAHO INC.
P.O. BOX 1625
IDAHO FALLS ID 83415
USA

T. OHNO
NUCLEAR POWER ENG'G TEST CTR
BLDG. 4-3-13, TORANOMON, MINATO-KU
TOKYO 105
JAPAN

M. OHUCHI
JAPAN SYSTEMS CORP.
NOMIURA BLDG., 4-8 YOMBANCHO, CHIYODA-
TOKYO 102
JAPAN

T. OKUBO
JAPAN ATOMIC RESEARCH INST.
TOKAI-MURA, NAKA-GUN
IBARAKI-KEN 319-11
JAPAN

R. C. OLSON
BALTIMORE GAS & ELECTRIC CO.
CCNPP-NGF PO BOX 1535
LUSBY MD 20657
USA

A. OMOTO
TOKYO ELECTRIC POWER
1901 L ST., NW, STE. 720
WASHINGTON DC 20036
USA

N. R. ORTIZ
SANDIA NATIONAL LABS., DIV. 6410
P.O. BOX 5800
ALBUQUERQUE NM 87185
USA

J. PAN
UNIVERSITY OF MICHIGAN
2250 G. G. BROWN BLDG., MECH. ENG.
ANN ARBOR MI 48108
USA

R. K. PAPESCH
BECHTEL-KWU ALLIANCE
15740 SHADY GROVE RD.
GAITHERSBURG MD 20877
USA

C. PARK
BROOKHAVEN NATIONAL LABORATORY
BLDG. 130
UPTON NY 11973
USA

W. R. PEARCE
CONSULTANT
6846 GLENBROOK ROAD
BETHESDA MD 20814
USA

G. A. PERTMER
UNIVERSITY OF MARYLAND
DEPT. OF CHEMISTRY & NUCLEAR ENGR.
COLLEGE PARK MD 20742
USA

G. PETRANGELI
ENEA/DISP
VIA VITALIANO BRANCATI, 48.
ROME 00144
ITALY

J. L. PIERREY
CEA FRENCH ATOMIC ENERGY COMMISSION
CEN/FAR, BP NO. 6
FONTENAT-AUX-ROSES 92265
FRANCE

A. PINI
ENEA/DISP
VIA VITALIANO BRANCATI, 48
ROME 00144
ITALY

M. G. PLYS
FAUSKE & ASSOCIATES
16W070 WEST 83RD STREET
BURR RIDGE IL 60521
USA

M. Z. PODOWSKI
RENSSELEAR POLYTECHNIC INSTITUTE
TROY NY 12180-3590
USA

A. Y. PORRACCHIA
CEA FRENCH ATOMIC ENERGY COMMISSION
CEN CADARACHE-DERS/SEMAR BP NO. 1
SAINT PAUL LEZ DURANCE 13108
FRANCE

D. A. POWERS
SANDIA NATIONAL LABS.
P.O. BOX 5800
ALBUQUERQUE NM 87185
USA

N. PRASAD
WESTINGHOUSE POWER SYSTEMS DIVISION
P.O. BOX 2728
PITTSBURGH PA 15230-2728
USA

T. PRATT
BROOKHAVEN NATIONAL LABORATORY
BLDG. 130
UPTON NY 11973
USA

D. A. PRELEWICZ
ENSA, INC.
15825 SHADY GROVE RD. (SUITE 170)
ROCKVILLE MD 20850
USA

J. G. PRUETT
OAK RIDGE NATIONAL LABORATORY
P.O. BOX 2008
OAK RIDGE TN 37831-6135
USA

J. PUGA
UNITED ELECTRICIA, S. A. (UNESA)
FRANCISCO GERVAS, 3
MADRID 28020
SPAIN

C. E. PUGH
OAK RIDGE NATIONAL LABORATORY
P.O. BOX 2009
OAK RIDGE TN 37831
USA

W. J. QUAPP
WESTINGHOUSE HANFORD CO.
PO BOX 1970
RICHLAND WA 99352
USA

P. J. QUATTRO
MBZ, INC.
1175 HERNDON PKWY., STE. 150
HERNDON VA 22070
USA

Z. H. QURESHI
SAVANNAH RIVER LABORATORY
786-5A
AIKEN SC 29808
USA

H. J. REILLY
IDAHO NATIONAL ENGINEERING LAB
PO BOX 1625
IDAHO FALLS ID 83402
USA

L. RIB
LNR ASSOCIATES
8605 GRIMSBY CT.
POTOMAC MD 20854
USA

B. RIEGEL
GESELLSCHAFT FUR REAKTORSICHERHEIT
FORSCHUNGSBELANDE
D-8046 GARCHING
FRG

D. E. ROBERTSON
PACIFIC NORTHWEST LABORATORY
P.O. BOX 999
RICHLAND WA 99352
USA

S. B. RODRIGUEZ
EG&G IDAHO INC.
1646 GRANDVIEW #1
IDAHO FALLS ID 83402
USA

U. S. ROHATGI
BROOKHAVEN NATIONAL LABORATORY
BLDG 4758
UPTON NY 11973
USA

B. ROSENSTROCH
EBASCO SERVICES INC.
2 WORLD TRADE CENTER 89E
NEW YORK NY 10048
USA

S. T. ROSINSKI
SANDIA NATIONAL LABS, DIV. 6513
P.O. BOX 5800
ALBUQUERQUE NM 87185
USA

J. C. ROUSSEAU
CEA FRENCH ATOMIC ENERGY COMMISSION
CEN/GRENOBLE
GRENOBLE 38000
FRANCE

D. RUBIO
ELECTRIC POWER RESEARCH INSTITUTE
3412 HILLVIEW AVE.
PALO ALTO CA 94303
USA

K. A. RUSSELL
EG&G IDAHO INC.
1520 SAWTELLE
IDAHO FALLS ID 83415
USA

J. RUTHERFORD
CENTRAL ELECTRICITY GENERATING BD.
BOOTH'S HALL, CHELFORD ROAD
KNUTSFORD CHESHIRE WA16 806
UK

B. F. SAFFELL
BATTELLE COLUMBUS DIVISION
505 KING AVENUE
COLUMBUS OH 43201
USA

R. T. SAIRANEN
TECHNICAL RSCH CTR OF FINLAND
POB 169
HELSINKI SF-00181
FINLAND

K. SAKANA
JAPAN INST. OF NUCLEAR SAFETY
FUJITA KANKOU TORANOMON MINATO
TOKYO 105
JAPAN

K. SAKANO
JAPAN INSTITUTE OF NUCLEAR SAFETY
FUJITA KANKON TOR. BLDG. 3-17-1
TOKYO 105
JAPAN

A. SALA
HIDROELECTRICO ESPANOLA
HERMOSILLA 3
MADRID 28001
SPAIN

J. SALUJA
VIKING SYSTEMS INTERNATIONAL
2070 WM PITT WAY
PITTSBURGH PA 15238
USA

L. SCHOR
YANKEE ATOMIC ELECT. CO.
508 MAIN ST.
BOLTON MA 01740
USA

D. G. SCHRAMEL
UFK
WEBERSTR. 5
KARLSRUHE
FRG

S. SETH
MITRE CORP.
7525 COLSHIRE DR.
MCLEAN VA 22102
USA

W. J. SHACK
ARGONNE NATIONAL LABORATORY
BLDG. 212
ARGONNE IL 60439
USA

V. N. SHAH
EG&G IDAHO INC.
P.O. BOX 1625
IDAHO FALLS ID 83415
USA

R. H. SHANNON
CONSULTING ENGINEER
P.O. BOX 2264
ROCKVILLE MD 20852
USA

R. S. SHARMA
AMERICAN ELECTRIC POWER
ONE RIVERSIDE PLAZA
COLUMBUS OH 43017
USA

D. A. SHARP
SAVANNAH RIVER LABORATORY
AIKEN SC 29801
USA

D. L. SHAW
BALTIMORE GAS & ELECTRIC COMPANY
CALVERT CLIFFS NPP, P.O. BOX 1535
LUSBY MD 20657
USA

L. SHEN
ATOMIC ENERGY COUNCIL, ROC
NO 67, LANE 144, KEELUNG RD. SEC. 4
TAIPEI TAIWAN 107
ROC

G. L. SHERWOOD
U.S. DEPT. OF ENERGY
GERMANTOWN MD 21701
USA

P. SHEWMON
ACRS
2477 LYTHAM ROAD
COLUMBUS OH 43220
USA

K. SHIBATA
JAPAN ATOMIC RESEARCH INST.
TOKAI-MURA, NAKA-GUN
IBARAKI-KEN 319-11
JAPAN

K. SHIMIZU
HITACHI, LTD.
1-1 SAIWAI-MACHI
HITACHI
JAPAN

A. SHIMIZU
OHBAYASHI CORP.
777 RIVERVIEW DR., APT. 9
ROCHESTER PA 15074
USA

J. J. SHIN
EBASCO SERVICES, INC.
2 WORLD TRADE CENTER
NEW YORK NY 10048
USA

M. S. SHINKO
EMERGENCY RESPONSE TEAM
PO BOX 129
WASHINGTON GROVE MD 20880
USA

B. S. SHIRALKAR
GENERAL ELECTRIC CO.
175 CURTNER AVE (M/C 186)
SAN JOSE CA 95125
USA

D. A. SIEBE
LOS ALAMOS NATIONAL LABORATORY
P.O. BOX 1663, MS K555
LOS ALAMOS NM 87545
USA

E. G. SILVER
OAK RIDGE NATIONAL LABORATORY
P.O. BOX 2009, BLDG 9201-3
OAK RIDGE TN 37831-8065
USA

F. A. SIMONEN
PACIFIC NORTHWEST LABORATORY
P.O. BOX 999
RICHLAND WA 99352
USA

F. B. SIMPSON
EG&G IDAHO INC.
P.O. BOX 1625
IDAHO FALLS ID 83415
USA

L. SLEGERS
SIEMENS KWU
BERLINER STR 295-303
OFFENBACH 6000
FRG

G. L. SMITH
WESTINGHOUSE HANFORD CO.
P.O. BOX 1970 X0-44
RICHLAND WA 99352
USA

A. W. SNYDER
SANDIA NATIONAL LABS. ORG. 6500
P.O. BOX 5800
ALBUQUERQUE NM 87185
USA

P. SOO
BROOKHAVEN NATIONAL LABORATORY
BLDG 830
UPTON NY 11973
USA

H. SPECTER
NEW YORK POWER AUTHORITY
123 MAIN STREET
NEW YORK NY 10601
USA

J. E. SPEELMAN
ECN
3 WESTERDUINWEG, P.O. BOX 1
PETTEN NEW HOLLAND 1755 ZG
THE NETHERLANDS

K. E. ST. JOHN
YANKEE ATOMIC ELECTRIC CO.
1671 WORCESTER RD
FRAMINGHAM MA 01701
USA

H. STADTKE
JOINT RESEARCH CENTRE-ISPRA ESTABLISH
ISPRA 21020
ITALY

D. D. STEPNEWSKI
WESTINGHOUSE HANFORD CO.
P.O. BOX 1970 NI-31
RICHLAND WA 99352
USA

E. J. STURBE
TRACTABEL
31 RUE DE LA SCIENCE
BRUSSELS 1040
BELGIUM

R. K. SUNDARAM
YANKEE ATOMIC ELECT. CO.
508 MAIN ST.
BOLTON MA 01740
USA

J. D. SUTTON
YANKEE ATOMIC ELECTRIC CO.
580 MAIN ST.
BOLTON MA 01740
USA

T. SUZUKI
TOSHIBA
SHINSUGITA 15060-KU
YOKOHAMA
JAPAN

I. SZABO
C.E.A.
C.E.N CADARACHE
ST. PAUL LES DURAN 43
FRANCE

A. TAKAGI
TOSHIBA
4921 NORWALK DR., APT V202
SAN JOSE CA 95125
USA

K. TASAKA
JAPAN ATOMIC RESEARCH INST.
TOKAI-MURA, NAKA-GUN
IBARAKI-KEN 319-11
JAPAN

J. H. TAYLOR
BROOKHAVEN NATIONAL LABORATORY
BLDG 130
UPTON NY 11973
USA

B. J. TOLLEY
COM. OF THE EUROPEAN COMMUNITIES (C)
200 RUE DE LA LOI
BRUSSELS 1049
BELGIUM

J. S. TONG
ATOMIC ENERGY CONTROL BOARD
PICKERING NGS OPERATIONS
PICKERING ONTARIO L1V2R5
CANADA

L. S. TONG
TAI
9733 LOOKOUT PLACE
GAITHERSBURG MD 20879
USA

F. M. TOUBOUL
CEA FRENCH ATOMIC ENERGY COMMISSION
CEN-SACLAY DEMT/SMTS/RDMS
GIF-SUR-YVETTE 91191
FRANCE

H. E. TRAMMELL
OAK RIDGE NATIONAL LABORATORY
104 OGLETHORPE PL
OAK RIDGE TN 37830
USA

J. D. TROTTER
GROVE ENGINEERING
15215 SHADY GROVE RD.
ROCKVILLE MD 20878
USA

C-K TSAI
WESTINGHOUSE POWER SYSTEMS DIVISION
P.O. BOX 355
PITTSBURGH PA 15230-2728
USA

T. TSUJINO
JAPAN ATOMIC RESEARCH INST.
TOKAI-MURA, NAKA-GUN
IBARAKI-KEN 319-11
JAPAN

B. D. TURLAND
UKAEA CULHAM
CULHAM LABORATORY
ABINGDON
UK

G. TYROR, DIRECTOR
UKAEA/SRD
WIGSHAW LANE, KNUTSFORD
WARRINGTON WA34NE
UK

R. E. UHRIG
OAK RIDGE NATIONAL LABORATORY
113 CONNORS DRIVE
OAK RIDGE TN 37830
USA

R. A. VALENTIN
ARGONNE NATIONAL LAB - BLDG. 208
9700 S. CASS AVE
ARGONNE IL 60439
USA

Ø. L.C.M. VAYSSIER
MINISTRY OF SOCIAL AFFAIRS
P.O. BOX 69
VOORBURG 2270MA
THE NETHERLANDS

O. VESCOVI
SIET
VIA NINO BIXIO 27
PIACENZA 29100
ITALY

G. L. VINE
ELECTRIC POWER RESEARCH INSTITUTE
3412 HILLYVIEW AVE.
PALO ALTO CA 94303
USA

D. S. WALLS
OAK RIDGE NATIONAL LABORATORY
P.O. BOX 2009, M5-8057
OAK RIDGE TN 37831-8065
USA

S. F. WANG
INST. OF NUCLEAR ENERGY RSCH.
PO BOX 3-3, LUNG TAN
TAIPEI TAIWAN 32500
ROC

O. J. WANG
WESTINGHOUSE HANFORD CO.
P.O. BOX 1970 X0-44
RICHLAND WA 99352
USA

R. WANNER
PAUL SCHERRER INSTITUTE
WUERENLINGEN CHS303
SWITZERLAND

E. A. WARMAN
STONE & WEBSTER
245 SUMMER ST.
BOSTON MA 02107
USA

K. E. WASHINGTON
SANDIA NATIONAL LABS.
P.O. BOX 5800
ALBUQUERQUE NM 87185
USA

W. L. WEAVER
EG&G IDAHO INC.
P.O. BOX 1625
IDAHO FALLS ID 83415
USA

E. O. WEINER
WESTINGHOUSE HANFORD CO.
P.O. BOX 1970, L2-57
RICHLAND WA 99352
USA

P. A. WEISS
SIEMENS AG / UB KWU
HAMMERBACHERSTR. 12+14
ERLANGEN 8520
FRG

H. J. WELLAND
EG&G IDAHO INC.
442 JOAN AVENUE
IDAHO FALLS IDAHO 83401
USA

E. T. WESSEL
CONSULTANT
312 WOLVERINE STREET
HAINES CITY FL 33844
USA

H. WESTPHAL
GESELLSCHAFT FÜR REAKTORSICHERHEIT
SCHWERTNERGASSE 1
D-5000 COLOGNE 1
FRG

A. M. WHITE
SAVANNAH RIVER LABORATORY
BLDG. 773-11A
AIKEN SC 29808
USA

J. D. WHITE
OAK RIDGE NATIONAL LABORATORY
P.O. BOX 2008
OAK RIDGE TN 37831-6009
USA

G. M. WILKOWSKI
BATTELLE COLUMBUS
505 KING AVE.
COLUMBUS OH 43201
USA

W. K. WINEGARDNER
PACIFIC NORTHWEST LABORATORY
P.O. BOX 999
RICHLAND WA 99352
USA

F. J. WINKLER
SIEMENS
RINGSTRASSE 19
SPARDORF
FRG

L. WOLF
KERNFORSCHUNGSZENTRUM, PHDR
POSTFACH 3640
7500 KARLSRUHE 1
FRG

A. J. WOLFORD
EG&G IDAHO INC.
P.O. BOX 1625
IDAHO FALLS ID 83415
USA

D. N. WOODY
SAVANNAH RIVER LABORATORY
AIKEN SC 29808
USA

R. O. WOOTON
BATTELLE COLUMBUS
505 KING AVE.
COLUMBUS OH 43201
USA

J. WREATHALL
SAIC
2929 KENNY RD.
COLUMBUS, OH 43221
USA

D. W. WRIGHT
ANCHOR/DARLING VALVE
701 FIRST ST.
WILLIAMSPORT PA 17701
USA

W. WULFF
BROOKHAVEN NATIONAL LABORATORY
BLDG 475B
UPTON NY 11973
USA

H. XU
BROOKHAVEN NATIONAL LABORATORY
BLDG. 130
UPTON NY 11973
USA

Y. YAMAMOTO
TAKENAKA CO.
21-1 8CHOME CHUO-KU
TOKYO
JAPAN

H. YASOSHIMA
JAPAN ATOMIC RESEARCH INST.
TOKAI-MURA, NAKA-GUN
IBARAKI-KEN 319-11
JAPAN

M. YOKOTA
JAPAN ATOMIC RESEARCH INST.
TOKAI-MURA, NAKA-GUN
IBARAKI-KEN 319-11
JAPAN

Y. YOSHIMOTO
HITACHI, LTD.
SAIWAI-CHO 3-H
HITACHI-SHI 316
JAPAN

R. W. YOUNGBLOOD
BROOKHAVEN NATIONAL LABORATORY
BLDG 130
UPTON NY 11973
USA

R. ZIPPER
GESELLSCHAFT FÜR REAKTORSICHERHEIT
SCHWERTNERGASSE 1
D-5000 COLOGNE 1
FRG

P. C. ZMOLA
C&P ENGINEERING
5409 NEWINGTON RD.
BETHESDA MD 20816
USA

R. ZOGRAN
MPR ASSOCIATES, INC.
1050 CONNECTICUT AVENUE, N.W.
WASHINGTON DC 20036
USA

PROCEEDINGS OF THE
SIXTEENTH WATER REACTOR SAFETY INFORMATION MEETING

October 24-27, 1988

TABLE OF CONTENTS - VOLUME 3

	<u>Page</u>
ABSTRACT.	iii
GENERAL INDEX	v
REGISTERED ATTENDEES.	vii

NUCLEAR PLANT AGING

Chairman: J. P. Vora (NRC)

Condition Monitoring and Aging Assessment of Class 1E Cables.	1
M. J. Jacobus (SNL)	
Time Domain Spectroscopy to Monitor the Condition of Cable Insulation.	21
F. I. Mopsik and F. D. Martzloff (NIST)	
Lessons Learned to Date from the Shippingport Aging Evaluation.	41
R. P. Allen and A. B. Johnson, Jr. (PNL)	
Aging Assessment and Mitigation for Major LWR Components.	59
V. N. Shah et al. (INEL), and J. J. Burns, Jr. (NRC)	
The Effects of Aging on the Fire Vulnerability of Nuclear Power Plant Components.	85
S. P. Nowlen (SNL)	
Nuclear Plant Aging Study of Residual Heat Removal Systems.	97
R. Lofaro et al. (BNL)	

NUCLEAR PLANT AGING

Chairman: M. Vagins (NRC)

Nuclear Plant Aging Research on the High Pressure Injection System.	109
L. C. Meyer and H. L. Magleby (INEL)	
Safety Implications of Diesel Generator Aging Management.	131
K. R. Hoopingarner (PNL)	
Aging Assessment of PWR Auxiliary Feedwater Systems	143
D. A. Casada (ORNL)	

NUCLEAR PLANT AGING
(Cont'd)

	<u>Page</u>
PRAAGE-1988: An Interactive IBM-PC Code for Aging Analysis of NUREG-1150 Systems	157
R. R. Fullwood and W. G. Shier (BNL)	
Utilization of Aging Program Results in Plant Inspections	175
W. Gunther and R. Fullwood (BNL)	

STRUCTURAL AND SEISMIC ENGINEERING

Chairman: A. J. Murphy (NRC)

Probability of Crack-Induced Failure in BWR Recirculation Piping.	185
G. S. Holman (LLNL)	
Guillotine Breaks Indirectly Caused by Seismically-Induced Failures.	213
G. S. Holman and T. Lo (LLNL)	
Piping and Fitting Dynamic Reliability Program.	247
D. Guzy (NRC), S. Tagart and Y. K. Tang (EPRI), W. English and H. Hwang (GE), K. Merz (ANCO), and V. DeVita (ETEC)	
Relay Studies - Exiting Data, Current Testing and Cabinet Amplification	265
K. Bandyopadhyay et al. (BNL)	
ASCE Working Group Activities on Stiffness of Concrete Shear Wall Structures	279
J. G. Bennett and C. R. Farrar (LANL)	
Assessment of Effects of Structural Response on Plant Risk and Margin.	293
M. P. Bohn and E. W. Klamerus (SNL)	
The Role of Parameter Uncertainty in Seismic Risk Assessment.	299
B. Ellingwood (Johns Hopkins Univ.)	
Progress Report on the Containment Integrity Programs	311
D. B. Clauss et al. (SNL)	
SHAM: High-Level Seismic Tests of Piping at the HDR.	339
C. A. Kot, M G. Srinivasan and B. J. Hsieh (ANL), L. Malcher and D. Schrammel (KfK), H. Steinhilber (Fraunhofer Inst.), and J. F. Costello (NRC)	
Evaluation of Aged Concrete Structures for Continued Service in Nuclear Power Plants.	363
D. J. Naus and M. F. Marchbanks (ORNL), and E. G. Arndt (NRC)	

MECHANICAL RESEARCH

Chairman: G. H. Weidenhamer (NRC)

	<u>Page</u>
Application of Signature Analysis for Determining the Operational Readiness of Motor-Operated Valves Under Blowdown Test Conditions	381
H. D. Haynes (ORNL)	
Assessment of Nonintrusive Methods for Monitoring the Operational Readiness of Solenoid-Operated Valves	399
R. C. Kryter (ORNL)	
Similarity Principles for Seismic Qualification of Equipment by Experience Data.	411
D. D. Kana and D. J. Pomerening (SWRI)	
Valve Testing for UK PWR Safety Applications.	437
S. Bryant, P. T. George and D. R. Airey (CEGB)	
Piping Support and Gate Valve Behavior During High Level HDR Simulated Seismic Tests	445
R. Steele, Jr. (INEL)	
Early Results of Gate Valve Flow Interruption Blowdown Tests.	467
K. G. DeWall (INEL)	

ENVIRONMENTAL EFFECTS IN PRIMARY SYSTEMS

Chairman: A. Taboada (NRC)

Environmentally Assisted Cracking in Light Water Reactors	491
W. J. Shack et al. (ANL)	
Initial Assessment of the Processes and Significance of Thermal Aging in Cast Stainless Steels.	519
O. K. Chopra and H. M. Chung (ANL)	
Shippingport Aging Studies - Results and Plans.	547
W. J. Shack, O. K. Chopra and H. M. Chung (ANL)	

Condition Monitoring and Aging Assessment of Class 1E Cables

M. J. Jacobus
Sandia National Laboratories
P.O. Box 5800
Albuquerque, NM 87185

ABSTRACT

Sandia National Laboratories is currently conducting long-term aging research on representative samples of nuclear power plant Class 1E cables. The objectives of this program are to determine the suitability of these cables for extended life (beyond 40 year design basis) and to assess various cable condition monitoring (CM) techniques for predicting remaining cable life. The cables are being aged for long times at relatively mild exposure conditions with various CM techniques being employed during the aging process. Following the aging process, the cables will be exposed to a sequential accident profile consisting of high dose rate irradiation followed by a simulated design basis loss-of-coolant accident (LOCA) steam exposure.

This paper covers two aspects of the research program: the electrical measurement techniques that have been developed and are being performed and some initial data that has been generated from these measurement techniques. The electrical measurements include insulation resistance, polarization index, capacitance, and dissipation factor.

INTRODUCTION AND OBJECTIVES

Many types of cable are used throughout nuclear power plants in a wide variety of applications. Past practice of cable qualification has typically included preoperational type testing consisting of highly accelerated thermal and radiation aging intended to put the cable in its end-of-life condition,

1 The Long-Term Cable Aging Program is supported by the United States Nuclear Regulatory Commission and performed at Sandia National Laboratories which is operated for the U.S. Department of Energy under contract number DE-AC04-76DP00789.

followed by simulated accident testing. Generally, the radiation and thermal aging are applied to the specimens sequentially, but some (primarily research) programs have applied the environments simultaneously.^{1,2,3,4}

Once cable installation and checkout is completed, cables are generally not subjected to any type of periodic maintenance or surveillance. The technical basis for a lack of maintenance and surveillance is the combination of qualification testing, installation verification, and operating experience. However, with outstanding aging issues and with significant interest in life extension of current nuclear plants, efforts to detect aging and predict continued functionality of cables (as well as other types of equipment) are needed. Most qualification efforts do not provide information that can be used to establish a valid, technically based CM program to verify a cable's ability to survive an accident environment and to support life extension.

The primary purposes of the current testing program are to assess the effectiveness of various cable CM techniques for predicting how cables will perform in an accident environment and to gain an indication of whether cable life extension beyond 40 years is practical. We are conducting simultaneous radiation and thermal aging on three test chambers to equivalent nominal lifetimes of 20, 40, and 60 years. After aging, a sequential accident exposure consisting of high dose rate radiation followed by a steam exposure will be performed. The data obtained from the monthly CM techniques will be correlated with observed performance of cables during the LOCA. This will provide information regarding appropriate cable CM acceptance criteria for typical nuclear cables.

In addition to the primary objectives, we also expect to derive additional insights from the test program, including the following: (1) the effects of low dose rate radiation exposure and low temperature, long time thermal aging on cable mechanical properties versus those obtained from more accelerated, but similar aging conditions on previous cable specimens in Sandia tests, (2) the LOCA behavior of cables aged for long times at low exposure conditions, (3) assessment of the conservatism associated with the current post-LOCA mandrel bend and dielectric withstand test, (4) evaluation of how cables age during long term simultaneous exposure to thermal and radiation aging, and (5) assessment of what additional qualification requirements might be necessary to qualify cables for life extension.

This paper discusses some electrical condition monitoring techniques that we have implemented. These include insulation resistance as a function of time and voltage and transfer function (capacitance and dissipation factor) as a function of

frequency. The remainder of this paper discusses more details of the experimental arrangement, implementation considerations for electrical measurement techniques, some initial data from the electrical measurements, and some future directions and conclusions.

EXPERIMENTAL ARRANGEMENT

Test Setup

The testing consists of two phases, a long term simultaneous thermal and radiation aging followed by a sequential accident exposure consisting of high dose rate radiation followed by a steam exposure. The cable products included in our study are listed in Table 1. This test program includes only aged samples. Three different sets of cable specimens are being tested: one aged to a nominal lifetime of 20 years, a second to 40 years, and a third to 60 years. Each cable has an exposed length in the test chamber of about 15 feet. Actual simulated lifetimes will vary because of the different activation energies of the specimens (a nominal activation energy of 1.15 was assumed in aging calculations). We chose artificial aging times of three, six, and nine months. The aging temperature assumes a plant ambient temperature of 55#C with no conductor heat rise. (Conductor heat rise during aging is rarely significant in nuclear power plant circuits subject to equipment qualification (EQ) because most EQ power circuits are not energized during normal operation and other circuits have minimal heat rise because of low current levels.) Based on the Arrhenius equation, the resulting aging temperature is 95#C. The radiation aging doses are 20 Mrads for the "20 year" cables, 40 Mrads for the "40 year" cables, and 60 Mrads for the "60 year" cables. The resulting dose rate for our test is about 9 krads/hr.

Outside air is heated and introduced into the chamber during aging to maintain a temperature of about 95-100#C and ambient oxygen concentrations. An air overpressure of about 5 psig is used to prevent any water leakage into the test chamber. Three independently controlled wall heaters inside the test chamber help to maintain temperature uniformity. We have also included short cable segments in the aging chambers. These will be used for tensile and elongation testing and for dielectric breakdown testing. These samples will be removed at one month intervals to assess their condition.

Accident testing consists of irradiation followed by a simulated design basis LOCA test. The accident dose is approximately 110 Mrads at a dose rate of between 0.3 and 0.5 Mrad/hr. The accident profile is similar to that in IEEE 323-1974 for "generic" qualification, except that the accident exposure is accelerated to seven days and no chemical spray is

Table 1: Cable Products Included in Test Program

<u>Supplier</u>	<u>Description</u>
Brand Rex	XLPE Insulation, CSPE Jacket, 12 AWG, 3/C, 600 V
Rockbestos	Firewall 3, Irradiation XLPE, Neoprene Jacket, 12 AWG, 3/C, 600 V
Raychem	Flamtrol, XLPE Insulation, 12 AWG, 1/C, 600 V
Samuel Moore	Dekoron Polyset, XLPO Insulation, CSPE Jacket, 12 AWG, 3/C and Drain
Anaconda	Anaconda Y Flame-Guard FR-EP EPR Insulation, CPE Jacket, 12 AWG, 3/C, 600 V
Okonite	Okonite Okolon, EPR Insulation, Hypalon Jacket, 12 AWG, 1/C, 600 V
Samuel Moore	Dekoron Dekorad Type 1952, EPDM Insulation, Hypalon Jacket, 16 AWG, 2/C TSP, 600 V
Kerite	Kerite 1977, FR Insulation, FR Jacket, 12 AWG 1/C, 600 V
Rockbestos	RSS-6-104/LE Coaxial Cable, 22 AWG, 1/C Shielded
Rockbestos	Firewall Silicone Rubber Insulation, 16 AWG, 1/C, 600 V
Champlain	Polyimide Insulation, Unjacketed, 12 AWG, 1/C
BIW	Bostrad 7E, EPR Insulation, CSPE Jacket, 16 AWG, 2/C TSP, 600 V

Abbreviations used in table:

XLPE - Cross-linked polyethylene
 CSPE - Chlorosulfonated polyethylene
 AWG - American Wire Gauge
 /C - number of conductors
 XLPO - Cross-linked polyolefin
 FR-EP - Flame retardant ethylene propylene
 CPE - Chlorinated polyethylene
 EPR - Ethylene propylene rubber
 EPDM - Ethylene propylene diene monomer
 TSP - Twisted shielded pair
 FR - Flame retardant
 BIW - Boston Insulated Wire

included. The planned accident profile has superheated steam conditions during the first 11 hours of the test. It then continues as saturated steam. Three separate accident tests will be performed, one using each test chamber.

Condition Monitoring Techniques

A number of different CM techniques are being used in this test program, but will only be described briefly here. These include the following:

a. Breakdown voltage. Breakdown voltage of cable segments will be performed using a voltage ramp rate of 500 V/s. The sections of cable to be used for these tests are aged and irradiated concurrently with those cables employed for in-situ and non-destructive testing. Specimens for the breakdown test are submerged during testing to provide a ground reference for the applied voltage. This dielectric withstand test is one measure of the ultimate electrical capability of the insulation.

b. Ultimate tensile strength and elongation. These measurements, in particular elongation, have historically been used by the cable industry to assess the thermal aging behavior of low voltage cable materials. These properties have also been extensively used to characterize the susceptibility of cable materials to dose rate and synergistic aging effects. These practices are used since elongation at break typically decreases with increased aging. In contrast, tensile strength may first increase, then decrease with age, and therefore has been less used by the industry to characterize aging behavior.

Our measurements are made with a Instron Model 1000 tensile test apparatus and use small test specimens (about six inches long) which are aged concurrently with the cable specimens. We generate tensile specimens by disassembling the cables prior to the start of the aging exposure. Therefore, we are only monitoring this parameter for those cables whose jacket is not bonded to the insulation.

c. Modulus profiling. The modulus is a measure of the slope of the stress vs. strain curve in the initial linear portion of the curve. Modulus profiling considers the variation of the modulus over the cross section of a specimen. Changes in insulation modulus have been shown to correlate with thermal aging degradation.⁹ However, for ethylene propylene rubber (EPR) materials, modulus has not always correlated well with radiation degradation. In certain circumstances, modulus profiling of cable specimens gives an indication of aging uniformity and hence is used in our test to help assess whether dose rate effects have been eliminated by test parameters. Consequently, modulus profiling is being used only on selected cable samples using a test apparatus developed at Sandia.⁹

d. Hardness testing. Hardness is a material's resistance to local penetration. It is measured with any of a variety of hardness testers. In this program, a Shore Durometer Type A2 will be used for the measurements. The modulus profiling technique will yield much more quantitative information, but the hardness tests will be included since they represent a very simple field measurement technique and have demonstrated some correlation to polymer degradation.¹⁰

e. Bulk density. Density measurements have demonstrated that insulation density tends to increase with aging by oxidation.¹¹ Thus, as for modulus, it may be subject to gradients resulting from oxygen diffusion effects. In this program, bulk density is being measured for selected samples and other techniques, such as modulus profiling, are being used to give an indication of the gradients resulting from oxygen diffusion. Small samples are being kept during the tests for later analysis of bulk density or density profile if deemed necessary.

f. Visual appearance. The visual appearance of the cables is thoroughly documented periodically throughout the aging exposure. In particular, evidence of discoloration, cracking, or any other abnormal condition is noted.

g. Additional techniques which may be used to a limited extent in this test program include indentation testing using Franklin Research Center's test apparatus developed under EPRI funding,¹² step voltage response of small samples (a technique advanced by the National Bureau of Standards^{6,7,8} to measure transfer function, with particular applicability at very low frequencies), thermogravimetric analysis (TGA), differential scanning calorimetry (DSC), and average molecular weight measurements.

The remaining CM measurements are being performed on-line during aging and will form the basis for the remainder of this paper. These measurements are all electrical and may be generally characterized as insulation resistance measurements as a function of voltage and time (i.e. up to one or five minutes depending on the test voltage) and transfer function as a function of frequency. Information which can be deduced from the insulation resistance measurements includes insulation resistance at a specific time (one minute is a time which is typically employed by the industry), polarization indices, and step voltage behavior (i.e. insulation resistance as a function of voltage). Parameters which can be calculated as a function of frequency from the transfer function are real and imaginary components of the complex transfer function, capacitance and dissipation factor, real and imaginary (loss) components of complex capacitance, power factor, loss angle, etc.

Some guidance for insulation resistance measurements is provided in industry standards. IEEE Std. 402-1974¹⁴ is one such standard, but it primarily applies to laboratory testing of small specimens in a test cell. IEEE Std. 4-1978¹⁵ provides general information for high-voltage testing. IEEE Std. 62-1978¹⁶ provides guidelines for field testing of power apparatus insulation.

For our tests, insulation resistance measurements are being performed between each conductor and ground with all other conductors connected to ground. Measurements are taken at 3 voltages, 50, 100, and 250 V. Leakage current (or insulation resistance) data is taken at discrete time points from 2 seconds to 1 minute for 50 and 100 V measurements and from 2 seconds to 5 minutes for 250 V measurements. Insulation resistance gives a measure of the resistive component of the dielectric impedance. It is typically used in industry as a go/no-go test of insulation. However, no technical basis is available to set an acceptance criteria related to age-related degradation.¹³ Rather, the test usually is used to assist detection of locally damaged cable (e.g. insulation windings that are wet, a gouged cable that is "sufficiently close" to the ground plane in the test, etc.).

Some common criticisms of insulation resistance measurements are that they are subject to uncontrollable temperature and humidity effects along the cable. Because they are dimensionless quantities, polarization indices are sometimes used to determine the condition of an insulation structure. A polarization index lower than normal suggests excessive surface leakage or deteriorated insulation.^{5,16} IEEE 62-1974¹⁶ indicates a definition of polarization index as the ratio of the insulation resistance at 10 minutes to the insulation resistance at 1 minute, which should normally be greater than 1. It should be noted, however, that other definitions of polarization index may be used. In this study two major polarization indices are being used. At all voltage levels, a polarization index ratio of 1 minute to 30 seconds is being used; at 250 V, a second polarization index ratio of 5 minutes to 1 minute is being used. Other polarization indices may be used depending on the behavior demonstrated by the cables.

Transfer function measurement techniques are described in References 17, 18 and 19. The transfer function gives an indication of the variation of dielectric impedance (principally due to the bulk cable capacitance and conductance) as a function of frequency. The imaginary component of the transfer function gives an indication of the dielectric charge/voltage characteristics at the given frequency, and the phase angle between the real and imaginary components gives an indication of the dielectric losses as a function of frequency. The tangent of the phase angle δ is commonly referred to as the dissipation

factor (DF) and is often measured only at a single discrete frequency. Dissipation factor also gives an indication of the power factor (PF) since the two are related as $PF=DF/(1+DF^2)$. If d is a small angle, then $PF|DF$.

References 17-19 describe a number of bridge techniques, with probably the most famous being the Schering Bridge. Typically in bridge techniques, a sinusoidal voltage is applied to a bridge containing the unknown sample as one leg. Other reference legs are adjusted until bridge balance is obtained and the unknown capacitance and resistance at the discrete frequency is calculated based on the reference values.

We are making capacitance and dissipation factor measurements using two different instruments, covering an effective range of frequency from about 0.3 Hz to 500 KHz. We use a Hewlett Packard Model 4192A Low Frequency (LF) Analyzer to make these measurements at the "higher" frequencies, ranging from about 100 Hz to 1 MHz, and we use a Hewlett Packard Model 3192A Spectrum Analyzer combined with a low noise preamplifier to make the measurements at the lower frequencies, from about 0.3-1000 Hz. The overlapping portion of the ranges provides a check between measurements made by two independent techniques. As with insulation resistance, the transfer function in our tests is evaluated between each conductor and ground with all other conductors connected to ground.

IMPLEMENTATION CONSIDERATIONS

Insulation Resistance

The test apparatus for measuring insulation resistance is shown in Figure 1. An HP Model 216 computer is used to control the data acquisition. A Keithley electrometer is used to measure the voltage across a dropping resistor which is selected on-line by the computer. The output of the Keithley is then fed, via the HP 3497A datalogger, to the computer for storage on disc. The datalogger also automatically selects the proper voltage level using the 0-250 Vdc power supply.

Probably the major difficulty with implementing the above system is the high insulation resistances which must be measured. Several techniques, which are perhaps not obvious from Figure 1, are used to overcome the difficulties associated with measuring high impedances. For illustrative purposes, assume that the insulation resistance to be measured is $10^{11} X$ at 100 V using the 60 MX dropping resistor. This value has been exceeded by some cables in our test, even at elevated temperatures. A typical relay has an isolation resistance of $10^9 X$ between open contacts and between open contacts and the coil.

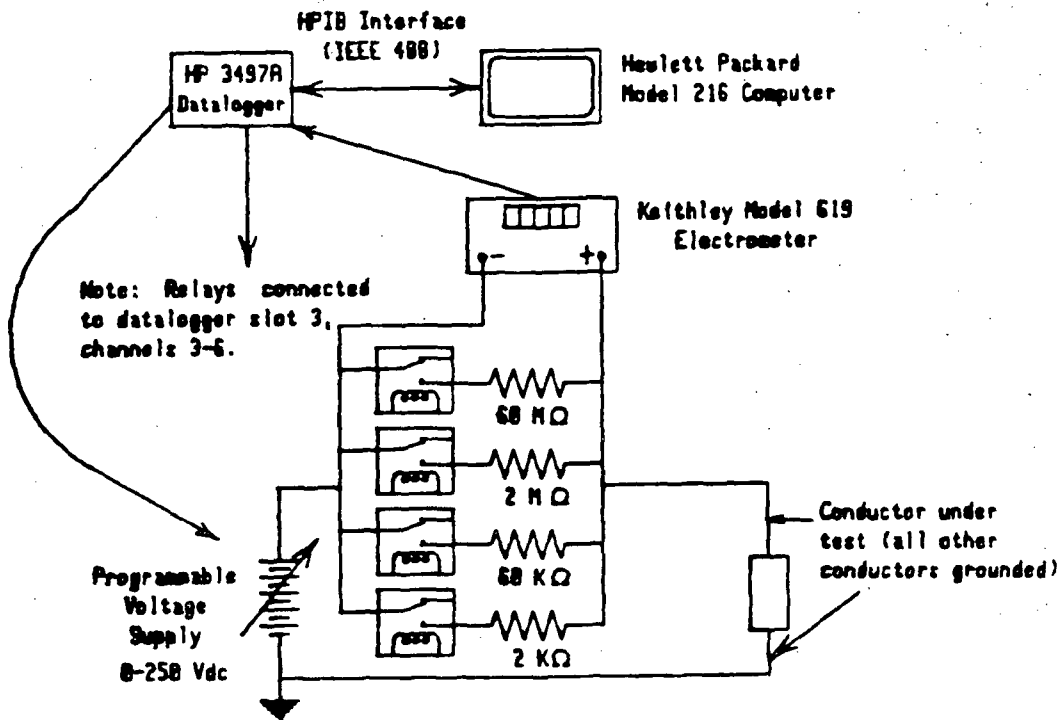


Figure 1 Circuitry to Measure Insulation Resistance

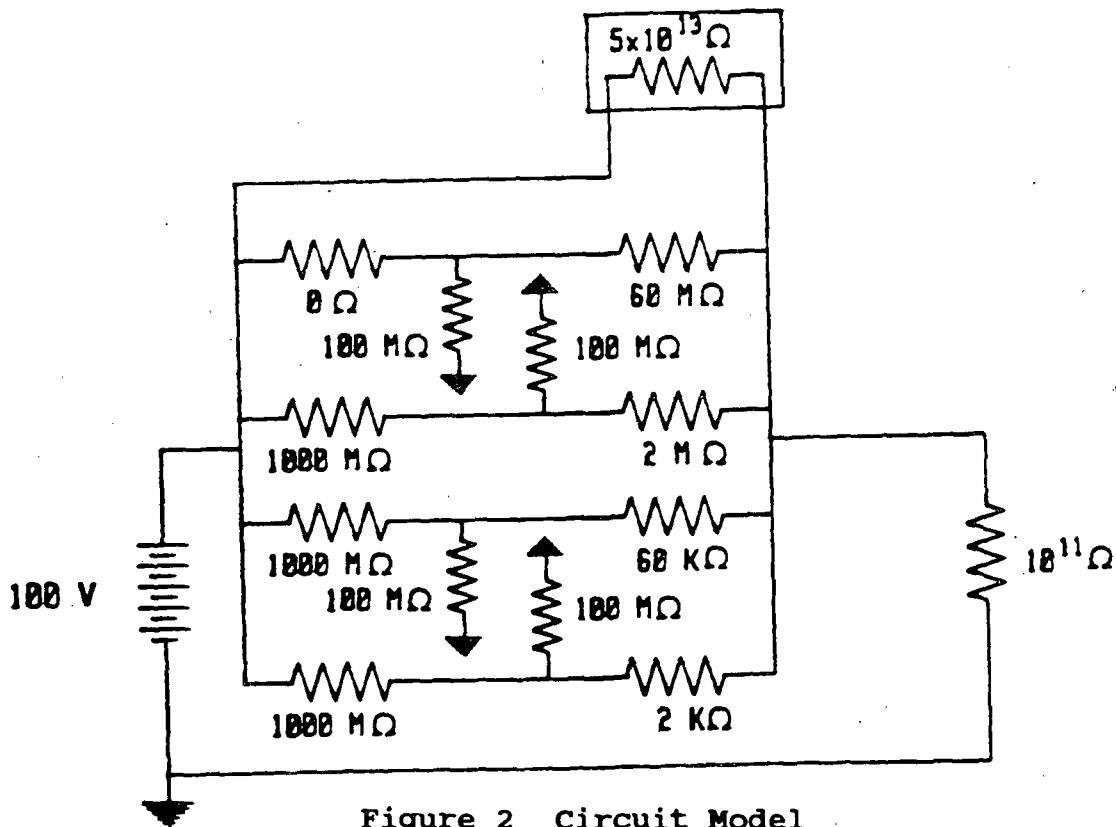


Figure 2 Circuit Model

Based on the above, Figure 2 is a circuit model which includes the input impedance of the Keithley, the relay insulation resistance across open contacts, and the relay isolation from the coil (which is essentially a ground connection). It should be noted that the relay coils are somewhat isolated from "plant" ground since they use rectified voltages which may float relative to "plant" ground. However, our experience has shown that this additional isolation is not significantly higher than 10^8 X. The effect of lack of isolation on the measurement is severe. Referring to Figure 3, we now have a parallel path to ground going in a reverse direction through the unused dropping resistors. This parallel path amounts to about 3.3×10^7 X, and the measured insulation resistance is then the parallel combination of the specimen and 3.3×10^7 X, or essentially 3.3×10^7 X. This is clearly unacceptable.

The above problems were solved using a specialized relay that is rated at a minimum isolation of 10^{14} X and is capable of switching 200 V at 0.5 A and carrying 1.5 A. The minimum breakdown voltage of the relay is 300 Vac across the contacts and 1000 Vac from the contacts to the coil. The manufacturer indicated that 250 Vdc and low currents should present no problem for the relatively few switching operations required of the relay in our application. Thus we decided to limit our test voltage to 250 V (we had initially planned to go as high as 1000 V using a manual instrument) and use these relays.

In addition to the 250 V limitation imposed by the relays, we are also limited to 250 V by the Keithley electrometer because its inputs must float to the high voltage (see Figure 2). An alternative to the Keithley limitation is to put it on the low (return) side of the circuit. Unfortunately, there is no real access to the return line as is implied in Figure 2. The grounded cables and the grounded test chamber form the ground reference for the measurement. As shown in Figure 3, the return path via the cables is accessible and the return current through the cables could be measured. However, the test chamber is grounded and cannot be isolated. Thus any leakage current to the chamber (i.e. anything except conductor to conductor leakage) would not be detected if the Keithley were on the low side of the circuit.

Many measurement techniques discussed in the literature, particularly those developed for use on small insulation samples, depend on being able to have

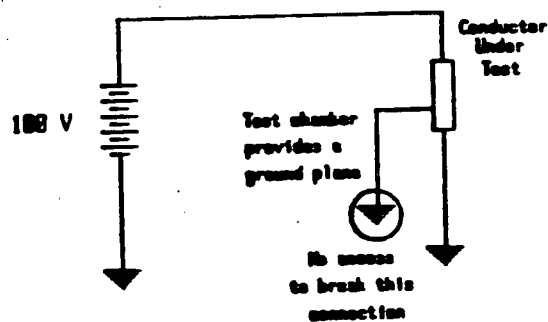


Figure 3 Effect of Grounds

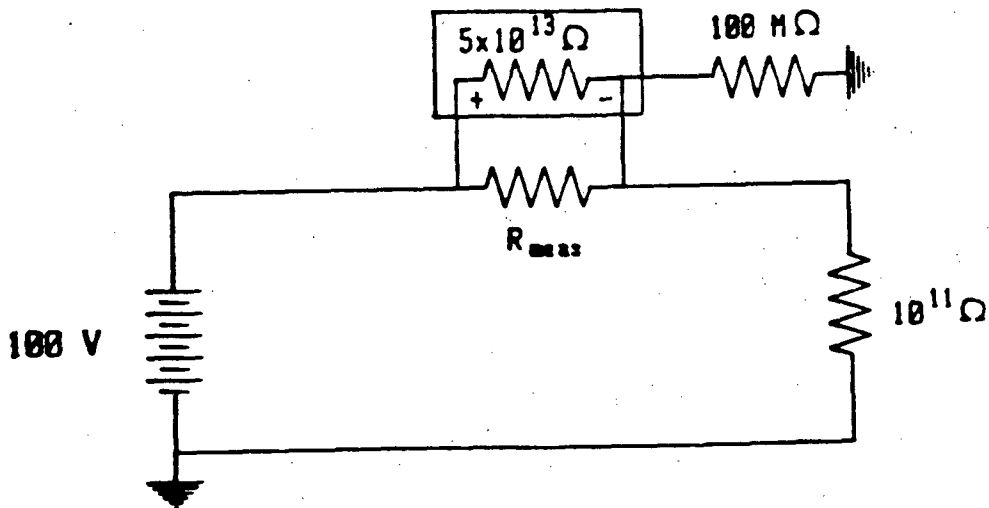


Figure 4 Model for Normal Keithley Connection

neither the cable under test nor the "ground plane" actually grounded, i.e. neither side of the insulation under test is connected to ground. Thus, field implementation of these techniques may be limited by the effect demonstrated in Figure 3. It may be possible to use highly isolated sources (e.g. batteries) to circumvent the grounding problem, but this is not discussed in the references.

An additional problem (already solved in Figure 1) is imposed by the Keithley itself. Anytime a high impedance measurement is being made, the characteristic impedances of the measuring device must be considered. The differential input impedance is sufficient, i.e. about $5 \times 10^{13} \text{ X}$, even when the 60 MX dropping resistor is being used. However, the impedance from the negative terminal of the Keithley to ground is only specified at 10^8 X . A model for the "normal" connection of the Keithley in this circuit is shown in Figure 4. As can be seen from this figure, the impedance of 10^8 X acts in parallel with the cable under test and again would essentially destroy the measurement. In Figure 1, the Keithley is connected in reverse of what would normally be expected, i.e. it measures negative voltages. In the case of reversed leads, the differential input impedance of $5 \times 10^{13} \text{ X}$ becomes the minimum insulation resistance to ground in parallel with the cable. The 10^8 X resistance simply becomes a shunt across the power supply and has essentially no effect on the measurement. The error due to the high impedance is on the order of 2% or less at cable insulation resistances of 10^{12} X . This is one of several effects that limit the upper range of the instrument.

A reasonable estimate of the maximum capability of the instrument as currently configured may be found from baseline

open circuit measurements. The typical minimum insulation resistance of the open circuit is 5×10^{12} X. This insulation resistance includes limitations from aspects discussed above, interconnecting wire contributions, and inherent instrument limitations. Without using any type of baseline correction, the open circuit insulation resistance is expected to cause maximum errors of about 20% when measuring insulation resistances of 1×10^{12} X, or less than 2% when making typical measurements at 1×10^{11} X or below.

Transfer Function

The transfer function is measured using the circuit shown schematically in Figure 5. Two different instruments are used to make the transfer function measurements, both being controlled by a Hewlett Packard Model 216 computer. At "higher" frequencies, over an effective range from about 100 to 500 KHz, the Low Frequency Analyzer is used (obviously we have some different perspectives of "low" frequency). This instrument uses an oscillator to excite the device under test in combination with a vector voltmeter to detect the complex voltage applied to the specimen and a vector ammeter to detect the complex current through the specimen. A four terminal network is used to make the measurement, which may be displayed in a variety of formats (i.e. capacitance, dissipation factor, conductance, magnitude and angle, etc.). This instrument is capable of making measurements on a cable even when one side of the insulation under test is at ground potential. However, it should be noted that different results are obtained when one side is grounded as compared to having both sides floating. The reason for this behavior is illustrated in Figure 6. In (a), neither side of the cable is grounded and the measurement is just the series combination of the two insulations between the conductors. In (b), with conductor #2 grounded, an additional path is introduced in parallel with the conductor #2 insulation to ground. This parallel path, which includes the jacket of multiconductor cables, consists of any paths to ground from conductor #1 except the path through the insulation of conductor #2. The significance of this path is particularly pronounced for single conductor cables which rely heavily on the parallel path to form a ground plane for the measurements. It should be noted that the effects illustrated in Figure 6 apply to any type of electrical measurement.

At lower frequencies, over an effective range from about 0.5 to 200 Hz, a Hewlett Packard Model 3582A spectrum analyzer (SA), driven by a white noise source is used. The white noise is provided by the spectrum analyzer and is fed to channel A of the analyzer. The input to channel B of the analyzer is from the signal across the nominal 1 MX resistor in series with the cable. The spectrum analyzer obtains the Fast Fourier Transform (FFT) of the transfer function between V_{in} and V_{out} and transmits the

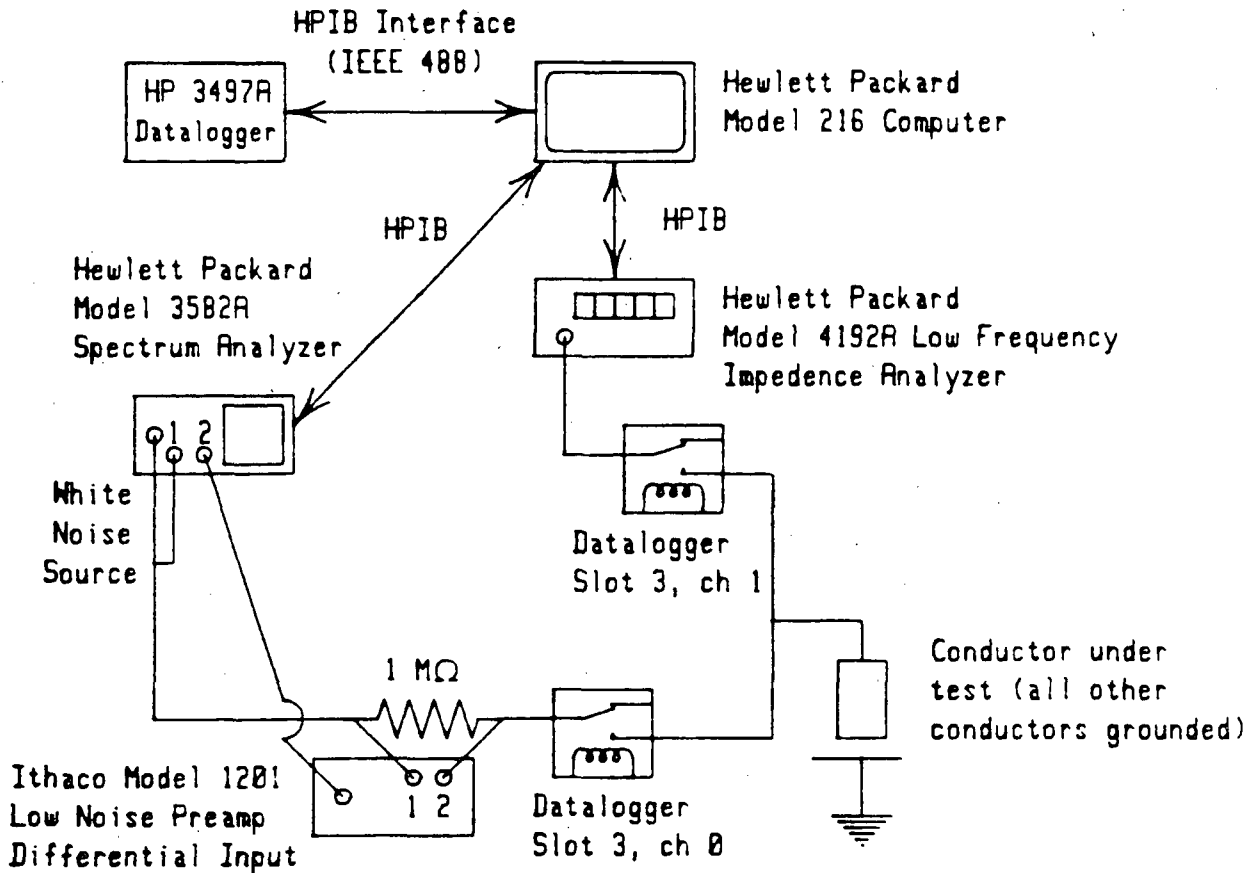


Figure 5 Schematic of Transfer Function Measurement Circuitry

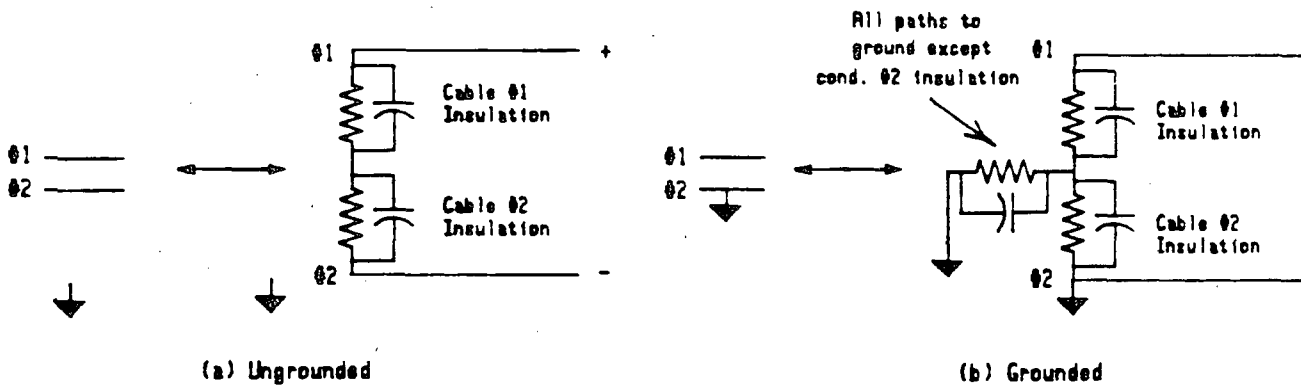


Figure 6 Comparison of Ungrounded and Grounded Configurations

amplitude ratio and phase difference between V_{in} and V_{out} to the computer. These data are then processed by the computer to provide measures of capacitance and dissipation factor (as a function of frequency) of the cable under test.

The buffer amplifier shown in Figure 5 is used in the voltage follower mode (output=input). The buffer amplifier has an input impedance of greater than 10^9 X in the differential mode and a input capacitance of about 8 pF. The input capacitance of the amplifier limits the upper frequency for effective measurements using the spectrum analyzer. For example, at 1000 Hz, impedance due to the capacitance is $1 / (2 * \pi * 1000 * 8 \times 10^{-12}) = 20 \times 10^6$ X. Although this impedance is a factor of 20 above the nominal 1 MX resistor and would only be expected to create errors on the order of 5%, in practice the phase shift associated with the capacitance can cause additional difficulty.

We are able to obtain dissipation factor data from the LF analyzer down as low as 30 Hz (by changing the instrument settings to display conductance rather than dissipation factor), but the data is somewhat variable and unreliable. However, the LF analyzer generally does not make effective dissipation factor measurements below about 100 Hz. To provide a reasonable overlap region for comparison, we wanted the SA system to make measurements up in the range of 1000 Hz. When we corrected data reduction routines for the amplifier input capacitance, we discovered that a more significant problem is that the calculation of dissipation factor from the spectrum analyzer data is extremely sensitive under some conditions, with the problem appearing to be most significant at higher frequencies. Thus, the two independent dissipation factor measurements seem to be least accurate in the overlap region. The sensitivity and amplifier input impedance problems are much less important in the calculation of capacitance and good agreement in the overlap region is expected.

EXPERIMENTAL DATA

Initial baseline measurements using the SA/LF system and the insulation resistance system have been completed on the six and nine month chambers. In addition, one, two, and three month measurements have been performed on the nine month chamber. Baseline measurements were performed at room temperature and at the aging temperature of about 100 #C. Baseline insulation resistance measurements on the nine month chamber at room temperature were made using a Hipotronics megohmmeter and measurements at the elevated temperature were made using an earlier version of the insulation resistance system described above. Because of the large amount of data generated by these measurements, only selected data is presented in this section.

Insulation Resistances and Polarization Indices

Table 2 presents selected results of the insulation resistance measurements for two cable products. All the measurements given in the table were taken at the aging temperature of about 100°C and all measurements are for the nine month chamber. Statistics presented are based on one standard deviation and are the directly calculated standard deviation (rather than the standard deviation of the mean). The discussion in the next paragraphs is based on some initial analyses of the data that has been acquired. Because all data collection and analysis has not been completed, the statements made should be considered as preliminary.

Table 2 indicates several trends for the cable products listed. First, the insulation resistances have shown a consistent decrease from month to month, as might be expected. Each month of exposure roughly corresponds to 7 years of natural aging (based on a set of assumed ambient conditions). This trend is consistent for most of the cables in the nine month chamber. The only statistically significant exception identified thus far is the Rockbestos FW III product (data not given in Table 2) which showed an increase of about 20-25% between the baseline and the one month data. Between the first and second month, however, the same product decreased in insulation resistance by about a factor of 5-7. The small initial increase in insulation resistance may have been a result of additional crosslinking of the irradiation XLPE. The decreases in insulation resistance shown in Table 2 over the three month period ranges from about a factor of 4 to a factor of 100.

The polarization indices for the Anaconda multiconductor cable show a substantial decrease from the baseline to the one month measurements. The baseline data on the six month chamber agrees quite well with the data presented here for the nine month chamber, but the one month data on the six month chamber has not yet been acquired. The single conductor Anaconda cable hints at the possibility of a long term decrease in polarization index, as do some of the other cable products tested. The polarization indices noted for the BIW cable product are fairly low and an alternative polarization index definition may produce somewhat larger numbers that may give a better indication of any trends.

Capacitance and Dissipation Factors

Capacitance and dissipation factor data is presented as a function of frequency for the Samuel Moore Dekoron Dekorad cable in Figure 7. In each of the plots, data from the two different measurement techniques is shown, the lower frequency data from the spectrum analyzer apparatus and the higher frequency data from the low frequency analyzer. Conductors 20-23 (Cond. #20-23 in figure) represent the averages of 2, 2-conductor samples, and

Table 2 Selected Insulation Resistances and Polarization Indices

Cable Type	IR (100 V)	IR (250 V)	PI (100 V)	PI (250 V)
Anaconda FR-EP (Based on two 3/C cables, i.e. 6 samples)				
Baseline	1.09x10 ¹¹ ± 0.05x10 ¹¹ X	9.35x10 ¹⁰ ± 0.07x10 ¹⁰ X	1.45±0.05	1.36±0.09
1 month	1.12x10 ¹⁰ ± 0.17x10 ¹⁰ X	1.19x10 ¹⁰ ± 0.18x10 ¹⁰ X	1.08±0.01	1.08±0.02
2 month	4.06x10 ⁹ ± 1.20x10 ⁹ X	4.30x10 ⁹ ± 1.46x10 ⁹ X	1.08±0.02	1.08±0.02
3 month	1.10x10 ⁹ ± 0.16x10 ⁹ X	1.14x10 ⁹ ± 0.17x10 ⁹ X	1.03±0.02	1.02±0.00
Anaconda FR-EP (One 1/C removed from 3/C, i.e. 1 sample)				
Baseline	1.09x10 ¹¹ X	1.05x10 ¹¹ X	1.17	1.16
1 month	2.04x10 ¹⁰ X	2.31x10 ¹⁰ X	1.09	1.13
2 month	1.21x10 ¹⁰ X	1.35x10 ¹⁰ X	1.08	1.16
3 month	1.03x10 ¹⁰ X	1.07x10 ¹⁰ X	1.08	1.08
BIW (Based on two 2/C cables, i.e. 4 samples)				
Baseline	7.92x10 ⁸ ± 0.21x10 ⁸ X	7.30x10 ⁸ ± 0.79x10 ⁸ X	1.08±0.01	1.04±0.00
1 month	5.62x10 ⁸ ± 0.06x10 ⁸ X	5.77x10 ⁸ ± 0.12x10 ⁸ X	1.02±0.00	1.03±0.01
2 month	2.01x10 ⁸ ± 0.08x10 ⁸ X	2.06x10 ⁸ ± 0.08x10 ⁸ X	1.01±0.00	1.01±0.01
3 month	4.27x10 ⁷ ± 0.29x10 ⁷	4.20x10 ⁷ ± 0.29x10 ⁷ X	1.00±0.00	1.00±0.00
BIW (Based on two 1/C removed from 2/C, i.e. 2 samples)				
Baseline	1.38x10 ⁹ ± 0.03x10 ⁹ X	1.59x10 ⁹ ± 0.07x10 ⁹ X	1.02±0.00	1.02±0.00
1 month	1.20x10 ⁹ ± 0.01x10 ⁹ X	1.28x10 ⁹ ± 0.01x10 ⁹ X	1.03±0.01	1.03±0.00
2 month	4.62x10 ⁸ ± 0.24x10 ⁸ X	5.03x10 ⁸ ± 0.27x10 ⁸ X	1.01±0.00	1.01±0.00
3 month	3.28x10 ⁸ ± 0.24x10 ⁸ X	3.67x10 ⁸ ± 0.29x10 ⁸ X	1.01±0.00	1.01±0.00

IRs at 1 min., PIs are ratio of IR at 1 min. to IR at 30 sec.

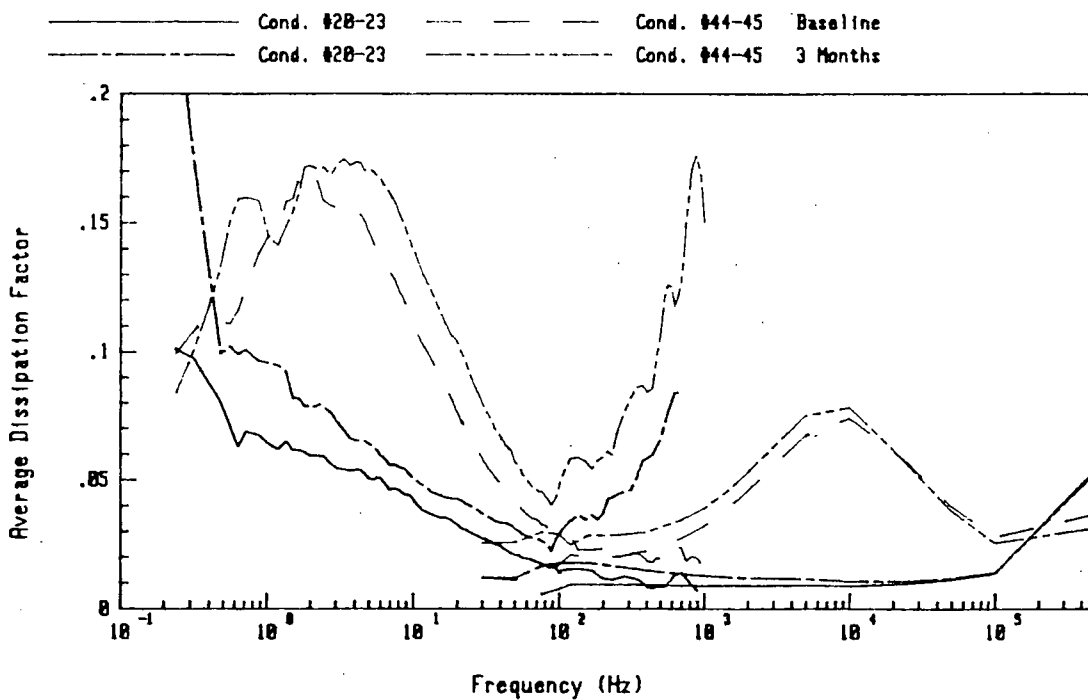
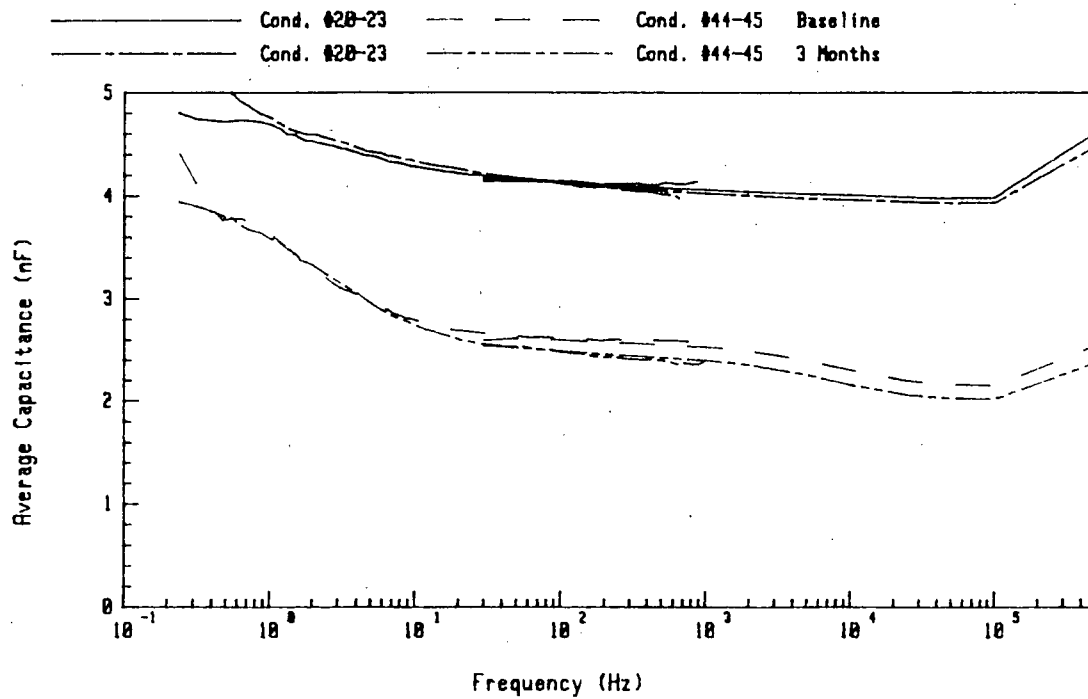


Figure 7 Comparison of Baseline and 3 Month Capacitance and Dissipation Factors as a Function of Frequency for a Single and Multiconductor Cable

conductors 44-45 (Cond. 44-45 in figure) represent the average of 2 single conductor samples. The figure indicates excellent agreement in capacitance between the two measurement techniques. The lower baseline capacitance of the single conductors as compared to the multiconductors was also observed for the BIW cable, but not for the Anaconda FR-EP cables. The capacitances for the entire length of cable under test indicate a per foot capacitance in the neighborhood of 60 pF/ft.

A peak in dissipation factor occurred at about 10^4 Hz for the single conductor cables but not for the multiconductors. This peak also occurred for many other single conductor cables (and is quite high in some cases), but has not yet been clearly observed for any multiconductors (considering the 9 month chamber baseline data). A loss factor peak (similar to dissipation factor) at about 10^4 Hz is indicated in Ref. 18 for a typical polymer. We expect that the "typical" plot in Ref. 18 is based on testing of small dielectric specimens as is most often done. It is thus interesting to note the similarity of single conductors to the small samples, with the multiconductor cables not behaving the same way. We will continue to watch and see if this trend is followed for other test conditions. A second peak, also observed only on some single conductors, occurred in the vicinity of several Hz. The dissipation factor as measured by the two different instruments indicates quite good agreement in the overlap region for the baseline measurements. However, the 3 month measurements indicate significant deviation between the two techniques, except in the immediate vicinity of 100 Hz. We believe that this is a result of the problems discussed earlier with both the spectrum analyzer at higher frequencies and the LF analyzer at lower frequencies. We will be investigating these problems further.

ADDITIONAL ANALYSIS OF TEST RESULTS

The test data collected during the aging and accident exposures will be analyzed to assess the following:

- a. the effectiveness of condition monitoring measurements made during aging in predicting cable performance in an accident environment;
- b. the impact of long-term, low exposure rate aging on cable performance as compared to the usual high exposure rate conditions employed in many tests; and
- c. the potential for life extension of popular cable products beyond the current 40-year design life.

CONCLUSIONS

A variety of electrical and mechanical condition monitoring techniques are being evaluated for their ability to predict

accident performance of cables based on measurements performed prior to beginning the accident exposure. This paper emphasized the practical elements of developing the automatic ranging insulation resistance measurement system and the automatic data acquisition system for determining transfer function as a function of frequency. In addition, some initial data generated from these electrical measurement techniques was presented.

We anticipate that test data provided by this experimental program will provide a foundation for development of in-situ condition monitoring techniques for estimating the remaining useful life of currently installed cable products. Additional insights from this program will include information on long term aging effects on complete cables (as compared to the commonly used tensile specimens) and the possibility for life extension of cables currently used in the nuclear power industry.

REFERENCES

1. L. D. Bustard, "The Effect of LOCA Simulation Procedures on Ethylene Propylene Rubber's Mechanical and Electrical Properties," NUREG/CR-3538, SAND83-1258, Sandia National Laboratories, Albuquerque, New Mexico, October 1983.
2. L. D. Bustard, et al., "The Effect of Thermal and Irradiation Aging Simulation Procedures on Polymer Properties," NUREG/CR-3629, SAND83-2651, Sandia National Laboratories, Albuquerque, New Mexico, April 1984.
3. L. D. Bustard, "The Effect of LOCA Simulation Procedures on Cross-Linked Polyolefin Cable's Performance," NUREG/CR-3588, SAND83-2406, Sandia National Laboratories, Albuquerque, New Mexico, April 1984.
4. P. R. Bennett, S. D. St.Clair, and T. W. Gilmore, "Superheated-Steam Test of Ethylene Propylene Rubber Cables Using a Simultaneous Aging and Accident Environment," NUREG/CR-4536, SAND86-0450, Sandia National Laboratories, Albuquerque, New Mexico, June 1986.
5. A. Sugarman, B. Kumar, and R. Sorensen, "Condition Monitoring of Nuclear Plant Electrical Equipment," EPRI NP-3357, Research Project 1707-9, NUTECH Engineers, San Jose, California, February 1984.
6. Letter F. I. Mopsik, National Bureau of Standards to M. J. Jacobus, Sandia National Laboratories, October 28, 1987.
7. F. I. Mopsik, "The Transformation of Time-Domain Relaxation Data Into the Frequency Domain," *IEEE Transactions on Electrical Insulation*, Vol. EI-20, p. 957 (1985).

8. F. I. Mopsik, "Precision Time-Domain Dielectric Spectrometer," *Rev. Sci. Instrum.*, Vol. 55, p.79, (1984).
9. K. T. Gillen, R. L. Clough, and C. A. Quintana, "Modulus Profiling of Polymers," *Polymer Degradation and Stability*, Vol. 17, p.31, (1987).
10. R. L. Clough, K. T. Gillen, and C. A. Quintana, "Heterogeneous Oxidative Degradation in Irradiated Polymers," NUREG/CR-3643, SAND83-2493, Sandia National Laboratories, Albuquerque, New Mexico, April 1984.
11. K. T. Gillen, R. L. Clough, and N. J. Dhooge, "Density Profiling of Polymers," *Polymer*, Vol. 27, p.225, 1986.
12. G. J. Toman and G. Sliter, "Development of a Nondestructive Mechanical Condition Evaluation Test for Cable Insulation," Presented at the International ANS/ENS Topical Meeting on the Operability of Nuclear Power Systems in Normal and Adverse Environments, Albuquerque, New Mexico, September 29-October 3, 1986.
13. G. C. Stone and M. Kurtz, "Interpretations of Megohmmeter Tests on Electrical Apparatus and Circuits," *IEEE Electrical Insulation Magazine*, Vol.2, p. 14, January, 1986.
14. IEEE Std. 402-1974, "IEEE Guide for Measuring Resistivity of Cable-Insulation Materials at High Direct Voltages," The Institute of Electrical and Electronic Engineers, Inc., 1974.
15. IEEE Std. 4-1978, "IEEE Standard Techniques for High-Voltage Testing," 6th ed., The Institute of Electrical and Electronic Engineers, Inc., 1978.
16. IEEE Std. 62-1974, "IEEE Guide for Field Testing Power Apparatus Insulation," The Institute of Electrical and Electronic Engineers, Inc., 1978.
17. ASTM D150-81, "A-C Loss Characteristics and Permittivity (Dielectric Constant) of Solid Electrical Insulating Materials," American Society for Testing and Materials, 1981.
18. R. Bartnikas, editor, *Engineering Dielectrics, Volume IIB, Electrical Properties of Solid Insulating Materials: Measurement Techniques*, American Society for Testing and Materials Special Technical Publication 926, 1987.
19. Rene Seeberger, "Capacitance and Dissipation Factor Measurements," *IEEE Electrical Insulation Magazine*, Vol.2, p. 14, January, 1986.

TIME DOMAIN SPECTROSCOPY TO MONITOR THE CONDITION OF CABLE INSULATION

F. I. Mopsik and F. D. Martzloff

National Institute of Standards and Technology
Gaithersburg, Maryland 20899

ABSTRACT

The use of Time Domain Spectroscopy, the measurement of dielectric constant and loss using time-domain response, for monitoring the aging of reactor cable insulation is examined. The method is presented, showing its sensitivity, accuracy and wide frequency range. The method's ability to acquire a great deal of information in a short time and its superiority to conventional single frequency data is shown. Different cable samples are examined before and after exposure to radiation and changes with exposure are clearly seen to occur. Also it is shown that a wide range of behavior can be found in different insulation systems. The requirements for performing valid measurements is presented. The need for controlled samples and correlation with other criteria for aging is discussed.

INTRODUCTION

As part of an industry-wide research program on nuclear power plant aging, NIST has been assessing test methods for evaluating the operational readiness of cables inside reactor confinement where they are subject to aging from many different stresses. These include not only the normal ones during operation, but also those during and after a loss of coolant accident, LOCA. Also, these methods must be not only sensitive to the state of the cables, but they must be nondestructive in the sense of not changing the remaining lifetime of the cables.

One simple method for evaluating the quality of electrical insulation has been insulation resistance, either AC or DC^{1,2,3}. This test has been incorporated in the ECCADS⁴ method as one of a battery of tests. While these measurements are definitely nondestructive with the excitation voltages normally used, the usual implementations are fairly crude in their ability to reveal what state the insulation is in.

One of the problems is that for such measurements, especially for polymeric insulation, there is no way to distinguish between dielectric relaxation and conductance on the basis of a result for a single time or frequency. Polymeric materials typically have relaxations on the same time scales as those used to measure insulation resistance. Furthermore, especially in semi-crystalline polymers and in compounded systems, there is no guarantee that interfacial polarization will not further complicate the results. As a

result, the measurements become a function of time or frequency. Interpretation of the results can become very difficult.

Despite these reservations, electrical measurements of the cable insulation remain very attractive for use in evaluating cable lifetimes. It is well known that radiation can change the dielectric properties of insulators from many causes. Radiation-induced damage can directly generate charge carriers. Oxidation in the presence of air resulting from radiation damage⁵ can change the level of loss and the time scale of relaxations. Cross-linking can definitely affect relaxation times. Non-radiative aging can also affect both dielectric relaxation and conduction.

If these changes can be measured and correlated with the useful lifetime of the cable insulation, then electrical measurements can have great potential⁶. They can be relatively easy to implement, are quite sensitive and should not require much invasion of the confinement. They certainly are nondestructive since the excitation voltages can be much less than the operating voltages. Furthermore, they allow a continuous history to be maintained. This history could be especially important if trends are needed to estimate lifetimes. This may be the case since very small changes in material composition can make large changes in the radiation response of polymeric materials.

The method reported in this paper is Time Domain Spectroscopy (TDS) which was developed at NIST (formerly the National Bureau of Standards) to measure the dielectric properties of polymers⁷. With one instrument, one can measure not only the AC properties of the insulation as a function of frequency, but also the time-dependent DC response. Furthermore, the instrument has high sensitivity, accuracy and a very wide time or frequency range. With one relatively short total measurement time of 10 minutes, one can recover not only the standard ASTM DC conductivity for a one minute charging time and the 60 Hz AC conductivity, but the entire time response from 10 μ s to 300 s as well as the loss spectrum over 7 decades in frequency from 10 kHz down to 0.001 Hz.

In this paper, we wish not only to describe the measurement method, but also some results on systems that have been exposed to different aging conditions. Significant changes will be shown to occur upon exposure to radiation, raising great promise for the method. We will also discuss the requirements for in-situ instrumentation.

DIELECTRIC SPECTROSCOPY

The basis for the Time-Domain Spectrometer is shown in Fig. 1. A step voltage is applied to a sample starting at a time $t = 0$. The induced charge, $Q(t)$, will be a function of time and can be used to define a time-dependent capacitance $C(t) = Q(t)/E^0$, where E^0 is the applied field. Then one can evaluate the complex frequency-dependent capacitance, $C^* = C'(\omega) - iC''(\omega)$, by the Laplace transform integrals

$$C'(\omega) = \int_0^{\infty} dC/dt \cos \omega t dt$$

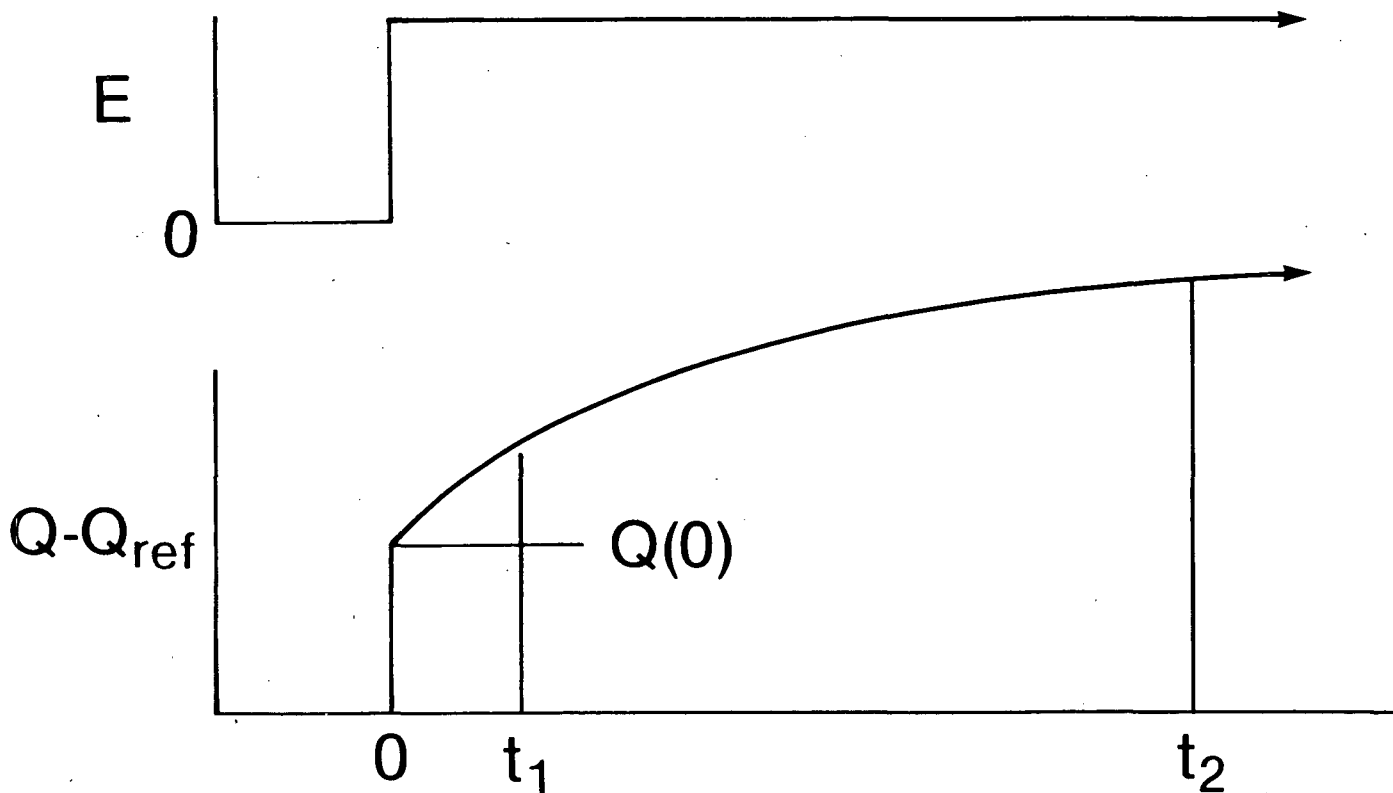


Figure 1: Applied field (top curve) and measured charge response for the time-domain measurement. $Q(0)$ is the measured charge immediately after the application of the field. The times t_1 and t_2 are the shortest and longest times of measurement and also define the frequency range of the measurement.

$$C''(\omega) = \int_0^{\infty} dC/dt \sin \omega t dt$$

Using the definition $C'' = G(\omega)/\omega$ and the capacitance C_g , which is the capacitance of the sample if it were a vacuum, one obtains the complex dielectric constant, $\epsilon^* = \epsilon' - i\epsilon''$ as

$$\epsilon^* = C'/C_g - iC''/C_g = C(\omega)/C_g - iG(\omega)/(\omega C_g)$$

where $G(\omega)$ and $C(\omega)$ are the conventionally measured capacitance and conductance for the equivalent parallel circuit.

Note that $dC(t)/dt$ for $t = 1$ min is the definition for conductance used by ASTM. If one were to record the data for all time, then a Laplace transform would give the complete frequency-dependent behavior of the sample. Also, true time-independent conductance can be not only incorporated in the actual measurement, but also in the evaluation of the integrals. If such a term is present, it is just the limiting value for long times or low frequencies. However, for any, given time, or equivalently any given frequency, a measured value can have other, unspecified contributions.

The Time Domain Dielectric Spectrometer is the realization of these principles. The actual setup is shown in Fig. 2. Two extremely stable step generators that produce positive and negative 100 V steps to parts-per-million accuracy within times on the order of 10 μ s allow measurements with respect to an adjustable, lossless reference capacitor. The charge detector converts the net charge flowing in the measuring circuit to voltage with comparable accuracy and response time. It has a bias current of less than 30 fA. The voltage is then digitized using a variable multi-rate quartz clock and acquired by the computer. The data are taken initially every 5 μ s for the first 2 ms. The time of measurement then increases by factors of ten for every decade of total measuring time to maintain nearly uniform logarithmic sampling.

Once the data set is acquired, it is then properly normalized and a numerical Laplace transform is applied. The method used in the Spectrometer was developed specifically for the instrument and preserves the full numerical accuracy of the data.⁸ As indicated in Fig. 1, the minimum and maximum times for data acquisition, t_1 to t_2 , 10 μ s to the stopping time, determine the maximum, 10 kHz, and the minimum, $1.8/(2\pi t_2)$ Hz, frequencies. Thus, in a measurement time that is less than 1/3 of a cycle of the lowest frequency of interest, one obtains the entire time and frequency behavior of the sample. Also, since a discrete FFT is not used, the frequency coverage is continuous and the results for any desired frequency within the measurement range are obtainable.

It is just this broad time and frequency coverage that is the power of the instrument. Conventional single time or frequency methods require measurement times not much different than the time used to obtain the entire

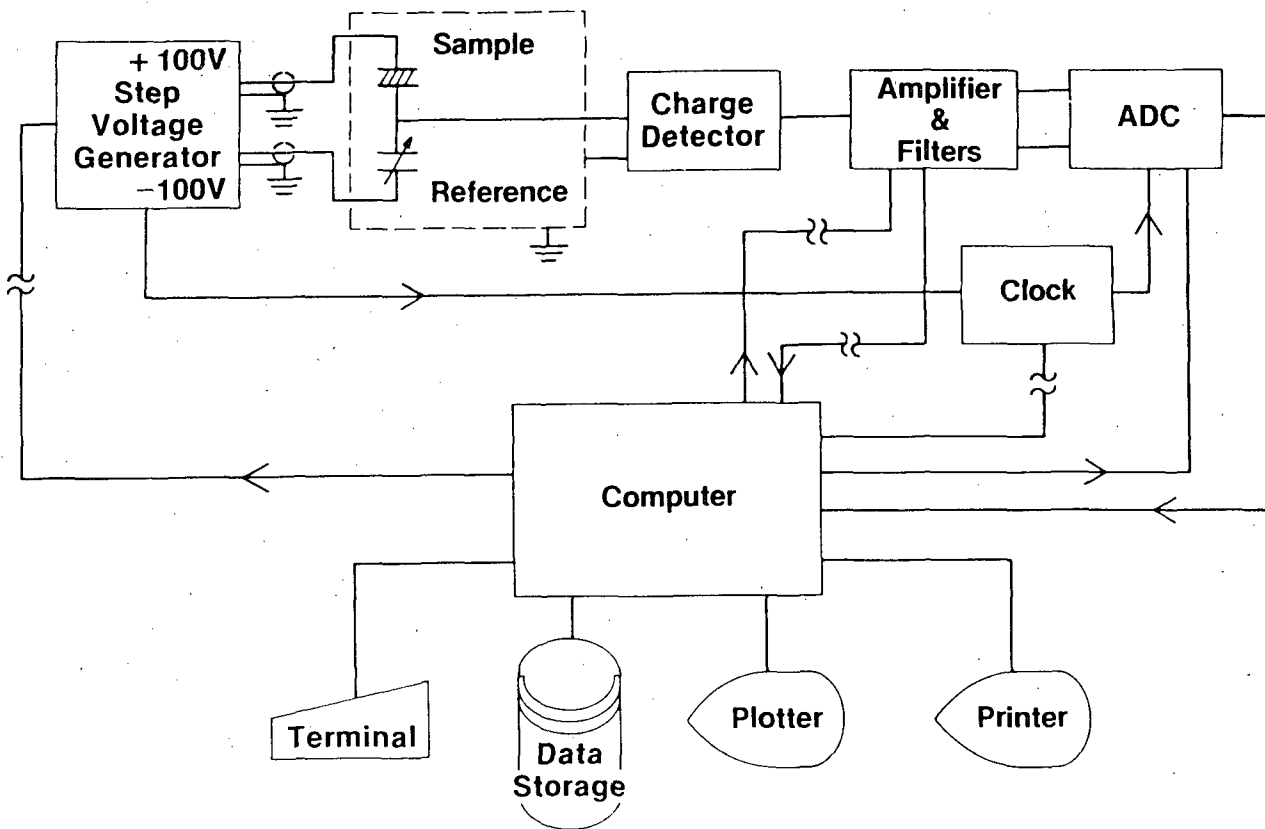


Figure 2: Block diagram of the Dielectric Spectrometer. The breaks in the data lines, the directions shown by arrows, represent optical isolators.

loss spectrum. They also have a much more restricted range of measurement. Often only a single time or frequency is used. For many applications, interpretation of such loss or conductance data can be very difficult but becomes much easier with broad frequency coverage.

The wide range of frequencies also allows different forms of data presentation. As dielectric loss changes slowly with frequency, small differences are hard to see. Also, it can be hard to determine when a true conduction process is present. Analysis is often helped by plotting the imaginary component of ϵ^* , ϵ'' , as a function of the real component of ϵ^* , ϵ' , in the complex plane. Frequency becomes a running parameter along the resulting line decreasing from left to right. A single dielectric relaxation process then becomes a closed curve along the real axis. The simplest relaxation, an exponential decay, becomes a semicircle along the real axis. A pure conductance becomes a vertical line. If there is no conductance or dielectric relaxation, all the points superpose on a single point. Examples of this representation will be shown later.

THREE-TERMINAL ADMITTANCE

The Spectrometer measures the equivalent three-terminal admittance between its generator and its charge detector. That is, the measuring path, as shown in Fig. 2, is between the leads from the generator and the detector. In particular, any admittances to ground are not included in the measurement. This capability is completely analogous to the measurements made with a conventional transformer bridge.

This capability can be seen by noting that the generator acts as a zero impedance source so that voltage applied to the sample is independent of the load across the generator. Therefore, a shunt admittance to ground on the generator lead, as long as it does not significantly change the settling time or exceed the current limits of the output stage, cannot affect the measurement.

Similarly, the charge detector measures the charge flowing to its input with the input held to ground potential within the accuracy of the input amplifier stage. As long as a shunt to ground on the detector input does not draw significant current at the offset levels present at the input, it, too, cannot affect the measurement.

This measurement configuration allows enclosure of the sample in a grounded, shielded holder. Just as important, especially at low frequencies, it allows the use of a guard ring on the sample. Guarding is done by placing an outer electrode completely around the one connected to the detector. Since the detector lead is nearly at ground potential, if the guard ring is connected to ground, any leakage currents along the surface of the sample are intercepted and excluded from the measurement.

The three-terminal configuration also allows the measurement of samples at the end of rather long leads with shunt admittances large compared to the sample admittance. It should be mentioned that there are real physical

limits to the length of the leads. One is that the series impedance of the leads is small in comparison with that of the sample. This condition is easily met in practice with any ordinary polymeric insulation. Another is that there is no significant propagation delay along the leads with a resulting wave reflection. For ordinary coaxial cable with propagation times of 5 ns/m, lead lengths much greater than 100 m would have to be known and accounted for, if suitable output capacity were available, and lengths much greater than 200 m could introduce degrading propagating reflections. If the highest frequency of interest is reduced by a factor of 10, then these restrictions would be reduced proportionally.

SAMPLES

To examine the usefulness of time-domain spectroscopy, samples of cable insulation were measured using the instrument at NIST. In particular, samples were sought that were obtainable both exposed and not exposed to a degrading environment. Three sets of samples were obtained: RG 149/U cable recovered from both the control room and reactor at Shippingport, samples of XLPO wire insulation artificially aged with 25 Mrad, and a set of five configurations of coaxial cable of cross-linked polyethylene, identified as Cables 1-5, that were artificially aged at 85°C and 25 Mrad. Cables 1-5 were available in the four treatments: unaged, heated to 85°C, exposed to 25 Mrad with no heat applied, and both heated to 85°C and exposed to 25 Mrad.

All the cable samples were measured by stripping the ends so that the center conductor was exposed on one end and the braid on the other. They were placed inside a shielded box with leads connecting to the braid and center conductor so that only the dielectric between the braid and center conductor was measured.

The XLPO insulation samples had their center conductor previously removed, and were both filled and colored in red, black and white. They were prepared by inserting 14 ga. tinned copper wire in the center with the wire warmed to 60°C and aided by a little lubricant. Silver-filled conducting paint was then applied around the insulation forming a large central low electrode surrounded by two smaller guard rings. The center wire was used as the high electrode. Just as was done for the cable samples, these samples were measured in a shielded box.

All the measurements reported in this paper were made at 50°C as a standard reference temperature. Measurements were made at lower temperatures with similar results but as would be expected, they were shifted to lower frequencies.

RESULTS

Shippingport Cable

These pieces of cable are conventional polyethylene coaxial cable. Because of their history, there is no way to know what the dose was. The dielectric loss as a function of frequency is shown in Fig. 3. The irradi-

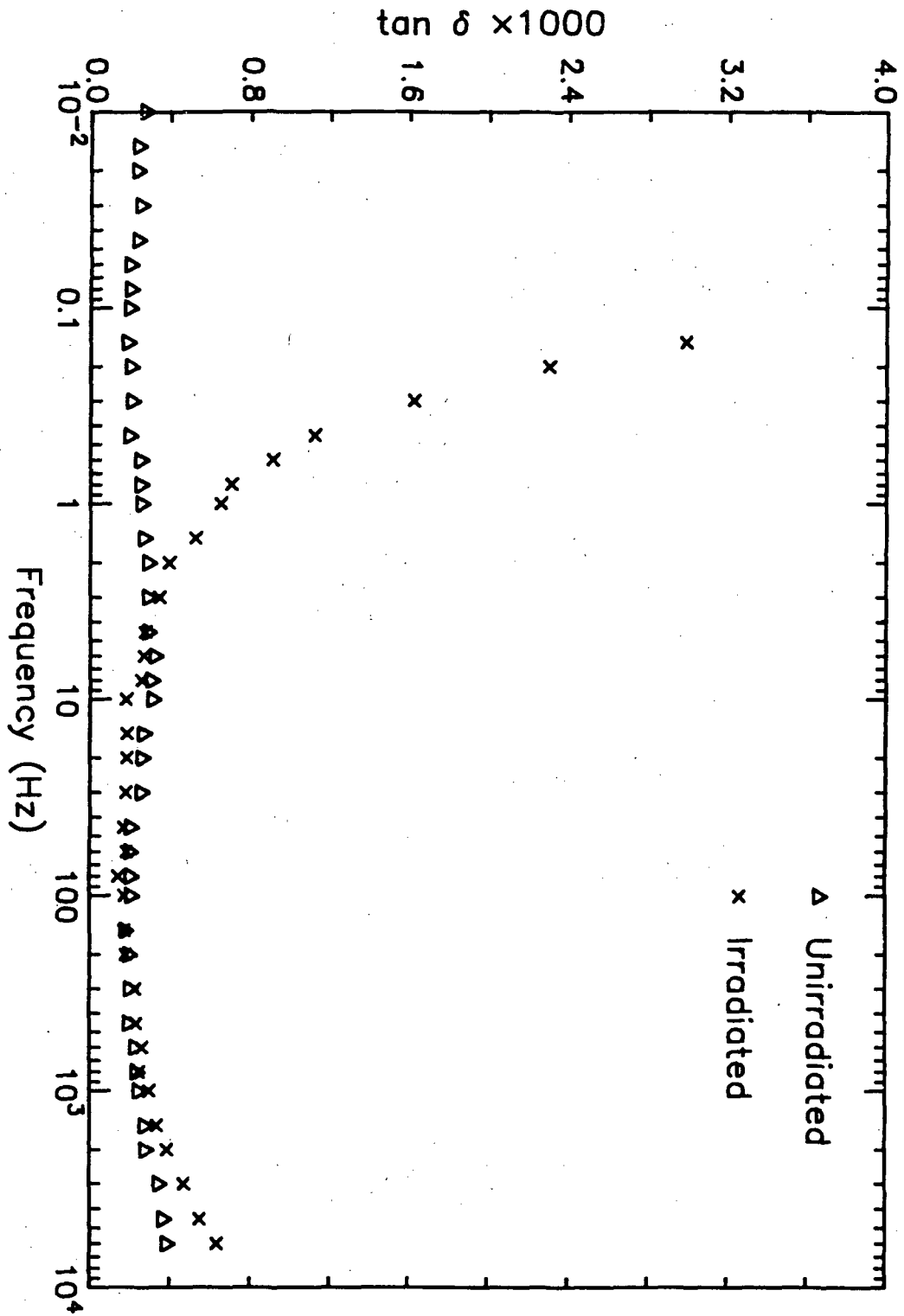


Figure 3: The loss tangent, ϵ''/ϵ' , for coaxial cables recovered from the Shippingport reactor. The irradiated cable came from inside the reactor while the unirradiated cable was from the same lot recovered from the control room. The upsweep at low frequencies is due to induced conductance.

ated cable showed cracking at the outer jacket and the polyethylene insulation showed definite yellowing and evidence of cross-linking. There is a clear upsweep in the data for the sample exposed to radiation as one goes to lower frequencies and is consistent with radiation-damage induced conductance. The sample from the control room is quite consistent with the behavior found in ordinary polyethylene cables. Because of the unknown exposure of the irradiated sample, comparison with the others is quite difficult. However, these results are indicative of the types of changes that can be expected. In particular, there is no way to know at what stage of its expected service life this cable was at since the records were not available and such cables were routinely changed on a regular basis.

XLPO Wire Insulation

The results for a representative sample of this material are shown in Figs. 4 and 5. These materials had exhibited little change in their mechanical properties upon exposure to radiation⁹ and simple physical examination showed no obvious differences. What is surprising in these data is the decrease in loss upon exposure to radiation, as seen in Fig. 4. However, the data for the untreated samples show very high loss values and are not those that would be expected from just a cross-linked polyolefin. In particular, the presence of filler material can create interfacial losses that are much larger than those from the polymer alone. The radiation could have either modified the filler, driven off some extraneous material or modified the polymer matrix to reduce the loss. Since these materials are known to be quite radiation resistant and within their expected lifetime dose⁹, it is hard to predict what would happen upon further exposure, but the low frequency loss would probably ultimately increase to higher values.

From Fig. 5, where data are shown in the complex plane, it is clear that other changes are taking place. There is an emerging dielectric loss process centered near $\Delta\epsilon' = 0.45$ and seen as a shoulder to the left of the low frequency loss that increases to the right. This shoulder is not present in the data for the unexposed sample. Also the slope of the curve at low frequencies is decreasing and is clearly deviating from the limiting behavior of a simple conduction process, which is a vertical line. While only the data for the white samples are shown, the results are similar for the other colors.

These insulation samples all show high initial losses. While the values of the loss are quite acceptable for power lines and low impedance circuitry, they could create problems in signal or sensor lines. Also, the loss levels in these samples are much higher than those found in the polyethylene cable from Shippingport, and very high compared to normal polyethylene. Therefore, if there were some radiation-induced conduction in the polymer matrix, it could be masked by the extra loss present, which must be due to additives and reappear after much higher doses.

Aged Coaxial Cables

Five different cable types, Cables 1-5, were measured. They were all made from cross-linked polyethylene and had some differences in construction.

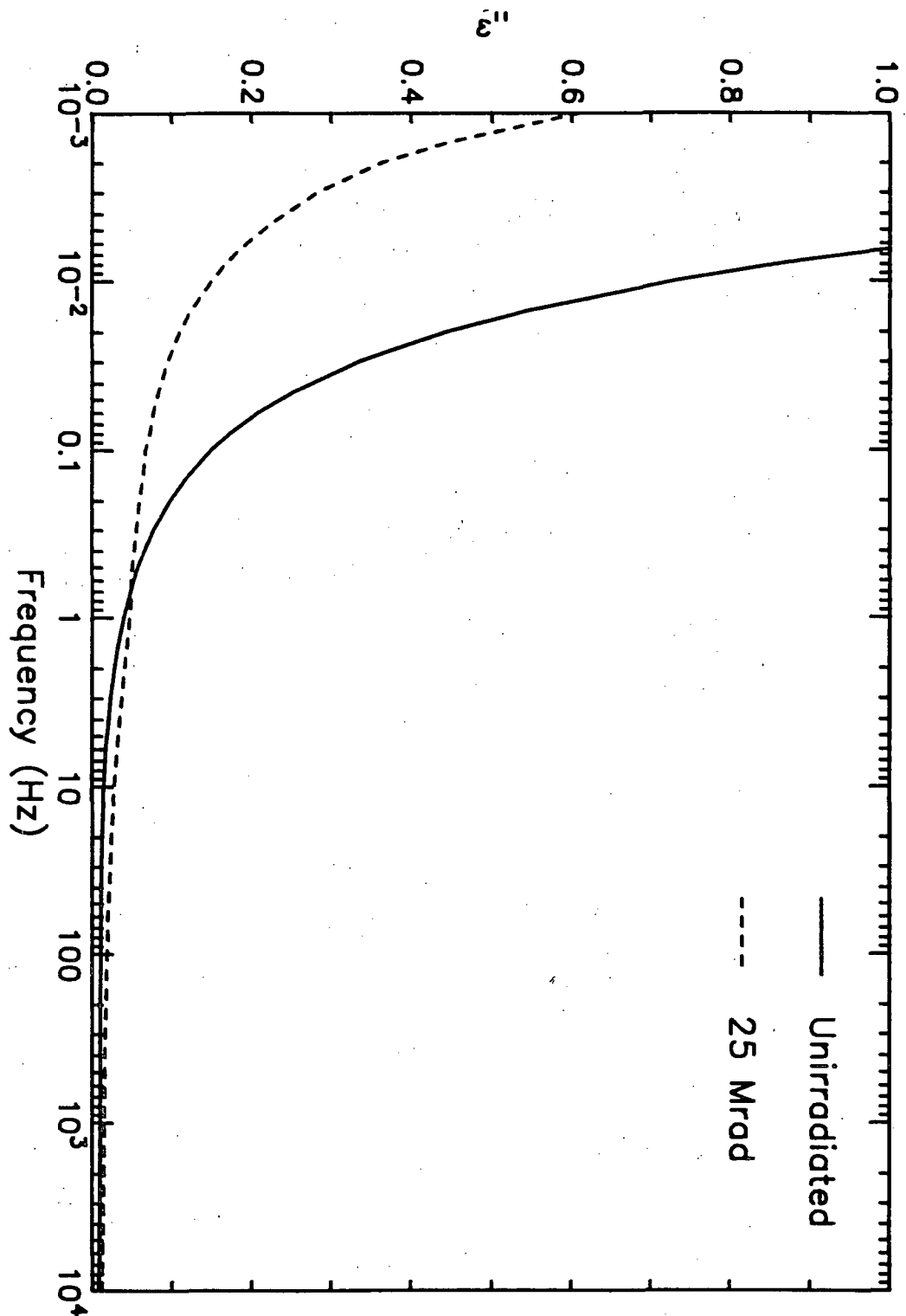


Figure 4: The loss index, ϵ'' , for XLPO wire insulation. The irradiated material was exposed to 25 Mrad. Note the decrease in loss with irradiation at low frequencies but the crossover above 1 Hz.

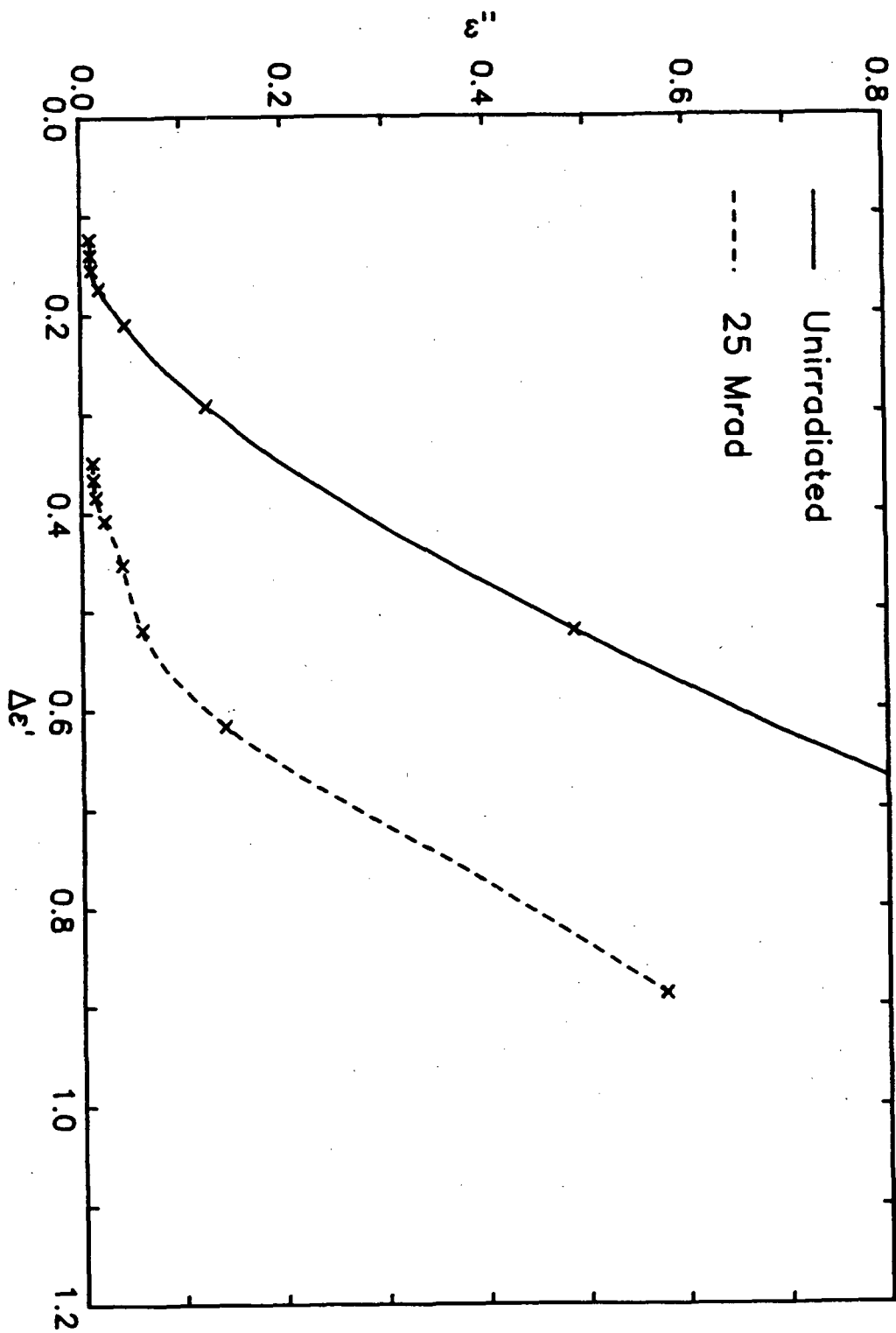


Figure 5: The loss index, ϵ'' , plotted against the real dielectric constant, ϵ' , for the same data as in Fig. 4. The crosses represent the frequency decades. The curves are arbitrarily displaced along the ϵ' axis for clarity. The shoulder for the irradiated sample near $\Delta\epsilon' = 0.5$ is due to a relaxation process.

Cables 1 and 2 also had flame retardant added to them. Visually the cables all appeared to have the normal translucence of polyethylene except for Cables 1 and 2 which were opaque and light in color. They were all available in the original unaged state, and with the treatments heat to 85°C, irradiated with 25 Mrad, and irradiated with heat. Representative data are shown in Figs. 6 - 9.

Initially, Cables 1 and 2 both show much higher loss than the other three which have loss values typical of very pure polyethylene. With only heat applied, the data all show small changes, although Cable 2 shows a significant drop in loss after heating. This particular cable, which had a conductive polymer layer just under the braid, showed migration of the conductive layer through the braid, even in the original state. The other cables showed almost no change at all, which would be expected for this polymer at these temperatures.

After treatment with both heat and radiation, the cables with flame retardant showed only small changes in loss, especially Cable 2 where the change was just measurable, as compared to the heated samples. The others, however, showed large increases in loss at low frequencies. If one looks at Fig. 9, which is the complex plane plot, the near verticality of the line for the sample with this treatment shows that this increase is due to induced conductance.

What is even more interesting is that the cable samples that were exposed to only radiation showed smaller changes than those exposed to both heat and radiation. All the samples showed smaller increases in conductance than those exposed to both heat and radiation. For Cable 2, where the initial background loss is larger than the induced conductance, one can observe only a decrease in the overall loss levels, as is apparent in Fig. 7. Since radiation damage is ultimately chemical in nature and very sensitive to such factors as oxygen^{5,9,10,11,12} and the presence of additives, including colorants¹³, this dependence on heat treatment can be expected.

DISCUSSION

It is clear that radiation does induce changes in cable insulation that can be monitored. Due to the limited number of samples that have been available, the limited range of treatments and the lack of a carefully controlled graded set of conditions, it is difficult to present more extensive conclusions. However, some factors should be noted.

The variability seen in the data and treatment is exactly what one hopes to accomplish with a good monitoring system. Particular note should be made of the aged cable samples where heat treatment greatly affected the aging behavior under irradiation. The variability seen from sample to sample is a more serious concern and must be addressed.

There should be no expectation that universally applicable criteria for lifetime can be found. Different polymers certainly will behave differently since they will allow different charge carrier mobilities, dipoles, and

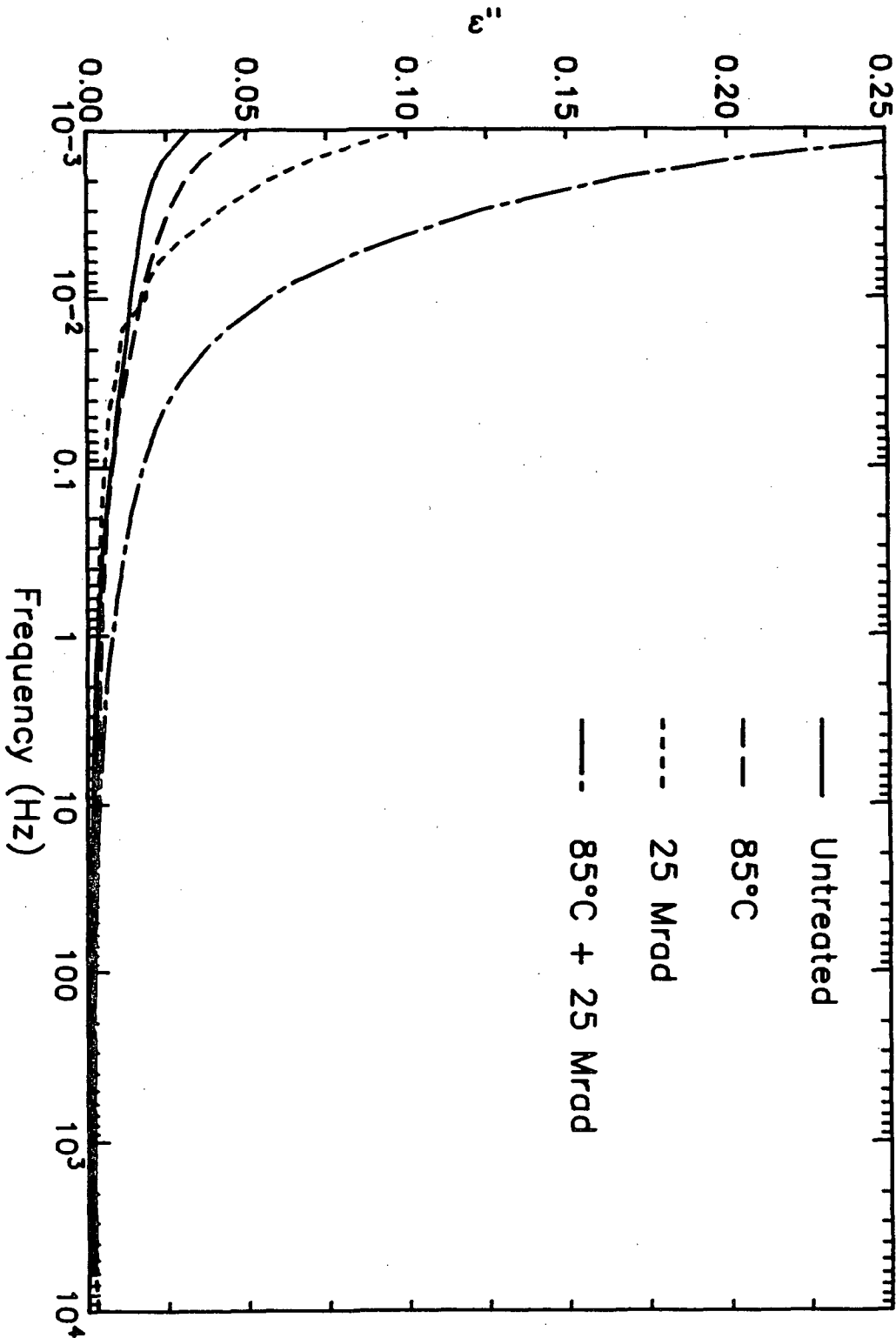


Figure 6: The loss index, ϵ'' , for Cable 1 (see text) as a function of frequency. Note the small increase in loss for the sample exposed only to radiation.

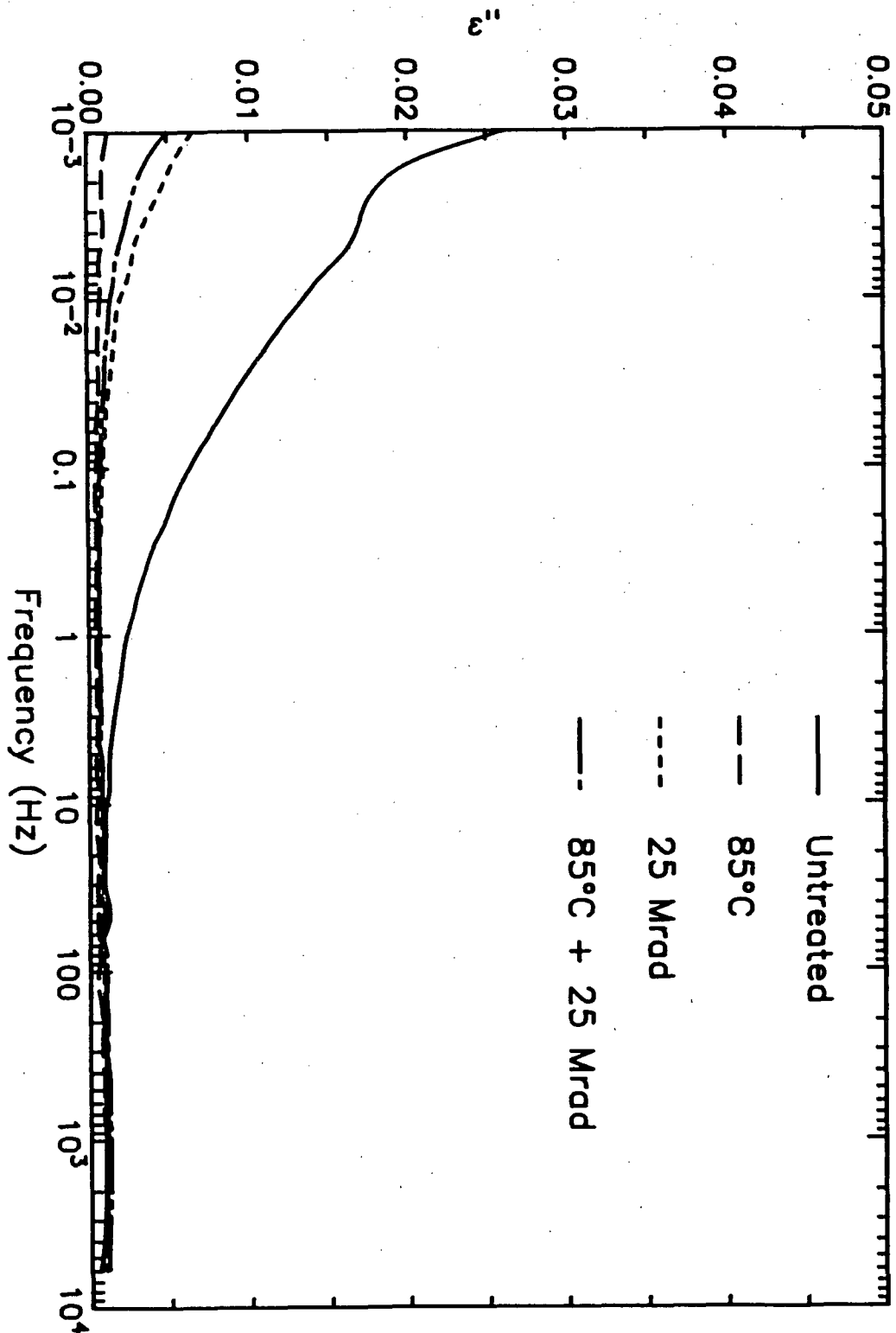


Figure 7: The loss index, ϵ'' , for Cable 2 as a function of frequency. The shoulder at 0.003 Hz is due to dipolar relaxation for the untreated cable. Note the decrease in loss for any treatment.

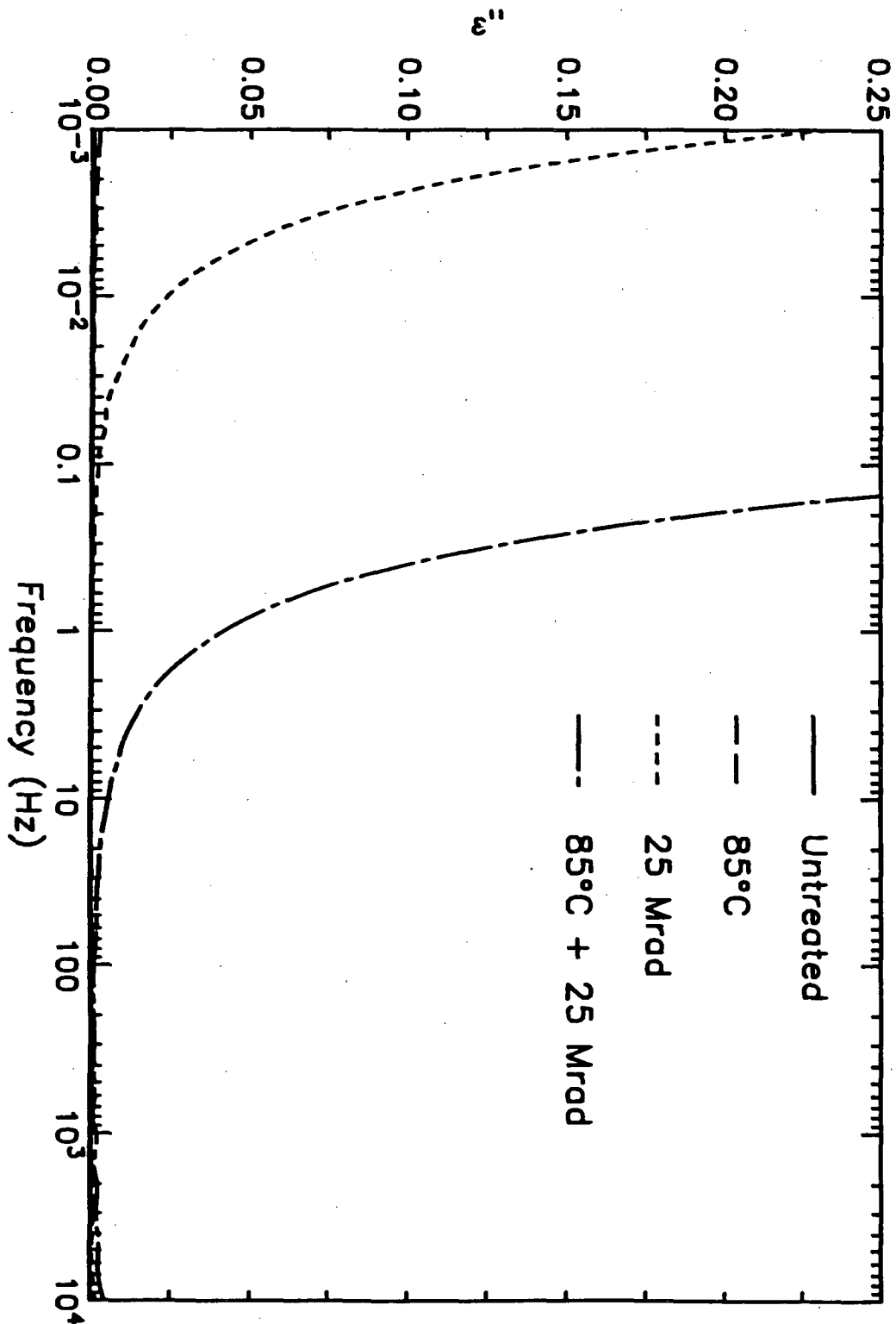


Figure 8: The loss index, ϵ'' , for Cable 4 as a function of frequency. Note the large increase in loss upon irradiation. The data for the untreated and heated samples are indistinguishable from 0 at this resolution.

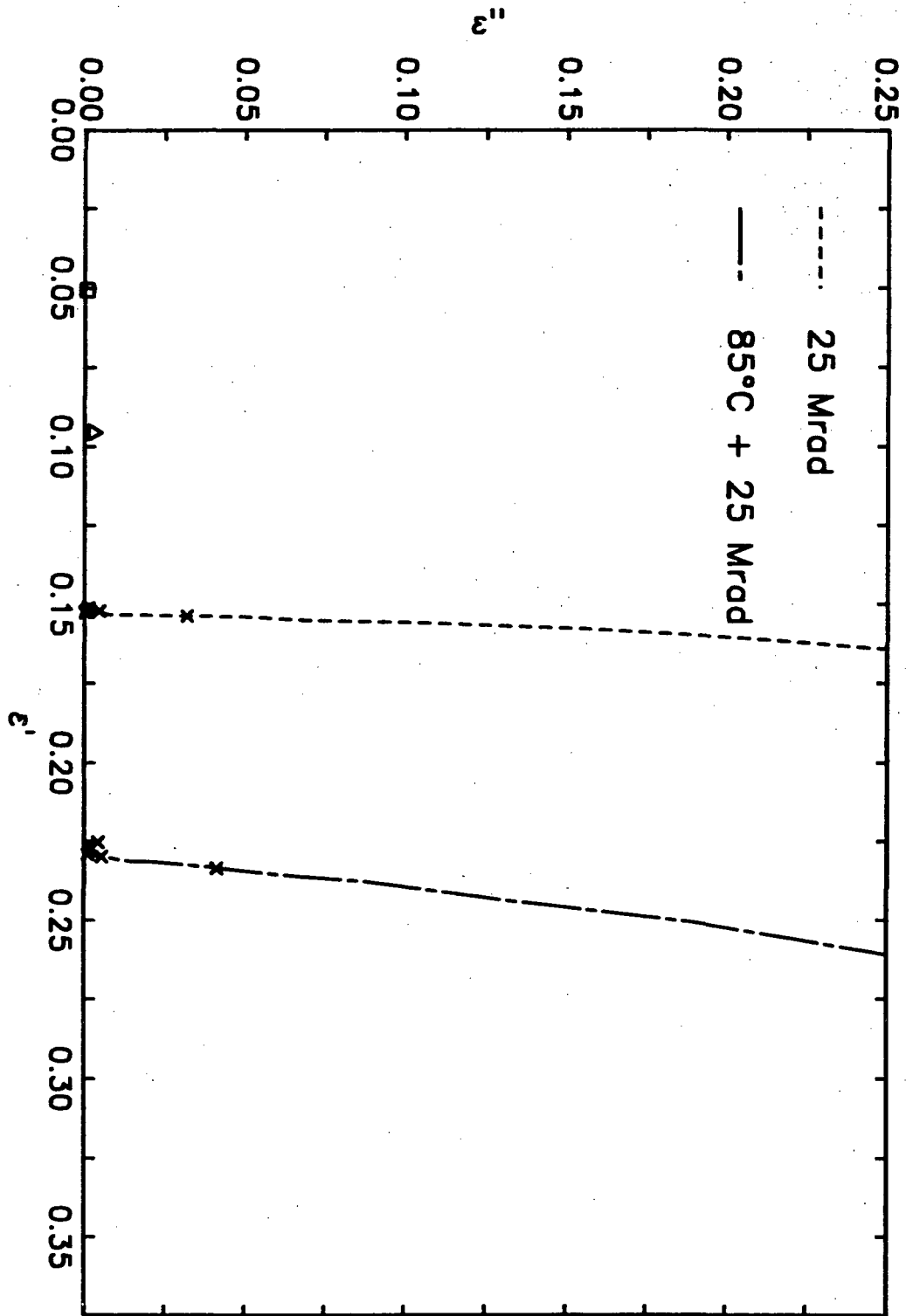


Figure 9: The loss index, ϵ'' , as a function of the real dielectric constant, ϵ' , for the same data as Fig. 8. The data have been arbitrarily displaced along the ϵ' axis for clarity. The data for the untreated and heated samples, represented as \square and Δ respectively, show no dispersion over the measured range. The x's near $\epsilon'' = 0.05$ mark the frequencies 0.01 and 1.0 Hz for the irradiated and irradiated with heat samples respectively.

molecular motions for a given condition. The correlations with mechanical properties will also differ. Major changes in additives, such as the absence or presence of fillers, flame retardants and others could do the same¹. However, sample to sample variations, whether they are due to exact formulation, which colorant is present, or other similar factors should change only the rate at which the properties change. This rate change is just what a good monitoring system is expected to follow and should not influence the validity of the estimation of lifetime. Further work is definitely needed in this area.

The definition of the lifetime of the cables is another area that needs to be addressed¹⁴. For some possible applications, the dielectric loss data can serve directly if they affect the transmission of any signals or power along the cable. For others, embrittlement, shrinkage or other mechanical failure can be more important and correlations of the TDS data are needed. Given a suitable definition, systems need to be examined as a function of life history so that these correlations can be made. This issue is not addressed in the work reported in this paper and no judgment has been made as to suitability of use.

Instrumentation for on-line monitoring also has to be addressed. One possibility is the use of monitoring specimens at critical spots along the cables with suitable shielded leads attached. Such a system could be interrogated at will at suitable times and be relatively immune to any interfering noise problems. Coaxial cables could simply be checked for their insulation by measuring between the center conductor and shield, although this would give only an average value. If the outer jacket is important or if it is a nonshielded system, electrodes would have to be designed and applied, possibly using the conductor already present as one electrode.

Finally, it is possible that TDS results may have their best application in laboratory situations using removable samples. Alternatively, data on test specimens could be used to establish a set of conditions for more conventional tests, such as DC conductivity for a set of charging times, that could be used to monitor lifetimes. Also, if simpler conductivity tests are made, some of the techniques used in TDS might prove useful. In particular, attention is called to the use of a charge detector and the three-terminal configuration.

CONCLUSIONS

TDS shows promise for the monitoring of electrical insulation systems during their lifetime. The main conclusion of this paper is that clearly defined changes do occur and they can be readily found. While there are large differences between different insulation systems, these should not be a major impediment to the use of dielectric loss data. Work has to be done to define the endpoint for useful life and relate this endpoint to measurable criteria. Also, work has to be done for proper test implementation. One possibility is that TDS data could be used to benchmark more conventional

tests on the insulation, such as conductivity, if used in a proper manner with explicit time dependence.

At NIST, we plan to extend our investigations using TDS. We are currently looking for samples with known and graded exposure to environmental conditions. Coordination with ongoing programs that yield results on the state of operational readiness is a necessity. We hope that such samples can be furnished on a cooperative basis so that the concept of lifetime estimation can be suitably validated.

We wish to acknowledge the support of USNRC Nuclear Plant Aging Research Program.

REFERENCES

1. Kuriyama, I., Hayakawa, N., Nakase, Y., et. al., "Radiation Resistance of Cable Insulating Materials for Nuclear Generating Stations", IEEE Trans. Elec. Insul., Vol. EI-13, 164,(1978).
2. Al-Hussaini, T. J. and Stoner, J. E., Jr., "On-Going Qualification of Cables in a Pressurized Water Reactor Environment", Nuclear Science Symposium, Orlando Florida, November 1, 1984.
3. Jeppeson, D., "Equipment Qualification Testing Methodology at Sandia Laboratories", NUREG/CP-0041, Vol. 5, U.S. Nuclear Regulatory Commission, NBS, Gaithersburg, MD, October 12, 1984.
4. Meininger, R. D., "Three Mile Island Technical Information and Examination Program, Instrumentation and Electrical Summary Report", EG&G-Idaho, Inc., GEND 050, DOE Contract No. DE-AC07-76ID01570, Idaho Falls, ID, July, 1985.
5. Kusama Y., Okada, S., Yoshikawa, et al, "Methodology Study for Qualification Testing of Wire and Cable at LOCA Conditions", Japan Atomic Energy Research Institute, Takasaki, Japan, October 12, 1982.
6. Sugarman, A. C., "Condition Monitoring of Electrical Equipment in Nuclear Power Plants", IEEE Trans. Energy Conv., Vol. EC-1, 1 (1986).
7. Mopsik, F. I., "Precision Time-Domain Dielectric Spectrometer", Rev. Sci. Instrum. 55, 79 (1984).
8. Mopsik, F. I., "The Transformation of Time-Domain Relaxation Data into the Frequency Domain", IEEE Trans. Elec. Insul., Vol EI-20, 957 (1985).
9. Bonzon, L. L., Wyant, F. J., Bustard, L. D., and Gillen, K. T., "Status Report on Equipment Qualification Issues Research and Resolution", NUREG/CR-4301, SAND85-1309, Albuquerque NM, November, 1986.
10. Gillen, K. T., Clough, R. L., Ganouna-Cohen, G., Chenion, J., and Delmas, G., Nucl. Eng. Design 74, 271 (1982).
11. Gillen, K. T., Clough, R. L., and Jones, L. J., "investigation of Cable Deterioration in the Containment Building of the Savannah River Nuclear Reactor", NUREG-2877, SAND81-2613, Sandia Laboratories, Albuquerque, NM, August, 1982.
12. Bustard, L. D., Chenion, J., Carlin, F., Alba, C., Gaussens, G., and LeMeur, M., "The Effect of Alternating Aging and Accident Simulation on Polymer Properties", NUREG/CR-4091, SAND84-2291, Sandia National Laboratories, Albuquerque NM, May 1985.

13. Clough, R. L., and Gillen, K. T., "Investigation of Cable Deterioration inside Reactor Containment", Nucl. Tech. 59, 344 (1982).

14. Ahmed, S., Carfagno, S. P., and Toman, G. J., "Inspection, Surveillance, and Monitoring of Electrical Equipment Inside Containment of Nuclear Power Plants - With Applications to Electrical Cables", NUREG/CR-4257, ORNL/Sub/83-28915-1, Oak Ridge National Laboratory, Oak Ridge, TN, September, 1985.

LESSONS LEARNED TO DATE FROM THE
SHIPPINGPORT AGING EVALUATION(a)

R. P. Allen
A. B. Johnson, Jr.

Pacific Northwest Laboratory(b)
Richland, Washington 99352

ABSTRACT

More than 200 naturally aged components and samples, ranging in size from small instruments and metallurgical specimens to one of the main coolant pumps, have been removed in conjunction with the decommissioning of the Shippingport Atomic Power Station and shipped to designated NRC contractors. In-situ assessments of selected Shippingport Station systems and components also have been conducted. Although the detailed evaluation of the naturally aged components and materials from the Shippingport Station is just beginning, there are a number of preliminary studies and results that are indicative of the value of the aging information that ultimately will be obtained. This paper presents background information on the Shippingport Station and its history, discusses the selection and relevancy of the naturally aged components and materials obtained through the Nuclear Plant Aging Research (NPAR) program, and illustrates the type of important plant aging information that can be derived from the in-situ studies and detailed evaluation of the components and samples from the Shippingport Station.

INTRODUCTION

The examination and testing of naturally aged nuclear power plant components is an important element of the U.S. Nuclear Regulatory Commission Nuclear Plant Aging Research (NPAR) Program strategy (USNRC 1985). The Shippingport Atomic Power Station, now in the latter stages of decommissioning, has been a major source of naturally aged materials and equipment for these NPAR evaluations and for other NRC programs. As the first U.S. large-scale, central-station nuclear plant, the Shippingport Station parallels commercial pressurized water reactors in reactor, steam, auxiliary, support, and safety systems. The 25-year service life (1957-1982) covers almost the entire period of currently operating reactors. Also, because of substantial

-
- (a) Work supported by the U.S. Nuclear Regulatory Commission, Office of Nuclear Regulatory Research.
 - (b) Operated for the U.S. Department of Energy by Battelle Memorial Institute under Contract DE-AC06-76RLO 1830.

modifications during the mid-1960s and 1970s, it offers unique examples of identical or similar equipment used side-by-side but representing different vintages and degrees of aging.

The entire Shippingport Station, including the structures and site support systems, is being completely dismantled (Schreiber 1987) under the direction of the U.S. Department of Energy (DOE) Shippingport Station Decommissioning Project Office (SSDPO), with the General Electric Company serving as the Decommissioning Operations Contractor. This represents a unique opportunity for NRC and its contractors to acquire naturally aged components and samples and to perform in-situ assessments to obtain critical information on plant aging.

SHIPPINGPORT STATION

The Shippingport Station is a pioneer in several respects. It was the first large-scale, central-station nuclear power plant in the United States and the first plant of its size in the world to be operated solely to produce electrical power from nuclear fission. It provided valuable information and training during initial operation with two different PWR cores, and then was converted to a light-water breeder reactor (LWBR) core to demonstrate the thermal breeding principle.

After completing its operational mission, the Shippingport Station became the first reactor of its size to be decommissioned by dismantlement, thus demonstrating the safe, cost-effective dismantlement of a large-scale nuclear power plant and providing valuable data for future decommissioning operations. Through the NPAR studies, the Shippingport Station also will make an important contribution to the continuing safety of operating plants.

The Shippingport Atomic Power Station is a 4-loop PWR with the same basic reactor, steam, auxiliary, support, and safety systems as current commercial PWRs. The primary system pressure and temperature were somewhat lower than normal parameters for a typical PWR. However, most components of interest for the aging studies (valves, inverters, cabling, etc.) are not influenced by the primary system operating conditions.

The Shippingport Station was constructed during the mid-1950s as a joint project of the federal government and the Duquesne Light Company (DLC) to develop and demonstrate PWR technology and to generate electricity. It is located on the south bank of the Ohio River at Shippingport, Pennsylvania, about 25 miles northwest of Pittsburgh on land owned by DLC. The reactor and steam generating portions were owned by DOE, and the electrical generating portion by DLC. The station began operation in December 1957 and was operated by DLC under supervision of the DOE Division of Naval Reactors until final shutdown on October 1, 1982. DLC paid DOE for the steam and marketed the electricity.

During its history, the Shippingport Station operated with two light-water cooled PWR cores (designated as PWR Core I and PWR Core II) and most recently with a LWBR core. PWR Core I began operation in December 1957 with a design

electrical power output of 68 MWe gross and operated until February 1964. PWR Core II was then installed and operated from April 1965 to February 1974 with a design electrical power output rating of 150 MWe gross. In 1976, a LWBR core was installed in the existing PWR vessel of the Shippingport Station. The LWBR core started operation in September 1977 and finished routine operation on October 1, 1982.

The two major core changes and the associated equipment and system upgrades thus provide a unique opportunity to compare identical or similar components that have operated side-by-side but represent different vintages and degrees of aging. For example, cells representing four vintages were in service in the same plant battery at the end of reactor operation.

COMPONENT SELECTION

Despite their value for plant aging studies, access to naturally aged components of the desired type and vintage is generally limited. One potential source is failed equipment from operating nuclear plants. The components are directly relevant to current plants and designs, but equipment of the specific type and with the age and service history desired for aging studies may not be available. Also the failure may compromise the aging evaluation unless the failure analysis itself is of prime interest.

Operational equipment could be removed from operating plants under a replacement arrangement, but this could be very costly and only feasible for a limited number of components. Similarly, selected in-situ aging evaluations could be conducted at operating plants, but these would be limited to the use of nondestructive techniques.

The best source of naturally aged components for aging studies is operational equipment from retired plants. A variety of components is available, including different vintages for replacement equipment. Not all components are Class 1E or typical of newer plants, but the older components are representative of equivalent vintage plants. In-situ tests can be performed without concern for equipment or operating schedules, and equipment and samples can be removed for detailed evaluation at other sites. The decommissioning of the Shippingport Station, particularly because it was managed by DOE, represented a valuable opportunity to conduct in-situ assessments at an aged reactor and to obtain a variety of naturally aged and degraded components and samples for detailed aging evaluations.

One of the major challenges of the Shippingport Station Aging Evaluation task was to select, out of the hundreds of possibilities, those specific components, samples, and in-situ evaluations that would be of most value to the NPAR Program and other NRC programs. The identification and selection of the specific components and samples to be acquired was accomplished primarily through seven site visits by NRC and contractor staff and industry consultants representing a range of disciplines and research interests. Table 1 lists the participants in one of these visits, together with their affiliation and area of expertise.

TABLE 1. Shippingport Site Visit - March 7, 1984

Name	Affiliation	Expertise
B. Morris	NRC/RES	Program Guidance, Elect. & Mech. Components
C. Serpan	NRC/RES	Materials, Vessel, Pipings, S. G., ND Examination
J. Vora	NRC/RES	Program Coordination, Elect. Components
G. Arndt	NRC/RES	Structures, Mech. Components
E. Brown	NRC/AEOD	Mechanical, Electro-Mech. Components
Z. Rosztoczy	NRC/NRR	PWR Systems, Relevancy, Elect. & Mech. Components
G. Murphy	ORNL	LWR Relevancy, Elect. & Mech. Components
R. Meininger	INEL	LWR Relevancy, Elect. Components
J. Taylor	BNL	LWR Relevancy, Elect. Components
D. Berry	SNL	LWR/NR Relevancy, Systems
V. Harris	WPPSS	LWR Relevancy, Systems, Elect. & Mech. Components, In Situ Monitoring - Testing
V. Bacanskas	FRC	Elect. Components (Breakers, Relays, Switchgear)
R. Allen	PNL	Project Coordination & Implementation

The component selection visits were preceded by extensive preparation, including site visits to meet with Naval Reactors personnel and review plant reports and records pertaining to Shippingport Station systems, components, and operating history. This information was compiled into a Shippingport reference manual and provided to the designated NPAR contractors for review. Other criteria used to select the specific components for evaluation included

- identical or similar equipment representing different vintages but the same function and operating environment
- equipment representing different models or manufacturers but the same vintage, function, and operating environment
- similar equipment operating in contrasting temperature and radiation environments
- equipment with performance concerns based on industry experience.

The relevancy of the Shippingport Station components to operating plant equipment designs, specifications, materials of construction, and operating parameters was an important factor in the component selection process. This criterion was addressed based on the following four considerations. First, it is impossible, by definition, to meaningfully evaluate naturally aged components if only current vintage equipment is considered to be relevant.

Second, the equipment from the Shippingport Station is directly relevant to the equipment used in equivalent vintage plants. Four commercial plants started operation within 5 years of the original Shippingport Station. Another 7 plants went on-line within 5 years of the PWR Core II upgrade, and a total of 62 reactors had begun commercial operation by the time the LWBR upgrade was completed in late 1977. Moreover, because these 62 reactors are the oldest plants in the United States, they represent the vintages of primary concern for near-term aging and life-extension evaluations.

Third, because the Shippingport Station service life covers almost the entire time span of currently-operating reactors, its equipment reflects a similar range of applicable codes, standards, and qualification testing. The original components represented the best off-the-shelf equipment commercially available at the time. In many cases, it is the same type of equipment used in other plants of that vintage. Conversely, the LWBR upgrade involved qualified components identical, in some cases, to equipment in current vintage plants.

Fourth, the Shippingport Station components and samples that were acquired for the NPAR Program were selected on an individual basis by experts, including industry consultants with a sound understanding of the equipment and materials used in plants of the vintages of importance to aging studies. Also, it should be recognized that even though the design of a specific component may change, an aging evaluation of a particular material or

subassembly from an earlier version may still be relevant to current equipment in terms of function, service environment, or a particular aging mechanism.

SITE ACTIVITIES

The NPAR Shippingport Station coordination activities began in July 1983. During the initial stages of the decommission operation, procurement specifications, technical manuals, operating reports, maintenance histories and other data and records relevant to the procurement, operation and maintenance of the components selected for acquisition were obtained to support the subsequent detailed aging evaluations. The written information was supplemented wherever possible by interviews with Shippingport Site personnel formerly involved in the operation and maintenance of plant systems and components.

As plant systems were deactivated, in-situ assessments of Shippingport Station systems and components were conducted. These included the pre-removal visual and physical examination of components, the testing of electrical circuits, and special measurements to assist in the selection of specific components for further evaluation. Then, as the progress of the decommissioning operations allowed, more than 200 Shippingport Station components and samples were removed and shipped to designated NRC contractors. The number and diversity of the items that were acquired for the NPAR studies and other NRC programs as part of the Shippingport Station NPAR coordination effort are illustrated in Table 2. Examples of these items are shown in Figures 1 through 7.

LESSONS LEARNED

In-situ assessments and the postservice examination and testing of naturally aged components are an integral and essential part of the NPAR program strategy. Only actual plant systems and naturally aged components reflect the full range of effects from plant and service factors such as external stressors, service wear, testing procedures, and maintenance practices.

The various types of plant aging information that can be derived from these system and component studies include the following:

- identification of equipment demonstrating satisfactory long-term performance with minimal aging effects
- aging rate data for expected degradation processes
- detection of unexpected aging mechanisms (surprises)
- basic insights on failure modes and mechanisms
- comparison data for validating aging projections from accelerated aging studies

TABLE 2. Items Acquired Through the NPAR Shippingport Station
Coordination Effort

<u>NRC Contractor</u>	<u>Number of Items</u>
<u>Pacific Northwest Laboratory (PNL)</u>	
• PV Nozzle Cutouts	5
• Coolant Purification Piping	2
• Rad Waste Piping	2
• B/D Instrument Piping	2
• Fuel Pool Piping	2
• Main Steam Piping	1
• Feedwater Piping	1
• Air System Piping	7
• SWS Heat Exchangers	2
• Contaminated Concrete	1 Drum
<u>Argonne National Laboratory (ANL)</u>	
• Main Coolant Pump	1
• Check Valves	4
• Manual Isolation Valves	3
• Hot Leg Pipe Section	1
• Cold Leg Pipe Section	1
• Spare Volute	1
• Spare Pipe Section	1
• NST Samples	11
• Reactor Chamber Steel	1 Drum
<u>Brookhaven National Laboratory (BNL)</u>	
• Motor-Generator Set	1
• Battery Chargers	2
• Inverters	3
• Motor Control Center	2
• Differential Relays	2
• Protective Relays	4
• Agastat Relays	5
• Scram Breakers	2
• MG-6 Relays	4
• DB-50 Breakers	2
• Circuit Breakers	8
• Current Transformers	2
• Potential Transformers	2
• 480/120 Transformers	2
• Constant Voltage Transformers	2
• Relay Panel	1
• Charger/Inverter Spare Parts	1 box

TABLE 2. (Cont'd)

<u>NRC Contractor</u>	<u>Number of Items</u>
<u>EG&G Idaho, Inc. (INEL)</u>	
• Motor Operated Valves	2
• Limit Switches	8
• Battery Cells	24
• Nuclear Instrumentation Channels	2
• Electrical Panel	1
• Thermocouple Signal Box	1
• Thermocouple Junction Box	1
• Power Lead Junction Box	2
• Power Cable	1
• Instrumentation Cable	2
• Rod Control Junction Boxes	2
• Selector Switches	3
• Pressure Switches	7
• Rosemount Transducers	3
• RTDs	8
• D/P Cells	6
• Transmitters	5
• Level Indicator	1
• Compensating Ion Chamber Detectors	4
• BF3 Detectors	4
• Electrical Stop Joints	6
• Electrical Cable (100')	3
<u>Oak Ridge National Laboratory (ORNL)</u>	
• Solenoid Valves	7
• Motor Operated Valves	6
• Check Valves	5
<u>National Bureau of Standards (NBS)</u>	
• Electrical Cable	4

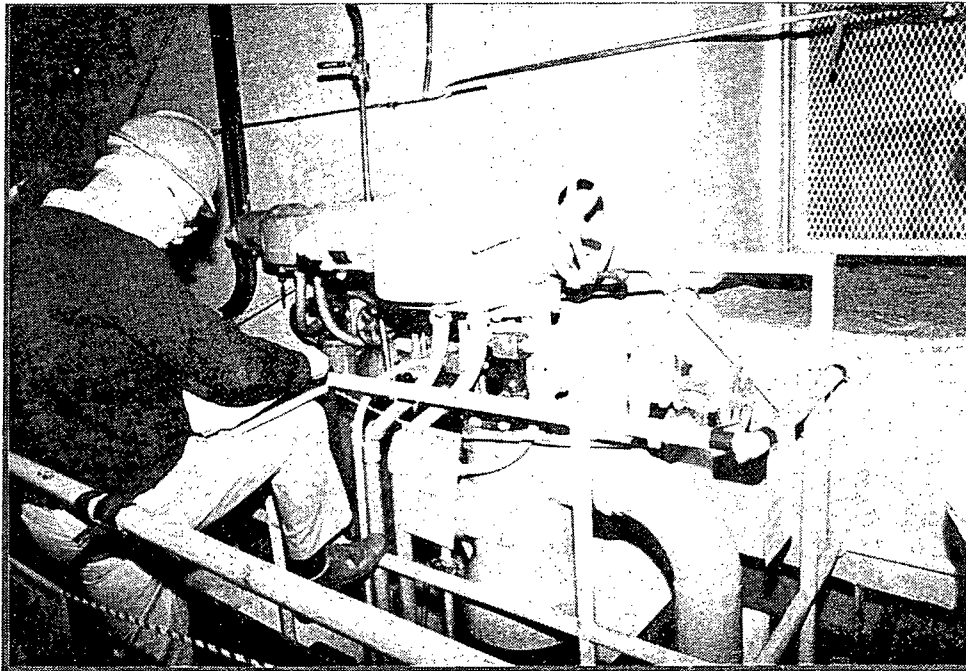
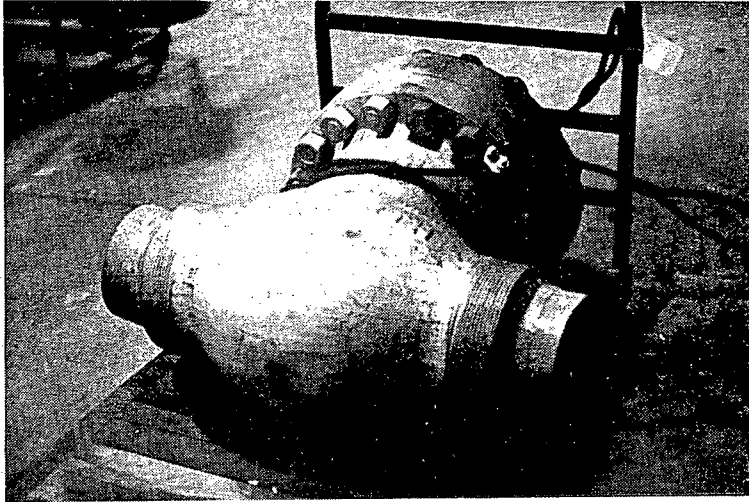


FIGURE 1. Check Valve (Top) and Motor-Operated Valve (Bottom) for NPAR Studies at ORNL

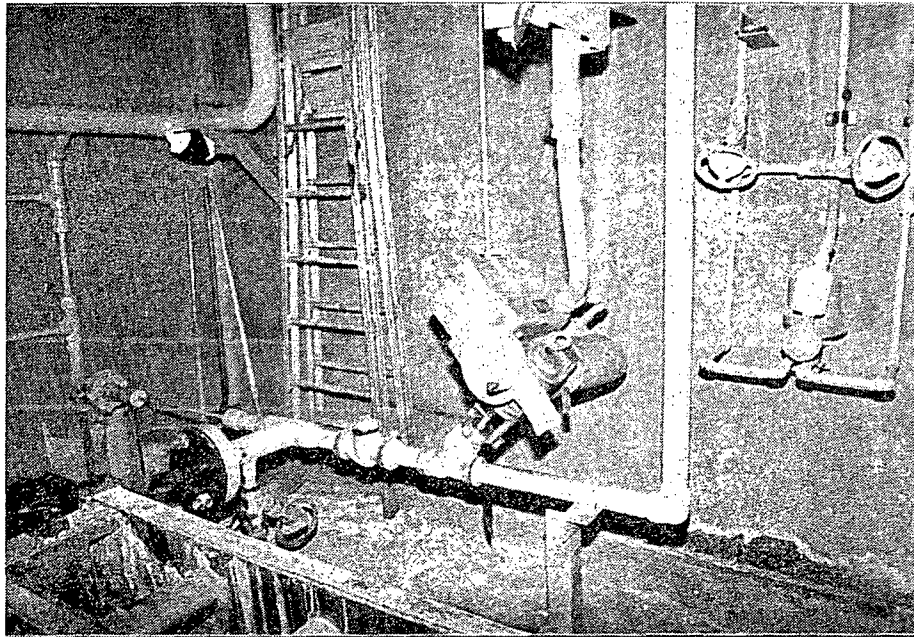
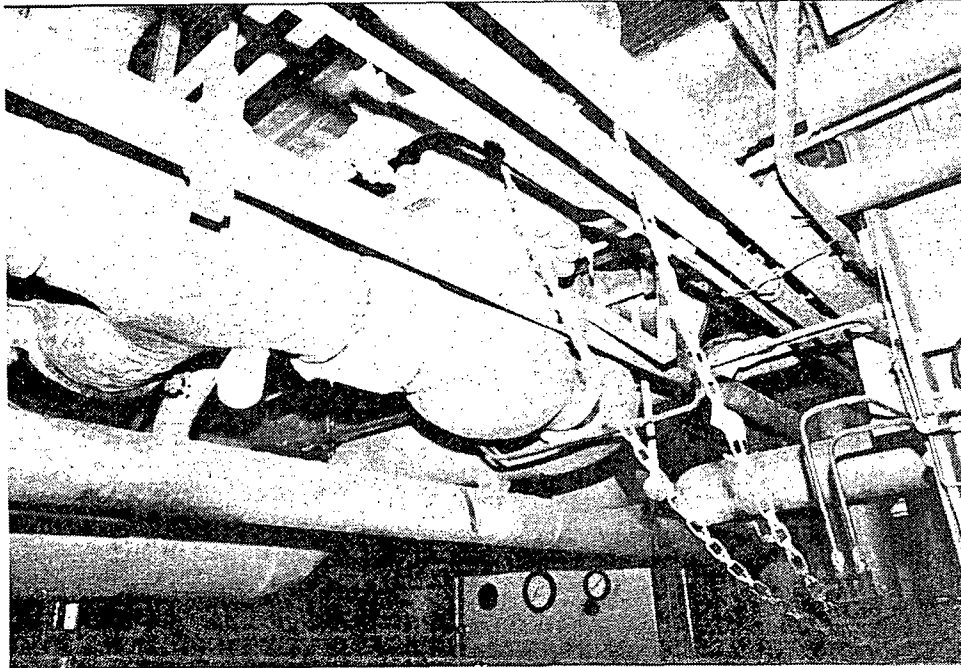


FIGURE 2. Original (Top) and Mid-1970s (Bottom) Vintage Motor-Operated Valves for Equipment Qualification Studies at INEL

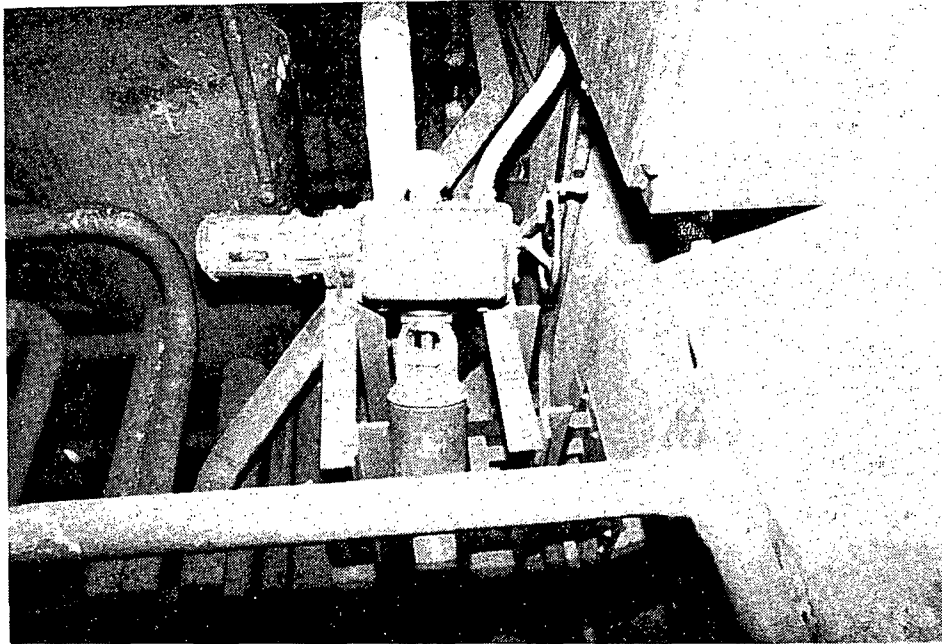
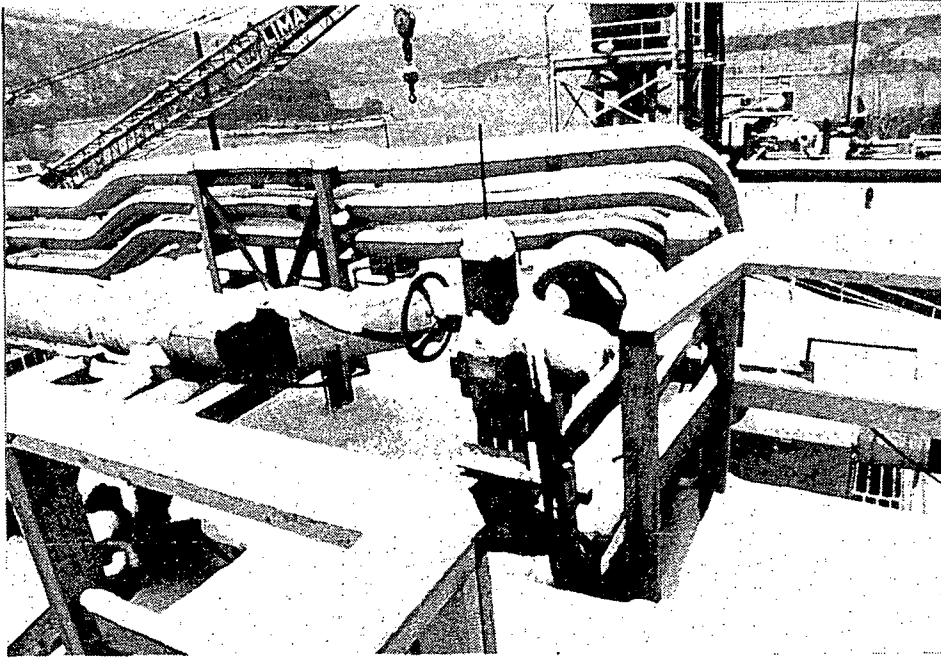


FIGURE 3. Similar Equipment (Motor-Operated Valves) Operating in Thermally Severe and Mild Service Environments

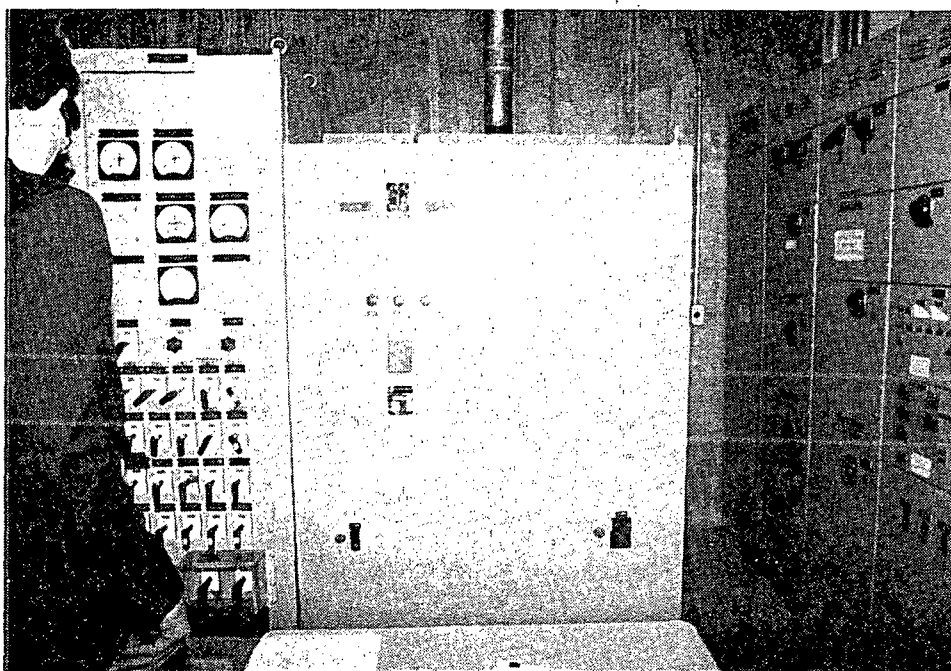
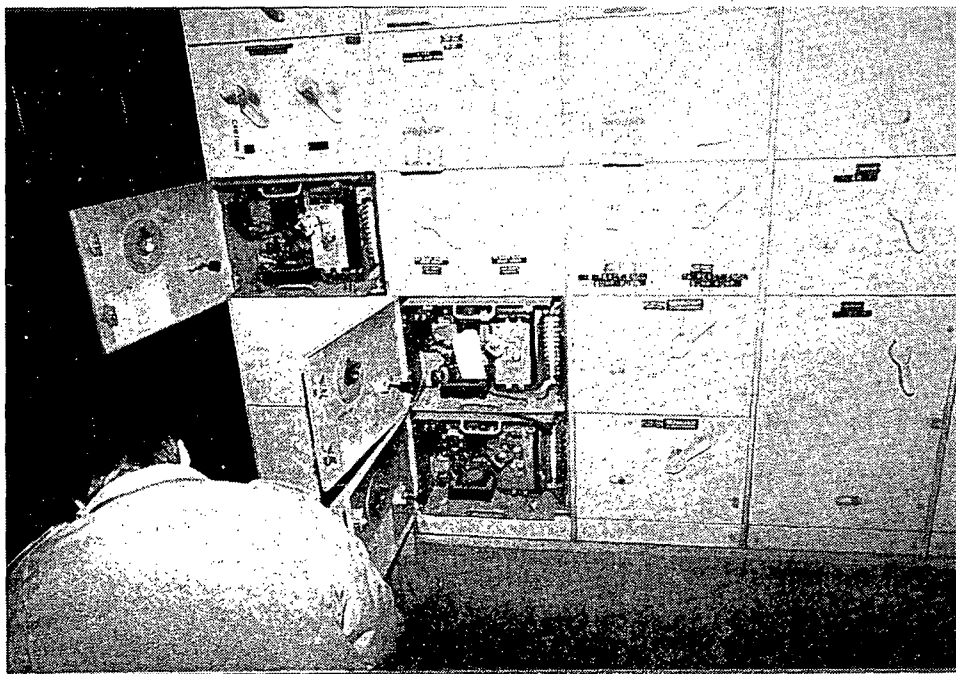


FIGURE 4. Original (Top) and Mid-1970s (Bottom) Vintage Electrical Equipment for NPAR Studies at BNL



FIGURE 5. Electrical Cable From Radiation (Top) and Control (Bottom) Areas for NPAR Studies at INEL and NBS

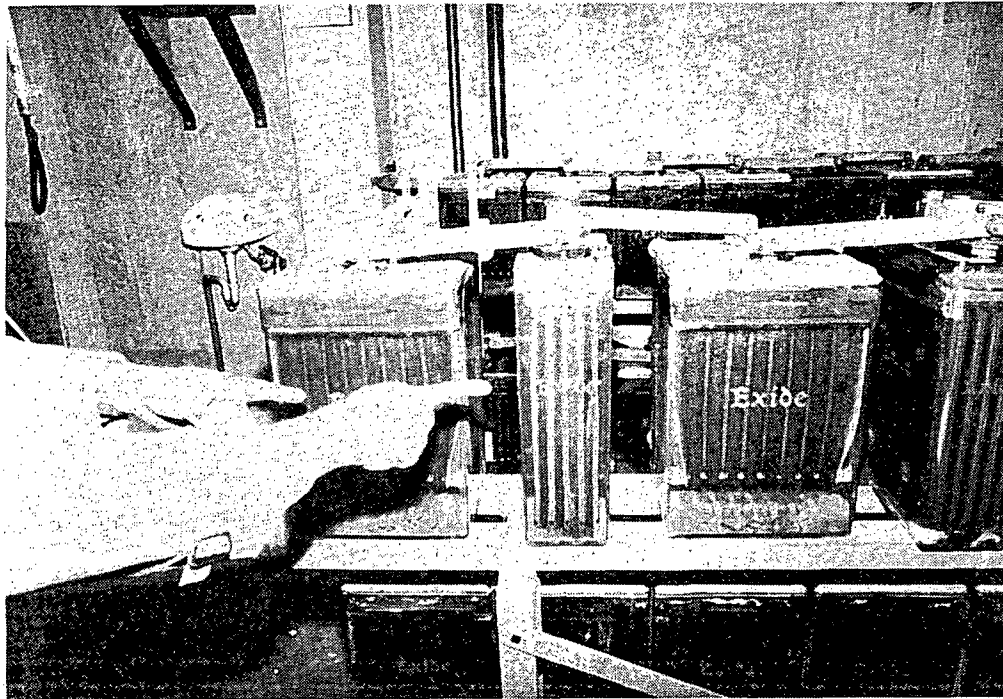


FIGURE 6. Original (Left) and Replacement (Right) Battery Cells from the Same Service Environment for NPAR Studies at INEL

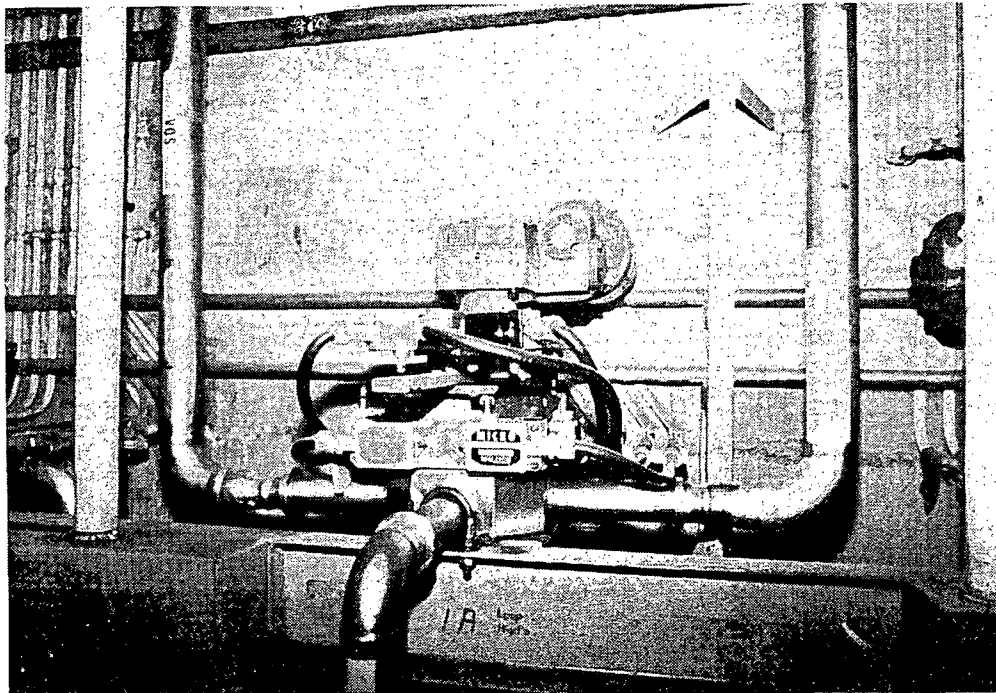


FIGURE 7. Original and Replacement Microswitches Operating in the Same Service Environment

Although the detailed evaluation of the naturally aged components and material from the Shippingport Station is just beginning, a number of preliminary studies and results are indicative of the value of the aging information that ultimately will be obtained. Examples include the following.

ELECTRICAL CIRCUITS

Idaho National Engineering Laboratory personnel conducted a comprehensive in-situ evaluation of 46 Shippingport Station electrical circuits and components (Dinsel, Donaldson and Soberano 1987). This electrical testing included more than 1600 individual measurements of voltage, effective series capacitance, effective series inductance, impedance, effective series resistance, dc resistance, insulation resistance, and time domain reflectometry parameters. The dual objectives were to determine the extent of aging or degradation of selected plant circuits and also to evaluate previously developed surveillance technology. Circuits evaluated included pressurizer heaters, control rod position indicator cables, primary system resistance temperature detectors, nuclear instrumentation cables, and motor-operated valves. The in-situ tests confirmed the effectiveness of the measurement system for detecting degradation of circuit connections and splices because of high resistance paths. The anomalies that were detected were attributed to corrosion, reflecting the termination of the surveillance/maintenance program for these circuits following plant shutdown. A similar rapid degradation of the plant battery cells upon removal from service was observed, further illustrating the critical role of proper maintenance in minimizing aging.

CAST STAINLESS STEEL

An Argonne National Laboratory (ANL) investigation of the microstructural characteristics of cast stainless steel from selected Shippingport Station primary system components (Shack, Chopra and Chung 1989) has helped clarify the thermal embrittlement processes that can occur at Light Water Reactor operating temperatures. The ferrite content of the cast stainless steel primary system main valves and coolant pump volutes was measured in situ to identify candidate materials for these thermal embrittlement studies. Nine components (Table 2) with ferrite contents in the 2 to 16% range were obtained and sent to ANL for detailed evaluation. The results of the postservice examinations of the naturally aged material will be compared with data previously obtained for laboratory-aged cast stainless steel to ensure that the mechanisms and kinetics of the aging processes are comparable. The availability of this naturally aged Shippingport Station material thus provides a direct means of validating aging projections based on the extrapolation of accelerated test data, and also has the potential of identifying unexpected aging processes and effects.

NEUTRON SHIELD TANK SAMPLES

A special sampling operation was conducted to obtain material from the inner wall of the Shippingport Station neutron shield tank (NST) for low-temperature, low-flux embrittlement studies. The NST is an annular water

tank 35-in. thick that surrounds the mid-section and bottom of the pressure vessel to reduce the neutron and gamma radiation in the reactor chamber. The inner and outer NST walls are 1-in. thick steel plate. A portable concrete coring system was used to cut a 7-in. diameter core from the outer NST wall using a bi-metal hole saw, core through the grout-filled tank using a 6.5-in. diameter diamond bit, and cut a 6-in. diameter core from the inner wall using a second hole saw. Eleven inner-wall disks were successfully removed from locations representing base metal and weld material exposed to different neutron flux levels. Evaluation of these samples will help resolve the issue of whether low-temperature, low-flux irradiation can produce an unexpectedly high degree of embrittlement of reactor pressure vessel support structures (Shack, Chopra and Chung 1989).

INVERTER/BATTERY CHARGER

Naturally aged inverters and battery chargers from the Shippingport Station were tested by Brookhaven National Laboratory as part of the NPAR Program (Gunther 1987). Component temperatures and circuit waveforms were monitored during steady-state testing and step load changes. A decrease in silicon controlled rectifier heat transfer capacity and an increase in output filter capacitor case temperature were noted and attributed to aging effects. However, it was concluded that aging had not substantially affected equipment operation. These results illustrate the use of naturally aged components to confirm the continued operability and satisfactory performance of plant equipment. This study also demonstrated the usefulness of circuit monitoring to detect impending failure in the incipient stage.

CHECK VALVES

Eighteen naturally aged check, solenoid and motor-operated valves representing a variety of types, sizes and vintages were obtained from the Shippingport Station for NPAR studies at Oak Ridge National Laboratory. The first component evaluated was an 8-in. piston lift check valve from the safety injection system. Although it was in a loop that operated only during system tests, detailed examination revealed a characteristic wear pattern indicative of significant service with the piston opened about 25% of its normal travel. This is an example of the value of naturally aged components in detecting unexpected aging effects.

MOTOR-OPERATED VALVES

A naturally aged 8-in. diameter gate valve and operator from the Shippingport Station were refurbished and requalified at the Idaho National Engineering Laboratory and then tested as part of an internationally sponsored seismic research program (Steele, MacDonald and Arendts 1987). The valve was installed in the decommissioned Heissdampfreaktor, located in the Federal Republic of Germany, and subjected to seismic loadings in addition to normal internal pressure and flow loads. The structural integrity of the valve and operator was not affected by the seismic excitations. However, some

opening/closing anomalies were detected using this valve that would not be revealed by normal in-plant valve testing (Steele, Arendts and Weidenhamer 1988).

RADIOLOGICAL ASSESSMENT

In addition to the evaluation of naturally aged components, the decommissioning of the Shippingport Station provides a valuable opportunity to study the composition, distribution and inventory of residual radionuclides in contaminated piping, components and materials. Samples of piping and concrete from selected Shippingport Station systems and surfaces have been obtained for radionuclide source term measurements at Pacific Northwest Laboratory (Table 2). A preliminary assessment of the corrosion film on the primary coolant piping samples (Robertson and Thomas 1988) disclosed comparatively low concentrations of long-lived activation products and very low fission product and transuranic radionuclide concentrations, reflecting the high integrity of the fuel cladding during reactor operation.

CONCLUSIONS

The detailed evaluations of naturally aged components and materials from the Shippingport Station that are now in progress are providing important plant aging information. These studies can confirm and quantify expected degradation mechanisms and failure modes, or provide assurance that components and materials will be minimally affected by aging. Because naturally aged components and materials experience the actual external stressors, service wear, testing procedures and maintenance practices, their evaluation is the only way to verify degradation models, to validate aging projections based on the extrapolation of accelerated test data, or to detect unexpected aging mechanisms that could significantly impact component or system safety performance.

Eventual outputs from current and future investigations of Shippingport Station components and materials may include the addition of aging perspectives to regulatory guides, standards and codes; improved performance indicator monitoring; improved maintenance guidelines; and other major contributions to the evaluation of the effects of aging on plant safety and to the technical basis for plant life extension.

REFERENCES

- Dinsel, M. R., M. R. Donaldson and F. T. Soberano. 1987. In Situ Testing of the Shippingport Atomic Power Station Electrical Circuits. NUREG/CR-3956, EG&G Idaho, Idaho Falls, Idaho.
- Gunther, W. E. 1987. Testing of a Naturally Aged Nuclear Power Plant Inverter and Battery Charger. Technical Report A-3270-10-87, Brookhaven National Laboratory, Upton, New York.
- Robertson, D. E. and C. W. Thomas. 1988. "Radionuclide Source Term Measurements for Power Reactor Decommissioning Assessment." In Proceedings of the Fifteenth Water Reactor Safety Information Meeting, Ed. A. J. Weiss, pp. 67-88, NUREG/CP-0091, Vol. 6, National Technical Information Service, Springfield, Virginia.
- Schreiber, J. J. 1987. "Shippingport Station Decommissioning Project: An Overview and Status Report." In Proceedings of the 1987 International Decommissioning Symposium, Ed. G. Tarcza, pp. I-35 to I-42, USDOE CONF-871018, Vol. 1, National Technical Information Service, Springfield, Virginia.
- Shack, W. J., O. Chopra and H. Chung. 1989. "Shippingport Aging Studies - Results and Plans." In Proceedings of the Sixteenth Water Reactor Safety Information Meeting, Ed. A. J. Weiss, National Technical Information Service, Springfield, Virginia.
- Steele, R., Jr., P. E. MacDonald and J. G. Arendts. 1987. "Dynamic Load Effects on Gate Valve Operability." In Proceedings of the Fourteenth Water Reactor Safety Information Meeting, Ed. A. J. Weiss, pp. 31-40, NUREG/CP-0082, Vol. 3, National Technical Information Service, Springfield, Virginia.
- Steele, R., Jr., J. G. Arendts and G. H. Weidenhamer. 1988. "Performance of a Piping System and Equipment in the HDR Simulated Seismic Experiments." In Proceedings of the Fifteenth Water Reactor Safety Information Meeting, Ed. A. J. Weiss, pp. 389-413, NUREG/CP-0091, Vol. 3, National Technical Information Service, Springfield, Virginia.
- U.S. Nuclear Regulatory Commission. 1985. Nuclear Plant Aging Research (NPAR) Program Plan. NUREG-1144, U.S. Nuclear Regulatory Commission, Washington, D.C.

Aging Assessment and Mitigation for Major LWR Components^a

V. N. Shah, A. G. Ware, D. A. Conley, P. E. MacDonald
Idaho National Engineering Laboratory

J. J. Burns, Jr.
U.S. Nuclear Regulatory Commission

Abstract

This paper summarizes some of the results of the Aging Assessment and Mitigation Project sponsored by the U.S. Nuclear Regulatory Commission, Office of Nuclear Regulatory Research. The objective of the project is to understand the aging degradation of the major light water reactor (LWR) structures and components and develop methods for predicting the useful life of these components, so that the impact of aging on the safe operation of nuclear power plants can be evaluated and addressed. Researchers are accomplishing this objective by integrating, evaluating, and updating the available aging-related information. This paper discusses current accomplishments and summarizes the significant degradation processes active in two major components: pressurized water reactor pressurizer surge and spray lines and nozzles, and light water reactor primary coolant pumps. This paper also evaluates the effectiveness of the current inservice inspection programs and presents conclusions and recommendations related to aging of these two major components.

Introduction

One hundred eight commercial nuclear power plants are currently licensed to operate in the United States. The oldest one is the Yankee Rowe plant, which has been in operation for 28 years. Five other plants have been in operation for more than 20 years. Twenty-two plants have been in operation between 15 and 20 years. Several time-dependent degradation mechanisms not accounted for in the original designs have caused failures in these plants. For example, high-cycle fatigue caused a steam generator tube to rupture, corrosion caused significant wall thinning of a metal containment, erosion-corrosion caused catastrophic failure of a "nonnuclear" portion of a pressurized water reactor (PWR) feedwater line, and thermal fatigue caused a through-wall crack in a PWR safety injection pipe between the safety injection nozzle and the first check valve.

^a Work sponsored by the United States Nuclear Regulatory Commission, Office of Nuclear Regulatory Research, under DOE Contract No. DE-AC07-76ID01570.

Therefore, the need to understand and manage aging has become a major focus for the research sponsored by the U.S. Nuclear Regulatory Commission (USNRC). An important part of the USNRC research effort is the Nuclear Plant Aging Research (NPAR) Program that is being conducted at several national laboratories, including the Idaho National Engineering Laboratory (INEL).

The NPAR Program is sponsoring the Aging Assessment and Mitigation Project at the INEL. The objectives of the project are to develop an understanding of the aging of major light water reactor (LWR) structures and components and to identify the technical issues associated with aging. The project is concerned with integration, evaluation, and updating of the current information related to the time-dependent degradation or aging of the major LWR structures and components so that the technical issues that may impact safety can be identified and addressed in an effective and timely manner. This information will provide the basis for the development of life assessment procedures that will assist the USNRC in the formulation of license renewal policy, as well as in other regulatory applications.

The Aging Assessment and Mitigation Project is being carried out in five steps. The five steps are:

1. Identify and prioritize the major reactor components according to their relevance to plant safety.
2. Identify the degradation sites, mechanisms, stressors, potential failure modes, and current inservice inspection methods.
3. Assess emerging inspection, surveillance, and monitoring methods that can be used to detect, quantify, and trend aging degradation. Evaluate current and emerging maintenance programs to mitigate aging damage.
4. Develop LWR structure and component life assessment procedures.
5. Support development of technical criteria for license renewal.

The first two steps of the five-step approach have been completed,^{2,3} and some progress has been made on the remaining three steps. This paper summarizes the qualitative results of step 2 for two major components: PWR surge and spray lines and nozzles⁴, and LWR coolant pumps⁵. Design, stressors, degradation sites and mechanisms, potential failure modes, and current inservice inspection methods are briefly described for each component. Conclusions and recommendations follow. Similar information for the remaining LWR structures and components of interest can be found in References 2 and 3.

Aging Assessment of PWR Surge and Spray Lines and Nozzles

The pressurizer controls the reactor coolant system (RCS) pressure by maintaining the temperature of the pressurizer liquid at the saturation

temperature corresponding to the desired system pressure. During heatup, the increase in the volume of the RCS coolant causes an insurge into the pressurizer through the surge nozzle. During cooldown, the pressurizer spray system, which is fed from one or two of the RCS cold legs, is activated to reduce the pressure. During reactor power transients, insurges and outsurges through the surge nozzle take place, and if pressure increases above a predetermined setpoint, the spray system is activated automatically.

Design of Surge and Spray Lines and Nozzles

The surge line is typically a 250 to 350-mm (10 to 14-in.) diameter pipe made of Type 316 stainless steel. In some PWRs the surge line is made of centrifugally cast stainless steel. The surge line connects the hot leg of the primary piping to the bottom of the pressurizer. The spray line is typically a 60 to 100-mm (2.5 to 4-in.) diameter Type 316 stainless steel pipe that connects the top of the pressurizer to one or more of the cold legs. The typical layout of the spray and surge lines, shown in Figure 1, includes long horizontal or near horizontal runs of piping. The nozzles at both ends of the surge and spray lines are called surge and spray nozzles, respectively.

The spray system consists of a main spray line and an auxiliary spray line. The main spray line is connected to the cold legs through the main spray and bypass valves. During normal operation, a small amount of continuous flow that bypasses the main spray valves and flows through the bypass valves is maintained by the driving head of the reactor coolant pumps. The bypass valves, if properly sized, pass a sufficient amount of coolant to ensure full flow in the spray line so the temperature difference between the spray line fluid and the pressurizer spray nozzle remains at a minimum. The auxiliary spray line is connected to the charging lines which are connected to the cold legs as shown in Figure 1. Actuation of the main spray valves depressurizes the reactor coolant system during cooldown. At low coolant temperatures and pressures, when the main spray system is no longer available because the reactor coolant pumps stop running due to net pump suction head (NPSH) limitations, the auxiliary spray system is activated to complete the depressurization. The temperature of the main spray is equal to the cold leg temperature, and it varies from 288 C (550 F) to about 227 C (440 F) during cooldown. The auxiliary spray temperature is normally at 205 C (400 F), but it can be as low as 50 C (120 F) at the time charging flow is initiated. In the design basis transients, it is assumed that the auxiliary spray temperature can be as low as 5 C (40 F).

Because the pressurizer is made of low-alloy carbon steel, the welds at the pressurizer ends of the spray and surge lines are dissimilar-metal welds. In Combustion Engineering (CE) and Babcock & Wilcox (B&W) plants, the primary loop piping is made of low-alloy carbon steel, so the welds at the hot leg end of the surge line and cold leg ends of the spray line are also dissimilar-metal welds. Figures 2 and 3 show typical surge and spray

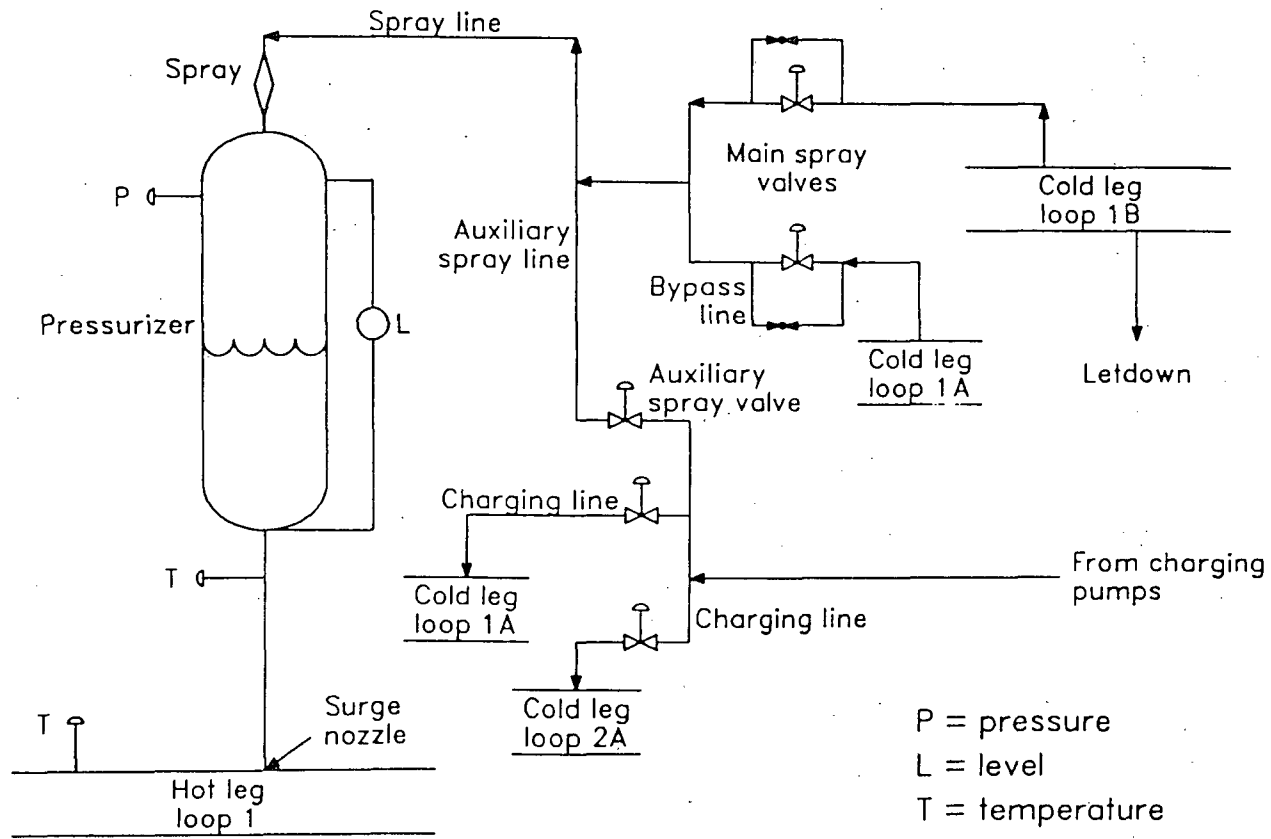
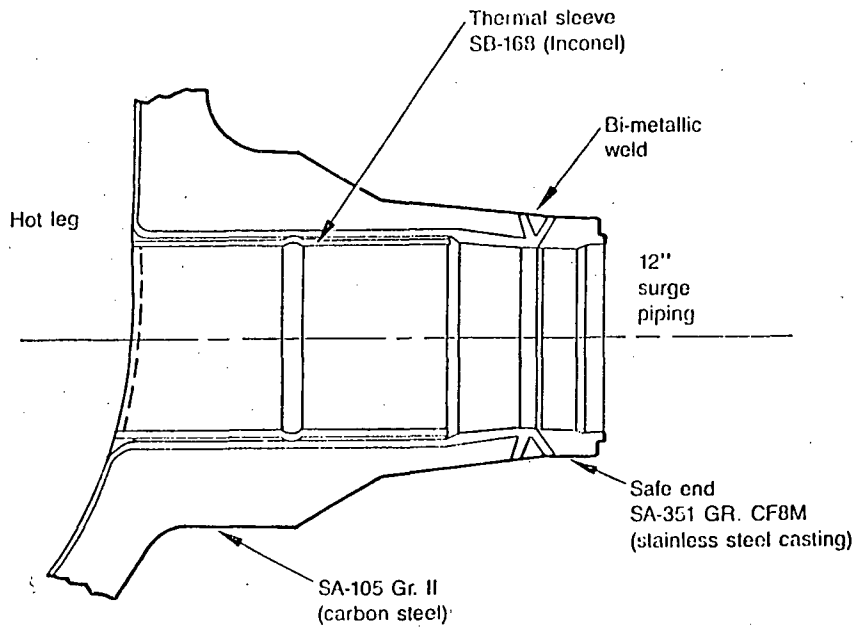


Figure 1. System schematic of spray and surge systems.

LN88026-1



Figures 2. Typical CE surge nozzle at hot leg (12 in. Schedule 160).

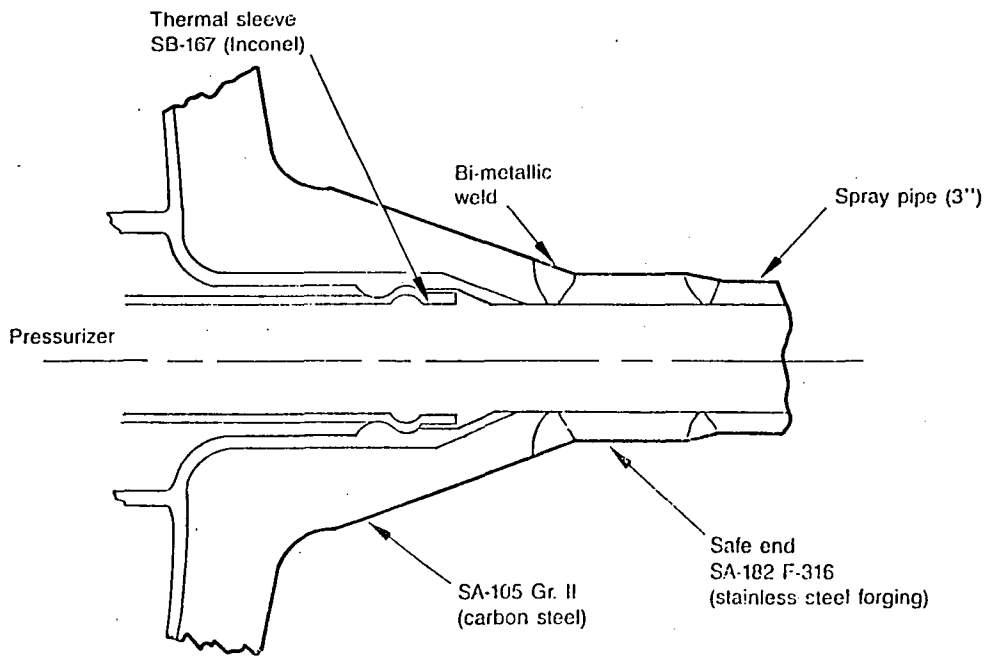


Figure 3. Typical CE spray nozzle (3 in. Schedule 160).

nozzles in CE plants. Thermal sleeves are included in the design of both surge and spray nozzles to protect nozzle walls from transient thermal loads.

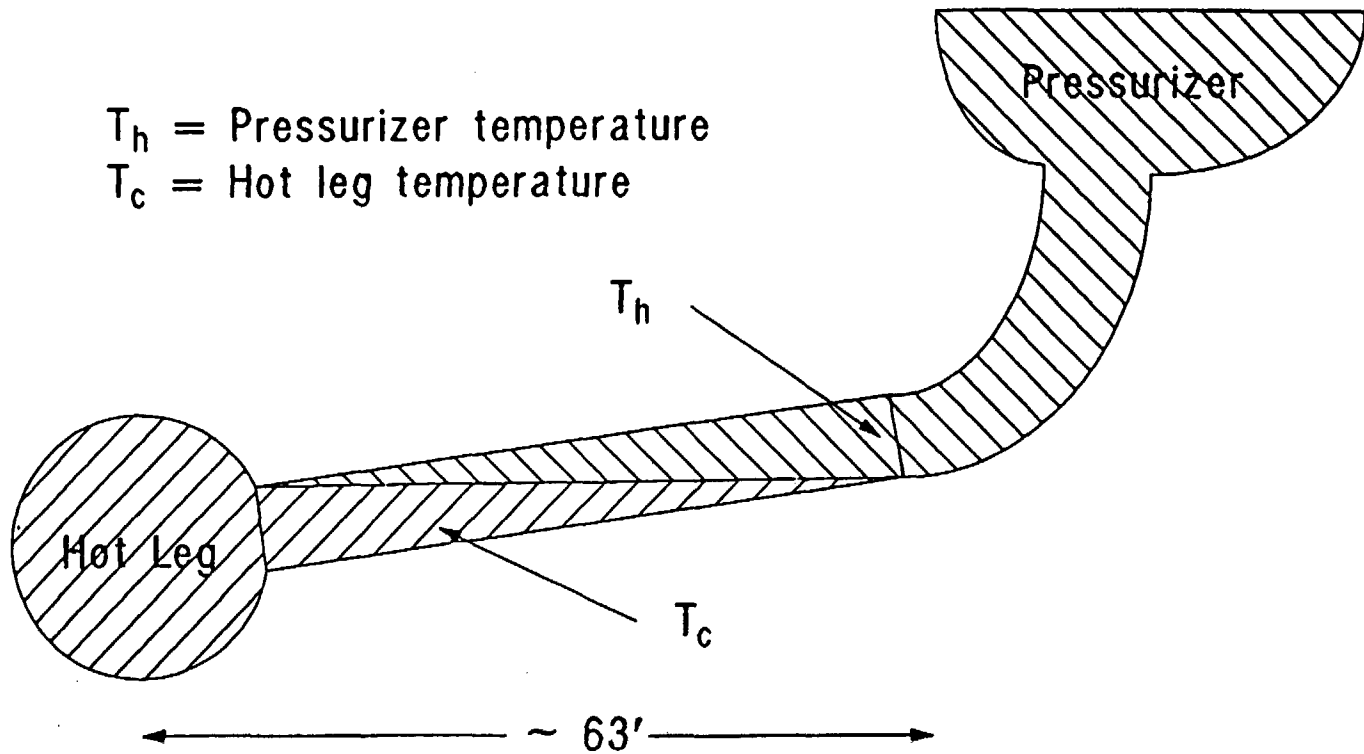
Degradation Mechanisms in Surge and Spray Lines and Nozzles

Operating transients, thermal shocks, stratified flows, and flow-induced vibrations cause fatigue damage to surge and spray lines, nozzles, and thermal sleeves. All of these stressors except stratified flows were considered in the original design of the surge and spray lines. Recent analysis results show that these lines have high cumulative fatigue usage factors resulting from the low-cycle fatigue damage caused by the design basis transients.⁶ For example, design basis transients alone will produce a fatigue usage factor of about 0.7 in the surge nozzle weld at the pressurizer end.

Stratified flows have also caused significant low- and high-cycle fatigue damage, but were not accounted for in the original design of the surge and spray lines. The design analysis of the surge lines assumed that the surges would sweep the surge line, but the actual flow pattern appears to be stratified, as indicated in Figure 4. Stratification in the surge line occurs during heatup and cooldown when the differences between the pressurizer and hot leg temperatures are high. Temperature swings of up to 177 C (350 F) in the upper portion of the surge line have been recorded.⁷ French field and laboratory tests have confirmed the presence of stratified flows in surge lines.⁸ Four U.S. utilities have also measured significant surge line stratification. At one plant, thermal stratification caused the horizontal portion of the surge line to deflect downward, closing the gaps between the pipe and the pipe whip restraints and resulting in permanent deformation of the pipe.⁹

Leak-before-break evaluations of typical PWR pressurizer surge lines subjected to low-cycle fatigue damage caused by the design basis transients showed that double-ended guillotine pipe breaks are highly unlikely to occur. However, stratified flows are not included in the design basis transients. Leak-before-break evaluations of surge lines subjected to both design basis transients and stratified flows need to be performed.^{6,10,11}

Low flow conditions during heatup, cooldown, and hot standby operation are likely to cause a significant thermal stratification in the spray line. Cyclic use of the main and auxiliary sprays and improperly sized bypass valves can also cause thermal stratification in the spray line. Temperature differentials as large as 288 C (550 F) may take place during cooldown. Excessive thermal stresses and pipe movement have been reported at some power plants. Stratified flows in relatively short horizontal sections of piping can be prevented by replacing them with sloped sections. In one plant a 10 ft long horizontal section of spray line has been replaced with piping having a 30 degree slope. The leak-before-break approach may not be workable for small diameter piping such as spray lines because it is difficult to maintain a sufficient margin between leakage-detectable crack length and critical crack length.



ECO00509

Figure 4. Temperature Stratification in Horizontal Run of Surge Line.

The surge lines made of cast stainless steel are also susceptible to thermal embrittlement. More information on the thermal embrittlement mechanism is presented later, in the section on LWR coolant pumps.

Inservice Inspection

Volumetric and surface examination of 25% of all the butt welds in the RCS piping and nozzles is required during each inspection interval,¹² which is usually a 10 year interval. Inspection of the same welds is required during each inspection interval. The welds selected for examination should include all dissimilar-metal welds, welds having a cumulative fatigue usage factor equal to or greater than 0.4, and welds having a stress intensity that exceeds $2.4 S_m$, where S_m is the maximum allowable primary membrane stress intensity. Therefore, the welds at the pressurizer end of the surge and spray lines are inspected during each inspection interval. In addition, the welds at the hot and cold leg ends of the surge and spray lines in CE and B&W plants are inspected. However, nozzle welds with high fatigue usage factors should be examined more frequently than presently required.

A system leakage test of the pressure retaining components, including the surge and spray lines and nozzles, is required during each refueling outage. This test is conducted at a test pressure equal to or greater than the normal pressure associated with 100% rated reactor power, i.e. 2250 psi. In addition, a system hydrostatic test is required during each inspection interval (usually 10 years) at a test pressure specified in Table IWB-5222-1 of Section XI of the ASME Code.¹³ Test specifications require that the minimum test temperature for either of the tests not be lower than the minimum temperature for the associated pressure specified in the plant Technical Specifications.

Fatigue is the major degradation mechanism for the surge and spray lines and nozzles. However, no detailed records of the transients causing fatigue damage are maintained; without such information it is difficult to estimate the actual fatigue damage experienced by the surge and spray lines and nozzles. We recommend that surge and spray lines be more extensively monitored. On-line monitoring of coolant temperatures, pressures, and flow rates, and pipe wall temperatures at nozzles and in horizontal portions of the piping during operational transients, thermal shocks, and stratified flows would provide data that could be used to determine actual fatigue damage. Stratified flows are likely to cause high fatigue damage in both base metal and welds. We recommend that acoustic emission methods be developed to detect fatigue crack growth in the base metal and welds. These methods provide global information regarding the defects in the piping and are capable of detecting growth of very small flaws that are not detectable by other nondestructive testing methods. Loose parts monitoring techniques should be used to determine if the thermal sleeves have broken loose from the nozzle.

Aging Assessment of LWR Coolant Pumps

The primary function of LWR coolant pumps is to circulate coolant through the reactor such that core-heated fluid can be passed to a turbine (in BWR plants) or to a steam generator (in PWR plants). The reactor coolant pumps are the only rotating heavy machines on the nuclear side of a plant and are critical pressure boundary elements. This section discusses the aging degradation of three pump components: the pump casing, closure studs, and pump shaft.¹⁴ The pump shaft seals are not discussed here because they are replaced or refurbished relatively frequently.

Reactor Coolant Pump Design and Fabrication

The design of a reactor coolant pump falls into one of three categories or types, as shown in Table 1: PWR primary coolant pumps, i.e., Types F and E; and BWR recirculation pumps, i.e., Type C. The major difference in the reactor coolant pump designs is in the pump casing geometry. The PWR Type F pump casings require thicker pressure retaining walls [100 to 200 mm (4 to 8 in.)] because, as shown in Figure 5, the casing walls are not structurally supported. The PWR Type E and BWR Type C pump casings are shown in Figures 6 and 7, respectively; their casing walls are thinner [67 to 75 mm (2.5 to 3 in.)] because of the structural reinforcements in their designs. The massive size of the pump casing helps to maintain the close tolerances required by the pump internals during operation.

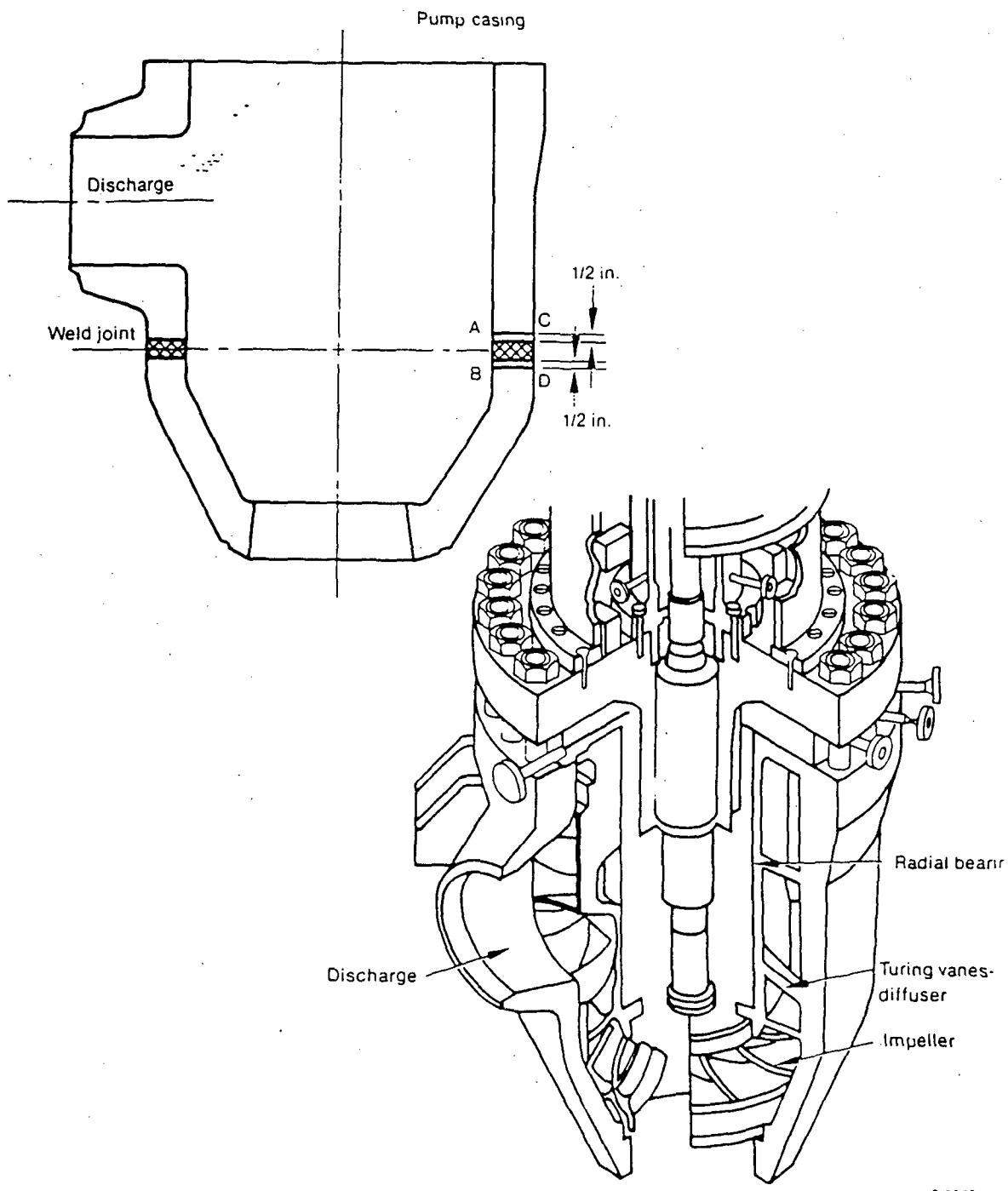
All reactor coolant pumps are fabricated from statically cast austenitic stainless steel, either Grades CF8, CF8M, or CF8A, except the ones at the three units of the Palo Verde plant. The pump casings at Palo Verde are fabricated from forged carbon steel and clad with stainless steel. The sections of the Type F pump casing made of cast stainless steel are welded by an electroslag method, which introduces high residual stresses that may exceed the yield strength of the material. However, no post-weld heat treatment is performed to reduce or eliminate the residual stresses at the fabrication welds in Type F pumps; a post-weld heat treatment is not an ASME requirement for a stainless steel weld. Later designs of Type F pump casings were modified to decrease or eliminate the number of weldments, as it became practical to manufacture larger casting sections.¹⁵ The carbon steel pump casings are subjected to post-weld heat treatment, and all Type E and Type C pump casings are subjected to full-solution heat treatment, which eliminates almost all residual stresses.

Thermal barriers or heat exchangers, or both, are used to limit the reactor coolant heat reaching the mechanical seal cavity. In the earlier Types E and C pumps, the hot reactor coolant was mixed with cold cooling water at the top of the thermal barrier. The resulting turbulent mixing introduced high-cycle (1 to 25 Hz) thermal fatigue loads on the pump shaft surface.

Two concentric Type 304 stainless steel flexitallic (stainless steel-graphite asbestos material) gaskets are used for sealing between PWR coolant pump covers and casings. A leak-off line is installed between the

TABLE 1. MANUFACTURERS AND NSSS VENDORS FOR REACTOR COOLANT PUMPS

Pump Type	Manufacturer	NSSS Vendor
Type E	Byron-Jackson	Babcock & Wilcox (3 plants) Combustion Engineering
Type F	Westinghouse	Westinghouse (all plants) Babcock Wilcox (2 plants)
	Bingham-Willamette	Babcock & Wilcox (2 plants)
	Combustion Engineering/ Klein, Schanzlin, and Becker	Combustion Engi- neering (Palo Verde Plants)
Type C	Byron-Jackson Bingham-Willamette	General Electric



8-0948

Figure 5. PWR Type F Coolant Pump.

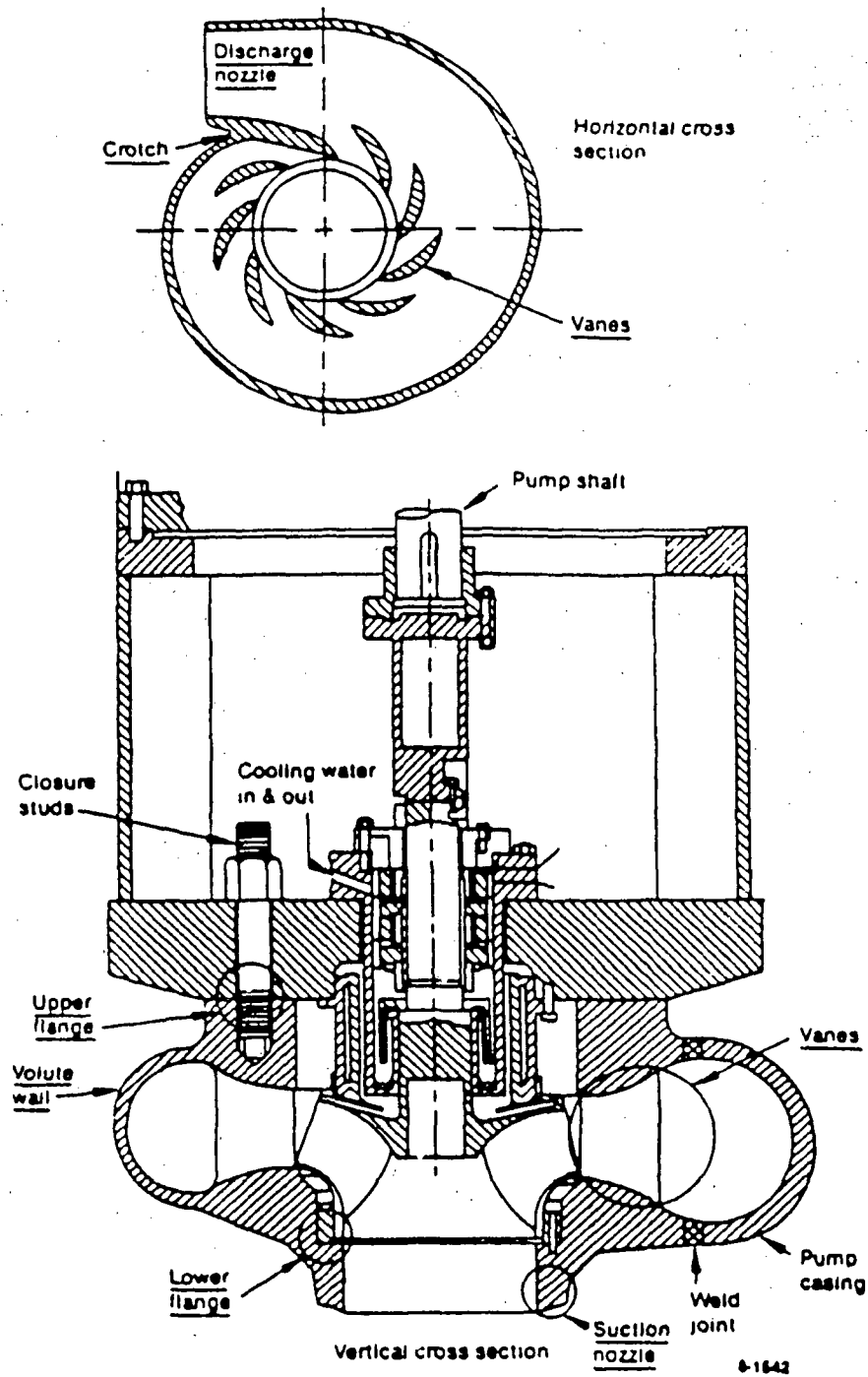
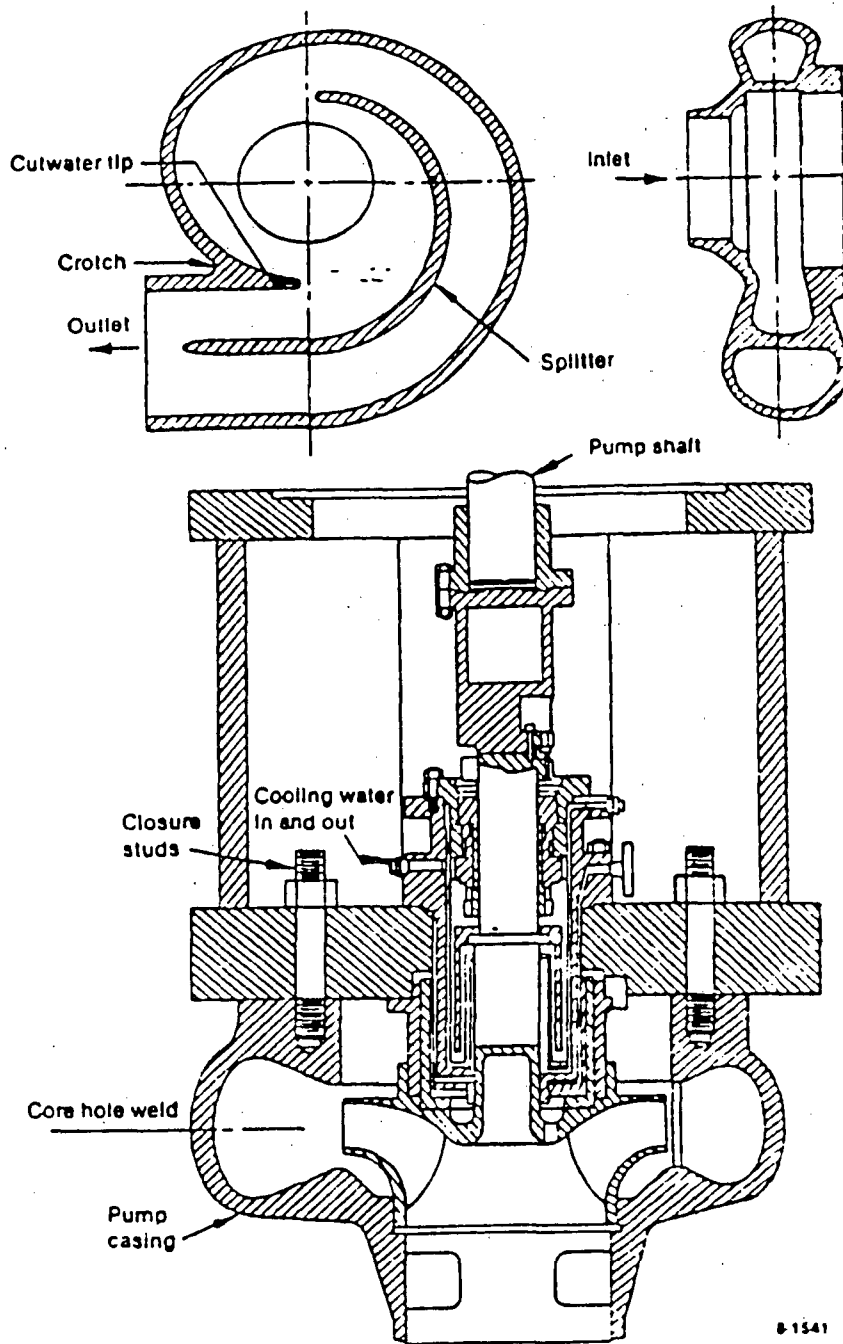


Figure 6. PWR Type E coolant pump (locations of maximum stress intensity are underlined).



8-1541

Figure 7. BWR Type C coolant pump.

gaskets to detect any leakage of reactor coolant. Only one gasket is used in BWR coolant pumps. Leaking reactor coolant, if not checked, may cause corrosion of the closure studs, which are made of low-alloy steel, either SA193 Grade B7 or SA540 Grade B23. Reactor coolant pump main closure studs are long [740-mm (29-in.) for Type E pumps]¹⁶, and their nominal diameter may vary from 90 to 140-mm (3.5 to 5.5-in.).

Aging of Reactor Coolant Pumps

Thermal Embrittlement. Thermal embrittlement is a major degradation mechanism for cast stainless steel reactor coolant pump casings. Cast stainless steels, i.e., Grades CF8, CF8M, and CF8A, have austenitic-ferritic microstructures and are subject to thermal embrittlement due to prolonged exposures at reactor operating temperatures, especially PWR temperatures. Thermal embrittlement of the base metal results in a slow loss of material toughness over extended periods of time and is influenced by coolant temperature, time of exposure at temperature, chemical composition, volume fraction of ferrite content, and ferrite distribution (spacing) in the microstructure. The loss of material toughness is caused by the formation of an alpha-prime phase in the ferrite. Since only the ferrite phase is embrittled by long-term exposure at LWR operating temperatures, the overall embrittlement depends on the amount and spacing of ferrite present in the base metal of the pump casing. A larger ferrite content and spacing will result in an increased thermal embrittlement. A high percentage of ferrite (18 to 22% is not uncommon) can be present in the cast stainless steel components.

The weldments in the pump casing are not very sensitive to thermal embrittlement. The initial toughness of the weldments in the pump casing is significantly lower than that of the unaged base metal, and the ferrite content of the weldments is generally lower than that of the base metal. In several older plants, the weldments in the pump casing and stainless steel RCS piping have less than 3% ferrite,^{17,18} whereas in newer plants a minimum of 5% ferrite is required.^{5,17} These requirements for minimum ferrite content avoid microfissuring in weldments.

Laboratory tests show that the loss in toughness of thermally aged cast stainless steel components can be recovered by annealing at 550 C (1022 F) for one hour, followed by rapid cooling (quenching) to lower temperatures.^{19,20} The short-term annealing process dissolves the alpha-prime phase. However, rapid heating and cooling of the pump casing is not feasible, and slow heating and cooling to and from the annealing temperature will cause formation of several other phases in the ferrite, resulting in additional loss of toughness. Therefore, annealing of the aged cast stainless steel components is not an acceptable solution.

Fatigue. The pump casing is subjected to thermal and mechanical fatigue damage caused by the system operating transients and pump vibrations. In Type F pumps, the weldments are susceptible to fatigue damage because of the high residual stresses, whereas in Types C and E pumps the susceptible sites are likely to include some portion of both the base metal

and weld region, because of the different geometric configuration and complex welds with no residual stresses. Figure 6 shows the locations of the maximum stress intensities in Type E pumps.¹⁵ In addition, the presence of microfissures in low-ferrite (<3%) weldments may adversely affect the fatigue strength of the pump casings in older plants. However, the fatigue damage is expected to be quite small in the absence of microfissures, because to ensure dimensional stability the pump casings have a thickness greater than that required for structural integrity.

The pump shafts are also susceptible to fatigue damage caused by the alternating bending stresses from the asymmetric distribution of static pressure and by the rapidly varying thermal stresses caused by the turbulent mixing of hot reactor coolant 288 C (550 F) with cooling water 52 C (125 F) in the cover thermal barrier. Thermal stresses from turbulent mixing, alternating bending stresses, and high residual stresses at the local welds are responsible for the initiation and propagation of fatigue cracks. Axial and circumferential cracks have been found on some PWR and BWR pump shafts.^{21,22,23} Axial cracks are caused by the turbulent mixing of the coolants, whereas circumferential cracks, which usually occur in the grooves on the shaft surface, are caused by alternating bending stresses. Hairline cracks have been found in the Type F pump shafts at the Palo Verde-1 plant. Heat-induced stress and the shaft's chrome plating have been mentioned as factors causing the cracks.²⁴

Boric Acid Corrosion. PWR pump body closure studs are susceptible to corrosion by borated primary coolant leakage across the pump casing-to-cover gasket. Such leakage has caused significant corrosion damage to the studs, and in carbon steel pump bodies it may also cause corrosion of the base metal.²⁵ Boric acid corrosion of the studs will increase the rate of leakage which, in turn, will lead to excessive corrosion of studs. In one PWR plant, boric acid corrosion reduced seven reactor coolant pump studs from a nominal diameter of 90 mm (3.5 in.) to between 25 and 37 mm (1.0 and 1.5 in.)¹⁶ The corrosion occurred in the area of the stud adjacent to the top surface of the lower flange. Visual inspection revealed that the severely corroded studs had an hour-glass appearance. Visual inspection of closure studs at other PWR plants has revealed that the studs in all different pump designs are susceptible to boric acid corrosion. Installation of instrumentation for actively monitoring the leak-off lines between the gaskets is necessary to detect leakage. If the leak-off line installed between the gaskets is plugged or not instrumented, no indication of reactor coolant leakage from the inner gasket will be available.

The major causes of gasket leakage are poor maintenance, minor corrosion of the stainless steel portion of the gasket, and poor gasket spring-back.⁵ Implementing the following recommendations would upgrade the maintenance procedures for the closure studs and thus improve plant reliability: use gaskets with improved spring-back characteristics, control cleanliness during gasket installation, and use proper fastener lubrication and tensioning practices.

Stress Corrosion Cracking. The cast stainless steel pump casing and its weldments have excellent resistance to stress corrosion cracking. However, if very low levels of ferrite are present at the welds because of the filler material and weld procedures used, both repair and fabrication weldments in pumps could be sensitized and become susceptible to environmentally induced stress corrosion cracking.²⁶ The full-solution heat treatment reduces or eliminates the sensitization in the weldments in Types E and C pump casings. All repair welding performed after the full-solution heat treatment of the casings is limited to a low heat input no greater than 19,700 J/cm (47.4 Btu/in.). This practice prevents additional sensitization and also reduces residual stresses. Therefore, the susceptible sites in the Types E and C pump casings will be at the weldments connecting the pump casing to the reactor coolant piping, if the ferrite content is very low.

Leakage of reactor coolant across the pump casing-to-cover gasket may wet the insulation and cause a chloride attack on the pump casing. To prevent a chloride attack, the insulation must meet chloride concentration acceptance criteria.²⁷ In addition, if leakage takes place, adjacent areas of the pump casing might become susceptible to stress corrosion cracking.

Inservice Inspection

Pump Casing. At least one reactor coolant pump from the RCS is generally disassembled for inspection and maintenance at the end of an inspection interval. Inservice inspection requirements for the pump casing include surface and volumetric examination of repair and fabrication welds. The cast stainless steel pump casings are difficult to inspect with conventional ultrasonic testing methods because of the elastic anisotropy caused by the different grain structures in the castings and because of the severe attenuation of the ultrasonic wave caused by the coarse grains in the steel. Therefore, radiography is generally used for volumetric examination of cast stainless steel pump casing welds. The indication detected by radiography must be considered as a worst flaw, i.e., a surface flaw with an aspect ratio of 0.5, because radiography can only detect the presence of a flaw; it cannot determine the location or size of the flaw. Triangulation radiography may be used to locate the flaw.

The extent of the thermal embrittlement of cast stainless steel components may be such that the critical flaw size decreases to the size of an existing flaw. The critical flaw size may become too small to reliably detect using current inservice inspection methods and therefore, advanced ultrasonic testing (UT) methods are being developed to detect a flaw and determine its size, orientation, and location.^{26,28} These advanced UT methods will be more effective than radiography.

The inservice inspection requirements were originally developed for Type F pump casings, which have high residual stresses at the welds. However, these requirements may not be practical or meaningful for Types C and E pumps having different geometric configurations and fabrication methods, with complex welds but low residual stresses.

As discussed previously, a reactor coolant leak across the pump casing-to-cover gasket can make adjacent areas of the pump casing susceptible to stress corrosion cracking. Damage to the affected area can be detected by penetrant testing.

Pump Shaft. LWR coolant pumps are generally equipped with two vibration monitors mounted at the top of the motor stand in a horizontal plane to detect radial vibrations of the pump. Proximity probes have also been used for vibration monitoring to detect circumferential cracks in the pump shaft. Monitoring of pump motor frame vibrations has also been successfully used to indicate damage to the pump shaft.^{21,22}

The inspections done during shutdown should include surface and volumetric examination of the pump shaft. Several utilities have used the conventional UT technique to inspect pump shafts, but the results have been inconclusive and misleading. A new UT technique, the modified cylindrically guided wave technique, is being developed by the Southwest Research Institute for shaft inspection, and the initial results of its use are promising.^{29,30}

Pump Closure Studs. Inservice inspection requires volumetric examination of all the bolts, studs, nuts, and bushings during each inspection interval. However, the conventional UT techniques are not effective in revealing corrosion wastage of the studs.³¹ Therefore, inservice inspection requirements, which are currently limited to volumetric examinations, should be supplemented with visual examinations. If the insulation covering the studs is removable, removal will facilitate visual examinations. Use of the cylindrically guided wave technique developed by the Southwest Research Institute may be considered, because it is capable of detecting both flaws and corrosion wastage in the long studs.³² Examination of the flange surfaces is required when a mechanical joint is disassembled.

Summary, Conclusions, and Recommendations

Problems associated with time-dependent aging, such as fatigue, radiation and thermal embrittlement, corrosion, and other effects, have occurred in U.S. light water reactors as they have matured. Therefore, effectively managing the aging-related problems in older plants has become a major focus of the research sponsored by the USNRC.

The Aging Assessment and Mitigation Project is being carried out at the Idaho National Engineering Laboratory to help the USNRC understand, detect, and mitigate the aging of the major light water reactor components. A qualitative assessment of the degradation processes active in the major components has been completed.^{2,3} The assessment of the degradation processes active in PWR pressurizer surge and spray lines and nozzles, PWR primary coolant pumps, and BWR recirculation pumps is presented in this paper. Table 2 summarizes the stressors, degradation sites and mechanisms, and potential failure modes for the PWR surge and spray lines and nozzles. The conclusions and recommendations related to aging degradation of these components are as follows:

TABLE 2. SUMMARY OF DEGRADATION PROCESSES FOR PRESSURIZER SURGE AND SPRAY LINES AND NOZZLES

Rank	Degradation Sites	Stressors	Degradation Mechanisms	Potential Failure Modes	ISI Methods
1	Pressurizer Surge Line and Nozzle	Thermal transient stress loadings	Low and high cycle thermal fatigue	Crack initiation and propagation leading to possible through-wall leak, pipe rupture	Piping and nozzle welds inspected volumetrically at each of the four 10 year intervals
		Stratified flow stress loadings, thermal striping		Thermal sleeve cracking	
		Thermal Shock	Mechanical fatigue	Thermal sleeve cracking, crack initiation in nozzle	
		Flow induced mechanical vibration		Through-wall leakage	
Temperature	Thermal embrittlement				
2	Pressurizer Spray Line and Nozzle	Thermal transient stress loadings	Low and high cycle thermal fatigue	Crack initiation and propagation leading to possible through-wall leak.	Piping and nozzle welds inspected volumetrically at each of the four 10 year intervals
		Stratified flow stress loadings (pipe only) thermal striping		Thermal sleeve cracking.	
		Flow induced mechanical vibration	Mechanical fatigue	Thermal sleeve cracking, crack initiation in nozzle	

1. Stratified flows cause significant fatigue damage to the horizontal portions of the surge and spray lines, but were not accounted for in the original design. Therefore, we recommended that the horizontal portions of the piping subjected to stratified flows be analyzed to determine whether a catastrophic rupture rather than a leak-before-break can take place.
2. Some of the nozzle welds have a fatigue usage factor as high as 0.7 from design transients alone. If stratified flows are taken into account, the fatigue usage factor will be much higher than 0.7. Therefore, more frequent inservice inspection of nozzle welds with high fatigue usage factors is needed.
3. Because stratified flows are likely to cause fatigue damage to the base metal in the horizontal sections of the surge and spray lines, inspection of the high stress regions in the base metal need to be included in the inservice inspection program.
4. Acoustic emission techniques should be developed to reliably detect the growth of fatigue cracks. These techniques can then be used along with other nondestructive testing methods to characterize these cracks.
5. Fatigue is a major degradation mechanism in the surge and spray lines and nozzles. However, detailed and accurate records of the transients causing fatigue damage are not available. This lack of information makes it difficult to estimate the actual fatigue damage. Data provided by on-line monitoring of coolant temperatures, pipe wall temperatures, and other parameters could be used to accurately determine the accumulated fatigue damage.
6. Full flow and continuous spray during plant cooldowns would mitigate the fatigue damage to the spray lines.
7. Properly sized bypass valves can provide full flow during normal operation and mitigate fatigue damage to the spray lines.
8. Where a horizontal run is short enough, replacing the horizontal section of piping with a sloped section can prevent stratified flows.
9. Thermal sleeves play an important role in protecting nozzle walls from thermal transients. Loose-parts monitoring methods should be used to ensure that thermal sleeves have not broken loose from the nozzles.

Table 3 summarizes the stressors, degradation sites and mechanisms, and potential failure modes for LWR primary coolant pump casings, shafts, and closure studs. The conclusions and recommendations related to aging degradation of these components are as follows:

TABLE 3. SUMMARY OF DEGRADATION PROCESSES FOR PWR COOLANT PUMPS

<u>Rank</u>	<u>Sites Degradation</u>	<u>Stressors</u>	<u>Degradation Mechanisms</u>	<u>Potential Failure Modes</u>	<u>ISI Methods</u>
1	Pump body (casting) ^a	Temperature, system operating transients, LWR environment	Thermal aging, fatigue, stress corrosion cracking	Through-wall leakage, unstable ductile tearing	Volumetric, surface
2	Closure studs	Leakage of borated coolant in PWR	Corrosion, wastage	Leakage, breakage	Volumetric
3	Pump shaft	Alternating bending stresses, rapidly changing thermal stresses, and residual stresses	Fatigue	Breakage (contained by pump body)	Surface, volumetric

a. Wrought carbon steel pump bodies make up a very small percentage of those in the field and have not had a long enough service history to be reflected here.

1. Thermal embrittlement is the primary degradation mechanism that affects the reactor coolant pump bodies made of cast austenitic-ferritic (duplex) stainless steel. A high ferrite content (18 to 22% is not uncommon) makes a thick pump casing more susceptible to damage from thermal embrittlement. Since thermal embrittlement causes the slow loss of material fracture toughness, the actual degree of thermal embrittlement needs to be determined so that the structural integrity of the pump casing can be assessed. We recommend the development of a model for estimating degradation in fracture toughness as a function of coolant temperature, time of exposure at temperature, chemical composition, and ferrite content and its spacing in the microstructure.
2. Ferrite distribution through the statically cast, thick-wall, stainless steel components is not uniform. Therefore, data for the ferrite distribution in a pump casing are needed so that the actual degree of thermal embrittlement can be determined.
3. The existing flaws in statically cast components are shrinkage flaws introduced during fabrication. Thermal embrittlement may be such that an existing flaw can reach critical dimensions, leading to failure of the casing. Characterization of the flaws would help to ensure the continued structural integrity of the pump casing. Advanced UT methods are needed for this purpose.
4. ASME Section XI, Table IWB-3518-2, provides standards for allowable planar flaws in cast stainless steel pump casing welds. Similar standards are needed for the flaws in the base metal, and such standards should take into account degradation from thermal embrittlement.
5. Laboratory tests show that the loss of toughness caused by thermal embrittlement can be recovered by annealing at 550 C (1022 F) for one hour, followed by rapid cooling to lower temperatures. However, annealing of the pump casing is feasible only with slow heating and cooling to and from the annealing temperature. This process will cause formation of several other phases in the ferrite, resulting in additional loss of toughness. Therefore, annealing of pump casings is not an acceptable solution.
6. The cast stainless pump casings have excellent resistance to stress corrosion cracking. However, if very low levels of ferrite are present at the welds because of the filler material and weld procedures used, both repair and fabrication welds become susceptible to stress corrosion cracking. Since the Types E and C pump casings are subject to full-solution heat treatment, the susceptible sites will be at the weldments connecting the pump casing to the reactor coolant piping, if the ferrite content is very low. The ferrite content in the pump casing welds should be determined.
7. Weldments in Type F pumps and high-stress regions in Types C and E pumps are susceptible to fatigue damage. In addition, the presence of microfissures in low-ferrite (<3%) weldments may adversely affect the

fatigue strength of the pump casing and should be taken into account. The fatigue damage is probably quite small in the absence of microfissures.

8. The ASME Section XI inservice weld inspection requirements were originally developed for the Type F pumps, which have high residual stresses at the welds. However, these requirements may not be practical or meaningful for Types C and E pumps. The high stress regions in Types C and E pumps are likely to include some portion of both the base metal and weld regions. Surface examination of the high stress regions is recommended.
9. Leakage of borated water across LWR primary coolant pump case-to-cover gaskets has resulted in corrosion and wastage of pump closure studs. In carbon steel pump bodies, this leakage is also likely to cause corrosion of the base metal. The corrective actions to prevent leakage include the use of gaskets with better spring-back characteristics, proper gasket installation and cleanliness control, and proper stud tensioning practices. The leak-off lines between the inner and outer gaskets should be left unplugged and be instrumented so that leakage can be detected.
10. ASME Section XI, Table IWB-2500-1, requires volumetric examination of the closure studs. However, the conventional ultrasonic techniques are not effective in revealing corrosion wastage of the studs. Therefore, current inservice inspection requirements for the closure studs should be supplemented with visual examinations. The use of the cylindrically guided wave technique developed by the Southwest Research Institute may be considered because it is capable of detecting both cracks and corrosion wastage in the long studs.
11. Use of conventional ultrasonic techniques to inspect pump shafts gives inconclusive and misleading results. Field application of the modified cylindrically guided wave technique for shaft inspection needs to be evaluated. Monitoring of the pump motor frame vibrations is recommended. Such monitoring can detect damage to the pump shaft.

References

1. J. P. Vora, Nuclear Plant Aging Research (NPAR) Program Plan, Rev. 1, NUREG-1144, September 1987.
2. V. N. Shah and P. E. MacDonald (eds.), Residual Life Assessment of Major Light Water Reactor Components - Overview, 1, NUREG/CR-4731, EGG-2469, June 1987.
3. V. N. Shah and P. E. MacDonald (eds.), Residual Life Assessment of Major Light Water Reactor Components - Overview, Volume 2, NUREG/CR-4731, EGG-2469 (Draft), June 1988.

4. E. A. Siegel and M. H. Bakr, "Pressurized Water Reactor Pressurizer Surge and Spray Lines and Nozzles," in Residual Life Assessment of Major Light Water Reactor Components - Overview, Volume 2, V. N. Shah and P. E. MacDonald (eds.), NUREG/CR-4731, EGG-2469 (Draft), June 1988, pp. 81-110.
5. F. R. Drahos, W. L. Server, and B. F. Beaudoin, "Light Water Reactor Coolant Pumps," in Residual Life Assessment of Major Light Water Reactor Components - Overview, Volume 2, V. N. Shah and P. E. MacDonald (eds.), NUREG/CR-4731, EGG-2469 (Draft), March 1988, pp. 8-29.
6. Westinghouse Electric Corporation, Application of the Leak-Before-Break Approach to Westinghouse PWR Piping, EPRI NP-4971, December 1986.
7. Surge Line Thermal Cycling Observed During Reactor Coolant System Pressurization, Heatup, and Cooldown, INPO SER 25-87, September 8, 1987.
8. Meeting Minutes of Task Group on Fatigue in Operating Plants, ASME Section XI, August 29, 1988, Colorado Springs, CO.
9. "Unexpected Piping Movement Attributed to Thermal Stratification," USNRC Information Notice No. 88-80, October 7, 1988.
10. Babcock and Wilcox Company, Application of Leak-Before-Break Approach to PWR Piping Designed by Babcock and Wilcox, EPRI NP-4972, January 1987.
11. Combustion Engineering, Inc., Application of Leak-Before-Break Analysis to PWR Piping Designed by Combustion Engineering, EPRI NP-5010, February 1987.
12. ASME Code Section XI, Table IWB-2500-1, Pressure Retaining Welds in Piping.
13. ASME Code Section XI, Table IWB-5222-1, Test Pressure.
14. V. N. Shah, W. L. Server, and P. E. MacDonald, "Aging Assessment of LWR Coolant Pumps," presented at the International Nuclear Power Plant Aging Symposium, Bethesda, MD, August 30 to September 1, 1988.
15. D. T. Umino and A. K. Rao, Long-Term Inspection Requirements for PWR Pump Casings, EPRI NP-3491, May 1984.
16. "Degradation of Reactor Coolant Pump Studs," U.S. Nuclear Regulatory Commission IE Information Notice No. 80-27, June 1980.
17. U.S. Nuclear Regulatory Commission, "Control of Ferrite Content in Stainless Steel Weld Metal," Regulatory Guide 1.31, Revision 3, April 1978.

18. Personal communication with E. Landerman, Westinghouse, Pittsburgh, PA, September 1988.
19. O. K. Chopra and H. M. Chung, "Effect of Low-Temperature Aging on the Mechanical Properties of Cast Stainless Steels," in Properties of Stainless Steel in Elevated Temperature Service, M. Prager (ed.), ASME, MPC-Vol. 26, PVP-Vol. 132, December 1987, pp. 79-112.
20. Personal Communication with Dr. W. J. Shack, Argonne National Laboratory, Chicago, IL, August 1988.
21. S. M. Stoller Corporation, "RCP Shaft Fractured, Cap Screws Cracked, Broken - Fabrication, Thermal and Weld Stresses, IGSCC, Insufficient Preload," Nuclear Plant Experience, PWR-2, p. 52.
22. S. D. Leshnoff and P. C. Riccardella, "Reactor Coolant Pump Shaft Crack Investigations at TMI-1," presented at the EPRI Reactor Coolant Pump/Recirculation Pump Monitoring Workshop, EPRI Component Monitoring and Diagnosis Technology Transfer Center, Toronto, Canada, March 29, 1988.
23. Personal communication with F. R. Drahos, Consultant, September, 1988.
24. E. Hiruo, Inside NRC, No. 25; December 7, 1987, p. 8.
25. S. M. Stoller Corporation, "RCP Gasket Leaked - Closure Studs Corroded," Nuclear Plant Experience, PWR-2, V.A.89.
26. G. R. Egan et al., Inspection of Centrifugally Cast Stainless Steel Components in PWRs, EPRI NP-5131, June 1987.
27. U.S. Nuclear Regulatory Commission, "Nonmetallic Thermal Insulation for Austenitic Stainless Steel", Regulatory Guide 1.36, February 23, 1973.
28. P. Jeong and F. Ammirato, "Nondestructive Examination of Coolant Pump Welds - Ultrasonic Examination of Cast Stainless Steel Components," presented at the Pressure Vessel and Piping Conference, Pittsburgh, Pennsylvania, June 19-23, 1988.
29. Electric Power Research Institute, "Cylindrically Guided Wave Technique (CGWT) for Pump Shaft Inspections," Technical Brief, 1987.
30. G. M. Light, E. A. Bloom, and S.-N. Liu, "Application of the Cylindrically Guided Wave Technique," presented at the Pressure Vessel and Piping Conference, Pittsburgh, Pennsylvania, June 19-23, 1988.
31. U.S. Nuclear Regulatory Commission, "Boric Acid Corrosion of Carbon Steel Reactor Pressure Boundary Components in PWR Plants," Generic Letter 88-05, March 1988.

32. G. M. Light, N. R. Joshi, and S.-N. Liu, "Stud Bolt Inspection Using Ultrasonic Cylindrically Guided Wave Technique," Improved Technology for Critical Bolting Applications, E. A. Merrick and M. Prager (eds.), ASME, New York, July 1986, pp. 31-38.

Notice

This paper was prepared as an account of work sponsored by an agency of the United States Government. Neither the United States Government nor any agency thereof, or any of their employees, makes any warranty, expressed or implied, or assumes any legal liability or responsibility for any third party's use, or the results of such use, of any information, apparatus, product or process disclosed in this paper, or represents that its use by such third party would not infringe privately owned rights. The views expressed in this paper are not necessarily those of the U.S. Nuclear Regulatory Commission.

The Effects of Aging on the Fire Vulnerability of
Nuclear Power Plant Components*

SAND88-2969C

Steven P. Nowlen
Sandia National Laboratories
Albuquerque NM 87185

Abstract

Sandia National Laboratories, under the sponsorship of the U. S. Nuclear Regulatory Commission, has initiated an effort to identify and investigate potential nuclear power plant fire safety issues associated with plant aging. The issues of potential concern, which have been identified, are the effects of aging on (1) the vulnerability of electrical equipment to fire induced damage; (2) the propensity with which electrical equipment will initiate, or contribute to the severity of, fires; and (3) the integrity of passive fire protective features. Efforts in this program were initiated late in fiscal year 1988. For fiscal year 1989 efforts will focus on the investigation of the effects of aging on cable damageability and cable flammability. This paper presents the findings of a limited review of past electrical equipment fire aging research and a summary of planned activities for fiscal year 1989.

Introduction

A program at Sandia National Laboratories (SNL) has been initiated by the U. S. Nuclear Regulatory Commission (USNRC) to investigate potential issues associated with plant aging and fire safety. Work on this program was initiated late in fiscal year 1988 (FY-88), and hence, only limited and quite preliminary investigations have to date been completed. One of the potential issues of concern identified to date is the effects of aging on the vulnerability of electrical components to fire initiation and fire growth. A second potential issue is the effects of aging on the vulnerability of electrical equipment to fire induced damage, short of actual burning. For these first two issues the electrical equipment of interest includes both cables and other Class 1E equipment. The third issue of potential concern identified to date is the effects of aging on the integrity of passive fire protection measures such as cable coatings, cable tray wrap systems, and fire barrier penetration seals. This paper describes the results of a review of past fire aging studies, and presents a description of efforts to be undertaken during FY-89.

* This work was supported by the U. S. Nuclear Regulatory Commission and was performed at Sandia National Laboratories, which is operated for the U. S. Department of Energy under contract number DE-AC04-76DP00789.

Review of Previous Studies

As an initial step in the execution of this program, a review of past efforts associated with fire-related aging issues has been initiated. While the results of this review have not been entirely evaluated and information regarding certain efforts has not yet been received, certain useful insights have been gained. In general, three sources of relevant information have been identified. The first is two limited USNRC-sponsored efforts at SNL directly concerned with the effects of aging on cable flammability. The second source is information developed by the manufacturers of cables and cable insulations. The third source is information available as a result of other aging-related investigations, such as those associated with equipment qualification studies, not directly concerned with potential fire issues, but which provide applicable insights.

Under USNRC sponsorship two studies directly associated with the investigation of the effects of aging on cable fire behavior, quite limited in scope, were conducted in the past. In the first study¹ the investigations focused on the loss of halocarbon fire retardant additives from cable insulations caused by both thermal and radiation aging. It was found that certain materials were subject to the loss of these flame retardant materials with aging. For ethylene propylene rubber (EPR), this loss of fire retardant also resulted in a moderate increase in flammability as measured by the ASTM Limiting Oxygen Index Test.² Conversely, while chlorosulfonated polyethylene (CSPE) also demonstrated a pronounced loss of fire retardant additives, the cables also demonstrated a pronounced reduction in actual flammability. This reduction in flammability was attributed to a loss of other volatile compounds during the aging process. This study demonstrated that while cable formulations can be expected to change because of an aging process, the simple examination of a particular fire retardant additive content does not necessarily indicate the effects of aging on actual flammability.

In the second USNRC-sponsored study,³ the effects of both thermal and radiation aging on certain key fire behavior parameters were investigated. In this study sample formulations considered typical of cable insulations were produced using various fire retardant additives. As in the previous USNRC study, the basic compounds were EPR and CSPE. The flammability parameters investigated included critical ignition energy, heat of combustion, and rate of mass release. The results obtained were not at all consistent, as illustrated in Figure 1. This inconsistency can be attributed to at least two factors. First, only a limited number of samples were tested. Second, the samples tested were thin discs of the given material. Testing was performed in a small-scale thermal exposure apparatus developed at Factory Mutual Research Corporation (FMRC). It has since been demonstrated by FMRC that this apparatus can experience difficulty while testing thin unrestrained samples, as in this program. Such samples tend to curl during heating causing an uncontrolled change in the samples' exposure profile and thus biasing test results. As a result of these inconsistencies, only limited insights resulted. One significant

conclusion drawn from this study was that the presence of fire retardants in the sample formulations did not affect the results of the aging process as measured by change in elongation.

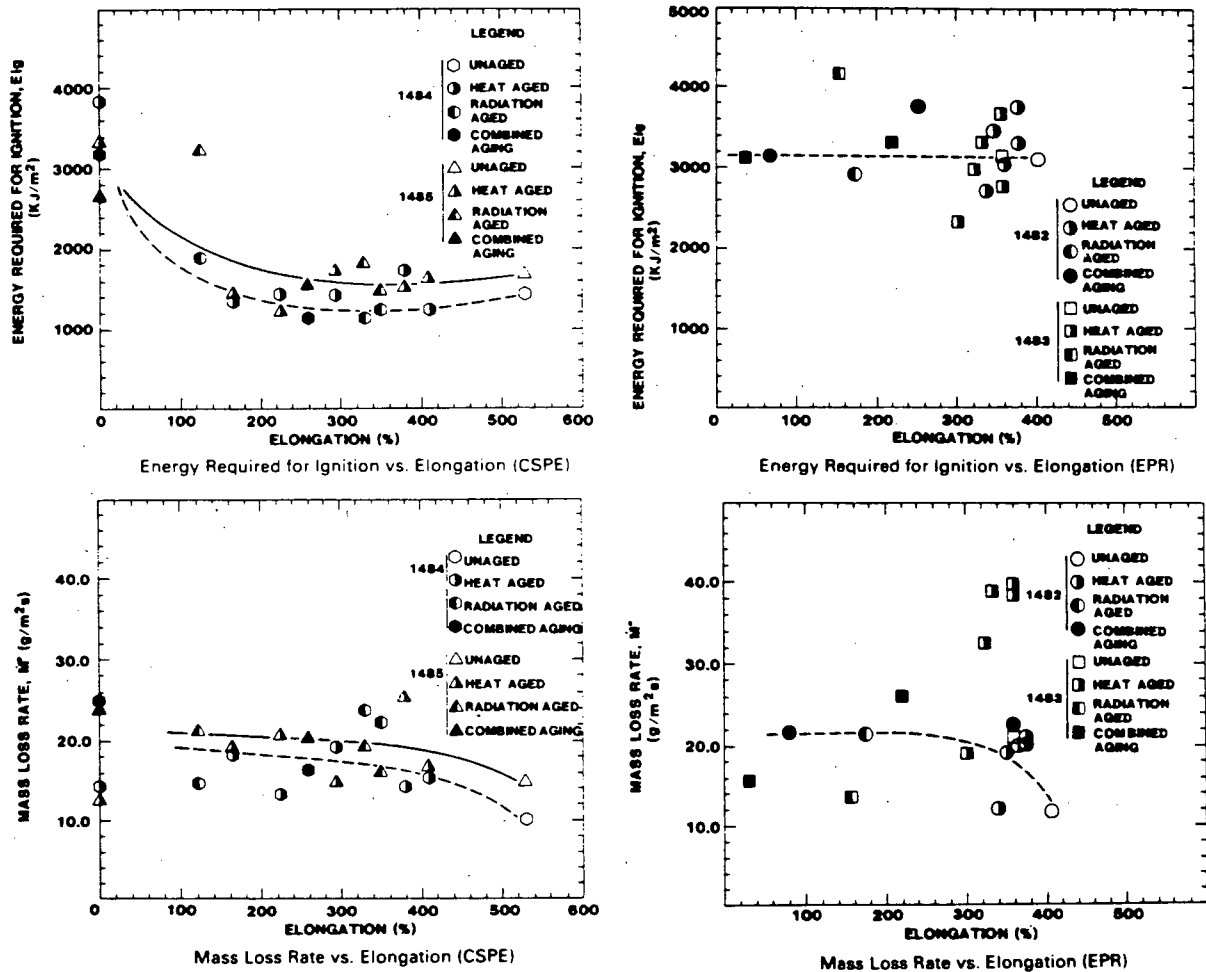


Figure 1: Typical flammability results from reference 3 showing energy required for ignition and mass loss rate in the combustion mode at an external exposure heat flux of 60 kW/m² for two base formulations of cable insulation materials.

The second source of relevant information identified is the cable manufacturing industry itself. In particular, researchers at RAYCHEM Corporation indicate that fairly extensive investigations have been conducted for certain cable types. Requests have been made for the results of these investigations, and the individuals involved have indicated that the information will be made available. However, to date no information is currently available regarding these investigations. As a part of FY-89

efforts other manufacturers will be contacted in an effort to identify additional sources of relevant information.

In addition to these efforts specifically associated with fire issues a large number of equipment qualification studies associated with component aging, though not directly associated with fire issues, have been conducted.⁴ These past studies are of interest since they indicate what types of materials are most vulnerable to age-related effects with respect to non-fire properties, and since these past efforts have also developed and investigated the techniques for artificially aging a sample material. These insights will be drawn upon as appropriate in the formulation and execution of the program plan.

Projected Activity for Fiscal Year 1989

For FY-89 efforts will focus primarily on two areas of investigation. These are (1) the effects of aging on cable damageability and (2) the effects of aging on cable flammability. Cable damageability is the potential for inducing electrical faults in a cable as a result of secondary fire effects (i.e., thermal heating and suppression effects) rather than actual involvement in the fire. Cable flammability is the behavior of cables directly involved in the fire and the propensity with which cables will initiate and/or contribute to fire growth and fire intensity. The investigation of cable aging behavior is of particular interest for several reasons. First, cables represent the largest single combustible fuel source in most plant areas. Second, virtually every plant system will involve cabling. Third, in the analysis of fire risk it is often plant locations that represent pinch points for the routing of redundant cable trains (such as the control room, cable spreading rooms, and containment penetration areas) which dominate plant fire risk. This also implies that cables will often be the critical safety system components exposed to the most severe environments in a fire situation. Finally, previous studies^{5,6,7,8} have indicated that cabling is vulnerable to relatively low thermal exposure levels.

While FY-89 efforts are expected to focus primarily on cable aging issues other types of Class 1E equipment will be tested in the future. During FY-89 efforts to identify and procure such equipment will be initiated. Other potential issues, those associated with passive fire protective features and barrier penetration seal integrity, will not be investigated until later fiscal years.

Cable Damageability Investigations

In the investigation of the effects of aging on cable damageability, unaged, naturally aged, and artificially aged cable samples will be experimentally evaluated. Initial testing will be performed on three conductor 12AWG cables. Each cable conductor will be energized using one phase of a 208 VAC three phase Y-connected power source. This will result in 120 VAC potential between each conductor and ground, and a 208 VAC potential between any two conductors. The cable samples will then be

subjected to an elevated, steady-state temperature environment and the time to electrical failure will be monitored. Electrical failures will be monitored by measuring the voltage across current limiting resistors for each cable conductor. This monitoring scheme will also provide a measure of the leakage current behavior over time, and will allow for the identification of the failure mode (i.e., conductor-to-conductor shorts, or conductor-to-ground shorts). The monitoring system is shown schematically in Figure 2.

A thermal environment test chamber developed under previous USNRC fire safety research efforts will be used in these tests. This chamber is capable of producing transient temperature excursions of up to 600°F per minute, though in these tests steady-state environment testing will be performed by preheating the chamber prior to sample insertion. This chamber has also been used to expose containment components to transient high flux thermal radiation conditions in combination with high temperature, high humidity, and high pressure conditions typical of both single and multiple hydrogen burn scenarios.⁷

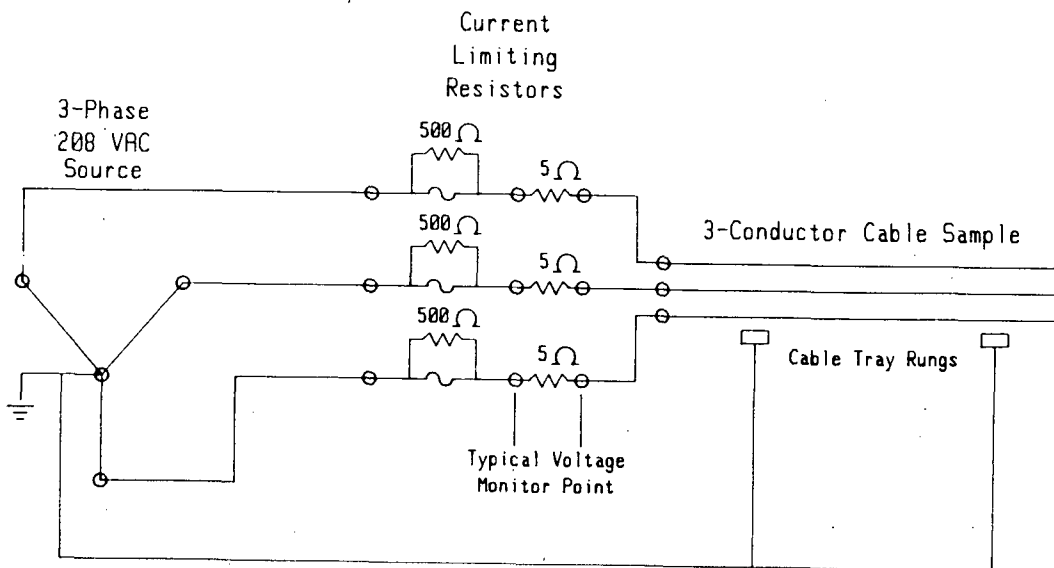


Figure 2: Schematic representation of cable energizing and failure monitoring system.

As an output of these tests, curves of the time to electrical failure versus exposure temperature for both the aged and unaged cable samples will be developed. This format for presentation has been used in previous cable damageability studies⁸ at SNL. Figure 3 illustrates typical results that were obtained in these previous experiments. These particular plots are for a cross-linked polyethylene (XPE or XLPE) insulated and jacketed cable, and for a polyethylene/polyvinylchloride (PE/PVC) cable.

Present plans call for the testing of at least four different cable types. For each cable type, approximately 25 artificially aged and 25 unaged samples will be tested. The testing of naturally aged cable samples will be dependent on the availability of such samples. Each test will consist of one aged and one unaged sample so that slight variations in test conditions from test to test will not bias the comparative results. The first tests for each cable type will establish the threshold of continuous use operability. Temperatures of exposure will then be increased in 50°C steps to approximately 200°C above the threshold temperature. At these higher temperatures, it is anticipated that ignition of the cable samples will be observed.

In addition to this information on cable damage, two additional aspects of the cable behavior will be monitored. First, the transient thermal response of the cables will be monitored through the use of dummy cable samples instrumented with thermocouples. Dummy samples will be used in order to ensure that the presence of thermocouples does affect the failure of the monitored samples. This information will be useful in the development of cable thermal response models. Limited transient environment exposure testing may also be performed in order to establish credible cable failure criteria applicable to realistic, transient fire environments. Second, as it is anticipated that at the higher exposure temperatures ignition of the cable samples will occur, visual observations will indicate cable ignition time as a function of exposure temperature for both aged and unaged cable samples.

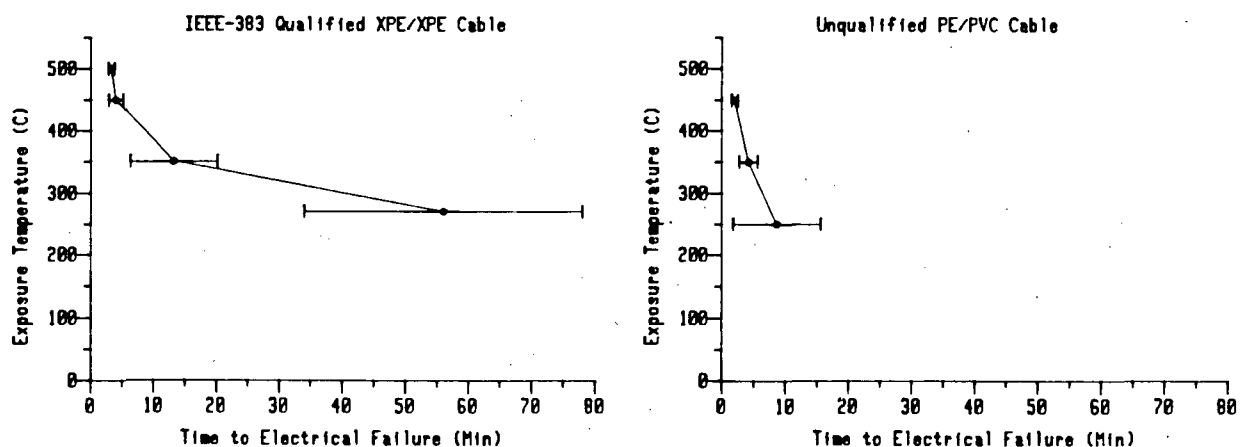


Figure 3: Typical time to failure plots from previous fire research efforts at SNL.

Cable Flammability Investigations

The second aspect of cable fire aging effects to be investigated in FY-89 is cable flammability. What distinguishes flammability from damageability

in that cables need not burn to suffer electrical failure. Flammability is associated with the behavior of cables directly involved in the fire. It is concerned with factors such as the ease of ignition of cables and the rate at which a fire may grow within a cable array.

Following the 1975 Browns Ferry cable fire, the USNRC endorsed the use of low flame spread cables as certified by the IEEE-383 cable flame spread test. Manufacturers of cable insulations modified their formulations in order to meet this criteria. Thus, most cable formulations in use today will pass this standard test without significant spread of fire. For this effort it will be necessary to induce fire spread so that real differences between aged and unaged cables can be observed. Towards this end, a slightly more severe exposure condition than that of the IEEE-383 standard test will be utilized. Efforts conducted at Factory Mutual Research Corporation (FMRC) will be utilized as the basis for establishing the appropriate exposure conditions.

In the FMRC tests⁵ two factors were changed from those specified in the IEEE-383 standard test. First, FMRC utilized two vertical cable trays separated by approximately one foot, each loaded with a single layer of cables, and backed by insulating boards. In the IEEE-383 test only a single vertical cable tray is utilized with an open back in which large gaps are left between individual cables. Second, the configuration of the burner used as the exposure source was changed to a propane sand burner rather than the standard propane ribbon burner. No change in the intensity of the source fire was made. A sand burner will produce a diffusion flame rather than a premixed gas jet flame. This diffusion flame is more representative of actual fire conditions and produces a somewhat more severe thermal exposure condition for the cables. With the standard ribbon burner in its standard configuration, much of the fuel is literally jettted through the cable array and effectively produces no heating effect. Thus, increasing the output of the standard burner does not necessarily produce a more severe exposure as this jetting effect is also magnified. In the FMRC tests the sand burner is placed between the two vertical cable trays. The diffusion flame produces a more uniform heating of the lowest section of the cable array. Figure 4 provides a schematic comparison between the two test methodologies.

In the modified configuration the cables are subjected to a more severe thermal environment than that of the standard test in that (1) the two tray configuration induces a higher thermal feedback to the burning cables, and (2) the sand burner's diffusion flame provides a somewhat more effective heating source than the standard ribbon burner even though total exposure fire intensity is identical. In the FMRC tests, use of this configuration resulted in the ability to further screen cable formulations which had passed the IEEE-383 standard test. Cables were segregated into (1) those which would not propagate fires, (2) those which were marginal fire propagators, and (3) those which readily propagated fire under these conditions.

Using this test methodology, side-by-side testing of aged and unaged cables

will be undertaken at the SNL fire test facility. These tests should demonstrate any effects of aging on the cable flammability characteristics under realistic exposure conditions. If cable materials are identified for which a pronounced effect is observed, aged samples may be exposed to the standard IEEE-383 flame spread test to determine if these cables have lost their ability to pass this test as well.

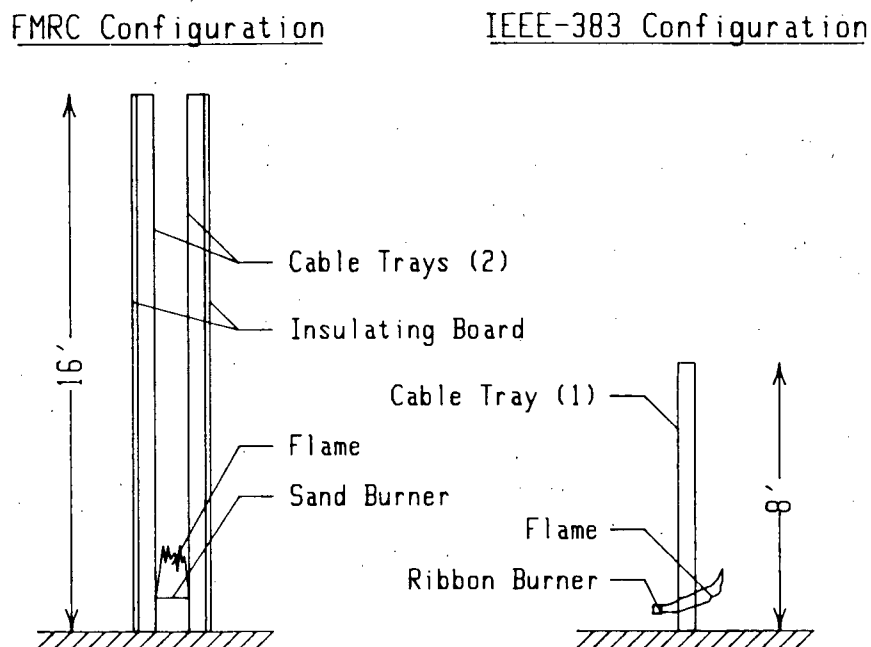


Figure 4: Simple schematic highlighting primary difference between FMRC and IEEE-383 vertical cable flame spread test methodologies.

Investigations of Other Class 1E Equipment

In addition to cables, there will be other Class 1E equipment for which fire related aging effects may be noted. In particular, motors, control circuitry, transformers, and rotating equipment may be subject to either an increased vulnerability to fire induced damage or to the initiation of a fire. During FY-89 a prioritized listing of such equipment will be developed. This listing of equipment will be based on (1) the importance of particular components to plant safety, (2) the prevalence of that equipment in plant safety areas, (3) the potential vulnerability of the equipment base materials to age related degradation, and (4) a review of the experience base on age related equipment degradation. It should be noted that previous efforts under the USNRC Fire Protection Research

Program have performed similar screening analyses.¹⁰ These results will be utilized as appropriate in this study.

Once this prioritized list has been established, procurement of test samples will be initiated. Procured samples will include both new, and to the extent possible, naturally aged components. These samples will then be tested for thermal endurance in a manner similar to that used for the cable samples. Limited efforts⁵ have been performed related to this issue and will be drawn upon as appropriate. The questions of the susceptibility to equipment induced fires is quite difficult to assess experimentally. For example, under the USNRC Fire Protection Research Program considerable effort was expended to develop a repeatable experimental methodology for electrically initiating a electrical control panel cable fire.¹¹ No firm plans in this area have yet been developed.

Summary

In the review of available information on fire aging issues, it was found that only cable flammability effects have been investigated, and that those investigations that have been conducted were quite limited. Further, the information available on age-related cable flammability is inconsistent and inconclusive. Some results indicate an increased flammability with aging while others indicate a decreased flammability. These results are dependent on both the material formulations and on the test procedures and aging schemes utilized. No efforts to investigate the other fire aging issues, those of the effects of aging on other Class 1E equipment and passive fire protective features, have to date been identified. Current data is not adequate to draw conclusions with respect to the significance of any of the above issues.

Efforts to be performed in Fiscal Year 1989 will focus on two cable aging issues, cable damageability and cable flammability. Damageability is related to the potential for inducing electrical faults in cables that may not be directly involved in a fire. Flammability relates to the behavior of cables actually involved in a fire and the propensity with which cable insulations will become involved in and contribute to fire intensity and fire growth. Cables are the focus of initial investigations due to their prevalence in plant systems, their dominance of combustible fuel loadings in most plant areas, their demonstrated vulnerability to relatively low thermal exposure conditions, and their highly visible roll in the analysis of plant fire risk.

Damageability studies will involve steady-state thermal exposure testing of both aged and unaged cable samples. Initial testing will involve energized three conductor cables for which the time to electrical failure as a function of exposure temperature will be measured. The mode of cable failure, conductor-to-conductor shorts versus conductor-to-ground shorts, will also be monitored.

Flammability studies will involve the use of an intermediate-scale vertical flame spread test configuration. This configuration is similar to, but

somewhat more severe than, the standard exposure configuration specified in the IEEE-383 flame spread test. This more severe exposure condition should result in observable flame spread, even for most cables certified as low flame spread by IEEE-383 testing. Thus, any change, either increase or decrease, in the cable insulation flammability should be readily observed as well.

Efforts will also be initiated in FY-89 to establish a prioritized list of other types of Class 1E equipment to be evaluated in subsequent fiscal years. This equipment is expected to include motors, control circuitry, small transformers, and rotating equipment. Once a prioritized list has been developed test samples will be procured. Thermal damageability testing of this equipment is anticipated as a part of FY-90 efforts.

In addition to the issues of Class 1E equipment damageability and flammability, the age-related degradation of passive fire protection features is also of potential concern. These passive features include cable coatings, cable tray wrap systems, and fire barrier penetrations seals. The potential for age-related degradation of these systems could result in a loss of protective features effectiveness and reliability, thus increasing overall plant fire risk. These efforts do not fall within the scope of currently planned activities.

References

1. Salazar, E. A., et.al., NUREG/CR-2314, Aging With Respect to Flammability and Other Properties in Fire-Retarded Ethylene Propylene Rubber and Chlorosulfonated Polyethylene, March 1982, Sandia.
2. Standard Method For Measuring the Minimum Oxygen Concentration to Support Candle-Like Combustion of Plastics (Oxygen Index), ASTM D 2863-76, American National Standards Institute, 1976.
3. Clough, Roger L., NUREG/CR-2868, Aging Effects on Fire-Retardant Additives in Organic Materials for Nuclear Plant Applications, August 1982, Sandia.
4. Bonzon, L. L., et.al., NUREG/CR-4301, Status Report on Equipment Qualification Issues Research and Resolution, November 1986, Sandia.
5. Jacobus, M. J., NUREG/CR-4596, Screening Test of Representative Nuclear Power Plant Components Exposed to Secondary Fire Environments, June 1986, Sandia.
6. Wheelis, W. T., NUREG/CR-4638, Transient Fire Environment Cable Damageability Test Results, Phase I, September 1986, Sandia.
7. King, D. B., et.al., NUREG/CR-4783, Safety-Related Equipment Survival in Hydrogen Burns in Large Dry PWR Containment Buildings, March 1988, Sandia.

8. Chavez, J. C., "Steady-State Environment Cable Damage Testing," A Letter Report to the USNRC, July 14 1984, Sandia.
9. Newman, J. S., et.al., "Classification of Electrical Cables Based on Vertical Fire Propagation," 37th International Wire and Cable Symposium, Reno, NV, November 15-17 1988, Factory Mutual Research Corporation.
10. Wanless, J., NUREG/CR-4310, Investigation of Potential Fire-Related Damage to Safety-Related Equipment in Nuclear Power Plants, November 1985, Sandia.
11. Spletzer, B. S., Horine, F., NUREG/CR-4570, Description and Testing of an Apparatus for Electrically Initiated Fires Through Simulation of a Faulty Connection, June 1986, Sandia.

Nuclear Plant Aging Study of Residual Heat Removal Systems

R. Lofaro, W. Gunther, M. Subudhi and J. Taylor

Brookhaven National Laboratory
Upton, New York 11973

ABSTRACT

The effects of aging on Residual Heat Removal systems in Boiling Water Reactors have been studied as part of the Nuclear Plant Aging Research program. The aging phenomena has been characterized by analyzing operating experience from various national data bases. In addition, actual plant data was obtained to supplement and validate the data base findings.

Time-dependent failure rates were calculated for several components to identify aging trends. A computer program was developed and implemented to model a typical RHR system and perform time-dependent Probabilistic Risk Assessment calculations. Using the time-dependent failure rates calculated from the data, the effects of aging on system unavailability and component importance were investigated.

INTRODUCTION

The Nuclear Plant Aging Research (NPAR) program was established by the Nuclear Regulatory Commission to address concerns related to aging effects on the safety and reliability of nuclear power plants. The goals of the program are to characterize aging and service wear effects and identify methods of detecting and mitigating them. Initial work under the NPAR program focused on specific components [1-8], whereas more recent work has addressed complete systems [9].

This paper presents preliminary technical results from the phase I evaluation of the effects of aging on Residual Heat Removal (RHR) systems in boiling water reactors. The goal of the phase I work is to characterize the aging phenomena by identifying predominant failure causes, modes and mechanisms, as well as time-dependent aging trends.

RHR SYSTEM DESIGN AND OPERATION

There are several different RHR system designs currently in use in the United States, however, the most common is the two loop design. Each loop has two pumps and one heat exchanger along with numerous valves and instrumentation (Figure 1).

The RHR system can typically operate in several different modes, however, low pressure coolant injection (LPCI) and shutdown cooling (SDC) are the two most commonly aligned modes. This study focussed on these two modes.

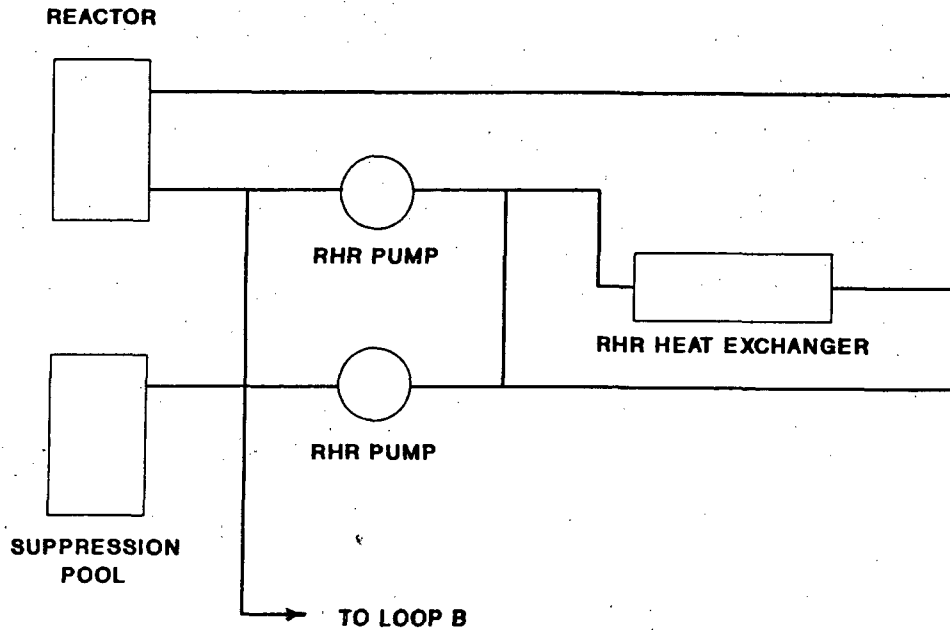


Figure 1: Typical RHR System Design

In the LPCI mode, the RHR pumps take suction from the suppression pool and inject the coolant directly into the reactor bypassing the heat exchanger. This mode is automatically initiated following a loss of coolant accident (LOCA).

In the SDC mode, the RHR pumps take suction from the reactor recirculation loop, deliver the coolant to the heat exchanger where it is cooled, and then inject it back into the reactor. This mode is used during normal cool down of the reactor and is manually initiated.

AGING ANALYSIS

To evaluate the effects of aging on RHR system performance, past operating experience from various sources was obtained and reviewed. Data were obtained from national data bases, such as the Nuclear Plant Reliability Data System (NPRDS) and Licensee Event Reports (LER's). To mitigate the limitations of the data base information, each event was reviewed to assure consistency in aging determinations and interpretations of failure characteristics. In addition, actual plant data from an operating BWR were obtained and analyzed to supplement and validate the data base findings.

The NPAR definition of aging [10] was applied to each of the failures to determine if the failure was aging related. The fraction of failures that could be attributed to aging was then determined for each of the data sources. As shown in Figure 2 for the NPRDS data, large aging fractions were found indicating that aging degradation is present in RHR systems and is a significant contributor to failure.

The data were further sorted to identify the methods by which the failures are currently detected (Figure 3). It was found that tests and inspections detected the predominant number of failures (65%). However, approximately 27%

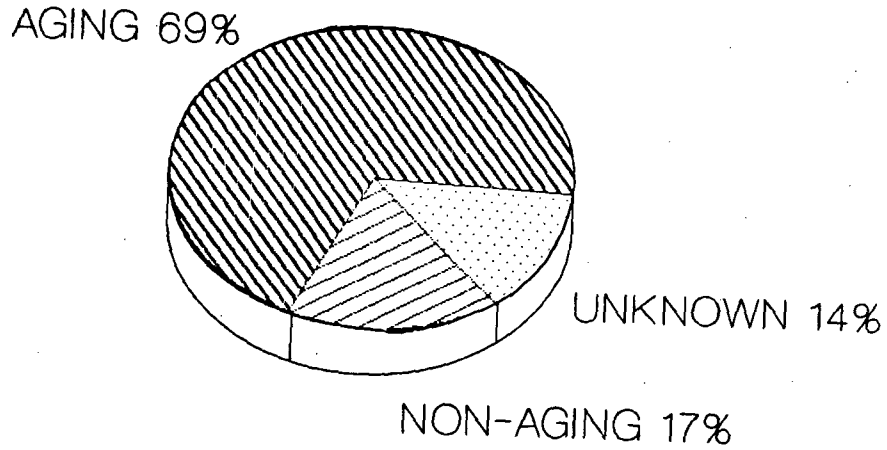


Figure 2 Fraction of Failures Related to Aging

of the failures were not detected until they resulted in some operational abnormality. This could include events such as the failure of a valve to transfer on demand or an instrument giving an incorrect indication. This finding shows that current test, inspection and maintenance practices do not detect all aging degradation before it results in failure.

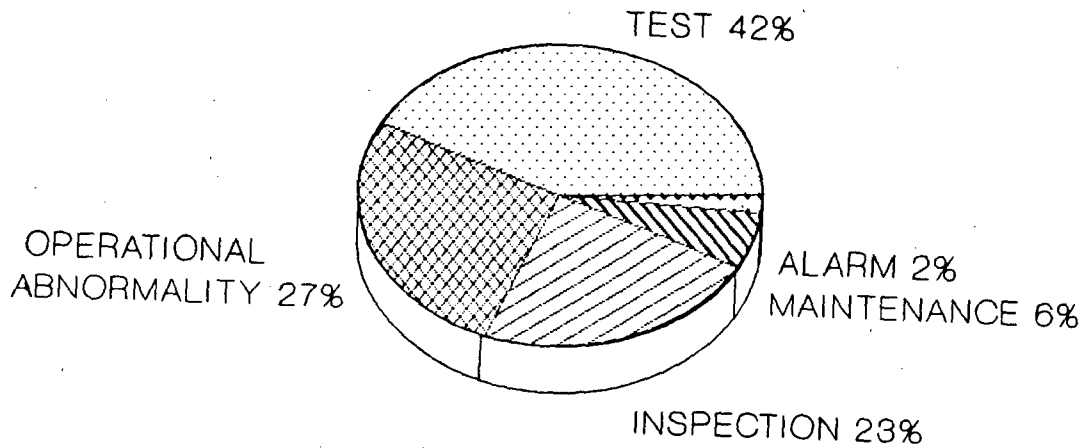


Figure 3: Failure Detection Methods

To determine the effect of the failure at the system level, the data were categorized into four groups (Figure 4). Approximately half of the failures resulted in degraded system operation. This implies that the system could still perform its design function, however, the failure would eventually need attention or it would worsen and possibly result in loss of system function. Failures in this category included minor events, such as valve packing leaks, as well as relatively significant events, such as radiation leakage from heat exchangers. The data also showed that approximately 21% of the failures resulted in a loss of redundancy. This is significant since it increases the probability that the system could become unavailable which could adversely impact plant risk.

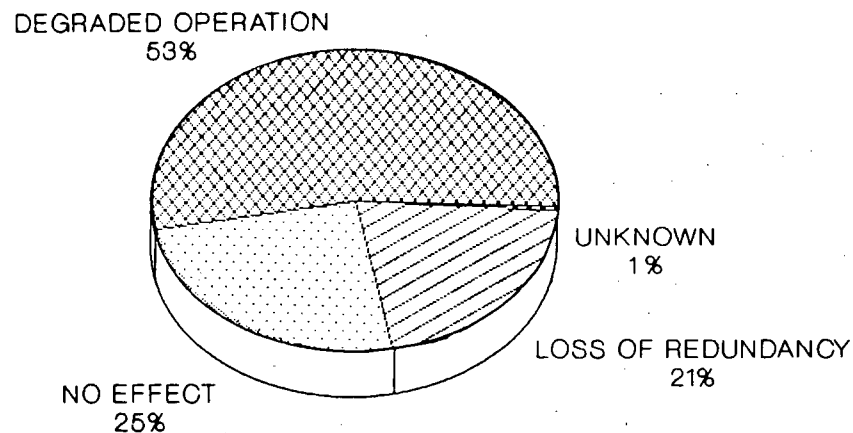


Figure 4: System Level Failure Effects

An important effect of RHR failures identified from the LER's is that they can result in radiological release (Figure 5). Although small in number, these failures are significant since each was aging related. The failures typically involved heat exchanger tube leakage caused by corrosion. Since corrosion is a time intensive aging mechanism, this type of failure can be expected to become more common as plants age if current methods cannot detect the degradation in a timely manner.

The predominant cause of failure was identified by categorizing the events into three classes; normal service, human error and other. Normal service included all causes related to degradation mechanisms the component is normally expected to be exposed to. This includes the typical aging mechanisms such as wear, corrosion, fatigue and calibration drift. The data were then sorted according to plant age to examine the time-dependent effects on cause of failure. As shown in Figure 6, the predominant cause of failure was found to be normal service for all plant ages. This is consistent with the large aging fraction discussed previously which indicates that aging degradation is a significant

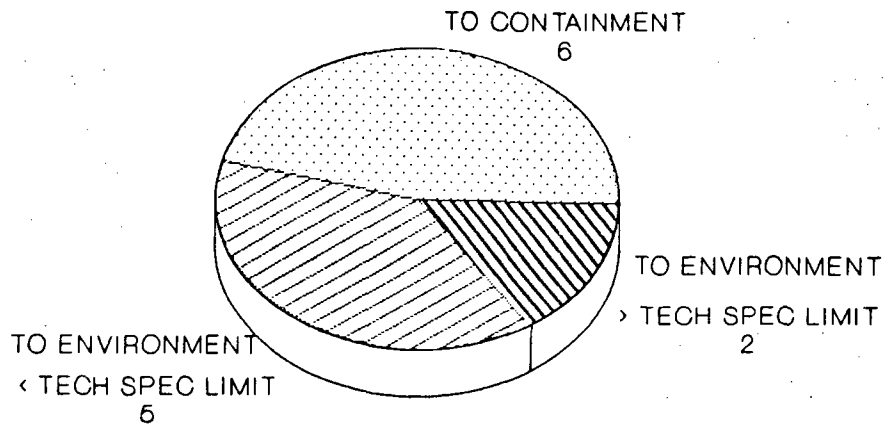


Figure 5: RHR Failures Resulting in Radiological Release

contributor to failures in the RHR system.

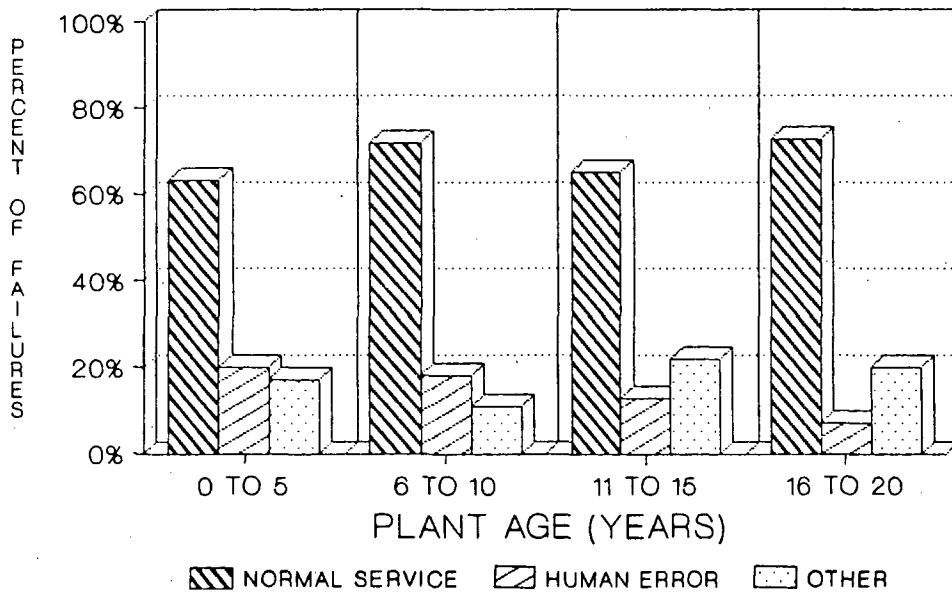


Figure 6: Failure Causes Versus Plant Age

Figure 6 also shows that the percentage of failures caused by normal service remains relatively constant with time. Therefore, no dramatic increases in failures with age are evident from past experience. This could be attributed to several factors including the predominant standby status of the RHR system which reduces exposure to operating stresses, as well as the relatively stringent test and inspection requirements on the system.

The predominant failure mechanisms were also identified from the data (Figure 7). Wear and calibration drift accounted for over half of the failures. Wear was typically associated with mechanical components, such as valves, pumps and heat exchangers, while calibration drift was typically associated with electrical components such as switches and sensors. It should be noted, however, that numerous other mechanisms are present in the RHR system which can lead to aging related failures. In order to detect all aging degradation, monitoring methods would have to be very diverse.

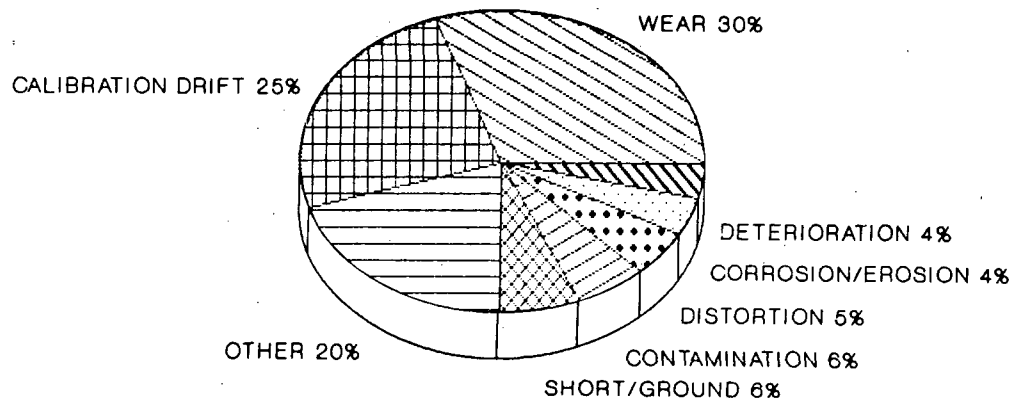


Figure 7: Failure Mechanisms

The data were further sorted to identify the components most frequently failed (Figure 8). Results showed that valves were the predominant component failing, followed by instrumentation/ controls and supports. These data are not normalized, therefore, population effects contribute to these results. However, it is noted that each of the components have a large fraction of failures which are aging related.

To identify the time-dependent effects of aging on component failures, the data were normalized to account for population and operating hours/demands. Time-dependent failure rates were then calculated for several of the RHR components. The calculations were performed by sorting the component failures by mode and plant age for individual plants. Linear regressions were then performed to obtain a failure rate curve for each plant. Results were then averaged over all plants to obtain generic failure rate curves. Upper and lower bounds were calculated using the standard error of the averages.

Figure 9 presents the time-dependent failure rate for motor operated valves (MOV's) failing to transfer. As indicated, the initial failure rate at age 0 is in good agreement with other commonly used sources, such as WASH-1400.

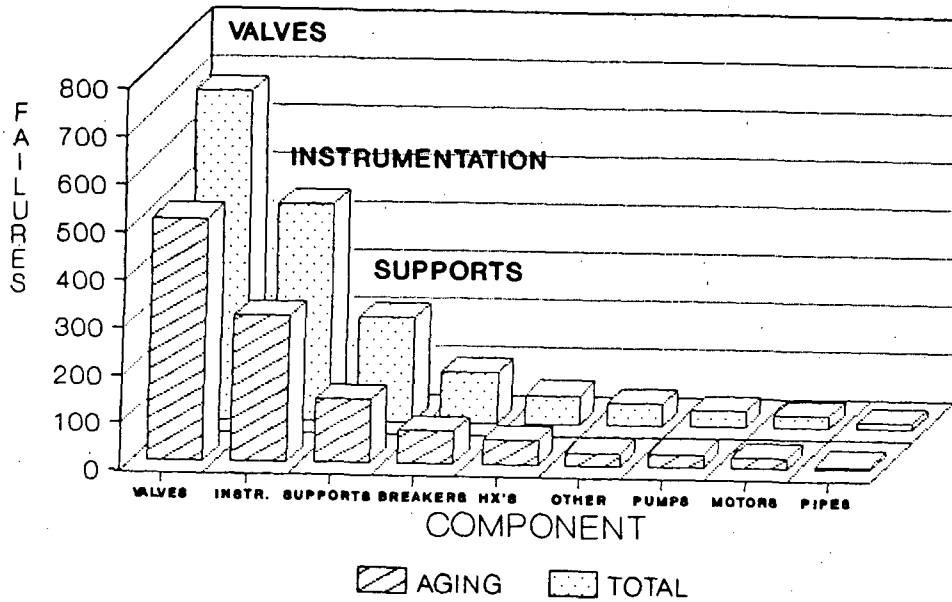


Figure 8: Failures Per Component

However, as component age increases the failure rate tends to increase also. For MOV's this increase was found to be 11% per year. In comparison with previous studies [9], in which failure rate increases as high as 20% to 30% per year were found, the increase found here for MOV's was judged to be moderate. Failure rate increases for other mechanical components were found to be moderate or low, including 8% and 17% per year for heat exchangers and pumps, respectively.

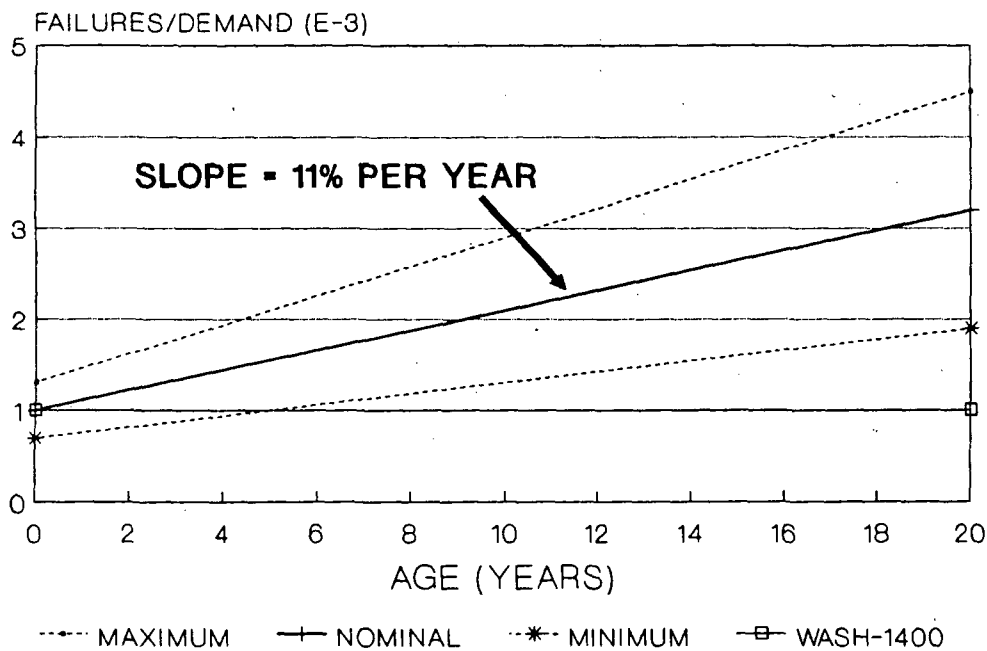


Figure 9: Time-Dependent MOV Failure Rate

Time-dependent failure rates were also generated for several electrical components. Figure 10 shows an example for level switch loss of function. As indicated, the failure rate did not show any increase with age for this component. Similar results were obtained for other electrical components with pressure and level sensors also showing no increase with age and pressure switches showing only a 3% increase per year.

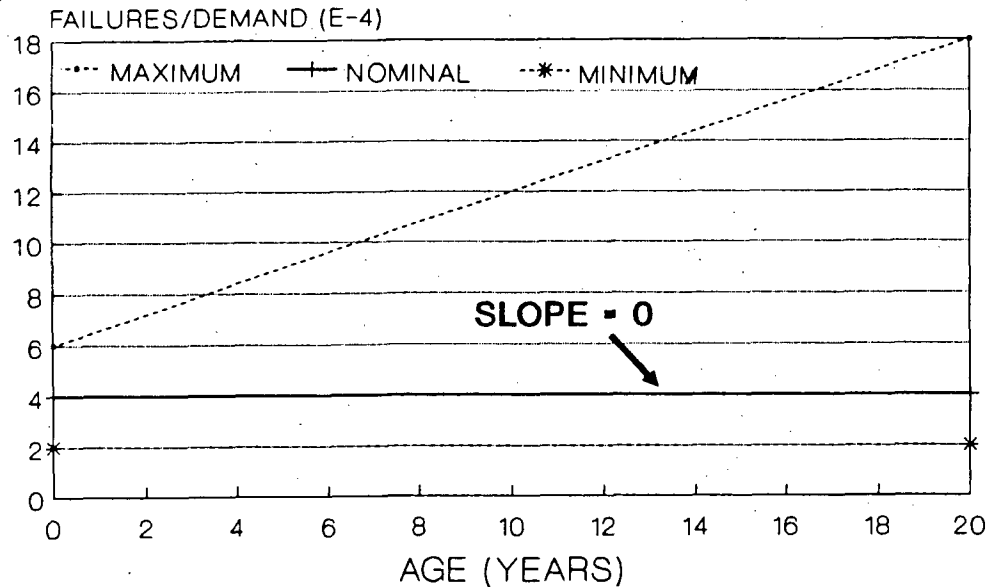


Figure 10: Time-Dependent Level Switch Failure Rate

To examine the effects of the increasing failure rates at the system level, a computer program was developed which performs time-dependent probabilistic risk assessment (PRA) calculations. The program (PRAAGE-1988) modeled the Peach Bottom RHR design in the LPCI mode and the SDC mode. Using the failure rates calculated from the data and extrapolating them, system unavailability projections were made over a 50 year period.

In Figure 11, the unavailability projection for the LPCI mode of RHR is presented. This projection accounts for aging of the two most important components contributing to system unavailability; MOV failure to transfer and pressure sensor loss of function. Failure rates used for all other contributors were the constant generic values originally found in the PRA. As shown, the LPCI unavailability was found to increase by a factor of approximately 2 over the 50 year time period. A similar projection was made for the SDC mode which resulted in an unavailability increase of approximately 4 times. The components aged for the SDC mode calculation were pumps, MOV's and pressure sensors, which were the leading contributors to system unavailability in this mode.

In a previous study [9], unavailability projections were made for the component cooling water (CCW) system, which is a continuously operating system. Comparing the results with the findings from this study (Figure 12) it is seen

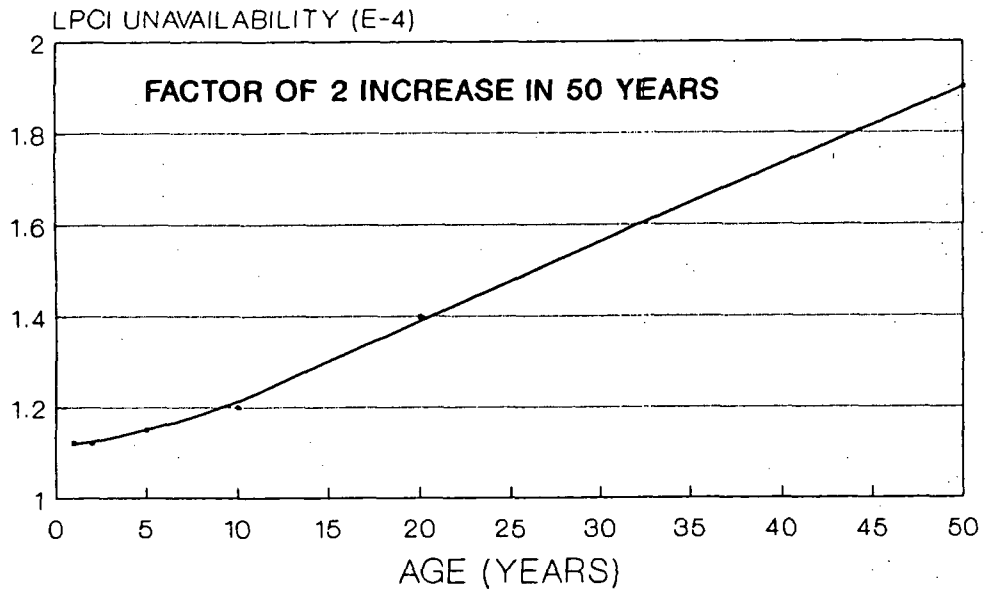


Figure 11: LPCI Unavailability Versus Age

that the unavailability increase for the CCW system is significantly higher than for the RHR system. It must be noted that these results are based on analysis of only two specific systems, therefore generalized conclusions cannot be made. However, the results shown here do indicate a potential trend for the unavailability of standby systems such as RHR to be less severely affected by aging than continuously operating systems such as CCW.

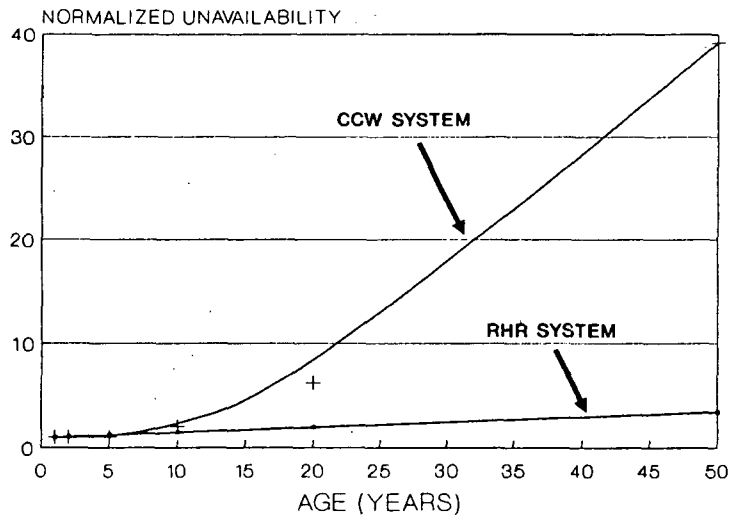


Figure 12: Normalized Unavailability Versus Age

The apparent mitigation of aging effects in the RHR system can be attributed to several factors. Since the system is predominantly maintained in standby status, exposure to operating stresses such as wear and erosion is reduced. Although these mechanisms are still present, they do not result in failures as rapidly as they would in a continuously operating system. This would result in a slower increase in failure rate with age for components in the standby system. In addition, since the RHR system is a safety related system, the test and inspection requirements are relatively stringent. This could be beneficial in that aging degradation may be detected before it results in a failure.

CONCLUSIONS

An analysis of past operating experience for RHR systems has shown that a significant number of failures are related to aging. The predominant cause of failure is normal service, which includes all operating and environmental stresses the system is normally expected to be exposed to. The predominant failure mechanisms are wear and calibration drift, which are associated with mechanical and electrical components, respectively. The components most frequently failed include valves and instrumentation/controls.

An evaluation of the time-dependent effects of aging on component failure rates and system unavailability has shown the following:

- Mechanical components show a low to moderate increase in failure rate with age. This may be attributable to their predominant standby status which reduces exposure to operating stresses such as wear and erosion. It may also be attributable to the relatively stringent test and inspection requirements placed on the RHR system.
- Electrical components such as switches and sensors show little or no increase in failure rate with age. This may be attributable to the relatively stringent test and inspection requirements placed on the RHR system. It may also be due to frequent replacement which is common with components such as these.
- Aging effects produce a moderate increase in the unavailability of the RHR system. Comparison with previous work has shown the potential for the unavailability of standby systems such as RHR to be less severely affected by aging than the unavailability of a continuously operating system.

Although the time-dependent aging effects found in this study have been judged to be moderate, it must be noted that this analysis was performed only at the system level. As part of the future phase II work, the results from this study will be used to analyze the effects of aging at the plant level. The impact of aging at the plant level will depend on many factors, however, it is possible that even a moderate increase in RHR unavailability can have a significant impact on plant risk. It is, therefore, important that this be addressed in the phase II work.

REFERENCES

1. Gunther, W.E., et al., "Operating Experience and Aging-Seismic Assessment of Battery Chargers and Inverters," NUREG/CR-4564, June 1986.
2. Subudhi, M., et al., "Improving Motor Reliability in Nuclear Power Plants," NUREG/CR-4939, June 1987.
3. Taylor, J. et al., "Seismic Endurance Tests of Naturally Aged Small Electric Motors," BNL Report A-3270-11-85, November 1985.
4. Subudhi, M., et al., "Operating Experience and Aging-Seismic Assessment of Electric Motors," NUREG/CR-4156, June 1985.
5. Greenstreet, W.L., et al., "Aging and Service Wear of Motor Operated Valves Used in Engineered Safety Feature Systems of Nuclear Power Plants," NUREG/CR-4234, June 1985.
6. Greenstreet, W.L., et al., "Aging and Service Wear of Check Valves Used in Engineered Safety Feature Systems of Nuclear Power Plants," NUREG/CR-4302, December 1985.
7. Bacanskas, V.P., "Aging and Service Wear of Solenoid-Operated Valves Used in Safety Systems at Nuclear Power Plants," NUREG/CR-4819, March 1987.
8. Adams, M.L., "Aging and Service Wear of Auxiliary Feedwater Pumps for PWR Nuclear Power Plants," NUREG/CR-4597, July 1986.
9. Higgins, J., et al., "Operating Experience and Aging Assessment of Component Cooling Water Systems in Pressurized Water Reactors," NUREG/CR-5052, July 1988.
10. NUREG-1144, "Nuclear Plant Aging Research (NPAR) Program Plan," U.S. Nuclear Regulatory Commission, Revision 1, September 1987.

NUCLEAR PLANT AGING RESEARCH ON THE
HIGH PRESSURE INJECTION SYSTEM^a

LeRoy C. Meyer
H. L. Magleby

Idaho National Engineering Laboratory
EG&G Idaho, Inc.
Idaho Falls, ID 83415
(208) 526-8385

ABSTRACT

This paper presents the results of a review of light water reactor High-Pressure Injection System (HPIS) operating experiences reported in the Nuclear Power Experience Data Base, Licensee Event Reports, Nuclear Plant Reliability Data System, and plant records. The purpose of the review is to evaluate the potential significance of aging as a contributor to degradation of the HPIS. Tables are presented that show the percentage of events for HPIS classified by cause, component, and subcomponents for pressurized water reactors. A representative Babcock & Wilcox plant was selected for a detailed study. The U.S. Nuclear Regulatory Commission's Nuclear Plant Aging Research guidelines were followed in performing the detailed study that identifies components susceptible to aging, stressors, degradation mechanisms, and failure modes for the HPIS. In addition to the engineering evaluation, the risk-significant components were determined and the aging contribution to risk was evaluated for the HPIS studied. The risk analysis utilized an existing PRA, the linear aging model and generic failure cause data.

NOMENCLATURE

B&W	Babcock & Wilcox
BIT	Boron Injection Tank
BWST	Borated Water Storage Tank
CE	Combustion Engineering
CM	Corrective Maintenance
ECCS	Emergency Core Cooling System

^aWork sponsored by the United States Nuclear Regulatory Commission, Office of Nuclear Regulatory Research, under DOE Contract No. DE-AC07-76ID01570.

ESFAS	Engineered Safety Feature Actuation System
HPI	High-Pressure Injection
HPIS	High-Pressure Injection System
I&C	Instrumentation and Control
IIR	Incident Investigation Report
ISI	Inservice Inspection
ISM&M	Inspection, Surveillance, Monitoring, and Maintenance Practice
IST	Inservice Testing
LER	Licensee Event Report
LOCA	Loss-of-Coolant Accident
LPIS	Low-Pressure Injection System
MOV	Motor Operated Valve
NPAR	Nuclear Plant Aging Research
NPE	Nuclear Power Experience
NPRDS	Nuclear Plant Reliability Data System
PRA	Probabilistic Risk Assessment
PWR	Pressurized Water Reactor
SIT	Safety Injection Tank

INTRODUCTION

This paper presents the highlights of a review of operating experiences and practices of commercial nuclear power plants to determine the significance of aging as a contributor to degradation of the High-Pressure Injection System (HPIS). Further details on this work are given in Reference 1. This study primarily covers Pressurized Water Reactors (PWRs). The Nuclear Plant Aging Research (NPAR) guidelines provided the framework for the study.² System aspects of the HPIS are stressed with specific component data utilized only to the extent needed to support the system study. The HPIS interfaces with many other systems in performing its functions. These systems include the Class 1E power, service water, instrument air, low-pressure injection, and the Engineered Safety Features Actuation System (ESFAS). As with other safety systems, the HPIS is a fail-safe design with redundant channels and high system reliability.

However, failures in other systems can contribute to the HPIS unavailability. Data for this study were obtained from generic data bases, which includes the Nuclear Plant Reliability Data System (NPRDS), Licensees Event Reports (LERs), Nuclear Power Experience (NPE), and maintenance records from one cooperating utility.

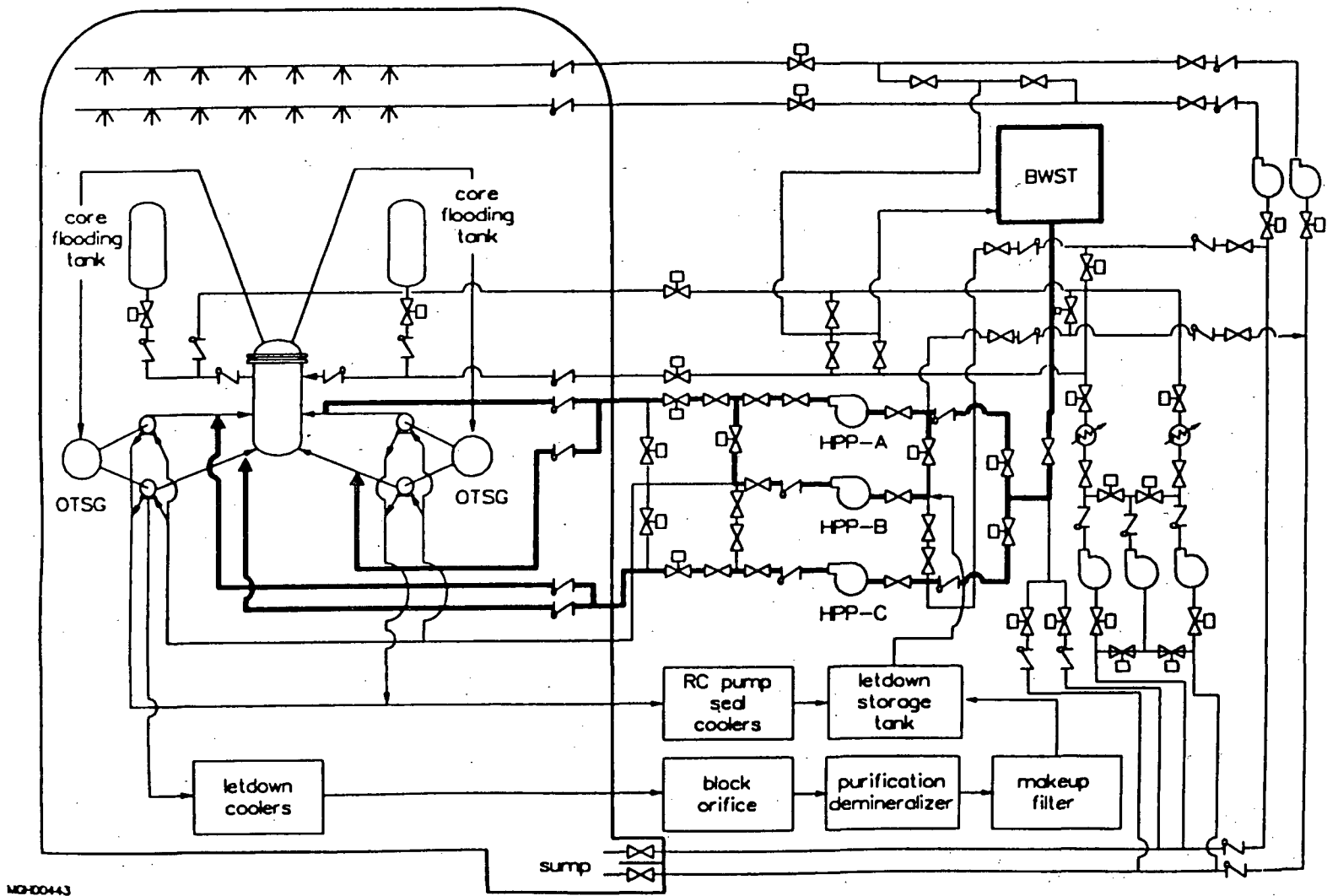
The specific objectives for the study were:

- Identify specific problems related to aging
- Determine the stresses, degradation mechanisms, and potential failure modes for major HPIS components
- Review the Inspection, Surveillance, Monitoring, and Maintenance practices (ISM&M)
- Recommend improved ISM&M and identify performance parameters or functional indicators potentially useful in detecting aging degradation.
- Identifying the risk significant component and contribution of aging to HPIS risk.

SYSTEM DESCRIPTION

The HPIS along with the Low-Pressure Injection System (LPIS) and the Core Flooding System collectively form the overall Emergency Core Cooling System (ECCS), which is designed to prevent core damage from a Loss-of-Coolant Accident (LOCA). High-pressure injection is necessary to prevent uncovering the core for small LOCAs, where high system pressure is maintained, and to delay uncovering the core for intermediate-sized LOCAs. The HPIS can also be used to cool the core following a non-LOCA reactor shutdown (e.g., transient). This mode of HPIS operation would be utilized only if normal and emergency secondary heat removal via the steam generators cannot be achieved.

The HPIS consists of three motor-driven high-pressure centrifugal pumps, with two primary suction and discharge paths. The HPIS described is for B&W plants and those Westinghouse plants which use the HPI pump both during normal operation for supply makeup water and during emergencies for injection. It is recognized that other standby HPISs may only have two HPI pumps and work at lower pressures. The detailed system configuration for a Babcock & Wilcox (B&W) plant is shown in Figure 1, with the High-Pressure Injection (HPI) mode of operation highlighted. For most conditions, flow from one pump is sufficient. For special cases, two pumps may be required for the system to fulfill its safety function. The HPIS is capable of supplying flow at relatively high reactor cooling system pressure. For the PWR studied, the emergency mode of operation is initiated if the reactor system pressure decreases to 1500 psig, or if reactor building pressure increases to 4 psig. The emergency HPI flow path is from the borated water storage tank through the HPI pumps and into the four cold legs of the



MD-00443

Figure 1. ECCS with high-pressure injection system highlighted.

reactor coolant loops. Once initiated, the emergency mode of operation will continue until manually terminated.

In addition to emergency functions, part of the HPIS is also used during normal plant operation. Together, the HPIS and related systems perform the following functions:

- Provides makeup and purification that maintains the volume of the reactor coolant within acceptable limits during most modes of operation, including chemical control and control of soluble boron for long-term reactivity control
- Provides seal injection water for the reactor coolant pumps
- In the event of a reactor coolant system accident, provides HPI of borated water for emergency core cooling and plant shutdown
- Provides long-term cooling following a LOCA using the high-pressure recirculation system and the low-pressure recirculation system.

The HPIS emergency operation is controlled by the ESFAS. An initiating signal is received from the ESFAS that is automatically sent to the appropriate controllers for pumps, motor-operated valves, and pneumatic-operated valves.

OPERATING EXPERIENCE

The NPE data base was reviewed to determine the most frequent cause of failures and to identify the components with the most frequent failures. The data base does not have a separate system classification for HPI. The HPI system is included in the ECCS system and the summaries reported in this paper include some failures from the standby core spray system and the LPIS. The data from the NPE will be, therefore, referred to as ECCS data in this paper.

The review of operating experience from the NPE data base has identified the most frequent cause of component failure as maintenance error. This is followed by design error, mechanical disability, and local Instrumentation and Control (I&C) events, as shown in Table 1. The ECCS component events ranked by frequency of occurrence are presented in Table 2. The four components with the highest frequency of failure are valves (35%), I&C (19%), pumps (19%), and piping (7%). The recorded failures in the NPE and LER data base for these components will be discussed briefly.

Valves--For the NPE data base command faults were the leading cause for ECCS events involving valves, which includes electrical power or any support system that prevents the valve from performing its intended function. Command faults accounted for 32% of the ECCS failures involving valves.

TABLE 1. ECCS FAILURE CAUSES FOR PWRs FROM NPE DATA BASE

<u>Cause</u>	<u>Percent</u>
Maintenance error	28
Design error	13
Mechanical disability ^a	10
Local I&C failure ^a	4
Set point drift ^a	4
Chemistry out of spec	4
Subcomponent sticking ^a	4
Short/ground ^a	3
Weld failure ^a	3
Blockage ^a	3
Other	24
Number of events	1552

a. Potentially aging related.

TABLE 2. ECCS COMPONENT FAILURE RANKING FOR PWRs FROM NPE DATA BASE

<u>Component</u>	<u>Percent</u>
Valves	35
I&C	19
Pumps	15
Pipe	7
Electrical	4
Heat exchanger	2
Pipe support	2
Tank	2
Other	2
Number of events	1552

A summary of HPIS valve failures from LER data is given in Table 3, where 40% of the valve failures are classified as potentially aging related. In this potentially aging related category of failures, mechanical controls (parts out of adjustment) occurred most frequently (8%), followed by seat or disk failure (6%), and packing failure (5%).

Instrumentation and Control--I&C failures reported in the NPE data base included the sensors, electronics, and motor control centers for valves and pumps. In this category, instrumentation accounted for 58% of the I&C failures, valve controls 22%, pump controls 6%; the rest were miscellaneous control circuits.

Pumps--The LER data base listed 44 events which involved the main HPIS pumps. Out of these, 22 events were caused by control, maintenance, and design error. The remaining events had no single dominant cause. About 20% of the events were potentially aging related.

Piping--The HPIS piping events from NPE data base, after eliminating design, construction, and maintenance errors (which accounted for 37%), were due primarily to weld failures (15%), corrosion (7%), and vibration (5%). The rest of the events were spread over many causes.

The NPRDS data for B&W and Westinghouse plants for frequency of failure and system effects are presented in Figure 2. The pie diagram for the HPIS event-cause category shows aging accounted for 21.3% of the events, design (11.8%), test and maintenance (8%), human related (2.6%), and all the rest were lumped under Other, which takes into account a large number of unknowns some of which may be aging related. The system effects diagram shows that the HPIS was unaffected for 42.8% of the component events and only 0.7% of the component events actually caused loss of total system function. Other system effects included loss of subsystem channel (24.2%), degraded system operation (19%), and loss of redundancy (13.3%).

Plant data from the Incident Investigation Reports (IIRs) followed the same pattern for frequency of events as the other data bases, as shown in Table 4. However, the maintenance records listed many more events. While the top four components with the highest frequency of events were the same for all the data bases, the ranking was different for the maintenance data. The maintenance data base ranked I&C first; pipe, supports, and nozzles second; then valves and pumps. This indicates that many minor problems associated with I&C and pipe hangers received corrective maintenance before major failures occurred. The plant-specific data is given in Table 5 in terms of number of Corrective Maintenance (CM) requests. A subbreakdown is also given for each of the major components. The routine maintenance and miscellaneous items, which had 171 maintenance requests, included such things as changing filters and repairing cabinet hardware.

The narrative descriptions in the NPE data base were reviewed to determine if failures have occurred as a result of conditions specific to the HPIS. Several failures were reported that resulted from the charging

TABLE 3. SUMMARY OF HPIS VALVE FAILURES^a

<u>Failure Cause</u>	<u>Percent</u>
Potentially Aging Related	
Mechanical controls (Parts failed or out of adjustment)	8
Seat or disk failure	6
Packing failure	5
Pilot valve failure	3
Torque valve failure	3
Motor operator failure	3
Leaking/ruptured diaphragm	3
Normal wear	3
Seal gasket failure	2
Limit switch failure	1
Excessive wear	1
Solenoid failure	1
Corrosion	<u>1</u>
Total	40
All Other	
Command faults	32
Personnel operations	6
Personnel maintenance	4
Construction	3
Design	3
Other and unknown	<u>12</u>
Total	60

a. Data source is LERs.

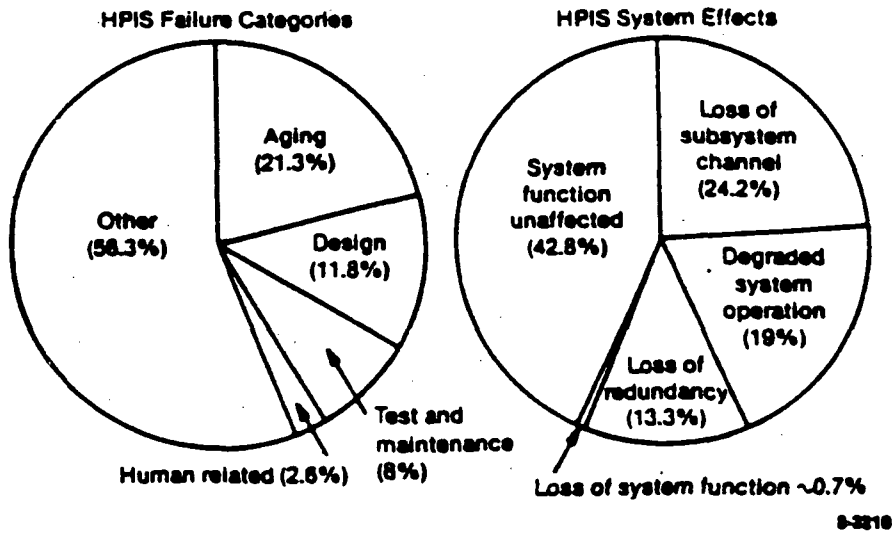


Figure 2. HPIS experience from NPRDS.

TABLE 4. DATA BASE RANKING OF MOST TROUBLESOME HPI COMPONENTS

Component	a	b	c	d
	NPE	NPRDS	IIR	CM
Valves	1	1	1	3
I&C	2	2	2	1
Pump	3	3	3	4
Pipe, supports, nozzles	4	4	4	2

- a. Nuclear power experience.
- b. Nuclear plant reliability data systems.
- c. Internal investigative report.
- d. Corrective maintenance.

TABLE 5. HPI PLANT DATA

Item	Number of CM Requests	Subbreakdown of CM Requests
Routine Maintenance (miscellaneous)	171	--
Pipe Maintenance	55	--
Flange leaks	--	(22)
Hangers	--	(17)
Pipe, penetration, orifice	--	(12)
Snubbers	--	(4)
Instrumentation	53	--
Sensors, monitors	--	(38)
Sensing line leaks	--	(15)
Valves	25	--
Mechanical problems	--	(12)
Packing replaced	--	(11)
Valve operator	--	(2)
Control Circuits, Breakers, Switches, Leads	21	--
Pumps	18	--
Vibration	--	(7)
Pump repair	--	(4)
Mechanical seals	--	(4)
HPI pump repair	--	(1)
Boron accumulation	--	(1)
Pump motor	--	(1)
Other	13	--
Pump coolers	--	(7)
Bolts	--	(3)
Gaskets	--	(3)
Total	356	--

of cold water into a hot system and from the handling of the water with a high boron concentration. The four most significant failures are discussed below.

High-pressure injection/makeup nozzles have developed through wall cracks. The cracks resulted from thermal fatigue. The thermal fatigue was caused by turbulent mixing of hot and cold coolant and thermal shock of the hot safe-end wall during normal makeup. All cracks were associated with loose thermal sleeves. Improved thermal sleeve design and increase in minimum continuous makeup flow to prevent thermal stratification have been employed for failure mitigation.

Elbows in the safety injection piping between the cold leg and the first check valve have developed through wall cracks in the heat-affected zone of the elbow weld to the safety injection piping and in the base metal of the elbow. The cracks resulted from high-cycle thermal fatigue caused by cold makeup water leaking through a closed globe valve at a pressure sufficient to open the check valve. Mitigation methods are being evaluated. Installation of a globe valve downstream of the check valve to isolate the injection line during normal make-up rather than the existing valve is being considered.

Motor Operated Valves (MOVs) and check valves have failed to operate due to boron crystallization on the valve stems, in the valve packing and in the valve body. The reason for crystallization was not always reported in the NPE and investigations may not have identified the cause. However, most causes were reported as packing leaks. The valves were usually cleaned and placed back in service. One incident reported additional heat trace was added to prevent future failures.

Injection boron concentration has been diluted from leaking valves. Leaks have been reported for both check and globe valves. Dilution of the Boron Injection Tanks (BITs) for Westinghouse plants and Safety Injection Tanks (SITs) for Combustion Engineering (CE) plants have been reported. A few dilutions have been reported for Borated Water Storage Tanks (BWSTs) and for the Babcock & Wilcox (B&W) plants. Improved monitoring of the tanks and repair of the valve seats have been implemented as mitigation measures.

AGING ASSESSMENT

The motor operated valve data from the NPRDS for Westinghouse plants had enough events (56 total) to show an aging trend as shown in Figure 3 when the data is plotted in 5-year increments. This is also shown in Table 6 along with data for check valves, manual valves and HPIS pumps. The check valves and manual valves showed no trend on aging failures. The HPIS pumps had a significant increase in the number of failures in the 10- to 14.9-year period for both aging and other causes.

The aging assessment of the HPIS involves a number of factors that include stresses, degradation mechanisms, and failure modes. A summary of

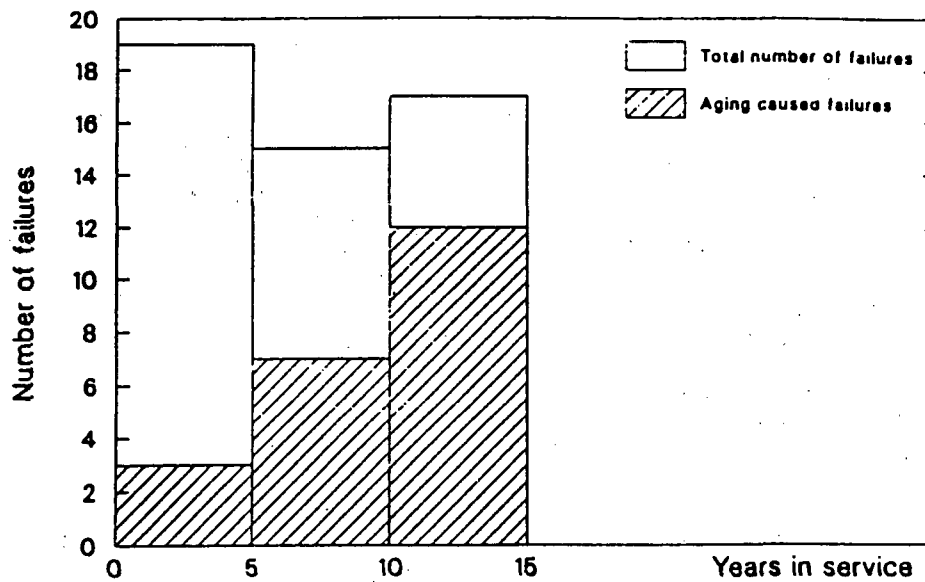


Figure 3. Failure data for HPIS motor operated valves in 5-year increments (data source in NPRDS).

TABLE 6. COMPONENT FAILURES IN 5-YEAR INCREMENTS

NPRDS Data for Older Westinghouse Plants

Component	Failure Classification	Number of Failures			Total
		0-4.9 Years	5-9.9 Years	10-14.9 Years	
MOV	Other	16	8	5	29
	Aging	3	7	12	22
	Total	19	15	17	51
CV	Other	7	4	9	20
	Aging	2	1	2	5
	Total	9	5	11	25
Manual valves	Other	3	3	3	9
	Aging	1	4	2	7
	Total	4	7	5	16
Pump (centrifugal) <500 gpm	Other	4	7	14	25
	Aging	4	4	15	23
	Total	8	11	29	48

these various factors in the aging process along with the Inservice Inspection (ISI) methods is given in Table 7.

Stressors acting on the various components contribute to the aging process. Stressors associated with maintenance, operation, and testing includes inadvertent HPIS actuation, water hammer, and thermal cycling. Environmental stresses include abnormal temperatures or pressures, incorrect water chemistry, boric acid crystals, and vibration. Electrical stresses include external environment of temperature, humidity and limited radiation, abnormal voltages and electrical transients affecting I&C. Mechanical stresses include pipe misalignment, vibration, and dynamic loading from valves closing.

Degradation mechanisms for the HPIS passive components (piping, thermal sleeves, and nozzles) include fatigue, crack initiation and propagation, and thermal embrittlement. Valves are subjected to wear, foreign material, mechanical linkage problems, and seat or disk degradation. Air-operated valves main degradation mechanism due to contaminated air supply is moisture or oil in the air. For I&C, the degradation mechanisms are loose connections, corrosion of terminals, and catastrophic component failures. Pumps degrade through wear, vibration, and fatigue.

The potential failure modes for the HPIS valves and pumps are failure to operate when needed; inadvertent operation when not called for; and, during operation, a failure to operate as required. Secondary modes would include leaks, blockage, or command faults. The piping and other passive components have failure modes of leaks, cracks, or loose parts. For I&C, the failure modes are opens, shorts, or failure to operate.

The inservice inspection methods for the HPIS components include visual inspection for leaks, volumetric inspection, and operational tests.

Materials in the HPIS susceptible to aging include seals and packing material in pumps and valves. Any carbon steel materials in other systems that are exposed to boric acid for some period of time will corrode. Electrical components in the I&C subsystem are subject to degradation of insulation, corrosion, and wear failures. The stainless steel piping aging is due to thermal stresses and fatigue. Material wear in pumps, valves, and relay contacts is a normal aging process.

INSPECTION, SURVEILLANCE, MONITORING, AND MAINTENANCE

The surveillance requirements in the technical specifications for a plant and the American Society of Mechanical Engineers (ASME) Boiler and Pressure Code comprise the testing requirements for the HPIS. Additional inspections for leaks may be performed periodically, as well as functional tests on major components if required by the utility. For example, after maintenance, functional tests may be necessary to verify operation. Monitoring consists of comparing the performance of similar channels and visual inspections for leaks in piping valves and pumps. Current maintenance practices by utilities follow the recommendations by vendors for

TABLE 7. SUMMARY OF AGING PROCESSES FOR HPIS

Major Component	Stressors	Degradation Mechanisms	Potential Failure Modes	ISI Methods
Nozzles and thermal sleeves	System operating transients, thermal cycling, vibration, water hammer	Fatigue crack initiation and propagation	Leaks through wall, loose parts	Visual inspection, volumetric inspection
Valves and valve motor operators	External environment, system operation transients, maintenance and testing	Electrical insulation and seals hardening, wear, foreign material, mechanical linkage faults, boron crystallization	Leakage, fail to operate, blockage, command faults	Visual inspection, operational and inservice tests
Air-operated valves	Systems operating transients, contaminated air supply	Sticking, blockage, fouling from water and oil in air supply	Fail to operate	Visual inspection, operational tests
I&C	External environment, electrical transients, thermal cycles, maintenance, vibration	Electrical insulation and seals hardening, corrosion, loose connections, failure (catastrophic)	Open, shorts, fail to operate	Testing
Pumps	External environment, systems operating transients, thermal cycles	Wear, vibration, fatigue	Seal leaks, fail to start, fail to run	Inservice testing, visual inspection
Pipe supports	Vibration, water hammer	Fatigue, loosening of connections	Breaking loose	Visual inspection
Piping	Vibration, water hammer, thermal cycles	Thermal fatigue, abrasive wear	Through the wall leakage or cracks	Visual inspection, volumetric inspections

major components, such as valves and pumps. The B&W plants that have experienced nozzle cracking have also indicated enhanced inspection and surveillance of the nozzle and associated piping welds.

Section XI of the ASME defines the Inservice Testing (IST) used by the plants. Pumps are tested quarterly unless a relief request is granted. For these tests vibration, differential pressure, and flow are measured. Bearing temperatures are also measured but on a less frequent schedule. Vibration is an excellent indicator of pump degradation and is a good monitor for pump aging. Periodic measurements of the electrical characteristics of the motor are not required by Section XI. A check at one plant indicated that monitoring is not done. Pump vibration and performance are not sensitive measurements for electrical insulation and other motor electrical degradation. Electrical characteristic measurements would be required to detect such aging.

Valves are tested quarterly unless a relief request has been granted. For these tests, stroke time is measured, usually without differential pressure. The measurements are often made crudely using a stop watch. Such tests would not be effective as a monitor for aging. Periodic measurement of the electrical characteristic for motor operators is not required by Section XI. For resolution of IE Bulletin 85-03 most plants are using diagnostic equipment to verify torque switch settings. Although the use of this equipment often includes electrical measurements of the operator, the tests are usually only done once for verification and are not usually repeated periodically. For valve testing to be a useful monitor for aging, more accurate measurements of stroke time and periodic measurement of electrical characteristics of the motor operator will be needed.

Section XI also defines the Inservice Inspection (ISI) for welds. Welds are to be inspected volumetrically each 10 years. The cracks in the HPI nozzles and elbows were detected by leaks not by the ultrasonic inspection of the ISI program. The ultrasonic techniques specified by Section XI were found to be inadequate to detect cracks resulting from thermal fatigue. The instrument gain had to be increased significantly and the 45-degree transducer had to be supplemented by a 60-degree shear wave transducer in order to detect the cracks. Also, one crack developed in the base metal of the elbow. Section XI only requires inspection of welds. Inspection of high-stress areas of base metal may be needed.

HPIS AGING SYSTEM UNAVAILABILITY ASSESSMENT

This aging assessment is based on the linear aging model⁴ and utilizes data from the Probabilistic Risk Assessment (PRA)⁵ for the representative plant studied and generic failure cause data on HPIS components from a composite of 9 PWR plants which were 10 years old or older.⁶ This approach is an approximate method that uses PRA results (steady state models) to evaluate aging risk. The PRA results provided the system fault trees and baseline data. The baseline data was then combined with the time

dependent failure cause data to provide the aging assessment. The software tool for this work was the Integrated Reliability and Risk Analysis System (IRRAS).⁷

The fault trees and event data from the PRA were loaded into a PC and the IRRAS program run to determine the cut-sets for the significant sequences. The outputs of the program that were used in this analysis included the probability that the HPIS fails to provide injection water when required and the risk achievement importance measure for each event. The probability that the HPIS fails to provide injection water was obtained from the cut-set quantification. The risk achievement ratio importance measure is used to identify the components which contributed significantly to unavailability of the system.

The example illustrated is for the HPIS failure to provide injection water on demand when one of three HPI pumps are required. The base case was run first using the failure data from the PRA. This base case data was assumed for the first 5-year interval.

The aging acceleration parameter was used for subsequent calculations in 5-year increments out to 40 years. Each active component in the system had an aging acceleration factor calculated for it based on the generic failure cause data for that type of component.

The equation for aging acceleration parameter "a" based on the moments considerations from Reference 4 is

$$a = \frac{4}{3} \frac{f}{1-f} \frac{\bar{\lambda}}{t}$$

where

- $\frac{4}{3}$ = constant from the deviation
- f = nonrandom fraction of failures of the component which are caused by aging mechanisms
- t = average time to failure
- $\bar{\lambda}$ = mean failure rate.

Probability calculations were then performed for 5-year increments of time using the following general equation

$$P_n = P_{n-1} + [(\Delta T)(a\tau)]$$

where

- P_n = new probability for the new 5-year increase

- P_{n-1} = probability for the previous 5-year increment
- ΔT = five years
- τ = twenty-four hours (mission time)
- a = acceleration parameter.

The full detailed procedure used for the risk assessment will be in the final report on the HPIS (Reference 1).

The calculated HPIS unavailability is plotted for the operating time period from 5 years to 40 years in Figure 4. The HPIS unavailability at 5 years was 5.59×10^{-5} and for 40 years had increased to 1.35×10^{-4} .

The risk achievement (RA) ratio was used to identify the components that contributed significantly to system unavailability. The RA is an indication of how much the HPIS unavailability goes up if the specific event was totally unreliable (failure probability equal to 1.0). The Risk Achievement Ratio is determined by evaluating the minimal cut-set upper bound (sequence frequency) with the basic event failure probability set to 1.0 and dividing it by the minimal cut-set upper bound evaluated with the basic event failure probability set to its true value. In equation form this is

$$RA = F(1)/F(x)$$

where

- RA = risk achievement ratio
- $F(1)$ = minimal cut-set upper bound (sequence frequency) evaluated with the basic event failure probability set to 1.0
- $F(x)$ = minimal cut-set upper bound (sequence frequency) evaluated with the basic event failure probability set at its true value.

The component events and their risk achievement ratios are presented in Table 8. The components associated with the events are shown in Figure 5. Only four component events are identified as contributing significantly to the unavailability of the system. These are HP-24 MOV, HP-25 MOV, HP-101 CVO and HP-102 CVO. If both valves (MOV-24 and MOV-25) fail to open, the borated water would be unavailable to the HPIS. Similarly, if both of the check valves (CV-101 and CV-102) failed, the borated water would be unavailable. These four component events were the only ones that had a RA of greater than three for the case modeled (one of three pumps required). An RA of three was considered a conservative runoff point for identifying significant components.

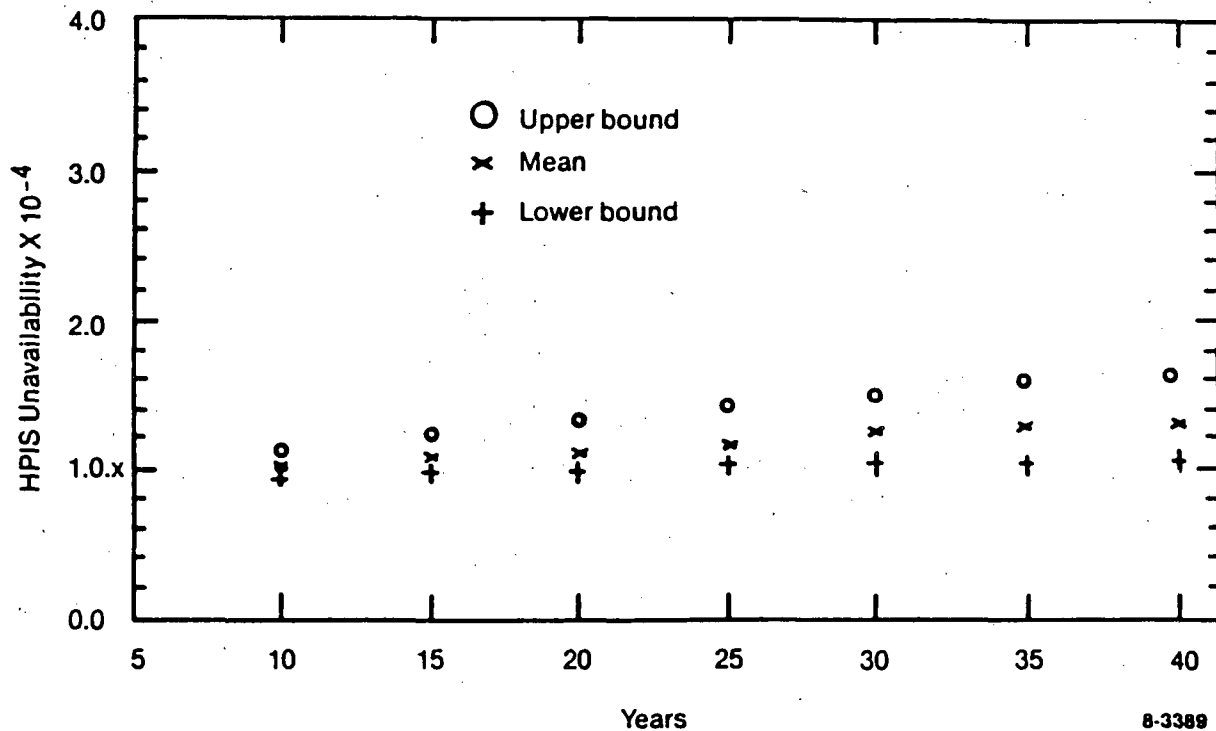


Figure 4. HPIS unavailability taking aging into account.

TABLE 8. RISK SIGNIFICANT COMPONENT EVENTS AND RISK ACHIEVEMENT RATIOS FOR HPIS (ONE OF THREE PUMPS REQUIRED) AT 5 YEARS AND 40 YEARS PLANT LIFE

Component Event	Risk Achievement Ratio	
	5 Years	40 Years
HP-24 MOV	70.9	67.0
HP-25 MOV	70.9	67.0
HP-101 CVO	71.3	67.6
HP-102 CVO	71.3	67.6

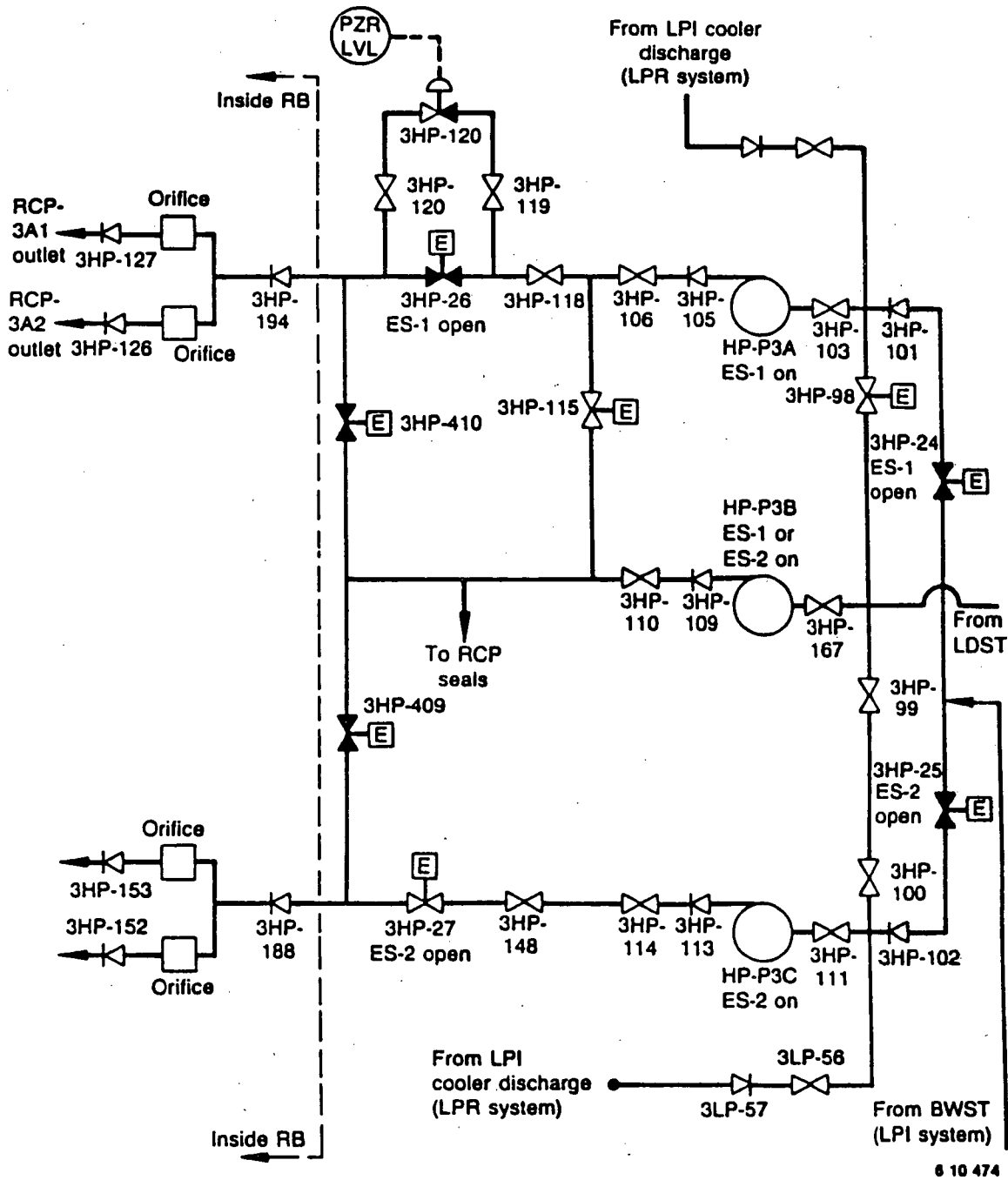


Figure 5. Part of the HPIS used during normal and emergency operations with components that contributed to system unavailability shaded.

This approach is suitable, as presented, for exploratory investigations and prioritizations of aging risk-important equipment. More advanced aging reliability models with better methods of computing "a" and which are related to aging degradation phenomenology, are needed to replace the moments method for some equipment (especially in the case of the threshold behavior).

CONCLUSIONS

The specific problems related to aging were: (a) through-wall cracks have occurred in the makeup nozzle and safety injection line elbow from thermal fatigue, (b) valves have failed to operate due to boron crystallization, and (c) injection boron concentration has been diluted from leaking valves.

An evaluation of major components identified that about 20% of report HPIS failures are related to aging. Less than 1% of reported failures caused loss of system function and valves are the component with the highest frequency of failures.

Inspection and surveillance review has identified that electrical measurements on pump motors and valve operators (for MOVs) could be used to detect aging. Also, that improved inservice testing of valves is needed to detect aging and assure operability with load. The detection of cracks caused by thermal fatigue requires enhanced ultrasonic testing methods. In addition, inspection of base metal in high-stress regions is needed to detect cracks in those areas.

The risk evaluation identified that valves contributed significantly to unavailability of the system and that aging caused little change in system unavailability.

REFERENCES

1. L. C. MEYER, Nuclear Plant-Aging Research on High-Pressure Injection Systems, NUREG/CR-4967, EGG-2514, Idaho National Engineering Laboratory (to be published).
2. Nuclear Plant Aging Research Program Plan, NUREG-1144, Rev. 1, 1987.
3. A Prioritization of Generic Safety Issues, NUREG-0933, 1983.
4. W. E. Vesely, Risk Evaluation of Aging Phenomena: The Linear Aging Reliability Model and Its Extensions, NUREG/CR-4769, May 1987.
5. Oconee PAA, A Probabilistic Risk Assessment of Oconee 3, The Nuclear Safety Analysis Center, Electric Power Research Institute Palo Alto, California and Duke Power Company, Charlotte, North Carolina, NSAC 60, Vol. 1, Vol. 2, Vol. 3, and Vol. 4, June 1984.

6. B. M. Meale and D. G. Satterwhite, An Aging Failure Survey of Light Water Reactor Safety Systems and Components, NUREG/CR-2473, Vol. 2, July 1988.
7. K. D. Russell and M. B. Sattison, Integrated Reliability and Risk Analysis Systems (IRRAS) User's Guide--Version 2.0, draft NUREG/CR-5111, EGG-2535, March 1988.

NOTICE

This paper was prepared as an account of work sponsored by an agency of the United States Government. Neither the United States Government nor any agency thereof, or any of their employees, makes any warranty, expressed or implied, or assumes any legal liability or responsibility for any third party's use, or the results of such use, or any information, apparatus, product or process disclosed in this paper, or represents that its use by such third party would not infringe privately owned rights. The views expressed in this paper are not necessarily those of the U.S. Nuclear Regulatory Commission.

SAFETY IMPLICATIONS OF DIESEL GENERATOR AGING MANAGEMENT

K. R. Hoopingarner

Pacific Northwest Laboratory^(a)
Richland, Washington 99352

ABSTRACT

Significant safety improvements can be achieved in diesel-generator management related to aging, testing, and other important regulatory concerns. This paper reports on the progress of aging research related to nuclear service diesel generators, which developed data and information supporting the recommended safety improvements.

The key to diesel-generator safety improvements is the development of a new balanced approach where testing, inspections, monitoring and trending, training, and maintenance all have appropriate importance. Safety improvement is projected in a management program that concurrently achieves three goals: first, the reduction of the fast-start stressor by regulatory and utility actions; second, the establishment of more appropriate testing and trending procedures; third, the adoption and use of reliability-centered maintenance activities. This paper describes the recommended safety improvements and the positive role of utility management in the process and outlines a new recommended regulatory approach.

Diesel generator aging and wear is the subject of research sponsored by the Nuclear Plant Aging Research (NPAR) Program under the U.S. Nuclear Regulatory Commission (NRC), Office of Nuclear Regulatory Research. The research was conducted by Pacific Northwest Laboratory (PNL), which is operated for the U.S. Department of Energy by Battelle Memorial Institute.

INTRODUCTION

Diesel generators are essential for supplying power for cooling and related emergency needs in nuclear power plants. The general size of these engines is in the range of 5,000 to 10,000 hp, or about 3,000 to 8,000 kW. Each nuclear power reactor typically has two diesel generator units.

(a) Pacific Northwest Laboratory is operated for the U.S. Department of Energy by Battelle Memorial Institute.

Diesel generators were identified as components with a high-risk significance in many generic and plant-specific studies, and as a consequence, were included in the Nuclear Plant Aging Research (NPAR) Program. This program is sponsored by the U.S. Nuclear Regulatory Commission (NRC)^(a). The objectives of the NPAR research activities were to find the causes of aging effects and propose ways of managing potential corrective actions.

Phase One Research

The diesel-generator study task was assigned to the Pacific Northwest Laboratory (PNL), and the first phase of the aging evaluation of nuclear service diesel generators has been completed. The NRC has published this evaluation in two volumes (Hoopingarner et al. 1987). The preliminary results of the first phase were presented at the Fourteenth Water Reactor Safety Information Meeting. The important failure causes were identified, and the corrective actions utilized by the utilities were presented. The safety emphasis given at this meeting is illustrated in Figure 1. This

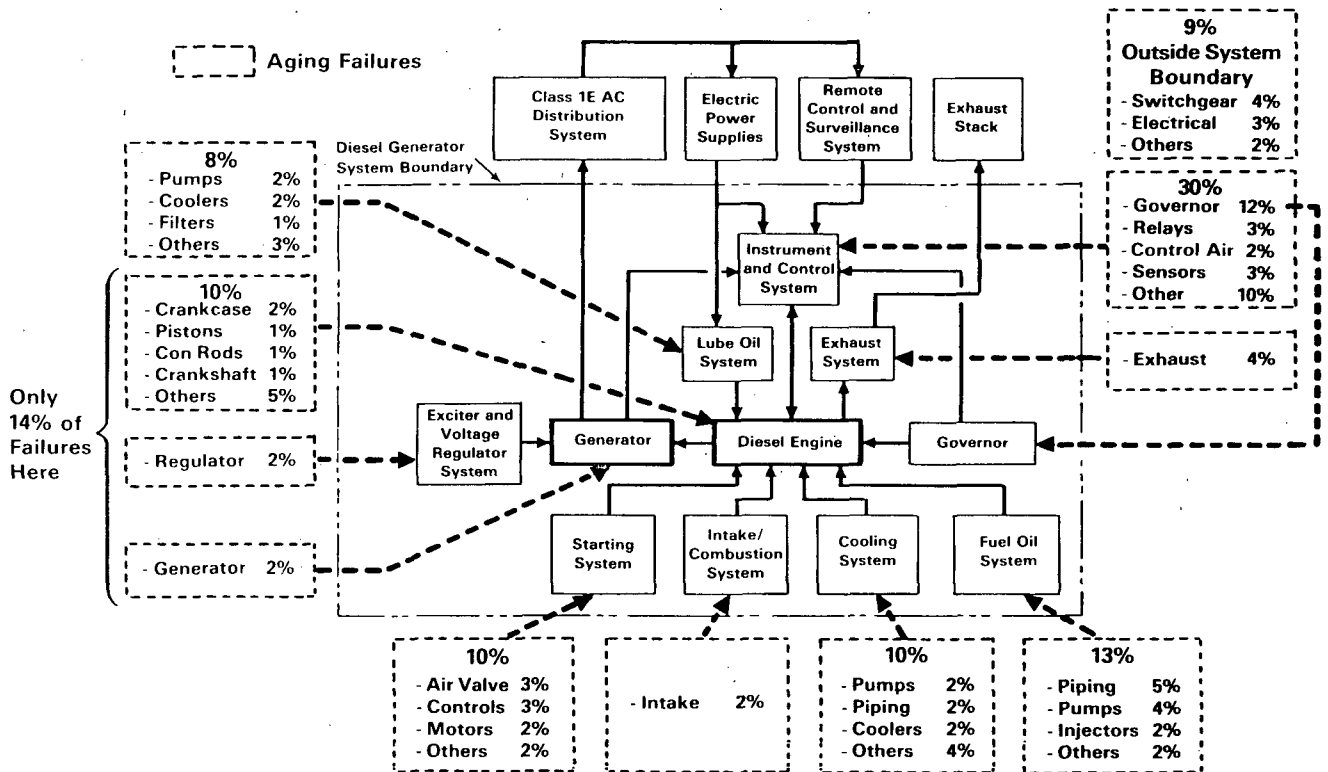


FIGURE 1. Aging Failures Associated with Systems and Components

(a) Under Contract DE-AC06-76RLO 1830, NRC FIN: 82911.

diagram shows the important diesel-generator systems and components and gives the related failure percentages for each. The key point is that the most significant safety improvement should occur when management and maintenance attention is directed to the components and systems with the higher failure rates.

Phase Two Research

The most recent work on diesel-generator testing and aging mitigation has been published by PNL as a Technical Evaluation Report (Hoopingarner et al. 1988). This second phase of the diesel-generator research is ongoing to determine why these engines appear to wear or age faster than non-nuclear service diesel engines. The data and additional information will be discussed in some detail in this paper, together with a comprehensive aging mitigation plan for diesel generators.

One important direction and emphasis of the current phase two research has been to apply the aging findings to the broader issues of "Station Blackout" (USI-A-44) and "Diesel Reliability" (GI-B-56). When aging effects are avoided or corrected, there are inevitable safety improvements related to operability, reliability, and other safety concerns. Thus, the NPAR program has developed important data and recommendations to share with utility and regulatory personnel regarding these issues.

Another emphasis of the aging research has been to address diesel-generator testing and associated aging effects. Current regulatory requirements mandate that nuclear service diesels should start in 10 to 12 seconds and be fully loaded within 45 seconds. Typically, these engines are tested at least once a month to ensure that they will indeed meet such rapid loading conditions. This testing, often identified as "fast-start" testing, has now been identified in the NPAR research as a leading cause of rapid wear, or "aging," for certain components in the diesel engines. This is not a new problem. In September 1982, the NRC staff prepared a summary of diesel-generator experience for the Advisory Committee on Reactor Safeguards recommending that a) routine test starts on a 3-day frequency should be eliminated, and b) testing should be focused on identifying unreliable diesel generators and then major repair action should be pursued, rather than just more testing (NRC 1985). The recommendations in this paper should eliminate this fast-start stressor and the associated aging and safety effects.

DIESEL-GENERATOR MANAGEMENT PROGRAM

The resolution to the station blackout issue requires the utilities to implement a diesel-generator reliability program. The proposed resolution to the generic diesel reliability issue further defines some of the reliability elements. The NPAR aging research on diesel generators generally supports the findings and resolutions proposed for these two issues. There are differences in some of the details, which is to be expected, because the NPAR

research was based upon aging and the issue research methodology was dissimilar. However, the recommended NPAR diesel-generator management program developed to address plant aging is an adequate reliability program which addresses these two issues.

Safety Issues Addressed

The diesel-generator management program, developed as part of the aging mitigation effort in the NPAR research, was intended to specifically address the following safety issues and problems:

- The statistical basis used to determine diesel-generator aging degradation and associated reliability appears to have three serious flaws: 1) changes from acceptable reliability to unacceptable reliability cannot be readily detected in time periods appropriate for regulatory, or utility, action; 2) the general ground rules for rigorous statistical analysis are not achieved, especially the need for uniform lot samples, the relationship of sample size to lot size (large number of failure causes and components), and the fact that the sampling process itself (testing) affects the analysis and the results; and 3) the false indication rate, with errors both high and low, has too large a probability for effective regulation. The cumulative probabilities of false indication, over many years, is very high.
- The program results should be predictive to help detect aging and indicate future operability and reliability with a high confidence. Incipient failures should be detected, rather than progressing to a system failure.
- The program should eliminate or reduce the fast-start stressor problem.
- The program should address failures related to unnecessary major engine overhauls. Data indicate failure rates may be increased for some period following major maintenance and overhauls.
- The issues related to station blackout and diesel reliability should be a consideration.
- Aging of fuel and lubrication oils should be addressed, as well as other common mode failures.

Recommended Program

Diesel generator management programs should incorporate the following basic program elements:

- Modified monthly testing should include a slower start and gradual engine loading with a recommended run time of about 10 hours or more.
- The monthly test goal should be to obtain the true operating condition parameters of the engine and generator system.
- Condition monitoring and trending is needed.
- Improved maintenance practice details should include adequate training, appropriate inspections, and safety-related preventative maintenance.
- Experience from non-nuclear diesel-powered stations and marine applications, as well as successful nuclear emergency power units with the better reliability records, should be considered.
- Failure correction methods and practices should find the root cause of the system failures and, to the extent practical, implement permanent repairs and avoid future engine and generator failures.
- There should be a defined central management responsibility.

The above program elements should be combined into an integrated model program. This model program is similar to the overall program and good practices already in place at many of the small non-nuclear diesel-powered units used by some electrical utilities. Regulatory overview of the diesel-generator system should focus on how a utility's submitted program conforms to the model program and on how well the utility manages the program. This approach would conform to the requirements for other nuclear plant safety-related equipment. Some of the more important elements of the management program are detailed in the following paragraphs.

Monthly Testing

The fast-start testing and loading of nuclear station diesels results in conditions found to be unique of all of the stressors found in the NPAR aging study: it was possible to eliminate this aging stressor, rather than only mitigating its effects, as is the case with all of the others. Replacing fast-start and fast-load testing with a new monitoring and trending program, including a slower engine test-start speed profile, results in many benefits. The direct benefits of a slower engine speed profile include significantly less piston ring and cylinder wear, reduced harmful overspeeds for the turbocharger and the generator, less valve camshaft and bearing wear, and less threat of an engine trip due to the initial and unavoidable overspeed with the fast-start speed ramp.

Aging and reliability concerns were reviewed by diesel experts who were familiar with the data, information, and proposed recommendations. They

were requested to evaluate the safety assurance of fast-start testing compared to slow-start testing to ensure that all important safety questions were addressed. The experts concluded that the recommended slower starts adequately tested all major components.

Monthly testing provisions should include modifications of hardware, technical specifications, and procedures to support the ability to start with a slower speed ramp designed to obtain synchronous speed in about 30 seconds. A prelube process is desirable before routine test starts. Two minutes at full operating oil pressure, is recommended. Test operation should be permitted at synchronous speed without loading for 2 to 5 minutes, while oil pressure and other important engine conditions are checked. It is recommended that operations at a reduced idle speed for the same purpose should be permitted.

Assuming synchronous speed and no observable faults, the test program should encourage gradual engine loading over a 5- to 30-minute period. Step loads representing actual site motor loads are useful but not essential for monthly testing.

Recommended testing procedures require reasonably stable engine test conditions, a minimum of 3 sets of data, and about one hour between data sets. There are about 50 parameters of interest for condition monitoring, collecting 3 data sets will result in approximately 150 data points for each evaluation test period. Hoopingarner et al. (1988) gives more information and a complete listing of these test parameters. Table 1 is a sample of these test parameters for the engine cooling water.

TABLE 1. Sample of Monthly Test Parameters

Engine Cooling Water	Requirements	
	Required	Optional
Water pressure to engine	X	
Water temperature to and from engine	X	
Water pressure to and from engine water cooler	X	
Water temperature to and from engine water cooler (could be radiator)	X	
Water pressure to and from raw water cooler	X	
Water temperature to and from raw water cooler	X	
Water pressure to and from turbocharger		X
Water temperature to and from turbocharger	X	
Water pressure to and from turbocharger after cooler	X	
Water temperature to and from turbocharger after cooler	X	
Water pressure and temperature to and from L.O. cooler	X	
Jacket water pump pressure (to and from)		X

Monitoring and trending evaluation procedures require an immediate data review to ensure that all tests parameters are within the operational, or normal, range. If not, corrective maintenance should be scheduled. Long-range trending analysis may be done later. Such trending should be completed on a periodic basis, but not longer than quarterly to ensure that adequate safety margins exist. Engine loads should be gradually reduced at the end of the monthly tests period and terminated at about 25% load or at the manufacturer's recommended level. Post-operational lubrication is recommended, applicable manufacturer's guidelines should be followed. Optional fast-starts, overload tests, and additional stops and starts may be performed on a warm and well-lubricated engine with much less aging and wear effects. These additional tests should be reserved for the plant outage periods, which occur on approximately an annual basis.

Condition Monitoring and Trending

For improved safety the diesel-generator monitoring and trending program should detect many potential failures in incipient states before the component or system actually fails.

The recommended program of testing, monitoring and trending is a forward-looking process, which gives very good assurance of future system operability. Such a program, often called "condition monitoring," was recommended by the diesel experts consulted during the NPAR aging study.

A conditioning monitoring and trending program should be designed to evaluate monthly about 50 diesel engine parameters. These recommended parameters are defined in Hoopingarner et al. (1988, Appendix A). They are essentially the important pressures and temperatures of the oil, water, and the intake and exhaust subsystems. These parameters should be compared to normal and safe operating range values for each of the 50 data points recommended. At the end of the monthly test, assuming all parameters are in the normal range, near-term diesel-generator operability may be predicted. Deviations from normal indicate that maintenance should be scheduled. Longer-term operability trends may be predicted by trending and plotting the data over long-time periods. Estimates of when certain data points will no longer be within the normal operating range will indicate when future maintenance or engine overhaul should be scheduled.

Recommended Maintenance Improvements

The first maintenance improvement recommended for increased safety purposes and aging mitigation is to avoid teardown of the engines for inspection purposes only. Various studies have shown that periodic engine disassembly without specific failure correction needs have an overall adverse influence on the system failure rate (Prichard 1984). The decision to overhaul an engine should be based on an evaluation of the monitoring and trending data. A healthy engine, as determined by the new recommended test program, should

not be disassembled. The data support the conclusion that failures and associated safety risks are definitely not improved by periodic overhaul of a well-running engine.

Improved diesel-generator maintenance should not be viewed as individual items for correction, but rather as one overall maintenance program. The NPAR data and information developed point to general improvements needed to reduce aging and increase reliability in parts of the overall maintenance process. Improved assurance of engine reliability is obtained if maintenance is directed to 1) repair defects and obvious failures, 2) perform recommended engine service and inspections without engine disassembly, and 3) perform maintenance to correct components identified by the monitoring and trending program.

Training levels and maintenance management practices vary among the licensees, but a need for improvement in specific areas was noted in the NPAR research. The most important safety benefits related to training need to be addressed. To avoid maintenance-induced aging problems, PNL has recommended that engine and governor maintenance training be improved. Operator training to overcome failure-to-start and -run problems and to show how to manually start the engines is also perceived as a need. The ability to manually start the engines by bypassing a failed component, such as a control system or air start valve, is a significant safety benefit for station blackout considerations.

At least two persons should be given maintenance training equivalent to that offered by the diesel engine and governor manufacturers. Such persons should be at the plant maintenance/engineering level and could then help train others. The systems, components, and stressors most likely to be involved in diesel generator aging and failures have been identified in the research on aging. Additional training on those items with the higher failure percentages, such as the instrument and control system and the governor, should give the best results.

Another maintenance point is that normal engine vibrations have a severe influence on the control-system instruments and calibration. Vibration was the diesel generator stressor found in the PNL research to cause the highest percentage of failures. It is recommended that engine preventive maintenance should be increased to mitigate the aging and wear results of this vibration, and that the preventive maintenance efforts should emphasize engine and engine-skid-mounted instruments. The aging research has developed information related to vibration and the other important stressors and the corresponding inspections and preventative maintenance items which should be the most effective (Hoopingarner et al. 1988).

Experience from non-nuclear diesel powered applications was factored into the recommendations presented to the NRC on maintenance, inspections, operations, and testing practices. This overall perspective is important in recommending better practices with corresponding safety improvements. A final maintenance observation is that proposed failure corrections need to be

carefully evaluated to ensure that in each case the true cause is known and is being fixed, rather than a repair of a symptom of the real problem. This requires a good management approach and the willingness to invest the resources necessary to operate a good diesel-generator program as outlined in this paper.

REGULATORY CONSIDERATIONS

The NPAR aging study was intended to develop data and recommendations for NRC consideration related to potential safety problems caused by the aging process. The general application was not foreseen for use of the diesel research information for diesel reliability improvements, plant technical specification modifications, improved resource application by the NRC and the utilities, and specific recommendations to change some regulatory requirements. All of these end uses of the research have been accomplished or are under active consideration. Collectively, the safety implications of all of these changes and recommendations are important.

Current requirements for fast-start testing, fast engine loading, and overload testing need to be reconsidered. In association with certain nuclear plant technical specifications, these requirements may lead to greater future safety problems and unreliability. Requirements for routine testing should define slow-start testing, slower engine loading, and diesel overload testing objectives that can be supported by the study results.

The plant standard technical specifications related to the diesel-generator system should be modified to add to safety assurance. The research information confirms opinions developed by industry and regulatory personnel over many years of experience that current technical specifications are not always conservative nor effective. In particular, those related to fast engine starting and loading, frequent sensor calibration, engine startup during abnormal plant conditions, frequent starts and special test requirements need to be carefully evaluated. This process has been started.

After consideration of the study data, nuclear regulatory guide documents addressing diesel-generator requirements should be withdrawn, combined into a new single guide document or modified as appropriate.

Diesel statistical probabilities, especially statistics based on 100 valid start and run tests, are very difficult to defend on a technical basis due to the very long time period needed to collect the data (maybe 5 years). A better regulatory approach is a monthly operational readiness test ("health checkup") of the diesel generator system as outlined in this paper.

SUMMARY

There are significant positive safety implications if diesel generator management is improved and diesel generator operational readiness is assured.

Under the new management approach recommended, licensees would be required to have an approved diesel generator program which would represent a balanced approach where testing, inspections, monitoring and trending, training, and maintenance all have appropriate importance. The regulatory overview should not be prescriptive, but rather should compare the licensees overall program against an acceptable program made up of the elements outlined and recommended in this paper.

REFERENCES

1. Hoopingarner, K. R., J. W. Vause, D. A. Dingee and J. F. Nesbitt. 1987. Aging of Nuclear Station Diesel Generators: Evaluation of Operating and Expert Experience. Volumes 1 and 2. NUREG/CR-4590, PNL-5832, prepared by Pacific Northwest Laboratory for the U.S. Regulatory Commission, Washington, D.C.
2. Hoopingarner, K. R., B. J. Kirkwood, and P. J. Louzecky. 1988. Study Group Review of Nuclear Service Diesel Generator Testing and Aging Mitigation. PNL-6287, Pacific Northwest Laboratory, Richland, Washington 99352.
3. Nuclear Regulatory Commission (NRC). 1985. Safety Evaluation by the Office of Nuclear Reactor Regulation, Related to Amendment No. 48 to Facility Operating License No. NPF-7, Virginia Electric and Power Company, Old Dominion Electric Cooperative, North Anna Power Station, Unit No. 2, Docket No. 50-339. Nuclear Regulatory Commission, Washington, D.C.
4. Prichard, J. W. 1984. Equipment Age-Reliability Analysis. Naval Engineers Journal, pp. 65-70.

AGING ASSESSMENT OF PWR AUXILIARY FEEDWATER SYSTEMS

D. A. Casada

Oak Ridge National Laboratory
Oak Ridge, Tennessee

Abstract

In support of the Nuclear Regulatory Commission's Nuclear Plant Aging Research (NPAR) Program, Oak Ridge National Laboratory is conducting a review of Pressurized Water Reactor Auxiliary Feedwater Systems. Two of the objectives of the NPAR Program are to identify failure modes and causes and identify methods to detect and track degradation. In Phase I of the Auxiliary Feedwater System study, a detailed review of system design and operating and surveillance practices at a reference plant is being conducted to determine failure modes and to provide an indication of the ability of current monitoring methods to detect system degradation. The extent to which current practices are contributing to aging and service wear related degradation is also being assessed. This paper provides a description of the study approach, examples of results, and some interim observations and conclusions.

I. Introduction

The Nuclear Regulatory Commission's Nuclear Plant Aging Research (NPAR) program was initiated to ensure that aging and service wear related degradation of nuclear power plant systems and components could be understood, recognized, and effectively mitigated. Oak Ridge National Laboratory (ORNL) is presently conducting a study of Pressurized Water Reactor Auxiliary Feedwater (AFW) Systems in support of the NPAR program. This paper describes the methodology that is being utilized in the ORNL review of AFW Systems, gives examples of results achieved to date, and identifies some interim conclusions that may be drawn from the results.

II. AFW System Functions

A typical AFW System for a four loop plant is shown in Figure 1. In reality, there is no such thing as a "typical" AFW System, due to variations resulting from a number of factors, including different steam generator numbers and configurations, evolving regulatory requirements, and designer preferences. There are, however, some common design functions which are supported by the AFW System.

"The submitted manuscript has been authored by a contractor of the U.S. Government under contract No. DE-AC05-84OR21400. Accordingly, the U.S. Government retains a nonexclusive, royalty-free license to publish or reproduce the published form of this contribution, or allow others to do so, for U.S. Government purposes."

The AFW System is a safety related system that is used for heat removal from the Reactor Coolant System (RCS) by delivering water to the Steam Generators. The AFW System is required to operate following a number of anticipated transients and design basis accidents, including loss of normal feedwater, feedwater line break, small break loss of coolant accident, steam generator tube rupture, station blackout, and others. The AFW System is depended upon, in conjunction with main steam line safety valves and main steam line power operated relief valves or atmospheric dump valves, to provide sufficient heat removal to allow the RCS to be initially stabilized in hot standby conditions and then subsequently cooled and depressurized to hot shutdown conditions where the Residual Heat Removal System can be placed into service.

In addition to providing for heat removal from the RCS, the AFW System must also be capable, either automatically, or with operator assistance, of isolating a faulted or ruptured steam generator. This capability is required to ensure that (1) adequate flow can be delivered to intact steam generators, (2) containment overpressurization or overheating does not occur due to continuing steam release, and (3) the steam generators do not overflow.

Another postaccident function of the AFW System is to provide a liquid barrier between any potential steam generator tube leakage and the environment by maintaining steam generator water level above the top of the steam generator tubes. The liquid barrier ensures that iodine in the fluid leaking from the primary to the secondary side will be "scrubbed" prior to release. In the calculation of radioactive release rates, an iodine decontamination or partitioning factor of 0.01 is typically applied when accounting for releases through main steam line safety or relief valves.

In addition to the posttransient and accident functions, the AFW System is often used in support of normal plant start-up and shutdown evolutions. The reason that the AFW System is often used instead of the main feedwater system during these periods is that at zero or very low power levels, operation of the main feedwater system is difficult due to the fact that flow rate demands are extremely low relative to feedwater pump capability.

It should be noted that some plants have nonsafety related start-up feedwater pumps that are normally used in the support of plant start-up and shutdown. In such cases, the AFW System is frequently referred to as the Emergency Feedwater System, and would normally be operated only for testing or in response to an automatic demand.

III. Study Methodology

A. Background

AFW Systems, as well as other engineered safety features systems, are designed to withstand the most deleterious single failure. The design basis accident analyses, which are performed to secure and maintain operating licenses, must demonstrate that unacceptable consequences do not result even if

the most limiting single failure (normally the failure of an entire train of all engineered safety features systems) occurs concurrently.

One of the key aspects of the assumptions related to the single failure criterion is that all failures which would degrade a system must be detectable. IEEE-379 observes that "The detectability of failures is implicit in the application of the single failure criterion." The Standard provides the following "generic statement" about the single failure criterion:

"The system shall be capable of performing the protective actions required to accomplish a protective function in the presence of any single detectable failure within the system concurrent with all identifiable, but nondetectable failures, all failures occurring as a result of the single failure, and all failures which would be caused by the design basis event requiring the protective function."

Two notable events of recent years in which the AFW systems played vital roles, the Davis-Besse loss of main and auxiliary feedwater and the San Onofre loss of power and water hammer, involved *multiple* failures that were common mode in nature, and resulted in conditions outside of analyzed bounds. Operator actions, including actions outside of the control room in the Davis-Besse episode, were required to reestablish AFW flow to the steam generators. Many of the failures in these two events were preexistent, and could have been detected. While there are many lessons to be learned from these and other events, one clear lesson is that the continuing validity of the single failure criterion and design basis licensing analyses are directly and heavily dependent upon the adequacy of the testing and maintenance programs.

B. General Approach

The approach that is being used at ORNL in the AFW System study is the relatively simple principle that degradation or failure that is detected can and will be corrected. Of course the converse of this principle is that degradation or failure that is not detected will, in all likelihood, not be corrected.

In order to assess the extent to which current utility practices are able to detect degradation or failure within the AFW System, ORNL is reviewing the AFW System design, operating, maintenance, and testing program for a plant owned by a cooperating utility. While it is recognized that there are a broad range of AFW System designs, as well as operational support programs, it is felt that a detailed review of a specific plant's programs can provide some valuable insights into the ability of current industry practices, on a generic basis, to detect degradation or failure.

C. Scope

Each of the major components that must function properly in order for the AFW System, as a whole, to operate as required is being reviewed. The components being reviewed include not only those that are part of the AFW System proper, but also interfacing system components that directly support the AFW System function. The interfacing components include steam generator blowdown

isolation valves, main feedwater isolation valves, main steam line safety valves, main steam line power operated relief valves, alternate pump suction source isolation valves, AFW turbine steam supply valves, as well as the instrumentation and controls associated with the reviewed components.

Each component's required function is first established based upon the system design basis functional requirements. The failure modes for each of the components are then identified, based upon the functional requirements. It should be noted that the established failure modes are only those which would result in substantial train degradation or train failure. As an example, a valve packing or bonnet leak would not comprise a failure, but failure to reposition upon demand would.

With the failure modes established, operating, surveillance, and maintenance practices associated with each component are reviewed to determine the extent to which degradation or failure mechanisms that are related to each failure mode are detectable. This portion of the review also assesses, qualitatively, the relative impact that testing itself would have upon component aging and service wear.

IV. Example Component: Trip and Throttle Valve

As noted earlier, each of the major AFW System components is being assessed as a part of the system review. One of the key components that is present in most plants' AFW systems is the turbine Trip and Throttle (T&T) valve. In order to illustrate the review process, a description of and some review observations relative to the T&T valve are provided. The description and discussion presented here are specifically applicable to the reference plant being reviewed by ORNL in the AFW System study. It should be recognized that many of the design features are generic, while others are plant specific.

A. T&T Valve Description and Functions

The T&T Valve is a 3-inch globe valve with a 125 VDC motor operator. As its name implies, the T&T valve can be used for control purposes, by throttling, or it can be used as a fast trip device to protect against turbine overspeed.

The T&T valve at the reference plant is normally closed. It opens in response to a number of signals, including:

- Safety Injection
- Low-Low Level in 2/4 Steam Generators
- Emergency Bus Undervoltage
- Loss of Main Feedwater Pumps
- Manual Start Signal

The first three of the above signals are safety related automatic start signals. The loss of main feedwater pump start signal is also automatic, however, a portion of the channel is nonsafety grade.

The T&T valve also trips to provide turbine overspeed protection. The tripping function is accomplished by an unlatching of the valve from its motor operator. Valve closure following the unlatching is accomplished by the combined forces from a yoke spring and the weight of the valve. Valve closure and sealing is also provided by the valve flow path orientation (steam entry is above the seat, and exhaust is below the seat).

T&T valve tripping is initiated when an overspeed condition is sensed by either an electronic speed monitor or a mechanical speed sensor. The nominal setpoints for these trips are 4300 RPM for the electronic overspeed, and 4900 for the mechanical overspeed. Normal operating speed is 3970 RPM.

The electronic overspeed trip is actuated by energization of a solenoid which unlatches the valve from its operator. Following an electronic overspeed trip, the valve motor automatically drives to the shut position, thereby relatching the valve and the operator. Once the motor and valve are relatched, the valve can be reopened, and in fact, will automatically reopen if a start signal is still present.

The mechanical overspeed trip is initiated when turbine speed is sufficient to activate a triggering device (based upon centrifugal force associated with the turbine speed) which operates mechanical trip linkage. This trip linkage ultimately unlatches the valve from its operator in the same manner as the solenoid action. However, when a mechanical overspeed occurs, local operator attention is required in order to reset the mechanical trip linkage at the turbine before the T&T valve can be reopened.

In addition to the automatic open and trip functions for the T&T valve, the reference plant design includes an automatic steam supply transfer function which requires T&T valve action. Normally, only one steam generator is aligned to supply steam to the turbine. In the event that the turbine driven pump does not achieve a designated discharge pressure within a specified time period following the opening of the T&T valve, an automatic sequence is initiated to transfer the turbine steam supply from the normal steam generator to an alternate steam generator. This automatic function is included in the design as a means of assuring that the turbine driven pump can be driven by an intact steam source, even if the normal steam supply source is not able to drive the turbine (for instance, in the case of a broken feed or steam line). A turbine driven pump start in which the automatic transfer is required is designed to proceed as follows:

- T&T valve opens (in response to automatic start signal)
- T&T valve stem actuated limit switch starts a timer. (Note that if required discharge pressure is reached prior to the time the timer cycle is completed, the remainder of the sequence will not occur.)
- T&T valve closes
- Normal steam supply valve closes
- Alternate steam supply valve opens
- T&T valve reopens

Each of the steps in this sequence must be complete before the succeeding step is initiated. The sequence minimizes the possibility of depressurizing two steam generators.

The T&T valve motor operator is also provided with thermal overload protection. By design, the overload switches are bypassed on any automatic start signal. The torque switch in the valve opening circuit is entirely bypassed for all strokes, including manual initiated opening, and the valve opening is halted by an open limit switch. The torque switch in the closed direction is bypassed except for the final 2% to 3% of stroke.

T&T valve stem limit switches provide control and indication inputs to several support functions associated with the AFW system:

- Enable the ramping function of the governor valve control circuit
- Provide a start signal to the turbine driven pump room ventilation fan
- Start the timer for the automatic steam supply transfer circuit
- Enable the automatic closure feature for the valve's motor operator in the event of an overspeed trip
- Provide close signal Steam Generator Blowdown isolation valves
- Provide a permissive signal to allow opening of the alternate pump suction source isolation valves in the event of low suction pressure
- Provide local and main control board indication of valve position

B. T&T Valve Manual Controls and Indication

The T&T Valve is provided with the following remote and local manual controls:

- Main Control Board (MCB) valve control handswitch which can be used to open or close the T&T valve.
- MCB valve trip pushbutton. Depressing the pushbutton has the same effect as an electronic overspeed trip.
- Transfer switch located at a local control panel. This switch allows transfer of T&T valve control to local. It should be noted that with the control transferred to local, all of the valve automatic open functions, as well as the electronic overspeed trip, are blocked.
- Pushbuttons at local control panel. There are pushbuttons to open, close, stop, and trip the T&T valve. The "stop" pushbutton can be used to interrupt valve stroking at any point in the open or close stroke, thereby allowing the valve to be used in its throttling/control function. Note that these pushbuttons are only enabled if control has been transferred to the local control panel by use of the transfer switch.

The following indication and alarms are provided for the T&T Valve:

- Valve position indicating lights at MCB and local control panel
- MCB Annunciator for electronic overspeed trip
- MCB Annunciator for mechanical overspeed trip
- Plant process monitoring computer indicates: T&T Valve open; No power to T&T Valve; No power to speed control

C. T&T Valve Failure Modes

Generic failure modes for motor-operated valves would include failure to open, failure to close, and failure to operate as required. For purposes of the AFW System study, the designated failure modes are more specific, and are based upon the individual component functional requirements. Based upon the functional requirements of the T&T valve, the following failure modes were designated:

<u>Failure Mode</u>	<u>Description</u>
1	Valve operator fails to open in response to an automatic AFW turbine driven pump start signal.
2	Valve operator fails to complete the close-open strokes in response to automatic steam supply transfer signal (i.e., fails to close or fails to reopen).
3	Valve electronic overspeed trip function fails to trip the valve before the mechanical overspeed trip occurs, thereby requiring local resetting (and preventing automatic restart).
4	Valve fails to open sufficiently to allow adequate flow.
5	Valve stem operated switches fail to provide input signals to other AFW related equipment or functions.

A few characteristics of these failure modes are worth mentioning. First of all, it should be clear that there could be multiple failure causes or sources for each of the failure modes. For example, for Failure Mode 1, the valve operator could fail to open due to a corroded set of contacts, a preexisting unlatched valve/operator condition, a ground in the motor windings, a faulty limit switch, or a multitude of other reasons. (Of course, each of these failure causes or sources would have their own set of causal factors.)

Secondly, these failure modes, as well as the nondetectable failures which will be discussed later, are specific to the reference plant. While it is felt that the failure modes and nondetectable failures provide some valuable insights, it must be recognized that these are not necessarily generic. For example, while the reference plant opens the normally closed T&T valve to start the turbine driven pump, other plants have the T&T valve normally open, and start the turbine driven pump by opening upstream isolation valves. For such plants, failure of the T&T valve to open in response to automatic start signals would clearly not be a failure mode.

A final observation about the identified failure modes is that the number of failure modes could be increased or decreased, depending upon individual preference. For example, Failure Modes 1 and 2 could be combined into a single failure mode that might read "Valve operator fails to open or close in response to an automatic signal." Alternatively, Failure Mode 2 might be broken down into two failure modes--failure to close for the steam supply transfer and

failure to reopen for the steam supply transfer. The critical factor is that all mechanisms that could prevent the valve from accomplishing its required functions must be addressed.

D. Surveillance Practices

There are four tests which are used to demonstrate operability of the T&T valve. The T&T valve is stroked by a number of other tests; however, those tests are not used to demonstrate operability of the T&T valve, but rather that other components are operable.

Test A, which is performed on an 18-month (refueling) frequency, is intended to verify that the T&T valve opens in response to each automatic open signal. The test does, in fact, verify that the T&T valve opens for all signals except for the emergency bus undervoltage signal. The test allows jumpering of either of two sets of contacts (the set is selected at operator discretion) that close in response to undervoltage conditions on the associated emergency bus. There is no other testing which verifies that the contacts do indeed close for undervoltage conditions.

Test B, which is performed primarily on a quarterly basis, meets the requirements of ASME Section XI valve testing by measuring valve stroke times. Consistency between remote indication and actual valve position is verified every two years.

Test C, which records response time data in conjunction with the valve stroking that occurs in Test A, is used to determine the overall turbine driven pump response time.

Test D, a calibration procedure which is primarily oriented toward the turbine governor valve, is performed on an 18-month frequency. This test verifies that operation of the mechanical trip linkage, by use of a trip lever located at the turbine, interrupts power to the valve operator, and that power is restored when the mechanical trip linkage is reset. The test also verifies the stroke length of the T&T valve and the proper setting of a stem actuated limit switch which enables a ramping function for the governor valve. The electronic overspeed trip setpoint is checked by use of a speed input signal simulator (note that the turbine is not running for this test).

Based upon a review of procedures that are used to demonstrate operability of the T&T valve, as well as other procedures which would result in operation of the valve, it is estimated that the T&T valve receives approximately 50 full strokes (where a full stroke involves opening and then closing the valve) per year. In some cases, the valve is stroked a number of times (estimated to be as many as 11 for Test A) in the conduct of a single procedure. It should be noted that precautions are included in some of the test procedures, as well as a general operating procedure that DC motor operated valves should not be continuously stroked for more than five minutes (where continuous stroking would be a stroke in either direction followed by a stroke in the opposite direction within one minute).

E. Nondetectable Failure Examples

After reviewing the T&T valve design and functional requirements and establishing failure modes based upon these requirements, a thorough review of the test procedures which implement the associated Technical Specification Surveillance Requirements, along with a review of pertinent operating and maintenance procedures was conducted. The procedures review indicated that there are a number of potential sources of failure or degradation which could exist and not be detected by current practices. As an example, four failure sources that could affect the first two of the above identified Failure Modes, and that would not be detected by current practices, are presented below.

<u>Potential Failure Source</u>	<u>Description</u>
A*	The thermal overload settings are improper.
B*	The bypassing of the thermal overload switches on automatic start signals does not occur.
C	The T&T valve does not open in response to emergency bus undervoltage conditions.
D	The automatic steam supply transfer sequence fails.

* If either the thermal overload settings or the thermal overload bypassing was verified as part of a plant procedure, adequate protection would be afforded. As it turns out, neither is checked.

Potential Failure Sources A, B, and C represent degradations which are pertinent to Failure Mode 1, "Valve operator fails to open in response to an automatic AFW turbine driven pump start signal." Potential Failure Sources A, B, and D represent potential degradation or failure sources which are pertinent to Failure Mode 2, "Valve operator fails to complete the close-open strokes in response to automatic steam supply transfer signal (i.e., fails to close or fails to reopen)."

There are some important points that should be made about these four non-detectable potential sources of failure. First, some of the potential failure sources represent only one part, or one type of part, while others represent a large number, and broad spectrum of parts. Potential Failure Sources B and D provide contrasts that are useful for illustrating this point.

Potential Failure Source B involves only two similar sets of contacts that are not checked. The contacts could fail due to any of several failure *mechanisms*, including sticking open or corroded contact surfaces, but only the single part is involved.

On the other hand, Potential Failure Source D represents a large number, and diverse spectrum of parts, ranging from limit switch contacts to the T&T valve motor. Some of the parts associated with Failure Source D, for instance the limit

switch contacts, are not checked. For other parts, such as the valve motor, which is verified to stroke open properly in periodic testing, the conditions associated with a steam supply transfer demand are more severe than the test conditions due to multiple valve strokes (for example, the motor supply cable would experience cumulative heating due to sequential valve stroking, thereby increasing resistance and reducing the voltage available at the motor, increasing the probability of motor failure).

Secondly, it is noteworthy that the potential failure sources include situations where only the T&T valve is involved as well as situations where multiple components or system interactions are involved. For instance, in Potential Failure Sources A and B, only the T&T valve is involved, while in the cases of Potential Failure Sources C and D, component and system interactions are involved. However, in all four cases, an undetected failure could exist which would prevent the T&T valve from operating as required, which in turn would prevent the turbine driven pump train from performing as required.

A third point is that while a potential failure source may apply to more than one failure mode, it does not necessarily apply equally. Note that Potential Failure Source A applies to both Failure Modes 1 and 2. However, in relation to Failure Mode 1, the T&T valve must only stroke open for a normal turbine driven pump start. But in relation to Failure Mode 2, the valve must initially stroke open, and then close and reopen for the steam supply transfer sequence. Failure due to degraded thermal overloads would be more likely for Failure Mode 2 than for Failure Mode 1.

Finally, it should be recognized that all four items represent conditions which could be overcome by local operator intervention, or possibly by remote operator action (see Section B, "T&T Valve Manual Controls and Indication"). Lack of knowledge of exactly why the T&T valve failed to open automatically following an emergency bus undervoltage condition, for example, would not prevent the operator from recognizing that the valve was not open (from MCB indication) and then opening the valve from the MCB, the local control panel, or by use of the valve handwheel.

V. Current Status of Work on Other Components

The AFW System Assessment is ongoing. The design, operating, and testing practices of many of the relevant components have been at least partially reviewed. The attached Table 1 provides a status of review for each of the components.

VI. Interim Observations and Conclusions

There are several tentative observations that can be drawn from the AFW System Study, based upon work completed to date.

1. There are potential degradation and failure sources for many of the components reviewed which would not be detectable by current practices. The examples cited above for the T&T valve are primarily related to instrumentation and control (I&C) circuitry. While it is too early to draw firm conclusions, it appears that many (more than half) of the potential failure sources that are not detectable by current practices

are related to I&C circuitry (as opposed to mechanical and hydraulic type degradation or failure, such as degradation of pump hydraulic capability).

2. Many of the potential failures sources which would not be detectable involve multicomponent or system boundary interactions, where testing of individual components does not adequately indicate system condition.
3. Most potential failure sources that are not detectable by current practices could be detected with little or no additional testing, from the standpoint of number or duration of tests.
4. Based upon the review to date, for some of the components the extent of testing is excessive to the point that the testing itself is a major contributor to aging and service wear-related degradation.

It can be tentatively concluded, therefore, that the quality of existing testing programs for the AFW System can be enhanced, while at the same time, the overall quantity of testing can be reduced.

Table 1. Review status of AFW components

<u>Component</u>	<u>Status of Review*</u>
Motor Driven Pumps	C
Turbine Driven Pump	P
Alternate Suction Source Valves	C
Steam Generator Level Control Valves	C
Pump Suction Check Valves	C
Pump Discharge Check Valves	C
Miniflow Check Valves	C
Other Check Valves	P
Turbine Steam Supply Valves	C
Turbine Trip And Throttle Valve	C
Turbine Governor Valve	P
Feedwater Isolation Valves	C
Feedwater Isolation Check Valves	C
Steam Generator Safety Valves	P
Steam Generator Power Operated Relief Valves	P
Steam Generator Blowdown Valves	C

*C - Review substantially complete.

P - Review partially complete.

PRAAGE-1988: An Interactive IBM-PC Code for Aging Analysis
of NUREG-1150 Systems

R.R. Fullwood and W.G. Shier
Brookhaven National Laboratory
Upton NY, 11973

ABSTRACT

Probabilistic Risk Assessments (PRA) contain a great deal of information for estimating the risk of a nuclear power plant but do not consider aging. PRAAGE (PRA+AGE) is an interactive, IBM-PC code for processing PRA-developed system models using non-aged failure rate data in conjunction with user-supplied time-dependent nuclear plant experience component failure rate data to determine the effects of component aging on a system's reliability as well as providing the age-dependent importances of various generic components. This paper describes the structure, use and application of PRAAGE to the aging analysis of the Peach Bottom 2 RHR system in the LPCI and SDC modes of operation.

1. Introduction

Aging, as it is used in this report, refers to the end-of-life region of the wearout curve (mortality curve) in which the probability of failure is no longer characterized by a constant failure rate but is increasing with time. The report Higgins, 1988, discussed in some detail the mathematical modeling of the wearout process and its approximation as a linear increase in the failure rate with time. The theory of linear aging was presented in Vesely, 1987, as being the result of Poisson-distributed assaults on a component until it finally fails. This assault model predicts a failure rate that linearly increases with time starting when the component is new. Higgins, 1988, using nuclear power plant experience data, showed that certain classes of components such as pumps and valves do not show such a simple dependence but characterization as two connected linear dependencies is required. The first segment is a constant failure rate, i.e., the failure rate is independent of time; the second segment is a continuation of the first but with a discontinuity in slope after which the failure rate linearly increases with time. Both the rate of increase and the location in time at which the break occurs are characteristic of the component.

System aging is the sum of failure rates of its components for each time step only in the special case of non-redundant systems. If a system is redundant, it ages at a rate that is the train aging rate raised to the power of the redundancy. For example, a system composed of three redundant trains each of which ages at a rate of 10%/year, will have a system aging rate of 30%/year. (This system effect is discussed further in Higgins, 1988). Because systems, not individual components, protect the public safety, aging analysis should be performed in a system context.

The first major modeling of two nuclear power plant, their systems and components to determine their risk and the reliability of the safety systems was WASH-1400. This was followed by further PRA methods development, PRA applications to regulatory issues and PRAs for many power plants. (Fullwood and Hall, 1988 provides a review of PRA development in this period.) A major

development in improving the quality of PRAs is the NUREG-1150 study for the analysis of which, PRAAGE-1988 is designed.

The Reactor Risk Reference Document, NUREG-1150 provides the results of major risk analyses to five different US plants (Surry, Zion, Sequoyah, Peach Bottom and Grand Gulf) using state-of-the-art methods. This work provides a data base and insights to be used for a number of regulatory applications: 1) Implementation of the NRC Severe Accident Policy Statement, 2) implementation of NRC Safety Goal Policy, 3) consideration of the NRC Backfit Rule, 4) evaluation and possible revision of regulations or regulatory requirements for emergency preparedness, plant siting, and equipment qualification, and 5) establishment of risk-oriented priorities for allocating agency resources.

The work presented here is a further application of the NUREG-1150 work by applying these system models to the investigation of aging in the residual heat removal system (RHR) at Peach Bottom -the oldest of the plants analyzed in NUREG-1150. Because of the quality of the PRA work in the NUREG-1150 models, one of the ground rules for the work presented here was to accept the PRA system models without modification in the form of system cutsets (Fullwood and Hall, 1988). The PRA system models are described in NUREG/CR-4450 and were provided to us along with the probability data by the Sandia National Laboratory. This information was transferred to a floppy disk for use in an IBM-PC and constituted the default data to be replaced by nuclear power plant experience data showing aging effects when obtainable from a companion study, Lofaro 1988 included in these papers.

Higgins, 1988 used an early version of PRAAGE (called PRAAGE-1987) for modeling the CCW system at Indian Point based on the Indian Point Probabilistic Safety Study (IPPSS). PRAAGE-1987 took advantage of certain symmetries in the cutsets to implement them in a unique, compact matrix format. While this worked well for this particular case, the method is not generally applicable and a major thrust of PRAAGE-1988 was a code that could operate directly with cutset input.

The organization of this paper is the introduction, just presented, the next section describes the design criteria for PRAAGE-1988. Section 3 presents structure of PRAAGE, section 4 describes how to use the code and section 5 presents results from its application to the RHR system in the LPCI and SDC modes of operation.

2. Design Criteria for PRAAGE

PRAAGE-1988 was designed on the bases of the experience with PRAAGE-1987 to include additional enhancements for current aging work. The principal criteria were:

- Perform an accurate analysis of the affects of aging of the Peach Bottom RHR system,
- Accept aging data in the bilinear form found to be necessary as reported in Higgins, 1988,
- Include any test and maintenance models that are developed in the data modeling,

- Be easily converted to analyzing the aging of other systems for which cutset and data block information are available. Easy convertability is taken to mean that it can be done in a few hours or less.
- Minimize the manual inputting of data,
- Be operable on all grades of IBM and compatible personal computers using the MDOS operating system with a disk drive and graphics adapter.
- User friendliness by instructing the operator and providing default values which the operator may choose to modify.
- Perform the calculations rapidly enough that the operation may be considered interactive. The current longest computation time is 30 seconds in which the unreliability, normalization and all the necessary importance information is calculated.
- Perform generic groupings of components. This is needed because component specific data are not available and such a large number of components is difficult to manipulate and interpret. Presently PRAAGE is dimensioned for 20 generic components. Generic components may be grouped by any ANDing and/or ORing of the four-element component name identifiers. The search mask for generic component construction is constructed in this fashion to assist the operator and avoid the possibility of typographical errors which would result in no component selection. PRAAGE assumes that the operator will select the generic components of present concern but that these selection may not include all components. Those components omitted are grouped as a "residual" generic component and treated the same as those specifically identified i.e. subjected to the aging and T&M models as will probability modification as a group.
- Allow individual component probability modifications.
- Record the parameters used in an aging analysis and the results,
- Print numerical and textual results,
- Provide graphical displays and printed output.

All of these criteria were met with the exception of test and maintenance modeling (T&M). This is a very complex problem because the aging data obtained from nuclear power plant experience reflects the effects of the T&M that is performed on each component in each plant. To introduce an explicit T&M model into PRAAGE would require that the effects of T&M be removed from the data and a generic T&M model be developed and applied in the system model.

Other limitations in current PRAAGE (which may be circumvented if need be) are:

- PRAAGE-1988 operates in the small probability approximation. This means that it will not calculate accurate results if probabilities are set to "1" as is commonly done to simulate a component outage. (This feature was provided in PRAAGE-1987 but was not used in PRAAGE-1988 for reasons of calculational simplification. Its inclusion would increase the code complexity and running times.)

- The data input to the cutsets are probabilities - not failure rates. If a component is modeled as failing during a mission time, the failure rate must be multiplied separately by the mission time. (PRAAGE-1987 identified and accepted both types of data and performed the necessary multiplication when needed. It will probably be necessary to modify the data representation if the T&M module is implemented.)

- The maximum problem sizes used to data sizes are 701 cutsets, 134 components, 20 generic components, and six time steps but the ultimate limitations have not been explored. It is likely that if overlay techniques are used in the code that much larger problems can be analyzed.

3. Structure of the Code

Figure 1 shows the computational flow that takes place in PRAAGE. The basic input information is obtained by down-loading a data block and the cutset

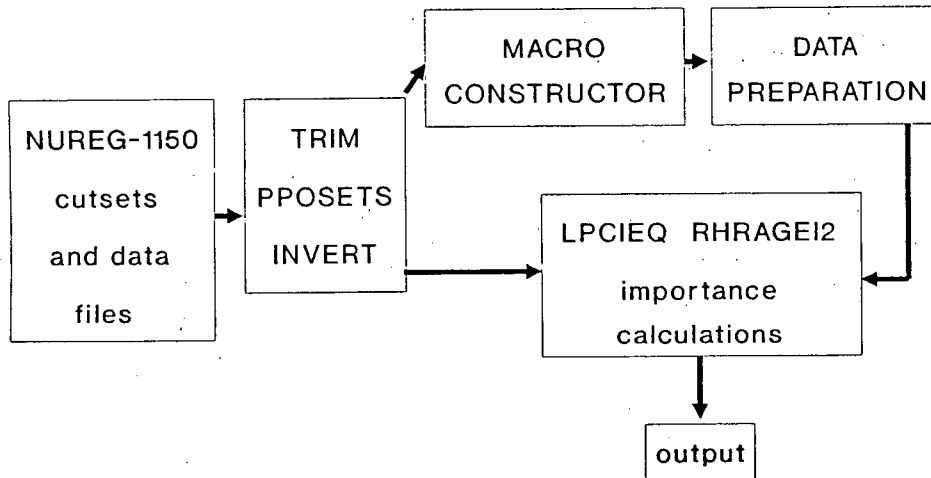


Figure 1
Computational Flows in PRAAGE

results from a SETS (Worell, 1985) code analyses of the fault trees representing the RHR mode being studied. The data block contains probability data (not failure rate) for 384 components. The 4 configurations of the RHR system are: LPCI, SDC, RHR and CSS. This work studied LPCI, which has 494 cutsets using 127 components and SDC which has 701 cutsets involving 134 components. Since memory requirements are a paramount concern in personal computer programming, the extraneous data is removed by the independent preprocessing code TRIM.

The new data block containing only data for the components in the cutset block being processed are stored on floppy disk to provide the input to PPOSETSI (Post Processor of SETS, Indexed). PPOSETSI converts the component names and

the component probabilities into indexed variables, $p[i,1]^1$, and $nam(i)$, respectively, for array processing. Beginning with the name of the first selected component, PPOSETSI looks at each component name in each cutset. If a match is detected, the cutset is modified by replacing the 16 character name with $p[i,j]$. This process continues until the whole equation block has been converted into a form using indexed variables. PPOSETSI goes a step further and decomposes the original cutset block which is one long equation into many separate equations - one for each cutset. This transformation is performed automatically to produce programming in the Pascal language. These many new equations are stored on floppy disk for reading into LPCIEQ which does the processing of the equations. In this sense PPOSETSI is a program that actually writes some of the Pascal programming language used in the LPCIEQ computer program.

PPOSETSI is followed by INVERT which takes the cutset file with the components identified by number and determines the cutsets in which a component appears. The results of this is to provide a directory to LPCIEQ for the grouping of cutset values to form the importances.

The cutset transfer to LPCIEQ is done in a very unusual fashion. The equations cannot be read in as string variables because these are programming instructions for LPCIEQ. The manner of entry is to read them into the LPCIEQ program as a block transfer in the editor mode. Further discussion of LPCIEQ will be deferred until completion of the discussion of the macro construction and data preparation.

The macro constructor code (MCROCON1) groups similar components for common treatment. A component name in the NUREG-1150 format is made up of 4 elements or subnames. These four subnames for the component respectively represent the system it is in, the dominant failure cause, the dominant failure mode and a unique identification for the component. MCROCON1 requests a name for the generic component and then lets the operator construct the generic component by ANDing and ORing the contents of each selected column. When the operator indicates completion, all components not selected for one of the generic groups are placed in the "residual" group. This is a fairly lengthy selection process, not to be frequently repeated, so the generic component groupings thereby constructed are saved to disk where they can be reused without having to repeat the generic grouping process. MCROCON1 also offers a simpler assembly process by selecting on first subname which is the system identification. There is good physical reason for the use of system groupings but it is also faster than individually tailoring the groupings and was very convenient for code development.

This menu also provides for a printout of generic component groupings but this is actually the compressed file used for generic component storage and transfer and is not easy to understand. So far, there has been no reason to make it more user-friendly but it is retained for its usefulness in code diagnostics. The first number indicates the number of components, next the number of generic

¹ The "i" index is the component designator; the second, "j" index, is the time designator for use in the aging analysis. Since PPOSETSI sets up the component probabilities for the components when new, the time index is set to "1".

components, then by the number of components in each group, by the component identifying numbers in each group and finally by the names of the generic components. If the first column construction method of generic component construction is selected, the name of the generic component is the same as the search mask.

This generic component code is passed to the data preparation code (DATAPREP) which allows the modification of the probability of failure at startup time ($t = 0$, $j = 1$) for each of the components by directly changing the values. The operator may modify the failure probabilities of all of the components in a group by the multiplication of their values by a common multiplier. (A common multiplier produces a proportional change even if the absolute value of each component probability is different). The parameters for each aging model are specified by the analyst in an interactive process. When aging model preparation is selected, the analyst is requested to select a generic component for aging model preparation. Then the analyst is requested to input the time at which aging starts followed by the aging slope in percent per year. This process is repeated until all generic components subject to aging have had their model specified. If no aging model is specified, it is assumed there is no aging (the aging slope is set to zero).

After the aging models have been specified, they are not automatically applied to the time zero probabilities but the analyst is required to order their incorporation. This is done to allow the analyst a last opportunity to modify the data. However to perform the aging analysis, the models must be implemented which results in the construction of the component failure probabilities for each time step. (The time steps are 0, 2, 5, 10, 20, and 50 and cannot presently be changed by the analyst without recompiling the code). These time dependent failure rates may be stored on floppy disk for use by LPCIEQ.

LPCIEQ may retrieve the time-dependent probability data as well as the generic component descriptor data from floppy disk or LPCIEQ may access the data from memory. If the latter is the case, it is necessary precede the running of RHRAGE by selecting and running MCROCON1 and DATAPREP.

LPCIEQ is rather slow starting (requiring about 30 seconds) because the code is calculating all 494 or 701 cutset equations involving 127 or 134 components for six aging times and executing a complex assembly process to construct the Birnbaum and Inspection importances. Upon completion, the remaining operations are very fast because the code is only grouping importances for the individual components into the generic component groupings and performing the necessary computations for the importance measure selected. When the calculation is complete, the results are automatically displayed. The results can be displayed, printed, graphed or saved to disk. The graphs may also be reproduced on a dot matrix printer.

4. Using PRAAGE-1988

Table 1 lists the present contents of the PRAAGE-1988 distribution disk. It is written in Turbo Pascal 4.0 (TP4 by Borland International). This code is considerably different from Turbo Pascal 3.0 which was the language used for PRAAGE87 as reported in Higgins, 1988. A major change in the codes was in discontinuing chaining and overlays in favor of "units". This is done by setting up an executive code, PRAAGE2.exe with a "uses" statement that names

Table 1
List of Codes Comprising the PRAAGE Ensemble
RHR/SDC Mode

Name	Size (kilobytes)	Purpose
PRAAGE2.exe	132608	Main program calling units
MAINTITL.tpu	1664	Global data file
MCROCON1.tpu	12736	Performs generic groupings
DATAPREP.tpu	21456	Data edit, aging and T&M
LPCIEQ.tpu	70608	Computes the cutset equations
RHRAGEI2.tpu	21600	Importance assembly and graph
GENCOMP1	660	Generic component identification
INVBLOK.pas	8491	Inverse file
NAM1PREP.PAS	104	First column component name
NAM2PREP.PAS	121	Second column component name
NAM3PREP.PAS	133	Third column component name
NAM4PREP.PAS	715	Fourth column component name
NAMBLOK	2093	Full component names
DATBLOK	3939	Default time zero data
AGEPDAT1	21802	Aging data file
BANNER.exe	47840	Title and synopsis
PRAAGE.bat	43	Calls BANNER and PRAAGE2

the "units" that it uses. Units can also use other units. These are compiled codes designated as "TPU" for Turbo Pascal Unit that contain a public section declaring variables and subroutines accessible to programs that have the units name in the uses statement. When the disk is loaded, the user simply types "PRAAGE". This calls PRAAGE.bat - a batch file which calls "BANNER.exe". This displays a full screen sign stating "Brookhaven National Laboratory presents PRAAGE - PRA applied to Aging" which is followed by a synopsis of the code. On a key press, the main program, PRAAGE2.EXE, is called. It calls MAINTITL.tpu to present a default problem title and request for identification of the default path and drive. With this information, it presents the main menu shown as Figure 2. These tasks may be performed in any order but if they are performed out of sequence, they use results stored from previous runs. If it is an entirely new

```

MAIN MENU
Select the Tasks to be performed for:
the NUREG-1150 Peachbottom RHR/SDC Aging Study
=====
1  Define the Generic component Groupings
2  Modify Individual or Generic component Groups,
    Aging and Test and Maintenance Models
3  Compute, Display, Print and Graph Age Dependent
    System Unavailability and Generic Component
    Importances
4  Quit

Select the Number of the Task to be Performed

```

Figure 2
The Main PRAAGE-1988 Menu

Generic Component Menu

- ```
=====
```
- 1: Construct Generic Component Grouping
  - 2: Construct Grouping from First Column of Component Id.
  - 3: Record the Constructed Groupings
  - 4: Print the Constructed Groupings
  - 5: Leave the Generic Component Construction

Select the Number Identifying Your Job

Figure 3  
Generic Component Construction Menu

problem, they must be run in sequence. If task 1 is selected, the menu shown in Figure 3 will be presented. Only the first 2 tasks are actually used in generic component definition. By far the most versatile is selection 1. If this is selected, PRAAGE asks for a name for the generic component which may contain 12 characters. Then the Figure 4 menu is presented in which a dialogue takes

```
Construction of a Generic Component (x1x-x2x-x3x-x4x)

What component i.d. position do you want to key on?
1
1 ACP, 2 CSS, 3 DCP, 4 DACTA, 5 DACTB, 6 DACTC, 7 DACTD,
8 ECW, 9 EHV, 10 ESF, 11 ESW, 12 HSW, 13 IAS, 14 LCI,
15 RBC, 16 RHR, 17 SDC, 18 LOSP,
Select part of the Generic Component Mask
1
You selected,"ACP", is that correct? (Y/N)
Do you wish to "and" this with another identifier? (Y/N)
```

Figure 4  
Menu for Forming a Generic component by ANDing and ORing

place between the analyst and the code. To understand the meaning refer to Figure 5 showing typical names for the components in the model. As stated earlier, the first column is the system designator, the second column is the cause, third, the mode and the last column is the unique identifier. In the dialogue shown, the analyst indicated to key on the first subnames. Then PRAAGE displayed all of the first subname designators and the operator selected "1" from this list. PRAAGE responded by saying that ACP (AC power) was selected and asking if this is correct. When the operator replied "Y" for yes, PRAAGE asked the operator if he wished to AND this with another designator. When the operator said "N" (no), PRAAGE displayed the information shown in Figure 6. After the display, PRAAGE asked the analyst if he wanted to OR the designator with something. If he said yes, then he could perform further ANDing operations to construct a composite mask using these logical operations. In this case, the operator said no and PRAAGE asked if another generic component is to be constructed. If he had said yes the whole process would have been repeated starting with a name for the generic component. Since no was designated, the construction process was ended. But note only a few components were included

ACP-PHN-LP-ESWG  
 ACP-TAC-LP-EDG1  
 ACP-TAC-LP-EDG2  
 ACP-TAC-LP-EDG3  
 ACP-TAC-LP-EDG4  
 CSS-MOV-MA-MV26A  
 DCP-BAT-LP-A2  
 DCP-BAT-LP-B2  
 DCP-BAT-LP-C2  
 DCP-BAT-LP-C3  
 DCP-BAT-LP-D2  
 DCP-BAT-LP-D3  
 DCP-INV-LP-24C  
 DCP-INV-LP-24D  
 DCP-PHN-LP-BATR  
 DCP-REC-LP-2  
 DCP-REC-LP-4  
 DGACTA  
 DGACTB  
 DGACTC

Figure 5  
Four Subname Component Naming Used in NUREG-1150

Construction of a Generic Component (x1x-x2x-x3x-x4x)

-----  
 What component i.d. position do you want to key on?

1

1 ACP, 2 CSS, 3 DCP, 4 DGACTA, 5 DGACTB, 6 DGACTC, 7 DGACTD,  
 8 ECW, 9 EHV, 10 ESF, 11 ESW, 12 HSW, 13 IAS, 14 LCI,  
 15 RBC, 16 RHR, 17 SDC, 18 LOSP,

Select part of the Generic Component Mask

1

You selected, "ACP", is that correct? (Y/N)

Do you wish to "and" this with another identifier? (Y/N)

-----Generic Name: acp Consists of:-----

Components selected are: 1 ACP-PHN-LP-ESWG

Components selected are: 2 ACP-TAC-LP-EDG1

Components selected are: 3 ACP-TAC-LP-EDG2

Components selected are: 4 ACP-TAC-LP-EDG3

Components selected are: 5 ACP-TAC-LP-EDG4

Components selected are: 135 ACP-BAC-LP-416A

Components selected are: 136 ACP-BAC-LP-416B

Components selected are: 137 ACP-BAC-LP-416C

Components selected are: 138 ACP-BAC-LP-416D

No. of acp items selected: 9

Do you want to "OR" with other selections as the same generic component (Y/N)

Do you want to construct another generic component? (Y/N)

Figure 6  
 Display of the Components Selected by the First Subname,  
 First Designator Mask

in the generic components defined. To avoid losing information, PRAAGE assigns the remaining components to a generic component called "Residual" so the minimum number of generic components is two.

If the operator had selected 2 in the generic menu, the screen would blink and state that the first column construction (i.e. system groupings) is complete.

In the laborious process of building the generic components by AND and OR groupings, the operator will probably want to save these definitions on disk. This is done by selecting item 3 in the generic component menu (Figure 3). If item 4 is selected (print the generic groupings), a rather cryptic printout results. The first number is the number of components, the second number is the number of generic components, The next number-of-generic component lines provide the decoding of the following string listing the numbers of the individual numbers of the components in the groups. This is followed by the names of the generic components that have been assigned.

Leaving the menu is executed by selecting "4" from the generic menu which returns to the main menu (Figure 2). Following the sequence, the operator selects "2" to modify the component probability data. The purpose of this menu (shown in Figure 7) is not just to edit data, inject the aging or T&M but it also

#### Individual and Generic Component Modification Menu

=====

- 1: Modify Components in Generic Component Groupings
- 2: Modify Individual Component Probabilities in PRA Order
- 3: Modify and Prepare the Aging Models
- 4: Modify and Prepare the Test and Maintenance Models
- 5: Implement Aging into the Probabilities
- 6: Implement Test and Maintenance into the Probabilities
- 7: Record the Time Dependent Probability Data Base
- 8: Display the Time Dependent Probability Data Base
- 9: Print the Time Dependent Probability Data Base
- 10: Leave the Component Modification

Figure 7  
Data Modification and Aging Model Menu

creates the remaining probabilities for the time steps. If this is not done RHRAGE will fail. If task 1 is selected, the editing is convenient by dealing with the components according to the generic component definitions. This results in the menu shown in Figure 8 being displayed. This lists the names of the generic components what were previously constructed. The operator can change selected generic components change in whatever order he chooses or if most of them will be changed, he can select "C" for cycle and it will cycle through the names thereby obviating the need for designating individual names. When a name is selected, the menu in Figure 9 is displayed showing not only the component name but also the current probability value. If the operator chooses to change these as a group, he enters a multiplier (positive but may be greater or less than one) and PRAAGE responds with a new menu displaying the effects of the operator's modification. If the change is wrong, it can be corrected by

The Generic Component Names Are:

```
=====
1 ACP 2 CSS 3 DCP
4 DGA 5 ECW 6 EHV
7 ESF 8 ESW 9 HSW
10 IAS 11 LCI 12 RBC
13 RHR 14 SDC 15 LOS
```

Select Number of Individual Generic Component for Change  
Or Type "C" to Cycle Or Type Q to Quit

Figure 8

List of Generic Component Names for Selecting Data Modification

Generic Component No.1 named ACP Is Composed Of:

```
=====
1 ACP-PHN-LP-ESWG 1.0E-0002;
2 ACP-TAC-LP-EDG1 2.2E-0002;
3 ACP-TAC-LP-EDG2 2.2E-0002;
4 ACP-TAC-LP-EDG3 2.2E-0002;
5 ACP-TAC-LP-EDG4 2.2E-0002;
135 ACP-BAC-LP-416A 1.1E-0005;
136 ACP-BAC-LP-416B 1.1E-0005;
137 ACP-BAC-LP-416C 1.1E-0005;
138 ACP-BAC-LP-416D 1.1E-0005;
```

Select # and Enter New Probability in "E" or 0.xx Format or "G"  
for Generic Multiplier, "Q" to Quit, or "N" for Next Cycle

Figure 9

Component Names Contained within a Generic Grouping

The Analyst Selects the Number of a Component whose Value is to be Changed

multiplying by the reciprocal of the previous change.

If it is necessary to change a probability value within a generic grouping, the operator may select "2" from the data modification menu and a listing of components by number, name and probability value is presented (not shown). From this, the operator selects the number of the component for modification. If this is done, PRAAGE repeats the old value and requests a new value in real format as shown in the menu. If a typo such as a letter is typed, a notice is displayed to retype the number. If integer format is used, no warning is displayed and no change is made. Then the values of the un-aged probabilities are as desired, PRAAGE returns to the main data modification menu and the operator designates task 3 to inject the aging models.

This results in the menu shown in Figure 10 being displayed (this Figure is the composite of considerable dialogue) and the operator is asked to designate a generic component for age modeling. In this case the operator chose item 1 and PRAAGE answered back that ACP was selected and asked for confirmation. PRAAGE then asks for the time that aging begins. The operator responds in real

format and PRAAGE repeats the entry so the operator can check it. PRAAGE then asks for the slope of the aging ramp in fractional (not percent) change per year in real format. The operator responds and PRAAGE repeats the response and asks the operator if another aging model is to be constructed for some other generic component. If the answer is no PRAAGE returns to the main data modification menu.

When PRAAGE is finished, undoubtedly, the operator will want to enter a T&M model but since this has not been done it will not be discussed.

Before leaving the data modification menu, it is essential that aging be

The Generic Component Names Are:

=====

|        |        |        |
|--------|--------|--------|
| 1 ACP  | 2 CSS  | 3 DCP  |
| 4 DGA  | 5 ECW  | 6 EHV  |
| 7 ESF  | 8 ESW  | 9 HSW  |
| 10 IAS | 11 LCI | 12 RBC |
| 13 RHR | 14 SDC | 15 LOS |

Select a Generic Component for Age Modeling Or Type Q to Quit

1

You Selected No. 1 named ACP

When Does the Aging Ramp Begin? (years from startup, x.x)

5.0

What is the Slope of the Ramp? (fraction/year, x.x)

0.1

You Specified Start 5.0E+0000 and Slope 1.0E-0001

Do You Want to Prepare Another Model?

Figure 10  
Implementing an Aging Model

implemented into the failure probability data to cause construction of all but the time zero probabilities which come from the data base as modified by the analyst. This is done by selecting tasks 5 and/or 6 in the main data modification menu. If task 7 is selected, the time dependent probability data will be saved to disk under a name of the operator's selection or a default name may be used.

If the operator wishes to see the data that will be used in RHRAGE, he selects task 8 and a printout results as sample of which is shown in Figure 11.

After the printout and return to the main data modification menu, the operator selects "9", returns to the main menu and selects "3" to go to RHRAGE for the importance calculations. After some preliminary questions the main importance menu is presented (Figure 12). Seven importance measures are displayed for selection. (Percent unavailability contribution per component as done in PRAAGE-1988 is not implemented.) In this figure, the analyst selected "2" for the Inspection Importance. Nearly immediately (since the individual importances were precalculated) the importances are displayed as shown in Figure 14. If the operator decides to print out the results, task 8 is selected from the main importance menu. If plotting is desired, task 9 is selected to result

The Age Dependent Probabilities Are:

| Prob. No./Initially | 2nd Year  | 5th Year  | 10th Year | 20th Year | 50th Year |           |
|---------------------|-----------|-----------|-----------|-----------|-----------|-----------|
| 1                   | 1.0E-0002 | 1.0E-0002 | 1.0E-0002 | 1.5E-0002 | 2.5E-0002 | 5.5E-0002 |
| 2                   | 2.2E-0002 | 2.2E-0002 | 2.2E-0002 | 3.3E-0002 | 5.5E-0002 | 1.2E-0001 |
| 3                   | 2.2E-0002 | 2.2E-0002 | 2.2E-0002 | 3.3E-0002 | 5.5E-0002 | 1.2E-0001 |
| 4                   | 2.2E-0002 | 2.2E-0002 | 2.2E-0002 | 3.3E-0002 | 5.5E-0002 | 1.2E-0001 |
| 5                   | 2.2E-0002 | 2.2E-0002 | 2.2E-0002 | 3.3E-0002 | 5.5E-0002 | 1.2E-0001 |
| 6                   | 8.0E-0004 | 8.0E-0004 | 8.0E-0004 | 8.0E-0004 | 8.0E-0004 | 8.0E-0004 |
| 7                   | 1.3E-0003 | 1.3E-0003 | 1.3E-0003 | 1.3E-0003 | 1.3E-0003 | 1.3E-0003 |
| 8                   | 1.3E-0003 | 1.3E-0003 | 1.3E-0003 | 1.3E-0003 | 1.3E-0003 | 1.3E-0003 |
| 9                   | 1.3E-0003 | 1.3E-0003 | 1.3E-0003 | 1.3E-0003 | 1.3E-0003 | 1.3E-0003 |
| 10                  | 1.3E-0003 | 1.3E-0003 | 1.3E-0003 | 1.3E-0003 | 1.3E-0003 | 1.3E-0003 |
| 11                  | 1.3E-0003 | 1.3E-0003 | 1.3E-0003 | 1.3E-0003 | 1.3E-0003 | 1.3E-0003 |
| 12                  | 1.3E-0003 | 1.3E-0003 | 1.3E-0003 | 1.3E-0003 | 1.3E-0003 | 1.3E-0003 |
| 13                  | 1.3E-0002 | 1.3E-0002 | 1.3E-0002 | 1.3E-0002 | 1.3E-0002 | 1.3E-0002 |
| 14                  | 1.3E-0002 | 1.3E-0002 | 1.3E-0002 | 1.3E-0002 | 1.3E-0002 | 1.3E-0002 |
| 15                  | 2.7E-0001 | 2.7E-0001 | 2.7E-0001 | 2.7E-0001 | 2.7E-0001 | 2.7E-0001 |

Press key for next page

Figure 11  
Time Dependent Probabilities after Aging Implementation

Select Importance Measures for:  
the NUREG-1150 Peachbottom LPCI Aging Study

```

=====
1 Birnbaum Importance
2 Inspection Importance
3 Percent Unavailability Contribution
4 Unavailability Budget Contribution
5 Vesely-Fussell Importance
6 Risk Achievement Worth Increment
7 Risk Reduction Worth Increment
8 Print Selection
9 Plot Part of Selection
10 Print Component Unavailability Fract.
11 Quit Menu

```

Figure 12  
Importance Measures Selection Menu

in a display such as shown in Figure 13. No provision for saving the results to disk has been made because the input data necessary for recalculation has been saved.

5. Description of the RHR System in the LPCI and SDC Modes

The function of the SDC mode of RHR is to remove decay heat during accidents in which the reactor vessel integrity is maintained. The RHR system is a two-loop system consisting of motor-operated valves (MOV) and electric motor driven pumps (Figure 14). There are two pump/heat exchanger trains per loop, with each pump rated at 10,000 gpm at a head of 20 psid. Cooling water is taken from the wetwell and flows through the heat exchanger for recirculation in the

reactor vessel in the SDC mode. In the LPCI mode, water is taken from the reactor vessel and flows through the heat exchangers for recirculation in the reactor vessel. These two systems are fault tree analyzed in NUREG/CR-4450 but these fault trees are not exhibited because of space limitations in this paper.

Some modeling assumptions that were employed in the fault tree preparation are:

- 1) SDC system failure from misaligned valves is neglected.
- 2) The fault tree considers components being out of service for maintenance. This is only considered to be possible if there is double blockage for high pressure piping and single blockage for low pressure piping.
- 3) Pump isolation due to spurious faults is neglected.
- 4) The control circuitry is not modeled in detail.
- 5) The pumps are assumed to fail when the suppression pool reaches saturated conditions.
- 6) Failure due to a test-diverting flow is neglected because this mode is manually initiated and aligned.
- 7) A suction path must be available from either the suppression pool or the reactor vessel path to start a pump.
- 8) Failure of the suppression pool from random failure plugging of the strainers is neglected.

#### 6. Using Nuclear Power Experience Data in the RHR Aging Investigation

After PRAAGE-1988 was working, it was tested by comparing its calculations with the same problem calculated by the SETS code for the system reliability which is the only parameter that both codes calculate. The agreement was extremely good. This was not surprising because both code work in the small probability approximation.

The next investigation was a study of the prioritization of components in the SDC and LPCI modes using the probability data from NUREG/CR-4450. (This was done before the BNL data investigation for the Peach Bottom RHR had been completed). Results from this are shown in Table 2. It will be noted that the dominant contributor to unavailability is the emergency service water system which may be regarded as external to the RHR. Table 3 is an examination of the LPCI with the effect of the supporting systems removed to exhibit the percent contributions to unavailability of components specific to the RHR in the LPCI mode. Table 4 shows a similar calculation for the SDC mode. Lofaro et al. (in these proceedings) compiled nuclear plant experience data to determine the aging rate as well as new non-aging failure frequencies. These are shown in Table 5. This results in the aging of the generic components as shown in Figure 13 and in the RHR system reliability aging (LPCI mode) shown in Figure 15.

Table 2  
Component Importances: LPCI Mode using PRA Data

| <u>System/Component</u>                | <u>Percent of Unavailability</u> |
|----------------------------------------|----------------------------------|
| ESW System:all modes                   | 53%                              |
| Pressure/Level Sensors: miscalibration | 18                               |
| MOVs: failure to transfer              | 7.9                              |
| MOVs: out for maintenance              | 5.0                              |
| Pressure Sensor: loss of function      | 4.1                              |
| Ventilation System: all modes          | 3.9                              |
| Diesel generators: failure to start    | 1.3                              |
| AC Power: all modes                    | 0.9                              |
| Level Sensor: loss of function         | 0.4                              |
| Pipe Segment Fault                     | 0.3                              |

Table 3  
LPCI Mode Component Importance using PRA Data

| <u>Component: Failure Mode</u>    | <u>Percent of Unavailability</u> |
|-----------------------------------|----------------------------------|
| Sensor: miscalibration            | 48%                              |
| MOV: failure to transfer          | 23                               |
| MOV: out for maintenance          | 15                               |
| Pressure Sensor: loss of function | 12                               |
| Pipe Segment Faults               | 1                                |
| Others                            | 1                                |

Table 4  
Component Importances: SDC Mode using PRA Data

| <u>Component: Failure Mode</u>     | <u>Percent of Unavailability</u> |
|------------------------------------|----------------------------------|
| MOVs: failure to transfer          | 56%                              |
| Pressure Sensors: loss of function | 24                               |
| MOVs: out for maintenance          | 12                               |
| MOVs: limit switch failure         | 3.7                              |
| Sensors: miscalibration            | 1.9                              |
| RHR Pumps: failure to start        | 0.54                             |
| RHR Pumps: failure to run          | 0.4                              |
| RHR Pumps: out for maintenance     | 0.3                              |
| Other                              | 1.2                              |

Table 5  
BNL Analysis of Failure Probabilities

| <u>Component</u>                  | <u>PRA mean value</u> | <u>BNL mean value</u> | <u>BNL maximum value</u> | <u>Aging Rate %/year</u> |
|-----------------------------------|-----------------------|-----------------------|--------------------------|--------------------------|
| MOV: failure to transfer          | 3.8E-3                | 1.0E-5                | 1.3E-3                   | 0.11                     |
| Pressure Sensor: loss of function | 2.5E-3                | 6.0E-4                | 8.4E-4                   | 0.02                     |

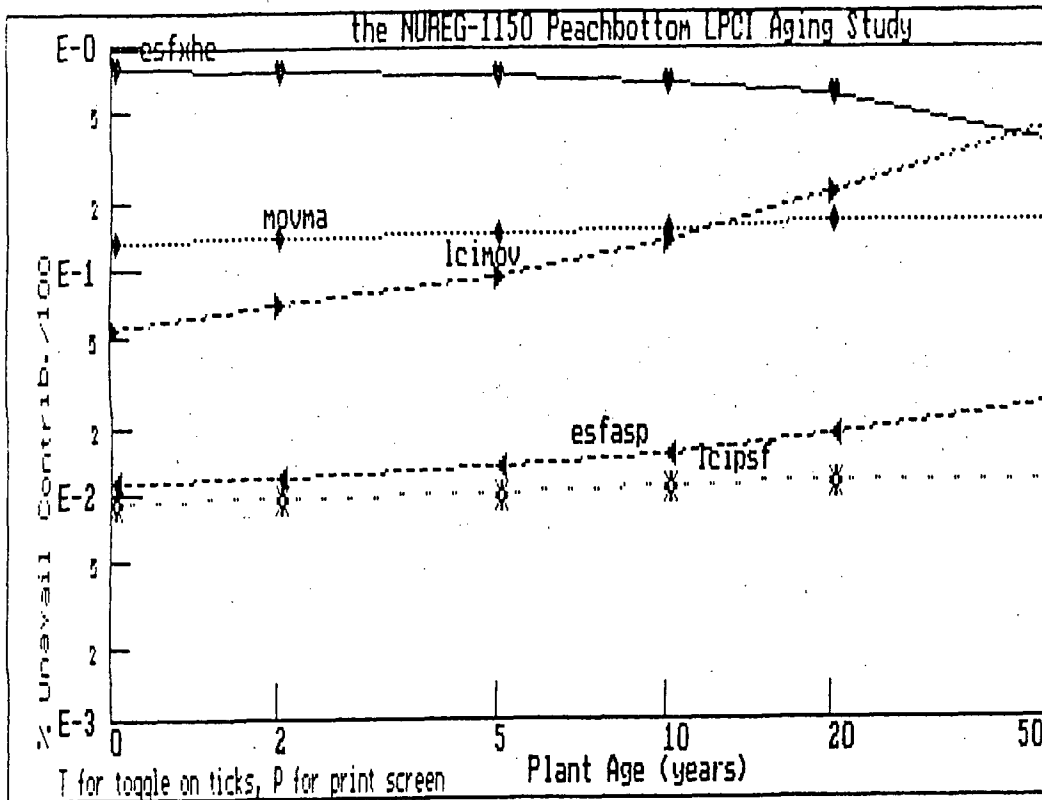


Figure 13

Copy of PRAAGE-1988 Graphical Output in Low Resolution (Acronyms are: esfxhe - engineered safety features (ESF) human errors, movma- MOV out for maintenance, lcimov - LPCI MOV, esfasp - ESF pressure sensor and lcisf - LPCI pipe section.)

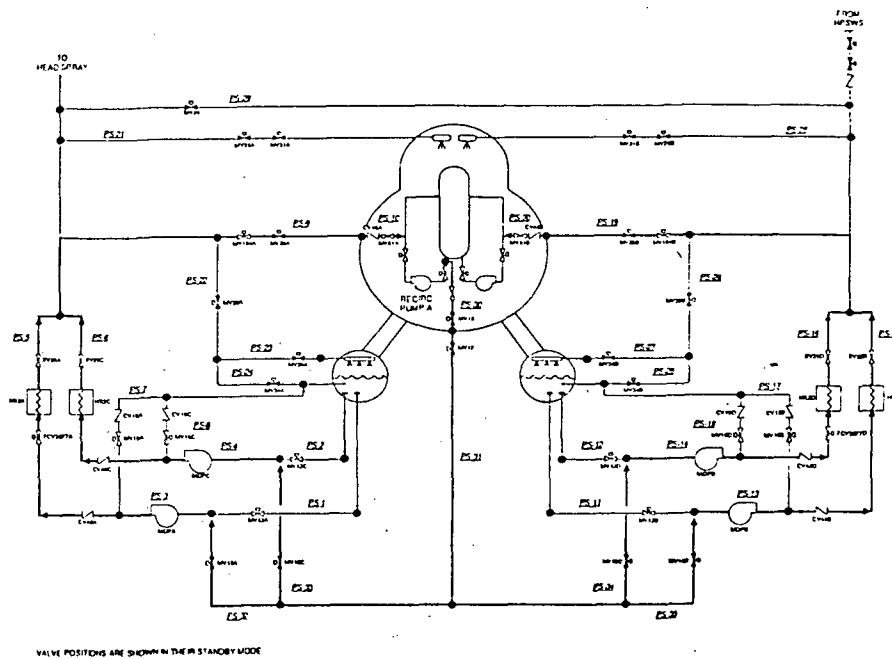


Figure 14

Simplified Schematic of the Residual Heat Removal System

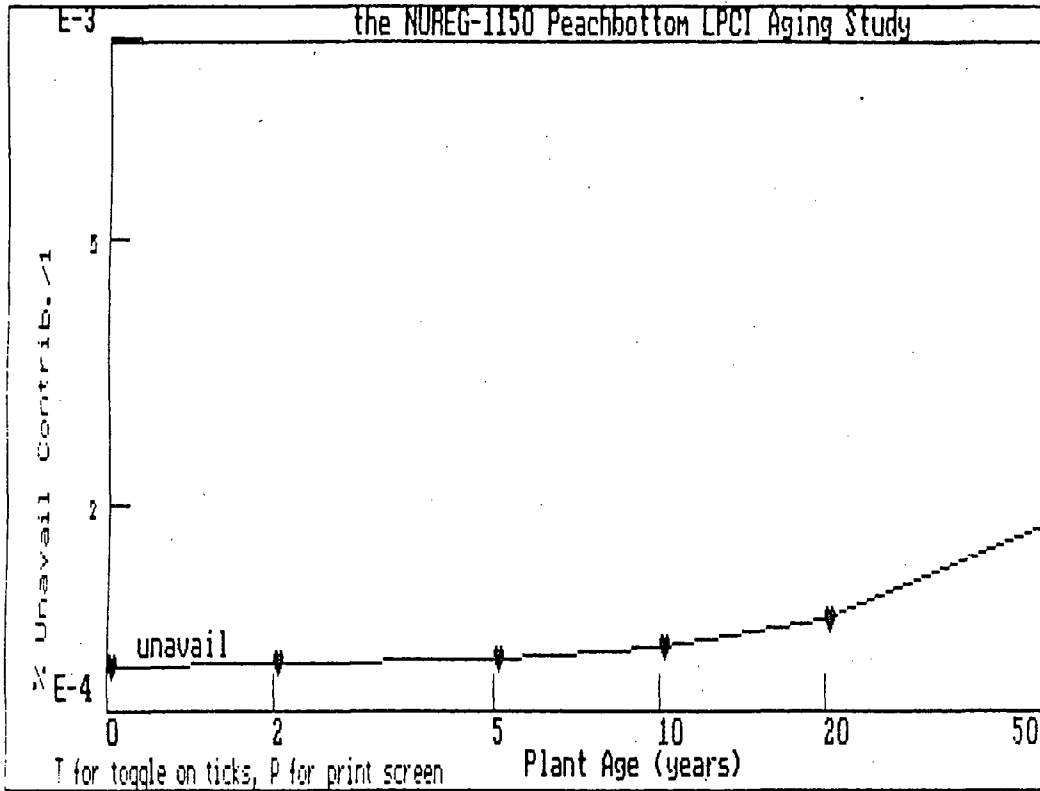


Figure 15  
The Effects of the Aging of the Components shown in Table 3  
on the RHR System in the LPCI Mode

## 7. References

Fullwood, R. and R. Hall, 1988, Probabilistic Risk Assessment in the Nuclear Power Industry, Pergammon Press, Oxford, G.B.

Higgins, J. et al., 1988, "Operating Experience and Aging Assessment of Component Cooling Water Systems in Pressurized Water Reactors," NUREG/CR-5052, July.

Vesely, W., 1987, "Risk Evaluations of Aging Phenomena: The Linear Aging Reliability Model and Its Extensions," NUREG/CR-4769, April.

Worrell, R.B., 1985, "SETS Reference Manual", NUREG/CR-4213.



## UTILIZATION OF AGING PROGRAM RESULTS IN PLANT INSPECTIONS

W. GUNTHER AND R. FULLWOOD  
Brookhaven National Laboratory  
Upton, N.Y. 11973

### ABSTRACT

Research conducted under the auspices of the U.S. Nuclear Regulatory Commission Nuclear Plant Aging Research (NPAR) Program has resulted in a large data base of component and system operating experience. This data base has been used to determine equipment aging susceptibility and the potential for equipment aging to impact plant safety and reliability. Methods of detecting and mitigating component and system aging have also been identified.

This paper discusses how the NPAR results could be used to focus inspection activities on age-sensitive components and systems and on the specific modes and mechanisms of age degradation. These activities range from the regular inspections conducted by resident inspectors to extensive special inspections such as the Safety System Functional Inspection typically conducted by a team of inspectors.

### BACKGROUND

The NPAR Program's goals are to obtain an understanding of the aging degradation process in components, systems, and structures, and assess methods for detecting and mitigating aging<sup>1</sup>. This hardware-oriented engineering research program uses a two phase approach. The phase 1 studies assess the nuclear power plant operating experiences to identify and characterize aging modes, mechanisms, and effects, and identifies measurable functional parameters which could be used to detect aging degradation in the incipient stage. The phase 2 research is an in-depth engineering study and assessment of aging detection and mitigation methods based on the testing of naturally aged equipment, a review of current nuclear power plant maintenance practices, and a cost/benefit analysis for applying recommendations.

Associated with each NPAR study is the need to determine the role of inspection, maintenance, and monitoring in counteracting aging and service wear effects. The role of maintenance in managing aging is an important area where NRC emphasis has been applied. A review by the NRC of maintenance performed at several plants resulted in the conclusion that "Most utilities do not perform condition monitoring due to inadequate knowledge of degradation mechanisms and the relationship between measurable parameters and predicted functional capability."<sup>2</sup> The output from NPAR in this area could assist the inspector in determining the extent of licensee inadequacies where appropriate.

To achieve the objective of integrating NPAR information into the NRC Inspection Program, several tasks must be accomplished. These tasks are to determine which NPAR information is relevant to areas addressed by the inspector; how the Inspection Program presently addresses component and system performance monitoring; and the format in which the NPAR information can be presented so that the material can be readily accessed and updated.

As illustrated in Figure 1, the information flow path depicted includes the following:

1. Determine NRC Inspection Program requirements: The results of a review of the NRC Inspection Manual are presented, highlighting those areas in which typical NPAR research results could be applied.
2. Complete NPAR Program Results: This paper presents examples of NPAR Program results which should be available to the inspector. Several information areas are discussed.
3. Develop the guidelines: For extracting information from the NPAR reports, guidelines have been established which include background information, operating experience, recommended maintenance, testing, and inspection, and references. This is intended to be a summary of NPAR information pertinent to an inspection of a nuclear power plant.
4. Application of Guidelines: To determine the effectiveness of the guidelines established for obtaining information from the NPAR reports, a trial application of the methodology will be implemented for two components-motors and inverters.
5. Information Transfer: The potential information transfer mechanisms are presented, including relationships to inspection modules, team inspections, and special subject area inspections.

This paper presents the research findings developed from completion of the first three tasks.

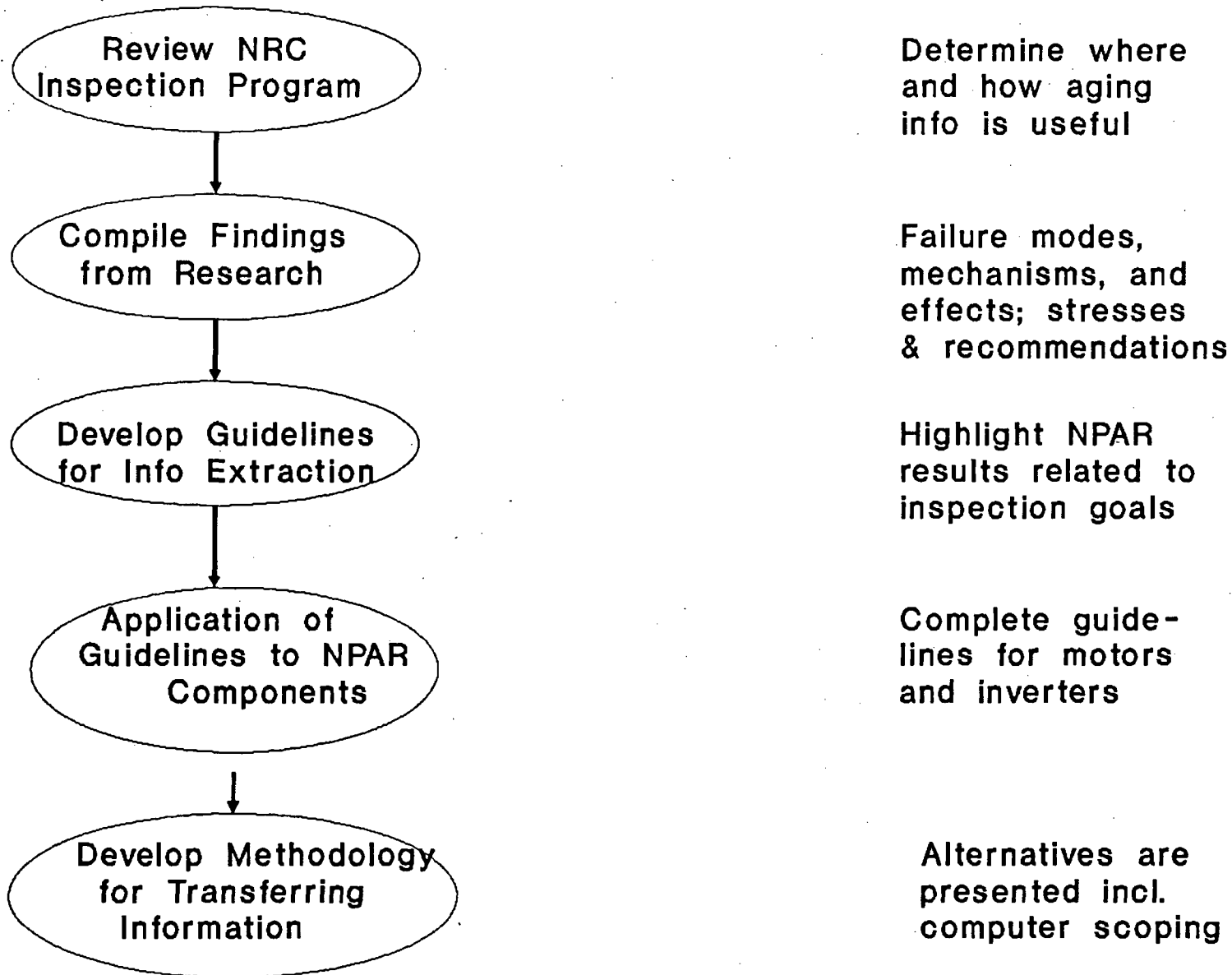


Figure 1 NPAR Information Integration Flow Chart

## Inspection Guidance to Address Nuclear Power Plant Aging

The NRC Inspection Program derives its objectives from the fundamental NRC responsibility of ensuring that planned and existing licensed operation of a nuclear power plant can be and are being conducted without undue risk to the public. The Inspection Program objectives include the following<sup>2</sup>:

- a. Identify conditions which may adversely affect public safety in order that appropriate corrective action can be taken
- b. Determine the level of effectiveness of licensee performance.
- c. Determine the status of compliance with NRC regulations and orders.

Through the use of inspection procedures, guidance is provided to inspectors in a variety of functional areas including Operations, Maintenance, Surveillance, and Modifications. Inspectors include Resident Inspectors, as well as other NRC personnel who may assist in specialized or team inspections.

Chapter 2515 of the NRC Inspection Manual was reviewed to determine areas of emphasis, and to ascertain where aging information could improve the inspection goals. It should be recognized that the utilities and the NRC require routine inspections with emphasis on monitoring, surveillance, detection, and preventive maintenance to assure that nuclear plants are operated safely. These provide potential indications of age related degradation.<sup>4</sup>

The NRC, through the regional offices, performs independent inspection of equipment and systems, as well as audits of each plant's inspection program and results. If necessary, augmented inspection teams are sent to a plant to resolve special issues and problems.

The NRC Inspection Program emphasis is on evaluating the performance of licensees by focusing on requirements and standards associated with administrative, managerial, engineering, and operational aspects of licensee activities. The Program recognizes that licensees may satisfy NRC requirements differently, and therefore expresses inspection guidance in the form of performance objectives and evaluation criteria.

### NPAP Information Relevant to Inspections

The NPAP Program can provide information to the Inspection Program to help guide the regional inspection activities in areas relevant to aging, aging detection, and mitigation of aging degradation. This work can provide guidance to NRC inspectors on equipment which is aging sensitive by identifying specific modes and mechanisms of age-related failures.

The types of information generated by NPAR which were found to be relevant to inspection needs include the following:

- functional indicators - NPAR reports identify parameters which can be monitored or measured to detect aging degradation. The inspector can apply these results to enhance visual inspections (walkdowns) and to evaluate licensee programs for assuring equipment and system operability.
- failure modes, causes, effects - operating experience data evaluated in NPAR studies can alert the inspector to prevalent system and equipment failure mechanism. The potential for failure rate changes with plant age is an NPAR output of interest to the inspector in evaluating preventive maintenance resources.
- stresses which cause degradation - an inspector can benefit from knowing the environmental and operational stresses which cause aging degradation.
- maintenance recommendations - the inspector is required to evaluate aspects of a licensee's maintenance program for a number of different inspections, including special team inspections. Each NPAR report contains a review of current maintenance practices, a summary of vendor-recommended maintenance, and recommendations for preventive and corrective maintenance which can be used to detect and mitigate the effects of aging.
- inspection prioritization - based on the failure rate determined through a detailed operating experience review and a model developed through Probabilistic Risk Assessment (PRA) techniques, NPAR system reports present the relationship between age degradation and plant risk. These results can be applied in the Inspection Program for redirecting inspection resources as the plant ages.

To further summarize where this NPAR information may be used, a matrix (Table 1) has been developed. This table shows the primary information categories applicable to the inspection areas reviewed. It should be noted, however, that the inspection procedures give the inspector a great deal of latitude to perform his responsibilities. Therefore, for any given inspection or inspector, the level of detail required may differ depending upon the specific circumstances. It therefore is recommended that as much potentially useful information as possible be made available.

**NPAR INFORMATION CATEGORIES**

| <u>Inspection Type<br/>(Procedure)</u>                        | <u>Background<br/>Info.</u> | <u>Oper.<br/>Exper.</u> | <u>Maint.<br/>Recom.</u> | <u>References</u> |
|---------------------------------------------------------------|-----------------------------|-------------------------|--------------------------|-------------------|
| 1. Safety System<br>Functional<br>Inspection<br>(SSFI)        | X                           | X                       | X                        | X                 |
| 2. Safety System<br>Outage Modi-<br>fication Insp.<br>(SSOMI) | X                           | X                       |                          |                   |
| 3. Operational<br>Safety Veri-<br>fication (71707)            | X(b)                        | X                       | X(a)                     | X                 |
| 4. Engineered<br>Safety Feature<br>System Walkdown<br>(71710) | X(b)                        | X(c)                    | X(d)                     | X                 |
| 5. Maintenance<br>Inspections<br>(62700 series)               |                             |                         | X(d)                     | X(e)              |
| 6. Surveillance<br>Inspections<br>(61700 series)              | X(f)                        |                         | X(d)                     |                   |

- (a) NPAR functional indicators
- (b) Age susceptible components and stresses
- (c) Dominant failure modes and mechanisms
- (d) Evaluation of current maintenance practices
- (e) Industry standards and guides for various components
- (f) Stresses associated with testing

**Table 1 Use of NPAR Results in Inspection**

Continuing work in the risk area within NPAR will provide additional information to the inspector for selecting aspects of the system for inspection which are of greatest safety significance, and will therefore result in the largest benefit. The potential exists that, based on input from the NPAR Program, inspection priorities for systems and components would change over the life of the plant. This would be due to several reasons including:

1. The aging degradation rate of some systems are high. Therefore, the licensee must allocate additional resources as the system ages in order to maintain acceptable safety and availability. The resources would likely be in the areas of maintenance and testing. The Inspection Program should be capable of verifying that these resources are adequate.
2. For systems which do not experience significant aging degradation, the inspection priority may remain the same or decrease as the plant ages. Other priority selection techniques, such as PRA, would remain viable.
3. Within a system, components age differently and therefore, the impact of a component on system availability will change over the life of the plant. The selection of major components for inspection within the system could be altered based on input from NPAR.

Figure 2 illustrates conceptually how inspection priorities could change based on the influence of equipment aging.

Three types of systems are illustrated. The first is the Reactor Protection System (RPS) representing an important safety related system which may not exhibit substantial degradation due to aging. The inspection activities associated with this type of system are assumed to be of high priority early in plant life, and despite minimal aging degradation expected due to the nature of the equipment (electronics), would continue to demand a high priority on inspection resources throughout plant life. This influence is strictly due to the importance of the system on plant risk.

A second type of system operates in a standby mode, i.e., Low Pressure Coolant Injection (LPCI) in a BWR. Because of its safety significance and the importance of properly aligning the system to assure automatic operation as required, the inspection priority will initially be high. This is influenced by the need to evaluate the licensee's capabilities to safely operate the facility by reviewing the operating procedures, operator training, and surveillance testing associated with the system. On the other hand, as NRC confidence is gained in the licensee's abilities, and it can be shown that this standby system experiences minimal degradation due to aging, it is conceivable that inspection resources dedicated to this type of system could decrease over the plant's operating life.

The continuously operating system is the third type of system considered in Figure 3, i.e., the Component Cooling Water (CCW) System in a PWR. A significant aging rate has been modeled for this type of system due to the continuous mode of operation, particularly for active components such as pumps, valves, and instrumentation. Despite having a low inspection priority early in plant life due to redundancy and system simplicity, an increase in inspection priority could be justified based on the deleterious effects of aging on system reliability and availability. The ability of the NRC Inspection Program to verify that licensee maintenance effectively manages the effects of aging to offset potential plant risk increase is of paramount importance.

Figure 3 illustrates that within a system, component importance can change with plant life due to the effects of aging. From the NPAR phase 1 CCW work a model was developed which incorporated failure rates for pumps, valves, and the exchangers based on actual operating experience data<sup>5</sup>. When plotted over the 40 year life of the plant, it was observed that the importance of pump operation to CCW availability became dominant. This type of information could therefore assist the inspector in determining priorities for a system inspection.

## CONCLUSIONS

It is concluded, based on the review of inspection procedures, that the NPAR data base can assist the inspector in focusing his activities on those components and systems most likely to affect plant safety as the plant ages. In addition, the NPAR data and research results can provide the inspector with criteria for determining the validity of findings and the completeness of licensee responses. Evaluating a licensee's administrative programs is another area where NPAR results can provide a reference, especially those reviews associated with operations, maintenance, and testing.

NPAR generated information which has a direct relationship with NRC Inspection Program requirements are:

- functional indicators
- failure modes, causes, and effects
- degradation causing stresses
- maintenance recommendations
- component and system risk impact as a function of time.

Examples of inspection procedures reviewed which could benefit from one or more of those NPAR results are:

- 71707, Operational Safety Verification
- 71710, Engineered Safety Feature System Walkdown
- 62700 series, Maintenance Program Inspections
- 61700 series, Surveillance Program Inspections
- Safety System Functional Inspection (SSFI)
- Safety System Outage Modification Inspection (SSOMI)

# SYSTEM INSPECTION PRIORITIES BASED ON NPAR INPUT

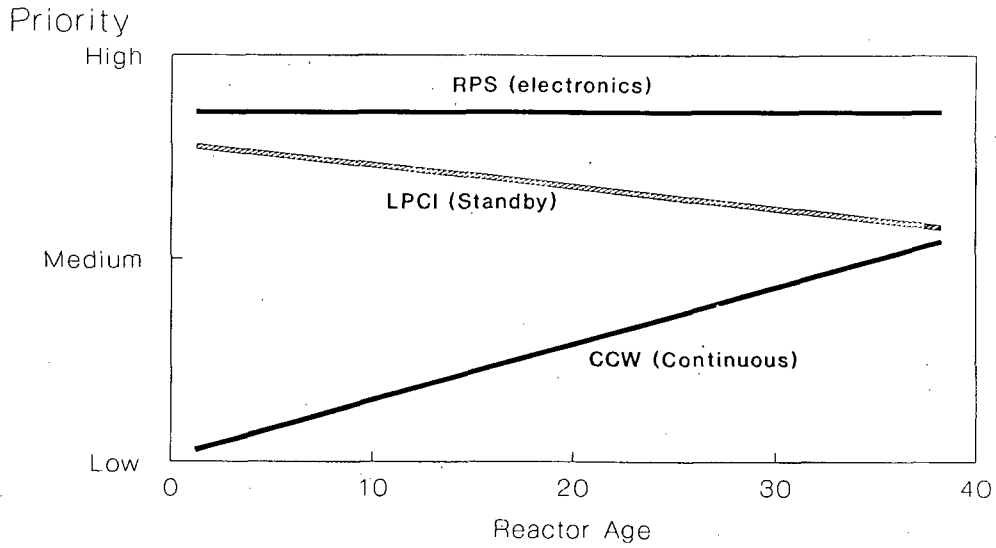


Figure 2 Potential Prioritization of System Inspections Based on NPAR Input

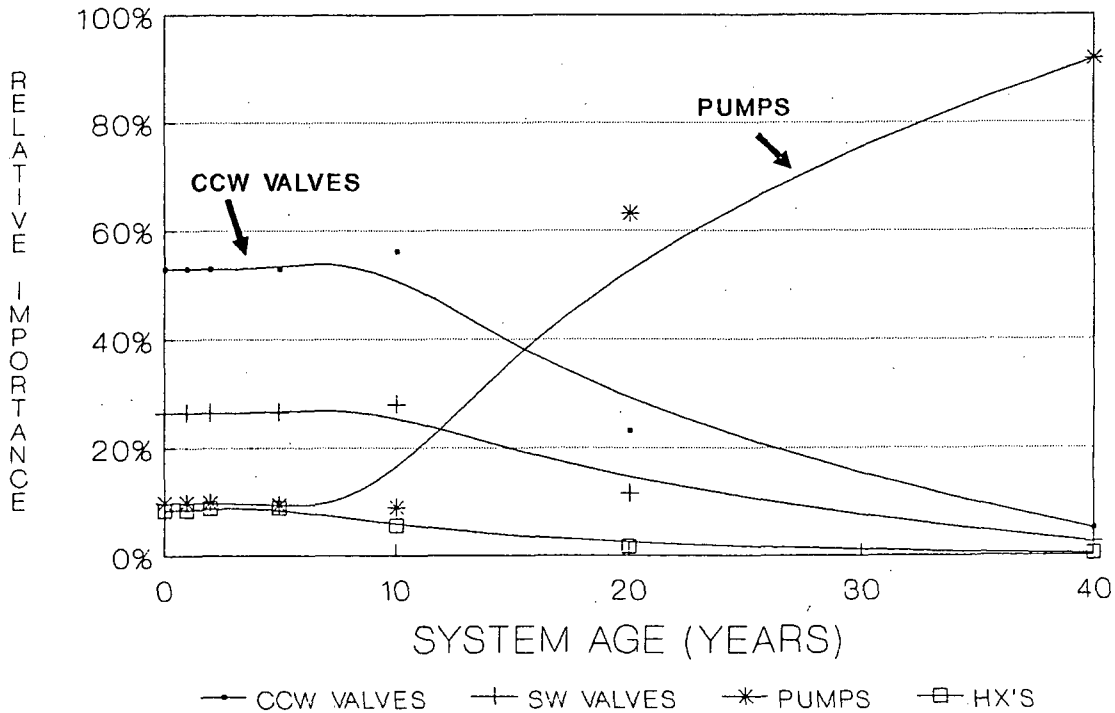


Figure 3 Inspection Importance of Components Within a System

## REFERENCES

1. NUREG 1144, Rev. 1, 9/87, "Nuclear Plant Aging Research (NPAR) Program Plan."
2. NUREG 1212, Vols 1 & 2, "Status of Maintenance in the U.S. Nuclear Power Industry," 1985.
3. NRC Inspection Manual, "Policy and Guidance for Development of NRC Inspection Manual Programs" Chapter 0030, 10/13/87.
4. Prepared Testimony Submitted by Lando N. Zech, Jr. to the Subcommittee on Energy and Power of the US House of Representatives, 11/10/87.
5. NUREG/CR-5052, "Operating Experience and Aging Assessment of Component Cooling Water Systems in Pressurized Water Reactors," 7/88.

# PROBABILITY OF CRACK-INDUCED FAILURE IN BWR RECIRCULATION PIPING\*

Garry S. Holman

Lawrence Livermore National Laboratory  
University of California  
Livermore, California / U.S.A.

## ABSTRACT

The Lawrence Livermore National Laboratory (LLNL) has estimated the probability of double-ended guillotine break (DEGB) in the reactor coolant piping of Mark I boiling water reactor (BWR) plants. Two causes of pipe break are considered: crack growth at welded joints and the seismically-induced failure of component supports. For the former a probabilistic fracture mechanics model is used, for the latter a probabilistic support reliability model. This paper describes a probabilistic model developed to account for effects of intergranular stress corrosion cracking (IGSCC). The IGSCC model, based on experimental and field data compiled from several sources, correlates times to crack initiation and crack growth rates for Types 304 and 316NG stainless steel against material-specific "damage parameters" which consolidate the separate effects of coolant environment (temperature, dissolved oxygen content, level of impurities), stress (including residual stress), and degree of sensitization. Application of this model to actual BWR recirculation piping shows that IGSCC clearly dominates the probability of failure in 304SS piping, mainly due to cracks that initiate within a few years after plant operation has begun. Replacing Type 304 piping with 316NG reduces failure probabilities by several orders of magnitude.

## 1. INTRODUCTION

The Lawrence Livermore National Laboratory (LLNL), through its Nuclear Systems Safety Program, has performed probabilistic reliability analyses of PWR and BWR reactor coolant piping for the NRC Office of Nuclear Regulatory Research. Specifically, LLNL has estimated the probability of a double-ended guillotine break (DEGB) in the reactor coolant loop piping of PWR plants, and in the main steam, feedwater, and recirculation piping of BWR plants. For these piping systems, the results of these investigations provide NRC with one technical basis on which to:

---

\* "This work was supported by the United States Nuclear Regulatory Commission under a Memorandum of Understanding with the United States Department of Energy."

- (1) reevaluate the current general design requirement that DEGB be postulated in the design of nuclear power plant structures, systems, and components against the effects of postulated pipe breaks. Recent NRC rulemaking actions, based in large part on the results of our PWR evaluations, now provide a means for eliminating dynamic effects of reactor coolant loop breaks (e.g., pipe whip, jet impingement) as a basis for PWR plant design.
- (2) determine if an earthquake could induce a DEGB and thus reevaluate the design requirements that pipe break loads be combined with those resulting from a safe shutdown earthquake (SSE). Recent deviations from the NRC Standard Review Plan, for example, now allow decoupling of SSE and DEGB loads for PWR reactor coolant loop piping.
- (3) make licensing decisions concerning the replacement, upgrading, or redesign of piping systems, or addressing such issues as the need for pipe whip restraints on reactor coolant piping.

In estimating the probability of DEGB, LLNL considers two causes of pipe break; pipe fracture due to the growth of cracks at welded joints ("direct" DEGB) and pipe rupture indirectly caused by the seismically-induced failure of critical supports or equipment ("indirect" DEGB).

## 2. BACKGROUND

Over the past several years, generic evaluations of reactor coolant loop piping were completed for PWR nuclear steam supply systems manufactured by Westinghouse, Combustion Engineering, and Babcock & Wilcox. In these evaluations, LLNL performed the following:

- (1) estimated the probability of direct DEGB taking into account such contributing factors as the initial size (depth and length) of pre-existing fabrication flaws, pipe stresses due to normal operation and sudden extreme loads (such as earthquakes), the crack growth characteristics of pipe materials, and the capability to detect cracks or to detect a leak if a crack were to penetrate the pipe wall. For this purpose, LLNL developed a probabilistic fracture mechanics model using Monte Carlo simulation techniques, implemented in the PRAISE (Piping Reliability Analysis Including Seismic Events) computer code.
- (2) estimated the probability of indirect DEGB by identifying critical supports or equipment whose failure could result in pipe break, determining the seismic "fragility" (relationship between seismic response and probability of failure) of each, and then combining this result with the probability that an earthquake occurs producing a certain level of excitation ("seismic hazard").
- (3) for both causes of DEGB, performed sensitivity studies to identify key parameters affecting the probability of pipe break. We also performed uncertainty studies to quantify how uncertainties in

input data affect the uncertainty in the final estimated probability of pipe break.

The results of these evaluations consistently indicated that the probability of a DEGB in PWR reactor coolant loop piping is extremely small, about  $1E-7$  events per reactor-year from indirect causes, and less than  $1E-10$  events per reactor-year from direct causes. It was also found that thermal stresses dominated the probability of direct DEGB, and that earthquakes contributed only negligibly. These results suggested that the DEGB design requirement -- and with it related design issues such as coupling of DEGB and SSE loads, asymmetric blowdown, and the need to install pipe whip restraints -- warranted reevaluation for PWR reactor coolant loop piping. Details of these investigations have been extensively documented elsewhere [1,2,3,4] and will not be discussed here any further.

The objectives and approach of the BWR study [5] were essentially the same except that additional potential failure mechanisms were added. LLNL limited its investigation to Mark I plants, which have recirculation piping particularly susceptible to the effects of intergranular stress corrosion cracking (IGSCC). Although our evaluations were all generally similar, two important aspects distinguished the BWR study from the earlier PWR evaluations:

- (1) the susceptibility of certain BWR stainless steels to stress corrosion cracking required development of an appropriate probabilistic model of corrosion phenomena. Stress corrosion is generally not perceived as a problem in PWR primary loop piping and, as a result, was not considered in our earlier evaluations.
- (2) the greater complexity and flexibility of BWR recirculation piping compared to PWR primary loops required that intermediate pipe supports (e.g., snubbers, spring hangers) be incorporated in the evaluation.

This paper will focus on the methods we developed to probabilistically model stress corrosion cracking and on application of the model to a "representative" BWR recirculation system (Fig. 1). The methods used to address failure of intermediate supports are described in detail in a companion paper [6] and will not be discussed here.

### 3. DOUBLE-ENDED GUILLOTINE BREAK CAUSED BY CRACK GROWTH

The probability of "direct" DEGB in reactor coolant piping is estimated using a probabilistic fracture mechanics model implemented in the PRAISE computer code and associated pre- and post-processing routines. Details of the model are documented elsewhere [7,8] and will not be repeated here, but can be summarized as follows.

For a given weld joint in a piping system, the probability of failure (i.e., leak or break) is estimated using a Monte Carlo simulation technique. As diagramed in Fig. 2, each replication of the simulation -- of which a typical simulation may include many thousand -- begins

with a pre-existing flaw having initial length and depth randomly selected from appropriate distributions. These distributions in turn relate the probability of crack existence. Fatigue crack growth is then calculated using a Paris growth model, to which are applied stresses associated with normal operating conditions and postulated seismic events. The influence of such factors as non-destructive examination (NDE) and leak detection is also considered through the inclusion of appropriate statistical distributions (e.g., probability of crack non-detection as a function of crack size). Leak occurs when a crack grows through the pipe wall, break when failure criteria based on net section stress (for austenitic materials) or tearing modulus (for carbon steels) are exceeded.

Completing all replications for a given weld joint and tabulating those cracks that cause failure yields the cumulative probability of failure as a function of time at that weld. If only pre-existing cracks are considered, then "stratified sampling" can be applied to assure that initial crack samples are selected only from those sizes that can potentially cause pipe break. Through this technique, very low failure probabilities (less than one in a million) can be reliably estimated from only a few thousand replications of the Monte Carlo simulation.

After the failure probabilities at all weld joints in a piping system have been estimated, a "systems analysis" combines these results with the non-conditional crack existence probability (a function of total volume of weld material) and seismic hazard (which relates the occurrence rates of earthquakes as a function of peak ground acceleration) to obtain the non-conditional probabilities of leak and DEGB.

This was the basic approach followed in our evaluations of PWR reactor coolant loop piping. One significant factor complicating the evaluation of BWR piping, however, was the need to include effects of intergranular stress corrosion cracking (IGSCC). When present, IGSCC not only accelerates the growth rate of existing flaws, but also causes new cracks to initiate after plant operation has begun. The effect of these "initiated" cracks on the probability of DEGB must be therefore be considered in addition to that of pre-existing flaws.

Recirculation piping in older BWR plants, particularly those characterized by the General Electric Mark I containment design, has been found in recent years to be susceptible to intergranular stress corrosion cracking. Stress corrosion cracking occurs in stainless steel piping (in the Mark I plants, Type 304) when the "appropriate" (in an adverse sense) conditions of "sensitization" -- material properties conducive to IGSCC that result from prolonged exposure to high temperatures during welding -- environment, and stress are met. Earlier versions of PRAISE treated the effect of IGSCC on pre-existing cracks through a simple relationship between growth rate and the stress intensity factor at the crack front; crack initiation was not modeled at all. It is important to note that this model was not applied in our

PWR evaluations because operating experience has indicated that IGSCC is not a problem in PWR reactor coolant loop piping.

#### 4. PROBABILISTIC MODEL OF STRESS CORROSION CRACKING

As part of our BWR study we developed an advanced IGSCC model for the PRAISE code [9]. This model is semi-empirical in nature, and is based on experimental and field data compiled from several sources. Using probabilistic techniques, the model addresses the following IGSCC phenomena:

- **crack initiation**, including the effects of environment, applied loads, and material type (i.e., sensitization). Crack location, time of initiation, and velocity upon initiation are all defined by appropriate distributions based on experimental data.

"Initiated" cracks are considered separately from pre-existing cracks until one of the following two criteria are satisfied: (1) the crack attains a depth of 0.1 inch, or (2) the velocity of the crack estimated according to the Paris growth law exceed the initiation velocity. Beyond this point, "initiated" and "fracture mechanics" cracks are treated identically.

- **crack growth rate**, including effects of environment, applied loads, and material type.
- **multiple cracks**. Because our earlier evaluations were based on pre-existing flaws only, each Monte Carlo replication included one crack only. Inclusion of crack initiation requires that multiple cracks be considered during each replication.
- **crack linking**. Treating multiple cracks requires that their potential linkage into larger cracks be considered. This is done using linkage criteria specified in Section XI of the ASME Boiler and Pressure Vessel Code.

The model covers not only the Type 304 stainless steel (304SS) found in most Mark I recirculation piping, but Type 316NG "nuclear grade" steel as well, a low-carbon alloy widely regarded as an IGSCC-resistant replacement for Type 304. Crack growth rates and times-to-initiation for each material are correlated against "damage parameters" which consolidate the separate influences of several individual parameters. The damage parameters are multiplicative relationships among exponential terms which individually describe the effects of the various phenomena on IGSCC behavior, including:

- **environment**, specifically coolant temperature, dissolved oxygen content, and level of impurities.
- **applied loads**, including both constant and variable loads to account for steady-state operation and plant loading or unloading, respectively.

- **residual stresses.** Steady-state pipe loads due to welding residual stresses are considered in addition to fatigue loads.
- **material sensitization.**

Figures 3 and 4 show, respectively, times-to-initiation and crack growth rates for 304SS, the material on which the initial development of the model was based. The solid curved lines in Fig. 4 show crack growth rates predicted by the earlier IGSCC model in PRAISE for oxygen concentrations of 0.2 ppm (typical during plant operation) and 8 ppm (typical during startup); the relatively close agreement implies that the earlier model gave reasonable crack growth rates despite its much simpler approach.

The damage parameters in the 304SS model were based on the results of both constant-load (CL) and constant extension rate (CERT) IGSCC laboratory tests. Many other factors were considered during initial model development, but were later excluded from consideration either because they were judged to be of secondary influence for 304SS, or because suitable operating data was not available to exercise them in a plant-specific evaluation. The model also assumes that growth rates and times-to-initiation measured under intentionally harsh laboratory conditions can be extrapolated to the relatively benign conditions found in actual reactors. We regarded this assumption as conservative, noting, for example, that some experimental observations [10] suggest levels of stress intensity factor below which stress corrosion cracking is effectively arrested or at least significantly reduced. Our original simplified model of IGSCC allowed for such "threshold" behavior (see Fig. 5), the present advanced model does not.

Although the present model was developed for 304SS, adapting the correlation scheme for 316NG was a relatively straightforward matter of defining new damage parameters based on appropriate laboratory data; the basic functional form of the model was otherwise left unchanged. Two features unique to the 316NG model are, however, noteworthy:

- where both CERT and CL data were available for 304SS, only CERT data was available for 316NG. These data were used to define constant-load growth rates and times-to-initiation in 316NG under the assumption that the creep behavior of both alloys is similar.
- as noted earlier, three conditions are necessary for IGSCC in austenitic steels: stress, environment, and sensitization. In 304SS, whenever stress corrosion cracking occurs in laboratory tests intended to simulate operating BWR conditions, it is most often intergranular. In 316NG, however, CERT specimens fail by transgranular stress corrosion cracking (TGSCC), whereas IGSCC is observed in fracture mechanics specimens. Since the relative influence of environment and loading on TGSCC in 316NG appears similar to that of IGSCC in 304SS, the available TGSCC data were used to predict cracking in 316NG.

Residual stresses are treated as a random variable in the Monte Carlo simulation. Distributions of residual stress as a function of distance from the inner pipe wall were developed from experimental data for three categories of nominal pipe diameter. For large lines (20 to 26 inches), residual stresses took the form of a damped cosine through the wall as based on data collected by General Electric and Argonne National Laboratory (see Fig. 5). The nominal tensile stress at the inner pipe wall is about 40 ksi. For intermediate-diameter (10 to 20 inches) and small-diameter (less than 10 inches) lines, a linear distribution was assumed through the pipe wall with respective inside wall stresses of 9.3 ksi and 24.4 ksi.

The 304SS model was benchmarked by comparing predicted leak rates under nominal BWR applied load conditions against actual leak and crack indication data made available to us by the NRC Office of Nuclear Reactor Regulation (NRR). During benchmarking we quickly ascertained that residual stress was the parameter most influencing the predicted leak rates, and we therefore opted to "tune" the model on this basis. A variety of schemes were considered before we settled on adjusting the stress magnitude (using a multiplication factor) to bring the model into agreement with the field data. Figure 6 compares predicted leak rates against field data for various adjustment factors, Figure 7 the number of NDE indications with depth a greater than 10 and 50 percent of the wall thickness  $h$ , based on the optimum stress adjustment factor. As Fig. 6 shows, surprisingly large reduction factors had to be applied to bring the model into line with the field data, suggesting that factors other than residual stress may be more influential than we first concluded.

Calculations performed during final development of the 316NG model revealed several interesting characteristics of its behavior compared to that of the less-resistant 304SS. For example, we performed analyses both for initiated cracks and for pre-existing cracks, the latter case reflecting only the effect of stress corrosion on crack growth and not only the addition of new "initiated" cracks to the overall population. Figure 8 shows a typical set of results from these analyses, in this case cumulative leak probabilities for an intermediate-diameter weld. Two observations are significant here:

- at any given time, the estimated failure probability in 304SS is some two to three orders of magnitude higher than in 316NG.
- the time required to reach a given leak probability is about six times as long in 316NG as it is in 304SS.

These results also show that where failure in 304SS is always dominated by initiated cracks (i.e., resulting from stress corrosion), in 316NG the initiated cracks dominate the probability of leak only after about 12 years. Once cracks are present, however, growth rates are nominally the same in either material. Consequently, the predicted difference in behavior between the two materials is due to differences in the times-to-initiation and in the number of initiated cracks, rather than differences in their "fracture mechanics" characteristics.

## 5. PROBABILITY OF FAILURE IN BWR RECIRCULATION LOOP PIPING

After we completed development of the stress corrosion model, we applied it to the recirculation loop piping in an actual Mark I BWR plant. We estimated the leak and DEGB probabilities both for an existing recirculation loop (Fig. 1), and for a proposed "replacement" loop (Fig. 9) fabricated from 316NG. Aside from its use of the more corrosion-resistant material, the replacement loop differs from the original by having fewer weld joints (about 30 compared to 50) and by eliminating entirely the pump bypass line (see Table 1).

During development of the IGSCC model, we found that its complexity greatly increased computer time requirements for its execution (up to three CPU hours per weld for the 20000 to 50000 Monte Carlo replications typical of our analyses) compared to our earlier PWR reactor coolant loop assessments. In order to keep the computational effort within practical bounds, we grouped the welds in the BWR pilot plant recirculation piping, taking those welds with the highest applied loads in each group. We then estimated the leak and DEGB probabilities at each of these representative welds and performed a systems analysis assuming that these leak and DEGB probabilities applied to all welds in the respective group. We followed a similar procedure for the proposed replacement system.

Practical considerations aside, the assumption of "worst case" stress conditions for each weld group offers reasonable assurance that the results of the analysis will be conservative. This conservatism is further enhanced by the fact that we did not include in-service inspection (ISI) in our evaluations (although PRAISE has this capability), nor did we consider how such IGSCC mitigating measures as weld overlay or inductive heating stress improvement (IHSI) might influence the estimated failure probabilities. Our main objective was to investigate the relative behavior of different material types under otherwise nominally identical conditions.

Figures 10(a) and 10(b) show, respectively, cumulative per-loop system leak and DEGB probabilities estimated by PRAISE for the existing loop configuration (i.e. including bypass piping). Results are given both for the original 304SS material and for the Type 316 nuclear grade. In the 304SS piping, leak is predicted to occur after about ten years of operation (i.e. the cumulative probability of leak approaches one). While it is important to keep in mind the conservatism of the analysis, this result is nonetheless reasonably consistent with some field observations. The corresponding probability of DEGB is on the order of  $1E-2$  after 10 years (or about  $1E-3$  per year), increasing only slightly (by about a factor of two) over the remaining 30 years of plant life.

If the 304SS is replaced with 316NG while keeping the original piping configuration (a fictitious intermediate step between the existing loops in our pilot plant and the replacement system actually proposed), corresponding leak and break probabilities are nominally zero after 10 years of operation. The probability of leak first

exceeds  $1E-4$  after about 12 years, increasing to about  $5E-1$  at the end of plant life. Two DEGB events (out of 25000 Monte Carlo replications) were predicted in the riser weld, the first of which occurred at about 30 years; all other weld groups experienced no DEGB events over the entire 40 years of plant life. The resultant end-of-life system break probability is about  $2E-3$  per loop, or about  $2E-4$  per loop-year; keep in mind that this result assumes (1) no "threshold" behavior, (2) no ISI over the 30-year period, (3) worst-case applied stresses, and that (4) all risers in the system behave identically. For the "replacement" loop configuration actually proposed, the end-of-life DEGB probability falls to about  $1E-3$  per loop ( $1E-4$  per loop-year), due to fewer welds in the new system (Fig. 11).

The bar charts in Fig. 12 show the relative contribution each weld type makes to the overall system probabilities of leak and DEGB; note that Fig. 12 does not depict the number of predicted failures, which were far fewer in the 316NG material than in the 304SS. In the existing loop configuration, about 80 percent and 20 percent of the breaks, and about 65 percent and 25 percent of the leaks, occurred at riser welds and bypass line welds, respectively. The remaining leaks predicted (about 10 percent of the total) were distributed, in descending order, among header, discharge line, and suction line welds.

In the proposed replacement system, virtually all leaks occurred in riser welds. System break resulted solely from riser DEGB as discussed above, which Fig. 12(b) reflects.

The relative contribution of different weld types is further illustrated by Fig. 13, which shows weld-by-weld leak probabilities for the existing loop configuration. Note in particular that the per-weld leak probabilities differ by up to one order of magnitude at 10 years, and by almost two orders of magnitude by the end of plant life. Note also that while the per-weld leak probabilities for riser and bypass piping behave similarly over time, the larger number of riser welds (20 compared to 10) and their somewhat higher per-weld leak probability are reflected in their dominant overall contribution to the probability of system leak (Fig. 12).

Figure 14 compares riser per-weld leak probabilities for 304SS and 316NG piping, in both cases based on the original loop configuration. Note the probability of leak in the 304SS weldment exceeds  $1E-4$  after only about 3 years of operation, while in Type 316NG this threshold is crossed only after some 15 years. The reason for this difference is clear from Fig. 15, which shows the total number of riser crack initiations in our evaluation (one weld, 25000 Monte Carlo replications) in both the 304SS and 316NG materials. Note that cracks initiate in 304SS within the first year of operation; by the time the first initiation occurs in the 316NG (about four years), nearly 1000 cracks have initiated in the less resistant material. The ratio of 316NG initiations to 304SS initiations falls to less than 100 at ten years, and to less than five by the end of plant life (see Fig. 16). By this time, however, piping in an actual plant would have gone through one or more ISI cycles.

Although the results presented here are only for the representative riser weld (i.e. the dominant contributor to the probability of system failure), they are characteristic of what we observed for the other welds considered. In all cases, the 316NG appears to owe its corrosion resistance mainly to the fact that (1) fewer cracks initiated than in the 304SS material, and (2) those that did initiate typically did so later in plant life. Once a crack initiates, however, its subsequent growth rate is not significantly affected by material type.

## 6. SUMMARY AND CONCLUSIONS

### 6.1 Discussion of Results

As part of our evaluations of reactor coolant piping for the Nuclear Regulatory Commission, we developed an advanced probabilistic model of stress corrosion cracking which we applied to the recirculation loops of a Mark I BWR plant. Based on the results of these evaluations, we were able to make the following general observations:

- if stress corrosion is not a factor, thermal fatigue is the main cause of pipe failure. Furthermore, the probability of break is similar to that in PWR reactor coolant loop piping (on the order of  $1E-10$  per reactor-year or lower). As for PWR reactor coolant loop piping, earthquakes contribute only negligibly to the probability of direct DEGB.
- when stress corrosion is a factor, corrosion-induced failure clearly dominates. Furthermore, the probability of pipe failure is dominated by residual stresses (i.e. uniform loads) rather than by stresses induced by applied loads. Our analyses further indicated that failure probability is very sensitive to the particular description of residual stress assumed in the analysis. This result may offer insight into field observations where nominally identical recirculation loops (e.g., in terms of configuration, materials, applied loads) may exhibit stress corrosion cracking in one plant and not in another. Such differences may be at least partly attributable to plant-to-plant differences in residual stresses caused by welding and "fit up" during pipe assembly.
- recirculation loops fabricated from Type 304 stainless steel are predicted to leak after about 10 years of operation. Although this result is based on conservative "worst case" stress assumptions and on the assumption of no in-service inspection over this period, it is also consistent with some field observations.

If the 304SS material is replaced by 316NG and the existing loop configuration is retained, the system leak probability at ten years (a "typical" ISI interval) is effectively zero. The end-of-life system leak probability (i.e. after another 30 years of operation) is about  $5E-1$  per loop, or about  $2E-2$  per loop-year assuming "worst case" applied stresses and no ISI.

- for recirculation loops fabricated from Type 304 stainless steel, the system probability of DEGB is about  $1E-2$  after ten years of operation (or about  $1E-3$  per loop-year), increasing to about  $2E-2$  by the end of plant life. Again, these results reflect "worst case" applied stresses and no ISI.
- for recirculation loops fabricated from Type 316NG stainless steel, the system probability of DEGB is zero for the first 30 years of operation, even under "worst case" applied stresses and no ISI. In our evaluation we predicted only two riser breaks (out of 25000 Monte Carlo replications), none in other weld types, which implies a per-loop DEGB probability on the order of  $1E-4$  per year or less over the final ten years of plant life, zero up to that time. Routine ISI over plant life could be expected to substantially lower the "late-life" probability of DEGB though early detection of potentially troublesome cracks.

Note that for 316NG, our "intergranular" stress corrosion model was actually based on laboratory data for transgranular stress corrosion cracking; we were unable to find suitable IGSCC data. Consequently, we would expect corrosion-induced cracking to more likely be transgranular rather than intergranular, and the probability of failure induced by "IGSCC" to actually be less than implied by our evaluations.

- for the replacement Type 316NG loop configuration, comprising fewer welds (about 30 compared to 50) and eliminating the bypass line altogether, the end-of-life leak and break probabilities drop by about a factor of two. Interestingly, the time-dependence of the system leak and break probabilities does not change significantly, reflecting the observation that the risers, rather than the bypass piping, dominate the probability of system failure.
- where failure in Type 304 piping is always dominated by initiated cracks (i.e., resulting from stress corrosion), in 316NG the initiated cracks dominate the probability of leak only after about 12 years. Once cracks are present, growth rates are nominally the same in either material. Consequently, the predicted difference in behavior between the two materials is due to differences in the number of initiated cracks and their later times-to-initiation, rather than how these cracks would grow once initiated.

## 6.2 Current and Future Applications

The NRC Office of Nuclear Reactor Regulation (NRR) recently published NUREG-0313, Rev. 2, which describes methods acceptable for controlling the susceptibility of BWR reactor coolant piping to intergranular stress corrosion cracking [11]. Although the NRR staff prefers replacement of sensitive piping with piping fabricated from IGSCC-resistant materials such as Type 316NG, enhancement of existing piping by appropriate combinations of repair (e.g., weld overlay, IHSI), prevention (e.g., hydrogen water chemistry), and augmented ISI

is also an acceptable option for plant licensees. For example, the NRR guidelines specify various inspection intervals and sample sizes, depending on IGSCC mitigating measures that have been applied to an affected piping system, but do not define the specific welds that must be inspected.

The results of our recirculation loop evaluation indicated that the likelihood of pipe failure (i.e. leak or break) can vary widely among the weld joints in a piping system. Consequently, the specific welds selected at any given inspection could have a significant influence on system safety. As part of a new project for the NRC Office of Nuclear Regulatory Research, we are using the PRAISE computer code, and in particular our probabilistic model of stress corrosion cracking, to establish an inspection priority for BWR recirculation loop welds on the basis of calculated leak rates for the "representative" Mark I BWR plant in our earlier evaluation. Although not intended in itself to define an "acceptable" piping inspection program, it will provide NRR with one technical basis for reviewing utility responses to NUREG-0313, Revision 2.

The usefulness of probabilistic evaluations in regulatory applications has already been demonstrated through recent NRC rulemaking actions based in large part on the results of LLNL piping reliability studies. Although not a part of our present work, future licensing assessments related to the issue of stress corrosion cracking might conceivably include the following:

- development of specific licensing criteria. It is presumed that the criteria now included in NUREG-0313, Revision 2, will provide the basis for future NRR licensing decisions pertaining to BWR piping susceptible to IGSCC. Probabilistic evaluations like the one discussed in this paper could conveniently be applied to more fundamentally define just what constitutes an "acceptable" piping inspection program.
- assessment of the effectiveness of the recommended inspection schedules relative to alternate inspection schemes (e.g. more or less frequent inspection, greater or lesser extent of inspection).
- assessment of the effectiveness, either relative or absolute, of various measures for enhancing the performance of piping susceptible to stress corrosion cracking.

In principle, our probabilistic approach could be applied without modification to the first two of these activities, although additional work to improve PRAISE code efficiency would be desirable. The approach could also be applied to the third given appropriate PRAISE code modifications, such as the capability to change residual stress patterns, coolant conditions, and pipe geometry at selected times during plant life to model, respectively, IHSI, hydrogen water chemistry, and weld overlay. Such capability would be a powerful tool for future licensing assessment and should be considered for further development and application.

## REFERENCES

1. **Probability of Pipe Fracture in the Primary Coolant Loop of a PWR Plant**, Lawrence Livermore National Laboratory, Report UCID-18967, NUREG/CR-2189, Vol. 1-9 (1981).
2. **Probability of Pipe Failure in the Reactor Coolant Loops of Westinghouse PWR Plants**, Lawrence Livermore National Laboratory, Report UCID-19988, NUREG/CR-3660, Vol. 1-4 (1984).
3. **Probability of Pipe Failure in the Reactor Coolant Loops of Combustion Engineering PWR Plants**, Lawrence Livermore National Laboratory, Report UCRL-53500, NUREG/CR-3663, Vol. 1-3 (1984).
4. **Probability of Pipe Failure in the Reactor Coolant Loops of Babcock & Wilcox PWR Plants**, Lawrence Livermore National Laboratory, Report UCID-53644, NUREG/CR-4290, Vol. 1-2 (1985).
5. **Probability of Failure in the Reactor Coolant Piping of BWR Plants**, Lawrence Livermore National Laboratory, Report UCID-20914, NUREG/CR-4792, Vol. 1-4 (1986/88).
6. G.S. Holman and T. Lo, "Guillotine Breaks Indirectly Caused by Seismically-Induced Failures", Lawrence Livermore National Laboratory, Report UCRL-98172 (May 1988). Presented at the NRC-MITI Technical Information Exchange Engineering Workshop, Tokyo, Japan, May 16-20, 1988.
7. D.O. Harris, et al., **Probabilistic Fracture Mechanics Models Developed for Piping Reliability Assessment in Light Water Reactors**, Lawrence Livermore National Laboratory, Report UCRL-15490, NUREG/CR-2301 (April 1982).
8. T. Lo, et al., "Failure Probability of PWR Reactor Coolant Loop Piping," Lawrence Livermore National Laboratory, Report UCRL-86249 (February 1984).
9. **Probability of Failure in BWR Reactor Coolant Piping, Vol. 3: Probabilistic Treatment of Stress Corrosion Cracking in 304 and 316NG BWR Piping Weldments**, Lawrence Livermore National Laboratory, Report UCID-20914, NUREG/CR-4792, Vol. 3 (November 1986).
10. W.J. Shack, "Effects of Impurities on Stress Corrosion Cracking in BWR Piping Systems", Argonne National Laboratory (May 1988). Presented at the NRC-MITI Technical Information Exchange Engineering Workshop, Tokyo, Japan, May 16-20, 1988.
11. W. Hazelton and W. Koo, **Technical Report on Material Selection and Processing Guidelines for BWR Coolant Pressure Boundary Piping**, U.S. Nuclear Regulatory Commission, NUREG-0313, Revision 2 (1987).

Table 1. Pipe diameters, number of welds in existing and proposed recirculation loop configurations for BWR pilot plant.

| Weld Group     | Diameter (in) | Welds/loop (existing) | Welds/loop (proposed) |
|----------------|---------------|-----------------------|-----------------------|
| Discharge      | 26            | 10                    | 11                    |
| Suction        | 26            | 6                     | 5                     |
| Header         | 20            | 5                     | 2                     |
| Risers         | 12            | 20                    | 12                    |
| Bypass         | 3             | 10                    | 0                     |
| Total per loop |               | 51                    | 30                    |

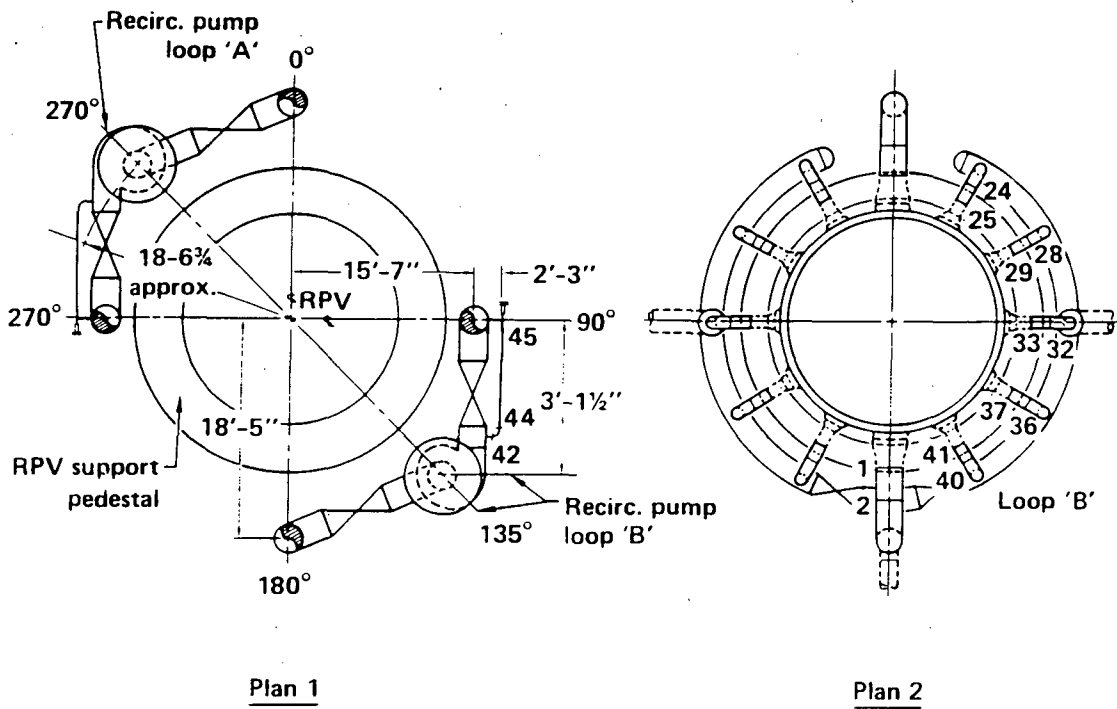
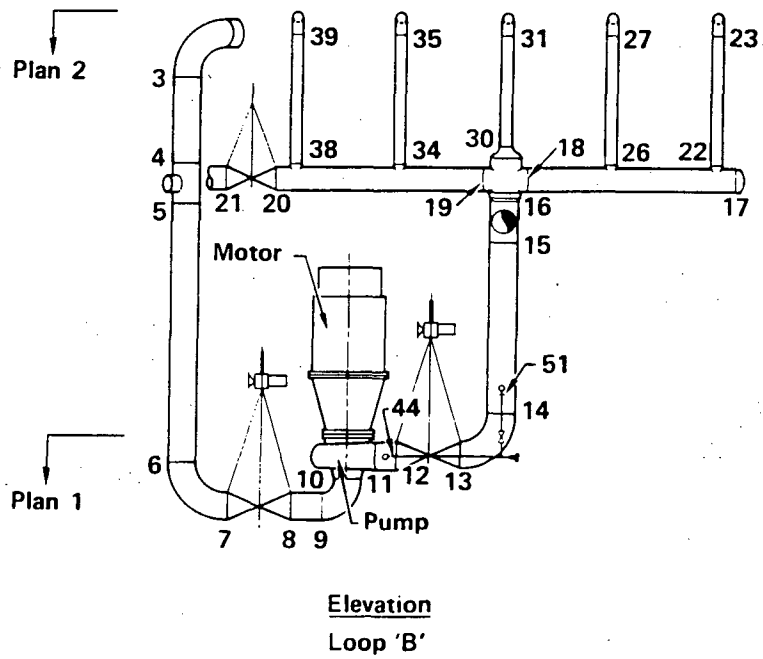


Fig. 1. Pilot plant recirculation system (existing configuration).

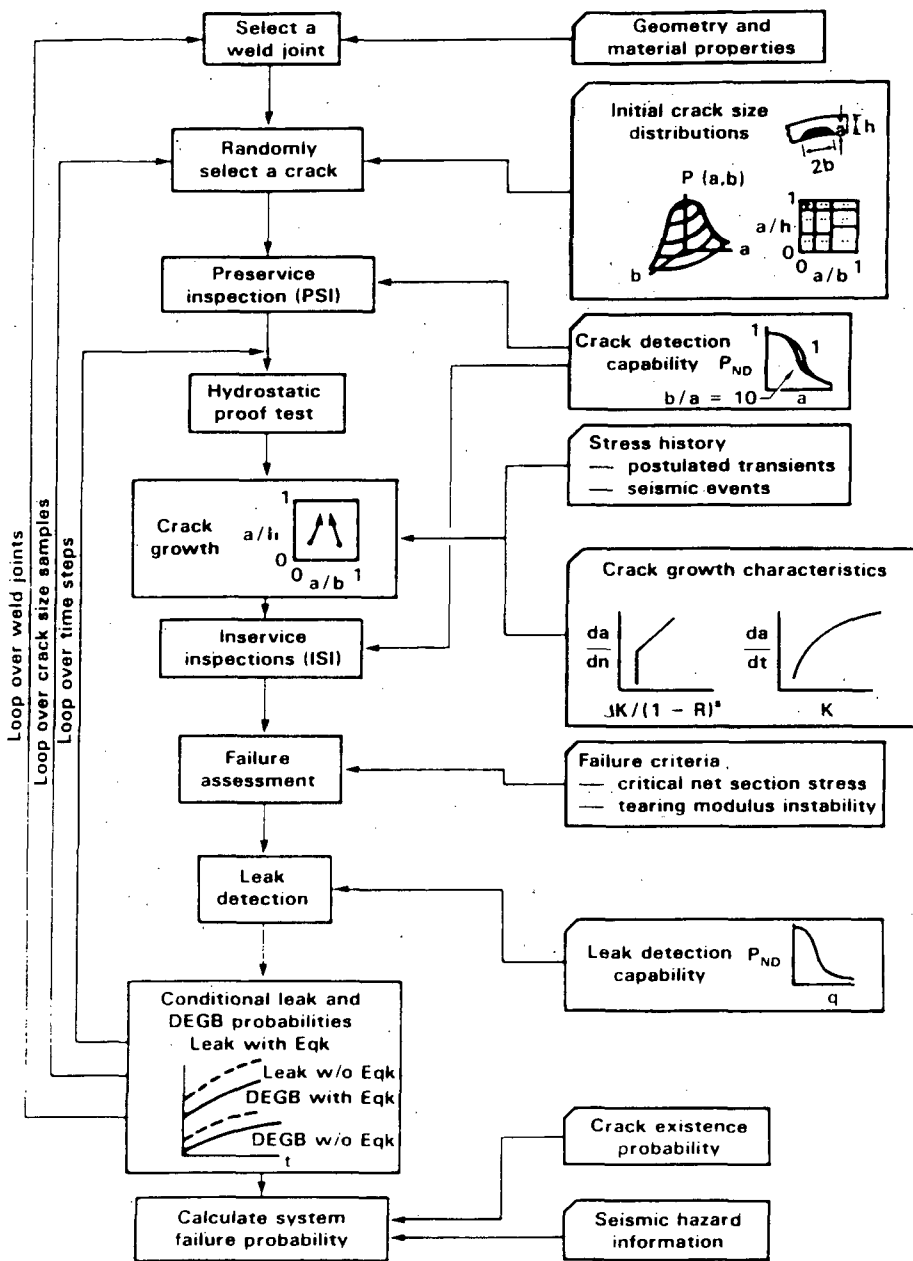


Fig. 2. Flowchart of the probabilistic fracture mechanics model implemented in the PRAISE computer code.

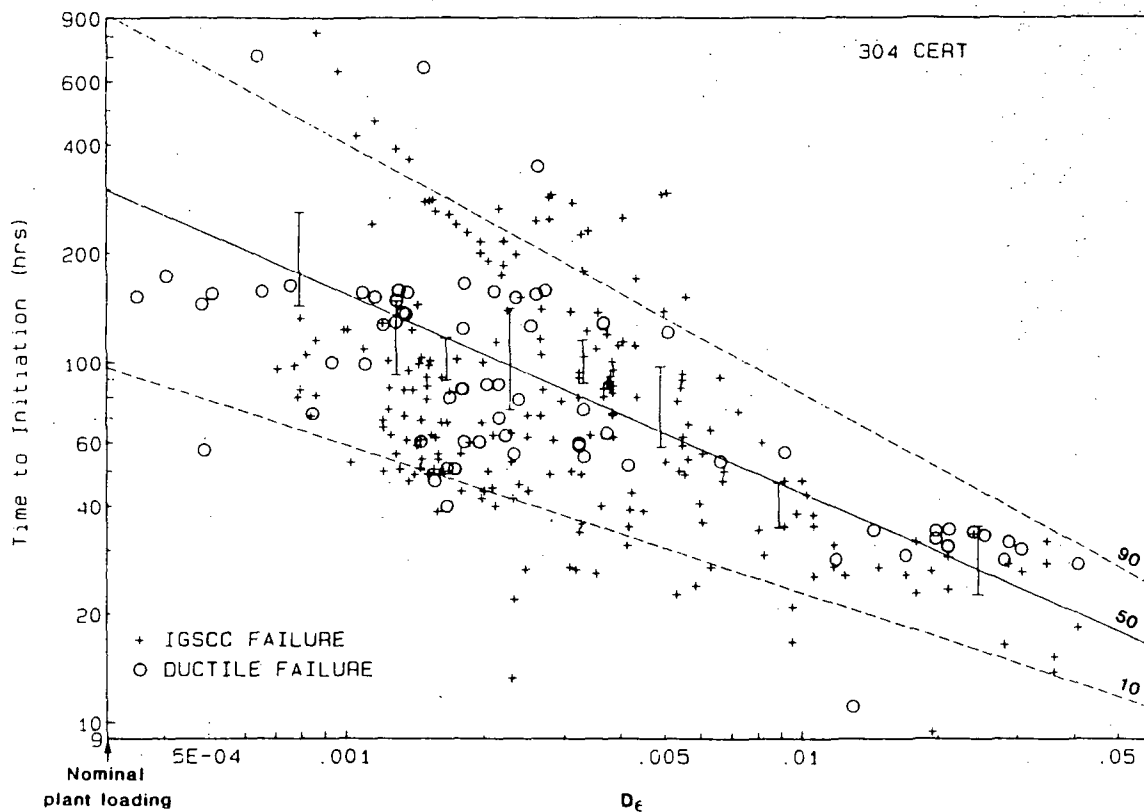


Fig. 3. Time-to-initiation for IGSCC cracks in 304SS as a function of damage parameter, plant loading/unloading.

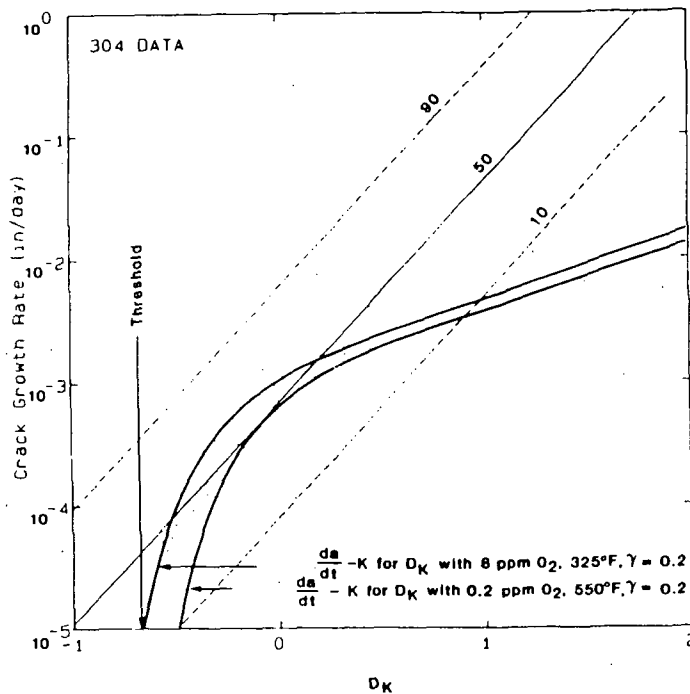


Fig. 4. IGSCC crack growth rate in 304SS as a function of damage parameter, steady-state operation. The solid lines represent crack growth rates predicted by the earlier IGSCC model in PRAISE.

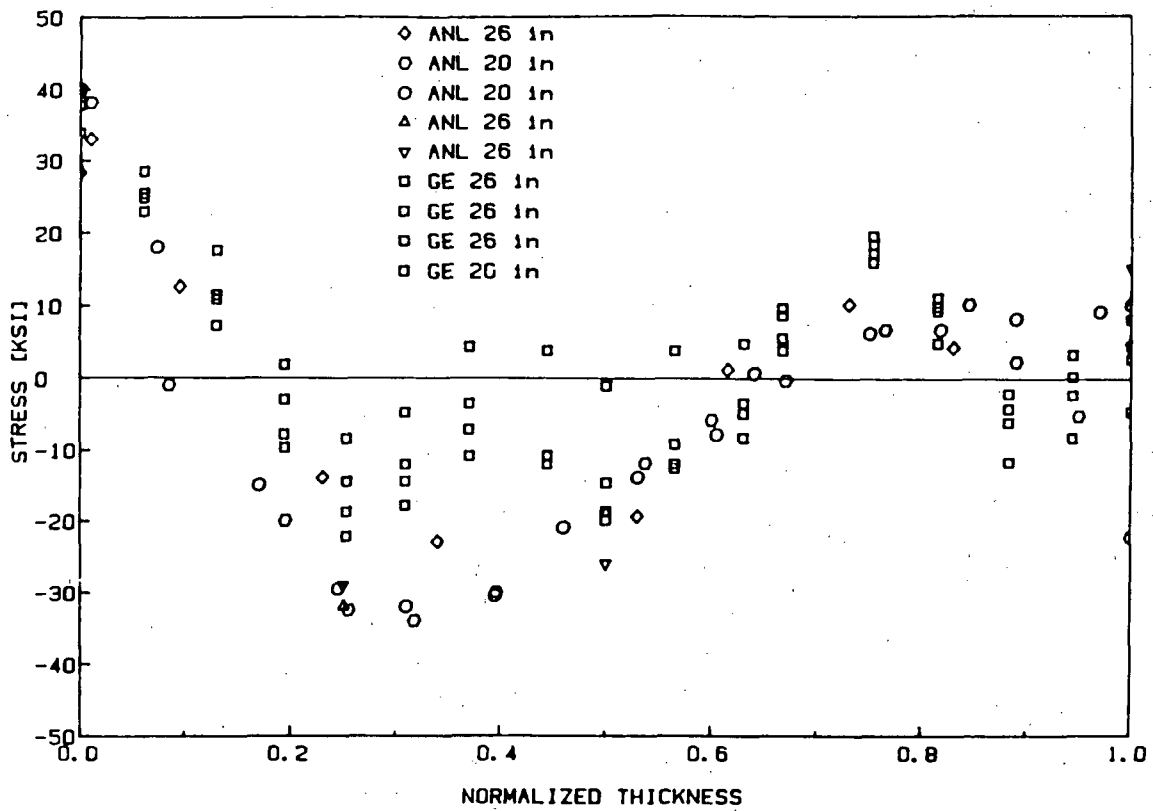


Fig. 5. Residual stress data for large-diameter (20 to 26 inches) piping as a function of distance from the inner wall.

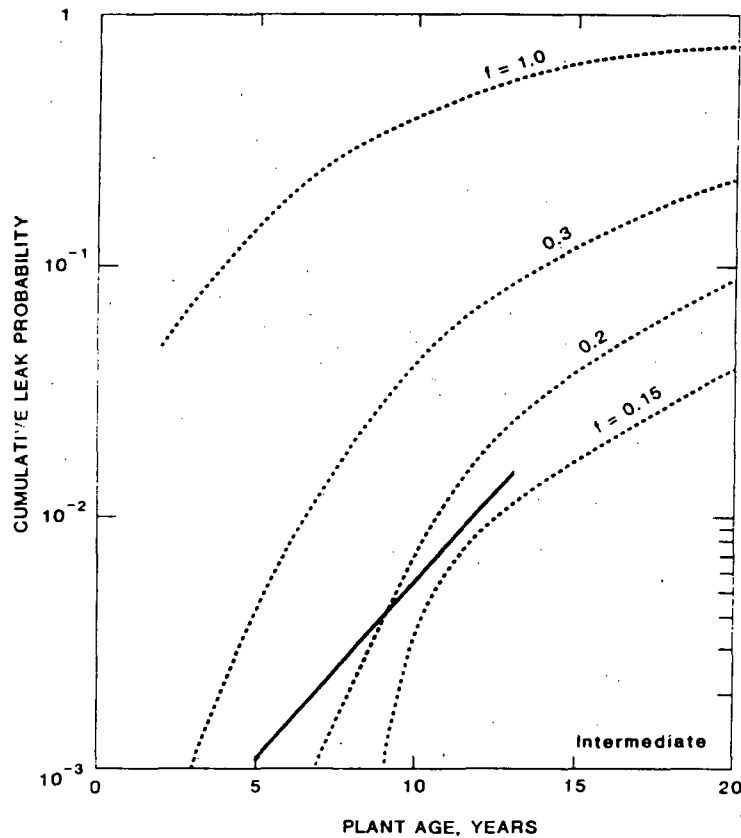
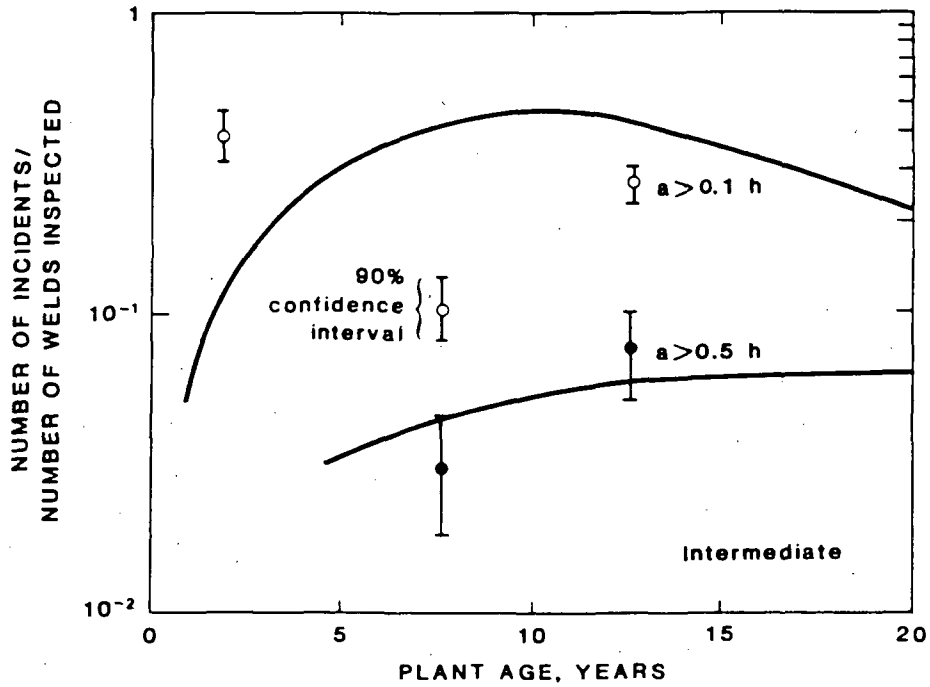


Fig. 6. Comparison of leak probabilities derived from field data with leak probabilities estimated by PRAISE for various values of residual stress adjustment factor (304SS).



- , ○ field data ( $a$  = crack depth,  $h$  = wall thickness) with 90% confidence interval
- crack size distributions estimated by PRAISE for  $a > 0.1h$  (top) and  $a > 0.5h$

Fig. 7. Comparison of crack indications derived from field data with PRAISE results based on optimum value of residual stress adjustment factor (304SS).

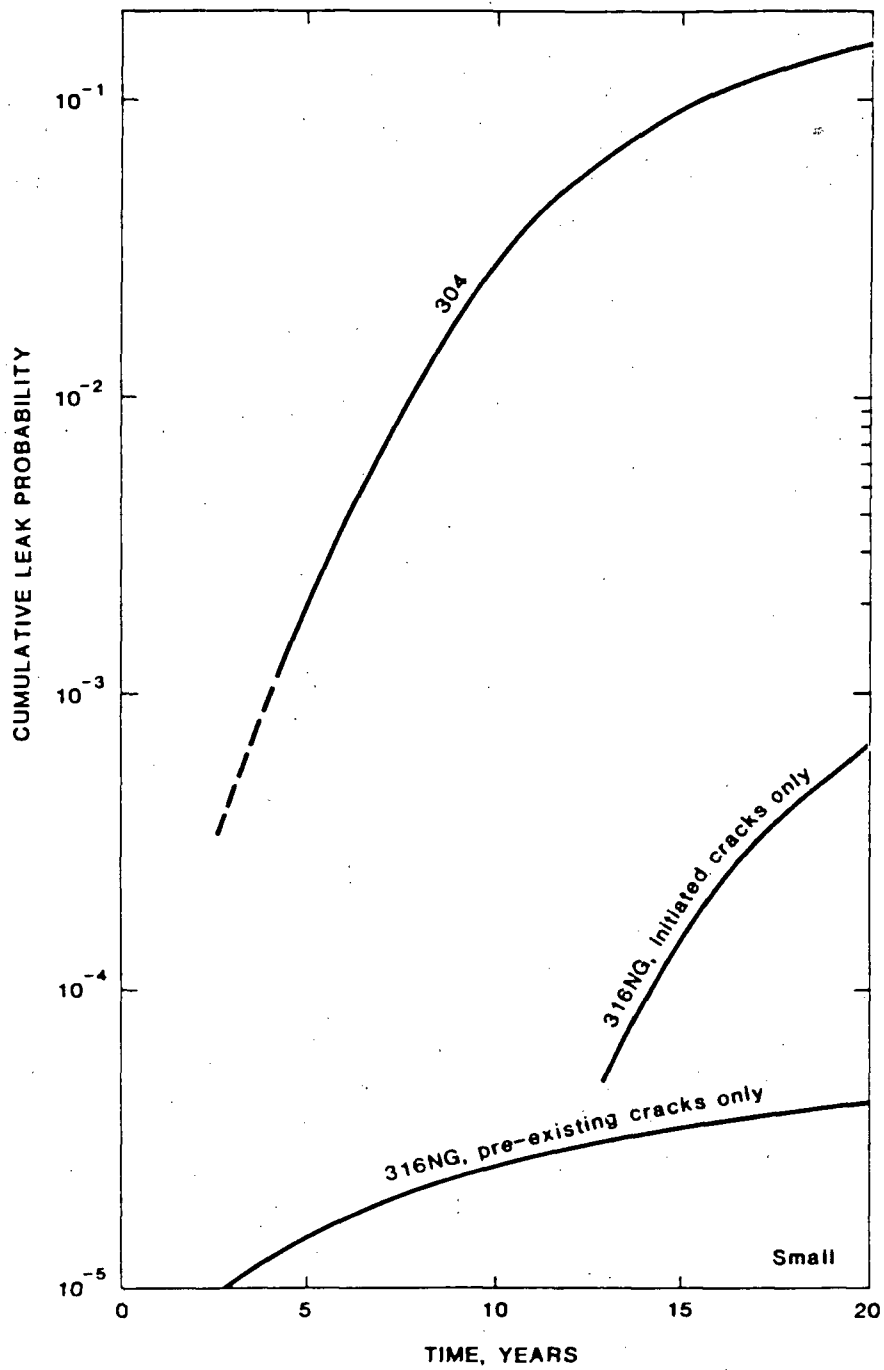


Fig. 8. Cumulative leak probability as a function of time for small-diameter weldments fabricated from Types 304 and 316NG stainless steel.

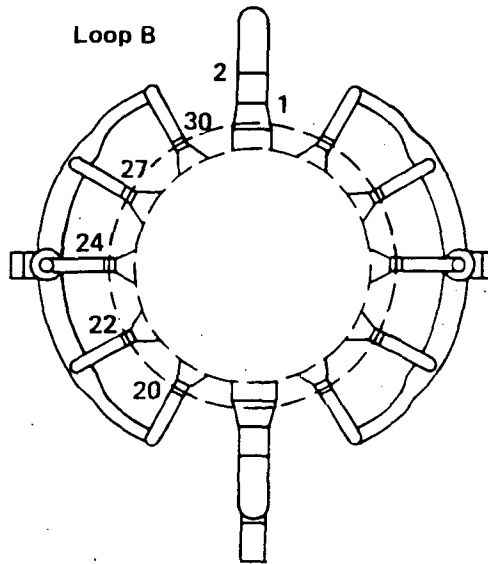
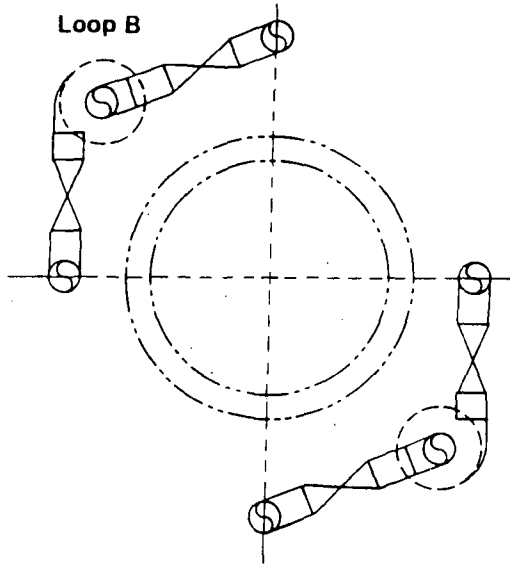
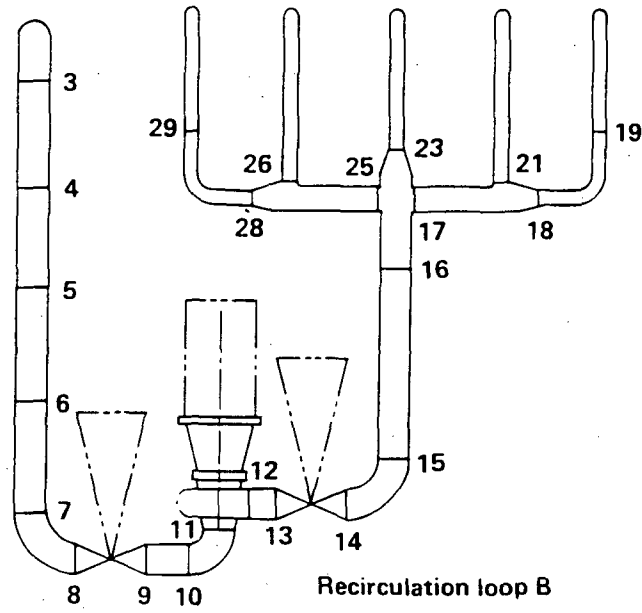


Fig. 9. Replacement recirculation loop configuration proposed for BWR pilot plant.

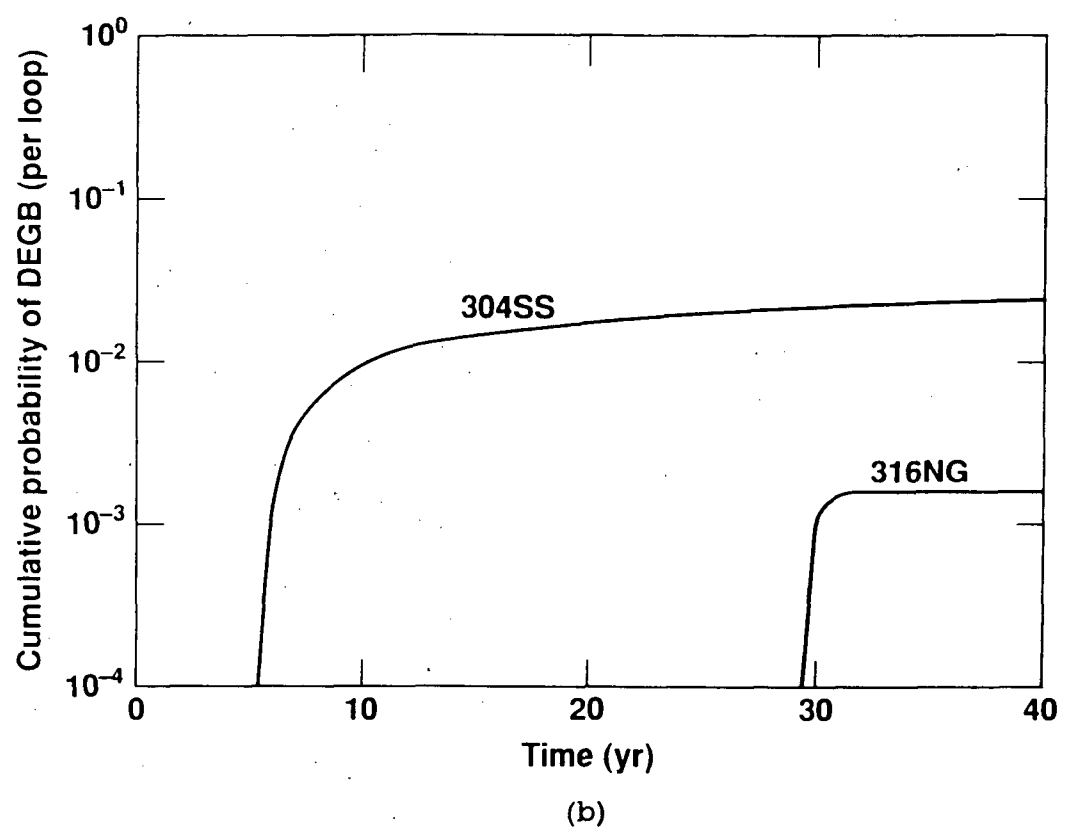
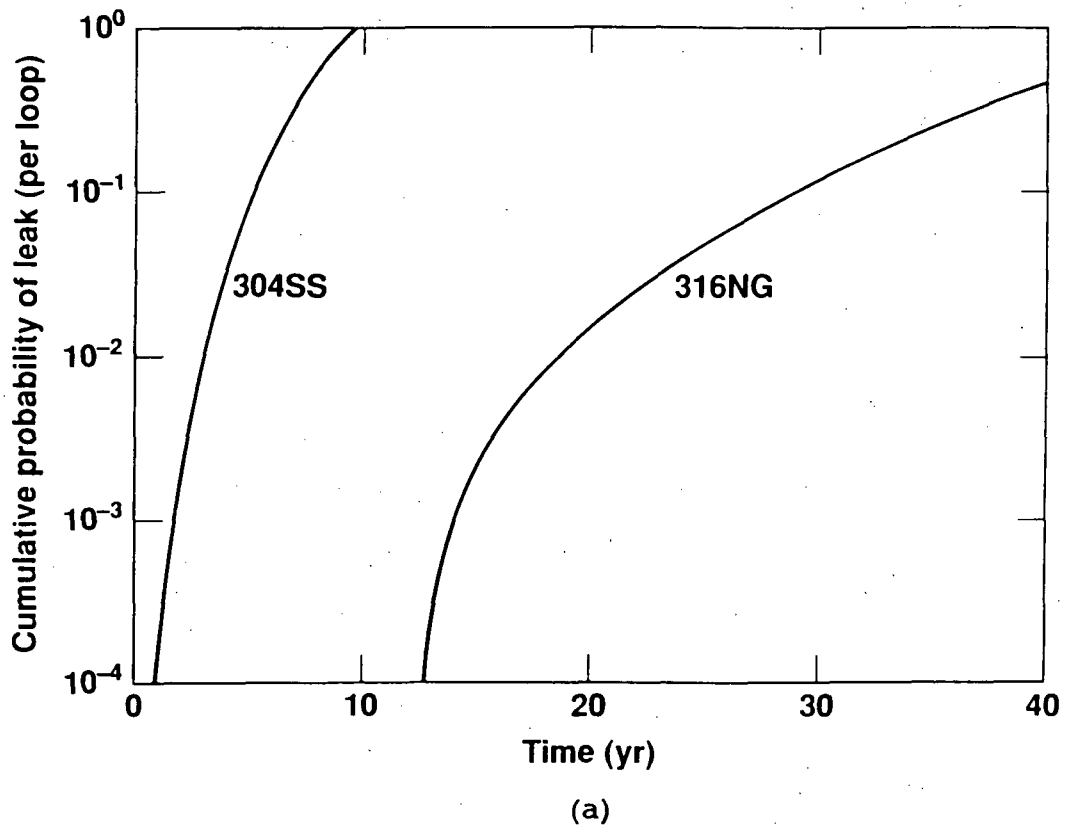


Fig. 10. Cumulative system probabilities of (a) leak and (b) DEGB for one pilot plant recirculation loop (existing configuration).

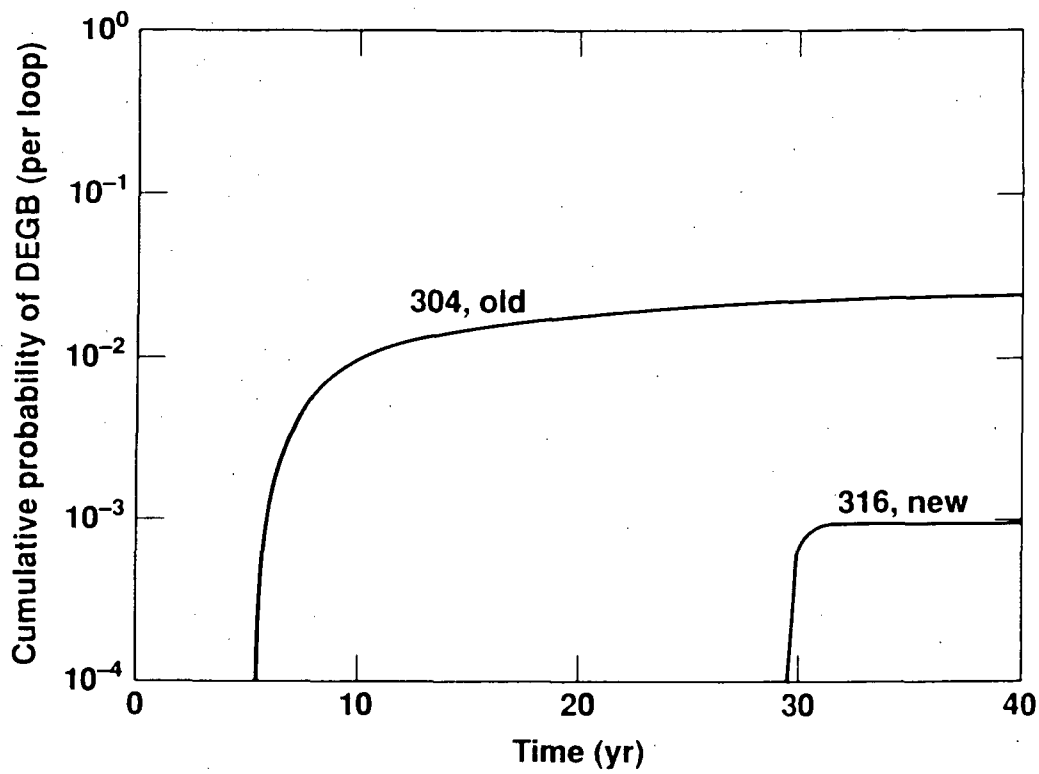


Fig. 11. Comparison of cumulative DEGB probabilities between existing recirculation loop and proposed replacement configuration.

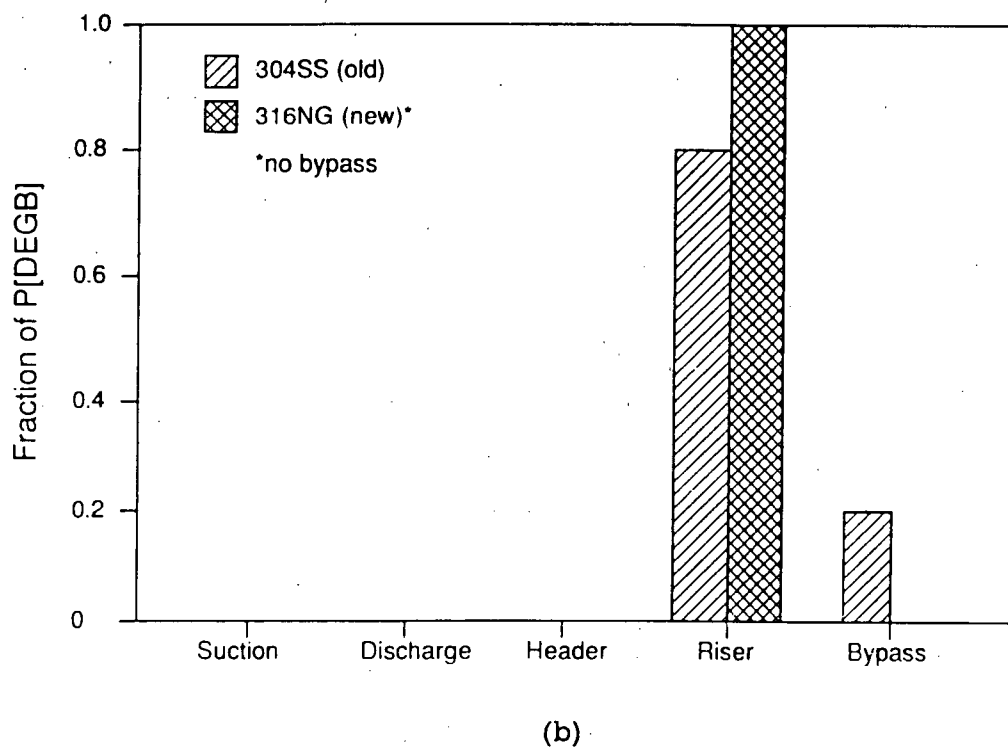
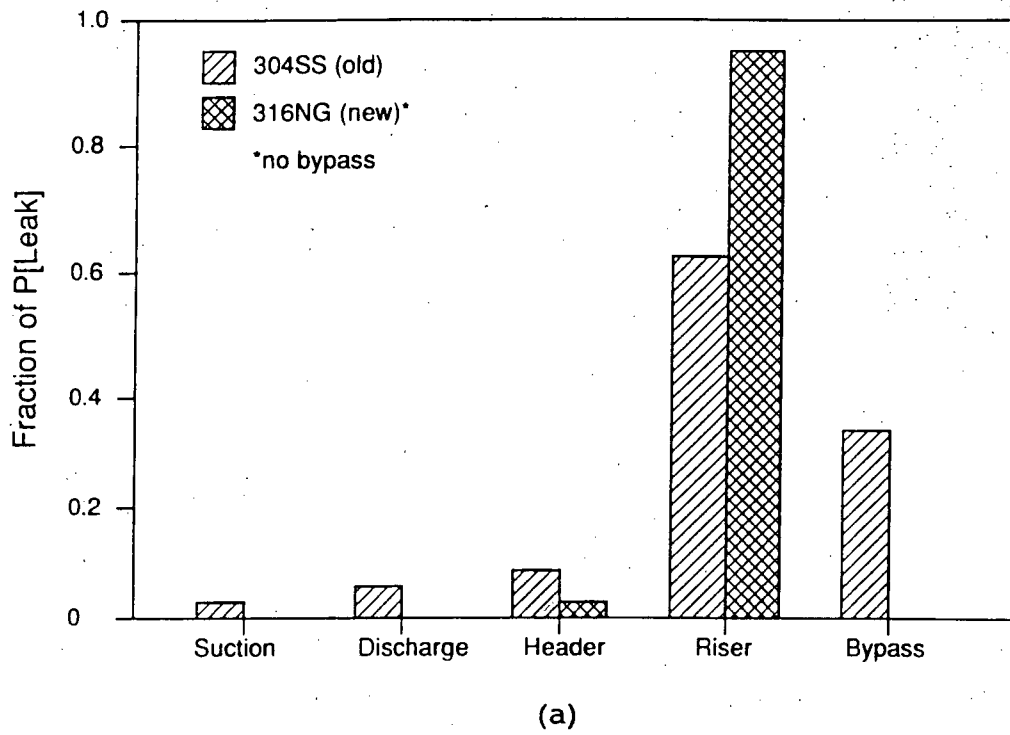


Fig. 12. Relative contribution of various weld types to system probabilities of (a) leak and (b) DEGB, existing recirculation loops and proposed replacement configuration.

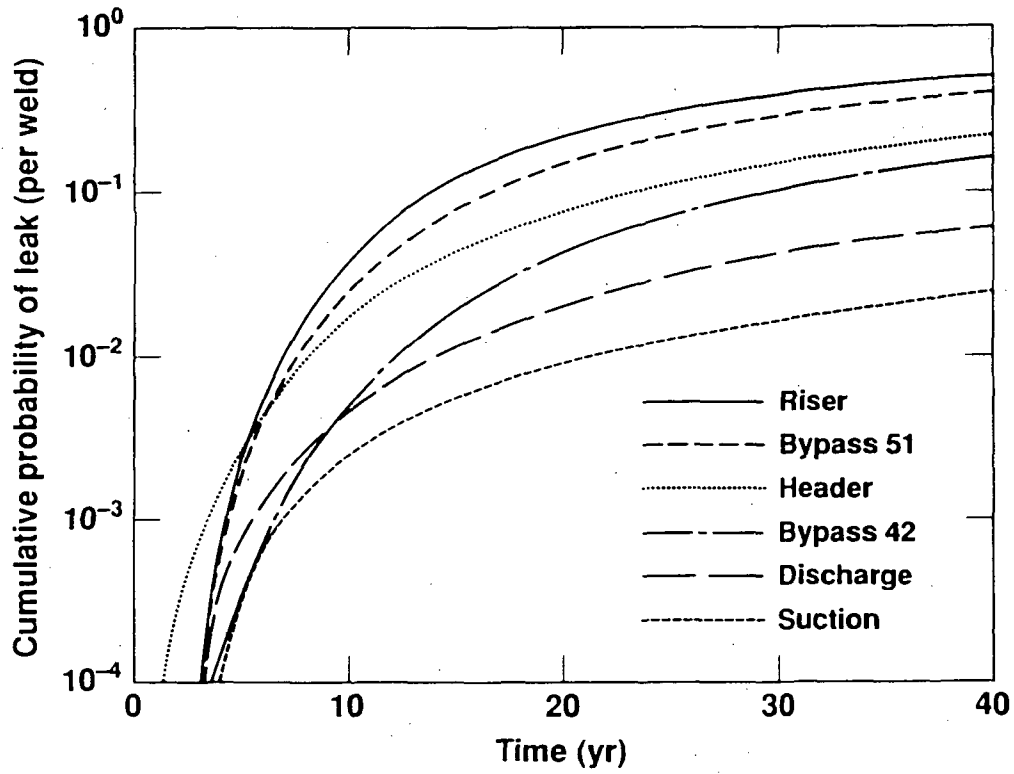


Fig. 13. Cumulative probabilities of leak for indicated welds (existing loop configuration).

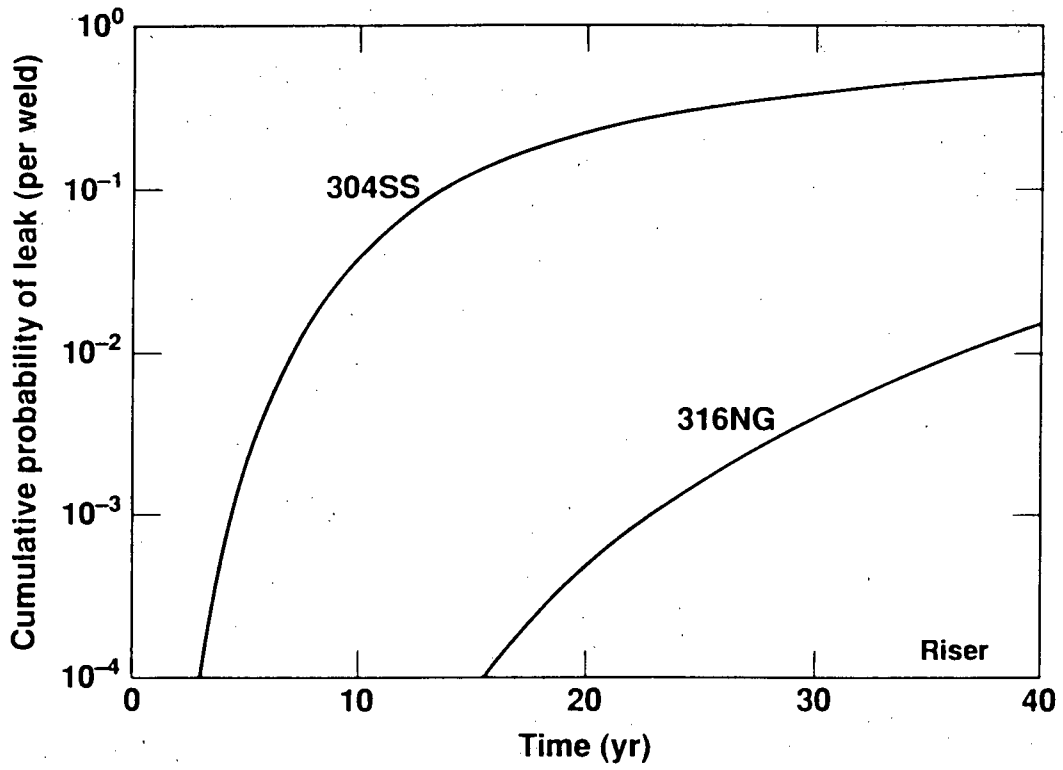


Fig. 14. Riser weld cumulative probability of leak, for Type 304 and Type 316NG stainless steel (existing loop configuration).

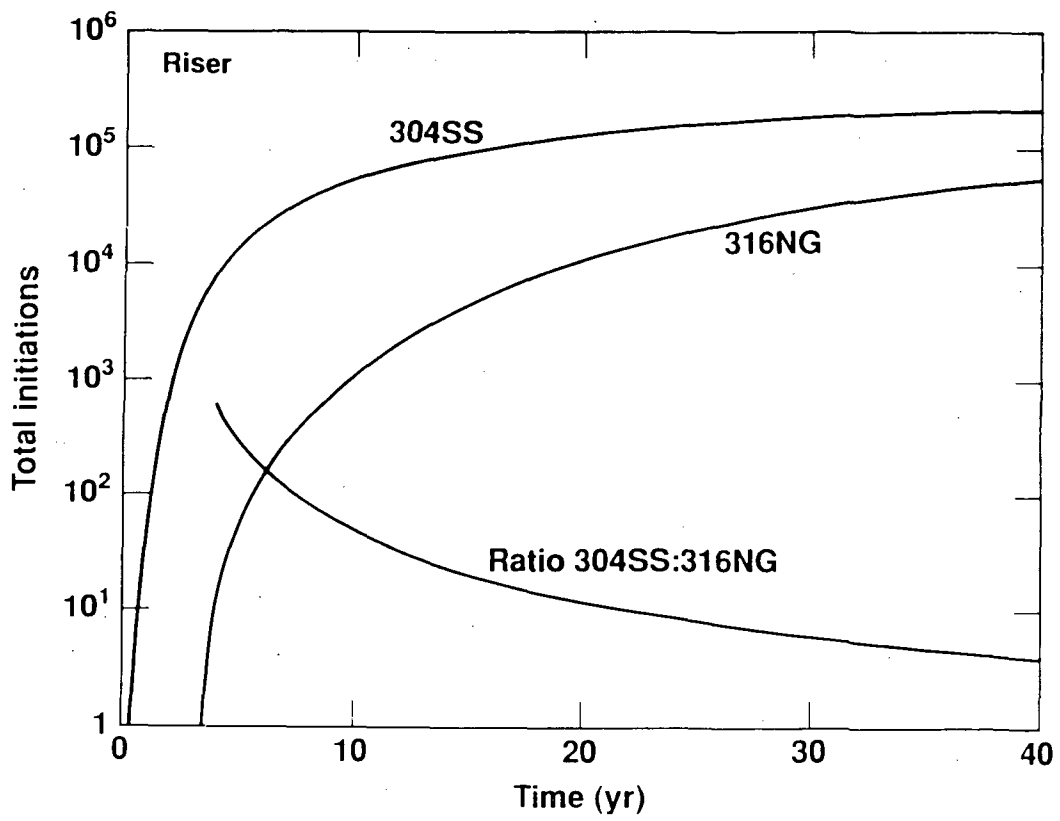


Fig. 15. Total riser weld initiations for Type 304 and Type 316NG material, existing loop configuration (25,000 Monte Carlo replications).

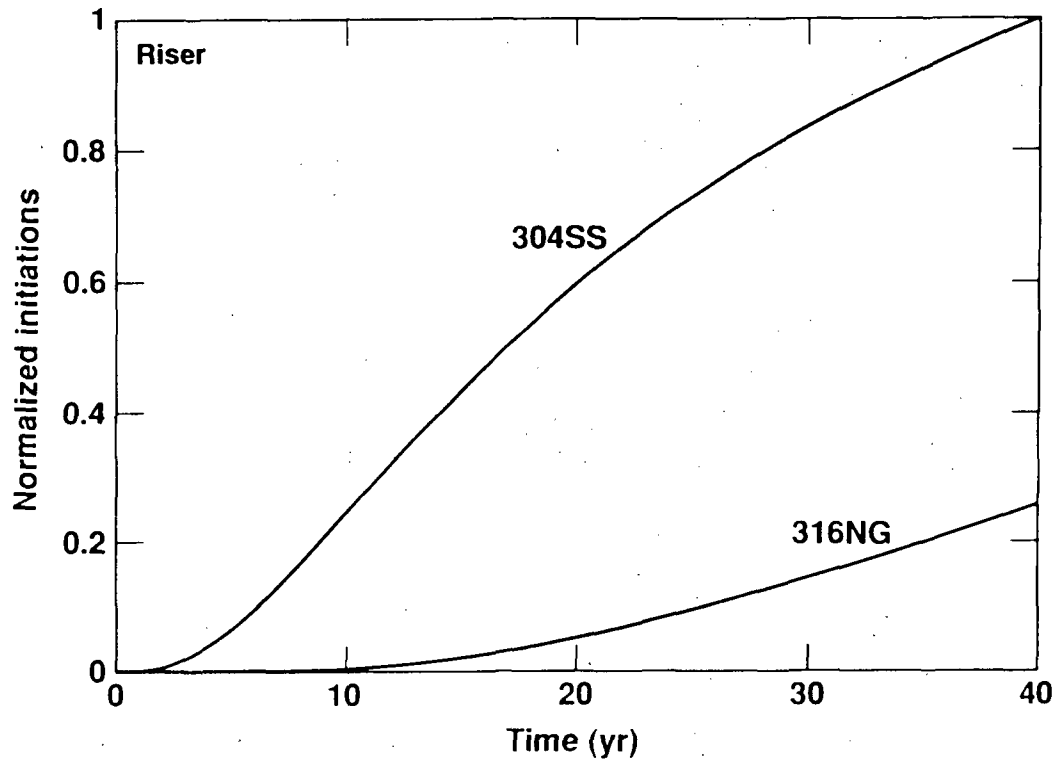


Fig. 16. Cumulative distribution of riser weld initiated cracks, normalized to Type 304 lifetime total.

# GUILLOTINE BREAKS INDIRECTLY CAUSED BY SEISMICALLY-INDUCED FAILURES\*

Garry S. Holman  
T. Lo

Lawrence Livermore National Laboratory  
University of California  
Livermore, California / U.S.A.

## ABSTRACT

The Lawrence Livermore National Laboratory has developed techniques for evaluating how piping support failures caused by earthquakes would contribute to the overall probability of piping system failure. These techniques have been applied to evaluate various reactor coolant piping systems in both PWR and BWR plants. These evaluations typically found that the likelihood of pipe break due to seismically-induced support failure is small, not only for the large, stiff piping found in PWR primary systems, but for more complex, more flexible piping systems as well. We have also applied these "reliability assessments" to specific regulatory issues such as the safety significance of various support failure scenarios, identifying individual supports whose failure would most seriously affect system integrity, and assessing system failure on the basis of realistic failure criteria. The usefulness of such evaluations in a regulatory context has been demonstrated through recent NRC rulemaking actions, which were based in large part on the results of LLNL piping reliability studies.

## 1. INTRODUCTION

The Lawrence Livermore National Laboratory (LLNL), through its Nuclear Systems Safety Program, has performed probabilistic reliability analyses of PWR and BWR reactor coolant piping for the NRC Office of Nuclear Regulatory Research. Specifically, LLNL has estimated the probability of a double-ended guillotine break (DEGB) in the reactor coolant loop piping of PWR plants, and in the main steam, feedwater, and recirculation piping of BWR plants. For these piping systems, the results of these investigations provide NRC with one technical basis on which to:

---

\* "This work was supported by the United States Nuclear Regulatory Commission under a Memorandum of Understanding with the United States Department of Energy."

- (1) reevaluate the current general design requirement that DEGB be postulated in the design of nuclear power plant structures, systems, and components against the effects of postulated pipe breaks. Recent NRC rulemaking actions, based in large part on the results of our PWR evaluations, now provide a means for eliminating dynamic effects of reactor coolant loop breaks (e.g., pipe whip, jet impingement) as a basis for PWR plant design.
- (2) determine if an earthquake could induce a DEGB and thus reevaluate the design requirements that pipe break loads be combined with those resulting from a safe shutdown earthquake (SSE). Recent deviations from the NRC Standard Review Plan, for example, now allow decoupling of SSE and DEGB loads for PWR reactor coolant loop piping.
- (3) make licensing decisions concerning the replacement, upgrading, or redesign of piping systems, or addressing such issues as the need for pipe whip restraints on reactor coolant piping.

In estimating the probability of DEGB, LLNL considers two causes of pipe break; pipe fracture due to the growth of cracks at welded joints ("direct" DEGB) and pipe rupture indirectly caused by the seismically-induced failure of critical supports or equipment ("indirect" DEGB). This paper will focus on methods used to estimate the probability of pipe break caused by support failure.

## 2. BACKGROUND

Over the past several years, generic evaluations of reactor coolant loop piping were completed for PWR nuclear steam supply systems manufactured by Westinghouse, Combustion Engineering, and Babcock & Wilcox. In these evaluations, LLNL performed the following:

- (1) estimated the probability of direct DEGB taking into account such contributing factors as the initial size (depth and length) of pre-existing fabrication flaws, pipe stresses due to normal operation and sudden extreme loads (such as earthquakes), the crack growth characteristics of pipe materials, and the capability to detect cracks or to detect a leak if a crack were to penetrate the pipe wall. For this purpose, LLNL developed a probabilistic fracture mechanics model using Monte Carlo simulation techniques, implemented in the PRAISE (Piping Reliability Analysis Including Seismic Events) computer code.
- (2) estimated the probability of indirect DEGB by identifying critical supports or equipment whose failure could result in pipe break, determining the seismic "fragility" (relationship between seismic response and probability of failure) of each, and then combining this result with the probability that an earthquake occurs producing a certain level of excitation ("seismic hazard").

- (3) for both causes of DEGB, performed sensitivity studies to identify key parameters affecting the probability of pipe break. We also performed uncertainty studies to quantify how uncertainties in input data affect the uncertainty in the final estimated probability of pipe break.

The results of these evaluations consistently indicated that the probability of a DEGB in PWR reactor coolant loop piping is extremely small, about  $1E-7$  events per reactor-year from indirect causes, and less than  $1E-10$  events per reactor-year from direct causes. It was also found that thermal stresses dominated the probability of direct DEGB, and that earthquakes contributed only negligibly. These results suggested that the DEGB design requirement -- and with it related design issues such as coupling of DEGB and SSE loads, asymmetric blowdown, and the need to install pipe whip restraints -- warranted reevaluation for PWR reactor coolant loop piping. Details of these investigations have been extensively documented elsewhere [1,2,3,4] and will not be discussed here any further.

The objectives and approach of the BWR study [5] were essentially the same except that different dominant failure mechanisms were added. LINL limited its investigation to Mark I plants, which have recirculation piping particularly susceptible to the effects of intergranular stress corrosion cracking (IGSCC). Although our evaluations were all generally similar, two important aspects distinguished the BWR study from the earlier PWR evaluations:

- (1) the susceptibility of certain BWR stainless steels to IGSCC (not a problem in PWR reactor coolant loops) required development of an appropriate probabilistic model of corrosion phenomena. This model is described in detail in a companion paper [6] and will not be discussed here.
- (2) the greater complexity and flexibility of BWR recirculation piping compared to PWR primary loops required that intermediate pipe supports (e.g., snubbers, spring hangers) be incorporated in the evaluation.

Thus, while our evaluations of indirect DEGB in PWR reactor coolant loops were limited to seismically-induced failure of so-called "heavy component" supports, our evaluation of BWR reactor coolant piping considered a second mode of "indirect" DEGB -- failure of intermediate pipe supports and supports for light loop components -- in addition to the failure of heavy component supports.

### **3. PIPE BREAK CAUSED BY FAILURE OF HEAVY COMPONENT SUPPORTS**

#### **3.1 General Discussion**

If earthquakes and pipe breaks are considered as purely random events, the probability of their simultaneous occurrence is negligibly low. However, if an earthquake could cause DEGB, then the probability

of simultaneous occurrence would be significantly higher. Our study of direct DEGB concluded that earthquakes were not a significant contributor to this failure mode. However, another way in which DEGB could occur would be for an earthquake to cause the failure of component supports or other equipment whose failure in turn would cause a reactor coolant pipe to break.

As shown schematically in Fig. 1, evaluating the probability of indirect DEGB involves the following three steps:

- (1) identify "critical" components whose failure could induce a DEGB. For each component, estimate the conservatism and the uncertainty in the calculated structural responses for various loading conditions, such as dead weight, thermal expansion, pressure, and seismic loads. In our PWR evaluations, we identified as critical components the reactor pressure vessel supports, the steam generator supports, and the reactor coolant pump supports; these components are often referred to as "heavy component" supports. Many other plausible causes of indirect DEGB unrelated to earthquakes (e.g., crane failure, pump flywheel missiles) were also considered as part of an in-depth pilot study, but were determined to be of negligible significance compared to heavy component support failure.

A BWR, of course, has no steam generators and the failure of coolant pump supports was considered separately as discussed later in this paper. Therefore, the only critical "heavy component" supports that we considered in our BWR indirect DEGB evaluation were those making up the reactor support structure. These included the lower support structure at the base of the RPV as well as the lateral stabilizers at the top of the vessel.

- (2) for each critical component, develop a fragility description for each failure mode. Each fragility description relates the probability of structural failure conditioned on the occurrence of an earthquake of given peak ground acceleration. Combine fragilities for individual components into an overall "plant level" fragility to account for all significant failure modes and the associated fragility descriptions.
- (3) calculate the non-conditional probability of indirect DEGB by convolving the plant level fragility with an appropriate description of seismic hazard. "Seismic hazard" relates the probability of occurrence of an earthquake exceeding a given level of peak ground acceleration.

Because it is conservative to expect that failure of a heavy component support would unconditionally result in pipe break, the "indirect DEGB" evaluation in this case becomes a "support reliability" evaluation. The following discussion, excerpted from Ref. 7, describes how this evaluation is performed.

### 3.2 Methodology

The probability of indirect DEGB,  $P[\text{DEGB}]$ , can be mathematically expressed by:

$$P[\text{DEGB}] = \int_0^{\infty} P\left[ \bigcup_{i=1}^n (C_i < R_i) \mid A = a \right] f_A(a) da \quad (1)$$

where:

- $\bigcup$  = "union" symbol
- $C_i$  = capacity of structural element "i" (e.g., RPV support, steam generator support)
- $R_i$  = random variable representing response of structural element "i" to peak ground acceleration  $a$
- $f_A(a) da$  = frequency of occurrence of an earthquake with peak ground acceleration between  $a$  and  $a+da$

Equation (1) is written assuming that there is perfect knowledge about the values of the parameters that define the probability terms. Since there is uncertainty in these parameter values, a subjective probability distribution of the probability of induced DEGB will be obtained by appropriately varying the parameter values.

The first term within the integral of Eq. (1) is the conditional probability of occurrence of DEGB due to structural failures for a given peak ground acceleration,  $a$ . It is defined as the probability of failure of at least one of the structural elements which can lead to DEGB of the RCL piping. Therefore, the focus in this study is only on those structural elements within the containment whose failure can result in DEGB. Among these, some elements may have large margins of safety against seismic failure and thus may not contribute significantly to the probability of DEGB. Therefore, critical elements are defined as those whose failure could contribute significantly to the probability of indirectly-induced DEGB. For PWR plants, these were identified as the steam generator supports, the reactor coolant pump supports, and the reactor pressure vessel supports [1].

The conditional probability of DEGB is evaluated by treating the failure events of individual structural elements as statistically independent. This gives a conservative upper bound on the probability of DEGB. Also, if one of the structural elements has a very high conditional probability of failure compared to other elements, the upper bound is a good approximation to the actual  $P[\text{DEGB}]$ .

### 3.3 Seismic Fragility

The conditional probability of failure of a structural element for a given peak ground acceleration is called the seismic "fragility" of the element (Fig. 2). The fragility evaluation in our DEGB evaluations was accomplished using information on plant design bases and by appropriately extrapolating the responses calculated at the design analysis stage to the failure levels of the structural elements.

Evaluation of the fragility is simplified by defining a random variable called the ground acceleration capacity. The ground acceleration capacity, denoted by  $A_C$ , is expressed as:

$$A_C = F * A_{SSE} \quad (2)$$

where  $F$  is the factor of safety on the design basis earthquake (usually the safe shutdown earthquake) and  $A_{SSE}$  is the peak ground acceleration at the safe shutdown earthquake. The factor of safety is defined as a ratio of the seismic capacity of the structural element  $C_i$  to the response,  $R_i$ , of the element due to the SSE. Since  $C_i$  and  $R_i$  are random variables, the factor of safety  $F$  is also a random variable.

The factor of safety  $F$  is modeled as a log-normally distributed random variable with the parameters, median  $F$  and logarithmic standard deviation  $\beta_F$ . Two basic types of variability are identified in describing the factor of safety: one that represents the inherent randomness and one that represents the uncertainty in the parameter value, e.g. the median. These variabilities are quantified by the logarithmic standard deviations  $\beta_{F,R}$  and  $\beta_{F,U}$ , respectively. Essentially,  $\beta_{F,R}$  represents the variability due to randomness of earthquake characteristics for the same peak ground acceleration and to the randomness of the structural response parameters which relate to these characteristics. The dispersion represented by  $\beta_{F,U}$  is due to such factors as:

1. Our lack of understanding of structural material properties such as strength, inelastic energy absorption capacity and damping, and
2. errors in calculated response due to use of approximate modeling of the structure and equipment, and inaccuracies in mass and stiffness representations.

For equipment supports, the factor of safety can be modeled as the product of three variables:

$$F = F_C * F_{RS} * F_{RE} \quad (3)$$

where the capacity factor  $F_C$  for the equipment support is a product of a strength factor  $F_S$  and an inelastic energy absorption factor  $F_{\mu}$ . The strength factor  $F_S$  represents the ratio of ultimate strength to the stress calculated for  $A_{SSE}$ . The inelastic energy absorption factor (ductility) accounts for the fact that an earthquake represents a limited energy source and structures or components are generally capable of absorbing substantial amounts of energy beyond yield without loss of function.

The structural response factor  $F_{RS}$  recognizes that in the design analyses, the structural response was computed using specific (and often conservative) deterministic response parameters for the structure. Because many of these parameters are random (often with a wide variability) the actual response may differ substantially from the design response calculated for a given peak ground acceleration. The more significant factors include variability in (1) ground motion and associated ground response spectra for a given peak free-field ground acceleration, (2) soil-structure interaction, (3) energy dissipation (damping), (4) structural modeling, (5) method of analysis, (6) combination of modes, and (7) combination of earthquake components.

The equipment response factor  $F_{RE}$  depends upon the response characteristics of the equipment (in this case, the nuclear steam supply systems including RPV, steam generators, reactor coolant pumps, and their supports) and is influenced by the same variables as those listed for structural response.

For each variable affecting the factor of safety, the median value as well as the associated random and modeling uncertainties  $\beta_R$  and  $\beta_U$  are estimated.

With the overall factor of safety  $F$  estimated as described above, the ground acceleration capacity of the structural element is then calculated using Eq. (3):

$$A_C = F_C * F_{RS} * F_{RE} * A_{SSE} \quad (4)$$

$$\beta_{A,R} = (\beta_{C,R}^2 + \beta_{RS,R}^2 + \beta_{RE,R}^2)^{1/2} \quad (5)$$

$$\beta_{A,U} = (\beta_{C,U}^2 + \beta_{RS,U}^2 + \beta_{RE,U}^2)^{1/2} \quad (6)$$

The ground acceleration capacity of each equipment support was modeled as the lowest capacity in all credible failure modes. This is a realistic assumption since the failure modes are highly correlated due to common structural material, method of fabrication, and correlation of input motion. Again, if the structural element of one of the failure modes has a very low capacity compared to other modes, this assumption leads to a good approximation of the probability distribution of the capacity.

### 3.4 Seismic Hazard

The remaining term within the integral of Eq. (1),  $f_A(a)da$ , is the annual probability that the peak ground acceleration at the plant site is between  $a$  and  $a+da$ . This is generally referred to as "seismic hazard" and is usually described by a set of curves plotting annual exceedance probability as a function of peak ground acceleration. The uncertainty in the hazard description is represented by assigning each curve a subjective weighting factor (or confidence limit). Our BWR evaluation and most of our PWR evaluations were based on generic hazard curves which we developed for the eastern United States (Fig. 2); west coast PWR plants were evaluated on the basis of site-specific seismic hazard information.

### 3.5 Discussion of Results

Applying this methodology to PWR reactor coolant loop piping, we found for all vendors that the probability of indirect DEGB was very small. For Westinghouse plants, the median probability of indirect pipe break was about  $1.0E-7$  per reactor-year for plants east of the Rocky Mountains (based on generic seismic hazard curves), and about  $3.0E-6$  per reactor-year for plants on the more seismically active west coast; "upper bound" (i.e. 90% confidence level) probabilities were typically about one order of magnitude higher. Equivalent results for Combustion Engineering and Babcock & Wilcox reactor coolant loops were comparable to the Westinghouse results.

In our BWR evaluation, we found that the probability of indirect DEGB due to heavy component support failure was about  $2E-8$  events per reactor-year, with a 90th-percentile value (confidence limit) of  $5E-7$  per reactor-year. We found that the "star" stabilizer at the top of the reactor pressure vessel, which restrains the RPV against lateral motion in the event of an earthquake, was the primary contributor to failure rather than the main support structure at the bottom of the vessel.

## 4. PIPE BREAK CAUSED BY FAILURE OF "INTERMEDIATE" PIPE SUPPORTS

### 4.1 General Discussion

Reactor coolant loops in PWR plants typically have small length-to-diameter ratios and, because of their stiffness, are supported solely by the major loop components (reactor pressure vessel, reactor coolant pumps, and steam generators); therefore, no additional supports are needed. However, recirculation loop piping in BWR plants is longer and smaller-diameter (typically 12 to 26 inches, although some systems include piping as small as 3 to 4 inches in diameter), and requires additional support from spring- or constant-load hangers. This piping may also have numerous snubbers to reduce stresses in the event that an earthquake occurs. Each recirculation loop at our BWR pilot plant, for

example, has a snubber pair each on the inlet and outlet lines, as well as a snubber triplet at the top and at the bottom of the recirculation pump.

The potential effect of intermediate support failure on estimating the probability of direct DEGB is two-fold:

- (1) support failure would redistribute applied stresses at weld joints, in turn affecting crack growth rates as well as the failure criteria used to define when pipe break occurs.
- (2) accounting for stress redistribution would require an individual probabilistic fracture mechanics evaluation for each support failure scenario, dramatically increasing the computational effort involved. For example, even if only four supports were addressed, sixteen separate PRAISE runs would be required to cover all possible combinations and permutations of support failure.

Our evaluations of "indirect" DEGB caused by heavy component support failure assumed that support failure unconditionally resulted in pipe break. This assumption was regarded as conservative, but nevertheless resulted in very low DEGB probabilities. To assume that failure of a snubber or a constant-load support would similarly cause a DEGB in BWR recirculation loop piping would be unreasonably conservative; in other words, a simple "support reliability" evaluation would no longer suffice. We therefore developed a more sophisticated approach to incorporate the effect of support fragility into the probabilistic fracture mechanics evaluation, which we used to investigate the effect of support failure on the probability of DEGB. Note that the need to incorporate support failure in the fracture mechanics evaluation blurs the distinction between "direct" and "indirect" DEGB, and leads us back to a more integrated approach for estimating the probability of pipe break.

#### 4.2 Methodology

Incorporating the effect of support failure on pipe failure probability is clearly a complicated problem demanding an accordingly complex analytic approach. Many questions can be asked:

- (1) What is the failure probability of a support for a given earthquake?
- (2) When does this support failure occur?
- (3) What is the response of the piping once a support fails?
- (4) What is the effect of this new response on the pipe failure probability?

- (5) If there is more than one support, how many supports will fail during an earthquake?
- (6) What is the failure sequence of these supports?
- (7) What is the piping response in such a scenario of multiple support failure? How is that going to affect the pipe failure probability?

It is difficult to answer these questions. The problem is further complicated by the fact that these questions are interrelated. For example, the support failure probability (Question 1) is affected by the piping and support responses (Question 3), which is in turn affected by the failure sequence of the supports (Question 6). Obviously, it is beyond our capability to address all of these questions. In this study, we made the following assumptions to simplify the problem to a manageable level.

- (1) All support failures occur at the same time and at the beginning of an earthquake. In other words, the piping system experiences the full duration of the earthquake for any given combination of support failures. This assumption is conservative. Thus, timing and the sequence of support failures in an earthquake are not considered. This assumption greatly reduced the complexity of the problem to a manageable size.
- (2) The supports experience the same stress distribution as if no support failure occurred during an earthquake. This allows the regular fragility development method to be applied to develop one fragility curve for each support for all levels of earthquake intensity. This assumption also allows one single set of in-structure response spectra or one single set of floor time-histories to be used in all seismic analyses.
- (3) The failure events of the supports are statistically independent of each other. The probability that certain supports will fail together in an earthquake is the product of their individual failure probabilities.

With these three assumptions, we are ready to perform the complicated, even though much simplified, assessment of pipe failure probability with the effects of seismically-induced support failure. Thus, the probability of pipe failure can be expressed as:

$$\begin{aligned}
 P[\text{PF}] &= P[\text{PF}|\text{no SF}] * P[\text{no SF}] + \\
 &\quad \sum_{i=1}^N \{P[\text{PF}|\text{SF}_i] * P[\text{SF}_i]\}
 \end{aligned}
 \tag{7}$$

where  $N$  represents the total number of support failure combinations, and  $SF_i$  represents the " $i$ "th combination of support failure. For example, a piping system with four supports will have a total of 15 support failure combinations (excluding the case of no supports failing): four cases of single-support failure, six cases of two-support failure, four cases of three-support failure, and one case of four-support failure.

To describe the general methodology as represented by Eq. (7), a flow chart is shown in Fig. 3. The analysis can be summarized in four major tasks.

- (1) Estimate support fragilities.
- (2) Calculate structural responses for all support combinations.
- (3) Estimate the conditional pipe failure probabilities at weld joints for all support conditions.
- (4) Perform system failure analyses for all support failure combinations.

In the first task, fragilities of the supports are estimated. The values of  $P[\text{no SF}|a]$  and  $P[SF_i|a]$  for a given earthquake peak ground acceleration level,  $a$ , can be calculated from the fragility curves of the supports. For each earthquake intensity,  $P[SF_i|a]$  is simply the product of individual support failure probabilities of the " $i$ "th combination scenario as stated in assumption number 3.  $P[\text{no SF}]$  is equal to 1.0 minus the sum of all cases of support failure probabilities.

In cases of support failure, the seismic responses of a piping system are different from that of the system without support failure. The structural responses for each case should be estimated separately depending upon the specific support failure combination. This estimation is the second task in assessing the effects of support failure. The regular seismic analysis process can be used starting with preparing the seismic analysis model, followed by either response spectrum or time history analysis, and ending with the calculated seismic stresses at each weld joint.

Once the seismic stresses are calculated, a probabilistic fracture mechanics analysis is then followed for each case of support failure combination. This analysis is the third task. This analysis yields the conditional failure probabilities at weld joints conditioned on the occurrence of an earthquake of specific intensity and the occurrence of a specific support failure scenario.

The probabilistic fracture mechanics methodology described earlier is a rather complicated procedure and the study of support failure effects does not warrant this level of sophistication. A simplified procedure was developed in this study to estimate the values of  $P[PF|\text{no SF}]$  and  $P[PF|SF_i]$  and is described in Ref. 8.

A system failure analysis, the last task in Fig. 3, can be performed to fold in the various results, such as the  $P[PF|SFi,a]$ ,  $P[SFi|a]$ , and the seismic hazard curves to calculate the probability of failure of a piping system for each support failure scenario. The probability of overall system failure, including all support failure scenarios, can therefore be obtained as simply the sum of the system failure probabilities of the cases according to Eq. (7).

### 4.3 Support Fragility

Three kinds of pipe supports were used in the the recirculation loops of the pilot plant; these supports are representative of those used in most vital piping in nuclear power plants (except PWR reactor coolant loops). These pipe supports are the rigid supports (or anchors), the spring hangers, and the hydraulic snubbers. The hangers and the snubbers are by themselves supported by structural members. These structural members are, by the requirements of manufacturers' design specification, much stronger than the hangers and the snubbers. Therefore, there is no need to examine the failure mode of the supports due to failure of these structural members in estimating overall support fragility.

The reactor pressure vessel provides a rigid support for the recirculation loops since the reactor vessel is massive and the recirculation loop comes out and returns back to the reactor vessel to form a loop. Failure of reactor vessel supports would most likely induce the recirculation loop to fail. The conditional failure probability of the piping (given that the reactor vessel has failed) can be assumed to be 1.0 in this case. This scenario is the same as for the PWR reactor coolant loops. Therefore, the falling down of the reactor pressure vessel is addressed in the same fashion as the earlier indirect pipe failure and is documented in Ref. 8. Here we focus our attention only on the cases where the conditional failure probability is not necessarily equal to 1.0.

Spring hangers are used to support the dead weight of the piping system; the snubbers are used to resist the seismic loads during an earthquake event. Two kinds of spring hangers were used. Constant spring hangers support the recirculation pumps, and variable spring hangers support the the coolant pipes. Hanger failure is not considered in this support failure analysis as discussed in the following reasoning.

The stiffness of the spring hangers is much less than the stiffness of the piping and the active snubbers. During an earthquake, movement of the piping system is mainly restricted by the snubbers and the rigid supports of the piping system. The increase in load in the hangers is expected to be insignificant compared to the snubbers. This expectation implies that there will be no significant difference in the hanger failure probabilities during operation or during an earthquake. On the other hand, the load in snubbers is zero at all times except during a seismic event, during which the load can be very high depend-

ing on the earthquake intensity. If a spring hanger did not fail before the earthquake, it is unlikely to fail before the snubbers fail during an earthquake. Therefore, it is reasonable to neglect hanger failure during an earthquake in this study.

Figure 4 shows the pilot plant recirculation loops, Fig. 5 the corresponding pipe support arrangement. The two loops A and B are essentially identical; in this demonstration analysis, we chose to study Loop B.

There are nine snubbers in four natural groups for the Loop B of the recirculation system, with bore diameters ranging from 3.25 to 6 inches. One snubber supports the suction line. Two are in the discharge line at the same location except in different orientations. There are three snubbers each for the pump motor at the top and the casing at the bottom of the recirculation pump. Each group as a unit provides support for a specific part of the piping system. It is reasonable to assume that if one in the group fails, the other snubbers in the same group would also lose their function. This conservative assumption simplifies the problem and makes it easier to handle than considering all nine snubbers as individual supports.

In this study the fragilities of all nine snubber supports were estimated first; then, the fragilities of the four support groups were calculated based on the assumption that the support (or the snubber) failure events are statistically independent (Fig. 6). If any one of the snubbers in a specific group fails, the whole group is assumed to have lost its function.

The particular snubbers used in the subject recirculation system offer an optional relief valve which, if installed, will protect the snubber from being damaged if the dynamic load exceeds the load limit set for the relief valve. The relief valve opens when the load reaches the preset limit so the hydraulic pressure will not continue to build up inside the cylinder. When the load reduces, the valve closes and the snubber is ready to take more load. Thus, a snubber functions like a elastic-plastic axial load member. The snubbers in the recirculation loops are equipped with such a relief valve and are set to open at 133% of the rated load. However, the test results indicated that the minimum valve opening load is actually 160% of the rated load. Under a very high earthquake load, it is possible that the load on the snubbers may exceed this valve opening load. In this situation, the snubbers behave like a non-linear structural member with a large energy absorption capability due to its plasticity effect.

Many failure modes of the subject snubbers were identified in our evaluation. Based on dynamic test results, the governing failure mode is the tensile failure of the threads at the piston rod end nut inside the cylinder. All of these failure modes (including the thread failure) showed higher capacity than the valve opening load. The minimum capacity of these failure modes is still about a factor of 1.8 or more than the relief valve opening load. This result is consistent with the

relief valve design concept of protecting the snubber assembly from being overstressed. The snubber with relief valve does not simply fail when the relief valve capacity is reached; the snubber just goes into "plastic" deformation. It would be grossly conservative to consider the relief valve opening load as the fragility level of the snubber. Therefore, the nut thread failure will be considered in this study as the best-estimate failure mode. However, fragility estimates based on a relief valve opening load were also developed for the purpose of a sensitivity study.

With the fragilities of the four support groups developed, the next step is to calculate the failure probabilities at different earthquake intensity levels for the various support failure scenarios or combinations. As stated earlier there are 15 cases of support failure scenarios for a system with four individual supports. These combinations are presented in Table 2. Table 3 shows the failure probabilities at different earthquake levels for various support failure combinations.

If we were to follow the indirect DEGB approach adopted in our evaluation of RCLs by assuming  $P[PF|SF]=1.0$ , taking the union of ("summing") the probabilities of the 15 cases of support failure (Cases 2 through 16 in Table 3) would yield the probability of the recirculation loop DEGB indirectly caused by failure of intermediate supports, i.e. lifetime indirect DEGB probabilities of  $2.4E-10$ ,  $3.2E-5$ ,  $4.3E-3$ ,  $5.8E-2$  and  $2.7E-1$  for seismic hazard cutoffs of 1, 2, 3, 4, and 5 times the SSE, respectively. Some of these indirect DEGB probabilities are very high and may not be realistic judging from the current state (i.e. no DEGB having occurred) of the recirculation loops in the United States. To more realistically assess how support failure would actually affect the likelihood of pipe failure, we evaluated seismic responses for each failure case and then performed a series of probabilistic fracture mechanics analyses.

#### 4.4 Seismic Responses Given Support Failure

To study the pipe failure induced by earthquake, we started with the calculation of the seismic stresses due to one earthquake level. Fifteen cases of seismic analysis of the recirculation loop B were performed and the corresponding pipe stresses were obtained using the response spectrum approach. Each case corresponds to one case of failure scenario of the support groups. Cases 2 to 16 of Table 2 show these combinations. Also included in Table 2 is Case 1, a support failure case in which no support failure occurs. All sixteen cases of seismic analysis were based on the OBE and a subsystem damping of 0.005. The seismic stresses due to other earthquake levels were estimated using the results of the design analyses and a series of response factors. In general, the suction line has the lowest average stress, and the risers have the highest. The discharge line has slightly higher average stress than the suction line. The discharge line is stiffer than the suction line because it has slightly thicker

wall thickness and is shorter in length even though both lines have the same outside diameter.

To get a general idea about the stress situation in the pipe if several supports failed during an earthquake, the ratios of the maximum normal stresses (on the pipe cross section) for various support failure to the normal stress for no-support-failure case were calculated at individual weld joints. These stress ratios are presented in Fig. 7. As this figure shows, the seismic stress increases significantly if the supports fail during an earthquake. However, many more supports failing in an earthquake does not necessarily generate much higher stresses in the piping system. The implication is that the support-failure cases with large number of support failures will most likely contribute little to the overall system failure probability because the probability of so many supports failing in a seismic event is very low.

#### **4.5 Simplified Analysis Method**

In principle, accounting for stress redistribution caused by the failure of intermediate supports would require a separate PRAISE (or equivalent) calculation for each support failure scenario ("case"), dramatically increasing the computational effort associated with a probabilistic fracture mechanics assessment. For the four support groups identified in our study, sixteen separate PRAISE runs would have been required to cover all possible combinations and permutations of support failure (including the case of no failure). As part of our study, we performed sensitivity calculations to determine the relative contribution of each support failure case to the overall system probability of DEGB. In order to minimize computational effort, we developed a simplified analysis method based on modified versions of the standard pre- and post-processing routines used by PRAISE. These routines, normally used, respectively, to develop the stratified sampling space used by PRAISE and to perform the "systems analysis", execute much faster than PRAISE itself. Improved computational efficiency comes at the expense of accuracy in the probabilistic results; however, because we were addressing only relative effects in these sensitivity calculations, we concluded that the simplified analyses were sufficient for our purposes. Details on the particular techniques used in these simplified analyses is provided in Ref. 8.

Following this simplified approach, the conditional failure probability for each weld joint was calculated for all 15 cases of the support failure scenario. The conditional failure probabilities of the weld joint for the no-support-failure case were not obtained in this fashion even though the same method applies, because they are already available from a rigorous PRAISE analysis of "direct" DEGB probability without support failure.

#### **4.6 Discussion of Results**

The conditional pipe failure probabilities of individual weld joints for each case of the failure scenario were calculated following the simplified methodology described above using the pipe stresses

obtained from the seismic analyses along with other operating stresses due to dead weight, pressure, and thermal expansion. System failure probability analyses were performed for each of these fifteen cases. These system failure probabilities were then combined with that of Case 1 following Eq. (7) to obtain the overall probability of seismically induced system failure.

The seismic hazard curve used in the system analysis was a generic curve based on an SSE of 0.16g peak ground acceleration. Because no seismicity data is available at very high levels of earthquake intensity (above one SSE), there is the question about how far the seismic curve should be extrapolated or truncated. That is, there exists a large modeling uncertainty in seismic hazard curves in the high earthquake intensity level.

To study the effect of different levels of extrapolation or truncation of the seismic hazard curve, several system failure analyses for various levels of truncation were performed. Five truncation levels were considered: 1, 2, 3, 4, and 5 times the SSE. The truncated seismic hazard curves are shown by the dashed lines in Fig. 8. The system failure probabilities are shown in Table 4 for the case when the effect of the relief valve is neglected. Table 5 presents the same results for the case in which the relief valve opening load is considered as the failure level of the snubbers.

In these tables, the probability of system failure (i.e. DEGB at any location in the system) for each of the fifteen support-failure scenarios (Cases 2 through 16) are presented for various seismic hazard truncations along with the probability of system failure for the no-support-failure scenario (Case 1). Note in Tables 4 and 5 that the total probability of system failure (at a given earthquake level) results from a union operation on the sixteen support failure cases (including that in which no supports fail), not a straight sum of the individual failure probabilities. Note also in Tables 4 and 5 that the overall ("total") probability of system failure decreases as the seismic hazard curve is truncated at lower levels. The maximum probabilities of overall system failure are  $4.8E-4$  and  $4.3E-6$  per plant lifetime, respectively, for the cases with and without the relief valve at the seismic hazard curve truncation level of five times the SSE.

At first glance, these results appear to contradict the purpose of the snubber relief valve, i.e. to protect the snubbers against extreme seismic loads and thereby reduce the likelihood of overall pipe system failure. It is important to consider, however, that with the relief valve, snubber "failure" -- defined as opening of the relief valve -- would only be momentary, i.e. snubber function would be recovered as soon as the seismic load dropped below the snubber load limit. Without the relief valve, snubber "failure" would be just that -- permanent loss of function -- and therefore the corresponding fragility, based on structural capacity rather than a pre-set load limit, is accordingly higher than for a snubber with the relief valve. The issue of momentary vs permanent loss of function was not accounted for in estimating

the respective probabilities of system failure; instead, for computational convenience, we treated relief valve "failure" as if it led to permanent loss of snubber function. How (or even if) momentary loss of snubber function would actually manifest itself as a pipe stress begins to address the time-dependent character of the seismic loads; evaluating this effect was beyond the scope of the current study. It seems reasonable, however, to expect that such pipe stresses would not act long enough to cause the pipe to fail, and that the actual probability of system failure would not only be significantly lower than that estimated above, but would also be lower than that for the same system equipped with snubbers having no relief valves.

The following paragraphs briefly summarize the findings of this study, which can be used to reduce the amount of work needed to assess accurately the effects of seismically induced support failures.

- (1) The maximum probabilities of overall system failure are  $4.8E-4$  and  $4.3E-6$  per plant lifetime, respectively, for the cases with and without the relief valve at the seismic hazard curve truncation level of five times the SSE (or about  $1.2E-5$  and  $1.1E-7$  per reactor-year, respectively, if a 40-year plant lifetime is assumed). These probability levels can be considered as the upper bound values. They are not very high probability values considering the fact that the case associated with the relief valve very conservatively assumes the valve opening load limit to be the "failure" (or fragility) level of the supports.

If we only consider earthquakes up to twice the SSE, the lifetime probabilities of failure with and without the relief valve drop to  $1.5E-6$  and  $6.4E-5$ , respectively (or about  $3.8E-8$  and  $1.6E-6$  per reactor-year, respectively).

- (2) The seismic stresses of cases when many supports fail during an earthquake are not significantly higher than those cases in which only one or two supports fail. It is unlikely that these cases will have any significant contribution to the overall system failure because the probability of so many supports failing in an earthquake is very small.
- (3) The welds which have high seismic stress in a no-support-failure case are most likely the dominate welds for the overall system failure probability. The welds with low seismic stress in Case 1 may have higher rates of stress increase for the with-support-failure cases from Case 1. However, the higher rate may still not make them major contributors to overall system failure.
- (4) The shape of the seismic hazard curve has a major effect on the overall system failure probability. Seismic hazard curves which do not extend far beyond the one SSE level indicate that evaluation of the no-support-failure case might be sufficient. Otherwise, the with-support-failure cases dominate. Following these observations, the effects of support failure may be assessed with the evaluation of a few carefully selected welds and support

failure combinations using the methodology presented in this section.

Besides the extrapolation or truncation of seismic hazard curves, a large modeling uncertainty also exists in the support fragilities. To study the effect of this uncertainty in support failure fragility, we considered two levels of uncertainties (90% and 10%) on the modeling uncertainty distribution of the support fragility. Table 6 shows the results for the 90% on the uncertainty distribution in the same format as Tables 4 and 5, which represent the median of the support fragility; as in Tables 4 and 5, the individual "SF" system failure probabilities will not necessarily sum to the total "SF" probability given. Not surprisingly, the overall system failure probability is again heavily dependent on the truncation level of the seismic hazard curve. At 90% on the modeling uncertainty distribution, the maximum overall system failure probability reaches  $1.7E-4$  per plant lifetime at the seismic hazard truncation level of 5SSE. It is close to the maximum probability of  $4.8E-4$  calculated for the case when the relief valve opening load was considered as the fragility level (see Table 5). This probability level is still not high.

## 5. SUMMARY AND CONCLUSIONS

We have developed detailed approaches for evaluating how piping support failures caused by earthquakes would contribute to the overall probability of piping system failure. Two different approaches are used, depending on the type of support considered:

- (1) a "support reliability" approach for heavy component supports, that is, supports whose failure could reasonably be expected to cause pipe failure under all circumstances, and
- (2) a more rigorous "piping reliability" approach, where the effect of support failure is incorporated directly into a probabilistic fracture mechanics evaluation to evaluate if and under what conditions support failure would cause a pipe to break.

These approaches have been applied to various reactor coolant piping systems in both PWR and BWR plants. The results of these evaluations have typically indicated that the likelihood of pipe break due to seismically-induced support failure is small, not only for the large, stiff piping found in PWR primary systems, but for more complex, more flexible piping systems as well. From the standpoint of addressing specific regulatory issues associated with piping behavior, a reliability approach also yields the following:

- (1) the relative contribution of various failure scenarios to the overall likelihood of pipe system failure, in other words, the "safety significance" of each failure scenario.

- (2) the relative "safety significance" of individual supports, in other words, identification of those supports whose failure would most seriously affect system integrity.
- (3) an assessment of system failure based on realistic failure criteria reflecting the actual behavior of the piping, rather than on simple exceedance of code allowable limits.

The usefulness of such evaluations in a regulatory context has already been demonstrated through recent NRC rulemaking actions, the technical justification of which was based in large part on the results of LLNL piping reliability studies.

#### REFERENCES

1. **Probability of Pipe Fracture in the Primary Coolant Loop of a PWR Plant**, Lawrence Livermore National Laboratory, Report UCID-18967, NUREG/CR-2189, Vol. 1-9 (1981).
2. **Probability of Pipe Failure in the Reactor Coolant Loops of Westinghouse PWR Plants**, Lawrence Livermore National Laboratory, Report UCID-19988, NUREG/CR-3660, Vol. 1-4 (1984).
3. **Probability of Pipe Failure in the Reactor Coolant Loops of Combustion Engineering PWR Plants**, Lawrence Livermore National Laboratory, Report UCRL-53500, NUREG/CR-3663, Vol. 1-3 (1984).
4. **Probability of Pipe Failure in the Reactor Coolant Loops of Babcock & Wilcox PWR Plants**, Lawrence Livermore National Laboratory, Report UCID-53644, NUREG/CR-4290, Vol. 1-2 (1985).
5. **Probability of Failure in the Reactor Coolant Piping of BWR Plants**, Lawrence Livermore National Laboratory, Report UCID-20914, NUREG/CR-4792, Vol. 1-4 (1986/88).
6. G.S. Holman, "Probabilistic Treatment of Stress Corrosion Cracking", Lawrence Livermore National Laboratory, Report UCRL-98173 (May 1988). Presented at the NRC-MITI Technical Information Exchange Engineering Workshop, Tokyo, Japan, May 16-20, 1988.
7. M.K. Ravindra and R.D. Campbell (EQE), G.S. Holman (LLNL), "Probability of Double-Ended Guillotine Break of Primary Coolant Piping Indirectly Induced by Earthquakes", EQE Incorporated, Newport Beach, California. Presented at the 8th International Conference on Structural Mechanics in Reactor Technology, Brussels, Belgium, August 19-23, 1985.
8. T. Lo, et al., **Probability of Failure in the Reactor Coolant Piping of BWR Plants, Vol. 2: Pipe Failure Induced by Crack Growth and Failure of Intermediate Supports**, Lawrence Livermore National Laboratory, Report UCID-20914, NUREG/CR-4792, Vol. 2 (1987).

Table 1. Parameters considered in developing component fragilities.

---

Structural Response

---

- Ground spectrum used for design
  - Structural damping
  - Site characteristics (rock or soil, shear wave velocity, thicknesses of different sites)
  - Fundamental frequency of internal structure if uncoupled analysis was performed
  - Interface spectra for NSSS points of connection to structure if uncoupled analysis was performed
  - Input ground spectra resulting from synthetic time history applied to structural model
- 

NSSS Response

---

- Method of analysis (e.g., time-history or response spectrum)
  - Modeling of NSSS and structure (i.e. coupled or uncoupled)
  - NSSS system damping
  - NSSS fundamental frequency or frequency range
  - If uncoupled analysis was performed, whether envelope or multi-support spectra were used
-

Table 2. Support failure combinations considered for recirculation loop B.

| Case No. | No. of support failure | Group 1               | Group 2                | Group 3         | Group 4                 |
|----------|------------------------|-----------------------|------------------------|-----------------|-------------------------|
|          |                        | SB4,5&6<br>Pump Motor | SB1,2&3<br>Pump Casing | SB10<br>Suction | SB12, BB12<br>Discharge |
| 1        | 0 SF                   |                       |                        |                 |                         |
| 2        | 1 SF                   | x                     |                        |                 |                         |
| 3        | 1 SF                   |                       | x                      |                 |                         |
| 4        | 1 SF                   |                       |                        | x               |                         |
| 5        | 1 SF                   |                       |                        |                 | x                       |
| 6        | 2 SF                   | x                     | x                      |                 |                         |
| 7        | 2 SF                   | x                     |                        | x               |                         |
| 8        | 2 SF                   |                       | x                      | x               |                         |
| 9        | 2 SF                   | x                     |                        |                 | x                       |
| 10       | 2 SF                   |                       | x                      |                 | x                       |
| 11       | 2 SF                   |                       |                        | x               | x                       |
| 12       | 3 SF                   | x                     | x                      | x               |                         |
| 13       | 3 SF                   | x                     | x                      |                 | x                       |
| 14       | 3 SF                   | x                     |                        | x               | x                       |
| 15       | 3 SF                   |                       | x                      | x               | x                       |
| 16       | 4 SF                   | x                     | x                      | x               | x                       |

Table 3. Probability of support failure at various levels of earthquake intensity.

| CASE | NO. SF | 0.5SSE    | 1SSE      | 2SSE      | 3SSE      | 4SSE      | 5SSE      |
|------|--------|-----------|-----------|-----------|-----------|-----------|-----------|
| 1    | 0 SF   | .1000E+01 | .1000E+01 | .9999E+00 | .9957E+00 | .9417E+00 | .7264E+00 |
| 2    | 1 SF   | .1729E-16 | .1879E-09 | .2100E-04 | .2381E-02 | .2833E-01 | .1207E+00 |
| 3    | 1 SF   | .2289E-17 | .4206E-10 | .8191E-05 | .1315E-02 | .2007E-01 | .1018E+00 |
| 4    | 1 SF   | .2432E-26 | .3912E-17 | .6131E-10 | .1177E-06 | .9775E-05 | .1767E-03 |
| 5    | 1 SF   | .3247E-18 | .9362E-11 | .2791E-05 | .5616E-03 | .9920E-02 | .5618E-01 |
| 6    | 2 SF   | .3958E-34 | .7902E-20 | .1720E-09 | .3130E-05 | .5686E-03 | .1229E-01 |
| 7    | 2 SF   | .4204E-43 | .7351E-27 | .1288E-14 | .2802E-09 | .2769E-06 | .2132E-04 |
| 8    | 2 SF   | .5566E-44 | .1645E-27 | .5022E-15 | .1547E-09 | .1962E-06 | .1799E-04 |
| 9    | 2 SF   | .5613E-35 | .1759E-20 | .5860E-10 | .1337E-05 | .2810E-03 | .6779E-02 |
| 10   | 2 SF   | .7432E-36 | .3937E-21 | .2286E-10 | .7383E-06 | .1991E-03 | .5720E-02 |
| 11   | 2 SF   | .7894E-45 | .3663E-28 | .1711E-15 | .6610E-10 | .9697E-07 | .9926E-05 |
| 12   | 3 SF   | .9624E-61 | .3092E-37 | .1055E-19 | .3683E-12 | .5558E-08 | .2171E-05 |
| 13   | 3 SF   | .1285E-52 | .7398E-31 | .4800E-15 | .1758E-08 | .5640E-05 | .6903E-03 |
| 14   | 3 SF   | .1365E-61 | .6882E-38 | .3593E-20 | .1574E-12 | .2747E-08 | .1198E-05 |
| 15   | 3 SF   | .1807E-62 | .1540E-38 | .1401E-20 | .8689E-13 | .1946E-08 | .1011E-05 |
| 16   | 4 SF   | .3125E-79 | .2894E-48 | .2943E-25 | .2069E-15 | .5514E-10 | .1220E-06 |

Table 4. Best-estimate seismically induced pipe failure probability (without relief valve) and the effects of seismic hazard curve extrapolation.

| CASE | NO. SF | 1SSE      | 2SSE      | 3SSE      | 4SSE      | 5SSE      |
|------|--------|-----------|-----------|-----------|-----------|-----------|
| 1    | 0 SF   | .5971E-11 | .7837E-11 | .8882E-11 | .9403E-11 | .9754E-11 |
| 2    | 1 SF   | .2289E-20 | .1184E-14 | .5064E-12 | .1303E-10 | .6170E-09 |
| 3    | 1 SF   | .2139E-20 | .6142E-14 | .1273E-10 | .9298E-08 | .8913E-06 |
| 4    | 1 SF   | .1153E-28 | .3215E-21 | .7304E-18 | .8469E-16 | .3060E-14 |
| 5    | 1 SF   | .1957E-19 | .9124E-11 | .1521E-06 | .7618E-06 | .1684E-05 |
| 6    | 2 SF   | .1070E-29 | .4974E-18 | .4923E-12 | .4169E-08 | .2147E-06 |
| 7    | 2 SF   | .1162E-37 | .1282E-24 | .1222E-18 | .3140E-15 | .1211E-11 |
| 8    | 2 SF   | .5697E-37 | .6615E-23 | .8322E-14 | .1063E-10 | .3116E-09 |
| 9    | 2 SF   | .9460E-29 | .1280E-14 | .3445E-09 | .1659E-07 | .1343E-06 |
| 10   | 2 SF   | .4688E-29 | .3737E-14 | .1909E-09 | .1162E-07 | .1106E-06 |
| 11   | 2 SF   | .1556E-37 | .5982E-23 | .1217E-13 | .5388E-11 | .1708E-09 |
| 12   | 3 SF   | .5456E-48 | .1082E-29 | .2183E-21 | .6912E-17 | .1299E-13 |
| 13   | 3 SF   | .5578E-40 | .3524E-22 | .3993E-12 | .3107E-09 | .1180E-07 |
| 14   | 3 SF   | .2756E-46 | .3475E-25 | .3991E-16 | .1491E-12 | .1942E-10 |
| 15   | 3 SF   | .5060E-47 | .6237E-26 | .2204E-16 | .1054E-12 | .1631E-10 |
| 16   | 4 SF   | .1137E-58 | .1034E-34 | .4881E-24 | .1413E-17 | .1919E-12 |
|      | TOTAL  | .597E-11  | .169E-10  | .152E-06  | .837E-06  | .429E-05  |

Table 5. Best-estimate seismically induced pipe failure probability (with relief valve) and the effects of seismic hazard curve extrapolation.

| CASE  | NO. SF | 1SSE      | 2SSE      | 3SSE      | 4SSE      | 5SSE      |
|-------|--------|-----------|-----------|-----------|-----------|-----------|
| 1     | 0 SF   | .5971E-11 | .7661E-11 | .7807E-11 | .7725E-11 | .7723E-11 |
| 2     | 1 SF   | .8357E-16 | .8601E-12 | .4645E-10 | .3140E-09 | .4685E-08 |
| 3     | 1 SF   | .7044E-14 | .6165E-10 | .5519E-08 | .4314E-06 | .9499E-05 |
| 4     | 1 SF   | .4109E-21 | .8925E-16 | .1309E-13 | .2275E-12 | .1967E-11 |
| 5     | 1 SF   | .1617E-14 | .1501E-07 | .3136E-04 | .5385E-04 | .6106E-04 |
| 6     | 2 SF   | .1210E-18 | .3489E-11 | .1723E-07 | .4012E-05 | .2111E-04 |
| 7     | 2 SF   | .1453E-25 | .2518E-16 | .1787E-12 | .1656E-10 | .4999E-08 |
| 8     | 2 SF   | .6352E-23 | .1793E-13 | .5753E-07 | .1378E-05 | .2970E-05 |
| 9     | 2 SF   | .2755E-19 | .1500E-08 | .5972E-05 | .2096E-04 | .2959E-04 |
| 10    | 2 SF   | .1217E-17 | .6045E-07 | .1732E-04 | .3994E-04 | .4789E-04 |
| 11    | 2 SF   | .4474E-25 | .2712E-14 | .3845E-07 | .6351E-06 | .1881E-05 |
| 12    | 3 SF   | .2157E-29 | .2089E-17 | .1293E-12 | .1652E-10 | .5534E-09 |
| 13    | 3 SF   | .5135E-24 | .4062E-12 | .2594E-05 | .1642E-04 | .2542E-04 |
| 14    | 3 SF   | .2814E-29 | .1123E-13 | .1085E-07 | .3476E-06 | .1457E-05 |
| 15    | 3 SF   | .4604E-28 | .2782E-13 | .2888E-07 | .5587E-06 | .1805E-05 |
| 16    | 4 SF   | .3676E-35 | .3285E-19 | .5362E-13 | .1328E-09 | .1005E-06 |
| TOTAL |        | .597E-11  | .770E-07  | .644E-04  | .243E-03  | .481E-03  |

Table 6. Effects of uncertainty in estimating support fragility on the seismically induced pipe failure probability (90% on the uncertainty distribution of the support fragility).\*

| CASE  | NO. SF | 1SSE      | 2SSE      | 3SSE      | 4SSE      | 5SSE      |
|-------|--------|-----------|-----------|-----------|-----------|-----------|
| 1     | 0 SF   | .5971E-11 | .7826E-11 | .8667E-11 | .8692E-11 | .8630E-11 |
| 2     | 1 SF   | .7160E-17 | .2048E-12 | .1863E-10 | .1769E-09 | .3576E-08 |
| 3     | 1 SF   | .9488E-17 | .1550E-11 | .6646E-09 | .1566E-06 | .6281E-05 |
| 4     | 1 SF   | .8799E-24 | .1249E-17 | .5221E-15 | .1862E-13 | .2755E-12 |
| 5     | 1 SF   | .1140E-15 | .2939E-08 | .1042E-04 | .2275E-04 | .2909E-04 |
| 6     | 2 SF   | .1442E-22 | .2137E-13 | .8870E-09 | .8669E-06 | .9661E-05 |
| 7     | 2 SF   | .2709E-29 | .8499E-19 | .3005E-14 | .8291E-12 | .5764E-09 |
| 8     | 2 SF   | .1891E-28 | .6442E-17 | .2969E-09 | .3929E-07 | .2181E-06 |
| 9     | 2 SF   | .1684E-21 | .7053E-10 | .8141E-06 | .5345E-05 | .1083E-04 |
| 10    | 2 SF   | .1189E-21 | .3024E-09 | .6652E-06 | .4997E-05 | .1063E-04 |
| 11    | 2 SF   | .6826E-29 | .7472E-17 | .5436E-09 | .2570E-07 | .1562E-06 |
| 12    | 3 SF   | .5561E-36 | .1801E-21 | .2738E-15 | .3024E-12 | .4243E-10 |
| 13    | 3 SF   | .4344E-29 | .4878E-15 | .4605E-07 | .1496E-05 | .5574E-05 |
| 14    | 3 SF   | .3715E-34 | .7422E-17 | .6277E-10 | .8530E-08 | .9609E-07 |
| 15    | 3 SF   | .9720E-35 | .1957E-17 | .5059E-10 | .8147E-08 | .9687E-07 |
| 16    | 4 SF   | .6712E-43 | .5549E-24 | .3917E-16 | .1286E-11 | .5471E-08 |
| TOTAL |        | .597E-11  | .332E-08  | .122E-04  | .511E-04  | .165E-03  |

\* no snubber relief valve

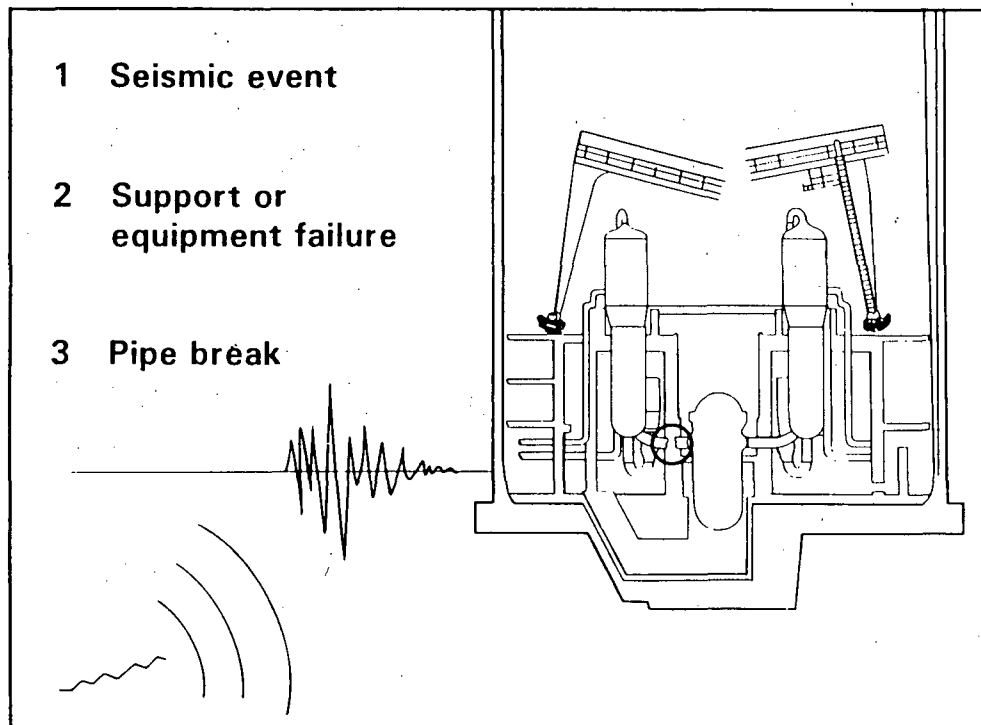
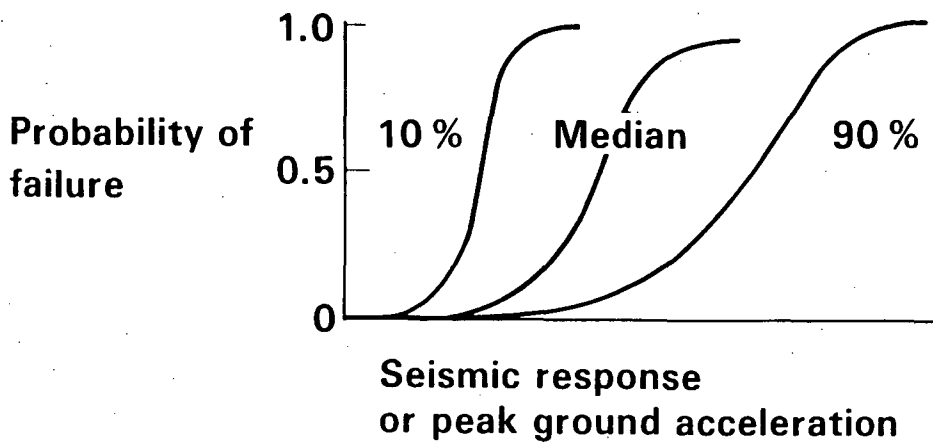
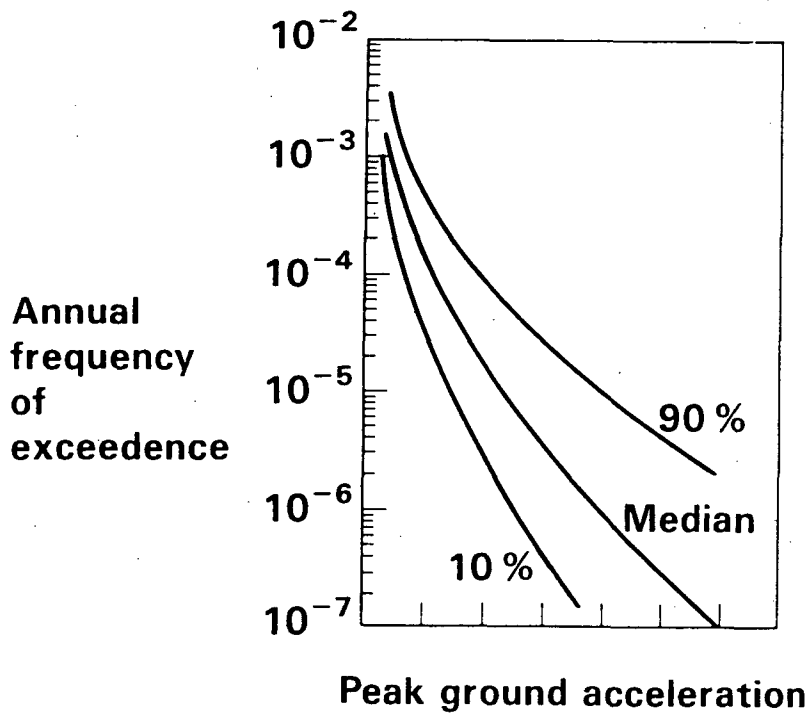


Figure 1. General approach for estimating probability of "indirect" DEGB due to seismically-induced failure of heavy component supports.



(a)



(b)

Figure 2. Typical descriptions of component fragility (a) and seismic hazard (b).

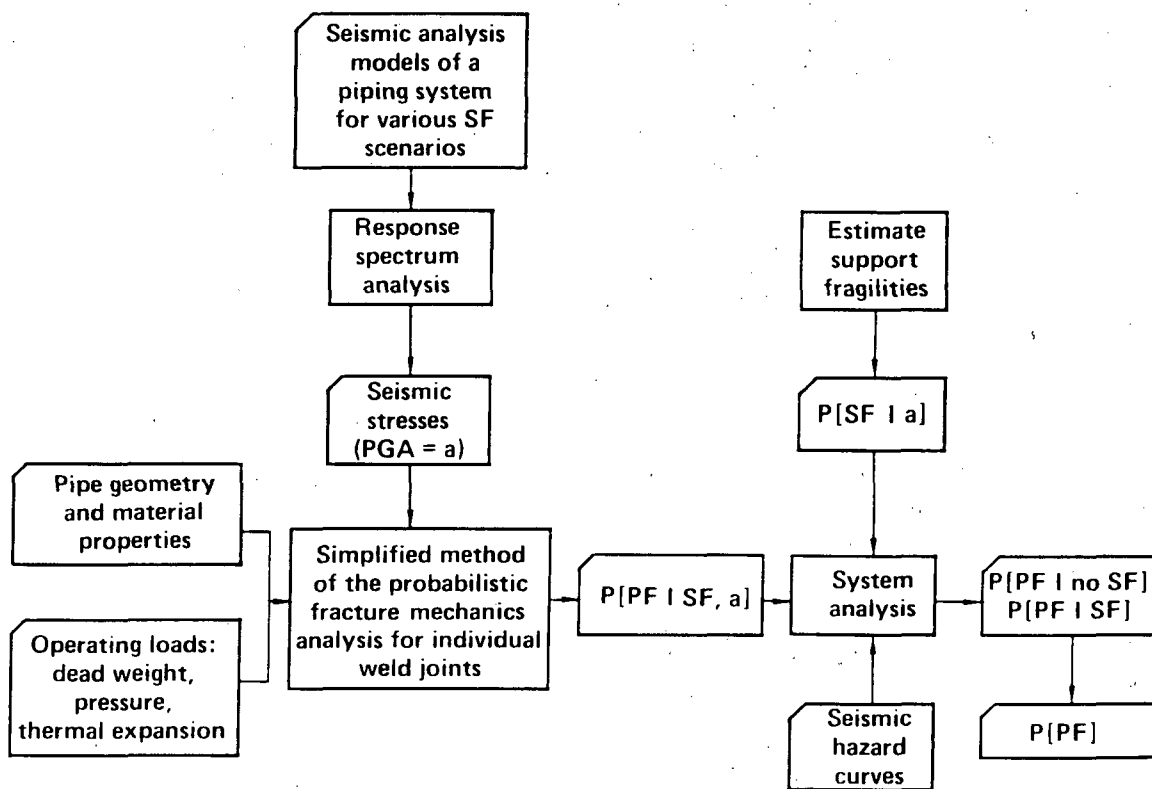


Figure 3. General approach used to study seismically-induced system failure considering the effects of support failure.

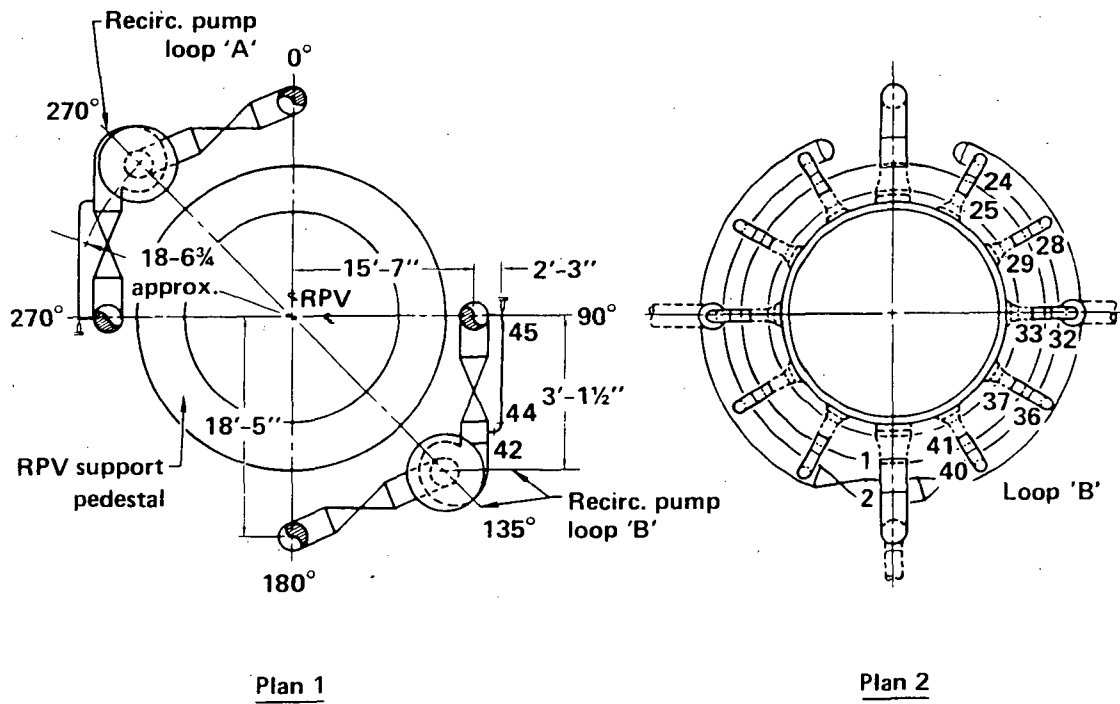
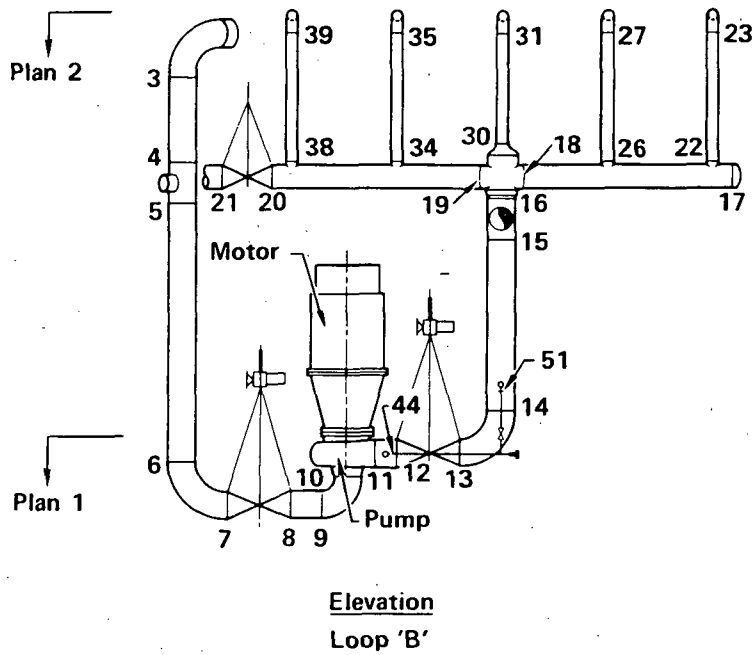


Figure 4. Pilot plant recirculation system.

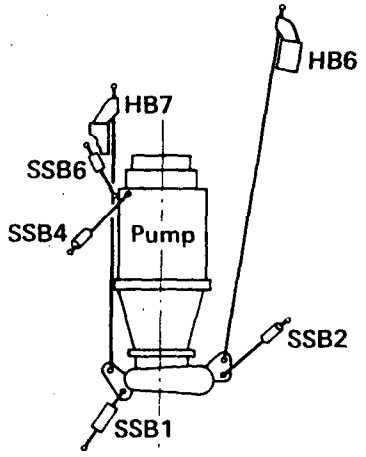
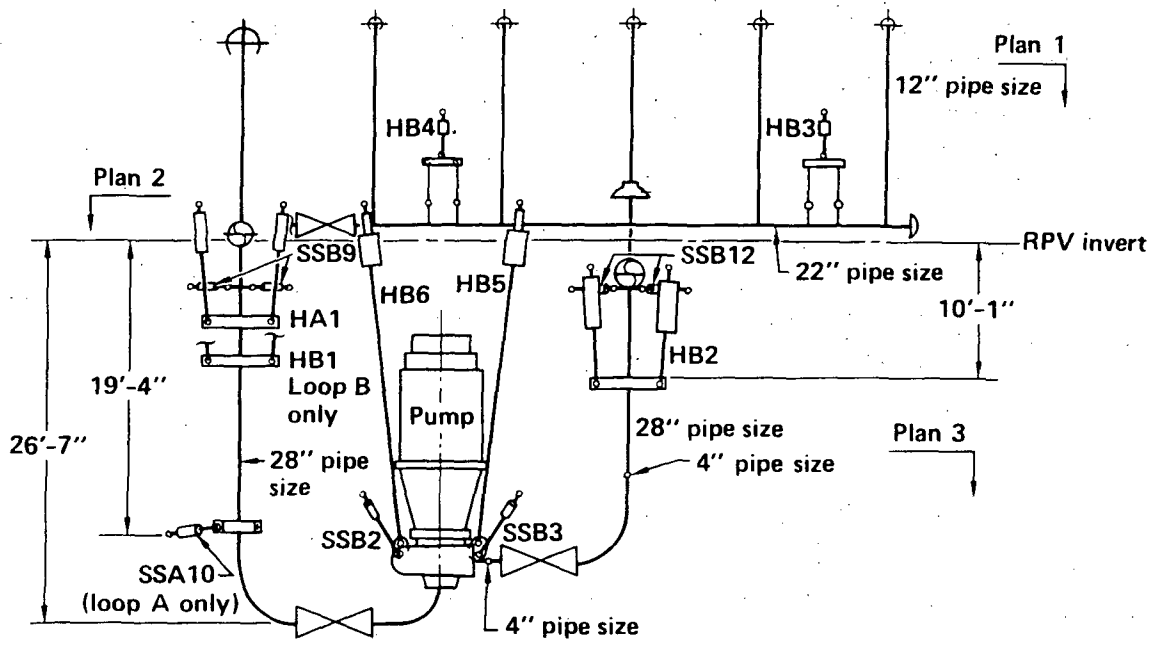


Figure 5. Supports of the pilot plant recirculation system.

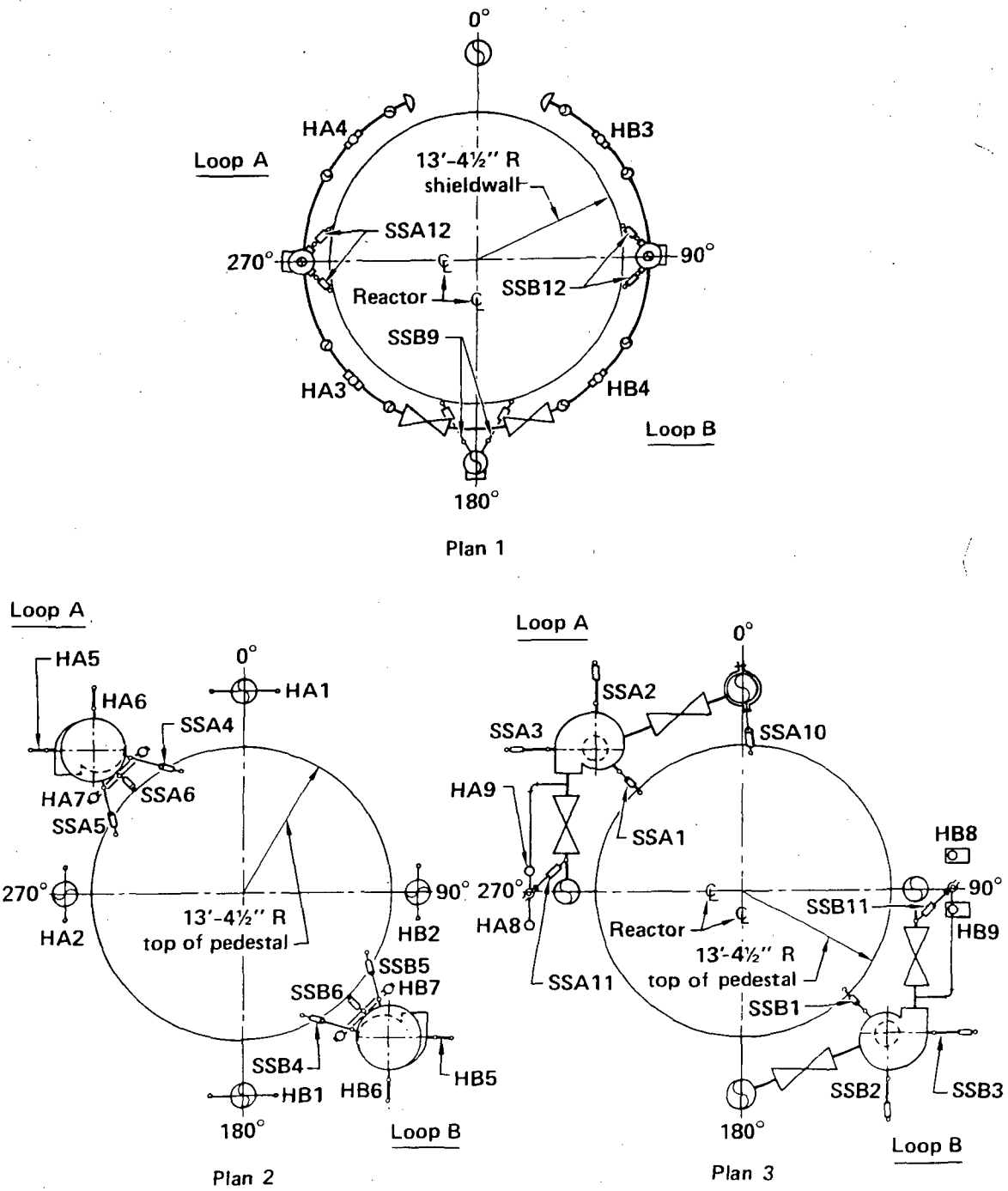
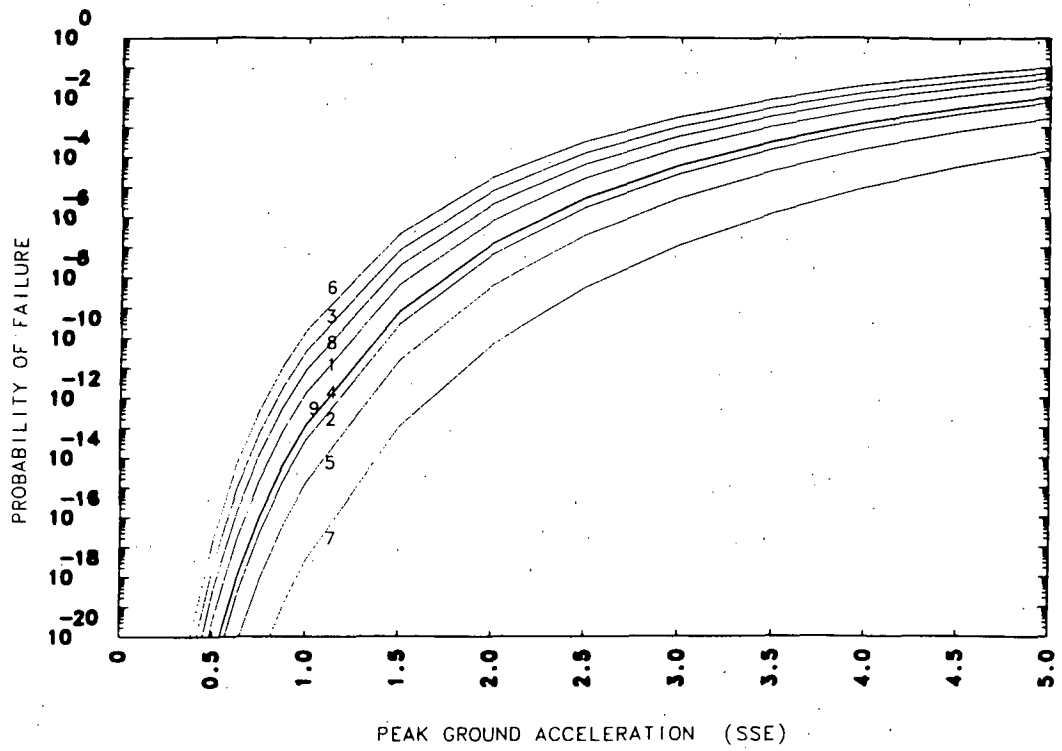
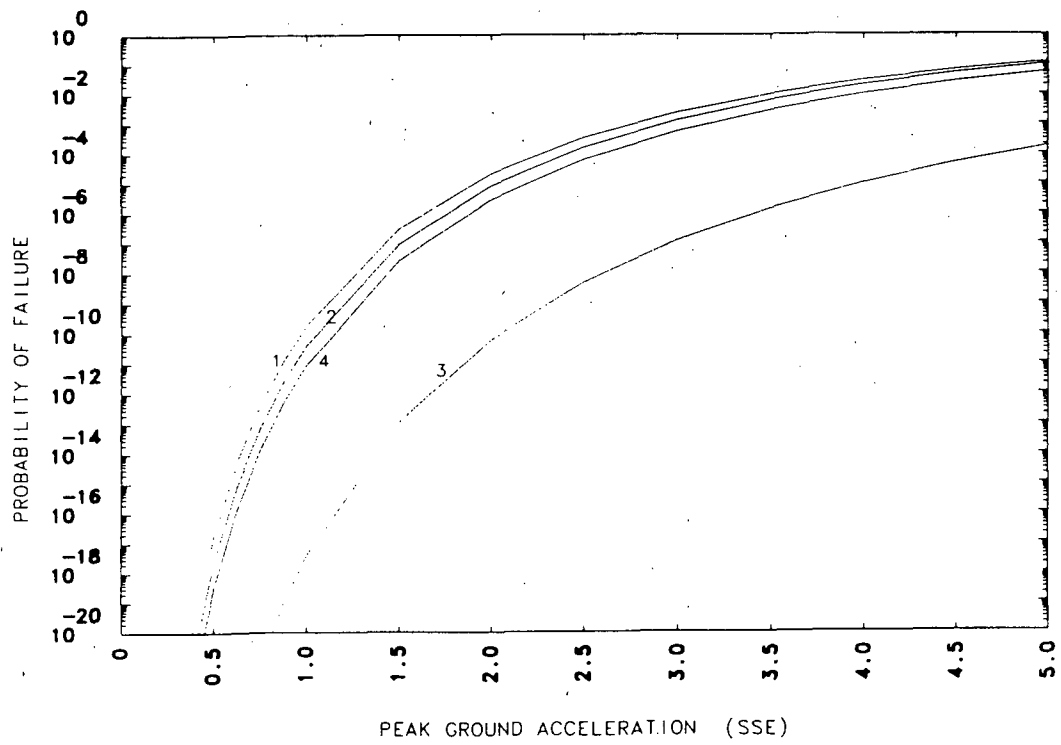


Figure 5 (cont.). Supports of the pilot plant recirculation system.

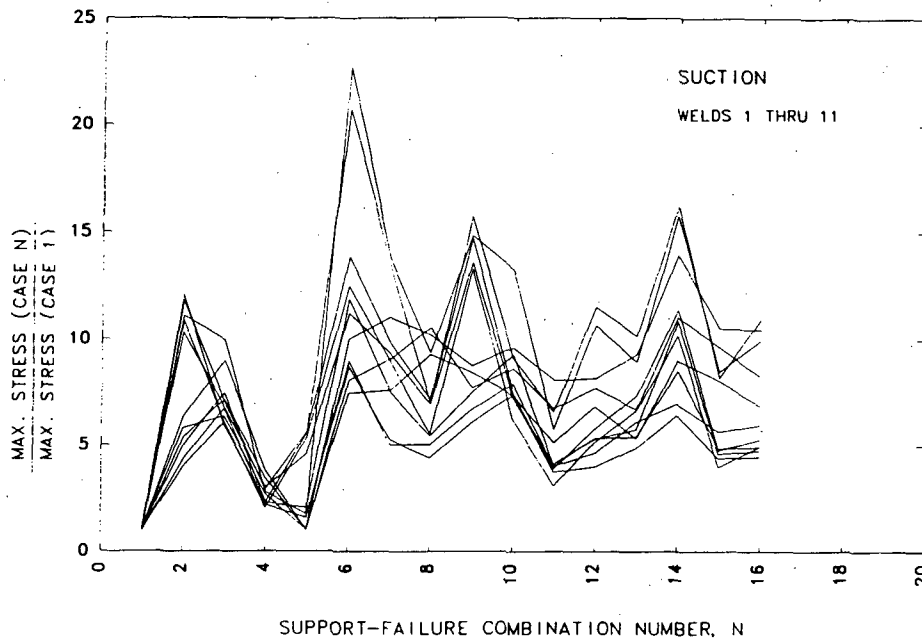


(a)

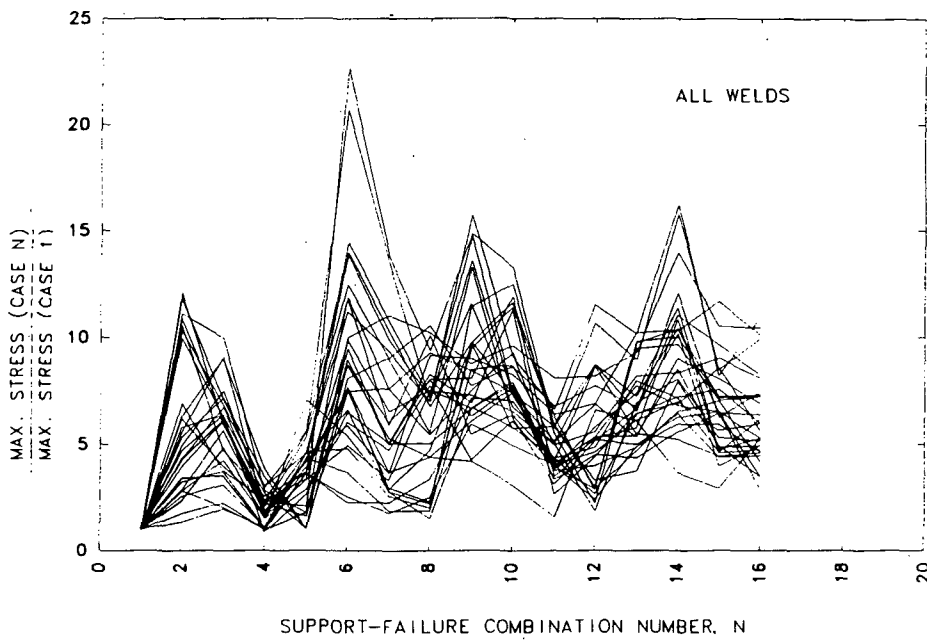


(b)

Figure 6. Failure probabilities of (a) nine individual pipe supports and (b) four support groups.



(a)



(b)

Figure 7. Increase in seismic stresses at (a) weld joints of the suction line and (b) all recirculation loop weld joints, due to support failure.

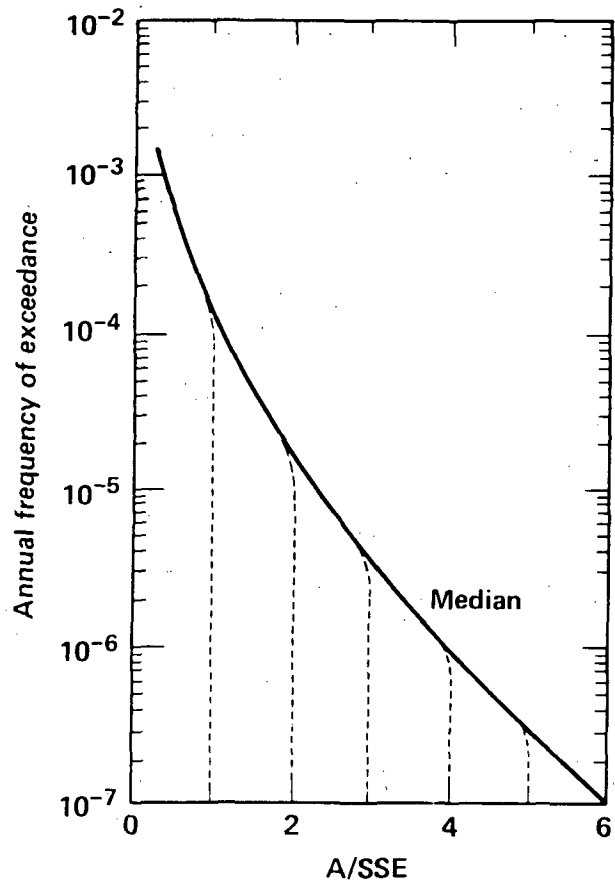


Figure 8. Seismic hazard curve used in intermediate support failure evaluation; dashed lines show truncations at indicated PGA levels.

## PIPING AND FITTING DYNAMIC RELIABILITY PROGRAM

D. Guzy, USNRC  
S. Tagart, EPRI  
Y. K. Tang, EPRI  
W. English, GE  
H. Hwang, GE  
K. Merz, ANCO  
V. DeVita, ETEC

### Introduction

In recent years, both industry and the NRC have been concerned about the appropriateness of our piping design rules for seismic and other dynamic loads. While experimental failure data was used to justify the ASME Code's piping stress criteria for static and fatigue loads, there was little available physical evidence of piping dynamic failure behavior when the current rules were written. The NRC Piping Review Committee recognized the need to obtain such data and recommended that the NRC support a test program in this area. This resulted in the NRC's cooperation with EPRI in the Piping and Fitting Dynamic Reliability Program (PFDRP). The PFDRP was initiated in 1985 with three main objectives: 1) to identify the failure mechanisms and failure levels of piping components and systems under dynamic loadings, 2) to provide a data base that will improve our prediction of piping system response and failure due to high level dynamic loads, and 3) to develop an improved and defensible set of piping design rules for inclusion into the ASME Code.

### October, 1988 Program Status

All the experimental tasks of the PFDRP have been performed. Forty-one piping components failure tests were completed by ANCO Engineers. Two piping systems were ruptured by high seismic-like loads at ETEC, and one of these systems was retested. The Materials Characterization Laboratory has finished testing over 140 fatigue ratchetting specimens. Also, piping system waterhammer tests have been performed by ANCO Engineers.

General Electric of San Jose, the prime contractor for the PFDRP, has completed most of the data reduction and analysis associated with these tests. Recommendations for improved piping rules for dynamic loads have been under development by General Electric and should be proposed formally to the ASME in the spring of 1989. The final reports for the PFDRP will be published by EPRI in 1989.

### ANCO Piping Component Tests

The the results of the forty-one piping component tests conducted at ANCO Engineers will form the primary basis for new ASME stress allowable criteria

for dynamic inertial loads in Class 1, 2, and 3 piping. While actual piping components were tested, the relative simplicity of the test articles was such that it allowed a great control of the dynamic input and measured response. And of course, a larger number of conditions and parameters were varied and tested than would have been economically possible with only pipe systems tests. It should be noted that current ASME piping stress criteria has been developed primarily on a "component" basis (e.g., Markl's fatigue tests).

At ANCO Engineers, piping elbows, tees, reducers, support connections, nozzles and lugs were dynamically tested to failure. Figure 1 shows a representative test article. The test specimens consist of both carbon and stainless steel 6-inch piping components with various thickness and internal pressures. Both in-plane and out-of-plane loadings were applied to the components; driven at one end by hydraulic actuators and having weights at the other end. High level time history inputs were repeated (usually more than twice) until the components ruptured.

The dynamic input loads for the component tests consisted of low frequency (seismic), mid-frequency (hydrodynamic), and high frequency (waterhammer) loads. The emphasis of this program has been placed on seismic loads. Figure 2 shows the "target" seismic input acceleration time history that has been used (with scaling of amplitude and frequency) for most of the pipe system and pipe component tests of the PEDRP. This time history was taken from an actual BWR design. The response spectrum (Figure 3) has an amplitude peak at 7-Hz and the zero period acceleration (ZPA) is  $0.4g$ 's at the SSE level.

Table 1 is a summary of the component tests. Note that repeated time history motions scaled typically 15 to 25 times higher than elastically calculated design limits were needed to cause rupture. Fatigue ratchetting has been the dominant failure mode for pressurized piping components and those unpressurized components that failed experienced low cycle fatigue or ratchet buckling due to mean stresses from gravity. Damage has all been related to cyclic effects.

All the pressurized components experienced swelling due to ratchetting, some times in several locations. Often, wall thinning was such that between high level tests, one could feel where the eventual failure location would be. Generally, cracking occurred independent of weld locations, but in some cases the weld location represented a geometric or stiffness discontinuity and this (rather than material effects) caused cracks to occur nearby. This was especially true for thin wall (Schedule 10) components where the higher stiffness of the weld seemed to concentrate stresses in the connecting piping.

The elbows of thicker schedule generally grew through-wall cracks in their bodies, as did the tees that were fixed at only one end. The tees fixed at both ends swelled in the bodies but cracked near the branch line weld.

Component Test 16 was perhaps the ultimate demonstration that fatigue-ratchetting, rather than collapse, controls failure of pressurized components. While other components were subjected to step increases of loads until the higher

level was reached, it was decided to give this relatively weak reducer assembly the highest sled input immediately. The reducer bulged and ruptured rather than collapsed.

### ETEC Piping System Tests

The PFDRP piping system tests verified that the conclusions reached from the component tests are applicable to prototypal piping systems. Nonlinear systems effects such as the redistribution of loads, system frequency detuning, and increased damping can be observed by such experiments. The test results also provide benchmark data for piping response prediction.

Figure 4 shows the PFDRP "System 1" test article. The material was A106 Grade B carbon steel. The piping system consisted primarily of 6-inch Schedule 40 piping, except for a 3-inch Schedule 40 cross-over piece and short sections of 6-inch Schedule 160 piping near the three actuator tables, or "sleds". Three short radius elbows were used for the bends near the sleds; these were installed instead of long-radius elbows to better ensure that failure would occur. The piping was supported by the connections to the three actuator tables and by a spring hanger attached near the middle. One actual motor operated valve was installed on the 3-inch cross-over piece and three heavy sections simulating other valve weights were installed on the 6-inch piping. The system was oil-filled and pressurized to 1000 psi prior to each test. The natural frequency of the system was 7.3 Hz, tuned to be slightly higher than the 7 Hz peak of the response spectrum of the load input. The system was instrumented with 59 strain gages, gages, 15 accelerometers, 6 displacement sensors and various pressure and temperature sensors.

The first test sequences were at low levels to check out instruments, valve operability, and to measure natural response frequencies. A high level, time history motion was next input that had "mid-frequency" loads like BWR hydrodynamic loads. (Although at high-levels, no damage was expected to, or did, occur due to this mid-frequency loading). For test sequences at the nominal "OBE", "SSE", and "5 SSE" levels, both identical and dissimilar sets of table inputs were used. The response data from dissimilar inputs could provide physical benchmarks for multiple input spectra analyses. One set of dissimilar table inputs had differences only in amplitude and another had differences in phasing. Altogether, 9 tests were run at OBE, SSE and 5 SSE levels.

A single "half table capacity" test was conducted with identical, synchronous inputs at all tables. As discussed below, damage (but not leakage) occurred in the system. This damage was purposely not repaired before the "full table capacity" test was run. The "full table capacity" test produced an actual rupture in piping and thus ended the testing sequence.

For the OBE and SSE level tests, no measurable permanent deformation occurred. For the 5 SSE tests, a small amount of yielding was measured with strain gauges, but no permanent gross deflection occurred. (Plastic behavior was very local and would not be detected with a "post earthquake" inspection.)

The motor operated valve was successfully opened and closed before, during, and after each of the nine OBE, SSE, and 5 SSE tests. It appears very clear that the piping system "functionality" was maintained even at the 5 SSE level. No leakage occurred, there would have been no loss of flow, and the valve operated properly.

During the "half table capacity" test, the spring hanger broke. Then the connecting bolts on the 3-inch motor operated valve's actuator failed resulting in the actuator flying off. The "half-table capacity" test caused measurable permanent deformation of the system, increased swelling at the three short radius elbows, but no leakage in the piping (or from the valve). Ultrasonic testing of the elbows detected no cracking. No loss of flow would have occurred from the piping damage of this test, but obviously the valve lost its functionality.

The "full table capacity" test was run with the piping system in the condition just discussed. At approximately 10 seconds into this test, the short radius elbow near Sled #4 ruptured. By the time the actuators were shut off in the "full-table capacity" test, the rupture had grown to a 300° circumferential tear in the crotch of the elbow (away from weld metal and heat affected zones). The loading was predominately torsional, which explains the circumferential tearing.

Approximately 5 seconds into the last test, the Sled #1 actuator ceased to provide force into the system due to the blow-out of a 2-inch pressure plug. Initial investigations indicate that the timing and location of this actuator failure was such that it probably did not make much difference in the overall results. To verify this and to provide information on the "repeatability" of these tests, System 1 was retested, having had new short radius elbows installed. The piping responses for the repeated 5 SSE and half-table capacity tests were similar to those seen in the original tests. During the full-table capacity test, failure occurred at the same location as in the original test. However, the crack orientation was different.

A typical ASME Code design analysis identified the failure location of System 1 as the highest stress point. Table 2 shows the stresses at this elbow calculated by linear response analyses using a broadened spectrum with 2% and 5% damping.

Figure 5 shows the PFDRP "System 2" test article. This is a 316L stainless steel system that was pressurized with oil to 1000 psi and driven dynamically by four input sleds. It is comprised of a 6-inch Schedule 40 main run and a 4-inch Schedule 40 branch line that connects to a fabricated nozzle. Unlike System 1 which had three separate locations of near equal high stress, System 2 was designed to be unbalanced in terms of stress distribution. That is, the elastically calculated stresses in the branch line near the nozzle connection (near Sled #1) were design to be roughly twice as great as the highest stresses elsewhere. The system was instrumented with 48 strain gages, 13 accelerometers, 7 displacement sensors and various pressure and temperature sensors.

The lowest modal frequency of System 2 was 4.1 Hz, but in a direction orthogonal to the input motion direction. The lowest modal frequency in the driven direction was 5.25 Hz. The seismic input time history was scaled to have a peak spectral frequency of 4.0 Hz.

After a series of low level input tests were run, a single nominal "SSE test" was run. This was followed by three "2 SSE tests" using identical and then varied sled input, a "mid-frequency" input test, and a sine sweep test. After these sequences were completed, it was noticed that a small crack had developed on the outside of the nozzle weld. It was decided to proceed with high load input without any repairs to this crack.

Next came another mid-frequency test followed by 3 "5 SSE tests" with varied and identical sled inputs. (The different combinations of sled motions has provided response data to be used in future benchmarking of multiple-input spectra techniques). The nozzle cracks grew during these tests, but little other damage was observed.

The next two high level tests used synchronous sled inputs. While no leakage occurred from the "half table capacity" test, the nozzle crack grew more and fatigue ratchet bulging was noticed at the higher stress location in the main run (near Sled #4). Through-wall cracks occurred on opposite side of the nozzle as a result of the "full table capacity" test. This last sequence resulted in leakage and thus the testing was considered completed. A summary of the calculate elastic stresses for each load level (with synchronous input) is given in Table 2.

It should be noted that while the sled motions driving the piping systems were unidirectional, there was considerable three-dimensional response observed.

#### General Observations from the PFD RP Component and System Tests

The results of the pipe component and pipe system experiments have shown surprisingly consistent general trends:

1. The results show that typical elastic piping design evaluations using the current ASME Code are very conservative for dynamic inertial loads. Margins to failure of 15 to 30 times the Level D design limit (referenced to calculations using 2% damping) were commonly observed.
2. Dynamic failure is dependent upon cyclic effects, even at input levels of incredible earthquake size.
3. Ratchetting and wall thinning led to the dynamic failure of pressurized piping.
4. Cross-sectional collapse (the basis for Eq. 9 of the ASME Code) did not occur. It seems that dynamic load reversal prevents collapse.

5. Failure locations were generally independent of weldment locations, except where geometric or stiffness discontinuity occurred at the weld.
6. "Loss-of-flow" failures did not occur. Swelling occurred in the pressurized piping and crimping was minimal in the unpressurized piping.
7. Extensive testing at OBE and SSE levels produce no detectable permanent deformation or damage. Even at the 5 SSE level, deformations were very localized and small.

Items 1 through 4 above indicate the need and justification for the future ASME Code criteria changes that will result from the PFDRP. Items 6 and 7 show the need to rethink piping "functionality" concerns.

#### MCL Fatigue-Ratchet Specimen Tests

The purpose of the specimen tests was to provide fatigue-ratchet data on a smaller, more fundamental, scale. The simplicity of the test articles allowed identification of material and temperature effects that can be integrated with the component test data, resulting in broader application base. The testing of two-bar and other test specimens have identified the influence of time dependent cyclic creep and mean stress on ratchet life. Several piping materials were tested.

Of the initial 140 specimen tests, 48 were conducted at 550°F. Ratchetting behavior at this high temperature was shown to be similar to the room temperature tests. This result helps confirm that conclusions from the component and system tests (conducted at room temperature) can be extended to higher temperatures. As recommended by the ACRS and its consultants, cast stainless steel specimens were later tested.

Results of the specimen tests will help establish strain limits below which dynamic ratchetting will not be expected to occur.

#### Waterhammer Tests

Two waterhammer tests were included in the ANCO component tests (see Table 1 and Figure 6). In addition, ANCO Engineers performed waterhammer tests on longer piping "systems". The tests showed that water slugs produce the greatest loads and cause responses that do not have the load reversal characteristics seen in "solid" waterhammer tests, or in the seismic and mid-frequency load tests. Thus design criteria for this type of waterhammer would need to be different from that for other dynamic loads.

#### Piping Design Criteria Development

General Electric is now engaged in the development and evaluation of alternative design rules for the dynamic load design criteria for ASME Class 1, 2, and 3 piping components. It should be noted that several piping consultants have provided direction to the PFDRP and both the ASME and PVRC standards

groups have monitored its progress. The NRC staff has been given several briefings, most recently in July 1988.

The revision of design rules for piping dynamic load design presents several challenges to those involved with the PFDRP, the ASME Code Committees, and the NRC. While the data show that current rules provide much more margins to failure than previously thought, no consensus exists on what margins should be kept in the new rules or how best to provide a balance of design with other piping loads. And while the current "Equation 9" approach has been shown to be inappropriate in terms of assumed failure mechanisms, it has the advantage of simplicity. It is hoped that the new rules can be used with simple calculation methods that somehow implicitly address the cyclic and nonlinear effects observed in tests.

The development of new piping design rules is in many ways hindered by not being allowed to begin with a "clean slate". We have a relatively long licensing history associated with the current ASME rules. While new piping design issues continually appear, these generally are found to be of minor significance when overall nuclear plant safety is considered. And however imperfect the current piping design procedures may be, they usually produce piping systems with sufficient "margins" to accommodate the unexpected or undesigned (and often more threatening) loads and conditions that piping systems are subjected to. Many prefer "to keep the devil we know rather than the one we don't". Thus careful study of the overall effects of piping design rule changes is needed before these changes can be accepted.

The upcoming proposed ASME Code revisions are expected to allow some reduction in the number of dynamic load supports used in piping system design. But it should be noted that the changes will be limited to piping stress evaluation. They will not, by themselves, alter existing design criteria for nozzle, equipment, and piping support loads. These latter criteria will become limiting considerations in piping system design until they are revised as well.

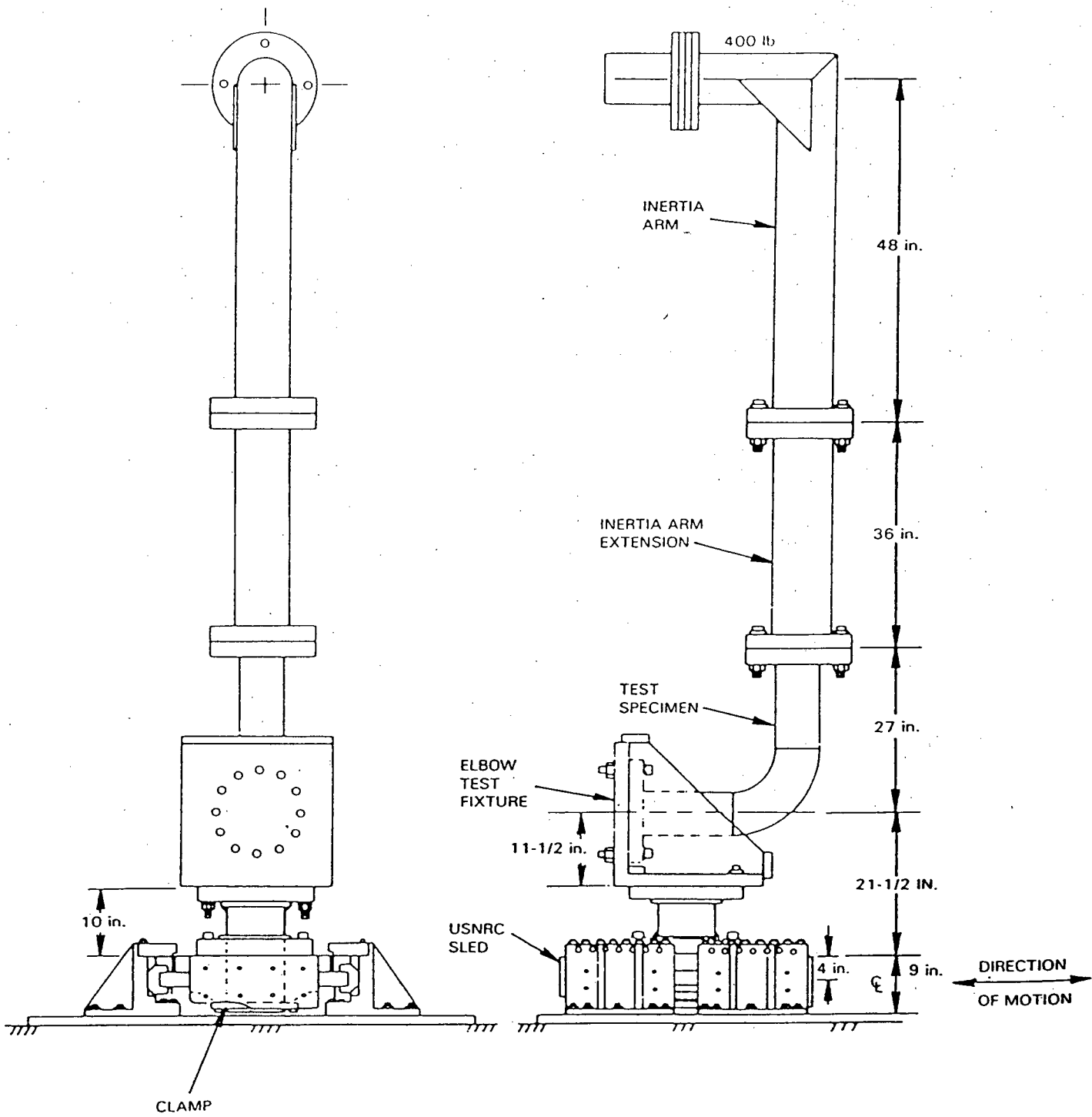


FIGURE 1 - Test 37 In-Plane Elbow Test Setup

# SEISMIC INPUT FOR COMPONENT & SYSTEM TESTS

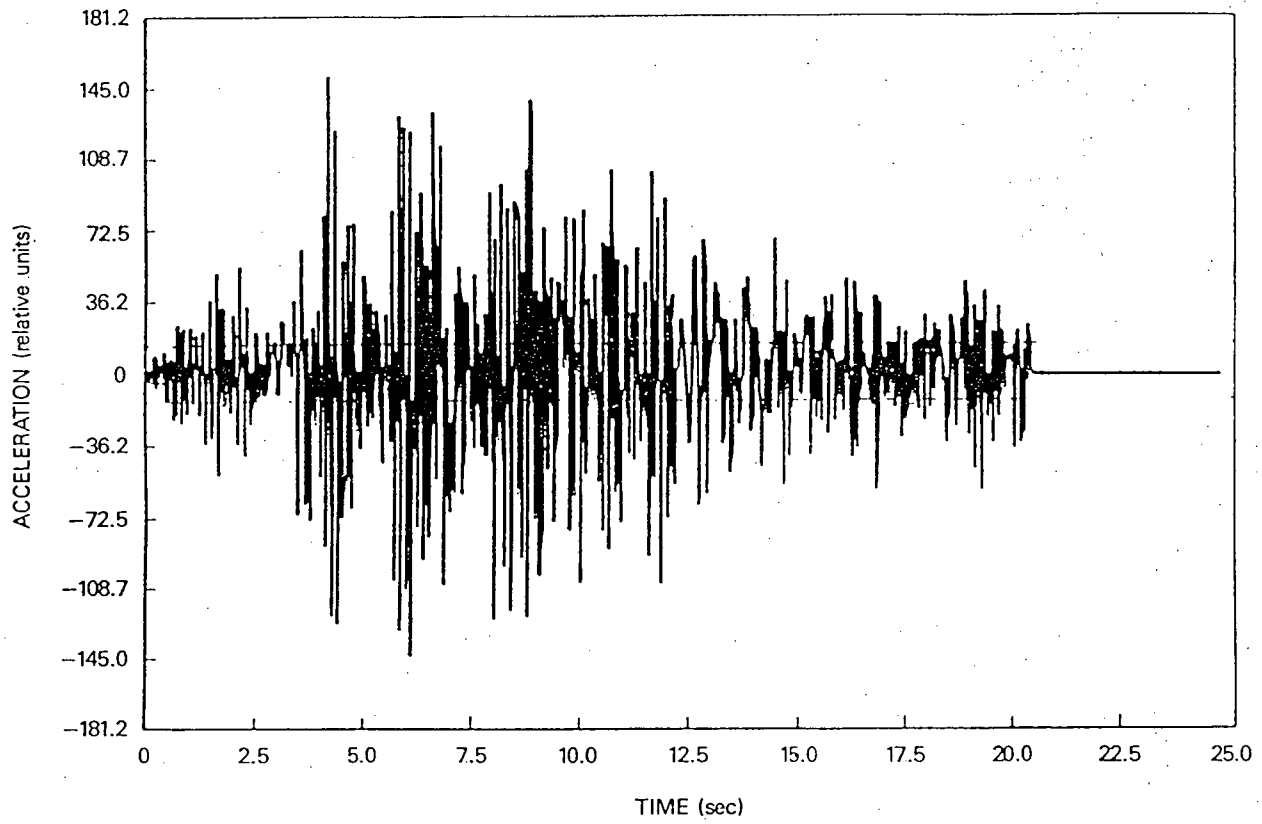


FIGURE 2 INPUT TIME HISTORY

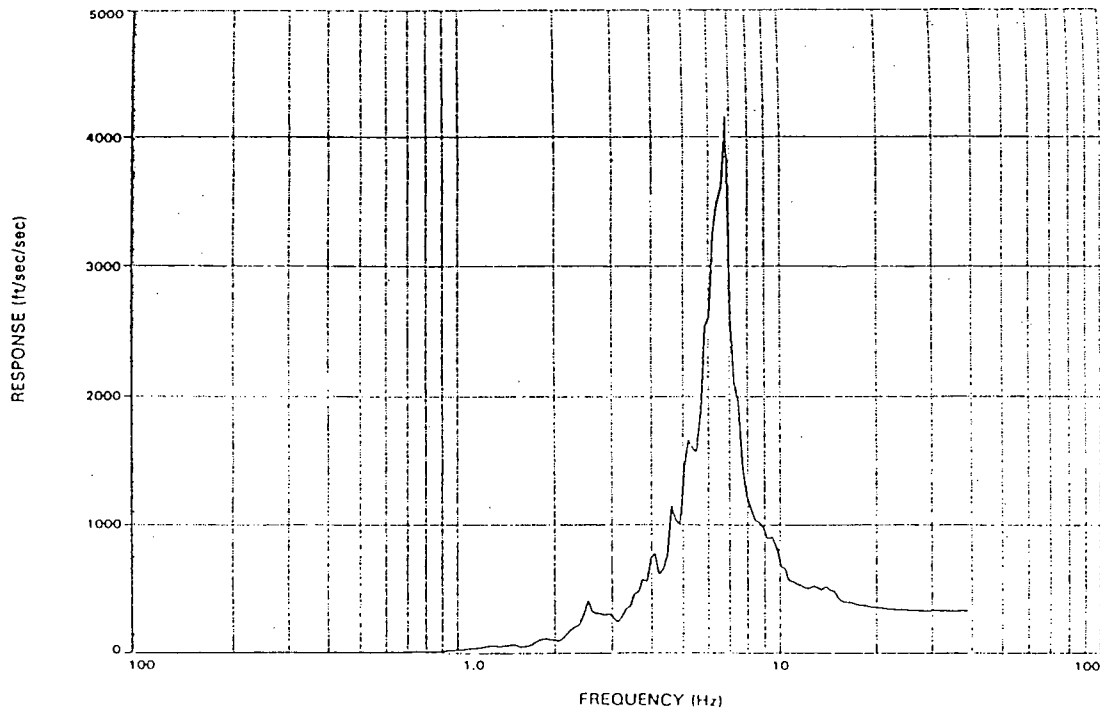


FIGURE 3 Response Spectra

TABLE 1  
PIPING AND FITTING DYNAMIC RELIABILITY PROGRAM  
COMPONENT TEST SUMMARY

| NO | TYPE       | MAT<br>SCH | RES<br>STR<br>X<br>(1) | PRESS | LOAD<br>DIR<br>/SIZE | DYN MOM<br>LIM MOM | LOAD<br>TYPE | P-P CYC<br>STRAIN<br>OD | INPUT X<br>LEVEL D | NO<br>TH | FAIL<br>MODE |
|----|------------|------------|------------------------|-------|----------------------|--------------------|--------------|-------------------------|--------------------|----------|--------------|
| 1  | Elbow      | CS<br>80   |                        | 1500  | I-P                  | 1.21               | SSE          | 2.5X(1)                 | 15                 | 5        | NF           |
|    | (Retest)   | 80         |                        | 2600  | I-P                  | 1.21               | SSE          | 1.5X(1)                 | 15                 | 0.5      | FR           |
| 2  | Elbow      | CS<br>80   |                        | 1500  | O-P                  | 1.04               | SSE          | 1.4X(1)                 | 15                 | 5        | NF           |
|    | (Retest)   | 80         |                        | 2600  | O-P                  | 1.04               | SSE          | 1.4X(1)                 | 15                 | 4.5      | FR           |
| 3  | Elbow      | SS<br>10   | 3.5                    | 400   | I-P                  | 2.36               | SSE          | 2.4X(1)                 | 21                 | 3.5      | FR           |
| 4  | Elbow      | CS<br>40   |                        | 1000  | I-P                  | 1.83               | SSE          | 2.0X(1)                 | 18                 | 2.5      | FR           |
| 5  | Elbow      | CS<br>40   | 13.8                   | 1700  | I-P                  | 2.06               | SSE          | 2.0X(1)                 | 21                 | 3.5      | FR           |
| 6  | Elbow      | SS<br>40   | 16                     | 1700  | I-P                  | 2.00               | SSE          | 2.0X(1)                 | 19                 | 3.5      | FR           |
| 7  | Elbow      | SS<br>40   | 9                      | 1000  | I-P                  | 1.80               | SSE          | 2.0X(1)                 | 23                 | 4.5      | FR           |
| 8  | Elbow      | SS<br>40   | 1.5                    | 0     | I-P                  | 1.80               | SSE          | 2.0X(1)                 | 24                 | 5        | NF           |
| 9  | Tee Fix-2  | SS<br>40   | 8                      | 1700  | O-P                  | 2.50               | SSE          | 2.2X                    | 21                 | 1.5      | FR           |
| 10 | Tee Fix-2  | SS<br>40   | 6.5                    | 1000  | O-P                  | 2.40               | SSE          | 2.2X                    | 21                 | 2.5      | FR           |
| 11 | Tee Fix-2  | SS<br>10   | 3                      | 400   | O-P                  | 1.00               | SSE          | 1.9X                    | 16                 | 0.5      | FR           |
| 12 | Tee Fix-2  | SS<br>40   | 11                     | 1700  | I-P                  | 2.30               | SSE          | 2.2X                    | 27                 | 2.5      | FR           |
| 13 | Short Elb. | CS<br>40   | 6                      | 1000  | I-P                  | 2.30               | SSE          | 1.9X(1)                 | 22                 | 2.5      | FR           |
| 14 | Tee Fix-2  | CS<br>40   | 10                     | 1700  | O-P                  | 2.46               | SSE          | 2.2X(2)                 | 18                 | 1.5      | FR           |
| 15 | Reducer    | SS<br>40   | 18                     | 1700  | 8x4                  | 1.18               | SSE          | 13X(3)                  | 13                 | 5        | FR           |
| 16 | Reducer    | SS<br>40   | 2.5                    | 1700  | 8x4                  | 1.72               | SSE          | 3.3                     | 30                 | 0.5      | FR           |

TABLE 1  
PIPING AND FITTING DYNAMIC RELIABILITY PROGRAM  
COMPONENT TEST SUMMARY

| NO | TYPE                   | MAT<br>SCH | RES<br>STR<br>X<br>(1) | PRESS | LOAD<br>DIR<br>/SIZE | DYN MOM<br>LIM MOM | LOAD<br>TYPE      | P-P CYC<br>STRAIN<br>OD | INPUT X<br>LEVEL D | NO<br>TH | FAIL<br>MODE |
|----|------------------------|------------|------------------------|-------|----------------------|--------------------|-------------------|-------------------------|--------------------|----------|--------------|
| 17 | Short Elbow            | CS<br>40   | 2.5                    | 1000  | TOR                  | N/A                | SSE               | 2.5X(1)                 | 20                 | 3        | FR           |
| 18 | Reinforced<br>Fab. Tee | CS<br>40   | 0.6*                   | 1000  | 8x4                  | 5.3                | SSE               | 0.80                    | 20                 | 0.3      | FR           |
| 19 | Elbow                  | CS<br>40   | 15*                    | 2300  | I-P                  | 2.1                | SSE               | 1.8                     | 22                 | 3.0      | FR           |
| 20 | Nozzle                 | SS<br>40   | 6*                     | 1000  | 12x4                 | 3.2                | SSE               | 1.9                     | 16                 | 1.9      | FR           |
| 21 | Guide Lug              | CS<br>40   | 5*                     | 1700  | 8x6<br>Circ.<br>Mom. | N/A                | SSE               | 1.5                     | 19                 | 0.4      | FR           |
| 22 | Guide Lug              | SS<br>40   | 5*                     | 1700  | 8x6<br>Circ.<br>Mom. | N/A                | SSE               | 2.3                     | 19                 | 0.5      | FR           |
| 23 | Strut                  | CS<br>40   | 1.5                    | 1000  | I-P                  | 2.3                | SSE               | 2.1                     | N/A                | 5        | NF           |
| 24 | Elbow                  | CS<br>40   | N/A                    | 1000  | I-P                  | 1.0                | Static<br>Closing | 2                       | N/A                |          | Collapse     |
| 25 | Elbow-Mid              | SS<br>10   | 4                      | 800   | Mix                  | 6.0                | RV2<br>Mid        | 1.4                     | 27                 | 7        | NF           |
| 26 | Elbow                  | CS<br>40   | 7                      | 1700  | I-P                  | N/A                | Sineswp           | 0.8                     | N/A                | 8        | FR           |
| 27 | Tee Fix-1              | SS<br>40   | 8                      | 1700  | O-P                  | N/A                | Mid +<br>Sine     | 0.3                     | N/A                | 9        | NF           |
| 28 | Waterhammer            | CS<br>40   | 1.8                    | 1700  | I-P                  | 2.7                | Solid Wh          | 2.2                     | 4.0(6)             | 3        | NF           |
|    |                        |            | 4.0*                   | 1000  | I-P                  | 3.1                | Water<br>Slug     | N/A                     | N/A                | 3        | Collapse     |

TABLE 1  
PIPING AND FITTING DYNAMIC RELIABILITY PROGRAM  
COMPONENT TEST SUMMARY

| NO              | TYPE         | MAT<br>SCH         | RES<br>STR<br>X<br>(1) | PRESS    | LOAD<br>DIR<br>/SIZE   | DYN MOM<br>LIM MOM | LOAD<br>TYPE      | P-P CYC<br>STRAIN<br>OD | INPUT X<br>LEVEL D | NO<br>TH | FAIL<br>MODE |
|-----------------|--------------|--------------------|------------------------|----------|------------------------|--------------------|-------------------|-------------------------|--------------------|----------|--------------|
| 29              | Waterhammer  | CS<br>40           | 1.8*                   | 1700     | I-P/<br>Strut          | 2.7                | Solid Wh          | 0.55                    | 4.0(6)             | 3        | NF           |
|                 |              |                    | 4.0*                   | 1000     | I-P/<br>Strut          | 2.8                | Water<br>Slug     | 0.40                    | N/A                | 3        | NF           |
| 30              | Elbow 1.4 Hz | SS<br>10           | 8.17                   | 0<br>410 | I-P 4 Hz<br>I-P 1.3 Hz | 1.7                | SSE               | 1.36<br>2.0             | 10                 | 3        | FR           |
| 31              | Elbow 4.1 Hz | SS<br>10           | 4.0                    | 410      | I-P                    | 2.7                | Sinesup<br>+ SSE  | 1.7                     | 23                 | 3.5      | FR           |
| 32              | Elbow        | SS<br>40           | N/A                    | 1700     | I-P                    | 3                  | Static<br>Opening | 0.5                     | N/A                | 3        | NF           |
| 33              | Pipe 15 Hz   | CS<br>40           | 4*                     | 1000     | N/A                    | 1.1                | Sinesup           | 1.1                     | N/A                | 10       | NF           |
| 34              | Pipe 6 Hz    | CS<br>40           | 6.5                    | 1000     | N/A                    | 1.8                | Sinesup<br>+SSE   | 1.95<br>2.16            | N/A<br>12          | 4        | FR           |
| 35              | Elb High Wt  | CS<br>40           | 13                     | 1700     | I-P                    | 1.65               | SSE               | 3.4X(1)                 | 18                 | 5        | FR           |
| 36              | Tee Fix-1    | CS<br>40           | 3*                     | 1700     | Thru-run               | 2.0                | SSE               | 1.0                     | 15                 | 0.5      | FR           |
| 37              | Elb 1.4 Hz   | SS<br>10           | 4                      | 0        | I-P                    | 1.03(4)            | SSE               | 2.0X(1)                 | 10                 | 2        | RB           |
| 38              | Tee Fix-1    | CS<br>40           | 20                     | 1700     | O-P                    | 1.92               | SSE               | 2.7X(3)                 | 20                 | 3.6      | FR           |
| 39              | Tee Fix-1    | SS<br>40           | 10                     | 0        | O-P                    | 1.84               | SSE               | 3.4X(3)                 | 21                 | 4        | NF           |
| 40              | Reducer      | SS<br>40           | 9                      | 0        | 8x4                    | 1.2                | SSE               | 3.3                     | 22                 | 2        | RB           |
| 41              | Elbow        | CS<br>40           | 10*                    | 1000     | I-P                    | 1.9                | SSE & SINE        | 2.7                     | 25                 | 2        | FR           |
| 170' Mini Sys 1 |              | CS<br>3"<br>Sch 40 |                        | 1700     | I-P                    | 1.5                | Solid Wh          | 1.2(7)                  | 1.8                | 6        | NF           |
|                 |              |                    |                        |          |                        | 1.9                | Water<br>Slug     | N/A                     |                    |          |              |
| 170' Mini Sys 2 |              | CS<br>3"<br>Sch 40 | 3"                     | 1000     | Mix                    | 1.5                | Solid Wh          | 1.1X                    | 1.8                | 6        | NF           |
|                 |              |                    |                        |          |                        | 1.9                | Water<br>Slug     | 1.7X<br>N/A             |                    |          |              |

## OBSERVATIONS

- o Collapse did not occur for any load input.
- o Failure mode was fatigue ratchet with leakage.
- o Eqv. Damping (35%) much greater than RG 1.61 (2%).
- o Seismic inputs much greater than reality.
- o Seismic loads, mid-frequency load and solid water hammer behave more like secondary than primary. Water slug load depend on load duration.

## SYMBOLS:

|          |   |                                                                                                                                                                                                                                              |
|----------|---|----------------------------------------------------------------------------------------------------------------------------------------------------------------------------------------------------------------------------------------------|
| WH       | = | Water Hammer                                                                                                                                                                                                                                 |
| I-P      | = | In-Plane                                                                                                                                                                                                                                     |
| O-P      | = | Out of Plane                                                                                                                                                                                                                                 |
| Fix-1    | = | Single End Fixed                                                                                                                                                                                                                             |
| Fix-2    | = | Both Ends Fixed                                                                                                                                                                                                                              |
| NO TH    | = | Number of high level input test runs to cause failure                                                                                                                                                                                        |
| FR       | = | Fatigue ratcheting failure                                                                                                                                                                                                                   |
| NF       | = | No failure                                                                                                                                                                                                                                   |
| RB       | = | Ratchet Buckling                                                                                                                                                                                                                             |
| FRT      | = | Fatigue ratcheting failure and followed by ductile tearing                                                                                                                                                                                   |
| Residual |   |                                                                                                                                                                                                                                              |
| Strain   | = | Measured by 2 inch scratch marks                                                                                                                                                                                                             |
| Input X  |   |                                                                                                                                                                                                                                              |
| Level D  | = | Calculated stress using linear response spectrum analysis, 2% Damping, $\pm$ 15% broadening and actual sled input. Use the calculated stress, $(B_2 M/Z)$ , divided by Level D allowable, $3S_m$ to determine multiple of Level D allowable. |

## NOTES:

- (1) For all the elbows, the measured strains are on the outside surface. For strain on inside surface, multiply the values by 1.5:  
The inside surface is 1.388 times of the outside, principal strain is 1.072 time of circumferential strain and the circumferential strain is 1.01 time of average strain over gage length 1/16".  
 $1.388 \times 1.072 \times 1.01 = 1.50$ . For 2" scratch mark, the factor 1.01 is increased to 1.52 and the multiplication is  $1.388 \times 1.072 \times 1.52 = 2.26$ .  
For ratchet strain on the inside surface, a factor of 2.0 over the tabulated values.
- (2) Gage failed too early, there is almost no data, use previous similar test run data.
- (3) Gage filed too early, it is not known if peak values have been obtained.
- (4) Weight stress over 1000 psi.
- (5) Test was stopped prior to crack to get sample.
- (6) Use measured moment instead of calculated moments. If calculated moment is used, the value will be reduced from 4.0 to 3.0.
- (7) Use twice of the maximum (O-P) value.

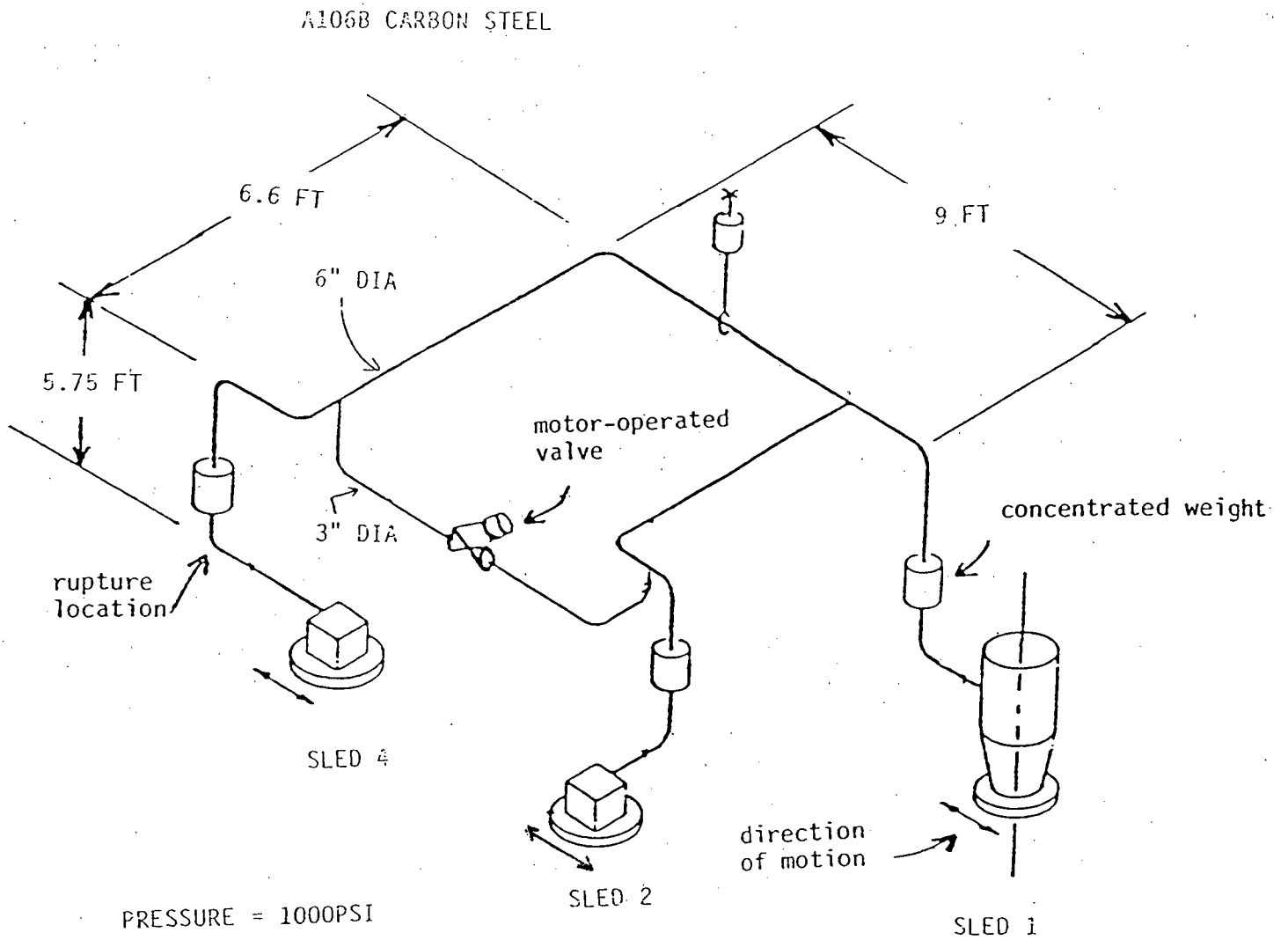


FIGURE 4 SYSTEM 1 CONFIGURATION



Table 2 - Calculated High Stresses of System Tests

Stresses are scaled from reference calculation using ratios of measured nominal input levels to the input level of the reference calculation. (High stress points coincide with rupture locations shown on Figures 4 and 5).

| <u>System 1</u>                                |              |                |                        |                        |                        |
|------------------------------------------------|--------------|----------------|------------------------|------------------------|------------------------|
|                                                | SSE<br>Input | 5 SSE<br>Input | Half Table<br>Capacity | Full Table<br>Capacity |                        |
| Calculated High Stress (ksi) using 2% Damping  | 47           | 320            | 1629                   | 2521                   |                        |
| Ratio to Class 1 Level D allowable (60 ksi).   | .78          | 5.3            | 27.2                   | 42.0                   |                        |
| Calculated High Stress (ksi) using 5% Damping. | 29           | 183            | -                      | -                      |                        |
| Ratio to Class 1 Level D allowable (ksi)       | .48          | 3.1            | -                      | -                      |                        |
| <u>System 2</u>                                |              |                |                        |                        |                        |
|                                                | SSE<br>Input | 2 SSE<br>Input | 5 SSE<br>Capacity      | Half Table<br>Capacity | Full Table<br>Capacity |
| Calculated High Stress (ksi) using 2% Damping  | 61           | 111            | 386                    | 661                    | 1261                   |
| Ratio to Class 1 Level D allowable (50.1 ksi)  | 1.2          | 2.2            | 7.7                    | 13.2                   | 25.2                   |
| Calculated High Stress (ksi) using 5% Damping. | 45           | 89             | 294                    | 483                    | 896                    |
| Ratio to Class 1 Level D allowable (50.1 ksi)  | .90          | 1.8            | 5.9                    | 9.6                    | 17.9                   |

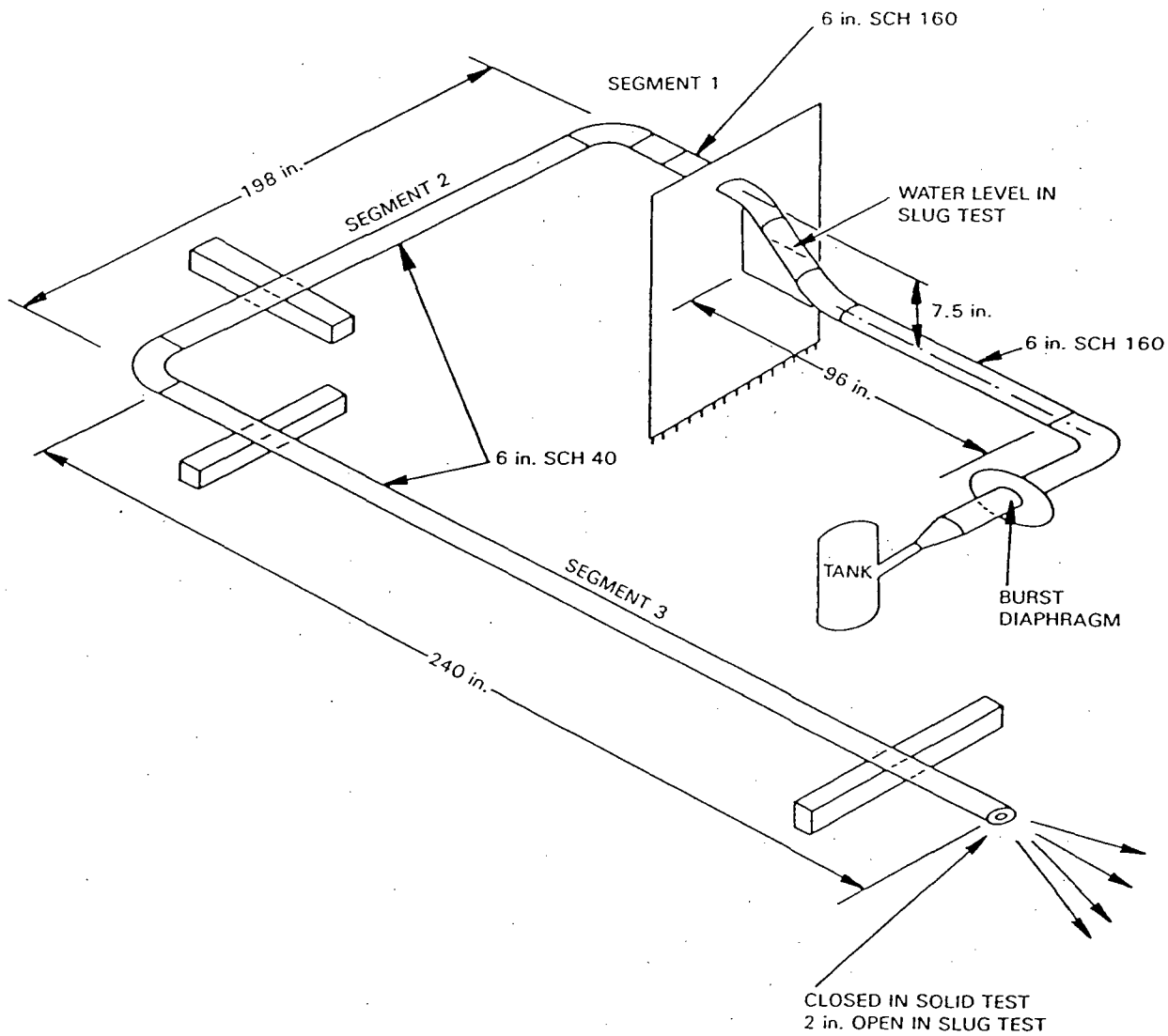


FIGURE 6 Test 28 Water Hammer Test Configuration



# RELAY STUDIES - EXISTING DATA, CURRENT TESTING AND CABINET AMPLIFICATION

K. Bandyopadhyay, C. Hofmayer, M. Kassir, S. Pepper  
Brookhaven National Laboratory  
Upton, NY 11973

## ABSTRACT

The seismic fragility of most electrical equipment is governed by the malfunction of relays. This paper discusses the combined study being performed at BNL by evaluating existing fragility test data, conducting a new relay test program and estimating the cabinet amplification at relay locations. Existing test data for relays have been collected and evaluated at BNL. The data base consists of results from a wide variety of test programs - single frequency, single axis, multifrequency, multiaxis tests. For most relays, the non-operating condition controls the chatter fragility limit. In order to characterize the effect of various parameters on the relay seismic capacity, a test program has been initiated at BNL. Selected test specimens will be tested to determine the influence of frequency of vibration, direction of motion, adjustments of relay parts, among others, on the relay capacities. The amplification study involves computing dynamic amplification factors at various device locations in motor control center and switchgear cabinets. Fragility and high level qualification data have been used for this purpose. This paper includes a summary of the amplification results.

## 1.0 INTRODUCTION

Evaluation of seismic fragility of electrical equipment being performed at Brookhaven National Laboratory (BNL) and elsewhere, indicates that for most equipment the fragility levels are governed by malfunction of relays. Therefore, a special study has been undertaken at BNL for understanding relay performance. To this end, evaluation of the existing relay test data, conducting a new relay test program and investigating the dynamic amplification of relay housing cabinets are being carried out at BNL. This paper discusses the data base, describes the testing methods and presents the cabinet amplification results.

## 2.0 DATA BASE TEST PROGRAMS

As part of the Component Fragility Program at BNL [1,2], a vast amount of relay test data has been collected from various sources. These tests were performed in the period 1973-1985. The test programs in the BNL data base can be grouped into two types depending on the testing methods and the available information as discussed in the following subsections.

### 2.1 Single Axis, Single Frequency Tests

Single axis, single frequency sine beat or sine dwell tests were performed on early vintage relays in the period 1973-75. Information is available for twenty five protective and auxiliary (including time delay) relay models. The relay specimens were tested at specific frequencies with increasing input level until they exhibited contact chatter at a pre-selected level (e.g. 1, 2 or 10

milliseconds) or until the capacity of the shake table was reached. The tests were repeated in different directions and for different electrical (i.e. energized and de-energized) and contact (i.e. normally open and normally closed) conditions. The vibration levels were measured in terms of the amplitude of the sine wave form and presented as a plot of input acceleration vs frequency. The discrete points in the plot are connected to provide a continuous fragility (or test equipment capacity) curve in the frequency range 1-35Hz. Figure 1 shows a set of typical test results for a relay model. The lower curve indicates the fragility chatter limit (2ms) for a normally closed contact of the sensing unit of the relay when de-energized and the upper curve corresponds to the shake table capacity curve which was exceeded for the energized condition. For the data base relays, the contact chatter fragility level was as low as 0.1g and as high as 3.0g sine beat input motion.

Single frequency test results reveal the frequency sensitive nature of relays. However, it is often difficult to use the input acceleration values to determine whether the data set envelops a required response spectrum, the common form of measure of the seismic demand in practice since the mid-1970's. Therefore, the use of the early test data is limited unless an appropriate conversion factor is developed.

## 2.2 Multiaxis, Multifrequency Tests

The data base contains multiaxis, multifrequency results from tests performed since the late 1970's. Most tests were performed with biaxial inputs - either phase incoherent or phase coherent. Triaxial input motion was used for the rest. The fragility levels due to relay chatter were determined for various electrical modes and contact conditions and expressed in terms of the test response spectrum (TRS). Some relay models did not exhibit chatter even at the shake table capacity vibration level. The multifrequency test data were of three different types and the nature of the data was also different as discussed in the following subsections.

### 2.2.1 Required Response Spectrum Tests

These tests were performed to meet a specific or a generic required response spectrum (RRS) and in the process the chatter fragility was reached. The corresponding vibration level was presented in terms of TRS data. These results are conservative in the sense that at some frequencies the relay may still withstand higher vibration levels.

### 2.2.2 IEEE Std 501 Tests

A large number of test programs were conducted following the generic procedure and the standard RRS shape recommended by IEEE Std 501 (ANSI C37.98) [3]. Since the late 1970's, the manufacturers have used this approach for seismic rating of their products. Typically, the ZPA is used as a single-valued fragility level such that the 5% damped spectral level is two and half times the ZPA. This is a very convenient and concise way of expressing the fragility limit and the seismic ratings (i.e. ZPA's) are readily available, sometimes even

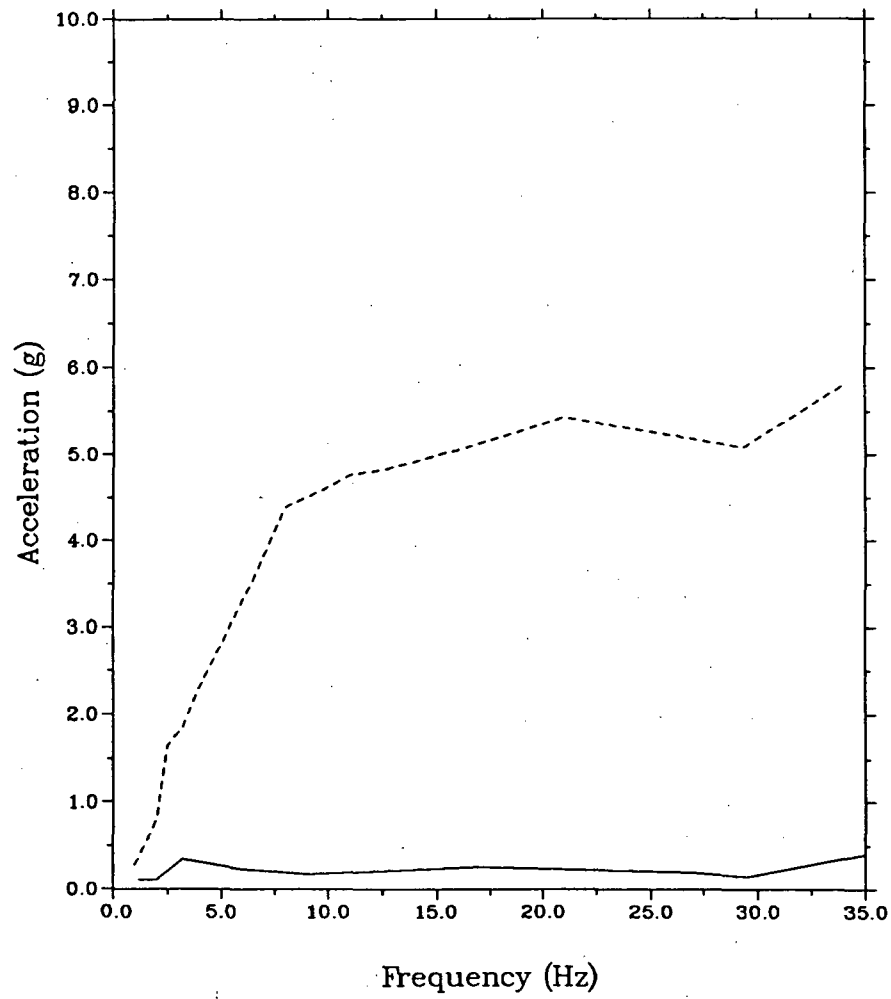


Fig. 1 Single Axis Sine Beat Test Amplitude

in manufacturers' catalogs and sales brochures. Also, the fragility levels of various relay models can be easily compared and the appropriate relay can be selected. However, the TRS data used for obtaining the seismic ratings are not easily available. The data base indicates a wide range of seismic ratings - from as low as 0.5g ZPA to as high as 6.0g ZPA. For many relays, the seismic rating is controlled by the capacity of the shake table rather than the capability of the relays.

### 2.2.3 Panel Tests

A large number of electrical panels were tested with relays mounted in them. Since for a long time it is known in the industry that relays are the typical weak links of electrical equipment, electrical channels and accelerometers are commonly used for selected relays to monitor the electrical performance of these relays and to measure the vibration level at the device locations. Such information is an important source of relay fragility data. The BNL data base contains relay information for equipment tested in the period 1977-80. The merit of the panel test data is that in application relays will be mounted in such panels and used in similar circuits. Therefore, the relay performance and the vibration level at locations recorded during panel testing are more direct, realistic and dependable, especially since the input vibration at the base of the equipment has been filtered through the cabinet structure. The limitation of the use of the panel test data is that the same relay located in another possible location in the same cabinet, or tested in another cabinet, may exhibit the fragility phenomenon corresponding to a different TRS data set due to different characteristics of the filtering medium. Another limitation of the panel test data is that since the purpose of the tests was not necessarily to determine the fragility threshold of a particular relay, the available information is most often either higher or lower than the threshold, e.g. either 20ms chatter or no chatter for a 2ms chatter criterion.

## 2.3 Sensitivity Parameters

The seismic fragility of relays depends on one or more parameters related to the design or the input motion. Some of these parameters are discussed in the following subsections.

### 2.3.1 Frequency of Vibration

Depending on the design, most relays are capable of withstanding a higher vibration level at one frequency than another. The frequency range in which a particular relay is weak may be low (e.g. less than 10Hz), medium (e.g. 10-30Hz) or high (e.g. greater than 30Hz) as illustrated by the chatter fragility sine beat input vs frequency curves for two different relay models shown in Figure 2. One curve shows sensitivity to low frequencies and the other curve shows sensitivity to medium and high frequencies.

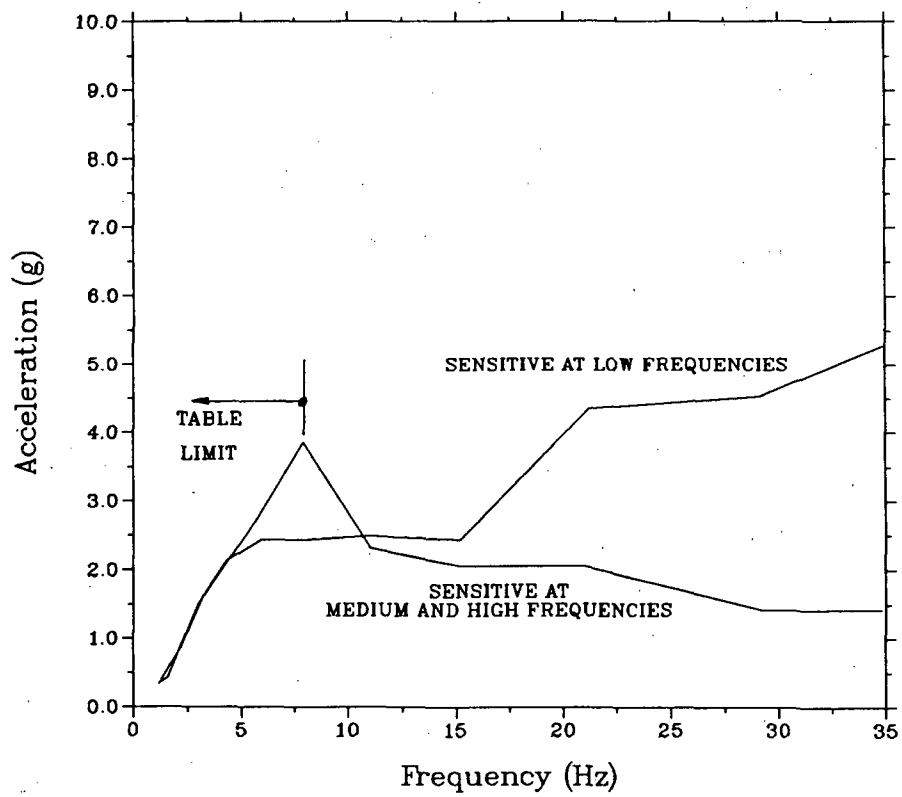


Fig. 2 Single Axis Sine Beat Test Amplitude Frequency Sensitivity

### 2.3.2 Chatter Duration

Depending on the chatter duration that can be accepted for a particular application, the fragility level may change. Single axis testing indicates that for most frequencies the vibration level is higher if a longer chatter can be accepted as demonstrated by Figure 3.

### 2.3.3 Direction of Vibration Input

Depending on the design of the operating mechanism, relays exhibit varying capacity levels in different directions. Typically they are weak in the direction of the contact movement. Figure 4 shows single frequency capacity test data of an auxiliary relay model in three orthogonal directions, front-to-back (FB), side-to-side (SS) and vertical (V). The front-to-back (FB) vibration controls the capacity level for the relay at high frequencies.

### 2.3.4 Electrical Mode

Most two-state relays chatter in the de-energized electrical mode at a lower vibration level than the energized mode. This is especially true for relays with hinged armature mechanisms since in the energized state the magnetic field of the coil tends to restrain the motion of the armature. Figure 5 shows single frequency capacity results of a popular auxiliary relay with a hinged armature mechanism for both the energized (E) and de-energized (DE) modes.

### 2.3.5 Contact State

The moving contact of an electro-mechanical relay needs to traverse the contact gap for a normally open contact before it closes by engaging the stationary contact. On the other hand, a normally closed contact becomes open immediately by disengaging the stationary contact. Therefore, for electro-mechanical relays, normally closed contacts typically chatter at a lower vibration level than normally open contacts. Figure 5 shows the single frequency capacity levels of a normally closed (NC) contact and a normally open (NO) contact of an auxiliary relay.

### 2.3.6 Adjustments

In a hinged armature mechanism, the magnetic force experienced by the armature must overcome the tension of the balance spring for movement of the moving contact. An adequate spring tension is required for normal operation and engagement of the moving contact. A stronger tension value tends to press the moving contact tight against the stationary contact and thereby makes the moving contact less susceptible to vibration.

The thin shaft of a rotary disk mechanism, on the other hand, is supported by two bearings and the disk tends to jump out of plane in a vibratory environment unless the play of the vertical shaft at the bearing is properly adjusted. One popular relay model was observed to exhibit such a phenomenon in a seismic test program resulting in malfunction of the relay.

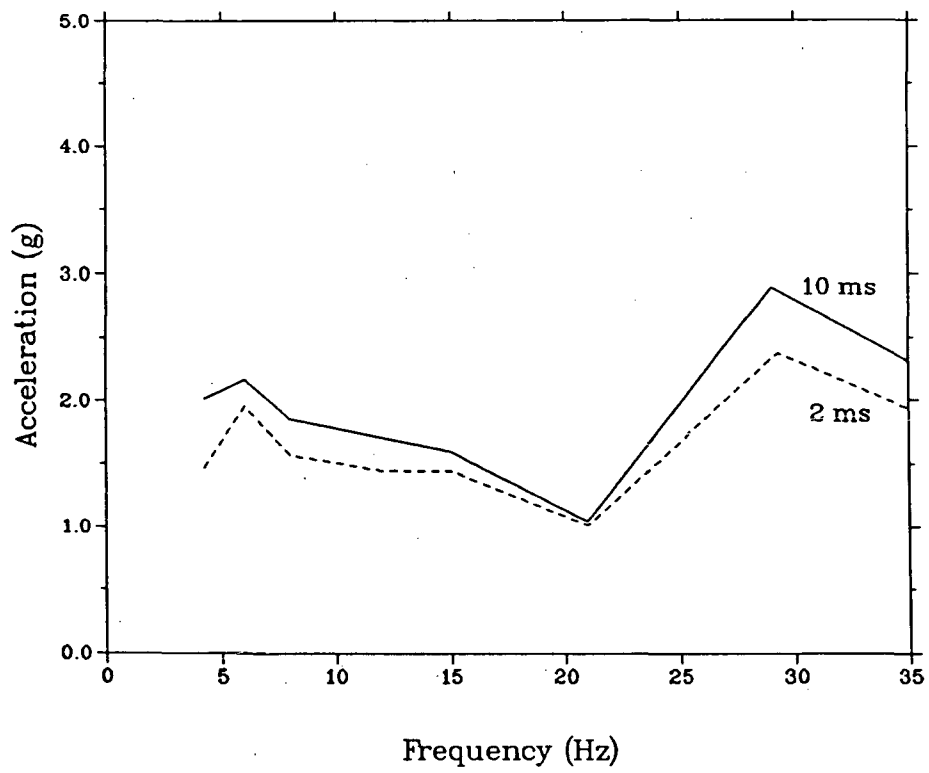


Fig. 3 Single Axis Sine Beat Test Amplitude Chatter Duration Sensitivity

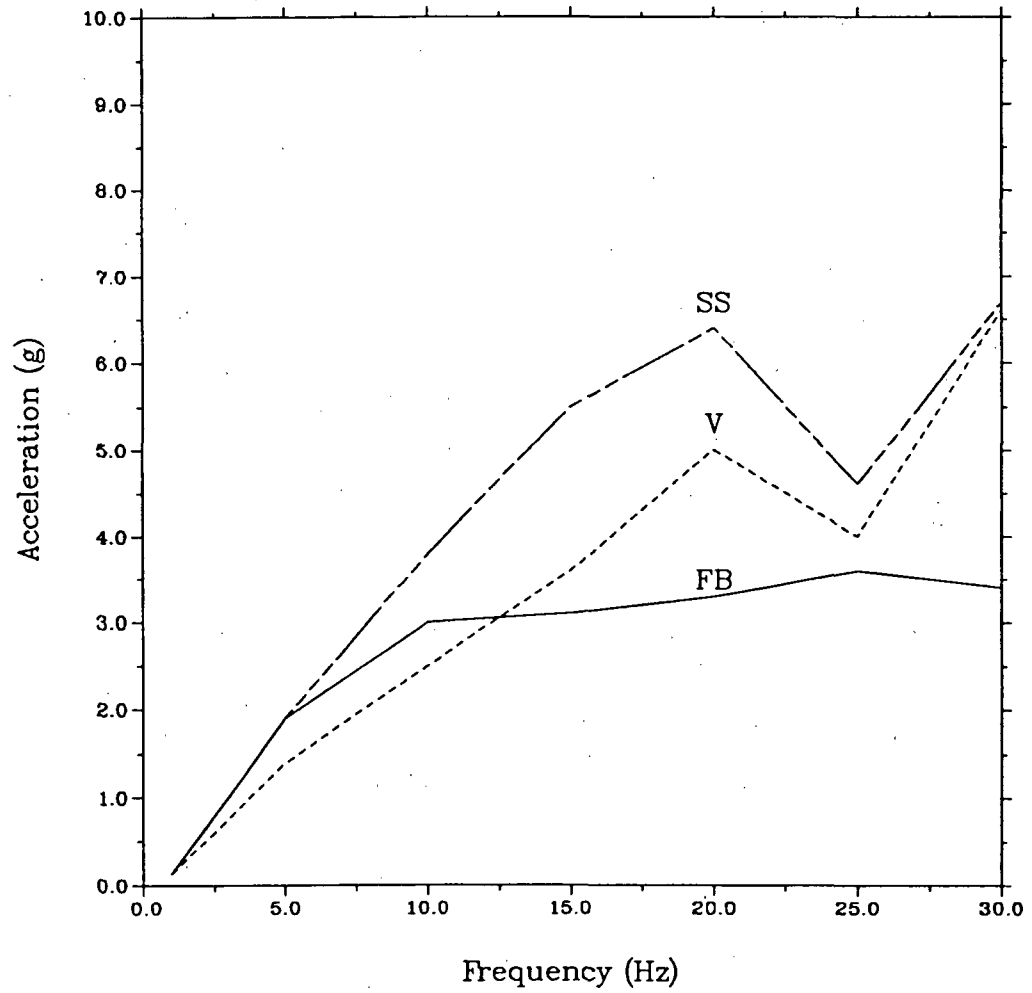


Fig. 4 Single Axis Sine Dwell Test Amplitude  
Input Motion Direction Sensitivity

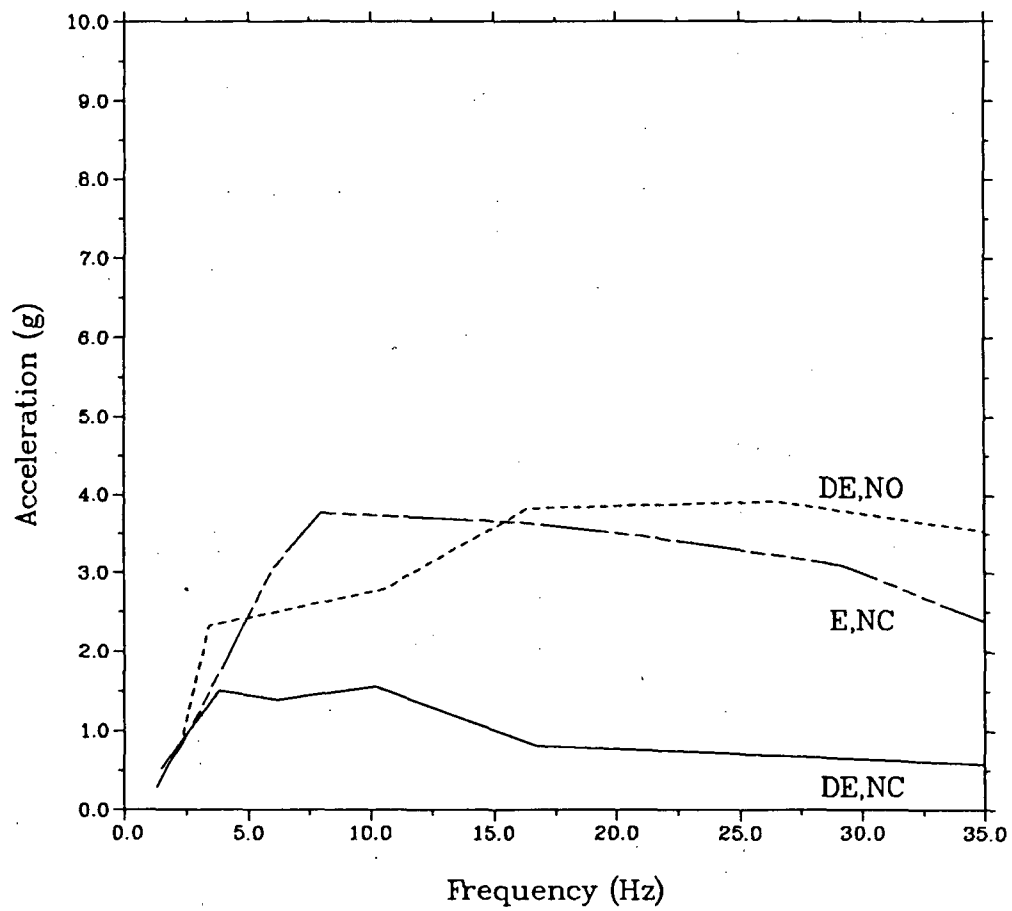


Fig. 5 Single Axis Sine Beat Test Amplitude  
Electrical Mode and Contact State Sensitivity

Thus, for different operating mechanisms, certain adjustments may influence the seismic capacity of a relay.

### 3.0 CURRENT TEST PROGRAM

Primarily, in order to further study the effect of parameters on relay fragility levels, BNL has initiated a relay test program. Establishing the correlation between single frequency fragility test inputs and multifrequency test response spectra, and confirming the similarity of relay models within a group are also objectives of the test program.

Single frequency sine dwell tests will be performed to study the effect of vibration frequency on the fragility levels. Nineteen popular models from three manufacturers will be tested. For ten models more than one specimen will be used to study the consistency of results.

Multifrequency tests will be performed with separate single axis, biaxial and triaxial inputs on twelve relay models. Spectral shapes will be matched with the respective single frequency fragility inputs so that the conversion factors relating the single frequency test inputs to the multifrequency test response spectra can be computed.

Four relay models from one manufacturer with three specimens for each will be tested with biaxial multifrequency input motion following the IEEE Std 501 (ANSI C37.98) spectral shape. The test is intended to confirm the same seismic rating for all four models.

All the above tests will be performed on new (current vintage) relay models. The effect of spring tension and contact gap adjustments will be studied by varying the respective parameters of two hinged armature relay models. The effect of end play adjustments will be tested on two rotary disk relays. All adjustment tests will be performed with single frequency inputs.

The initial single frequency tests will be conducted in all three orthogonal directions for all three electrical modes (i.e. operating, non-operating and transition) and two contact conditions (i.e. normally closed and normally open). All subsequent tests will be performed only in the weakest direction for the weakest electrical modes and contact conditions. A chatter duration of 2ms or greater will be used as the failure criterion to establish the fragility levels.

Upon completion of testing, the test data will be evaluated to draw conclusions regarding the effects of various parameters, the relation between single frequency and multifrequency results, and the similarity of relay models within the same seismic rating group. The results will be published in 1989.

#### 4.0 CABINET AMPLIFICATION

Since relays like most other devices are mounted on electrical cabinets which tend to amplify the input motion, the relay fragility data cannot be directly compared with the seismic demand specified at the base of the cabinet. If the amplified motion at the relay location is known from testing of the particular cabinet, that can definitely be used for comparison with the relay test data. In the absence of such specific information, a 'generic' amplification factor for the equipment class may be used to relate the relay test data to the input motion at the base of the housing cabinet. BNL has evaluated fragility and qualification level test data of nine motor control center and ten switchgear cabinets and computed amplification of the input motion at various locations in the cabinets measured in terms of response spectra. The factors have been obtained at various frequencies and presented as amplification spectra in NUREG/CR-5203 [4]. The input motion is amplified at the resonant frequencies of the cabinet structure and internals. Therefore, the amplification factor at a location in the cabinet is dependent on the frequency. A typical amplification spectrum peaks at the structural resonant frequencies and dips at other frequencies as illustrated by Figure 6. The amplification factors have been computed at many device locations in the respective data base cabinets and a summary of the deterministic and probabilistic results is presented in Table 1.

#### 5.0 CONCLUSIONS

The seismic fragility levels are to a great extent relay model specific. The existing data base provides fragility information for a large number of relay models manufactured at different time periods. However, the existing data are not adequate to address certain inconsistencies in the fragility results observed in the data base, probably due to the variation of the input motions or the specimen design or both. The relay test program will focus on these issues and is expected to clarify the influence of certain parameters. Both the existing and the new test data measure the relay capacity at its location. The amplification study provides the link between the motion at the relay location in an electrical cabinet and that at the base of the cabinet. Therefore, the three studies combined together will define the parameters controlling the seismic performance of relays and allow a proper and effective use of the existing relay data base.

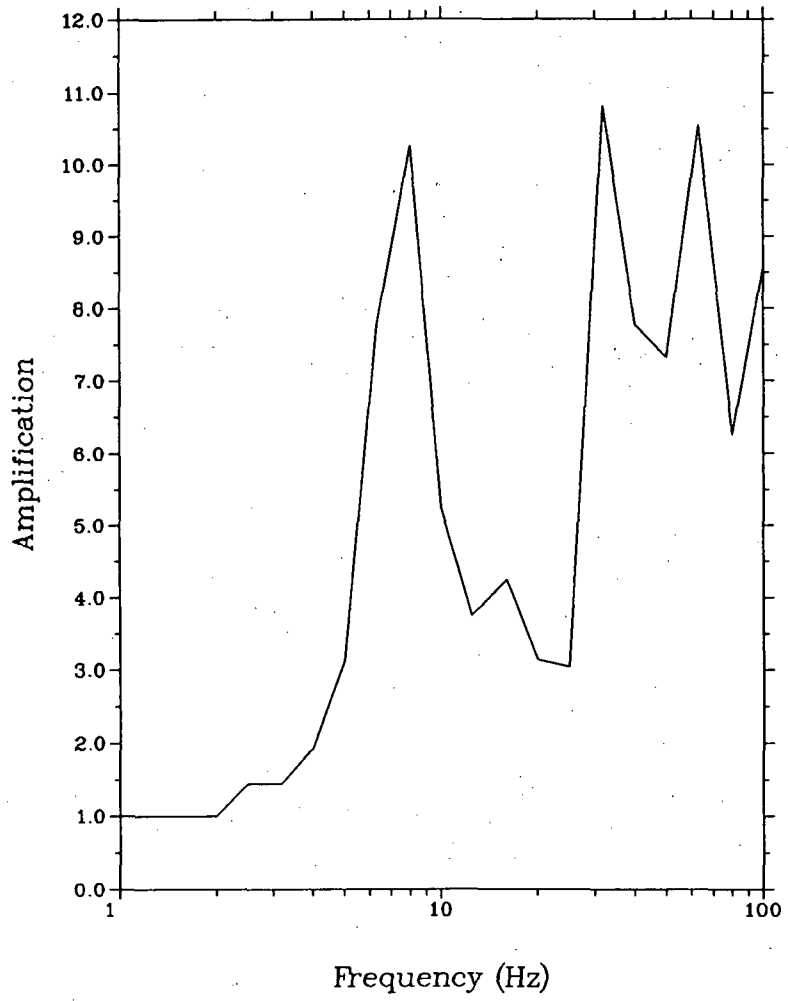


Fig. 6 A Typical Amplification Spectrum

TABLE 1

Summary of Amplification Results<sup>1,4</sup>

| Amplification <sup>2</sup> | Motor Control Center |        |                              | Switchgear |        |                              |
|----------------------------|----------------------|--------|------------------------------|------------|--------|------------------------------|
|                            | Maximum              | Median | High Confidence <sup>3</sup> | Maximum    | Median | High Confidence <sup>3</sup> |
| Peak                       |                      |        |                              |            |        |                              |
| 4-16 Hz                    | 7.7                  | 4.8    | 8.2                          | 20.0       | 7.4    | 16.7                         |
| 16-40 Hz                   | 8.3                  | 5.3    | 9.9                          | 27.3       | 11.2   | 31.6                         |
| 40-100Hz                   | 13.0                 | 5.7    | 15.8                         | 51.7       | 16.2   | 72.1                         |
| Average                    |                      |        |                              |            |        |                              |
| 4-16 Hz                    | 4.0                  | 3.0    | 4.7                          | 9.0        | 4.2    | 8.7                          |
| 16-40 Hz                   | 6.6                  | 3.7    | 7.7                          | 15.6       | 7.5    | 19.3                         |
| 40-100Hz                   | 9.3                  | 5.0    | 11.2                         | 28.3       | 12.3   | 45.0                         |
| Zero Period                | 4.8                  | 3.3    | 5.4                          | 16.7       | 5.8    | 15.2                         |

1 These results are applicable only within the limitations described in chapter 3, Section 3.3 of NUREG/CR-5203

2 The amplification parameters are defined in Chapter 2, Section 2.3 of NUREG/CR-5203

3 High (95%) confidence of a low (5%) probability of exceeding the listed values

4 Selection of the appropriate single-valued amplification factor is left to the user

#### REFERENCES

1. Seismic Fragility of Nuclear Power Plant Components (Phase I), NUREG/CR-4659, Vol. 1, June 1986
2. Seismic Fragility of Nuclear Power Plant Components (Phase II), Motor Control Center, Switchboard, Panelboard and Power Supply, NUREG/CR-4659, Vol. 2, December 1987
3. IEEE Standard Seismic Testing of Relays, ANSI/IEEE C37.98-1978
4. Dynamic Amplification of Electrical Cabinets, NUREG/CR-5203, June 1988

#### ACKNOWLEDGEMENT

This work is being performed under the auspices of the Division of Engineering, Office of Nuclear Regulatory Research, U.S. Nuclear Regulatory Commission. The authors wish to express their special thanks to Dr. John O'Brien, NRC Project Manager, for his continued support and guidance throughout the course of this program. The authors also sincerely acknowledge the cooperation of the organizations and the individuals who participated in the BNL program by providing valuable fragility data.

#### NOTICE

The findings and opinions expressed in this paper are those of the authors and do not necessarily reflect the views of the U.S. Nuclear Regulatory Commission.

# ASCE WORKING GROUP ACTIVITIES ON STIFFNESS OF CONCRETE SHEAR WALL STRUCTURES

by

Joel G. Bennett and Charles R. Farrar  
Advanced Engineering Technology

## ABSTRACT

This paper will review the history and activities of the ASCE Working Group on stiffness of concrete shear wall structures as influenced by the U.S. Nuclear Regulatory Commission (NRC) sponsored Seismic Category I Structures Program and their efforts to define a position for the "reduced stiffness" problem up through the May 1988 meeting. The group's activities and recommendations for accounting for this effect will be presented. This paper will present the authors' point of view. Therefore, no warranty is implied that it will represent the final Working Group position or the ASCE Dynamic Analysis Committee acceptance. The paper is offered in the spirit of presenting the group's activities for information to the NRC and to the civil engineering community.

---

## I. INTRODUCTION AND BACKGROUND FOR THE WORKING GROUP

The American Society of Civil Engineers (ASCE) has established an organization chart that maintains its technical leadership role in civil engineering through its professional development arm. Under the professional development arm, the Technical Activities Committee maintains management groups. Management Group B coordinates the activities of several technical divisions including the largest in membership, the Structural Division. The Nuclear Structures and Materials Committee operates within this division and further maintains a Committee on Dynamic Analysis. In May of 1986, through the efforts of Dr. Robert P. Kennedy, of RPK Structural Mechanics Consulting, and Dr. John D. Stevenson, of Stevenson and Associates, a Working Group on the stiffness of

reinforced shear walls was established from members of the Dynamic Analysis Committee. This Working Group was to be and is chaired by Dr. Robert C. Murray of the Lawrence Livermore National Laboratory (LLNL) and had its initial kickoff meeting, hosted by the Southwest Research Institute on November 20, 1986 in San Antonio, Texas. Such a Working Group had existed under this committee before, but it had never had been able to come to a consensus concerning the stiffness of shear wall structures. However, both Drs. Kennedy and Stevenson are members of a technical review group (TRG) for the Seismic Category I Structures Program sponsored by the U.S. Nuclear Regulatory Commission (USNRC), a research effort that had been ongoing at the Los Alamos National Laboratory since 1980. Both individuals were aware of the results of the research and felt that the time had come to reconsider some of the issues and findings that resulted from the reporting of that research.

Briefly, in FY 1980, the NRC established the Seismic Category I Structures Program to investigate the seismic structural response of low-aspect-ratio, shear-dominated nuclear power plant Category I structures. Testing of both single shear walls and box-like, scale-model microconcrete structures was completed by the end of FY 1984. Adequate reserve structural margin was reported, but measured natural frequencies were generally lower than would be predicted by a strength-of-materials analysis--many times by a factor of 2 or more. Both measured and frequency-implied structural stiffnesses were low as much as a factor of 4 or more. These findings generated considerable discussion and interest among the civil engineering community, particularly because the floor response spectra for Category I buildings might not be consistent with these findings. Some of these issues will be discussed further in this paper, but for members of the civil engineering community that accepted the "reduced stiffness" as being real and applicable to nuclear structures, the most likely source of the reduction has been cracking of the cross section. Furthermore, in early 1986, the ASCE Committee on Nuclear Standards had completed the ASCE Standard, Seismic Analysis of Safety-Related Nuclear Structures (ASCE 4-86) that was approved by ballot in September 1986. In this standard, the modeling of stiffness of reinforced concrete elements (Section 3.1.3) indicates that uncracked cross section properties may be used "provided that elements do not crack significantly." However, little or no consistency has been established about ways to implement this section.

With this background material, the authors will discuss the history and summarize the status of the Working Group activities in their efforts to establish an ASCE position paper on this topic.

## II. HISTORY OF WORKING GROUP'S ACTIVITIES AND PROGRESS

At the initial Working Group meeting, the first author presented a summary of the findings of the Seismic Category I Structures Program, including a discussion of the issues surrounding the "reduced stiffness" effects. The "reduced stiffness" issue arose from the reporting of program findings to the TRG at the end of FY 1984. At that time, results on items such as aging (cure time), effect of increasing seismic magnitude, etc., were reported, but the most important conclusion was that the so-called "working load" secant stiffness of the models was lower than the computed, uncracked, cross-sectional values by a factor of about 4. The term "working load" implies loads that produce stress levels equivalent to at least the operating basis earthquake, and up to the safe shutdown earthquake.

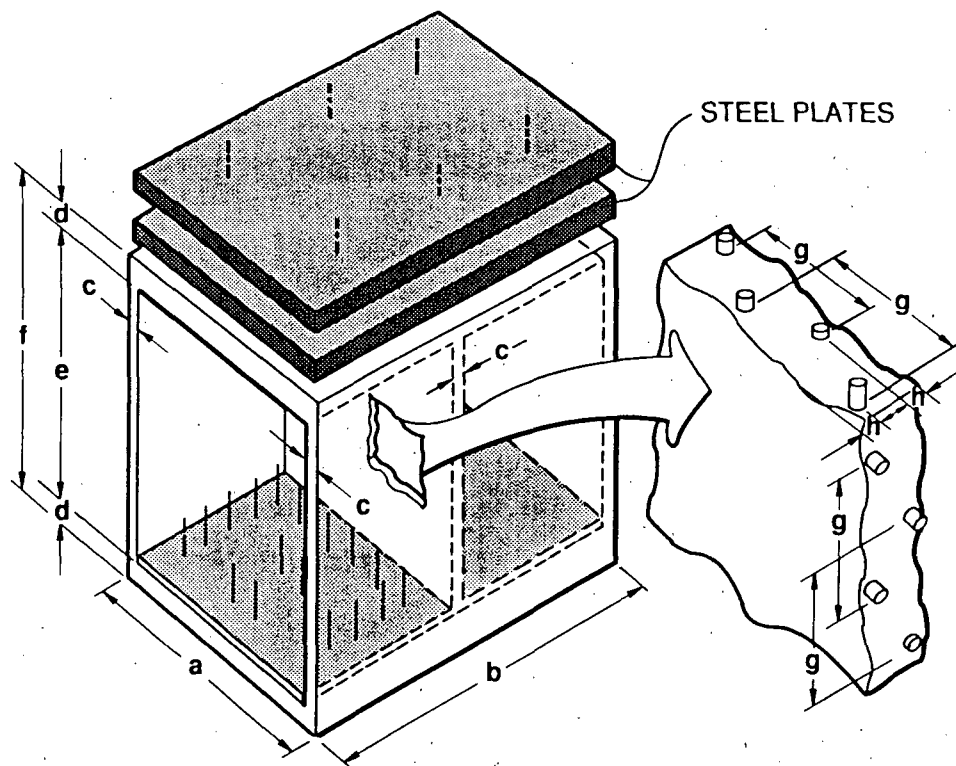
During their review of this program, the TRG pointed out the following:

1. Design of prototype nuclear plant structures is normally based on an uncracked cross-section, strength-of-materials approach that may or may not use a "stiffness reduction factor" for the concrete; however, should such a factor be used, it is never as large as 4.

2. Although the structures themselves appear to have adequate reserve margin (even if the stiffness is only 25% of the theoretical value), any piping and attached equipment will have been designed by using inappropriate floor response spectra.

3. Given that a nuclear plant structure designed to have a natural response of about 15 Hz may have a natural frequency of 7.5 Hz (corresponding to a reduction in stiffness of 4), and allowing further that the natural frequency may further decrease because of degrading stiffness, the natural response of the structure will shift well down into the frequency range for which an earthquake's energy content is the largest. This shift will result in increased amplification in the floor response spectra at lower frequencies, an effect that has potential impact on the equipment and piping design response spectra and their margins of safety.

Note that all three points are related to the difference between the measured and calculated stiffnesses of these structures. The ASCE Working Group was made aware of all of this information. In addition, the results for the first two structures in the TRG series of tests were presented. This series of tests was carried out basically at the request of the TRG as credibility experiments and consisted of a shear wall geometry like that shown in Fig. 1. A 1/4 scale model of this structure was also constructed and tested. The results for the first two structures are reported in Refs. 1 and 2, and drafts of those reports were provided to the Working Group at the kickoff meeting.



| STRUCTURE | DIMENSIONS (cm) |     |     |    |     |     |      |      | ADDED WEIGHT (kN) | REBAR diam (mm) |
|-----------|-----------------|-----|-----|----|-----|-----|------|------|-------------------|-----------------|
|           | a               | b   | c   | d  | e   | f   | g    | h    |                   |                 |
| TRG 1     | 58              | 75  | 2.5 | 5  | 58  | 68  | 0.6* | 1.3* | 26                | 0.11            |
| TRG 3,5   | 230             | 300 | 10  | 20 | 230 | 270 | 11*  | 3.8* | 170               | 10              |
| TRG 4     | 230             | 300 | 15  | 20 | 230 | 270 | 37   | 2.5  | 170               | 10              |
| TRG 6     | 230             | 300 | 15  | 20 | 61  | 101 | 18   | 2.5  | 170               | 10              |

\* ONE LAYER OF REINFORCEMENT DOWN THE CENTER OF THE WALL IN BOTH THE HORIZONTAL AND VERTICAL DIRECTION

Fig. 1. Geometry of the TRG-recommended credibility test structures.

The issues surrounding these results were summarized to the Working Group and are presented in Figs. 2, 3, and 4. Figure 2 shows the results of the tests performed in the Seismic Category I Structures Program and some other known data that were available at that time. This plot shows the actual measured (quasi-static test) or frequency-implied (base excited seismic test) "working load" secant stiffnesses normalized by the value that would be calculated from a strength-of-materials approach using an uncracked concrete cross-section. The values are plotted over a wide range of concrete moduli as determined for each model using the American Concrete Institute (ACI) recommended method of  $E_c = 57,000 \sqrt{f'_c}$  (psi), where  $E_c$  is the concrete modulus, and  $f'_c$  is the compressive strength of the concrete determined by cylinder testing.

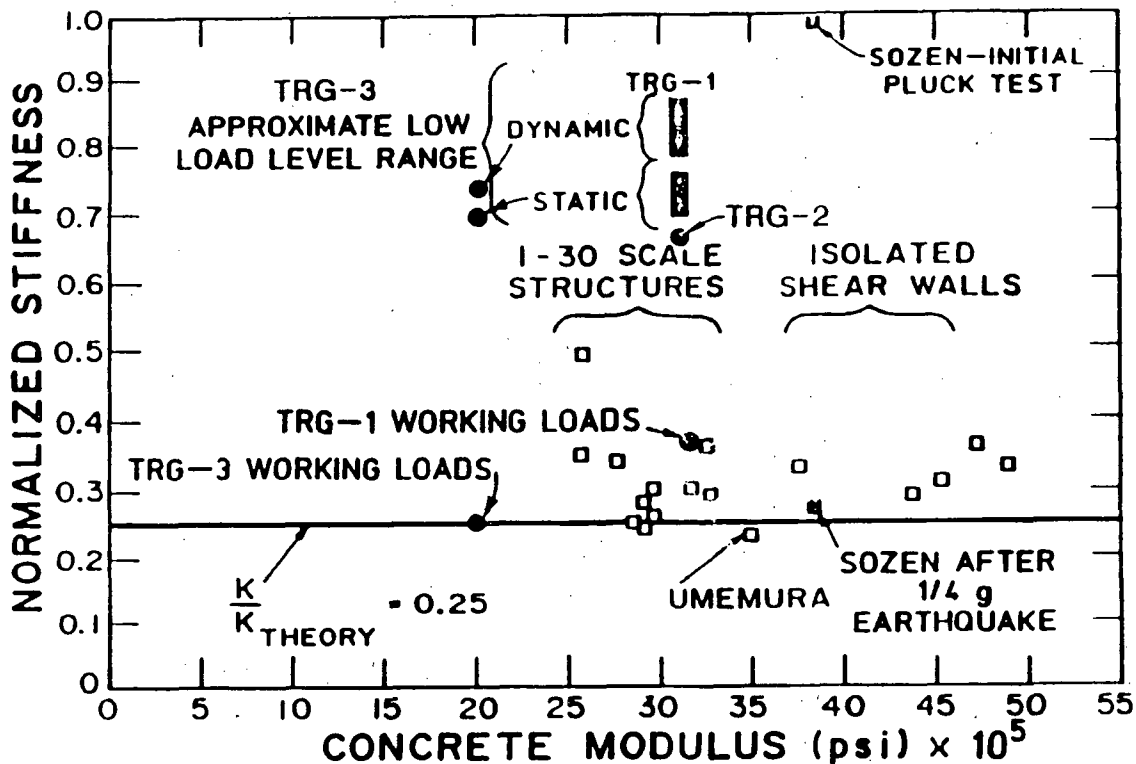


Fig. 2. Normalized stiffness of test data plotted versus concrete modulus (available at the ASCE Working Group kickoff meeting).

Figure 3 shows the floor response spectra that would be calculated for one of these tests (TRG-3), based on a stiffness determined from an uncracked cross-section, strength-of-materials analysis and a fixed-base boundary

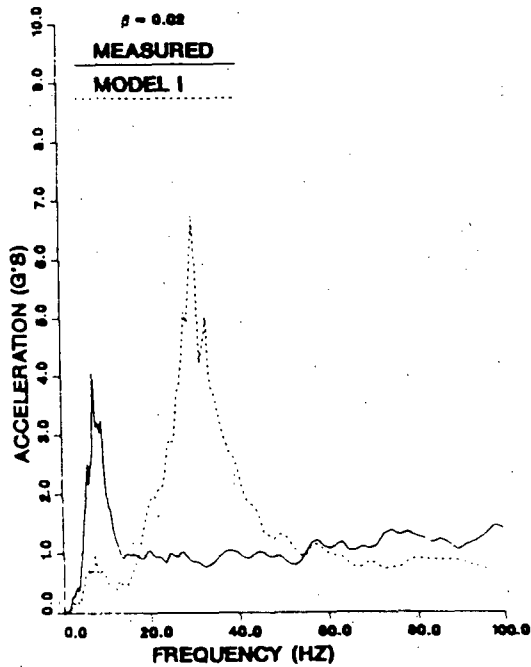


Fig. 3. Response spectra generated from measured floor acceleration compared with those that would be calculated by using a fixed base model and known material properties.

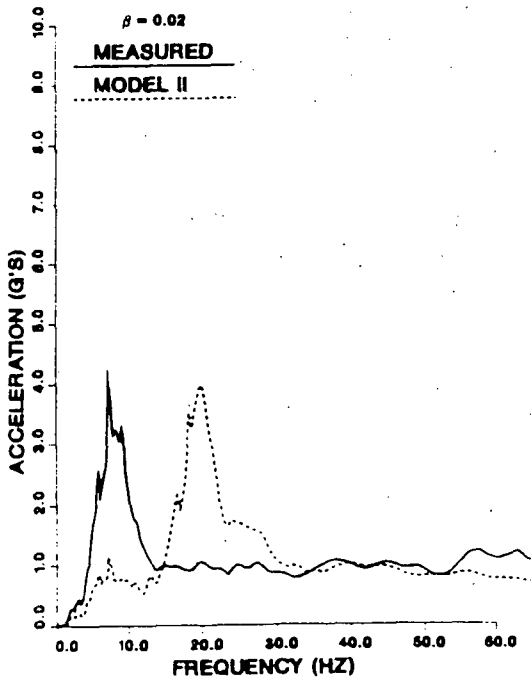


Fig. 4. Response spectra from a calculation that accounts for base rocking compared with those from measured data.

condition (dotted curve), versus the floor response spectra from the measured floor accelerometer record at the same location. Figure 4 shows the same comparison but with base connection springs included in the analysis. The Working Group immediately understood the potential effects of the frequency-shifted peak on piping and equipment design issue.

The course of action was then defined for the Working Group as follows: (1) collect any available supporting or conflicting data particularly on real structures, (2) carefully review available data, (3) develop an ASCE position paper, (4) polish and review the paper, and (5) publish the paper in an ASCE Journal. Appropriate assignments were made related to this action plan and the meeting was concluded.

The Working Group met next on May 7, 1987 in Palo Alto, California. The meeting was hosted by the Electric Power Research Institute (EPRI). At this meeting, Los Alamos presented the results of quasi-static cyclic testing of a large structure (TRG-4, 6-in.- thick walls) that was very carefully

constructed, handled, and tested in a controlled, thermal environment in an effort to minimize any cracking. These results showed that up until first cracking, the structural stiffness was in good agreement with analytical estimates.

Next, all data specifically relating to this issue were discussed. Particularly, model reactor containment tests conducted on a deep embedment structure by EPRI and Niagara Mohawk were discussed, but results relating to the reduced stiffness issue were not clear cut. These models are still available for further testing, however.

Diablo Canyon data were discussed. To get a match with measured low-level earthquake response, analytical models had to have both rock-structure interaction and basemat flexibility added. It was concluded that the low frequency response ( $< 4\text{Hz}$ ) of these structures can mask any reduced stiffness effects because of cracking.

Data taken on the University of California Santa Barbara North Hall during a 1978 earthquake were distributed to the Working Group and then discussed. The conclusion was that this structure is very complex and a large modeling effort would be required to make sense out of the data. It was felt that such an effort was beyond the resources and scope of the Working Group.

One of the other assignments that the group members undertook was to calculate a stiffness estimate for the TRG-3 test that had been carried out and presented at the prior meeting and to discuss factors that could contribute to a stiffness reduction. These discussions centered on:

- Base flexibility,
- Anchorage of the structure to the shaker table,
- Possible effects of gaps between anchors,
- Table flexibility, and
- Cracking level.

Details of the shaker table were requested by some members for possible future work on these topics.

Next, the group discussed a theory that had been published by A. K. Gupta of North Carolina State University, a corresponding member of the group, that the appropriate modulus of structural modeling for concrete may be  $1/2 E_{\text{initial}}$ . The group was "uneasy" about the concept in absence of more data and, because Gupta was not at the meeting, the discussion terminated.

The next order of business was to develop an outline for the position paper on how to calculate the stiffness of concrete shear wall structures. Figure 5 shows this outline as developed and distributed in the meeting minutes, along with principal assignments of responsibility. The difficult section of "recommendations" was postponed pending further data on the reduced stiffness effects, but it was agreed that the outline contained topics that had to be addressed.

OUTLINE AND ASSIGNMENTS

ASCE Position Paper on "How to Compute Shear Wall Stiffness"

Introduction (Kennedy/Murray)

Purpose of Paper

Effects on In-Structure Spectra

Typical Shear Wall (Nuta - east coast plants, Hadjian - west coast plants)

Geometry

Stress Levels

Reinforcement

Industry Practice (Singh)

Shear Stiffness

Flexural Stiffness

Special Effects (shear lag, shear area)

Reinforcement

Review of Experimental Data (Farrar)

Implications

Data Applicable

Strength of Materials Approach Applicable

Comparison of Practice with Data

Sources of Variability (Hashimoto)

Recommendations

Approaches

Stiffness Before Cracking

Stiffness After Cracking

Implication on Floor Spectra

Fig. 5. Outline of position paper as developed by the Working Group.

This meeting concluded with plans for the next meeting scheduled for Stone Mountain, Georgia, in October. At this point the group consisted of fourteen active members and one corresponding member.

At this meeting, results of a new test (TRG-5, 4-in. thick walls) by Los Alamos were presented. A portion of the meeting minutes read as follows:

The test was similar in geometry to TRG-4 with a 4-in. thick shear wall and one layer of rebar at the center of the wall (0.6% steel). TRG-5 was well instrumented and statically tested. Results were in good agreement with stiffness estimates by the strength-of-materials approach. This was the second of two well instrumented static tests that provided good agreement with theory.

The group summarized and prioritized the possible reasons for reduced stiffness measured in earlier tests as follows:

1. Models were cracked prior to testing;
2. Microconcrete versus real concrete/model size,
3. Dynamic tests versus static tests,
4. Base rotation.

The importance of normal stress in shear walls was discussed by the Working Group. The consensus points are indicated below:

- Tests were conducted at normal stress levels below 40 psi;
- Actual shear walls have normal stresses in the 30-70 psi range,
- At low levels, normal stress is likely to be a large contribution to stiffness reduction,
- Microconcrete may not develop aggregate interlock which could contribute to stiffness reduction.

The group went on to discuss several other details of the developing position paper, but were still having difficulty with the all-important section of recommendations. Two further quotes from the minutes are revealing in this respect:

Based on the available information examined so far, the Working Group has not established a position. We need to wait for more data to become available to resolve the open issues.

and,

An agenda for the next meeting was developed. Bob Kennedy agreed to invite Mete Sozen to the next meeting to stimulate discussion.

The Group had, at this point, developed into two factions that appear to be representative of the ASCE engineering community's reaction to the reduced stiffness issue. The one set believes that this effect is largely an experimental anomaly that does not occur in real structures. The other set generally believes that construction practices, differential settlement, thermal effects, and shrinkage (curing, aging), all contribute to cracking or microcracking of real concrete and that probably all concrete structures will exhibit a reduced stiffness, if not initially, then eventually. It was known that Dr. Mete Sozen, of the University of Illinois, had assembled data on earthquake response of R.C. structures over the years. The next meeting was scheduled for May, 1988 to be hosted by EPRI in Palo Alto, California, and as noted in the minutes, Sozen was to be invited.

By the May 1988 meeting, the final structure tested by Los Alamos as part of the TRG series, TRG-6, had been tested. This structure had a very low shear wall aspect ratio (0.25 height/length), 6-in.-thick walls and was lightly reinforced (0.25% by area each direction). The structure was so stiff, that at low load levels (<50 psi base shear), the instrumentation for measuring relative deformations was taxed to the limit. Nonetheless, the agreement between experimental and calculated stiffness values was again very good until first cracking. Thus, the Los Alamos presentation to the group once again raised questions about previously obtained data that showed reduced stiffness. Again, it was pointed out that everything possible was done with this structure in terms of construction, handling, and testing environment to obtain a theoretical value.

The first author believes that Mete Sozen's presentation was a turning point in the group's decision to deal with the reduced stiffness issue and to begin to come to a consensus on a set of recommendations. The basic presentation centers on a collection of data from Japan, from the University of Illinois, and from others; these data were plotted in Figs. 6-8 and presented by Sozen. Sozen argued that, according to these data, there is clearly a large variation in the expected value of the stiffness from a concrete shear wall, and not all nontheoretical measured results can be attributed to experimental error. This argument was very convincing and, following other presentations on potential base connection effects for the TRG-3 test, the group moved to grapple with a recommendation on stiffness variability.

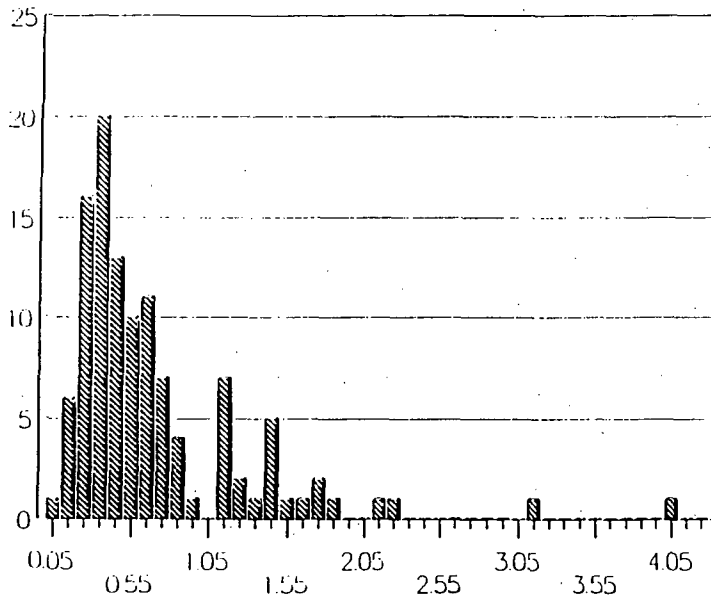


Fig. 6. Histogram of measured stiffness/  
calculated stiffness presented  
to the Working Group by Dr. Mete  
Sozen, University of Illinois.

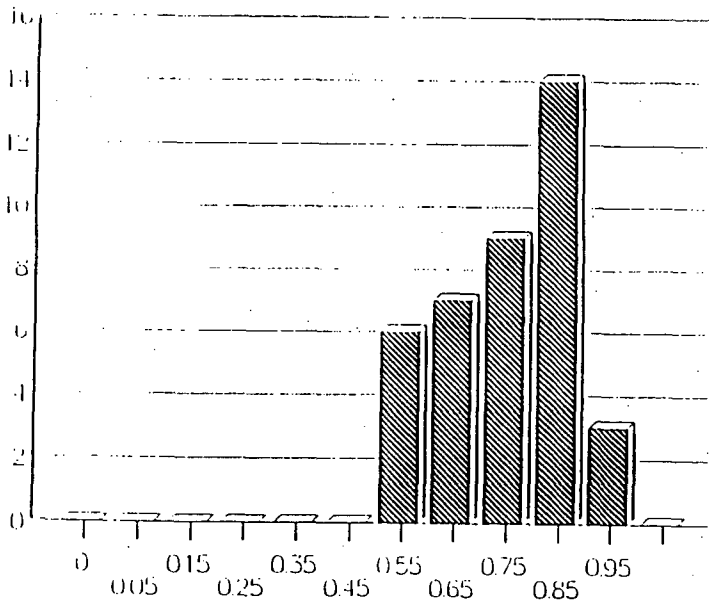


Fig. 7. Histogram of measured frequen-  
cies/calculated frequencies  
presented to the Working Group  
by Dr. Mete Sozen, University  
of Illinois.

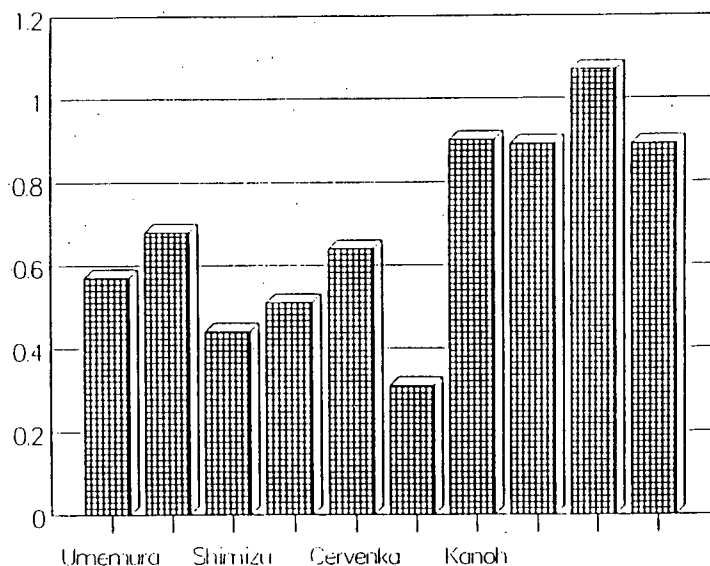


Fig. 8. Additional data on initial measured stiffness/calculated stiffness given to the Group.

### III. CURRENT STATUS OF THE WORKING GROUP'S POSITION

The current position (in the opinion of the authors) of the consensus of the Working Group revolves around Figs. 9 and 10.

In these sketches,  $K$  is the stiffness,  $f'_c$  is the design concrete compressive strength,  $K_{theory}$  is the uncracked cross-section strength of materials value,  $V_c$  is the ASCE calculated cracking load,  $\varphi$  is a parameter. The recommendation will likely be that, based on the fact that we cannot know the condition of the insitu structure (because of thermal effects, differential settlement, shrinkage, etc.), the normal design spectra should be produced by using the low, and high values of stiffness in Fig. 9 and equipment should be designed to meet the resulting enveloped spectra.

Figure 10 shows the expected stiffness behavior in terms of a load-drift curve. The values for the second knuckle of Fig. 10 have not been totally defined as yet.

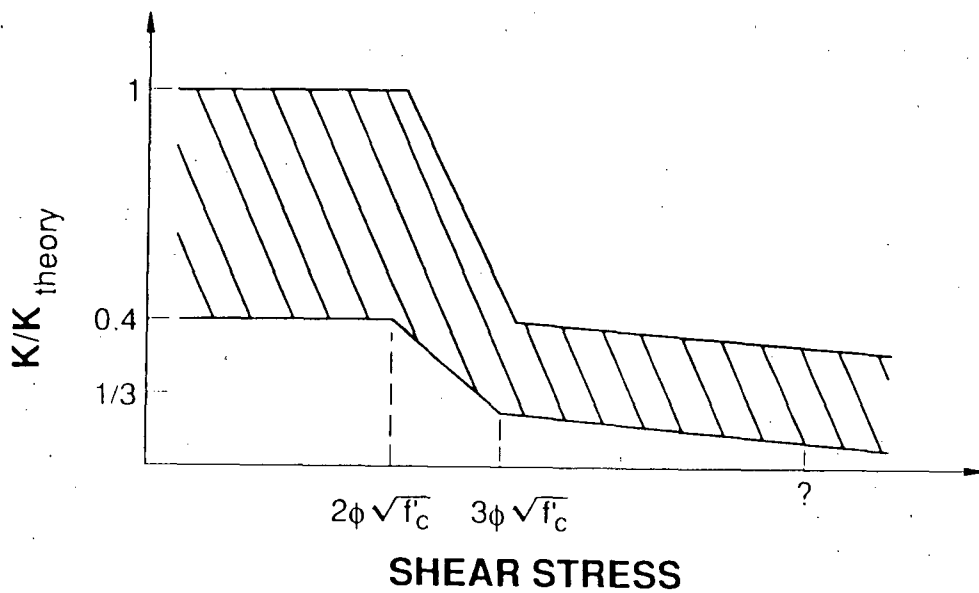


Fig. 9. Uncertainty band for stiffness of R.C. shear walls.

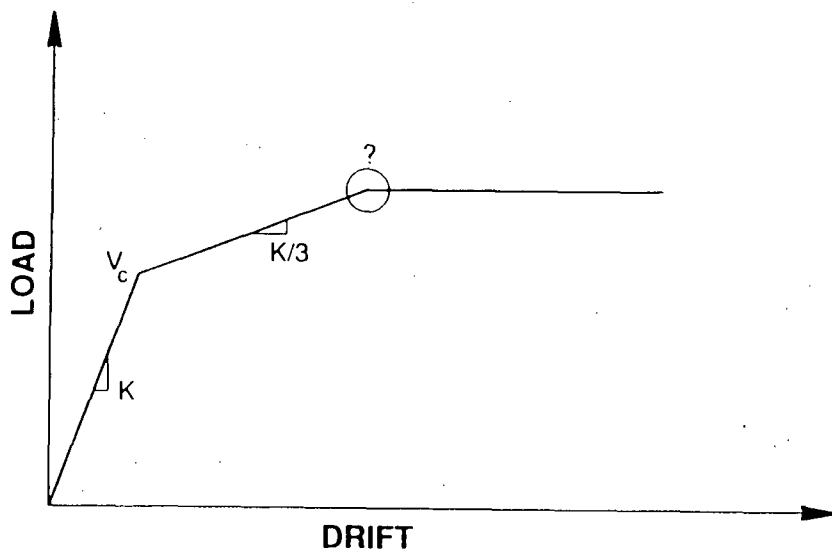


Fig. 10. Behavior of stiffness in terms of load drift.

#### IV. CONCLUSIONS

The research in the Seismic Category I Structures Program was initially directed at finding the margin-to-failure for low-aspect-ratio shear wall structures and at understanding of the seismic response of these structures. However, during the course of the investigation, the issue arose of how should shear wall stiffness be computed for analytical models that are used to generate spectra for equipment design. Here, the emphasis shifts toward being accurate rather than ensuring structural conservatism. The authors believe that this NRC-sponsored research will have an effect on both the design and safety analysis of these structures that will be beneficial in the long term. By working with the code committees, this research helps resolve this potentially important issue. This paper is presented in the interest of keeping both the U.S. NRC and the interested nuclear civil structure community advised of the Working Group's activities.

#### V. REFERENCES

1. J. G. Bennett, Richard C. Dove, W. E. Dunwoody, C. R. Farrar, P. Goldman, "The Seismic Category I Structures Program: Results for FY 1985," NUREG/CR-4998, December 1987.
2. J. G. Bennett, R. C. Dove, W. E. Dunwoody, C. R. Farrar, P. Goldman, "The Seismic Category I Results Program: Results for FY 1986," NUREG/CR-5182, September 1988.

ASSESSMENT OF EFFECTS OF STRUCTURAL RESPONSE  
ON PLANT RISK AND MARGIN

By

M.P. Bohn, E.W. Klamerus  
Sandia National Laboratories

I. Introduction

Since 1983, the U.S. Nuclear Regulatory Commission Office of Nuclear Regulatory Research has sponsored the Seismic Category I Structures Program at Los Alamos National Laboratories. This project has been primarily responsible for investigating the structural dynamic response of Seismic Category I reinforced concrete shear wall structures (exclusive of containment structures). In this program, both static and dynamic tests were performed on scale model concrete shear wall structures ranging from 1/10 scale to 1/42 scale. Both diesel generator buildings and auxiliary buildings were modeled and tested as reported in References 1 through 8.

In these tests, the structures were initially subjected to free vibration and small amplitude excitation to determine the fixed-base natural frequencies of the models. In addition, the models were subjected to a set of scaled earthquake time history simulations. To assess the effects of peak ground acceleration on building response, the amplitude of the simulated earthquake time history was increased in steps for successive tests.

As test results accumulated, it became clear that the initial natural frequencies measured were significantly less than would be computed analytically using the initial stiffness of concrete. Furthermore, during the simulated earthquake time history tests, measured structure stiffnesses were found to decrease with increasing peak ground accelerations. As a result, natural frequencies of the test specimens was found to be reduced by up to 50 percent of the computed natural frequency.

This reduction in natural frequencies represents a potentially important issue in the design and safety of nuclear power plants. For example, structure excitation could be greater if the reduced building natural frequencies more closely match the high energy content frequencies of an earthquake in that area. Also, safety related equipment could experience greater seismic loads, due to a shift in the floor spectra where the equipment is located.

In 1988, the U.S. NRC began the Assessment of Effects of Structural Response on Plant Risk and Margin program at Sandia National

Laboratories. The program will assess the impact of decreased natural frequencies on both the deterministic design calculations and the overall seismic plant risk for several prototypical power plants. This paper describes the scope of the program and its current status.

## II. Scope

The general approach chosen to assess the potential impact of the "frequency reduction" issue on power plant risk is as follows:

- Step 1. Choose existing seismic PRA(s) as base case(s).
- Step 2. Re-compute structure response with reduced fixed-base natural frequencies using best-estimate SSI calculations.
- Step 3. Re-evaluate capacity of structures with new median loads and uncertainty distributions.
- Step 4. Re-compute floor spectra for critical components (both median and uncertainty distributions).
- Step 5. Re-evaluate critical component fragilities.
- Step 6. Compute accident sequence probabilities with new structure and component fragilities and compare with original PRA results.

In Step 1, the decisions to be made involving the choice of seismic probabilistic risk assessments (PRAs) include the following: 1) The plant vintage, type (PWR or BWR) and the basis used for its original design. 2) Whether the plant is located on a rock or soil site. 3) Was a safety factor approach or a calculated dynamic response approach used to assign fragilities in the original PRA. Also, it is helpful to have available the details of structure and component fragility calculations for each power plant.

Three existing seismic PRAs are being re-evaluated. These will consist of a rock site Boiling Water Reactor (BWR), a rock site Pressurized Water Reactor (PWR), and a soil site PWR. The soil site PWR will be chosen to have a soil depth that is likely to enhance the effects of reducing the fixed-base natural frequencies of important structures. The potential sites for which some type of seismic PRA already exists are:

Rock BWR: Peach Bottom, Limerick, and Quad Cities.

Rock PWR: Seabrook, Millstone III, Indian Point, Maine Yankee, and ANO-1.

Soil PWR: Zion, Point Beach, Turkey Point, St. Lucie, and Surry.

Step 2 is to recompute the structural response. This is done by first obtaining design fixed base models of each important structure at a plant site and coupling these with best estimate soil models. Ten time histories matching original design spectra are then performed, which include variations in structure and soil properties, and the reduced building natural frequencies. The results obtained from Step 2 are: ten values (each) of story shears, slab accelerations and ten floor spectra for each floor, as shown in Fig. 1.

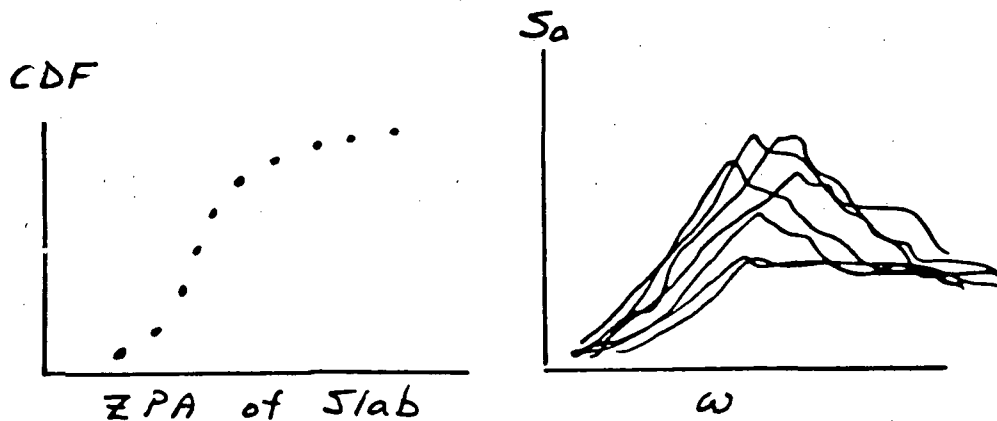


Figure 1. Distribution Plot and Floor Spectra

Step 3 involves re-evaluating the structure capacity. The structural capacity of most of these buildings, when subjected to earthquake ground motions, is governed by the strength of the shear walls. Therefore, the acceleration to failure is determined for each shear wall and governing walls are identified. Median loads and uncertainty distributions must be included to accurately determine the median and uncertainty of acceleration at structural failure.

In Step 4, the floor spectra is recomputed for each floor containing critical components using the model and results obtained in Step 2. The spectral acceleration ( $S_a$ ) at a given frequency for a specified floor elevation can then be found. When the " $S_a$ " is plotted for various PGAs, an almost linear representation can be found to correlate the PGA with the spectral acceleration. This representation, along with the variability, is shown in Fig. 2.

The results from Step 4 are used in Step 5, which is the re-evaluation of critical component fragilities. The original seismic PRA fragility derivations will be used, but modified to account for the new floor spectra. Some components may remain unchanged or experience even

smaller dynamic loads than were previously considered. However, in some cases the dynamic loading could be considerably increased if the natural frequency is reduced and the floor spectra shifts, as shown in Fig. 3.

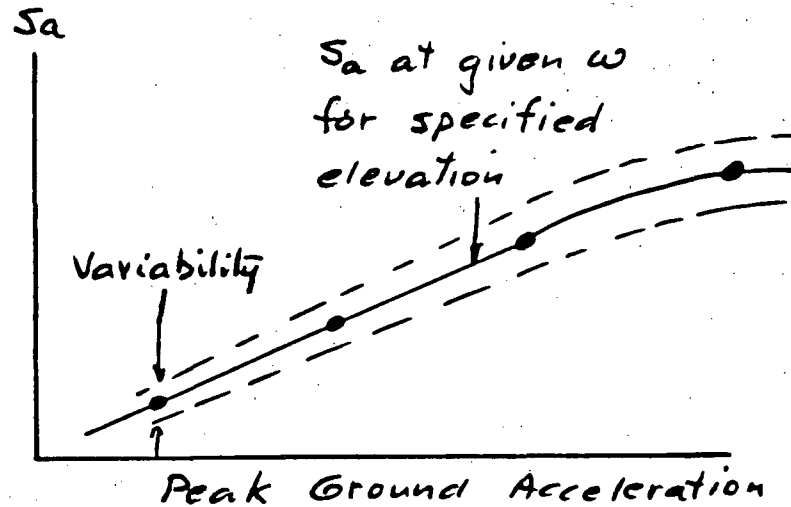


Figure 2. Response Location Acceleration with Uncertainty

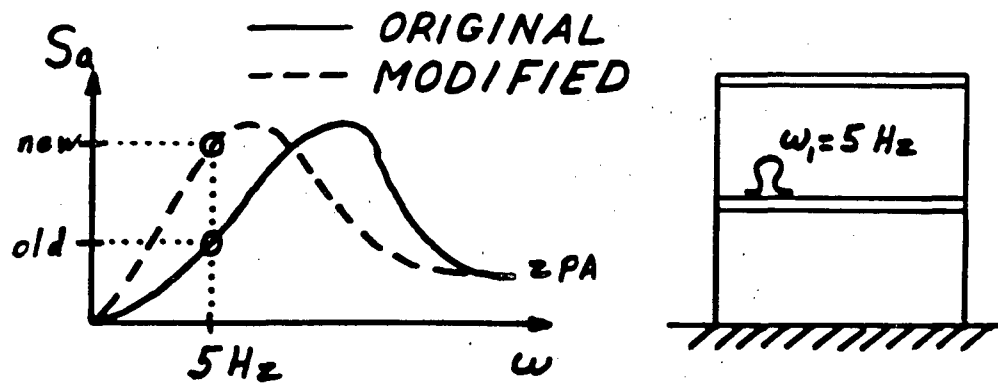


Figure 3. Effect of Frequency Spectra Shift

Step 6 is to compute new accident sequence probabilities and compare these with the original PRA results. The dominant accident sequences are re-evaluated using failure frequencies derived from the new fragility estimates derived in Steps 3 and 5. Uncertainty distributions for each accident sequence and for the total core damage frequency are generated. Finally, comparisons of accident sequence frequencies and core damage frequency (and their distributions) with the original seismic PRA results will be made to evaluate the impact of the "frequency difference" issue.

In addition to re-evaluating the existing seismic PRAs for the three plant sites described earlier, the effect of reduction of structural frequencies on deterministic seismic design margin will also be examined for the three sites. To do this, a design type calculation of structural loads and in-structure floor spectra is being performed for each site. Building models of the structures are being obtained from the original architect/ engineering firm or developed from plant drawings where necessary. The original site design spectra, load combination rules, methods of inclusion of soil-structure interaction, design material/soils properties, and damping values will all be used in the design process.

For the soil-site PWR, an analysis of all piping, nozzle and related component support forces will be made using a model of the complete Nuclear Steam Supply System (NSSS) coupled to the containment and internals structure models. This model will include the following: primary coolant loops, reactor vessel, pumps, steam generators, and pressurizer.

Both "as designed" and "reduced" natural frequency cases will be considered in the deterministic "design type" calculations. This is necessary to make an evaluation of the decrease in design margin of safety due to frequency reduction in the structures as well as safety related components.

### III. Conclusions

This project will be performed over approximately two years. The "probabilistic" and the "deterministic" re-evaluation for the first plant are planned for June 1989. These combined risk re-evaluations will provide a good estimate of the potential risk impact of the "frequency reduction" issue for existing commercial nuclear power plants. The design impact evaluations work will be affected by, and will have important implications for, a number of current or recently completed NRC, EPRI, and Industry programs. Therefore, it is important to establish formal interaction and cooperation early in the project to assure coordinated efforts and results.

#### IV. References

1. Endebrock, E. G. et. al., "Analysis and Tests of Small Scale Shear Walls FY-82 Final Report," Los Alamos National Laboratory Report, NUREG/CR-4274, 1985.
2. Dove, R. C. and Bennett, J. G., "Scale Modeling of Reinforced Concrete Category I Structures Subjected To Seismic Loading," Los Alamos National Laboratory Report, NUREG/CR-4474, 1986.
3. Dove, R. C. et. al., "Seismic Category I Structures Program Final Report, FY 1983-84," Los Alamos National Laboratory Report, NUREG/CR-4924, 1987.
4. Bennett, J. G., et. al., "The Seismic Category I Structures Program: Results for FY 1985." Los Alamos National Laboratory Report, NUREG/CR-4998, 1987.
5. Bennett, J. G. et. al., "Simulated Seismic Tests on 1/42- and 1/14-Scale Category I, Auxiliary Building," Los Alamos National Laboratory Report, NUREG/CR-4987, 1987.
6. Farrar, C. R. et. al., "Static Load Cycle Testing of a Four-Inch Wall TRG Type Structure," Los Alamos National Laboratory Preliminary Report (1987), to be published in 1988.
7. Bennett, J. G. et. al., "Seismic Category I Structures Program FY86 Final Report," Los Alamos National Laboratory Rough Draft Report, to be published in 1988.
8. Ltr, J. G. Bennett, Los Alamos National Laboratory to R. M. Kenneally, U.S. NRC (Document MEE-13:87:205), April 30, 1987.

# THE ROLE OF PARAMETER UNCERTAINTY IN SEISMIC RISK ASSESSMENT

Bruce Ellingwood  
Department of Civil Engineering  
Johns Hopkins University

## Abstract

Research is underway to examine the validity and limitations of seismic PRA methods through an investigation of how various uncertainties affect risk estimates, inferences and regulatory decisions. Indications are that the uncertainty in the basic seismic hazard at the plant site appears to be the single most source of uncertainty in core damage probability. However, when the fragility modeling and plant logic are uncoupled from the seismic hazard analysis in a margin study, fragility modeling assumptions may become important.

## Introduction

A seismic probabilistic risk assessment (PRA) of a nuclear plant contains a number of important ingredients. These include information on the seismic hazard at the plant site, the identification of dominant accident sequences leading to core damage, and fragility models to describe (conditional) failure probabilities of structures and mechanical and electrical equipment. This information must be integrated to determine point estimates or frequency distributions of the probability of core damage. Such probabilities might serve as one basis for regulatory decision-making. Each ingredient of a PRA contains sources of uncertainty. Some of these uncertainties are inherent in nature, i.e., they arise from the randomness or basic unpredictability in the conditions under which the plant must operate. Other uncertainties arise from limitations in data and information and the resulting assumptions that are made out of necessity in modeling any complex engineered system. In a nuclear plant, sources of uncertainty associated with the identification of the basic seismic hazard at the plant site and assumptions underlying the component fragility modeling are substantial.

When these modeling and informational uncertainties are propagated through a seismic PRA, the frequency distribution of the estimated core damage probability may span several orders of magnitude and the point estimates of risk, if required, may not be stable. The variability in estimated risk affects the credibility of PRA methods and the usefulness of the insights that might otherwise be gained. Research is being conducted to examine the validity and limitations of so-called Level I (McCann, et al, 1985) seismic PRA methods at their present stage of development. This research is aimed at determining how uncertainties due to inherent variability, modeling assumptions, incomplete data and errors affect risk estimates, inferences and regulatory decisions.

## Seismic Hazard, Fragility and Plant System Models

Several operating plants are being considered for purposes of examining how uncertainties affect estimates of seismic risk. One of these is the Limerick Generating Station (LGS), a BWR plant situated near Philadelphia, PA. It was selected for this study because the seismic PRA performed for LGS (included in the LGS Severe Accident Risk Assessment, or SARA (1983)) is well-documented and, moreover, has been subjected to an external published peer review (Azarm, et al, 1984).

The seismic hazard at the LGS is described by a relation between the effective peak ground acceleration (taken as the peak acceleration divided by 1.23 to account for the capability of the ground motion to cause damage) and the annual probability of exceeding that acceleration. Because of the uncertainty in the hypotheses regarding earthquake source mechanisms and attenuation in the Eastern United States, a family of hazard curves, with a likelihood assigned to each curve, is used to describe the earthquake hazard at the site, as illustrated in Figure 1. The development of this hazard curve family is described in Appendix A of the LGS SARA (1983).

The seismic fragility of a component is defined as its probability of failure, conditioned on a given value of effective peak ground acceleration. It has been customary to assume that the fragility of a component can be described by a lognormal distribution, with median  $A_R$  and logarithmic standard deviation  $\beta_R$ ; to take modeling uncertainties into account,  $A_R$  is assumed to have a lognormal distribution, with median  $A_m$  and logarithmic standard deviation  $\beta_U$ . Thus, the fragility of a component is actually described by a family of lognormal distributions (Kennedy and Ravindra, 1984). Table 1 summarizes the fragility parameters  $A_m$ ,  $\beta_R$  and  $\beta_U$  for key structures and components at the LGS; the development of these parameters is described in Appendix B of the LGS SARA (1983). The component numbering is identical to that in the LGS SARA (1983).

The assumption of a lognormal fragility model is convenient. It also is motivated, in part, by the observation that the capacity of many components can be expressed as the product of several random variables and thus might be approximately lognormal by virtue of the central limit theorem of probability. However, other fragility models also may be appropriate (Goodman, 1985); these may differ significantly from the lognormal model over their lower distribution fractiles, which are significant in risk analysis. For example, the Weibull distribution provides a possible alternate fragility model, one that might be justified on the basis of a weakest link failure hypothesis (Mann, et al, 1974).

The system analysis for the LGS is described in Appendix C of the LGS SARA (1983). The plant logic evaluation identified six dominant accident sequences leading to core damage. In a simplified form, these six sequences are described by the following Boolean expressions involving components identified in Table 1:

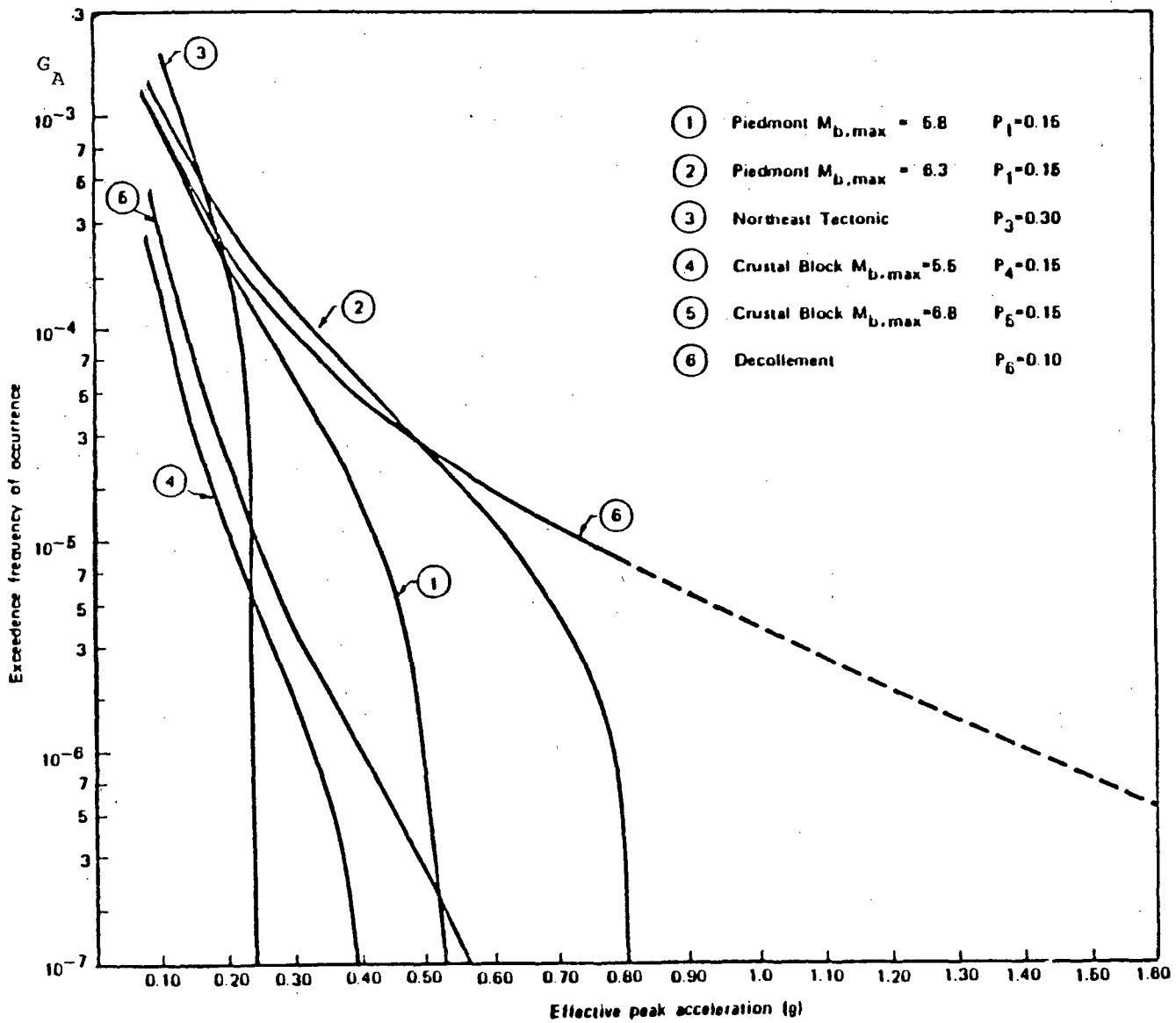


Figure 1. Annual Probability vs Acceleration  
at LGS Site (from LGS SARA, 1983)

$$TsEsUX = S1 * A$$

$$TsRpv = S6$$

$$TsRb = S4$$

$$TsEsCmC2 = S1 * (CR + S3) * (A + S10 + SLCR)$$

$$TsRbCm = S4 * (CR + S3)$$

$$TsEsW = S1 * \bar{A} * (\bar{S17} * WR + \bar{S2} * S17)$$

in which event A is failure of the emergency on-site electrical power system:

$$A = S11 + S12 + S13 + S14 + S15 + S16 + DGR$$

Terms DGR = 1.25-3/yr = random failure rate for the diesel generators; CR = 1.0-5/yr = random failure rate for the scram system; SLCR = 1.0-2/yr = random failure rate for the standby liquid control system; WR = 2.6-4/yr = random failure rate for the residual heat removal system. The ATWS sequences TsEsCmC2 and TsRbCm are different from those used in the LGS SARA (1983) and reflect comments from the peer review (Azarm, et al, 1984).

Table 1

LGS Component Fragility Parameters

| No. | Component                      | Cause of Failure       | $A_m(g)$ | $\beta_R$ | $\beta_U$ |
|-----|--------------------------------|------------------------|----------|-----------|-----------|
| S1  | Offsite power                  | Insulator breakage     | 0.20     | 0.20      | 0.25      |
| S3  | Reactor internals              | Lack of shroud support | 0.67     | 0.28      | 0.32      |
| S4  | Reactor enclosure structure    | Shear wall failure     | 1.05     | 0.31      | 0.25      |
| S6  | Reactor pressure vessel        | Loss of upper bracket  | 1.25     | 0.28      | 0.22      |
| S10 | SLC tank                       | Wall buckle            | 1.33     | 0.27      | 0.19      |
| S11 | 440-V bus/SG                   | Power circuit          | 1.46     | 0.38      | 0.44      |
| S12 | 440-V bus/transformer          | Loss of function       | 1.49     | 0.36      | 0.43      |
| S13 | 125/250-V DC bus               | Loss of function       | 1.49     | 0.36      | 0.43      |
| S14 | 4-kV bus/SG                    | Breaker trip           | 1.49     | 0.36      | 0.43      |
| S15 | Diesel generator circuit       | Loss of function       | 1.56     | 0.32      | 0.41      |
| S16 | Diesel generator heat and vent | Structural             | 1.55     | 0.28      | 0.43      |
| S17 | RHR heat exchangers            | Anchor bolts           | 1.09     | 0.32      | 0.34      |

The core damage event is defined as the union of the above six sequences:

$$CD = S4 + S6 + S1 * [A + (S17 + WR) + (S10+SLCR)*(S3+CR)]$$

The LGS core damage Booleans involve both seismic and random failures. They are dominated by electrical equipment failures but also include failures of plant structures and the reactor protection system (see Table 1).

### Analysis of Uncertainty

The capacity of each component in the core damage Booleans above is described by a family of fragility curves. When an accident sequence involving several components is considered, the sequence or plant level fragility is described by a family of curves as well. This sequence fragility family can be determined using a Latin Hypercube sampling technique (Iman and Conover, 1980) to propagate the uncertainties in the component fragilities through a particular sequence. Figure 2 illustrates the result of this process for sequence TsEsUX. The 95-percent lower confidence interval value of the 5-percentile sequence (or individual component) fragility is denoted the HCLPF, or high-confidence, low probability of failure value (Ravindra, Kennedy and Sues, 1985). The plant-level HCLPF is a key parameter in seismic margin studies (Budnitz, et al, 1985), in which the seismic hazard effectively is uncoupled from the fragility and plant logic models. The HCLPF for sequence TsEsUX is 0.33g, more than a factor of 2 above the design SSE of 0.15g for the LGS.

The plant level fragilities and seismic hazard curves are combined randomly, again using Latin Hypercube sampling, and are integrated to obtain a series of core damage probabilities,

$$P_{ij} = - \int_0^{\infty} F_{R_i} (a) \frac{dG_j}{da} da$$

These probabilities are rank ordered and plotted to determine the frequency distribution of core damage probability. Figure 3 illustrates the result of this process for core damage sequence TsEsUX. Identified in Figure 3 are the 5-, 50-, and 95-percentile values of P(TsEsUX) as well as the mean and median sequence probability. Three orders of magnitude separate the 5 and 95 percentile estimates, a reflection of the uncertainties in the modeling of the seismic hazard and component fragilities.

Table 2 summarizes the results of this analysis applied to the six sequences leading to core damage and to the core damage event itself. Sequence TsEsUX accounts for about 60 percent of the total mean core damage probability. Figure 3 indicates that the frequency distribution for P(TsEsUX) is strongly positively skewed, with the mean value occurring at about the 75th percentile of the frequency distribution and nearly an order of magnitude above the median (50th percentile) value. Similar results are observed for the other core damage sequences.

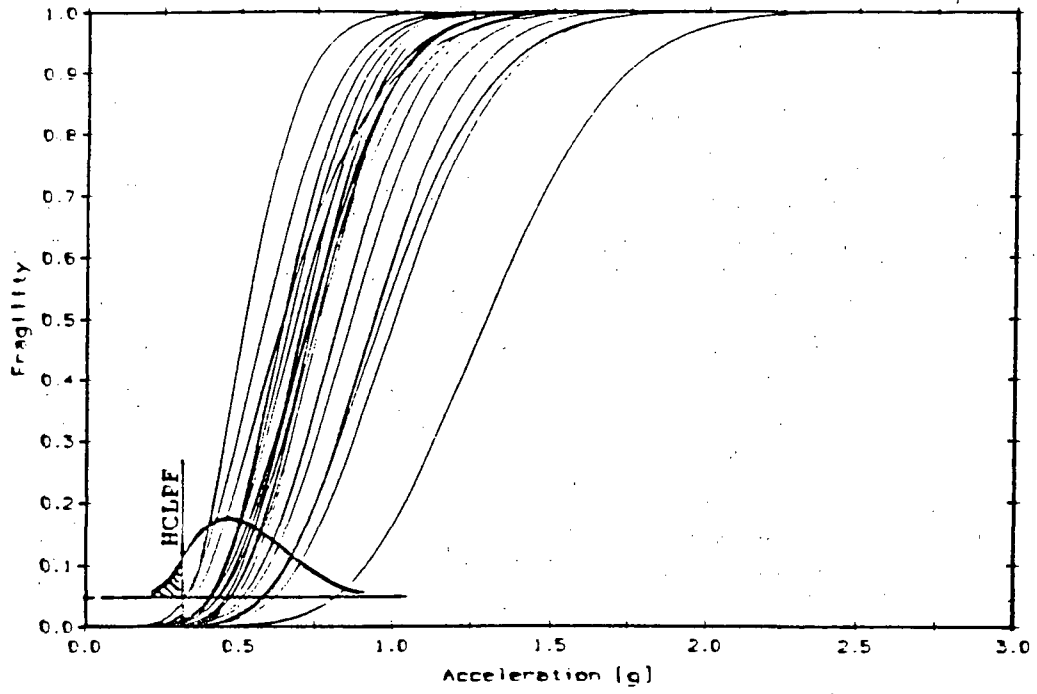


Figure 2.

Fragility for Sequence T E UX  
 $\xi_s$

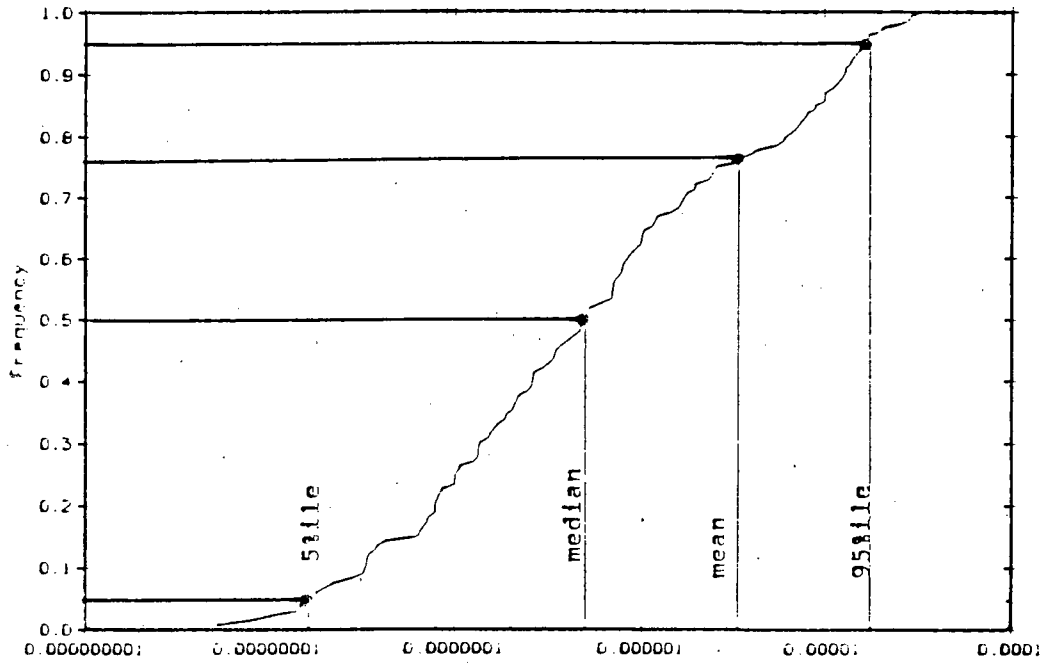


Figure 3.

Frequency Distribution for P(T E UX)  
 $\xi_s$

Table 2.

## Point Estimates of Core Damage Probability

| Sequence | 0.05   | 0.50   | 0.95  | Mean  |
|----------|--------|--------|-------|-------|
| TsEsUX   | 1.8-8  | 5.0-7  | 2.0-5 | 3.4-6 |
| TsRb     | 2.0-13 | 6.6-9  | 7.3-6 | 1.1-6 |
| TsRpv    | 1.5-16 | 1.9-10 | 3.5-6 | 4.7-7 |
| TsEsCmC2 | 4.7-12 | 1.0-8  | 8.6-6 | 1.5-6 |
| TsRbCm   | 3.7-17 | 2.9-10 | 4.4-6 | 6.0-7 |
| TsEsW    | 1.9-9  | 5.4-8  | 3.3-7 | 1.2-7 |
| SUM      | 2.0-8  | 5.7-7  | 4.4-5 | 7.2-6 |
| CD       | 2.7-8  | 7.2-7  | 2.4-5 | 5.0-6 |

Table 2 shows that the mean core damage probability provides a conservative point estimate of risk (with respect to the median) for a particular sequence or union of sequences (e.g., line CD in Table 2). Frequently, however, point estimates of core damage probability are obtained in seismic PRAs by simply adding the point estimates for the individual contributing sequences (e.g., line SUM in Table 2); in fact, this was done in the original LGS SARA (1983). Summing the means provides an estimate of mean core damage probability that is conservative but not excessively so (7.2-6 vs 5.0-6). However, summing medians results in an unconservative point estimate of median core damage probability, although the difference is minor in this case (5.7-7 vs 7.2-7). The mean is more desirable than the median as a point estimate of risk, if one is required, and propagates more consistently through the PRA (Lewis, 1985).

Table 3 provides a comparison of the differences in HCLPFs and core melt probabilities for sequences TsEsUX and CD that result from assuming lognormal and Weibull fragility models.

Table 3

## Comparison of Lognormal and Weibull Fragility Models

| Sequence | Model | HCLPF | 5%    | 50%   | 95%   | Mean  |
|----------|-------|-------|-------|-------|-------|-------|
| TsEsUX   | LN    | 0.33g | 1.8-8 | 5.0-7 | 2.0-5 | 3.4-6 |
|          | W     | 0.23g | 3.6-7 | 6.1-6 | 3.9-5 | 1.1-5 |
| CD       | LN    | 0.32g | 2.7-8 | 7.2-7 | 2.4-5 | 5.0-6 |
|          | W     | 0.21g | 7.9-7 | 1.3-5 | 5.2-5 | 1.7-5 |

The mean value of core damage probability increases by approximately a factor of 3, while the HCLPF decreases by about one-third. One would not expect a difference in risk of this magnitude to have a significant impact on regulatory decision-making in view of the large uncertainties manifested in the core damage probability frequency distribution. On the other hand, the difference in HCLPF might be significant in a seismic margins study, such as the one completed recently for the Maine Yankee Plant (Prassinis, et al, 1987), where the plant HCLPF is close to the review earthquake level.

The sequence probabilities in seismic PRA and margin studies usually are analyzed from the Boolean expressions assuming that failures of different components are statistically independent. However, the earthquake affects multiple plant systems simultaneously (McCann, et al, 1985), and the responses of neighboring components excited by a common earthquake may be statistically correlated. Although there are insufficient data to describe dependence in component behavior, the potential significance of statistically dependent failures may be investigated by assuming groups of component capacities to be perfectly correlated and comparing the resulting core damage probabilities or HCLPFs to the base (independent failure) case. Sequence TsEsUX is used in two example studies for this purpose. In the first, it was assumed that failures of: (1) components S11, S12, S13 and S14, which are all located in the reactor building, are perfectly correlated; (2) components S15 and S16, which are located in the diesel generator building, are perfectly correlated; and (3) components in different buildings are statistically independent. In the second, all components in TsEsUX were assumed to be perfectly correlated. The results are compared to the base case in Table 4. Note that the HCLPFs and fractiles of P(TsEsUX) are relatively unaffected by dependent failures for this sequence, which is dominated by unions of component failure events.

Table 4  
Statistically Dependent Component Failures - TsEsUX

| Case              | HCLPF | 5%    | 50%   | 95%   | Mean  |
|-------------------|-------|-------|-------|-------|-------|
| Independent       | 0.33g | 1.8-8 | 5.0-7 | 2.0-5 | 3.4-6 |
| Correlated (bldg) | 0.34g | 2.0-8 | 4.5-7 | 1.7-5 | 3.0-6 |
| Correlated (all)  | 0.32g | 2.1-8 | 4.3-7 | 1.6-5 | 2.9-6 |

The seismic hazard at the LGS site is described by the family of hazard curves shown in Figure 1. The most conservative of these curves (arising from the Decollement earthquake source hypothesis) is unbounded from above, while the remaining five curves have a maximum peak ground acceleration associated with an

assumption regarding the maximum possible earthquake. The existence (or lack thereof) of an upper bound on ground motion has been the object of some controversy. It should be noted that the seismic hazard curve families developed in more recent studies (e.g., Bernreuter, et al, 1987) generally do not contain an upper bound.

The sensitivity of core damage probabilities to the seismic hazard modeling was investigated by adopting two alternate ground motion hypotheses. In the first, the likelihood assigned to the Decollement hypothesis was increased from 0.1 to 0.3, the likelihoods associated with the remaining five being decreased in proportion. In the second, the likelihood assigned to the Decollement hypothesis was set equal to 1.0 and the frequency distribution for core damage probability reflects only uncertainty in component fragility modeling. The results of this analysis are presented in Table 5. There is a relatively small change in the 95-percentiles of P(TsEsUX) and P(CD) because the Decollement model is the determining factor for the upper fractiles of both frequency distributions. However, as the seismic hazard is collapsed into a single curve, the dispersion in core damage probability is reduced from three orders of magnitude to less than one, while the mean increases by about a factor of 3.

Table 5

Role of Uncertainty in Seismic Hazard

| Sequence | Hazard         | 5%    | 50%   | 95%   | Mean  |
|----------|----------------|-------|-------|-------|-------|
| TsEsUX   | p6 = 0.1(base) | 1.8-8 | 5.0-7 | 2.0-5 | 3.4-6 |
|          | p6 = 0.3       | 2.2-8 | 1.6-6 | 2.3-5 | 5.9-6 |
|          | p6 = 1.0       | 4.7-6 | 1.1-5 | 2.6-5 | 1.3-5 |
| CD       | p6 = 0.1(base) | 2.7-8 | 7.2-7 | 2.4-5 | 5.0-6 |
|          | p6 = 0.3       | 3.1-8 | 3.1-6 | 2.7-5 | 8.5-6 |
|          | p6 = 1.0       | 7.5-6 | 1.9-5 | 2.8-5 | 1.8-5 |

**Summary**

The seismic hazard at the LGS site appears to be the single most important factor in determining the frequency distribution of core damage probability. When the fragility modeling and plant logic are uncoupled from the seismic hazard analysis in a seismic margin study, the influence of the large uncertainty in the basic seismic hazard is eliminated. Other modeling assumptions and sources of uncertainty become relatively more important. For example, replacing the lognormal fragility model with an equivalent Weibull model may reduce the HCLPF estimate by 30%; including uncertainty in the logarithmic standard deviation  $\beta_R$  as well as in  $A_R$  may reduce the HCLPF by 10%. In seismic margin studies, fragility modeling assumptions may be far more important than they are in a Level I seismic PRA.

Questions have been raised in seismic PRAs concerning the potential impact of gross design and construction errors on estimates of seismic risk. Methodologies for dealing with such errors are in a developmental stage and supporting data are limited (Ravindra, et al, 1985). The error problem can be dealt with in approximation by postulating various error scenarios and their effects on the component fragilities, recalculating the HCLPFs or core damage probabilities, and comparing the results to the error-free case. Preliminary analyses indicate that plausible design/construction errors have little effect on mean core damage probabilities. However, such conclusions are valid only to the extent that errors can be incorporated through adjustments to component fragilities. In particular, errors in the plant logic models used as a basis for evaluating risk have yet to be evaluated.

### **Acknowledgement**

The assistance of J. O'Connor and M. Srinivasan, graduate students in the Department of Civil Engineering at Johns Hopkins University, in performing the calculations is gratefully acknowledged.

### **References**

- Azarm, M.A., et al (1984). "A Review of the Limerick Generating Station Severe Accident Risk Assessment." NUREG/CR-3493, U.S. Nuclear Regulatory Commission, Washington DC.
- Bernreuter, D.L., Savy, J.B. and Mensing, R.W. (1987). "Seismic Hazard Characterization of the Eastern United States: Comparative Evaluation of the LLNL and EPRI Studies." NUREG/CR-4885, U.S. Nuclear Regulatory Commission, Washington, DC.
- Budnitz, R.J., et al (1985). "An Approach to the Quantification of Seismic Margins in Nuclear Power Plants." NUREG/CR-4334, U.S. Nuclear Regulatory Commission, Washington, DC.
- Goodman, J. (1985). "Structural Fragility and the Principle of Maximum Entropy." **Structural Safety**, 3(1):37 - 46.
- Iman, R.L. and Conover, W.J. (1980). "Small Sample Sensitivity Analysis Techniques for Computer Models with an Application to Risk Assessment." **Communications in Statistics Part A - Theory and Methods**, A9(17):1749-1842.
- Kennedy, R.P. and Ravindra, M.K. (1984). "Seismic Fragilities for Nuclear Power Plant Studies." **Nuclear Engineering and Design**, 79(1):47-68.
- Lewis, H.W. (1985). "Medians and Means in Probabilistic Risk Assessments." **Nuclear Science and Engineering**, 91:220 - 222.
- Mann, N.R., Schafer, R.E. and Singpurwalla, N. (1974). **Methods for Statistical Analysis of Reliability and Life Data**. John Wiley and Sons, New York, NY.

McCann, M., et al (1985). "Probabilistic Safety Analysis Procedures Guide (Vol. 2)." NUREG/CR-2815, U.S. Nuclear Regulatory Commission, Washington, DC.

Prassinis, P.G., Murray, R.C. and Cummings, G.E. (1987). "Seismic Margin Review of the Maine Yankee Atomic Power Station." NUREG/CR-4826, U.S. Nuclear Regulatory Commission, Washington, DC.

Ravindra, M.K., Kennedy, R.P. and Sues, R.H. (1985). "Dominant Contributors to Seismic Risk: An Appraisal." NP-4168, Electric Power Research Institute, Palo Alto, CA.

"Severe Accident Risk Assessment 0- Limerick Generating Station (in two volumes)." Prepared for Philadelphia Electric Company by NUS Corporation, 1983.



# PROGRESS REPORT ON THE CONTAINMENT INTEGRITY PROGRAMS<sup>1</sup>

D. B. Clauss  
M. B. Parks  
J. R. Weatherby  
W. A. von Riesenmann  
Sandia National Laboratories  
Albuquerque, NM 87185

## Abstract

This paper will focus on recent progress in the Containment Integrity Programs, which are managed by Sandia National Laboratories for the U.S. Nuclear Regulatory Commission. The overall objective of these programs is to develop reliable methods for predicting the performance of LWR containment buildings for loadings beyond their design basis. The basic assumptions and an outline of the analysis methodology are presented. The mechanics of strain concentrations that lead to liner tearing in reinforced concrete containments are explained in terms of an analytical model that accurately represents the behavior of 1:6-scale model that was tested to failure. New insights into the leakage potential of personnel airlocks and equipment hatches based on test results and analyses are described.

## 1.0 Introduction

In commercial nuclear power plants in the United States, the containment building is the last engineered barrier to the release of radioactive material. In the unlikely event of a severe accident, temperature and pressure that significantly exceed the design basis loads may be developed inside a containment. The consequences of a severe accident are significantly affected by containment capability, as evidenced by the differing outcomes of the Three Mile Island and Chernobyl accidents. Consequently, evaluating the performance of the containment building under severe accident loads should have a significant role in accident management plans, emergency preparedness procedures, and safety assessment of a nuclear power plant.

For risk assessment studies, the measures of containment performance of primary interest include:

**Capacity** (Are the severe accident loads sufficient to cause a failure, i.e., a significant release of radioactive material? Does containment fail early or late in the accident sequence (this affects the inventory of radioactive material that is available for release to the environment)?

**Failure mode** (Is a catastrophic failure, which could damage or destroy important containment safety systems that could be used to "manage" an

---

1. This work was supported by the U.S. Nuclear Regulatory Commission and performed at Sandia National Laboratories, which is operated by the U.S. Department of Energy under contract number DE-AC04-76DP00789.

accident, possible? Is leakage from a penetration or some other source, wherein the containment still retains some functionality, more likely?)

**Failure location** (Are materials released directly to the environment or filtered through other structures, for example, the reactor auxiliary building?)

**Failure size** (How rapid is the rate of release of radioactive material to the environment? Is the leakage rate sufficient to preclude further pressurization of the containment building?)

Another useful measure of containment performance is the maximum pressure at which there is high confidence that there is a low probability of failure. This is perhaps the only containment performance question of interest for most emergency preparedness and accident mitigation issues.

The U.S. Nuclear Regulatory Commission (NRC) is sponsoring a number of programs, which are collectively known as the Containment Integrity Programs, that address the issue of light water reactor (LWR) containment performance for loads beyond the design basis. Sandia National Laboratories is managing four of these programs, including: (1) scale model tests of containment buildings, (2) tests of seals and mechanical penetrations, (3) analysis and methodology development, and (4) electrical penetration assemblies (EPA) tests. A related NRC-sponsored program at Idaho National Engineering Laboratory (INEL) involved an investigation into the performance of isolation valves [1].

The overall objective of these programs is to develop analytical and empirical methods for reliably predicting the performance of nuclear containment buildings subjected to hypothesized severe accident and other extreme loads. The emphasis is on methodology because containment performance must be evaluated on a case-by-case basis as there has been little standardization in containment designs in the U.S. Data generated by the experimental programs is used to evaluate analytical methods and to make improvements and modifications to the methods as necessary. The experiments have also led to important insights into which structural details affect containment performance significantly and how to best represent those details in mathematical models.

This paper will briefly review the status of methodology development and describe recent results in the following areas:

- Analytical models for predicting liner tearing;
- Tests on a full-size personnel airlock;
- Tests on inflatable seals.
- Analysis and testing of the leakage potential of unseating hatches;
- Comparison of calculated and experimental results for ovalization of penetration sleeves.

Some brief comments on the nature and scope of the work needed to complete the methodology conclude the paper.

## 2.0 Analysis Methodology

A flowchart of the analysis procedure that is proposed for use in evaluating the performance of containment buildings subject to severe accident loads is shown in Figure 1. A list of potential failure modes is given in Table 1. The flowchart suggests that separate analyses can be conducted to evaluate each potential failure mode, which offers a significant advantage in that much simpler mathematical models can be used. Thus, general shell failure can be evaluated independently of penetration seal failures or failure of bellows expansion joints. However, it should be noted that there is some interdependence of the analyses; for instance, the free-field shell response provides important boundary conditions for ovalization of penetration sleeves. Similarly, penetration insert plates cause significant strain concentrations in steel containments, which limit the structural capacity of the shell. The critical failure mode is determined by identifying the failure mode for which leakage initiates at the lowest pressure and temperature.

The flowchart also suggests other features of the analysis procedure:

Results are scenario dependent - the failure mode due to dynamic loading could be much different than that due to quasi-static pressurization, just as an accident scenario involving high temperatures may produce different results from one in which only moderate temperatures arise.

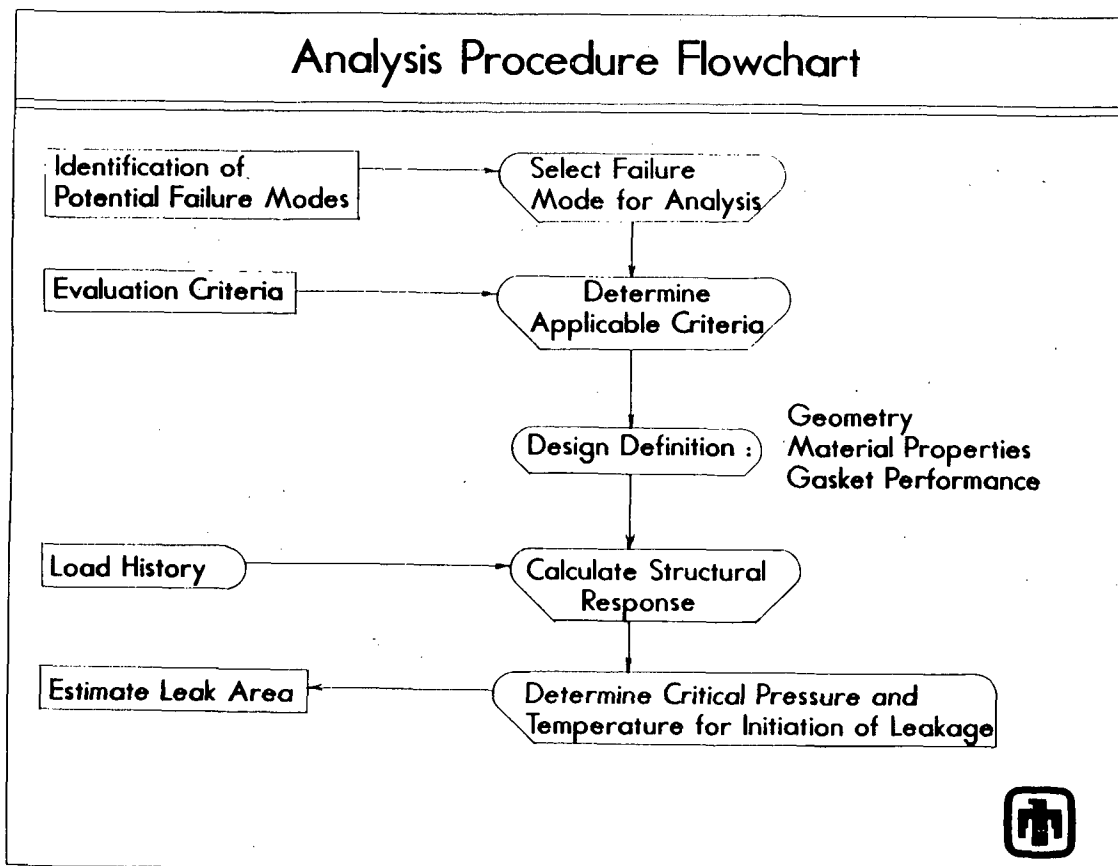


Figure 1. Containment Performance Analysis Flowchart

Results are design dependent - details of the containment design, which may differ even among nominally similar designs, can have an important effect on performance.

For these reasons, results of the scale model experiments and analyses should not be generalized. Containment performance must be evaluated on a case-by-case basis.

Table 1  
Potential Failure Modes of LWR Containments Subject to Severe Accidents

|                                                                                                                                                                                                                                                                                                                        |                                                                                                                                                                                                                                                                                                                                                                                  |
|------------------------------------------------------------------------------------------------------------------------------------------------------------------------------------------------------------------------------------------------------------------------------------------------------------------------|----------------------------------------------------------------------------------------------------------------------------------------------------------------------------------------------------------------------------------------------------------------------------------------------------------------------------------------------------------------------------------|
| <p>I. General Shell Failures</p> <p>A. Structural failure</p> <p>1. Steel containments:<br/>Shell tearing</p> <p>2. Reinforced concrete:<br/>Liner tearing<br/>Transverse shear failure<br/>Rebar failure</p> <p>3. Prestressed concrete:<br/>Liner tearing<br/>Shear failure<br/>Rebar failure<br/>Tendon failure</p> | <p>II. Penetration Failures</p> <p>A. Sealing failure</p> <p>1. Operable penetrations:<br/>Unseating of covers<br/>Sleeve ovalization<br/>Collapse of inflatable seals</p> <p>2. Fixed penetrations:<br/>EPAs<br/>Isolation Valves</p> <p>B. Structural failures</p> <p>1. Bellows expansion joints</p> <p>2. Buckling:<br/>Torispherical heads<br/>Pressure-seating hatches</p> |
|------------------------------------------------------------------------------------------------------------------------------------------------------------------------------------------------------------------------------------------------------------------------------------------------------------------------|----------------------------------------------------------------------------------------------------------------------------------------------------------------------------------------------------------------------------------------------------------------------------------------------------------------------------------------------------------------------------------|

The current stage of development is aimed primarily at predicting the initiation of leakage due to a failure mode listed in Table 1, although in some cases an estimate of leak area can also be made. Determination of leak rate is beyond current capabilities, in part due to difficulties in characterizing frictional effects and the irregular geometry typical of leak paths. Because leak rates on the order of the design-allowable leak rate (typically 0.1 to 1.5% mass/day) are not considered to be risk important, the important parameters affecting leakage in a severe accident are not necessarily the same as those in the design basis. For instance, the sensitivity of gasket performance to dust and surface finish is not important in severe accident analysis, whereas it may be in meeting design-allowables. The threshold at which leakage is considered to be risk significant in containment performance analysis is generally taken to be about 10% volume/day (e.g., see [2]).

Validation of analytical methods for predicting containment shell behavior is based on tests that have been conducted on scale models of steel and reinforced concrete containments [3,4,5]. Sandia and the NRC are currently cooperating with the Central Electricity Generating Board on a test of a 1:10-scale prestressed concrete containment model [6]. Separate effects tests are also planned to gain further insight into shell failure modes for reinforced and prestressed concrete containments.

The approach to evaluating penetrations has been based largely on the results of a survey and a scoping study conducted for Sandia by Argonne National Laboratory [7,8]. The primary emphasis has been on large diameter operable penetrations, such as equipment hatches, personnel airlocks, and drywell heads. These penetrations typically rely on elastomeric gasket materials of various geometries and contact force from either mechanical preload from bolts (pressure-unseating configurations) or internal pressure (pressure-seating configurations) to maintain an adequate seal and prevent leakage.

Current methods for severe accident analysis consider (at most) only two factors in evaluating the leakage potential of penetrations: (1) the relative position of the sealing surfaces and (2) the performance of the gasket material. The position of the sealing surfaces depends on the initial conditions<sup>2</sup> and on the deformations induced by pressure and temperature. Various levels of structural analysis are available to determine the pressure and temperature induced deformations. The performance of the gasket depends primarily on temperature and the effect of radiation and thermal exposure on the resiliency of the seal [9,10].

Investigation of fixed (including mechanical and electrical) penetrations has been more limited, mostly because a low priority was placed on these penetrations as a result of the Argonne study. Some testing has been conducted on isolation valves and electrical penetration assemblies under other NRC programs[1,11]; the results suggest that failures of these components need to be considered only for accident scenarios in which temperatures are sufficient to make the gasket materials unstable. Investigation into the behavior and capacity of bellows expansion joints is just now being initiated. Since significant plastic strains can be expected to develop before failure of the containment shell, bellows could be subject to lateral and axial deformations much larger than their design bases.

### 3.0 Recent Advances

#### 3.1 Liner Tearing in Concrete Containments

The overpressurization experiment on a 1:6-scale model of a reinforced concrete containment building, which was conducted at Sandia in July 1987, yielded extensive engineering data. The experimental results are reported in [12]. Several organizations submitted analytical predictions of the structural response of the 1:6-scale model before the overpressurization test was conducted [13]. By comparing the measured response to the predictions, much has been learned about the accuracy of the modeling assumptions applied in these analyses. More importantly, the test has revealed at least one set of structural details and mechanisms that can control the failure mode of containment buildings made of reinforced concrete.

During the experiment, numerous cracks or tears formed in the steel liner, which served as the pressure boundary for the structure. When the pressure inside the model reached 145 psig, leakage through tears in the liner became so large that the pressure could not be increased further. Virtually all leakage occurred through a single tear that initiated near

---

2. In most penetrations, metal-to-metal contact is maintained under operating conditions and design basis loadings, but in personnel airlocks, in particular those employing inflatable seals, the metal sealing surfaces are not in intimate contact.

the edge of a thickened insert plate that surrounds a series of three pipes that penetrate the containment wall. The tear propagated along the edge of the plate through a distance of 22" before arresting; a view of this tear after the model was depressurized is shown in Figure 2. The insert plate has a nominal thickness of 3/16" while the surrounding liner has a nominal thickness of 1/16".

The liner and insert plate are anchored to the concrete wall by headed studs. The purpose of the anchorage system in an actual containment is to prevent buckling of the liner in case it is exposed to high temperatures. In the 1:6-scale model, the studs were welded to the outer surface of the liner and insert plate in a square grid pattern (see Figure 3). As the concrete wall was cast, the heads and shanks of the studs were embedded in the concrete. Each stud in the region shown in Figure 3 is 3/4" in length and has a shank diameter of 0.135". On the liner near the insert plate and on the insert plate itself, the studs were placed with a 2" by 2" spacing. Away from the insert plate, the spacing changes to 6" by 6". The column of studs on the liner nearest to the insert plate were located approximately 0.5" from the edge of the insert plate.

Posttest finite element analyses of this region have been conducted to study and isolate the mechanism(s) responsible for the initiation of the tear. The results of the present investigation strongly suggest that the tear formed as the result of strain concentrations that arose at the base of studs due to high shear forces that were developed to resist the slip associated with the insert plate. In the analysis, the liner strains in elements adjacent to studs located near the insert plate reached magnitudes sufficient to cause liner tearing at an internal pressure between 143 and 148 psig. The analytical approach used in this investigation appears promising; however, additional validation is needed before the method can be generalized.

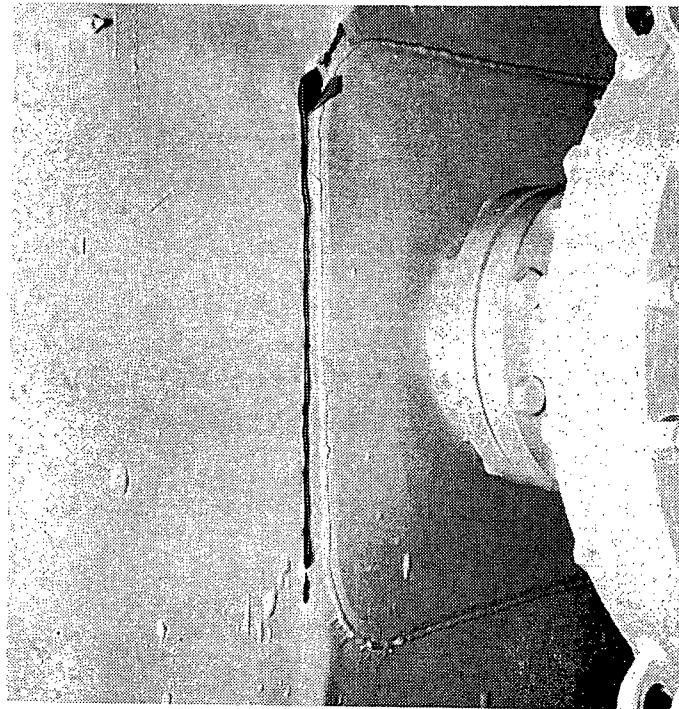


Figure 2.  
22-Inch Liner Tear Located Near a Piping Penetration in the 1:6-Scale Model

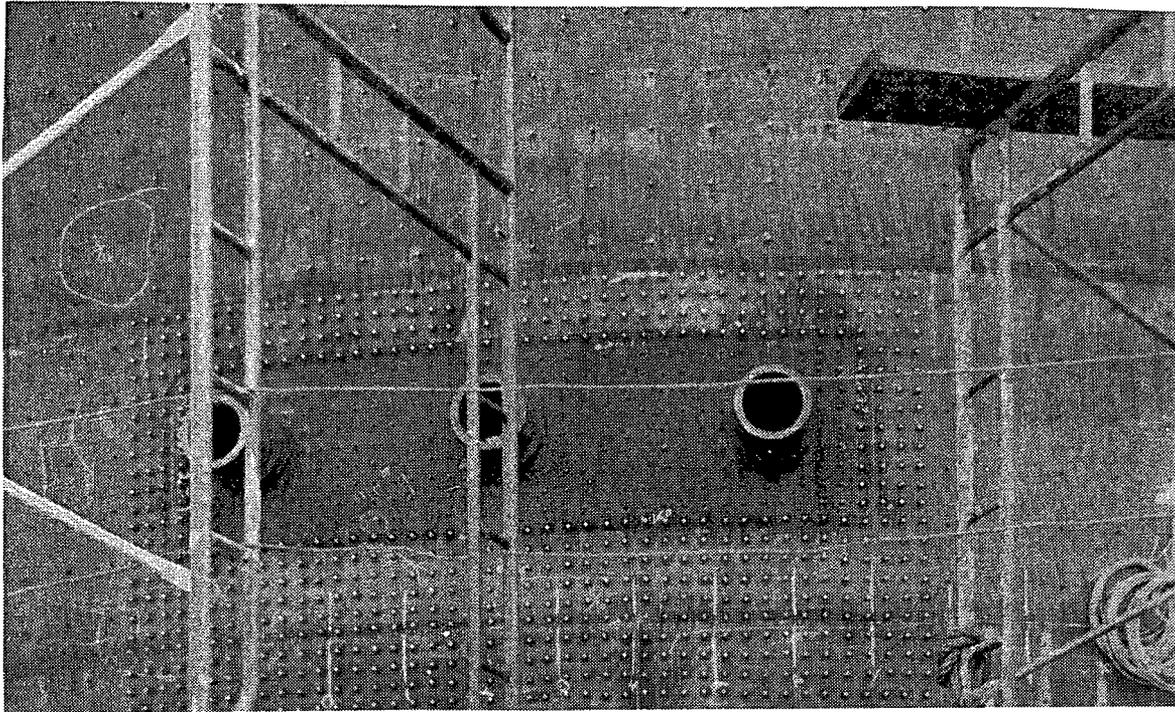


Figure 3. Arrangement of the Studs Near the Piping Penetration on the Concrete Side of the Liner Before Placement of Reinforcement and Concrete

At locations in the cylinder far away from piping penetrations, equipment hatches, and other discontinuities, the load carried by the studs was probably very small. Any deviation from zero load was the result of non-uniform deformations in the wall resulting from cracks in the concrete. Near the piping penetration, however, the situation was significantly different. The insert plate, because of its greater thickness, was stiffer than the surrounding liner and tended to stretch much less. As a result, the studs on and immediately surrounding the insert plate were put into shear as they attempted to force the insert plate to follow the vertical and circumferential expansion of the reinforced concrete wall. The highly concentrated forces from the studs produced large strains in the liner near the insert plate eventually causing the liner to tear. Further away from the insert plate, where the stud forces were small, the strains in the liner were more like those that would exist in a long, uniform cylinder.

Figure 4 shows the plane stress finite element model that was constructed to analyze the region surrounding the piping penetration. ABAQUS, a general purpose finite element code, was used for this investigation. The liner and insert plate were modeled using a 4-node bilinear quadrilateral element. Each stud was modeled using a discrete spring element which has the property that the line of action of the force in the element is parallel to the line segment joining the two nodes at each end of the element. The analysis was run using the nonlinear geometry option to account for finite strains.

Because the studs are modeled with spring elements, they introduce point loads into the mesh of quadrilateral elements. For this reason, the dimensions of the quadrilateral elements are crucial. As the mesh is refined, the strains for a given value of internal pressure will increase without bound in those quadrilateral elements that are connected to

springs. In the real structure, the stud forces are introduced over an area roughly equal to the cross-sectional area of the stud shank. Therefore, to avoid unrealistically high strains in the analysis, the minimum length of an element side should not be less than half the diameter of the stud shank. The smallest elements in the model are located between the first column of studs on the liner and the edge of the insert plate. Here, each element is 0.25" in length in the vertical direction, and 0.1" in length in the horizontal direction. Both dimensions are less than the stud radius (0.0675").

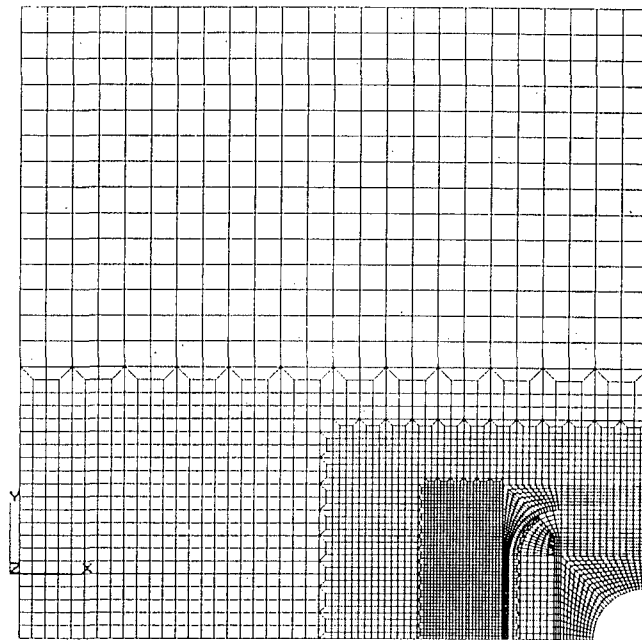


Figure 4. Plane Stress Finite Element Model of the Region Surrounding the Piping Penetration

In this calculation, the reinforced concrete wall was not modeled; instead, the motion of the wall was assumed to be identical to that of an infinite cylinder with a 1/16" thick liner and the same vertical, hoop, and seismic reinforcement found in the midsection of the 1:6-scale model. The infinite cylinder analysis was described in [13] and assumed that all load was carried by the rebar and liner; no tensile strength was attributed to the concrete. Assuming that the strains in the wall are uniform is equivalent to assuming that the amount of load transferred between the wall and insert plate via the anchorage system is negligible when compared to the vertical and horizontal loads carried by the reinforcement at a given internal pressure. As shown in Figure 5, the strains calculated in the infinite cylinder analysis were found to be in close agreement with the actual strains measured in hoop and vertical reinforcing bars located behind the insert plate. This supports the idea that the deformation of the wall is not significantly affected by the presence of the thickened insert plate.

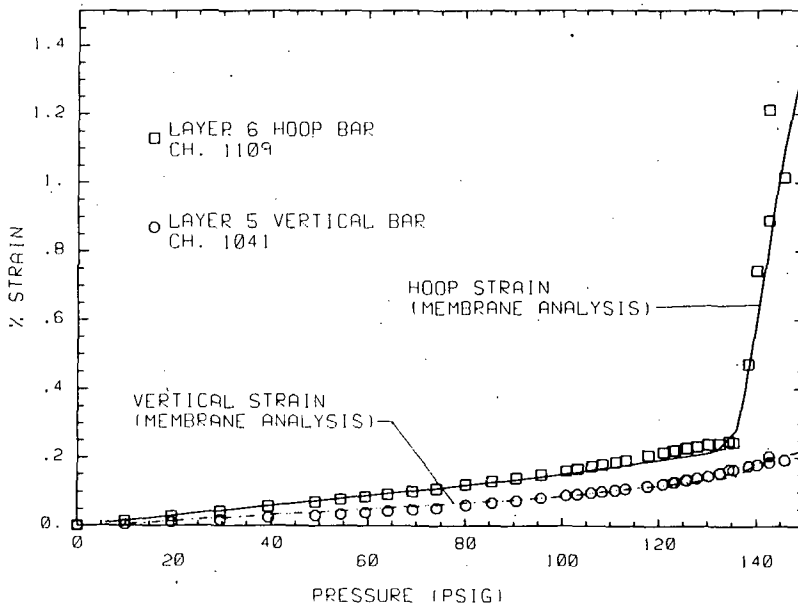


Figure 5. Comparison of Measured and Calculated Strains in the Hoop and Vertical Directions.

The boundary conditions applied to the edges of the model are listed in Table 2. In this table, a "no-slip" boundary condition in a particular direction implies that the liner is forced to follow the motion of the wall in that direction. For example, a no-slip boundary condition in the hoop direction implies that the displacement in the hoop direction is given by

$$u_h = x \epsilon_h \quad (1)$$

where  $u_h$  is the displacement in the hoop direction,  $x$  is the circumferential distance from the center of the pipe at the lower right corner of the finite element model, and  $\epsilon_h$  is the strain in the hoop direction given by the infinite cylinder analysis.

Table 2  
Boundary Conditions Applied to the Finite Element Model

| Boundary    | Boundary Condition |                    |
|-------------|--------------------|--------------------|
|             | Hoop Direction     | Vertical Direction |
| Left Edge   | no-slip            | no-traction        |
| Right Edge  | no-slip            | no-traction        |
| Top Edge    | no-traction        | no-slip            |
| Bottom Edge | no-traction        | no-slip            |
| Pipe Edge   | no-slip            | no-slip            |

An approximate load-deflection curve was constructed for the studs based on data obtained from shear tests performed on studs embedded in concrete [14]. Initially, both nodes on each spring element occupied the same location in the finite element model. One node on each spring was connected to either the liner or the insert plate. During the analysis, the motion of the second node on each spring was specified to follow the motion of the containment wall as determined from the infinite cylinder analysis.

A number of uniaxial tensile tests were conducted to determine the material properties of the liner and insert plate. The liner is made of A414 Grade D steel while the insert plate is made of A516 Grade 60 steel. Both materials have a yield strength of approximately 50 ksi. Both the A414 steel and the A516 steel show considerable strain hardening after yielding. The A414 steel reaches a true stress of 82 ksi at maximum load while the A516 steel exhibits slightly more hardening and reaches a true stress of approximately 92 ksi at maximum load. A total of four uniaxial tensile tests were conducted on the liner material: two in the rolling direction, and two in the transverse direction. The elongations at fracture were 21.3% and 30.0% in the rolling direction and 39.1% and 27.8% in the transverse direction [15].

In the finite element analysis, a piecewise linear relationship was used to define the stress-plastic strain curves of the two steels. The hardening of both materials was assumed to be zero when the equivalent plastic strain exceeded 15%. This is the strain level at which the maximum load was reached in uniaxial tensile tests on both materials.

As the containment wall deforms, forces develop in the studs as they attempt to force the stiff insert plate to follow the motion of the wall. The vector plots in Figure 6 show the relative magnitudes and directions of the forces that studs in the vicinity of the piping penetration exert on the liner and insert plate. Figure 7 shows in more detail how the stud forces vary as a function of internal pressure.

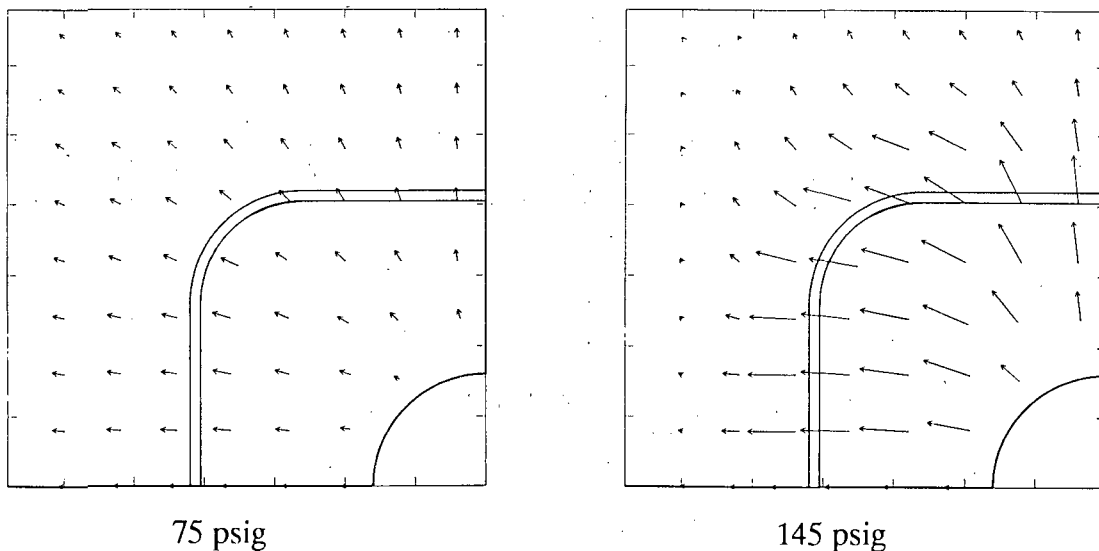


Figure 6. Magnitudes and Directions of the Forces Exerted by the Studs on the Insert Plate and Liner

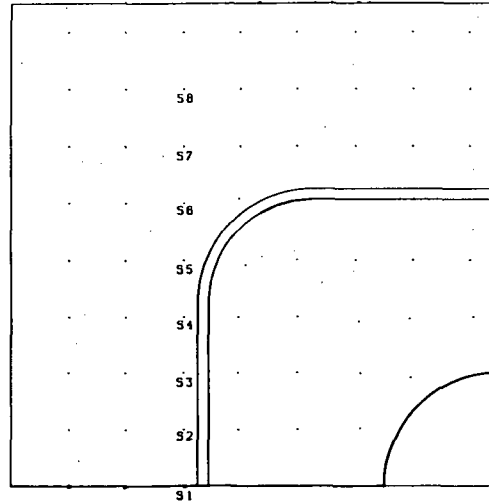
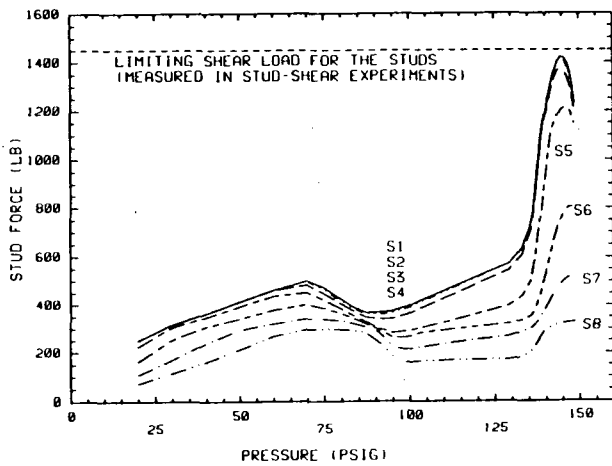


Figure 7. Stud Forces Acting on the Liner as a Function of Internal Pressure

In general, the forces in the first column of studs adjacent to the insert plate increase until reaching a local maximum at approximately 70 psig internal pressure. This corresponds to the pressure when the liner begins to yield locally around the first column of studs. The forces in studs S1 through S4 begin to increase again at 90 psig, and continue to rise until reaching a maximum of approximately 1400 lb at 145 psig internal pressure. Above this pressure, the load begins to rapidly decrease. This second region of decreasing load begins when the elements connected to studs S1 through S4 reach 15% equivalent plastic strain, which is the point where it is assumed that the liner material ceases to work-harden.

A contour plot of the maximum principal strain in the liner at 145 psig is shown in Figure 8. Along the straight, vertical segment of the insert plate boundary, the contours are virtually symmetric about horizontal lines that pass through the studs and about horizontal lines that pass halfway between the studs. The largest principal strains were reached in the elements connected to studs S1 through S4. The values of the maximum principal strain are approximately equal in those elements that are connected to studs S1, S2, and S3. The principal strains next to the fourth stud (S4) are slightly higher than the strains next to the first three studs making this the most likely site for tear initiation.

As the pressure increased, strains became increasingly localized in elements connected to the first column of studs. Figure 9 shows the maximum principal strain plotted as a function of position in the first row of quadrilateral elements next to the lower boundary of the mesh. In these plots, abrupt changes in strain clearly mark the location of each stud. Above 140 psig, the strain increased many times faster in Element A than in the other elements. Element A is connected to the liner stud that is closest to the insert plate.

The strains calculated in the analytical model were compared against an empirically-based fracture criterion developed by Manjoine [16]. Based on this fracture criterion and the calculated strains, the liner would begin to tear near the stud anchors at 143 psig. By 148 psig, the maximum principal strains in the liner near the stud anchors exceeded the strain at fracture measured in uniaxial tension tests of the liner material.

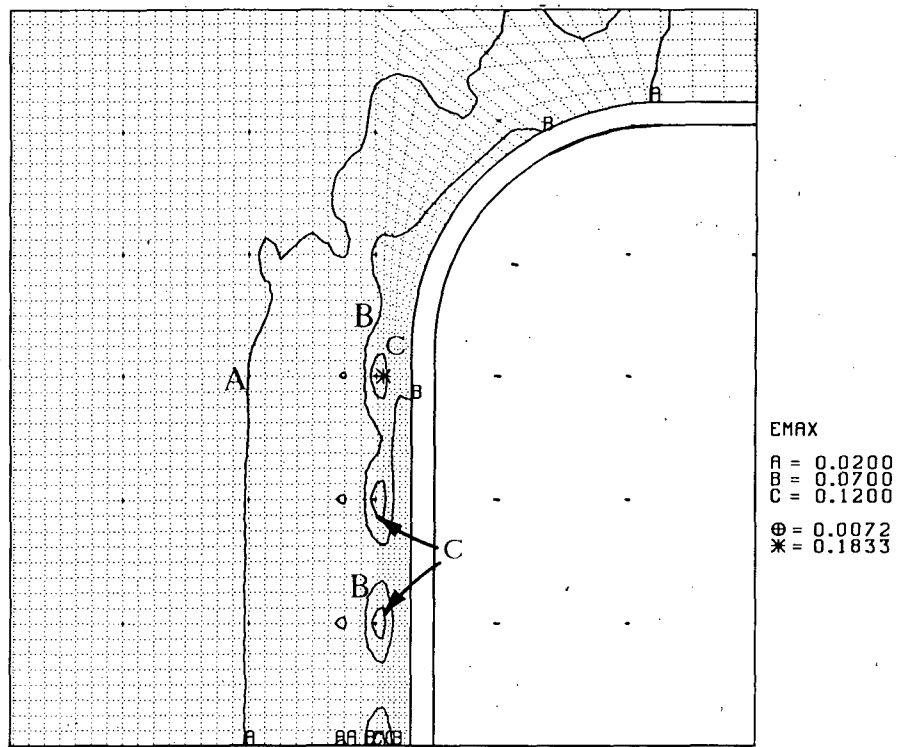


Figure 8. Maximum Principal Strains in the Liner at 145 Psig Internal Pressure

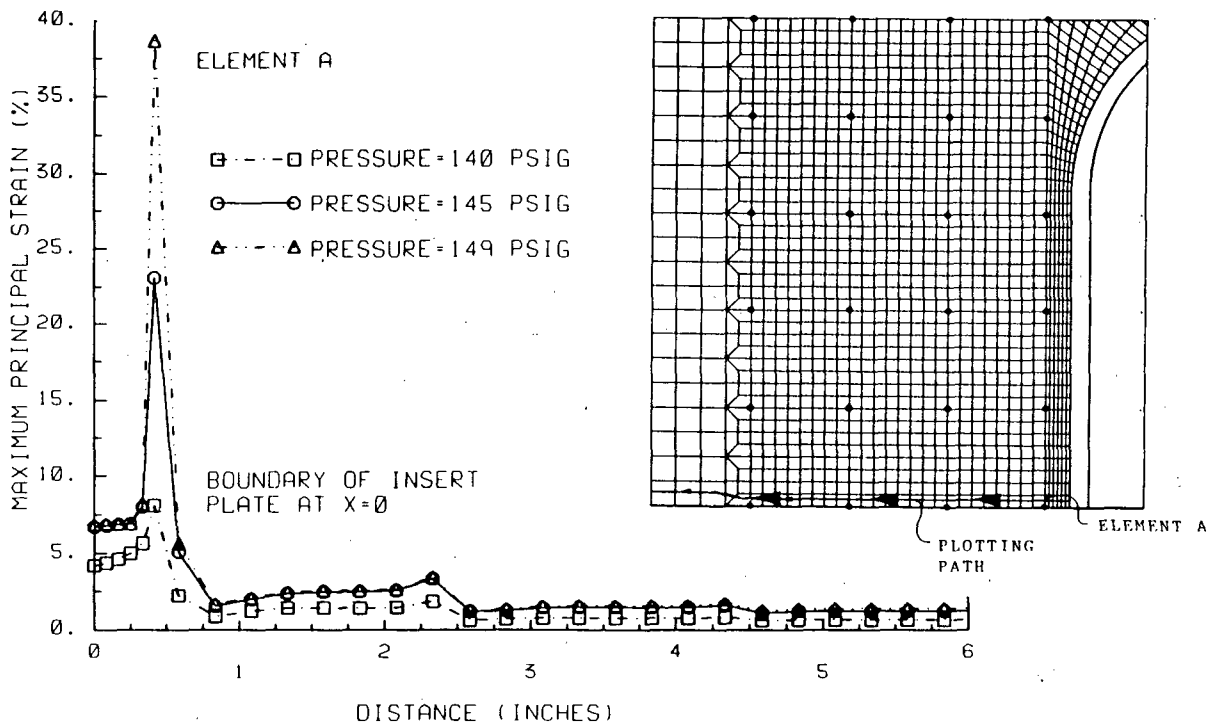


Figure 9. Maximum Principal Strain in the Liner as a Function of Distance From the Edge of the Insert Plate.

A finite element analysis of the liner surrounding a piping penetration in the 1:6-scale model has been described. Based on this investigation and posttest inspections of the model the following conclusions may be drawn:

- Forces introduced by the stud anchors caused the initiation of the 22" liner tear. The stud forces that caused the tear developed as the result of circumferential slippage between the liner and the reinforced concrete wall (which occurs near the insert plate).
- The tear initiated at one of the stud anchors in the first column of studs next to the insert plate. The state of strain is virtually the same around each of the first four studs in this column. Strains in the fourth stud up from the horizontal mid-plane are slightly higher than the strains next to the first three studs in this column.
- At the failure point, the regions of high strain ( $> 15\%$ ) were very small in size and confined to the material immediately surrounding the studs. The analysis as well as visual observations and thickness measurements support this conclusion.
- When an empirically-based failure criterion is used in conjunction with the finite element analysis, liner tearing is predicted to occur at approximately 143 psig internal pressure. Because the maximum strains increased rapidly above 140 psig in the analysis, any reasonable strain-based criterion of failure would predict liner tearing by 148 psig. The experimental evidence suggests that no tears were developed in the liner before 142 psig and the maximum pressure achieved in the test was 145 psig.

### 3.2 Personnel Airlock Test

In the Argonne survey of containment penetrations [7,8], personnel airlocks were identified as having a relatively high potential for leakage. Idaho National Engineering Laboratory came to similar conclusions in their analysis of specific containments and penetrations [17]. Because of the complex structural behavior and uncertainties with respect to gasket performance in an actual penetration, experimental validation of analytical methods was felt to be indispensable.

The airlock tested in this project was fabricated for the Union Electric Company's Callaway Unit 2, which was subsequently cancelled. The test program was carried out by CBI Research Corp. under contract to Sandia. The airlock consists of a sleeve or barrel, which is roughly 10 feet in diameter and 20 feet in length, and two door and bulkhead assemblies. The doors are 42" wide and 80" in height; a double dog-ear gasket in a pressure-seating configuration provides a seal with the bulkhead. A schematic of the door and bulkhead assembly is shown in Figure 10. The airlock was designed for a pressure of 60 psig and temperature of 340°F. The primary objective of the tests was to investigate the leak characteristics of an airlock under conditions consistent with severe accident loads. The experiments were also designed to provide data on the structural and thermal response of the airlock under elevated pressure and temperature conditions. The data will be used to develop and validate analytical methods.

The gaskets tested in this program (both doors) were subjected to an accelerated aging process to simulate radiation and thermal aging for a 40 year service life and a loss of

coolant accident. The gaskets were aged in place with the doors closed and latched. As a result of the aging, the cross-section of the gaskets was permanently deformed such that the original cross-section was hardly recognizable, as shown in Figure 11. Although this represents very extreme aging conditions, these gaskets were used throughout the test sequence.

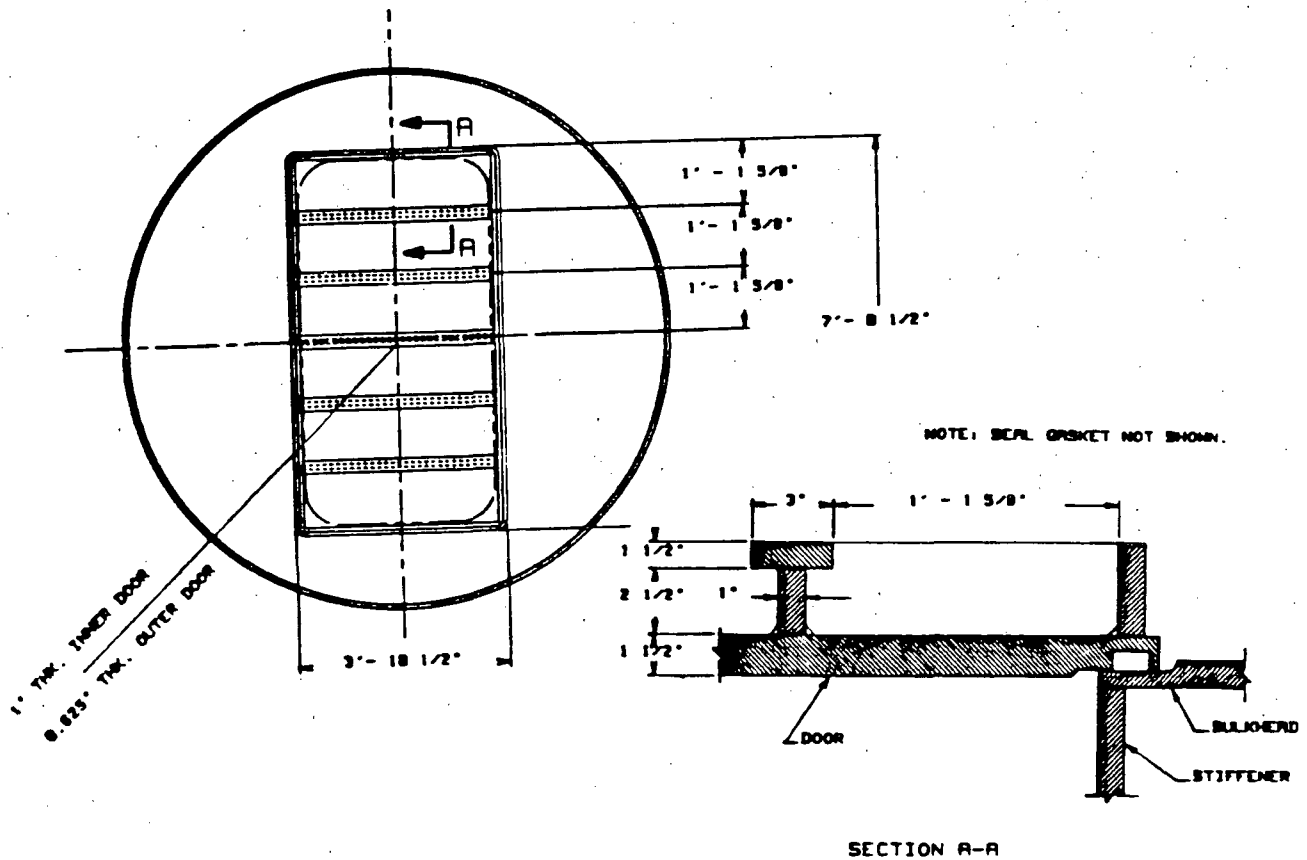
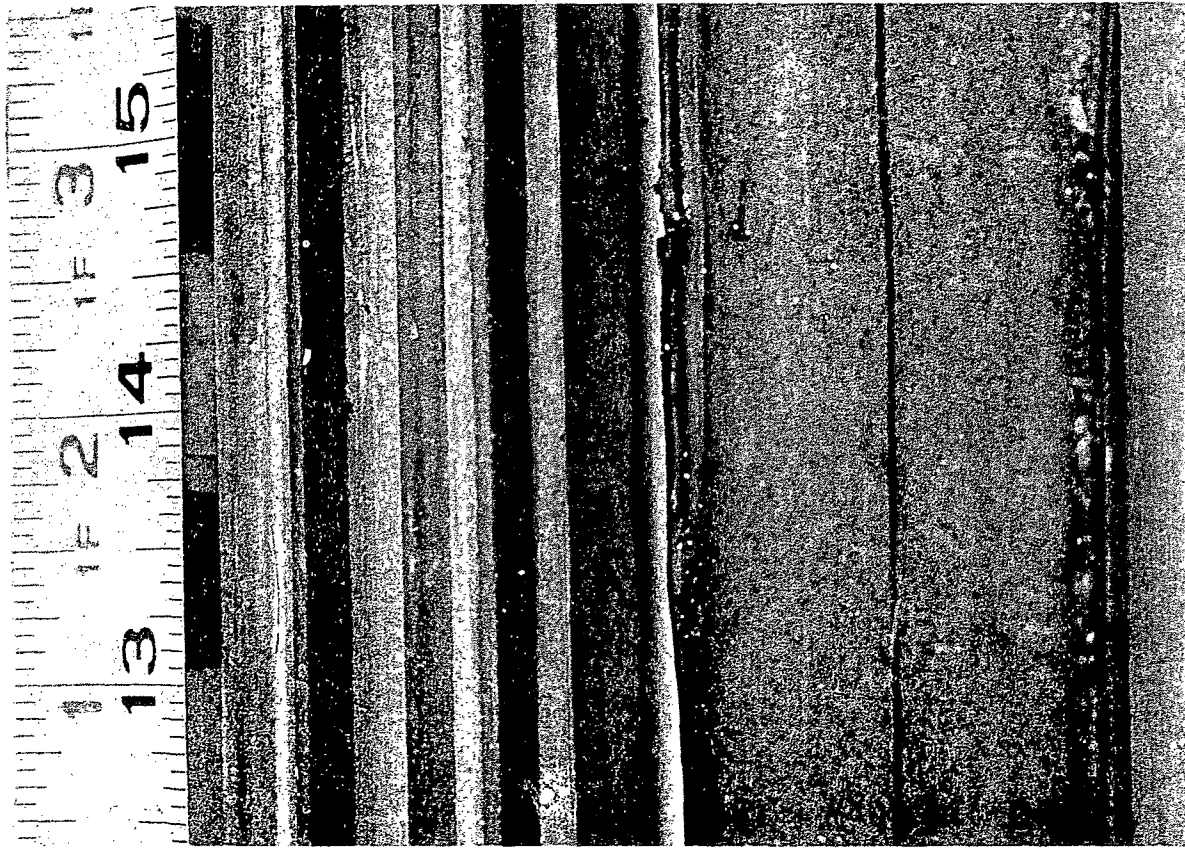


Figure 10. Schematic of Door and Bulkhead Assembly of Airlock Tested at CBI

The personnel airlock was extensively instrumented with 123 high temperature strain gages, 115 thermocouples, 89 displacement transducers, pressure transducers, and flow meters.

A total of nine tests were performed on the airlock using quasi-static loading. A number of tests were conducted at ambient temperature and design pressure in order to (1) check out the instrumentation systems, (2) verify the leak integrity of the airlock under design conditions, and (3) provide baseline measurements. During the most severe test, the inner door and bulkhead were exposed to a maximum pressure of 300 psig and a maximum air temperature of 800°F. The following observations were made:

- The structural integrity of the airlock was exceptional. None of the strain gages indicated yielding in any of the tests. Pretest analyses indicated that although some local yielding was possible, the maximum strain would not exceed 0.3% at 300 psig.



(Before Aging)

(After Aging)

Figure 11. Double Dog-Ear Gasket Before and After Aging

- Heat transfer effects are extremely important. Under forced convection conditions (quasi steady-state), the average temperature of the inner door was only 650° when the air temperature was 800°F. The temperature of the outer door and bulkhead never exceeded 200°F. Since gasket performance (and thus leakage potential) depends largely on temperature, this is an important finding.
- Up to a pressure of 300 psig and air temperature of 400°F, no leakage past the inner door was detected. This is quite remarkable considering the condition of the gasket after aging, but it is in line with expectations from the pretest analyses, which indicated that the separation displacement of the sealing surfaces would be less than .006" at 300 psig.
- A significant leak past the inner door, which resulted in the inner door being effectively bypassed, occurred after the inner door was held at 650°F for over two hours (corresponding to an air temperature of about 800°F) and the pressure was raised beyond 150 psig. There appears to be a threshold temperature at which the gasket material becomes unstable, which may correspond to ignition

or smoldering. A photo of the remains of the gasket after testing are shown in Figure 12. Nevertheless, it took significant pressure to break-up this material and create a significant leak path, which is due in part to the small separation of the door and bulkhead sealing surfaces.

- There was no measurable leakage past the outer door at any time during the test sequence.

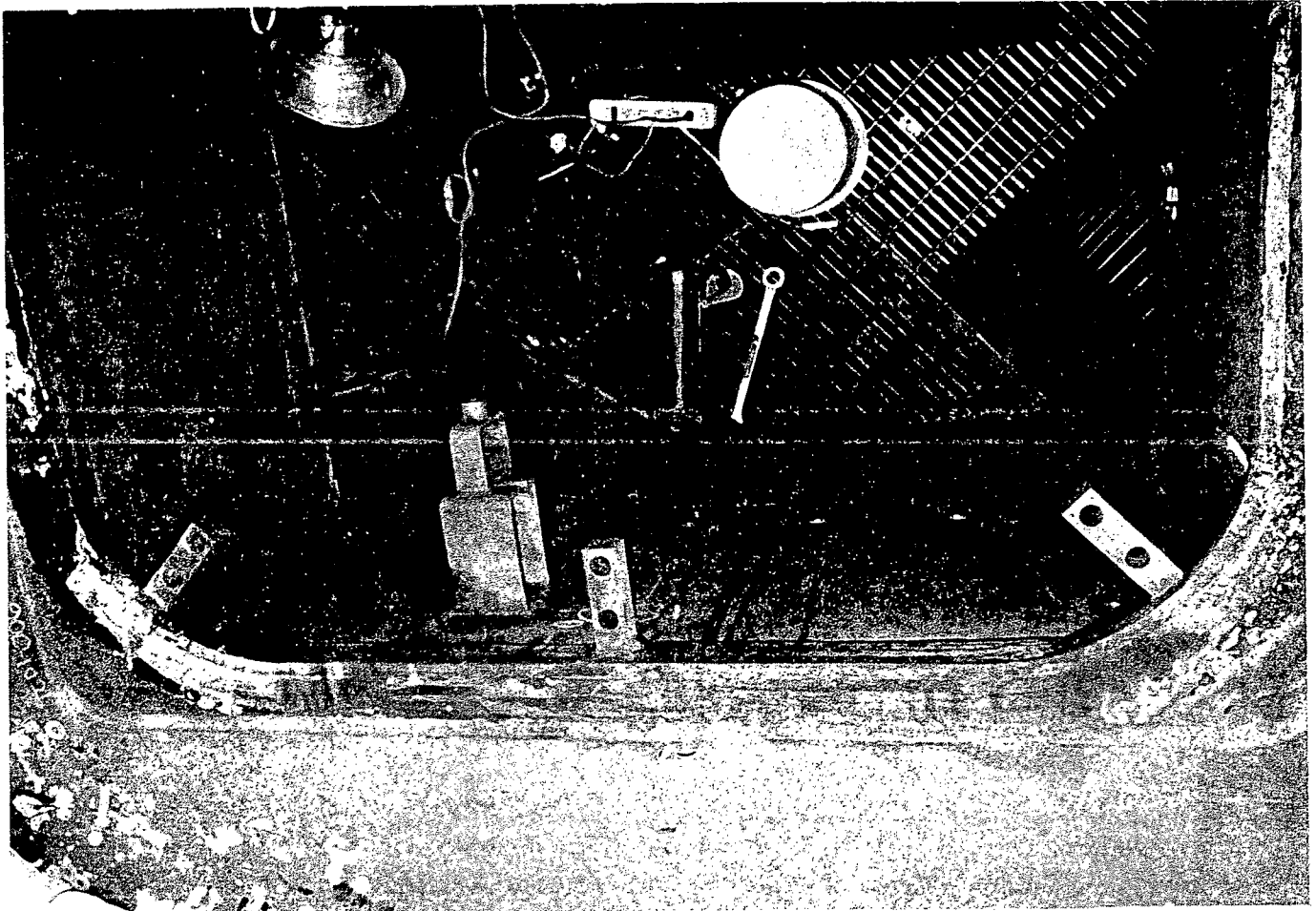


Figure 12 Posttest Photo of Inner Door Gasket

A complete data report is currently being prepared by CBI Research Corporation and should be published in early 1989. The test results are consistent with the analysis in that for the small separations predicted, leakage would be expected only if the gasket material becomes unstable. More detailed comparisons will be made when data reduction is completed. Unfortunately, a simplified analysis approach for airlocks does not seem possible: It appears that the complicated interaction between the door, bulkhead, and gasket can only be represented with 3-D finite element analysis. It should be noted that many older airlock designs are considerably less stiff and the sealing surface deformations may be substantially larger than in the airlock tested. Different designs must be evaluated by analysis or testing.

### 3.3 Tests on Inflatable Seals

Inflatable seals are used to prevent leakage around the perimeter of personnel and escape lock doors. They are fastened to the outer edge of the doors and, when pressurized with air, seal the gap between the door and the bulkhead. A typical application is shown in Figure 13. The pressure inside the seal is furnished by the instrument air supply system. After the door is closed and the seals are inflated, the seals are isolated from their pressure source by closed valves in the pressure lines. Thus, any increase in the seal temperature or in the external pressure applied to the seal will produce a corresponding increase in the seal pressure.

These seals are either currently installed or planned for use in eleven commercial power plant containment structures. All of the installations are in either PWR or BWR Mark-III type containments. Thus, only the severe accident pressure and temperature conditions expected for these containments need be applied during the inflatable seals testing. The actual internal seal pressures used in these containments varies from 50 to 110 psig.

Three different types of inflatable seals are currently available for use in nuclear containments. Cross sections of the three designs may be compared in Figure 14. The vendor found that the "old" design, shown in Figure 14(a), had undesirable amounts of leakage based on in-service experience. Leakage seems to occur along laps in the Kevlar reinforcement, which produce small but visible leak paths across the seal tube. Even though this type of seal design is no longer supplied to the nuclear industry, they may possibly still be in use in some containments.

In order to improve the seal performance, two techniques have been employed. In each case a 1/8" thick layer of EPDM E401 material has been added to the sealing surface to cover irregularities in the Kevlar reinforcement.

- For the seals already fabricated using the old design, a 1-1/2" wide by 1/8" thick layer of EPDM 404, 40 durometer material has been vulcanized to the sealing surface. The modified cross section is shown in Figure 14(b).
- A new design has been developed in which the added E401 material is incorporated as an integral part of the seal as illustrated in Figure 14(c). This type of seal is currently supplied for use in nuclear containments.

Because the new inflatable seal design (Figure 14(c)) is believed to provide a superior seal and because it is now furnished exclusively for nuclear containments, it was imperative that the test program include this type of seal. Also, because the old seal design (Figure 14(a)) may still be in use in some containments, it is also included in the test program. Inflatable seals with the added layer of E401 material (Figure 14(b)) were not tested since they were only supplied for a short period of time.

The inflatable seals test specimens are full scale in cross section. As shown in Figures 14(a) and 14(c), the cross-sectional dimensions of the old and new seal designs are practically identical; thus, the same size test fixture was used for both types of seals. Figure 15 is a schematic of the test setup. Pressure enters the fixture through circular openings on the inner side. Leakage past the inner seal may be measured through ports located between the seals; whereas, leakage past both seals may be measured through ports on the outer side of the test fixture. The overall shape of the test fixture is that of a short

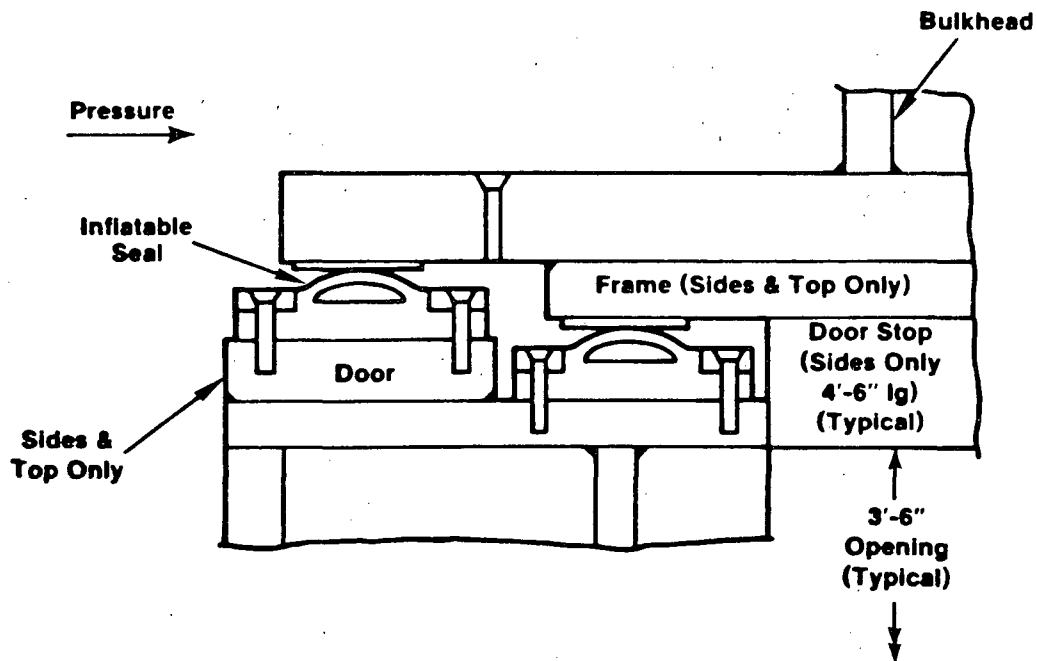
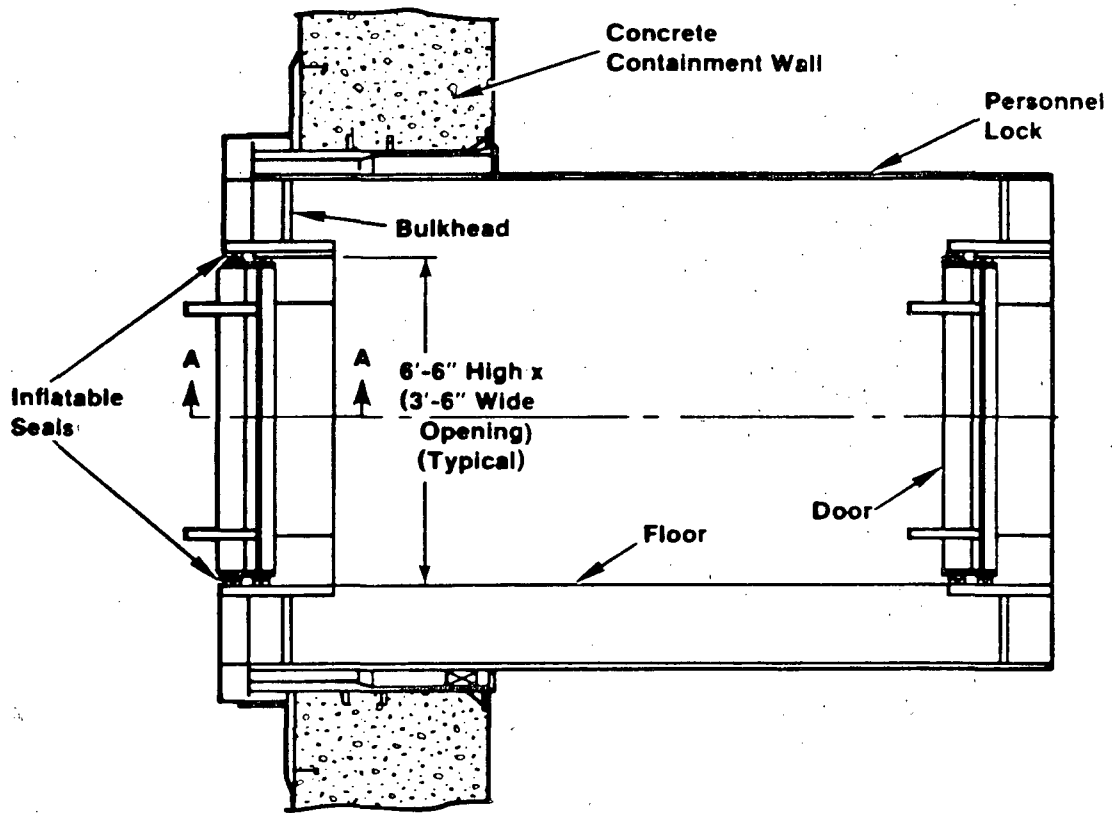
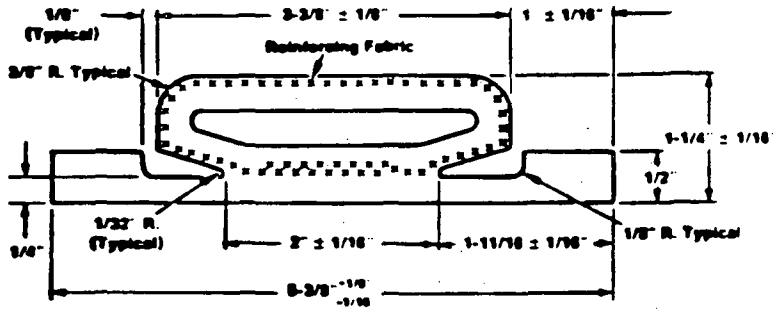
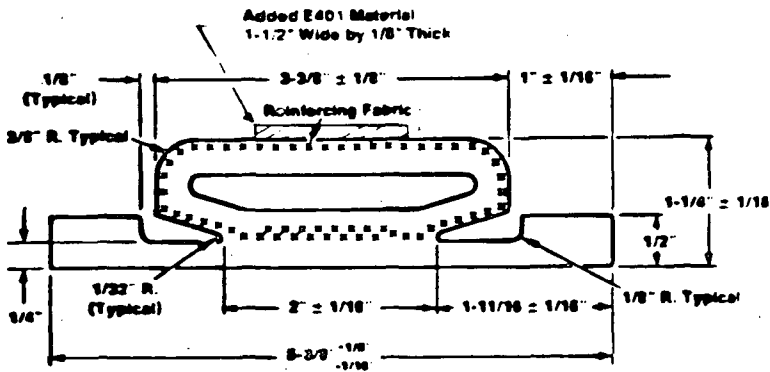


Figure 13. Typical Installation of Inflatable Seals in Personnel Lock Doors



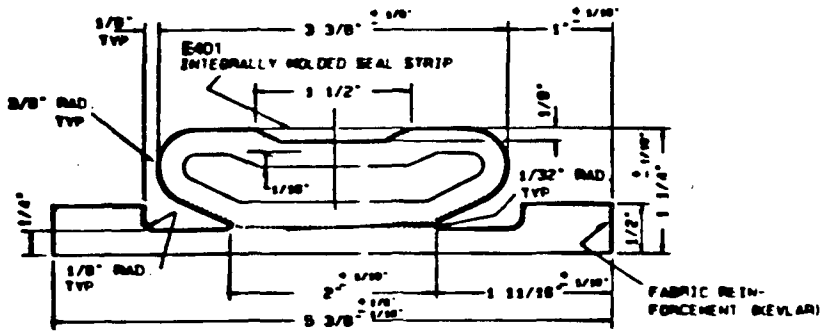
Material: EPDM E603

(a) "Old" Inflatable Seal Design



Material: EPDM E603 with added E401 layer

(b) Modified "Old" Inflatable Seal Design



Material: EPDM E603 with E401 insert

(c) "New" Inflatable Seal Design (Currently Supplied to Nuclear Industry)

Figure 14. Cross-Sectional Dimensions of Inflatable Seals

length of cylinder with an outer diameter of approximately 35-3/4" and a length of approximately 13". The plate to which the seals are attached is about 32" in diameter. Thus, the circumferential length of the seals is approximately 100" as compared to a total length of about 240" for a typical 6'-6" X 3'-6" personnel airlock door. (There are door stops along the vertical edges of the airlock door frames, which would inhibit leakage in these areas).

The primary objective of the inflatable seals test program is to determine the pressure and temperature conditions within the containment that would cause significant leakage past the inflatable seals. The internal seal pressure and temperature, containment (chamber) pressure, seal design, and aging conditions are all important parameters in determining the onset of significant leakage.

As outlined in Table 3, four different series of tests have been performed. Two series of tests were conducted for both the "old" and "new" seal designs. For each seal design, separate tests were performed for unaged and aged seals. The aged seals were first subjected to a total dose of 200 Mrads of gamma radiation at a dose rate of < 1 Mrad/hr followed by thermal aging at 250°F for 1 week. The intent of this aging process was to produce similar properties in the seal material as would be expected after being subjected to a loss of coolant accident at the end of a 10 year life.

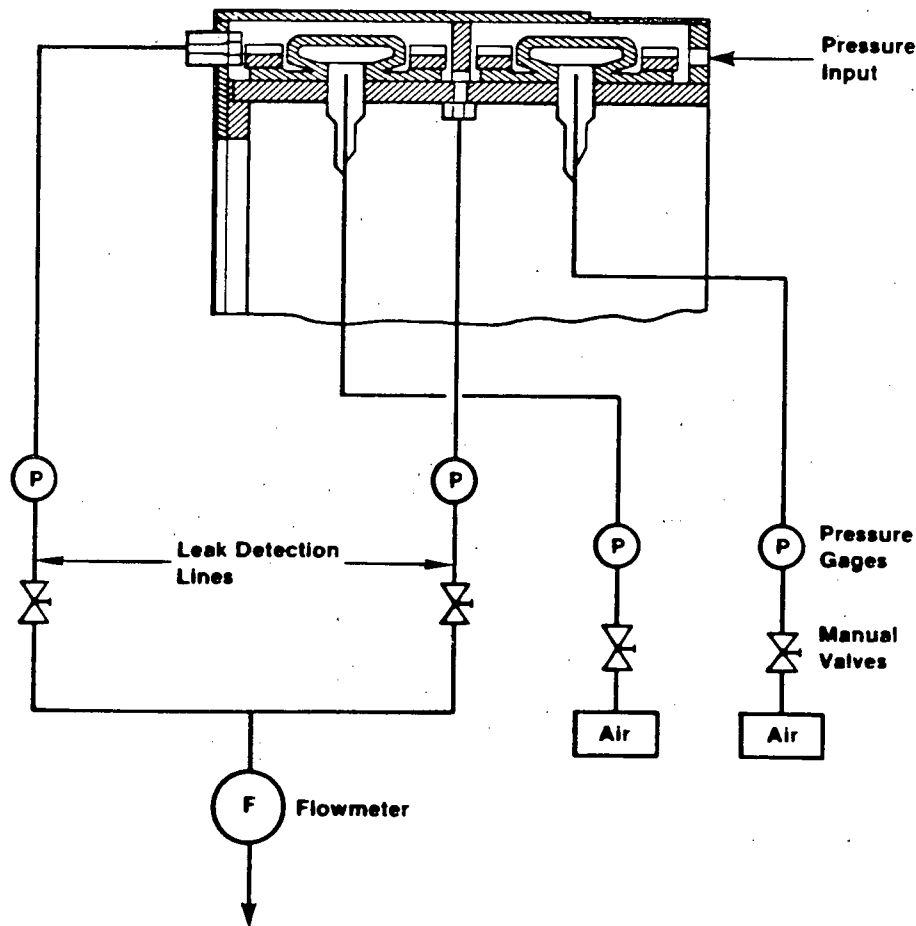


Figure 15. Schematic of Test Setup (Seals not Inflated in Figure)

Table 3  
Test Sequence

| <u>Test Series</u> | <u>Seal Design</u> | <u>Seal Condition</u> | <u>Loading</u>                 |
|--------------------|--------------------|-----------------------|--------------------------------|
| 1                  | Old                | Unaged                | Air, Room Temp. & 400°F        |
| 2                  | Old                | Aged                  | Air, Room Temp. & 300°F        |
| 3                  | New                | Unaged                | Air, Room Temp. & 300°F, 350°F |
| 4                  | New                | Aged                  | Air, Room Temp. & 300°F        |

For each test series, leakage tests were performed first at room temperature and then at elevated temperature. Tables 4 and 5 present a summary of the results of the room temperature and elevated temperature tests, respectively. In order to minimize the potential for seal damage and thus allow each pair of seals to be tested at several seal pressures, the room temperature tests were concluded when leakage past both seals reached approximately 10,000 standard cubic feet per day (scfd). (Leakage of 10,000 scfd corresponds to 1% volume per day of a 1x10<sup>6</sup> ft<sup>3</sup> containment volume at standard temperature and pressure.) The elevated temperature tests, on the other hand, were continued to failure of the seals, which normally occurred as a rapid increase in leakage past both seals from near 0 scfd to >>30,000 scfd. Posttest inspection after the elevated temperature tests usually revealed a tear in the outer seal tube near the valve stem, which prevented the seals from maintaining their internal pressure.

As can be seen by comparing Tables 4 and 5, the chamber pressure at which significant leakage begins, for a given initial seal pressure, is considerably higher at elevated temperature than at room temperature. This improvement may be attributed to the increase in seal pressure caused by increasing temperature and the "softening" effect of high temperature on the seal material. Also, for a given seal pressure, significant leakage usually began at higher chamber pressures for the "new" seal design than for the "old" seal design.

Table 4  
Summary of Room Temperature Tests - Test Series 1 Thru 4

| <u>Initial Seal Pressure (psig)</u> | <u>Chamber Pressure (psig) for Leakage of Approx. 10,000 scfd</u> |                      |                       |                       |                      |
|-------------------------------------|-------------------------------------------------------------------|----------------------|-----------------------|-----------------------|----------------------|
|                                     | <u>Test Series 1</u>                                              | <u>Test Series 2</u> | <u>Test Series 3a</u> | <u>Test Series 3b</u> | <u>Test Series 4</u> |
| 50                                  | 51.1                                                              | ----- <sup>3</sup>   | 93.0                  | 58.2                  | -----                |
| 60                                  | 65.4                                                              | 79.0                 | 98.5                  | 76.9                  | 100.5                |
| 70                                  | 79.0                                                              | -----                | 104.3                 | 97.4                  | -----                |
| 80                                  | 94.7                                                              | -----                | 125.1                 | 129.1                 | -----                |
| 90                                  | 109.9                                                             | -----                | 140.1                 | -----                 | -----                |
| 100                                 | 129.6                                                             | -----                | -----                 | -----                 | -----                |

3. Dashed line indicates that a test was not conducted at that particular seal pressure.

Table 5  
Summary of Elevated Temperature Tests - Test Series 1 Thru 4

| Seal Pressure at Room Temperature (psig) | Chamber Pressure (psig) at Which Leakage First Exceeded 10,000 scfd |               |               |               |               |
|------------------------------------------|---------------------------------------------------------------------|---------------|---------------|---------------|---------------|
|                                          | Test Temperature (°F)                                               | Test Series 1 | Test Series 2 | Test Series 3 | Test Series 4 |
| 50                                       | 400                                                                 | 132           | ---           | ---           | ---           |
| 90                                       | 300                                                                 | ---           | 180           | 180           | 138           |
| 90                                       | 350                                                                 | ---           | ---           | 145           | ---           |

### 3.4 Pressure Unseating Hatches and Heads

A pressure-unseating equipment hatch was included in the 1:6-scale reinforced concrete containment model that was tested at Sandia [14]; measurements of the bolt strain and separation displacement were made. Low pressure test results (at ambient temperature) have provided some confirmation of the analytical approach proposed for these types of penetrations (see [18]). Comparisons of measured and calculated bolt strains and separation displacements are shown in Figures 16 and 17. Since the 1:6-scale model survived high pressure testing with only limited structural damage, plans to conduct additional testing of this hatch subject to internal pressure and elevated temperature are being formulated. These tests should provide important data on temperature effects and conditions under which significant leakage initiates.

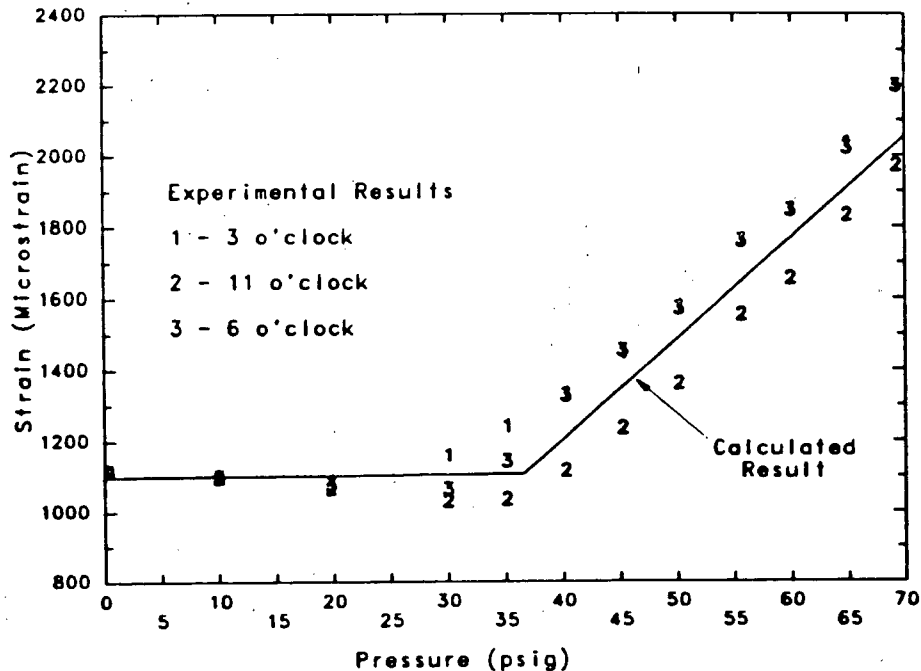


Figure 16. 1:6-Scale Reinforced Concrete Model  
 Measured and Predicted Bolt Strain in Pressure-unseating Equipment Hatch

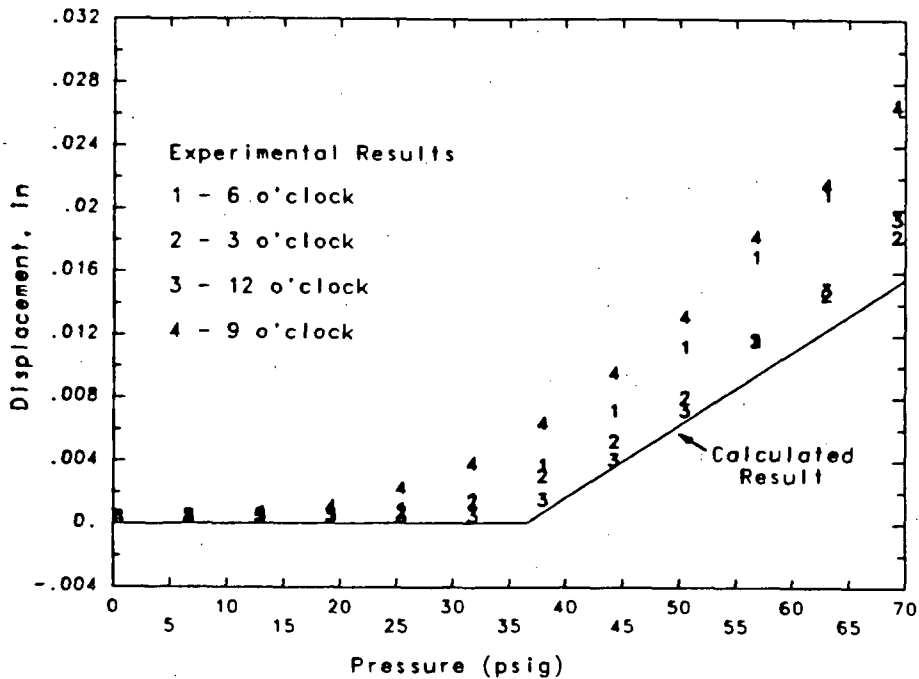


Figure 17. 1:6-Scale Reinforced Concrete Model  
Measured and Predicted Separation Displacement in Pressure-unseating Equipment Hatch

### 3.5 Ovalization

For penetrations in which the sleeve is an integral part of the sealing surface (typically the case in equipment hatches), ovalization of the sleeve represents a potential leakage mechanism. Experimental results of the 1:8-scale steel containment model and of the 1:6-scale reinforced concrete model, which both included scaled equipment hatches, have provided substantial validation of analytical models used to calculate ovalization and have suggested important conditions that must be met for ovalization to occur.

In a cylindrical containment shell, an equipment hatch sleeve will deform into an oval shape due to interaction with the containment shell provided that:

1. there are no significant constraints on radial deformation of the sleeve
2. for concrete containments, either the liner radius is uniform or the penetration sleeve is well anchored to the concrete wall.

If these conditions are met, the horizontal diameter of the sleeve increases while the vertical diameter decreases by a like amount; the deformations can become quite large (on the order of the sleeve wall thickness) after general yielding of the cylindrical containment shell. The mismatch caused by the sleeve sliding relative to the cover tensioning ring is greatest along the horizontal and vertical centerlines; as indicated in Figure 18, eventually the sleeve and tensioning ring will lose contact at these points, resulting in leakage. Changes in the diameter of the cover and its tensioning ring are typically quite small (except possibly for pressure seating hatches that are susceptible to buckling) and can

normally be neglected; thus leakage is expected to initiate when the ovalization is on the order of the sleeve thickness. Under these conditions, the performance of the gasket does not affect the leakage potential.

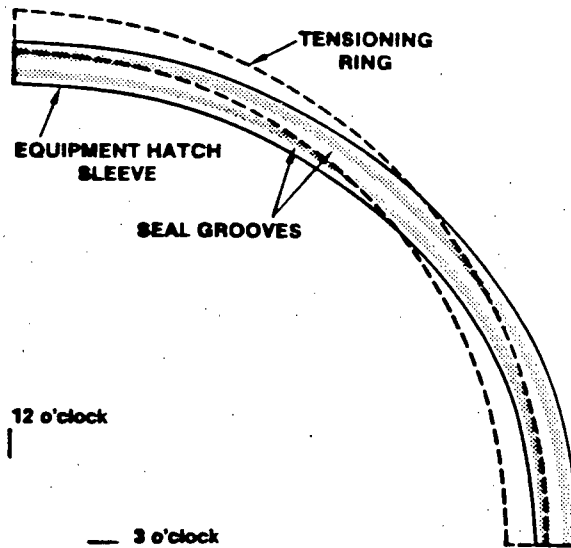


Figure 18. Schematic of Leakage Mode due to Ovalization of Penetration Sleeve

A simple approach of calculating ovalization was first developed in conjunction with the steel containment model testing [19,20]. The increase in the horizontal radius of the sleeve,  $\Delta r_H$ , can be approximated as

$$\Delta r_H = \epsilon_{ff} r \quad (2)$$

or

$$\Delta r_H = u_{ff} r / R_c \quad (3)$$

where  $\epsilon_{ff}$  and  $u_{ff}$  are the "free-field" or average membrane circumferential strain and average radial displacement of the shell at the elevation of the equipment hatch centerline,  $r$  is the original sleeve radius, and  $R_c$  is the containment shell radius. Comparison of the ovalization measured on equipment hatches in the containment model tests with results calculated from Equations 2 and 3 are shown in Figures 19 and 20. The free-field values,  $\epsilon_{ff}$  and  $u_{ff}$ , were calculated from axisymmetric finite element models. The comparisons demonstrate that this complex three-dimensional behavior can be accurately predicted by using results of axisymmetric finite element models in either Equation 2 or 3.

#### 4.0 Conclusions

A methodology for evaluating the performance of LWR containment buildings subject to pressure and temperature loads beyond the design basis has been outlined and recent advances have been described in detail. Analytical models that can be used to predict liner tearing appear quite promising, although further validation is necessary. Important tests on

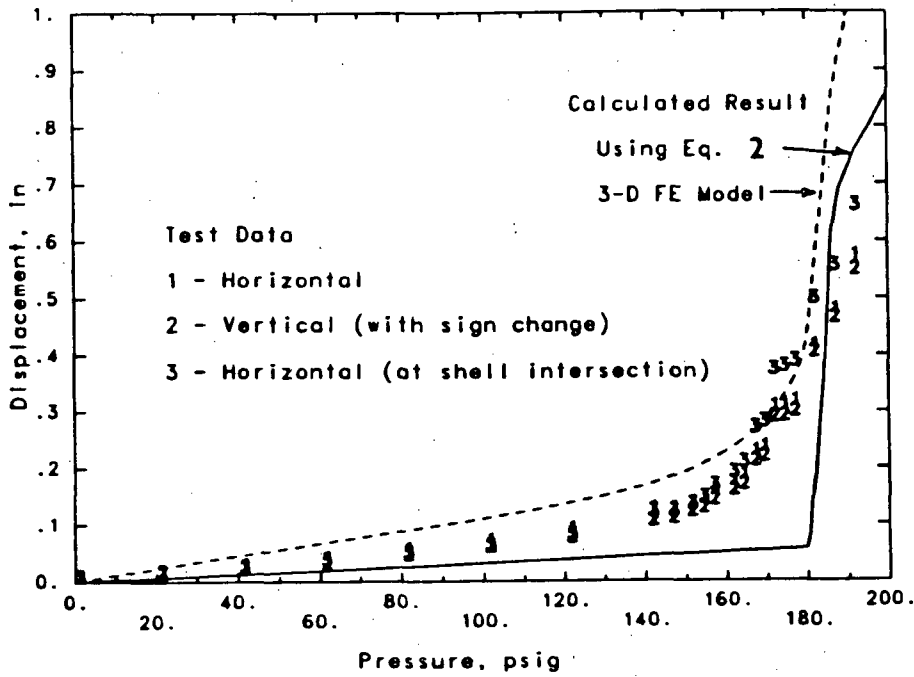


Figure 19. 1:8-Scale Steel Containment Model Measured and Calculated Ovalization of Equipment Hatch 2

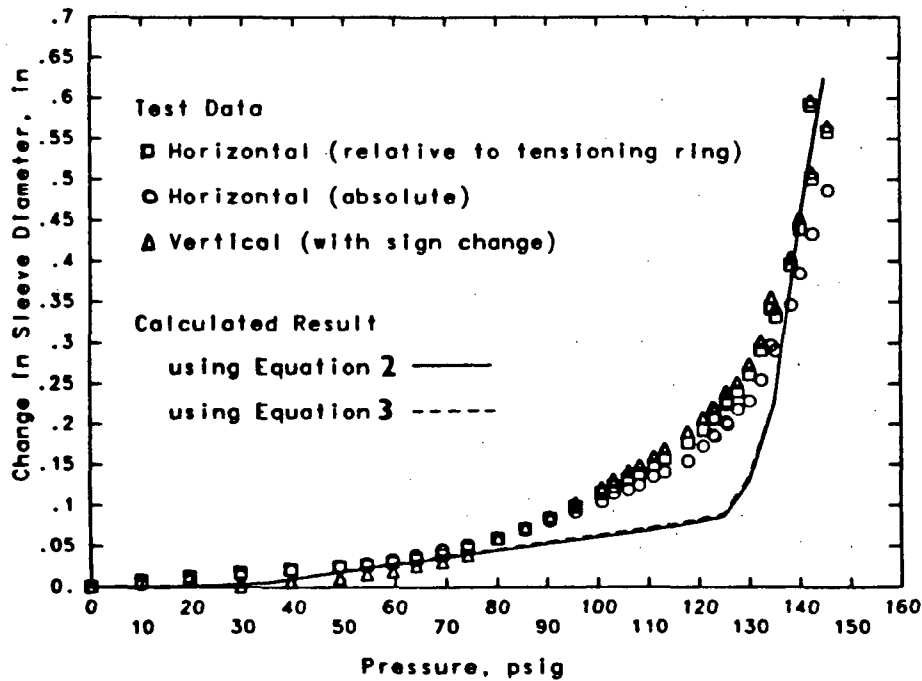


Figure 20. 1:6-Scale Reinforced Concrete Containment Model Measured and Calculated Ovalization of Equipment Hatch A

a full-size personnel airlock and on inflatable seals have recently been completed. Finally, new experimental validation of methods for evaluating the leakage potential in pressure unseating penetrations and in penetrations subject to ovalization have been described.

As is readily seen from the table of containment failure modes (Table 1), there are several areas in which the research needs to be initiated or further advanced. Investigation into the behavior of prestressed concrete containments depends in part on the testing of a 1:10 scale model by the Central Electricity Generating Board. Separate effects tests to address potential shell failure modes in reinforced and prestressed concrete containments other than those realized in the scale model tests is considered crucial to development and validation of any reasonable methodology. Finally, test validated methods for determining the behavior and performance of bellows expansion joints are needed to complete the methodology.

## 5.0 References

- [1] Steele, R., Jr. and Watkins, J. C., "Containment Purge and Vent Valve Test Program Final Report", NUREG/CR-4141, EG&G Idaho, Inc., Idaho Falls, Idaho 83415, September 1985.
- [2] Sebrell, W., "The Potential for Containment Leak Paths Through Electrical Penetrations Assemblies Under Severe Accident Conditions", NUREG/CR-3234, SAND83-0538, Sandia National Laboratories, Albuquerque, NM, July 1983.
- [3] Horschel, D. S., "The Design, Fabrication, Testing, and Analyses of Four 1:32-Scale Steel Containment Models", NUREG/CR-3902, SAND84-2153, Sandia National Laboratories, Albuquerque, NM, (to be published).
- [4] Clauss, D. B., "Comparison of Analytical Predictions and Experimental Results for a 1:8-Scale Steel Containment Model Pressurized to Failure", NUREG/CR-4209, SAND85-0679, Sandia National Laboratories, Albuquerque, NM, July 1985.
- [5] Cochrell, R. C., (ed.), Proceedings of the Fourth Workshop on Containment Integrity, Session E (Analyses Associated with Sandia 1:6-Scale Model Test), NUREG/CP-0095, SAND88-1836, Sandia National Laboratories, Albuquerque, NM, October 1988.
- [6] Smith, J., "The Design of a 1/10th Scale Model of a Sizewell B Primary Containment", Proceedings of the Fourth Workshop on Containment Integrity, NUREG/CP-0095, SAND88-1836, Sandia National Laboratories, Albuquerque, NM, October 1988.
- [7] Bump, T. R., et al., "Characterization of Nuclear Reactor Containment Penetrations - Preliminary Report", NUREG/CR-3855, SAND84-7139, Sandia National Laboratories, Albuquerque, NM, June 1984.
- [8] Shackelford, M. H., et al., "Characterization of Nuclear Reactor Containment Penetrations - Final Report", NUREG/CR-3855, SAND84-7180, Sandia National Laboratories, Albuquerque, NM, January 1985.

- [9] Brinson, D. A., and Graves, G. A., "Evaluation of Seals for Mechanical Penetrations of Containment Buildings", NUREG/CR-5096, SAND88-7016, Sandia National Laboratories, Albuquerque, NM, 1988.
- [10] Bridges, T. L., "Containment Penetrations Elastomer Seal Leak Rate Tests", NUREG/CR-4944, SAND87-7118, Sandia National Laboratories, Albuquerque, NM, July 1987.
- [11] Keck, J. D., and Thome, F. V., "Electrical Penetrations Assemblies Severe Accident Testing", Proceedings of the Intl. Topical Meeting on Operability of Nuclear Power Systems in Normal and Adverse Environments, pp 181-186, September 29-October 3, 1986.
- [12] Horschel, D. S., "Experimental Results from Pressure Testing a 1:6-Scale Nuclear Power Plant Containment", NUREG/CR-5121, SAND88-0906, Sandia National Laboratories, Albuquerque, NM, 1988.
- [13] Clauss, D. B., (ed.), "Round Robin Pretest Analyses of a 1:6-Scale Reinforced Concrete Containment Model Subject to Static Internal Overpressurization", NUREG/CR-4913, SAND87-0891, Sandia National Laboratories, Albuquerque, NM, April 1987.
- [14] Horschel, D. S., "Design, Construction, and Instrumentation of a 1/6-Scale Reinforced Concrete Containment Building", NUREG/CR-5083, SAND88-0030, Sandia National Laboratories, Albuquerque, NM, 1988.
- [15] Knorovsky, G. A., Hatch, P. W., and Gutierrez, M. R., "Evaluation of Materials of Construction for the Reinforced Concrete Reactor Containment Model", NUREG/CR-5099, SAND88-0052, Sandia National Laboratories, Albuquerque, NM, September, 1988.
- [16] Manjoine, M. J., "Creep-Rupture Behavior of Weldments", Welding Journal, Vol. 61, No. 2, February, 1982, p. 50.
- [17] Barnes, B. L., et al., "Leak Area Estimates for Power Reactor Containments During Severe Accident Conditions", Idaho National Engineering Laboratory, EGG-EA-6753, 1984.
- [18] Clauss, D. B., von Riesemann, W. A., and Parks, M. B., "Containment Penetrations", proposed for publication in proceedings of the NRC/MITI Technical Information Exchange Workshop, May 16-18, 1988, Tokyo, Japan.
- [19] Clauss, D. B., "Comparison of Analytical Predictions and Experimental Results for a 1:8-Scale Steel Containment Model Pressurized to Failure", Nuclear Engineering and Design, Vol. 90 (1985), pp 241-260.
- [20] Clauss, D. B., "Failure Mechanisms of LWR Steel Containment Buildings Subject to Severe Accident Loadings", Proceedings of the Third Workshop on Containment Integrity, NUREG/CP-0076, SAND86-0618, August 1986, Sandia National Laboratories, Albuquerque, NM.



# SHAM: High-Level Seismic Tests of Piping at the HDR

by

C. A. Kot, M. G. Srinivasan, B. J. Hsieh, Argonne National Laboratory;  
L. Malcher, D. Schrammel, Kernforschungszentrum, Karlsruhe, FRG;  
H. Steinhilber, Fraunhofer Institut für Betriebsfestigkeit, Darmstadt, FRG;  
J. F. Costello, U. S. Nuclear Regulatory Commission, Office of Research

## ABSTRACT

As part of the second phase of vibrational/earthquake investigations at the HDR (Heissdampfreaktor) Test Facility in Kahl/Main, FRG, high-level simulated seismic tests (SHAM) were performed during April-May 1988 on the VKL (Versuchskreislauf) in-plant piping system with two servohydraulic actuators, each capable of generating 40 tons of force. The purpose of these experiments was to study the behavior of piping subjected to seismic excitation levels that exceed design levels manifold and may result in failure/plastification of pipe supports and pipe elements, and to establish seismic margins for piping and pipe supports. The performance of six different dynamic pipe support systems was compared in these tests and the response, operability, and fragility of dynamic supports and of a typical U. S. gate valve were investigated. Data obtained in the tests are used to validate analysis methods. Very preliminary evaluations lead to the observation that, in general, failures of dynamic supports (in particular snubbers) occur only at load levels that substantially exceed the design capacity. Pipe strains at load levels exceeding the design level threefold are quite small, and even when exceeding the design level eightfold are quite tolerable. Hence, under seismic loading, even at extreme levels and in spite of multiple support failures, pipe failure is unlikely.

## 1. Introduction

The Heissdampfreaktor (HDR) Test Facility in Kahl/Main, Federal Republic of Germany (FRG), has been used since 1974 by the HDR Safety Project (PHDR) of the Kernforschungszentrum Karlsruhe (KfK), FRG, to perform vibrational, thermal hydraulic, blowdown, and other experiments related to the design and safety of nuclear power plants. As part of the current second-phase testing, high-level seismic experiments, designated SHAM, were performed on an in-plant piping system during the period of 19 April to 27 May 1988. These experiments were intended as a companion test series to the SHAG tests performed in 1986 [1,2], in which the reactor containment building was tested to incipient failure. Thus, the objectives of the SHAM experiments were to (i) study the response of piping subjected to seismic excitation levels that exceed design levels manifold and which may result in failure/plastification of pipe supports and pipe elements; (ii) provide data for the validation of linear and nonlinear pipe response analyses; (iii) compare and evaluate, under identical loading conditions, the performance of various dynamic support systems, ranging from very flexible to very stiff support configurations; (iv) establish seismic margins for piping, dynamic pipe supports, and pipe anchorages; and (v) investigate the response, operability, and fragility of dynamic supports and of a typical U.S. gate valve under extreme levels of seismic excitation.

The SHAM experiments were conducted as a cooperative effort among a number of organizations in Europe and the USA. These included KfK/PHDR, with the participation of the Fraunhofer Institut für Betriebsfestigkeit (LBF), Darmstadt, FRG, and the Kraftwerk Union (KWU), Offenbach, FRG; the Central Electricity Generating Board (CEGB), UK; the Electric Power Research Institute (EPRI), Palo Alto, California, with the participation of Bechtel Corp. and R. C. Cloud & Associates; and the U.S. Nuclear Regulatory Commission, Office of Research (NRC/RES), which supported the efforts of Argonne National Laboratory (ANL) and Idaho National Engineering Laboratory (INEL).

A brief description of the SHAM tests is provided, including the design of the experiments and hardware, the test procedures and approach, and the instrumentation and data acquisition. Since the experimental data are just now becoming available, only highlights of the test results are given primarily in the form of maximum response values. Also presented are very limited comparisons of experimental data and pretest analytical predictions. All results and conclusions presented here should be considered preliminary.

## **2. Description of the SHAM Experiments**

The test object in the SHAM experiments was the VKL (Versuchskreislauf) piping system that was already extensively tested in the SHAG experiments [1,2]. In the latter tests, excitation of the piping resulted from the shaking of the HDR containment building. In the SHAM experiments, direct, high-level shaking of the VKL piping was used. Therefore, some significant modification of the test loop was necessary.

### **2.1 Test Design and Set-up**

An isometric sketch of the VKL piping as used in the SHAM testing is shown in Figure 1. The VKL piping is located between the 18- and 24-m elevations in the HDR facility, and it consists of multiple stainless steel pipe branches ranging from 100 to 300 mm in diameter, with the main two flow loops connected to the HDU vessel and the DF16 manifold. A third major branch connects the DF16 manifold to the DF15 manifold. Aside from the pipe hangers and dynamic supports, the only points of fixity for the entire system, including the HDU and manifolds, are the supports at the bottom of the HDU and the nearly rigid attachment of the DF15 manifold. All extraneous piping leading to other flow systems in the HDR were disconnected for the SHAM tests. As in the earlier tests, the test loop again included an 8" U.S. gate valve from the decommissioned Shippingport Atomic Power Station. This valve was refurbished prior to testing at the HDR; and its motor operator was equipped with a new AC motor, torque switch, and torque spring prior to the SHAM testing.

The VKL piping was excited directly by means of two servohydraulic actuators rated at 40 tons (metric) of force each. As shown in Fig. 1, both actuators were acting in the horizontal x-direction at hanger location H5 and at location H25 (DF16 manifold). The excitation system was designed and furnished by LBF-Darmstadt, FRG, and included a computer-controlled hydraulic actuating/control system to provide predetermined displacement-time histories. Extensive pretest design calculations indicated that the hydraulic shakers should be capable of producing up to 6 g acceleration for the VKL piping, with a maximum displacement (stroke) of  $\pm 125$  mm [3].

Six different dynamic support systems of the VKL piping were designed by the various participants in the SHAM testing. These ranged from the very stiff U.S. system with rigid struts and snubbers to a very flexible HDR system with essentially only dead-weight supports. Two support configurations, provided by EPRI in collaboration with industrial partners, contained snubber replacement devices. The first of these, designed by Bechtel Power Corp., uses Energy Absorber (EA) devices, in which a set of specially designed steel plates is plastically deformed to dissipate energy and restrict pipe motion under seismic loading. The second snubber replacement system, designed by R. L. Cloud & Associates, Inc., includes Seismic Stops (SS). In their current design, these stops are simple telescoping-tube devices with preset internal gaps that allow a certain amount of motion to accommodate thermal effects. During seismic excitation, the motion is restricted/stopped by impacting on disc spring pads. Two other support configurations, designed by KWU and CEGB, rely only on rigid struts for dynamic restraint. Figure 2 shows an overview of all the support configurations with the location and type of dynamic support clearly indicated. All configurations used the same dead-weight hanger system shown in Fig. 1. Similarly, all configurations employed the same rigid struts at locations H4 and H23. These are horizontal struts in the z-direction and their primary function is to stabilize the input motions of the actuators, at H5 and DF16 respectively, so that they move only in the x-direction. The components of these supports were sized for the highest loads anticipated.

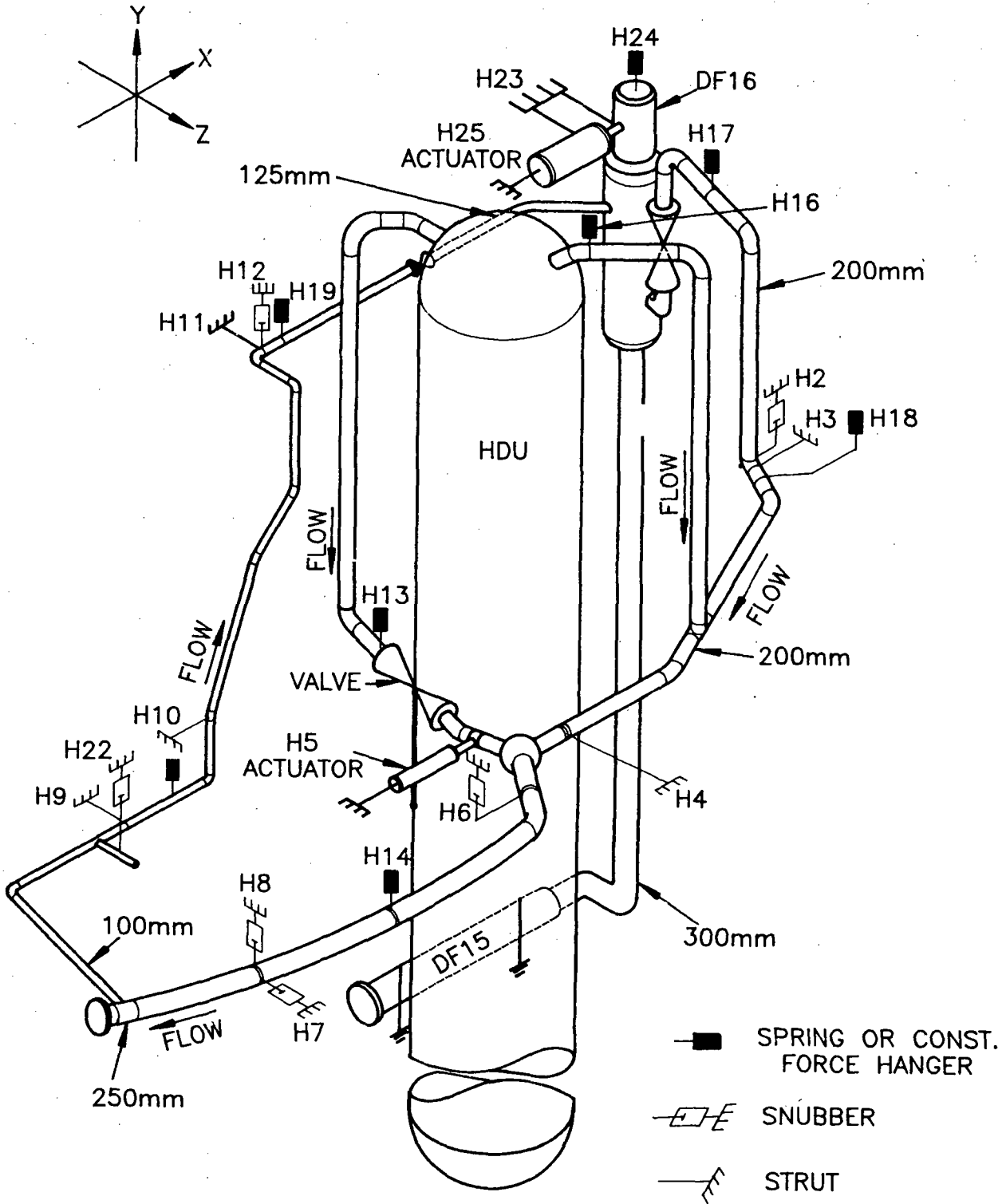


Fig. 1. SHAM Test Configuration – VKL Piping with US NRC Supports

| HANGER CONFIGURATIONS |                           |                 |                    |                    |                 |                |
|-----------------------|---------------------------|-----------------|--------------------|--------------------|-----------------|----------------|
| Hanger No.            | 1<br>HDR                  | 2<br>KWU        | 3<br>NRC           | 4<br>EPRI/EA       | 5<br>EPRI/SS    | 6<br>CEGB      |
| 2                     | —                         | —               | Snubber<br>PSA1    | —                  | Seismic<br>stop | —              |
| 3                     | —                         | —               | Strut<br>Size B    |                    |                 | —              |
| 4                     | Strut<br>Size 20          |                 |                    |                    |                 |                |
| 6                     | —                         | —               | Snubber<br>PSA 1/2 | —                  | Seismic<br>stop | —              |
| 7                     | —                         | —               | Snubber<br>A/D 150 | Energy<br>Absorber | Seismic<br>stop | Strut<br>RS-15 |
| 8                     | —                         | —               | Snubber<br>A/D 70  | Energy<br>Absorber | Seismic<br>stop | Strut<br>RS-7  |
| 9                     | —                         | Strut<br>Size B | Strut<br>Size A    |                    |                 | Strut<br>RS-7  |
| 10                    | —                         | Strut<br>Size B | Strut<br>Size A    |                    |                 | —              |
| 11                    | —                         | Strut<br>Size B | Strut<br>Size A    |                    |                 | —              |
| 12                    | —                         | —               | Snubber<br>A/D 40  | —                  | Seismic<br>stop | Strut<br>RS-15 |
| 22                    | —                         | —               | Snubber<br>PSA 1/4 | Energy<br>Absorber | Seismic<br>stop | —              |
| 23                    | Two Struts<br>2 x Size 20 |                 |                    |                    |                 |                |

Fig. 2. Dynamic Support Configurations for VKL Piping used in SHAM Tests

All dynamic support systems except that designed by CEGB were designed for the common HDR spectrum shown in Fig. 3. The actuators were displacement controlled, and the basic earthquake displacement history used was an artificially generated displacement-time function of 15 seconds duration (see Fig. 4), fitted to the preselected common Safe Shutdown Earthquake (SSE)-floor-response spectrum with a 0.6 g peak acceleration (ZPA), shown in Fig. 3. The supports for the U.S. stiff support system were designed by INEL with typical U.S. struts from Grinnell and snubbers from Pacific Scientific (PSA) and Anchor Darling Industries (A/D). INEL analyzed the VKL piping system for seismic response using a typical nuclear plant design approach and basing their allowables on the 1979 ASME Code. To permit the evaluation of seismic margins and failure modes of support components at reasonably low levels of earthquake excitation, the dynamic supports were sized for Level "C" allowables for the expected SSE loading. While the other support configurations, i.e., KWU, EPRI/EA, and EPRI/SS, were also designed for the same floor-response-spectrum and a ZPA of 0.6 g, they were sized for more conservative allowables. The HDR flexible support system was essentially not designed for seismic loading and only contained the rigid struts required to stabilize the hydraulic actuators (H4, H23). Finally, the CEGB hanger system was designed for the Sizewell B spectrum shown in Fig. 3 and was tested with displacement histories of 20-s duration, corresponding to that spectrum and the Allsites spectrum shown in Fig. 3.

To study the behavior and fragility of typical pipe mountings and anchorages, trunions were installed at locations H2 and H22 (see Fig. 1). At the same time, the anchor plates and anchors at these locations were replaced with typical U.S. hardware, sized for the design spectrum and SSE level.

## 2.2 Instrumentation and Data Acquisition

Nearly 300 channels of data were recorded, with major measurements being strains (142 channels), accelerations (90 channels), displacements (29 channels), and forces (27 channels). In addition, 10 channels were used to monitor the operating parameters of the U.S. 8" gate valve. All important aspects of the experiments were monitored; this included the excitation systems (actuators) where displacements, accelerations, and forces were measured. The pipe responses (accelerations) at the driving points were also measured. Displacement and forces of dynamic supports were recorded, as were the pipe accelerations at the point of support attachment. Additional accelerations and displacements were recorded at points where large responses were expected. Finally, strain measurements were made throughout the piping system. Again, pipe locations and elbows where the strain was expected to be high were selected. In particular, the first pipe elbow (Elbow 1) adjacent to the DF16 manifold (see Fig. 1) was monitored, as was the 100-mm pipe next to the reduction tee, and the elbow following that tee (Elbow 2). Stress coating, applied at some locations of the pipe, was monitored during the testing to provide early indication of severe straining. Details of the instrumentation can be found in the Test Design Report [3] and the Test Protocol [4].

During conversion to digital form the data were originally acquired at a rate of 625 Hz and filtered at 100 Hz. Before final storage in the computer of the HDR Central Measurement Facility (ZMA), the data acquisition rate was reduced by a factor of three; i.e., to 208.3 Hz; and the data were digitally low-pass filtered at 60 Hz. After plausibility checks and offset corrections, the data are now made available in this form to the users by the Central Evaluation Computer (ZAW) of KfK/PHDR.

## 2.3 Experiments Performed

Fifty-one individual experiments were performed with the VKL piping and the six different pipe support configurations. Two random excitation tests of 120-s duration, with each of the hydraulic actuators singly and separately (H5 and DF16) were performed for each hanger configuration. These tests provided dynamic characterization of the systems in the frequency range from 2 to 40 Hz. The maximum excitation level in these tests was approximately 0.3 g with a maximum actuator piston displacement of around  $\pm 3$  mm.

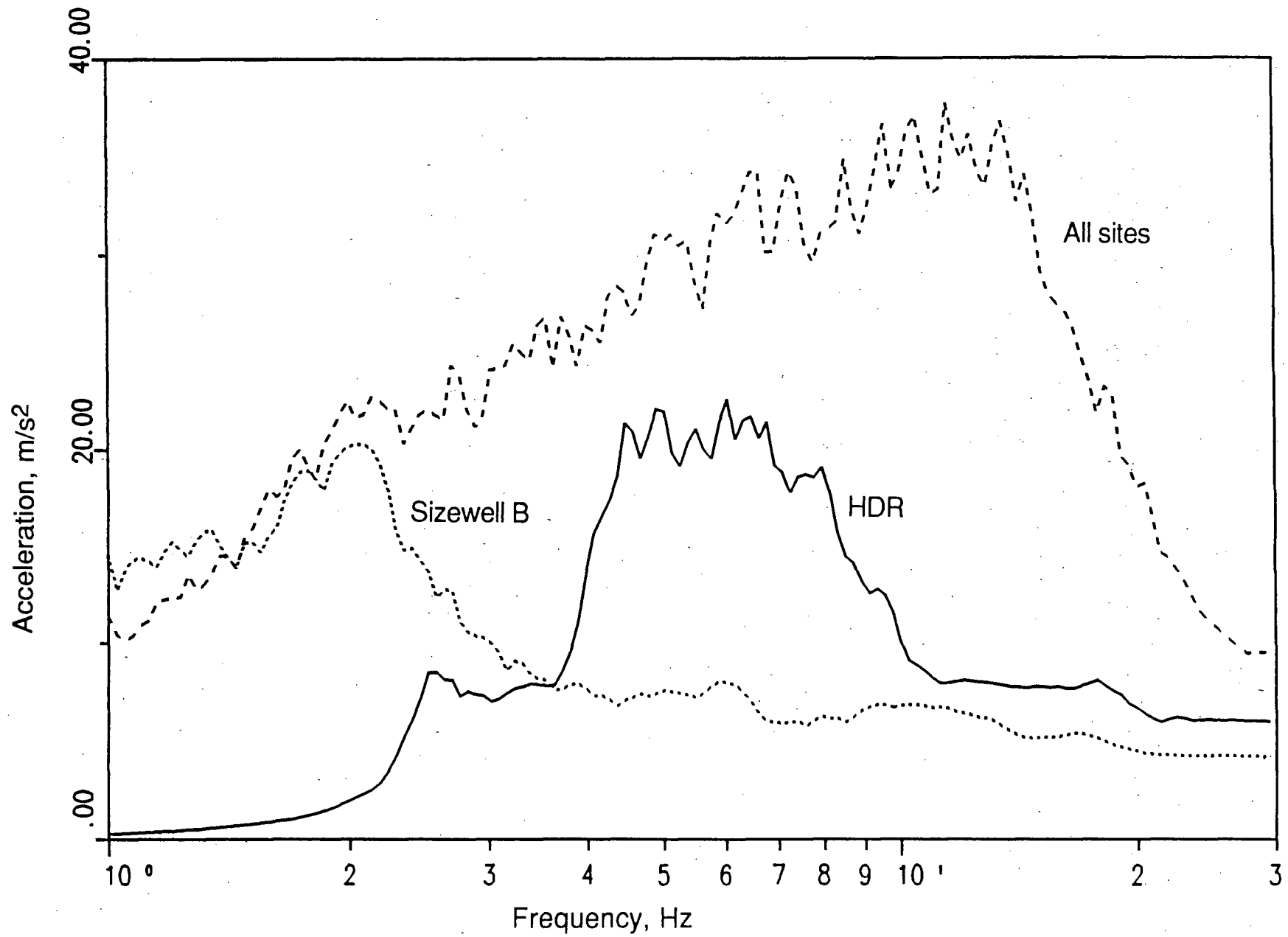


Fig. 3. Spectra of the Earthquake Excitations, 100%--SSE, 4% Damping

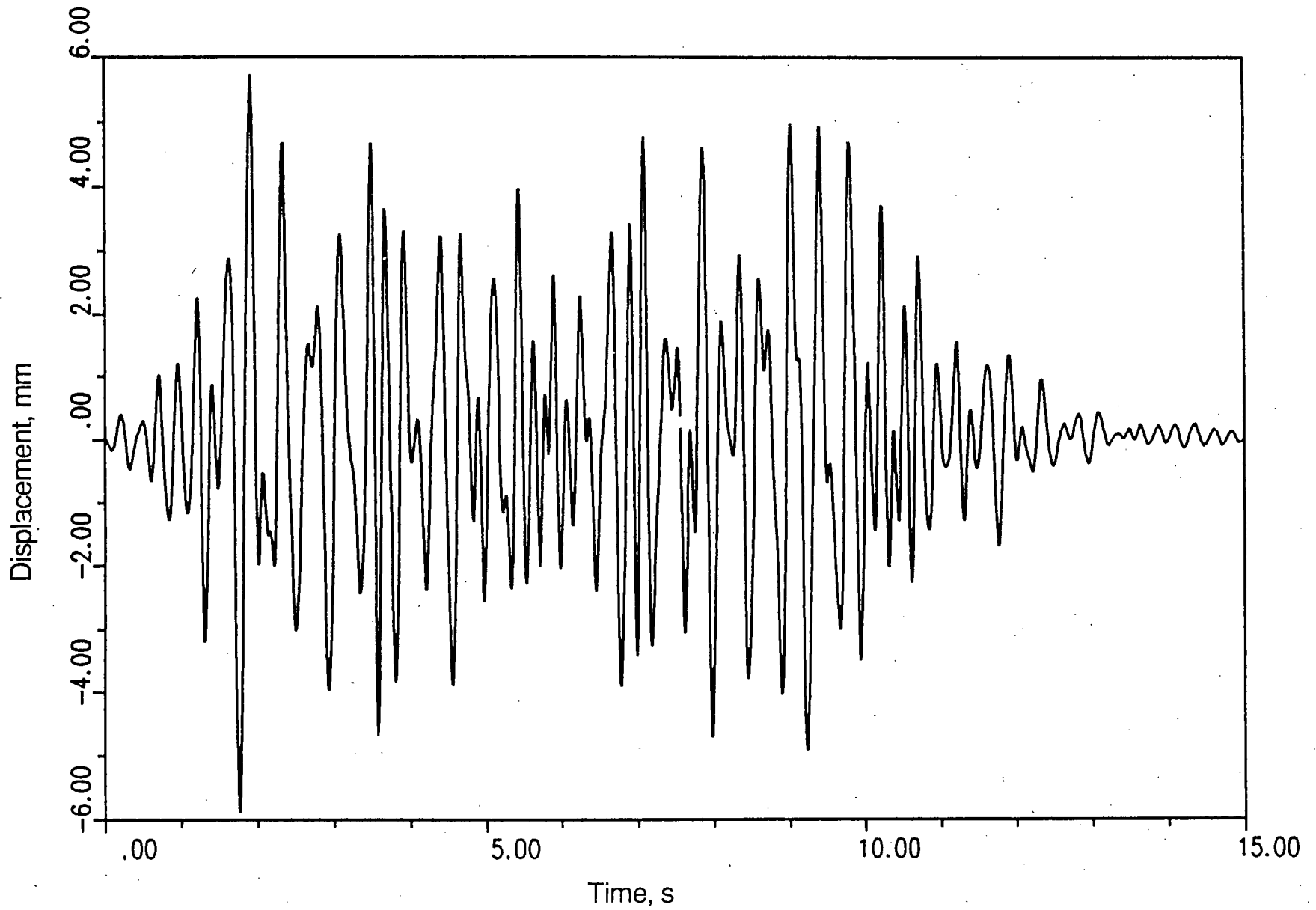


Fig. 4. Earthquake Displacement-Time History for the HDR 100%-SSE Spectrum

For all but the CEGB configuration, earthquake experiments were then performed at the low to intermediate level, i.e., at excitation levels ranging from one SSE (0.6 g ZPA) to three (four) SSE. These experiments were carried out with the 15-s duration displacement history based on the common HDR spectrum (see Fig. 4) scaled to the proper SSE level. The two hydraulic actuators (at H5 and DF16) were operated together and in phase; both were programmed to provide identical displacement histories. The purpose of these tests was to study the behavior of piping systems at load levels exceeding the design load and to compare the performance of different support configurations. To make these tests possible with all configurations, strains in the piping were required to remain below significant plastification, i.e., about 0.2% of strain. These tests were also intended to provide seismic-margin information for dynamic supports, and data for the validation of linear analyses.

Two configurations, namely the KWU system and a modified NRC system, were then tested to high levels of excitation (up to 800% SSE) again with scaled-up displacement histories and both actuators operating in phase. The modification of the NRC system consisted of providing a stiff bridging (welded box beam) between the DF16 manifold and the 200 mm J-pipe extending from it. This bridging was intended to prevent excessive straining of the first elbow adjacent to the DF16 manifold and to provide a more uniform load distribution throughout the piping system. The elbow in question exhibited the highest strains in the lower level tests and any eventual failure at this elbow would not be considered prototypical of real earthquake loading but rather as "engineered" by the hydraulic actuator excitation. The purpose of the high-level tests was to obtain information on possible pipe failure/plastification, seismic margins for piping, and pipe supports, and to provide data for the validation of nonlinear analysis methods.

The CEGB configuration was subjected to its own test program. Low- and intermediate-level earthquake tests were performed with displacement histories of 20-s duration derived from the Sizewell B and Allsites spectra (see Fig. 3). Intermediate- and high-level tests were also performed with sine burst histories. Finally, to provide a comparison with the other configurations, a 100% SSE earthquake test was performed with the displacement history derived from the common HDR spectrum.

### 3. SHAM Results

As indicated earlier, analysis of the very large volume of SHAM test data is just beginning. The following preliminary overview of the results is based primarily on the exposition of maximum responses for selected variables in the experiments. In order to obtain consistent and comparable results in the earthquake testing of all the support configurations that were subjected to the common HDR spectrum, it was our intention to control the input acceleration spectra for the two actuators within a tolerance of  $\pm 10\%$  in amplitude. Figures 5 and 6 provide the actual measured input spectra for the experiments at 100% and 300% SSE, respectively. Also shown in these figures are the desired tolerance bounds for the spectra. It can be seen that at 100% SSE, up to frequencies of about 10 Hz, the experimental spectra generally meet the stipulated requirements, with the actuator at DF16 producing less scatter than the one at H5. At higher frequencies, the tolerance criterion is not satisfied very well, and peaking of the spectra generally occurs between 15 and 20 Hz. The magnitude of this peak varies from configuration to configuration. At this time, it is not clear if this is indeed an input characteristic, or if the strong deviation from the desired spectra represents feedback from the piping system. Please note that displacement, and not acceleration, was the controlled variable. This point requires further investigation. In the 300%-SSE experiments, at the H5 actuator of the stiff U.S. NRC configuration, strong deviations from the desired spectrum can be seen even in the lower frequency range, with the peak amplitude overshoot being nearly twice as high as the intended value. Similar discrepancies have also been found for the 200%-SSE experiments. At higher levels of excitation (400, 600, and 800% SSE), the input spectra are similar to those at 100% SSE.

The large deviations from the expected spectra and the differences between various configurations make comparisons somewhat problematic. Approaches to overcome this problem must be

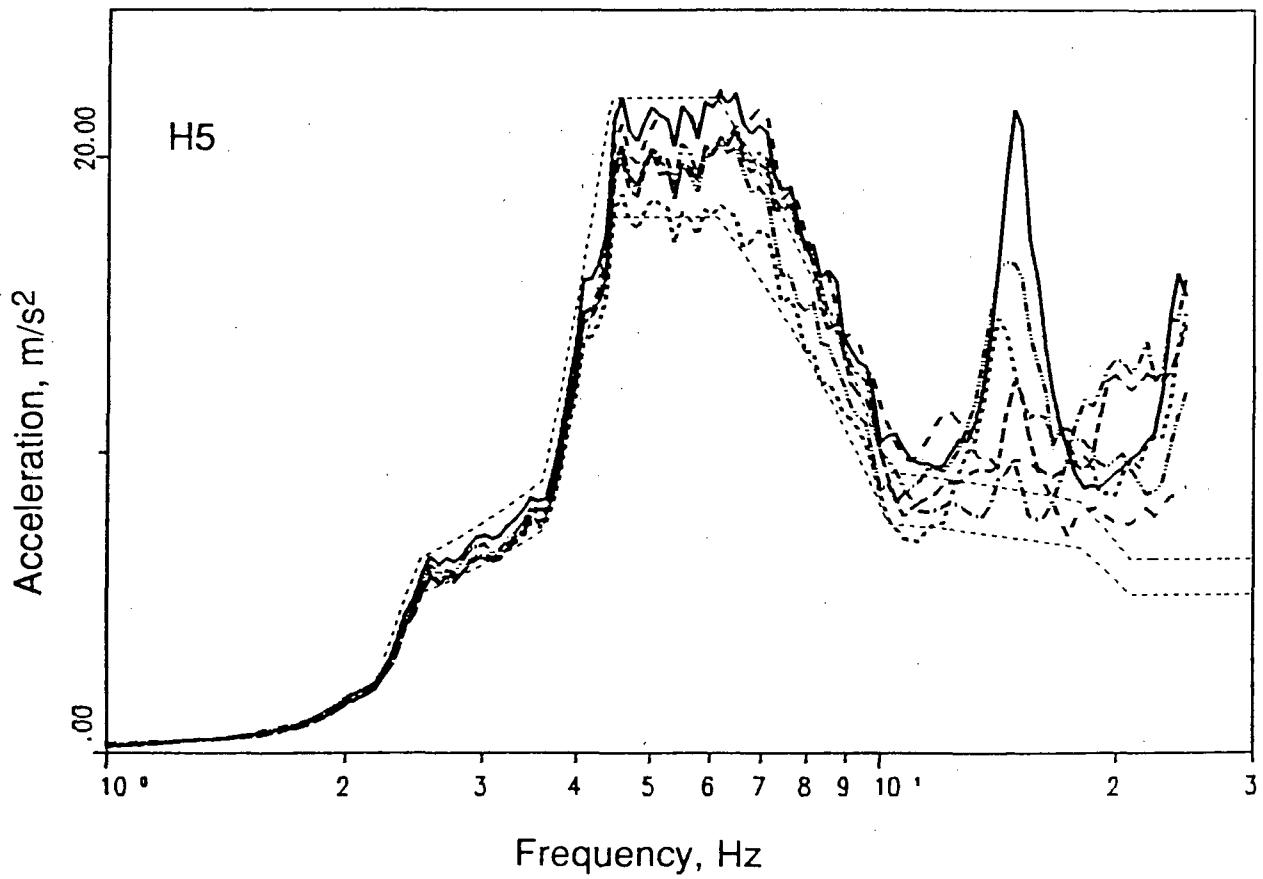
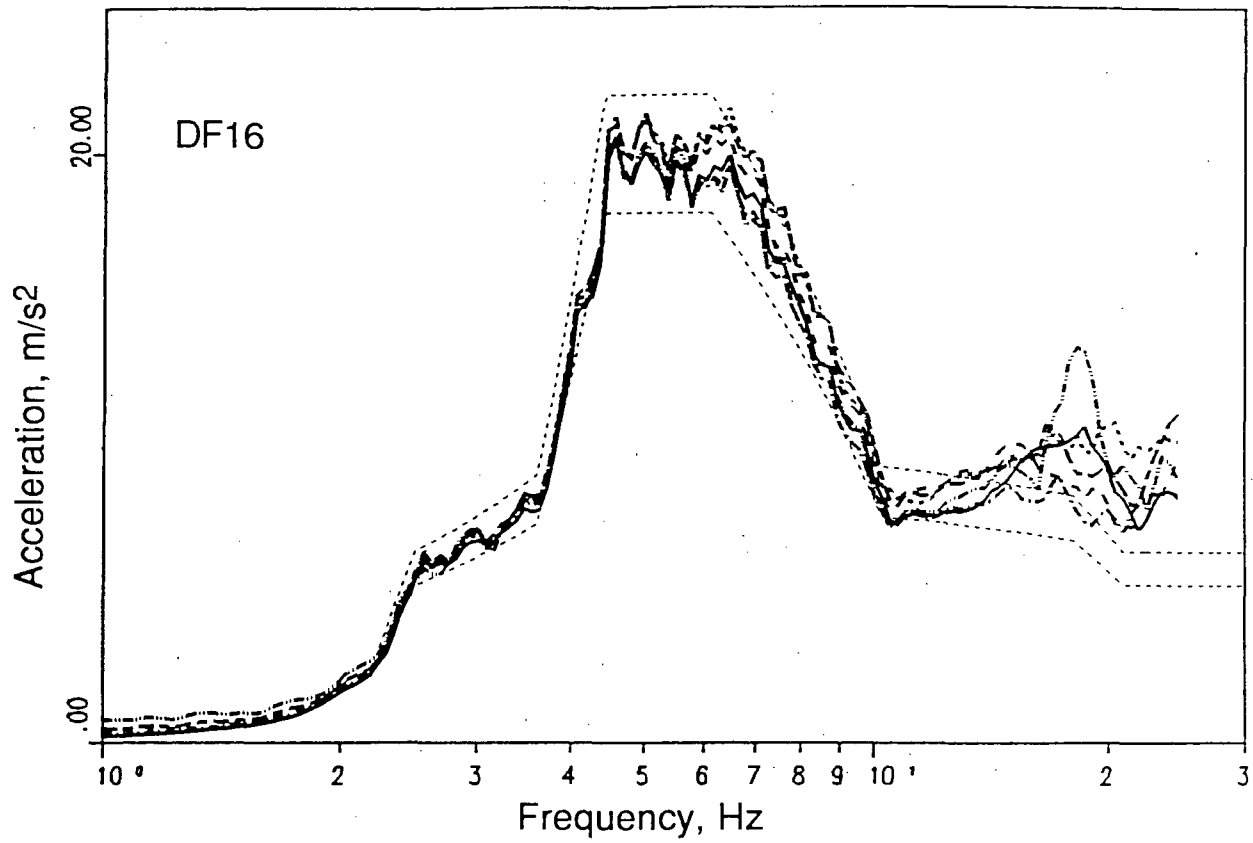


Fig. 5. Input Response Spectra for 100%-SSE Experiments, 4% Damping

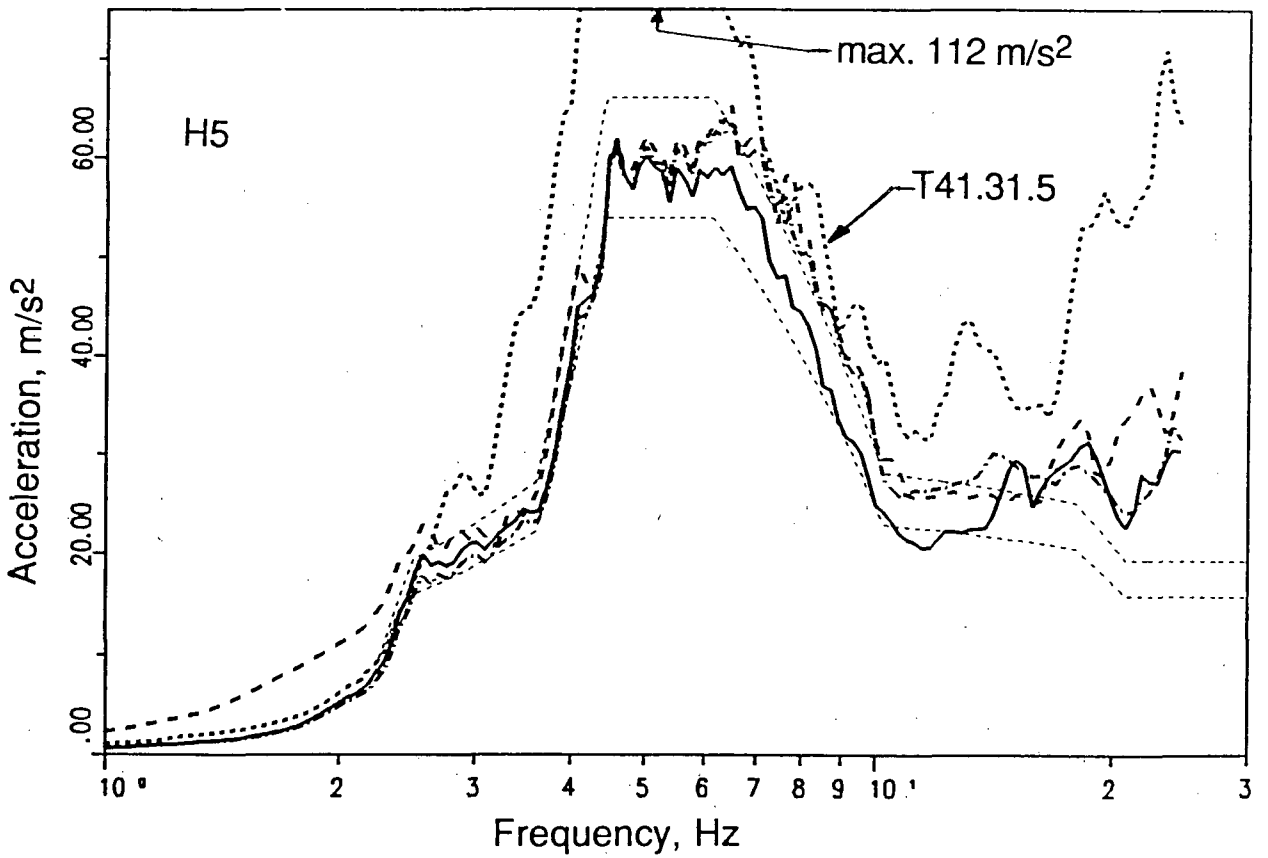
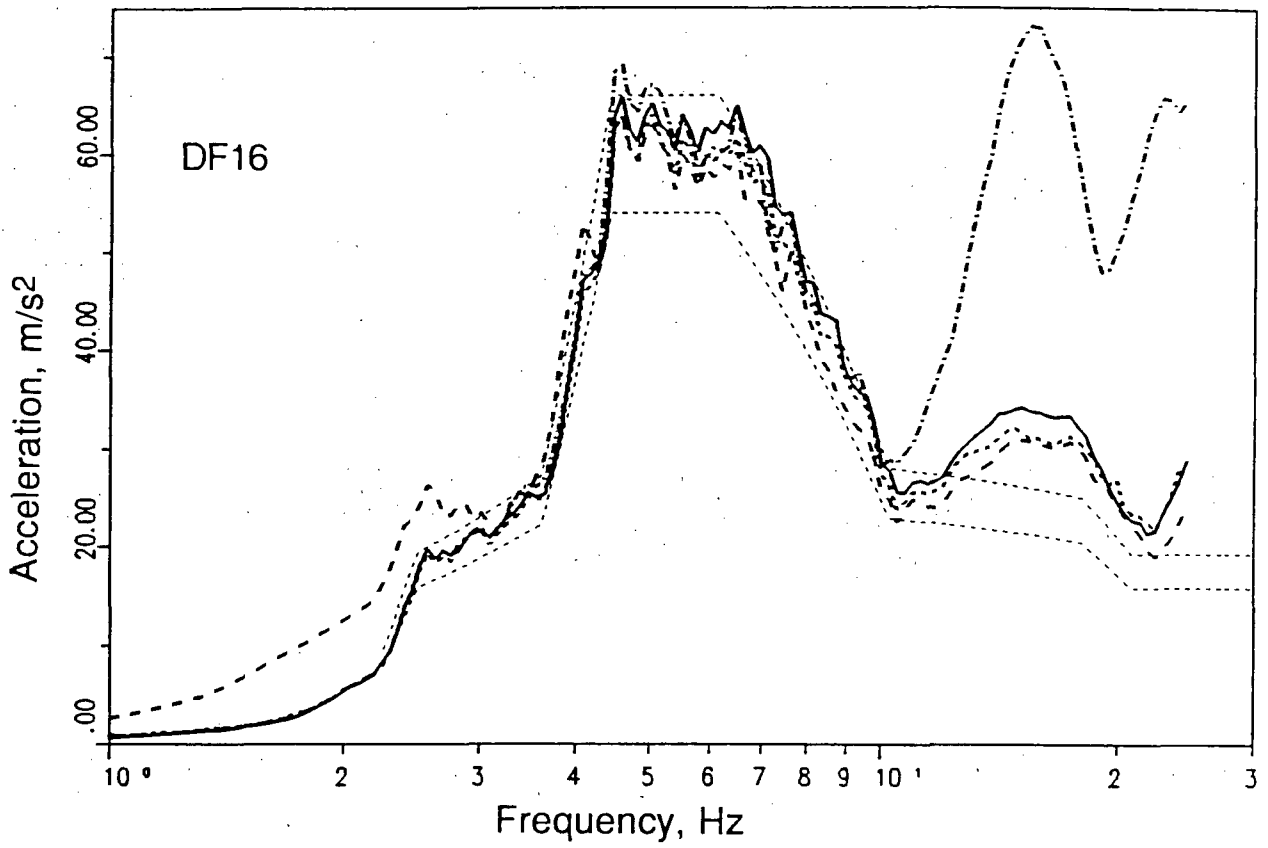


Fig. 6. Input Response Spectra for 300%-SSE Experiments, 4% Damping

developed. These difficulties should also be kept in mind when examining the results presented here and when drawing any conclusions.

### 3.1 Comparisons at 100% SSE

Figures 7 to 10 show peak response values for various variables at 100%–SSE–input load (HDR common spectrum, 0.6 g ZPA) for all six support configurations. When making comparisons, it should be remembered that the CEGB configuration was designed for a different spectrum, namely, the Sizewell B spectrum which peaks at lower frequency.

The differences in peak accelerations (Fig. 7) in the 200–mm pipe and at the valve are not large between configurations, the stiffest NRC configuration giving the lowest values at two location (QB116, QB940). On the 100–mm pipe, the more flexible configurations (HDR and CEGB) give higher responses at the elbow following the reduction tee (QB101) and at midspan (RS761). The situation is reversed at the top of the pipe run close to the DF16 manifold (QB112).

Figure 8 presents the peak forces at the actuators (H5 and DF16) and at the permanent struts H4 and H23. Two forces are given for the latter since this support consisted of two parallel struts. It can be seen that these two forces are not equal and that, for strut H23.1, the flexible configurations (HDR, CEGB) result in lower forces than the other hanger configurations. At actuator H5, only the most flexible HDR configuration differs significantly, whereas at actuator DF16, the peak forces vary from about 32 kN to 42 kN but no consistent variation with support system stiffness is apparent. At the other control support H4, the lowest force corresponds to the stiffest NRC support system and the most flexible HDR system gives the highest force.

Comparing the maximum bending stresses in the 200–mm piping (Fig. 9), one sees that the NRC configuration gives the highest stresses in the branch emanating from the DF16 manifold (QA100, QA102). On the other hand, in the pipe coming from the HDU (QA104, QA106) and at the valve (QA937), the NRC configuration gives the lowest stresses. In the smaller diameter pipe (Fig. 10), the bending stresses are consistently high for the more flexible configurations (HDR and CEGB), whereas the stiff NRC configuration, in general, exhibits the lowest peak stresses. The stress results are confirmed by the maximum strain measured in the elbows. Elbow 1 in the 200–mm pipe, next to the DF16 manifold, shows the highest strains for the stiff NRC configuration, while Elbow 2, in the 100–mm pipe directly following the reduction tee, yields the highest strains for the flexible configurations (HDR and CEGB).

Other comparisons made include the maximum forces in the rigid struts. In general, the stiff NRC configuration gives lower peak forces than the snubber replacement configurations and the more flexible KWU configuration. In particular, at hanger location H3, the force for the seismic stops exceeds that for the snubbers by more than a factor of two (14.4 vs. 6.6 kN). Finally, if forces at snubber locations are compared, one finds that the seismic stops result in the highest forces at four locations (H7, H8, H12 and H22). At H6, the peak seismic–stop force is somewhat lower than for the NRC snubber. At location H2, the seismic stop made no contact with the impact disc spring and no force was recorded.

### 3.2 Effect of Increasing Excitation

Only the KWU support configuration was subjected to the entire range of excitation levels from 100% to 800% SSE. While the modified NRC configuration, with the bridging between the DF16 manifold and 200–mm pipe, was also tested in the range from 200% to 800% SSE, multiple snubber failures occurred (H8, H12, H22) during the 600%–SSE test. These snubbers were not replaced for the 800% SSE test. Snubbers H8 and H12, which failed so as to permit free motion without resistance, remained installed, while snubber H22, which failed with resistance, was removed for the 800%–SSE test. During the latter test, snubber H7 also failed after 6.5 s, when it reached force levels of about 60 kN. Finally, the bridging failed in this test, at about 12 s, as did the anchors at location H2. At lower levels of excitation, snubbers H6 and H8 failed in the original unmodified NRC configuration during the 300%–SSE

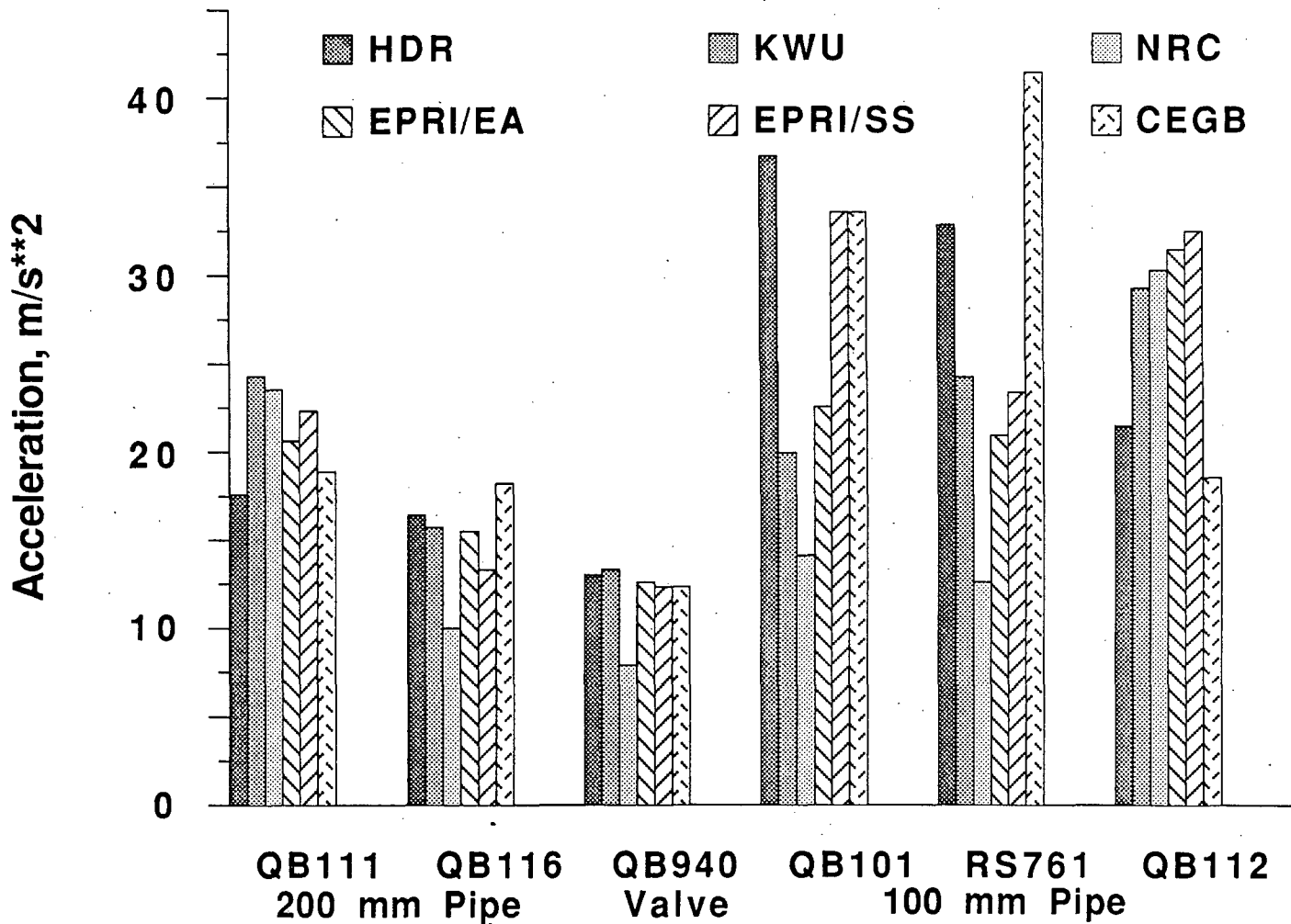


Fig.7 Comparison of Peak Accelerations of Support Configurations at 100% SSE

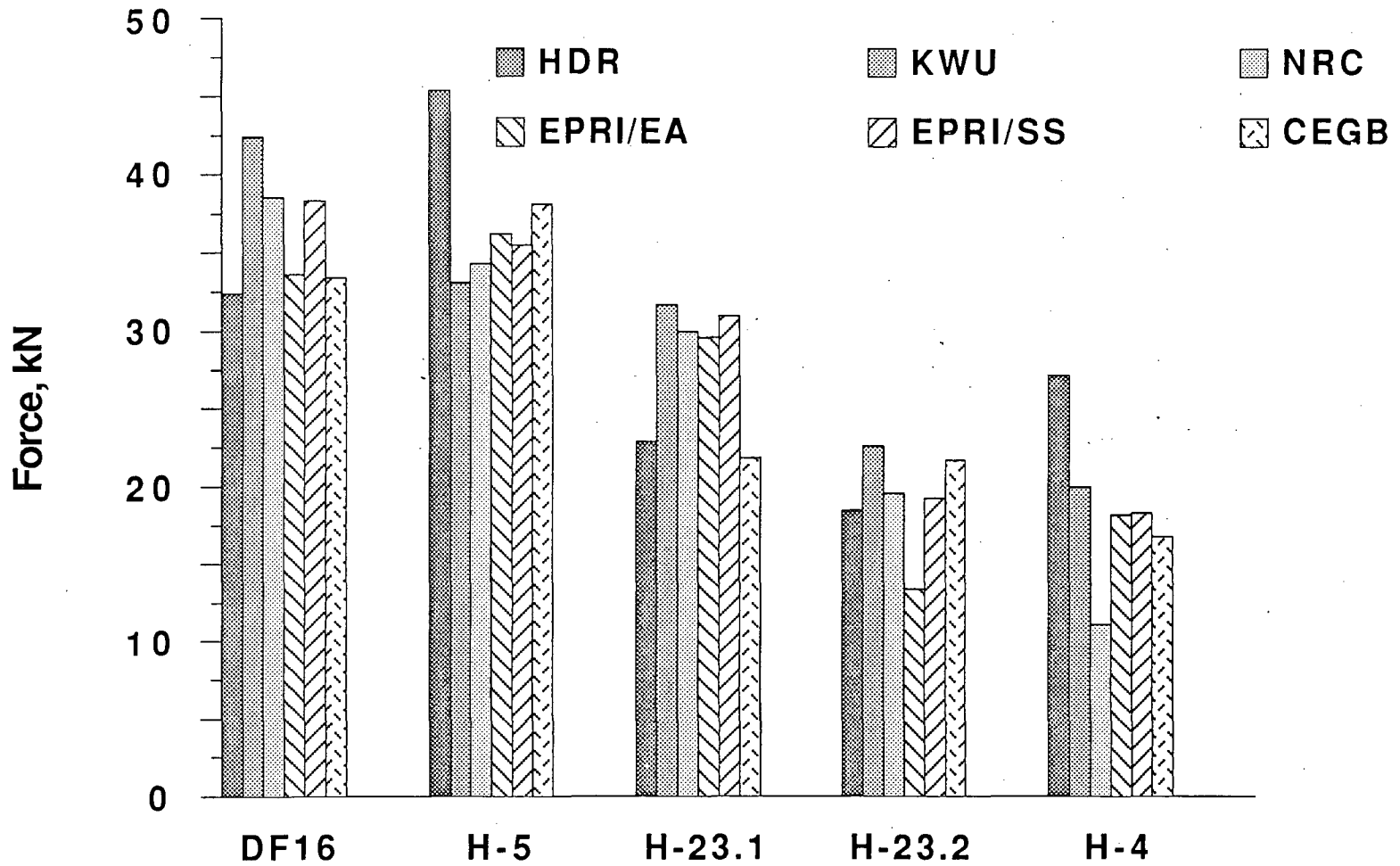
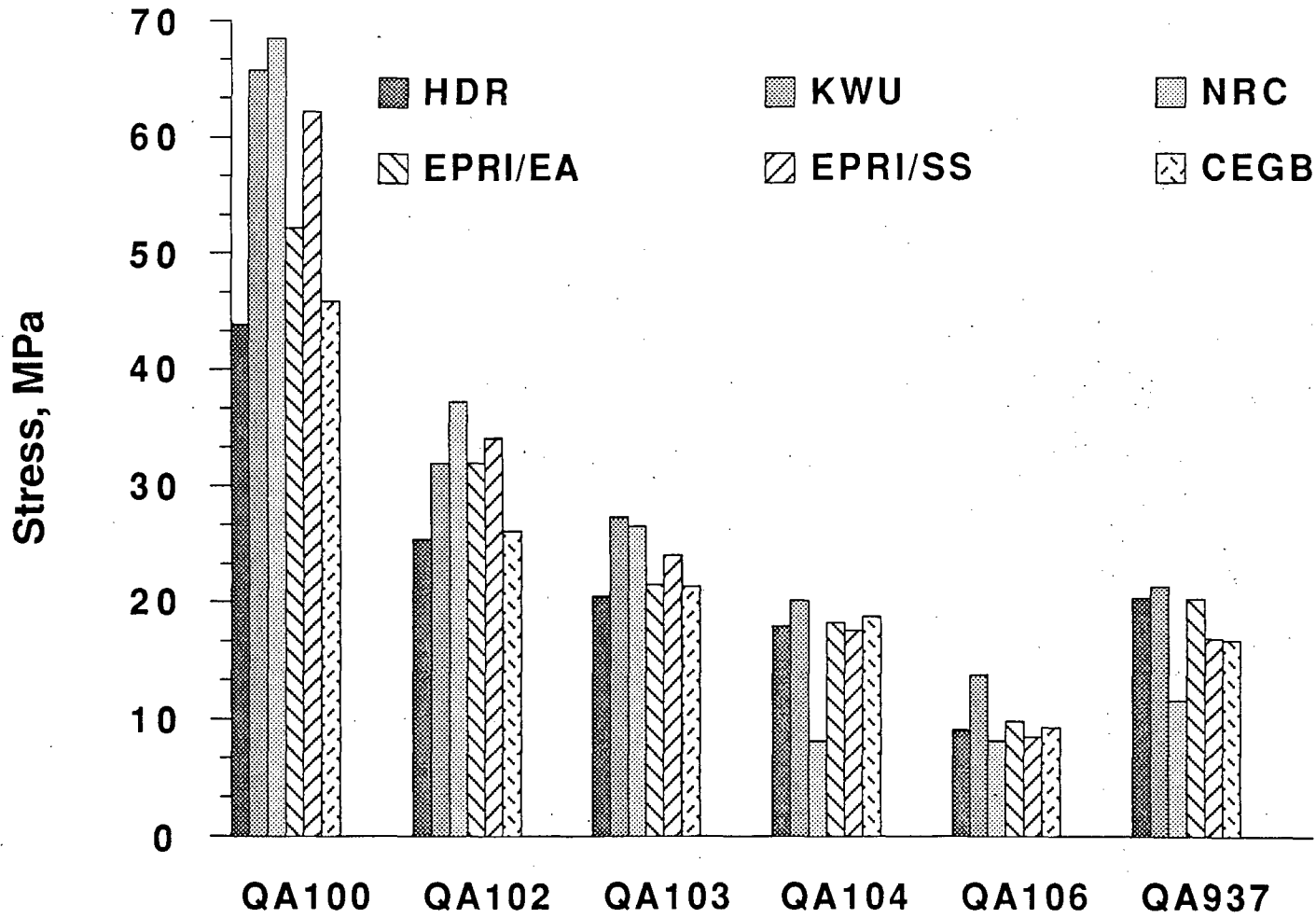


Fig.8 Comparison of Forces in the Common Struts and Actuators of Support Configurations at 100% SSE



**Fig.9 Comparison of Maximum Bending Stress in 200-mm Pipe and Valve of Support Configurations at 100% SSE**

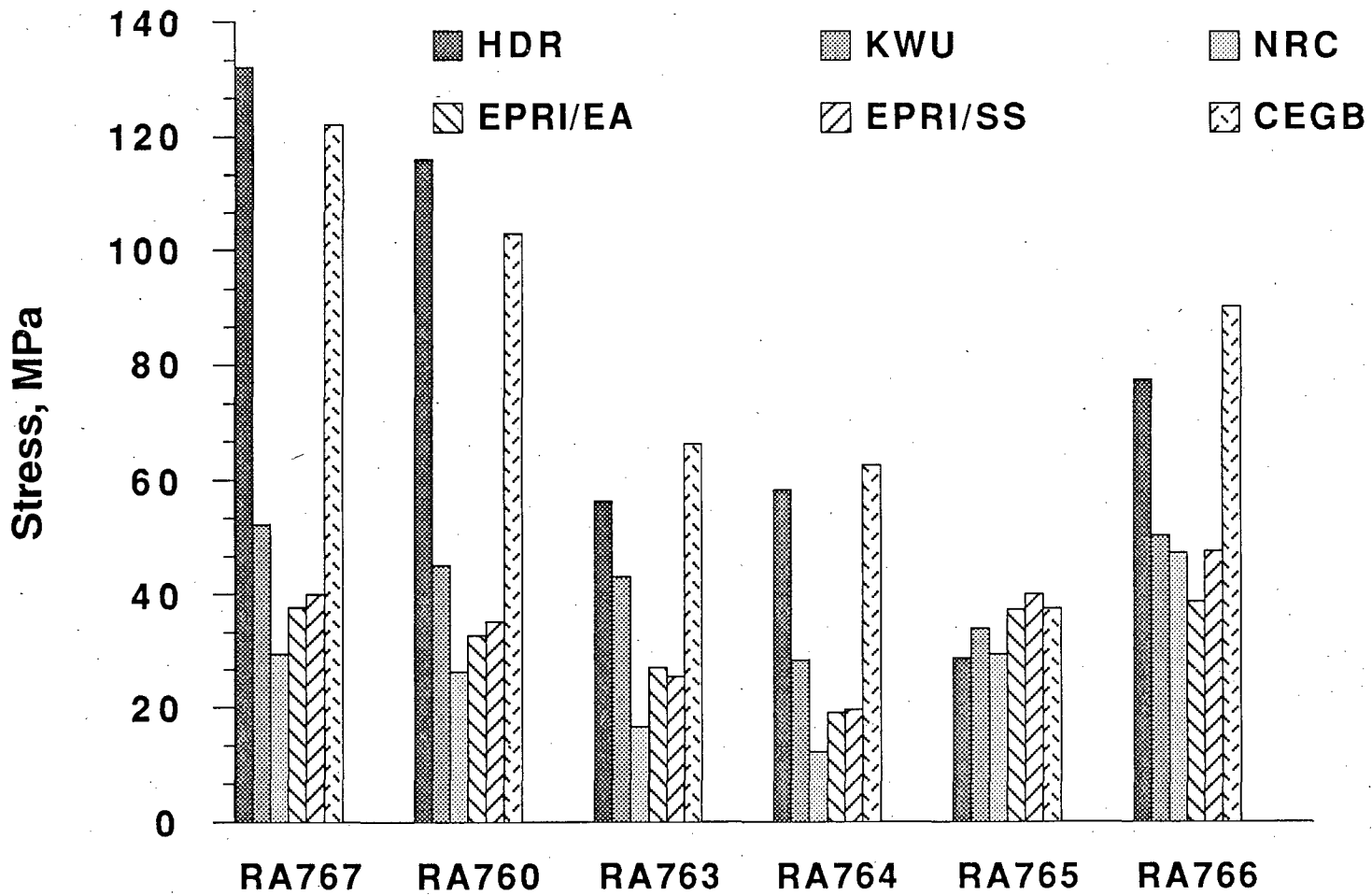


Fig.10 Comparison of Maximum Bending Stress in 100-mm Pipe of Support Configurations at 100% SSE

test. The other configurations did not experience support failures, in particular, none of the rigid struts failed in any of the tests. Since dynamic support failures may drastically alter the behavior of piping, the above-outlined events should be kept in mind when comparing the peak responses of the various support configurations.

Figure 11 presents the maximum bending stresses at location QA100, the most highly stressed straight-pipe section in the 200-mm pipe, directly adjacent to Elbow 1, next to the DF16 manifold. At excitation levels up to 300% SSE, most support configurations gave similar results, with the flexible HDR system exhibiting the lowest stresses. Installation of the bridging in the NRC system drastically lowered the response (see 200%-SSE level). The peak bending stresses for the KWU configuration increase nearly linearly, with the excitation level reaching a maximum of about 380 MPa at a load of 800% SSE. The stress level corresponding to a 0.2% offset strain for the pipe material is about 260 MPa, as indicated in Fig. 11. Thus, some plastification did occur in both the 600% and 800% tests. The plastification level (0.2% offset strain) was barely reached by the modified NRC configuration. Also in this case, the maximum bending stress increased faster than linearly with load level. However, this may be due to the aforementioned support failures. A very similar result was obtained for the maximum strains in Elbow 1.

A comparison of the maximum bending stresses at the most highly stressed straight-pipe section of the 100-mm pipe (RA767), shown in Fig. 12, reveals that the more flexible configurations (HDR and KWU) give the highest stresses at the lower load levels. Both the energy absorbers and seismic stops result in somewhat lower stresses than the snubber configuration. Again, the modification of the NRC system by bridging significantly lowers the bending stress (200% SSE). The stress increase for the KWU configuration is nearly linear with excitation level, whereas, for the modified NRC system, the stress increase with load is much steeper than linear. Again, this is probably due to support failure, particularly for the 800%-SSE case when the snubber at H7 failed and the NRC system nearly became the same support configuration as the KWU system. The peak recorded bending stress of 580 MPa for the KWU configuration exceeds the 0.2%-offset strain level by more than a factor of two. Thus, significant local plastification is to be expected at this section.

Examining the maximum forces in the rigid strut at location H10 (100 mm pipe) in Fig. 13, one can see that the more flexible KWU support configuration gives the highest values at all load levels. Again, the force varies almost linearly with excitation level. The modification of the NRC configuration reduces the strut force somewhat (200%-SSE case) and again, increases with load at a rate that is steeper than linear.

#### 4. Pretest Computational Efforts

As indicated earlier, a number of design calculations were performed prior to the SHAM experiments. Linear finite-element analyses were carried out in all cases and simplified modeling of the dynamic supports was used. Thus LBF, using the SAP5 code, performed experiment design and actuator performance calculations for the NRC, KWU, and HDR configurations. Using the NUPIPE II code, INEL designed the NRC support configuration and the actuator-stabilizing struts H4 and H23. Spectral and time history analyses were performed with typical design procedures for both the two-point excitation and actual earthquake input-loading at all supports. CEGB designed their support system with the ADLPIPE computer code. They also performed a design computation for the NRC configuration. Similar efforts were carried out by Bechtel and Cloud in the design of the EPRI/EA and EPRI/SS configurations, respectively. In both cases, in-house proprietary computer codes based on SAP and adapted to the specific support configurations were employed. Again, standard design procedures were followed, in which spectral analysis was performed with enveloping and peak-broadened input spectra.

The only true predictive calculations were carried out by ANL for the NRC support configuration. The piping analysis module of the SMACS code [5] was used in the analysis. The pseudostatic-mode approach was used in these calculations; this allowed for time-history analysis with independent support motion input. Again, the basic FE formulation was based on the SAP IV code. In addition, dead weight

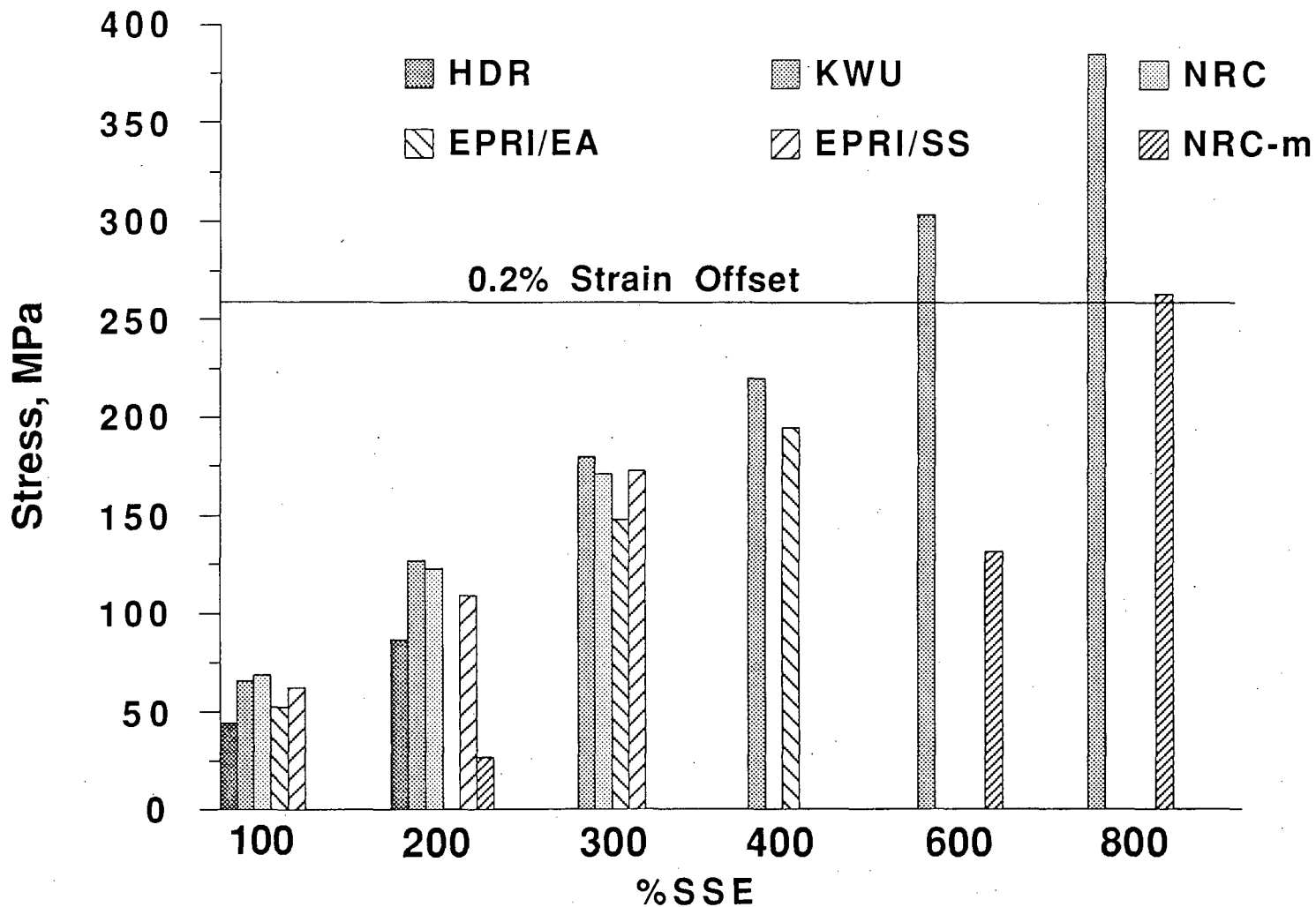


Fig.11 Maximum Bending Stress at Section QA100-200-mm Pipe  
Effect of Increasing Excitation Levels

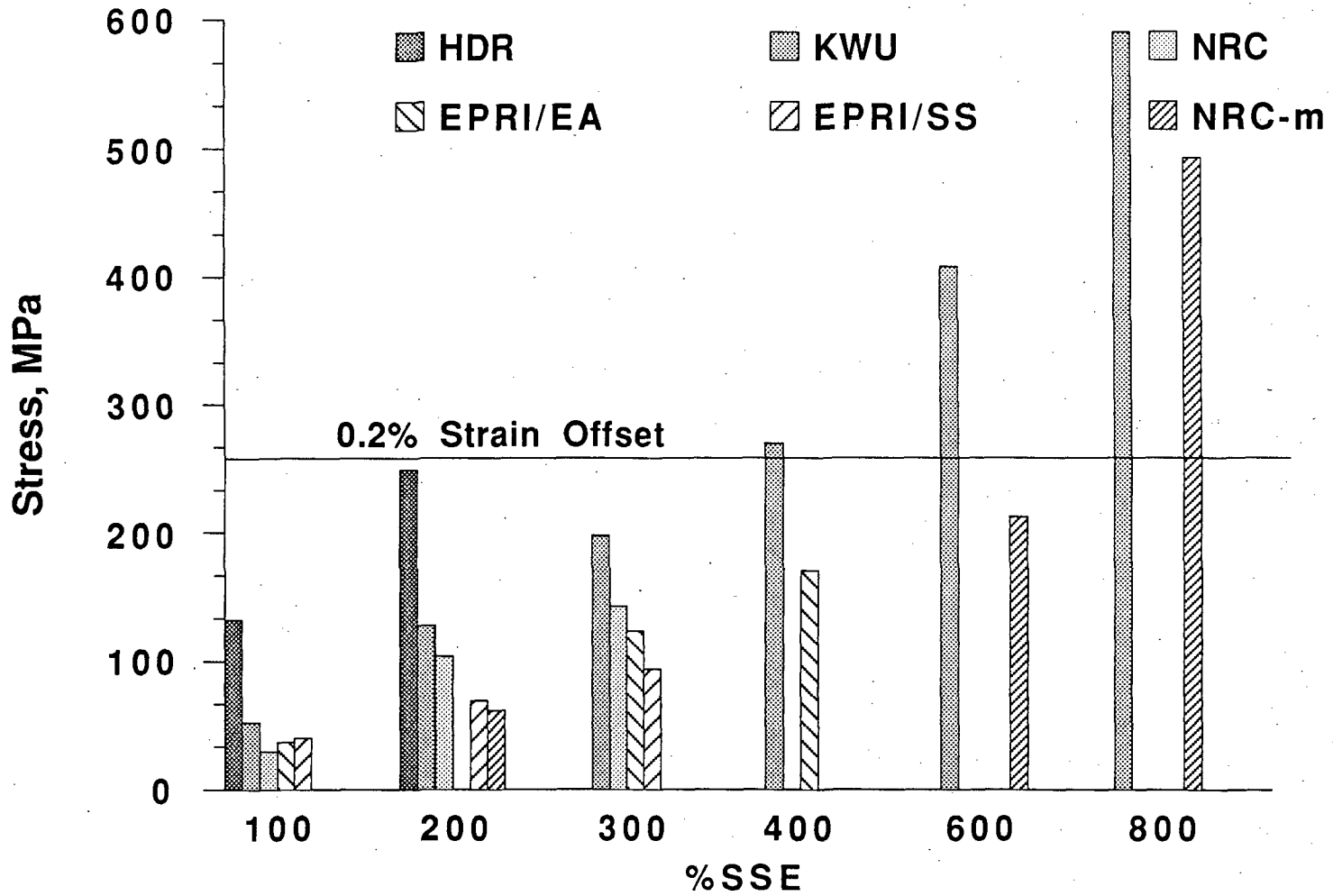


Fig.12 Maximum Bending Stress at Tee, RA767-100-mm Pipe:  
Effect of Increasing Excitation Levels

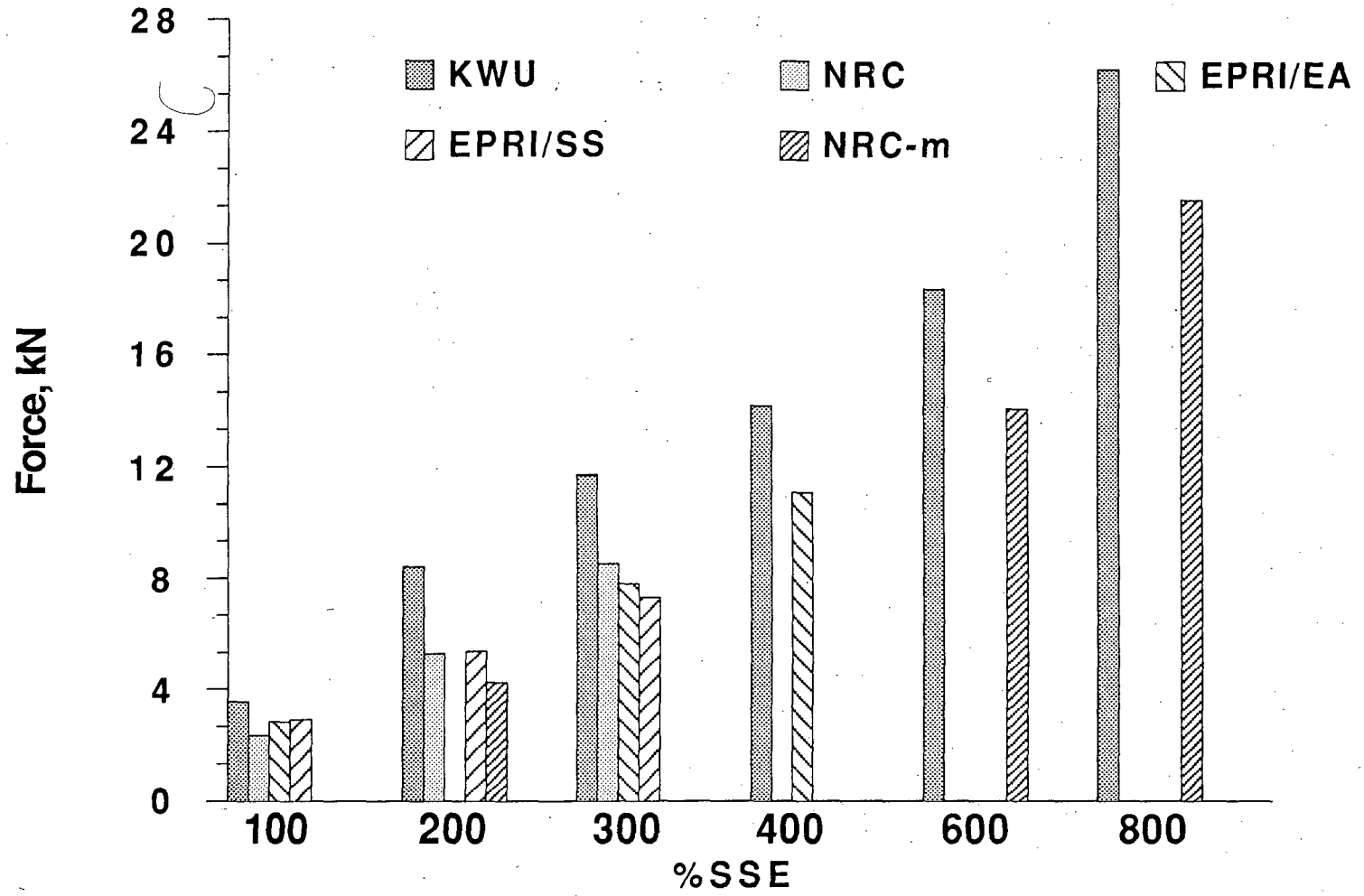


Fig.13 Maximum Forces at Hanger H10: Effect of Increasing Excitation Levels

stress and modal analyses were performed for the NRC system by means of SUPERSAP. The first eigenfrequency was found at about 5.56 Hz.

The peak response values as calculated by the SMACS piping analysis are compared with measured values in Figs. 14–16. The peak forces in the rigid struts of the NRC configuration at excitation levels of 100%–300% SSE are compared in Fig. 14, which shows that all peak forces were underpredicted, often by as much as a factor of two. A similar result was obtained for the permanent struts H4 and H23, where the discrepancies are even larger, with the measured value being 3 to 4 times larger than the calculated results.

The measured and calculated maximum snubber forces are compared in Fig. 15 for the excitation range from 100% to 300% SSE. Again, the calculation generally predicts substantially lower values than those measured. The exception is the snubber location H2, where the calculation overestimates the peak forces. The measured peak forces for the 300%–SSE excitation at locations H6 and H8, which are designated by arrows, are seen to be lower than the values obtained for the lower excitation levels of 100% and 200% SSE. Failure of these snubbers during the 300% SSE test is the most likely cause for this anomaly. Post-test inspection of the snubbers seems to confirm this supposition. Further analysis of the data is needed to investigate these failures in more detail.

Finally, Fig. 16 compares the calculated and measured peak bending stresses in the most highly stressed straight-pipe sections of the 200-mm (QA100) and 100-mm (RA767) pipe. Again, the calculations generally underestimate the stresses. Similar results are found when one examines the stresses at other locations in the pipe. While there are some locations, particularly in the 100-mm pipe, where the predictions overestimate the stresses at the 100%–SSE level; the situation in general reverses at higher loads, i.e., the calculations underpredict.

An explanation for the underprediction of the peak dynamic support forces can possibly be based on the fact that the analysis is linear and does not account for such nonlinear effects as minor impacts caused by gaps and play in the support hardware. However, the underprediction of the peak bending stresses cannot be readily explained at this time. The more conservative design calculations, performed by other investigators, exhibit some of the same deficiencies as the ANL "best estimate" prediction. Again, peak forces in many supports, and even peak stresses, are underpredicted. Much more detailed data analysis and post-test calculations are required to ascertain the precise causes for the differences between calculation and experiment. At this time, it can only be surmised that a contributing factor to these differences could be the large deviations of the experimental excitations (histories, spectra) from the ideal excitations assumed in the calculations. In particular, the differences in the excitations at DF16 and H5, observed in the tests, could be of significance.

## 5. Conclusions

The results given in the preceding sections are very preliminary and incomplete. Hence, it is not possible to present any final, quantitative and conclusive evaluations of either the support configurations, seismic margins, or pipe behavior. However, based on the total experimental performance of the SHAM test series, the following preliminary qualitative observations can be made:

- It appears that stiff support systems with snubbers and struts, such as the NRC configuration, offer no particular advantages over systems with snubber replacement devices (EPRI/EA and EPRI/SS) or reasonably compliant systems (KWU).
- Long, unsupported pipe runs may lead to excessive displacements and high stresses under seismic loading, as evidenced by the behavior of the HDR configuration.
- In general, failures of dynamic supports (in particular, snubbers) and of anchorages occur only at load levels that substantially exceed the design capacity.

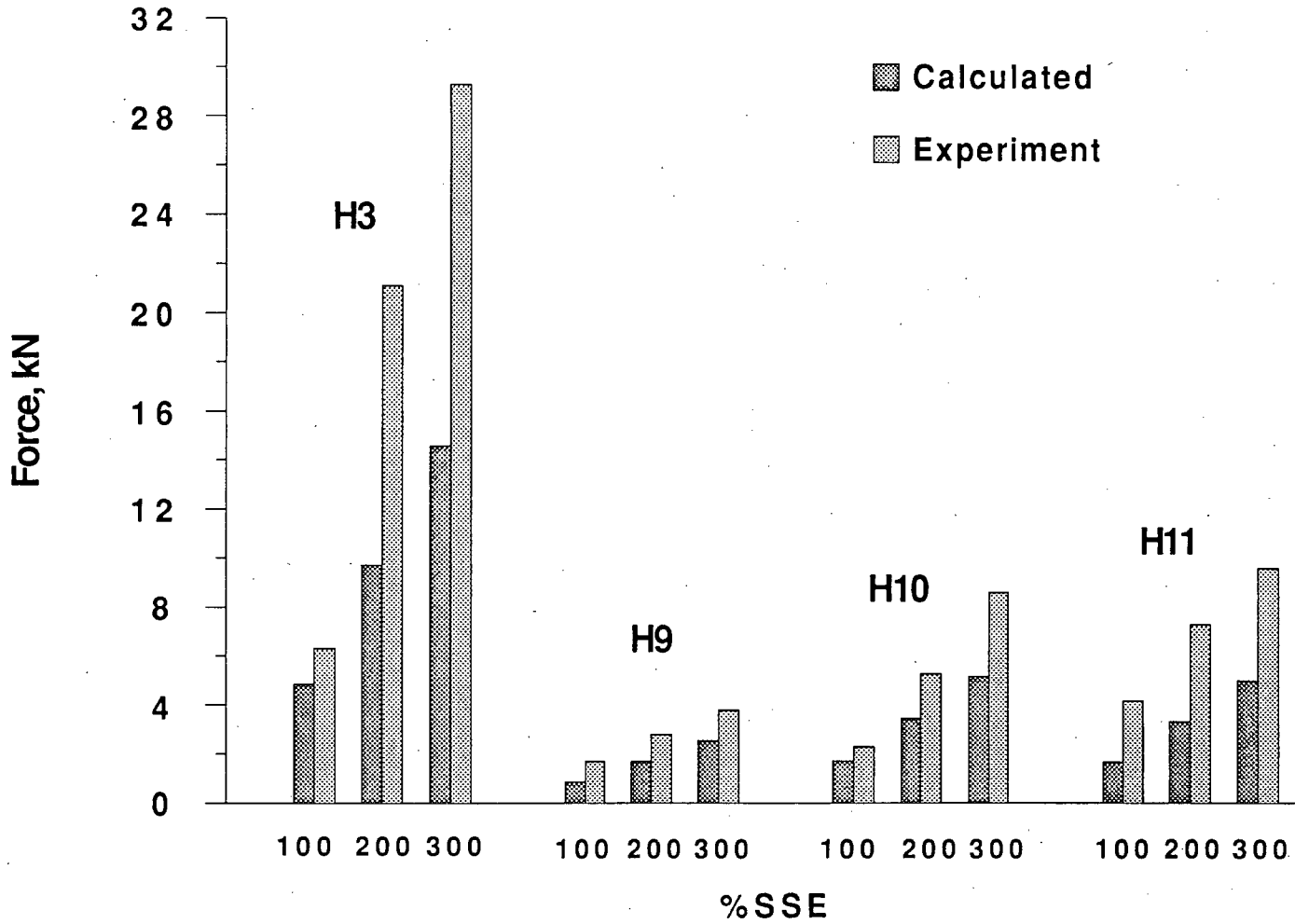


Fig.14 Calculated and Experimental Maximum Strut Forces:  
Effect of Excitation Level – NRC Configuration

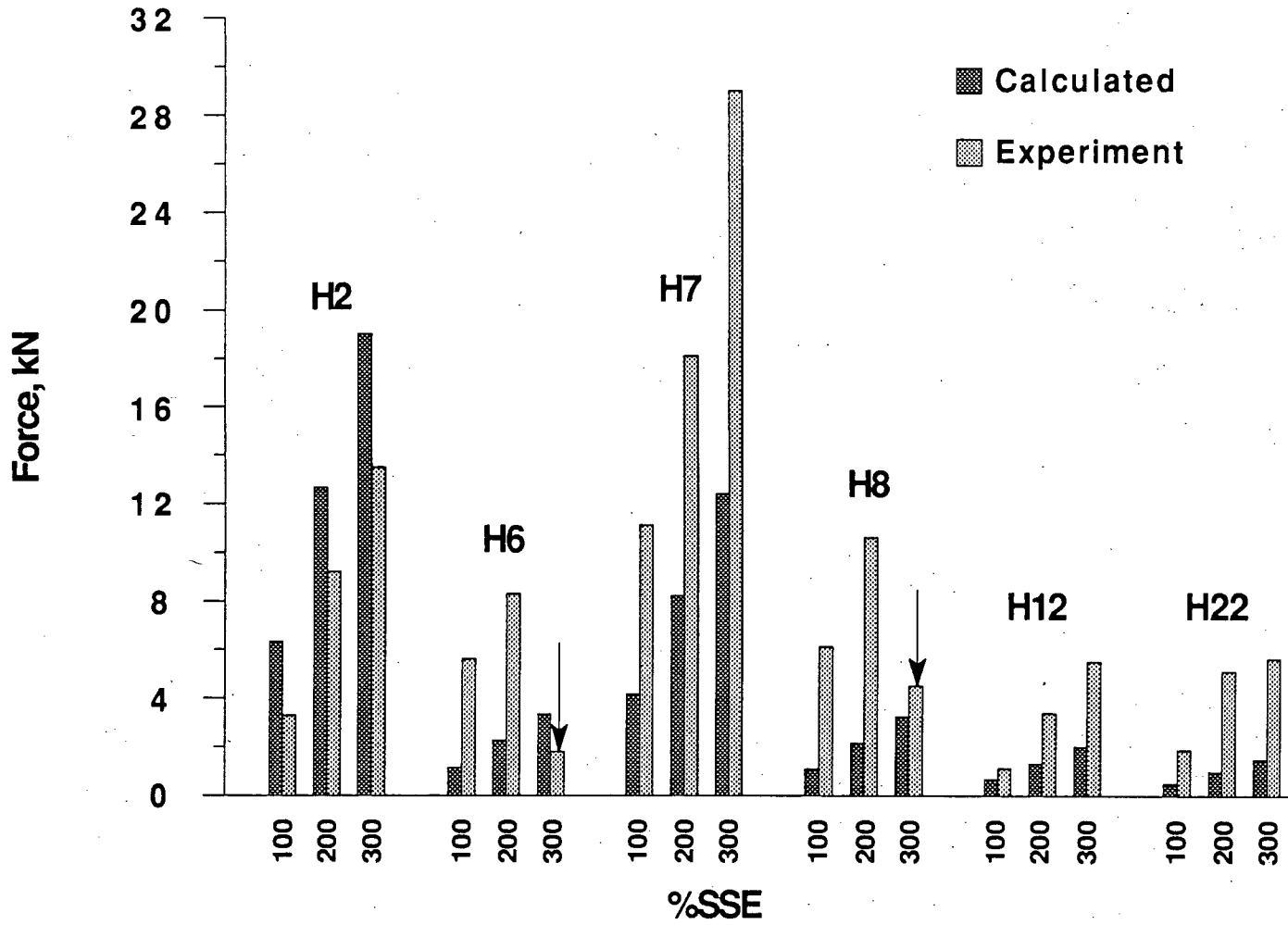


Fig.15 Calculated and Experimental Maximum Snubber Forces:  
Effect of Excitation Level – NRC Configuration

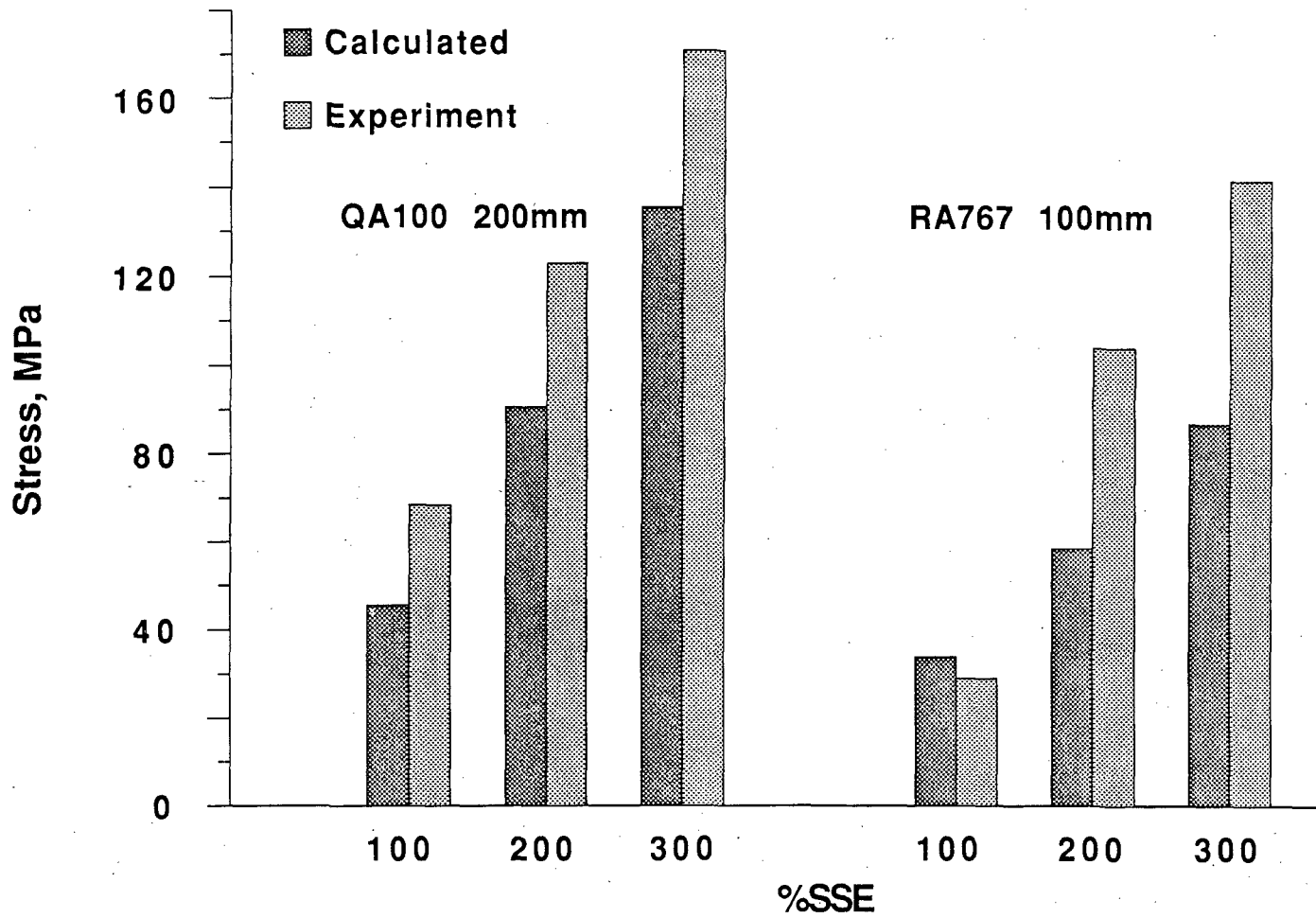


Fig.16 Calculated and Experimental Maximum Bending Stress:  
Effect of Excitation Level – NRC Configuration

- Pipe strains and deformations at excitation levels of up to 300% SSE remain quite small (about 0.3%) and even at extreme excitation levels of 800% SSE are quite tolerable (about 1.0%). This is true in spite of multiple dynamic support failures.
- Pipe failure under typical seismic loading histories, even at extreme load levels (800% SSE) and in spite of multiple serial support failures, is highly unlikely. It appears that significant strain ratcheting is only feasible by repeated high-load cycling such as may be produced by sine burst loading.
- Linear piping analysis appears to substantially underpredict the peak loads in dynamic supports, and is not necessarily conservative in estimating pipe stresses.

## References

1. L. Malcher and C. A. Kot, "HDR Phase II Vibrational Experiments," Proceedings of the U.S. NRC 14th Water Reactor Safety Information Meeting, NUREG/CP-0082, Vol. 3, pp. 295-312, NBS-Gaithersburg, MD, October 27-31, 1986.
2. C. A. Kot, L. Malcher, and H. Steinhilber, "Vibrational Experiments at the HDR: SHAG Results and Planning for SHAM," Proceedings of the U.S. NRC 15th Water Reactor Safety Information Meeting, NUREG/CP-0091, Vol. 3, pp. 251-277, NBS-Gaithersburg, MD, October 26-29, 1987.
3. L. Malcher, H. Steinhilber, and D. Schrammel, "Design Report - Servohydraulic Excitation of Mechanical Equipment, HDR Test Group SHAM, vs. No. T41," PHDR Work Report No. 4.338/88, March 1988.
4. H. H. Wenzel, L. Löhr, and R. Grimm, "Versuchsprotokoll Servohydraulische Anregung Maschinentchnik, Versuchsgruppe SHAM, Versuch T41," Vol. 1, PHDR-Arbeitsbericht Nr. 4.345/88, April 20 1988 to May 27, 1988.
5. J. J. Johnson, et al., Seismic Safety Margins Research Program, Phase I Final Report, "SMACS, Seismic Methodology Analysis Chain with Statistics (Project VIII)," NUREG/CR-2015, Vol. 9, UCRL-53021, 1981.

EVALUATION OF AGED CONCRETE STRUCTURES FOR CONTINUED SERVICE IN  
NUCLEAR POWER PLANTS

D. J. Naus and M. F. Marchbanks  
Oak Ridge National Laboratory (ORNL)  
P.O. Box 2009  
Oak Ridge, Tennessee 37831-8056

and

E. G. Arndt  
U.S. Nuclear Regulatory Commission  
Mail Stop NL/S-302  
Washington, DC 20555

ABSTRACT

Results are summarized of a study on concrete component aging and its significance relative to continued service of nuclear power plants (NPPs) beyond the initial period for which they were granted operating licenses. Progress is presented of a second study being conducted to identify and provide acceptance criteria for structural safety issues which the USNRC staff will need to address when applications are submitted for continued service of NPPs. Major activities under this program include: development of a materials property data base, establishment of structural component assessment and repair procedures, and development of a methodology for determination of structural reliability.

BACKGROUND

As of December 1987, there were ~119 nuclear power plants (NPPs) in the United States (US) either under construction, operating at low-to-full power, or awaiting an operating license. Together these units have a net generating capacity of ~110 GW(e). Presently nuclear power provides ~17% of the electricity in the US with the total expected to increase to ~20% in the not-too-distant future. Despite the increasing role of nuclear power in electricity production, the current trend is toward completion (or cancellation) of plants that are under construction. No nuclear plants have been ordered in the US since 1978. In fact, about 90 plants have been cancelled or indefinitely deferred. Therefore, assuming no life extension of present facilities, a potential loss of electrical generating capacity in excess of 75 GW could occur during the time period 2005 to 2020 due to the expiration of operating licenses (usually 40 years after issuance of the construction permit). A

---

\*Research sponsored by the Office of Nuclear Regulatory Research, U.S. Nuclear Regulatory Commission under Interagency Agreement 1886-8084-5B with the U.S. Department of Energy under Contract DE-AC05-84OR21400 with Martin Marietta Energy Systems, Inc.

"The submitted manuscript has been authored by a contractor of the U.S. Government under contract No. DE-AC05-84OR21400. Accordingly, the U.S. Government retains a nonexclusive, royalty-free license to publish or reproduce the published form of this contribution, or allow others to do so, for U.S. Government purposes."

potential timely and cost-effective solution is to extend the service life of the existing NPPs (Ref. 1 estimates plant life extension could save US electricity consumers about \$390B in 1986 \$'s). Since the concrete components provide a vital safety function in these facilities, any continued service considerations must include an in-depth assessment of the safety-related concrete structures.

## INTRODUCTION

Under the USNRC Nuclear Plant Aging Research (NPAR) Program,<sup>2</sup> a study was conducted to extend upon the work which was performed under an Electric Power Research Institute (EPRI) sponsored program at ORNL on concrete material systems in nuclear safety-related structures.<sup>3</sup> This study provided recommendations that would lead to subsequent development of a methodology for assessing and predicting the effects of aging on the performance of concrete-based materials and structures in NPPs. The approach followed was in accordance with the NPAR Program strategy to evaluate the long-term environmental challenges to light-water reactor (LWR) civil structures and consisted of six parts: (1) description of primary safety-related concrete components in LWRs; (2) review of the performance of concrete components in both non-nuclear and nuclear applications; (3) identification and discussion of potential environmental stressors and aging factors to which safety-related concrete structures may be subjected in an LWR environment; (4) review of the current state-of-the-art for inservice inspection, surveillance, and detection of concrete aging phenomena and structural adequacy; (5) discussion of remedial measures for the repair, replacement, or retrofitting of degraded concrete components; and (6) remarks concerning correlations between damage assessment and continued service evaluations. Results of this study were then utilized to help formulate the Structural Aging (SAG) Program being conducted at ORNL to provide the USNRC with structural safety issues and acceptance criteria for use in NPP evaluations for continued service.

## DESCRIPTION OF SAFETY-RELATED CONCRETE COMPONENTS IN LWRs

A myriad of concrete-based civil structures are part of an LWR system. Although the particular components may vary somewhat according to the selection of the nuclear steam supply system (NSSS) and containment concept, the seismic Category I structures generally fall into four primary categories: reactor containment buildings, containment base mats, biological shield walls and buildings, and auxiliary (balance-of-plant) buildings.

### Reactor Containment Building

The containment building is one of the most important structures of a NPP since it provides one of the final barriers against the release of radioactive fission products to the environment under postulated design basis accident

(DBA) conditions. Containment designs are based on the pressure and temperature loadings associated with a loss-of-coolant accident (LOCA), resulting from a double-ended rupture of the largest size pipe in the reactor coolant system. The containment is also designed to retain its integrity under low probability ( $< 10^{-4}$ ) environmental loadings. Additionally, the containment is required to provide biological shielding under both normal and accident conditions and to protect the internal equipment from external missiles.

Prior to 1965, installed capacity of nuclear power plants in the 50 to 400 MW(e) range utilized steel containments of various configurations. Their designs conformed to the ASME "Unfired Pressure Vessel Code" (Ref. 4), with the shells fabricated from welded steel plates up to 38 mm in thickness. Support for the reactor vessel and shielding requirements was provided by reinforced concrete. As the plant sizes were increased to 800 MW(e), shielding requirements increased, and the practical limit for fabrication of steel containments without requiring postweld heat treatment were exceeded. At this time, it also seemed prudent to combine the containment and shielding functions into a composite steel-lined reinforced concrete structure.

The first primary reinforced containments (RCCs) were built in the 1960's and typically consisted of a ~1.4-m-thick cylindrical reinforced concrete wall with an ~1.1-m-thick hemispherical dome and flat base slab. Grade 60 (Nos. 11, 14, and 18) steel reinforcing bars were normally utilized to resist hoop, axial, seismic, and shear loadings. Leak tightness was provided by a steel liner, which generally ranged from 6.35 to 12.7 mm in thickness depending on the location. Concrete compressive strengths generally ranged from 20.7 to 34.5 MPa. Later concrete was partially prestressed in the vertical direction only with mechanically spliced reinforcing steel in the hoop direction and dome.

Fully prestressed concrete containments (PCCs) were first built in the late 1960's. The PCCs came into use because: the possibility existed of improved optimization in selection of vessel geometry, fully prestressed concrete would remain in compression (crack free) under postulated incident conditions, and possibilities existed for reductions in costs and construction scheduling. Design improvements have progressed to a third-generation PCC which includes a hemispherical dome and increased capacity prestressing tendons; i.e., the number of buttresses and prestressing tendons have been reduced and the ring girder at the intersection of the dome and wall has been eliminated. Leak tightness is still provided by a steel liner. Steel reinforcing and concrete materials are essentially the same as those used for RCCs.

Table 1 summarizes the containment types for US power reactors and Figures 1 and 2 present schematics of typical BWR and PWR containments.

Table 1. Containment Summary

| Plant type | Containment designation | Steel | Reinforced concrete | Post-Tensioned concrete | Total |
|------------|-------------------------|-------|---------------------|-------------------------|-------|
| BWR        | Pre-Mark                | 1     | -                   | -                       | 1     |
|            | Mark I                  | 22    | 2                   | -                       | 24    |
|            | Mark II                 | 1     | 6                   | 2                       | 9     |
|            | Mark III                | 2     | 2                   | -                       | 4     |
| PWR        | Large Dry               | 9     | 11                  | 42                      | 62    |
|            | Ice Condenser           | 8     | 2                   | -                       | 10    |
|            | Sub-Atmospheric         | -     | 8                   | -                       | 8     |
| HTGR       | Primary                 | -     | -                   | 1                       | 1     |
| TOTAL      |                         | 43    | 31                  | 45                      | 119   |

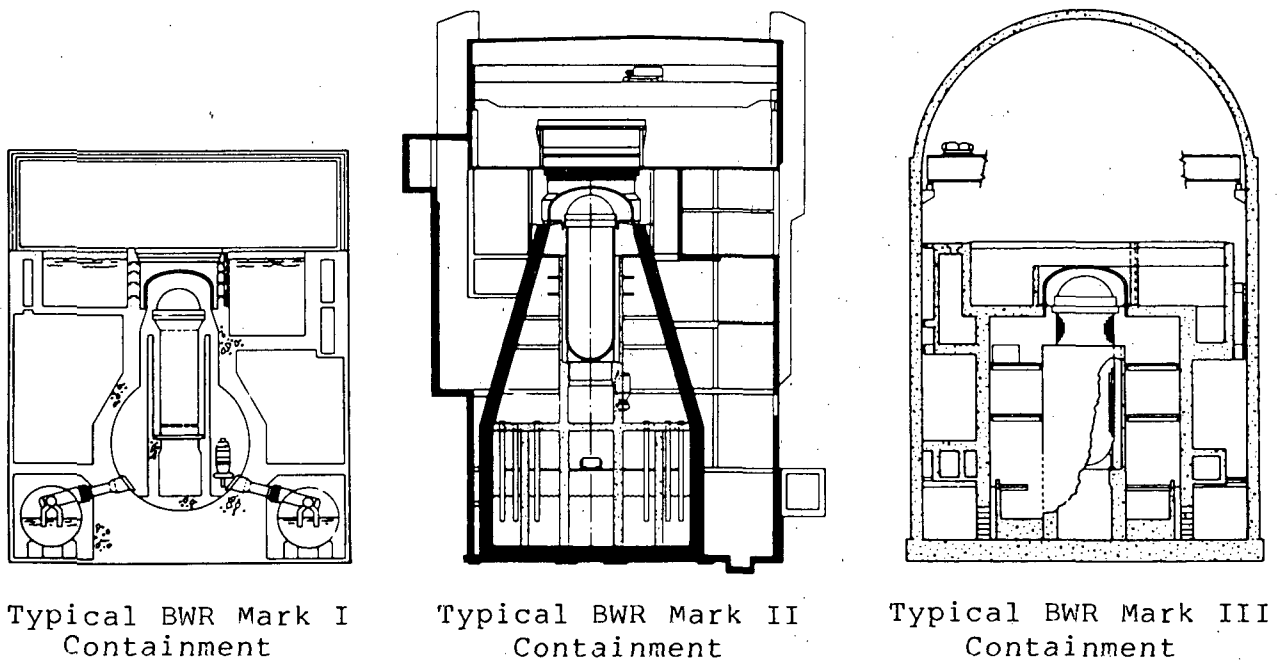
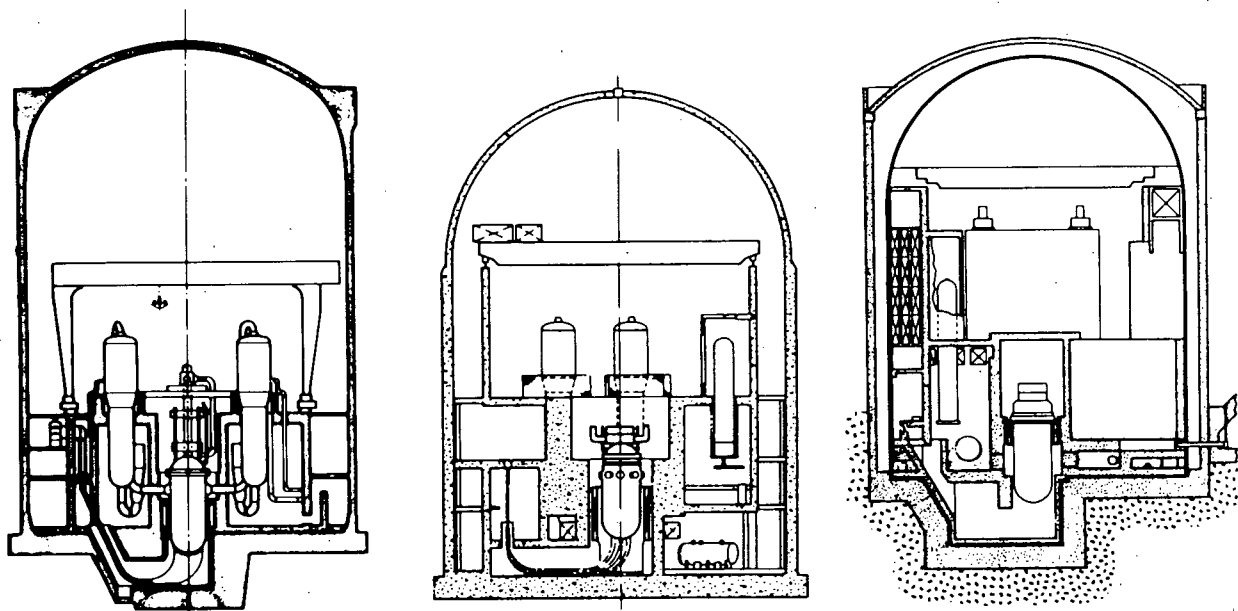


Fig. 1. Schematics of typical BWR containments.



Large Dry Containment

Sub-Atmospheric

Ice Condenser

Fig. 2. Schematics of typical PWR containments.

#### Containment Base Mats

Base mats for reactor containment buildings are fabricated of reinforced concrete. Depending on the siting conditions, the base mats may be founded on rock, soil or piles. Thickness requirements are controlled by the concrete shear capacity, maximum allowable compressive strength of the concrete, maximum allowable steel area, and allowable soil-bearing area. In general, base mats are circular in design with diameters which may be  $> 45$  m and thicknesses which range from  $\sim 2.6$  m to 6.0 m. Concrete and steel reinforcement materials for the base mats are essentially the same as used for the RCCs.

#### Biological Shield Walls and Buildings

Biological shield walls for commercial reactors are generally fabricated from standard weight reinforced concrete. Thicknesses of the shield walls typically range from  $\sim 1.5$  to 4 m, and the walls can either support all or part of the reactor pressure vessel weight. Steel reinforcement is provided to take flexural and seismic loads that would place portions of the wall in tension. Concretes having compressive strengths from 27.6 to 41.4 MPa are normally used for shield fabrication.

A shield building, or secondary containment, is a medium leakage reinforced concrete structure that surrounds the steel containment vessel. Typically the

building is a reinforced concrete cylinder (wall thickness ~0.9 m) with a base slab and spherical dome (dome thickness ~0.6 m.) Concrete and steel reinforcement materials are essentially the same as for the RCCs.

### Auxiliary Buildings

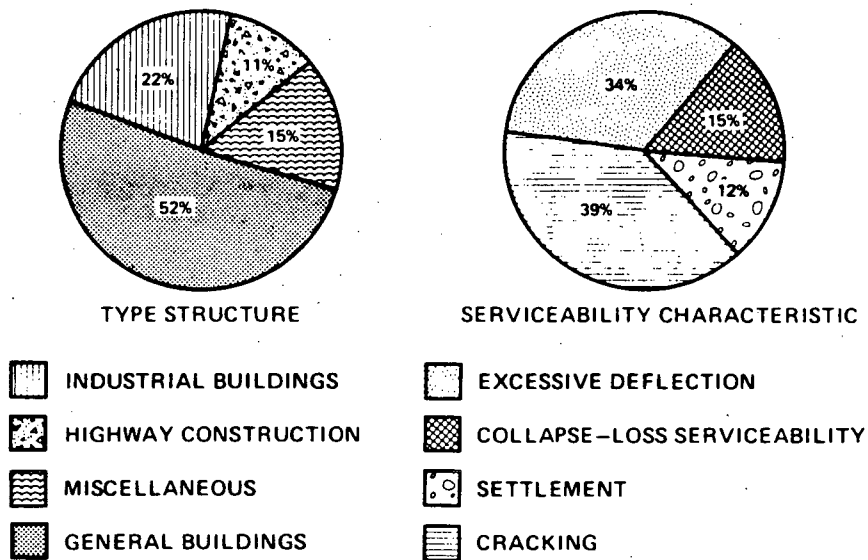
Auxiliary buildings, or balance-of-plant structures, include functional units such as the diesel generator building, control room or building, radwaste facility, turbine generator building, and circulating water structures. In general, these structures are box-shaped, shear-wall buildings constructed of reinforced concrete, but they may contain steel beams that support the floor slabs. Basic structural components include: exterior walls (~0.45 to 1.2 m thickness) which protect safety class equipment and piping from external events; internal walls (~0.3 to 1.2 m thickness) which resist internally generated loads, support gravity loads, and provide radiation shielding where required; base slabs (~1.8 to 8.2 m thickness); roof slabs (~0.46 m thickness); floor slabs (~0.3 to 0.9 m thickness); and columns which provide intermediate supports for floor slabs, and primary supports where walls are not available or unusually heavy floor loads occur.

### PERFORMANCE OF CONCRETE COMPONENTS IN BOTH NON-NUCLEAR AND NUCLEAR APPLICATIONS

Concrete in various forms has been utilized as a construction material for several thousand years. When fabricated with close attention to the factors related to the production of good concrete, the concrete will have practically infinite durability unless subjected to detrimental environmental influences. Problems do occur, however, that can result in concrete distress. To trend the type of problems that have been experienced with concrete materials and structures, the literature was reviewed with respect to performance of both general civil engineering structures and nuclear power plant applications.

### General Civil Engineering Structures

Extensive reviews of incidences of errors in concrete structures in North America (277 cases) and Europe (~800 cases) are reported in Refs. 5 and 6. Error profiles developed from these studies are presented in Fig. 3. From these results it was concluded that few structures actually fail in use, and that the errors which occurred were generally the result of either construction problems (improper rebar placement, poor concreting) or design problems (improper consideration of shrinkage or temperature effects, detailing). Also, most of the errors could have been prevented by improved quality assurance procedures. Although not aging related, if not detected, some of these problems could have increased with time.



MOST ERRORS COULD HAVE BEEN PREVENTED BY ADDITIONAL CHECKING

Fig. 3. Error profiles for concrete civil structures.

### Nuclear Power Plant Applications

A review of the performance of concrete components in NPPs was conducted by examining the open literature and several data sources: the nuclear power plant reliability data system, nuclear power experience, construction deficiency reports, periodicals, licensee event reports, and plant docket files. The results of this survey are summarized in Fig. 4. Although the vast majority of the problems detected did not present a threat to public safety or jeopardize the structural integrity of a particular component, a few incidences were identified that if not discovered and repaired could potentially have had serious consequences. These incidences were all related to concrete containments and involved two dome delaminations (Turkey Point 3 and Crystal River Unit 3), voids under tendon bearing plates (Calvert Cliffs), anchor head failures (Bellefonte, Byron, and Farley Units 1 and 2), and prestressing tendon wire corrosion (Fort St. Vrain). With the possible exceptions of the anchor head failures at Farley, which occurred about 8 years after posttensioning, and the prestressing tendon wire corrosion at Fort St. Vrain, which was discovered during a scheduled ISI 5 years after start of commercial operation, the errors were detected either during the construction phase or early in the structure's life, were of no structural significance or "easily" repaired, and were nonaging related.

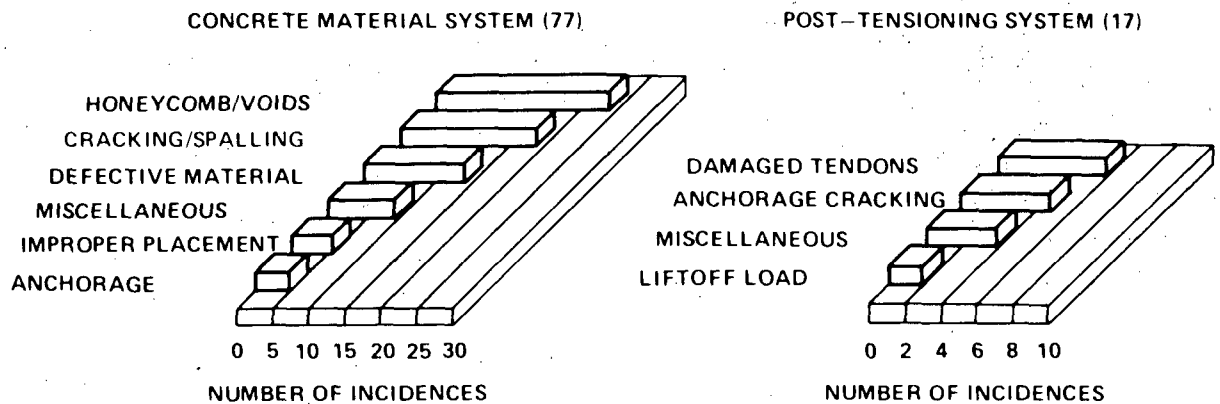


Fig. 4. Distribution of LWR concrete component problem areas.

#### POTENTIAL ENVIRONMENTAL STRESSORS AND AGING FACTORS

Nuclear power plants are generally designed for a plant life of about 40 years, which, with an anticipated availability factor of 80 to 90%, yields 32 to 36 full-power years. Over this period of time, changes in the concrete, reinforcing steel and prestressing steel material properties will occur in all likelihood as a result of aging or environmental effects. Concrete in many structures can suffer undesirable degrees of change with time, but these changes do not have to be detrimental to the point that the structure has deteriorated and is unable to meet its functional and performance requirements.

Mechanisms (factors) that, under unfavorable conditions, can produce premature concrete deterioration include: (1) freezing-thawing and wetting-drying, (2) aggressive chemical and groundwater exposure (sulfates, chlorides, leaching), (3) abrasion, (4) corrosion of embedments, (5) chemical reaction of aggregates (alkali-, cement- or carbonate-aggregate reactions), (6) vibrations, and (7) miscellaneous (unsound cement, shrinkage cracking). In addition, for concrete components utilized in nuclear-safety-related structures, an additional factor can be added, extreme environmental exposure (e.g., elevated temperature and irradiation). Table 2 summarizes predominant environmental stressors and the important material parameters affected for the concrete safety-related structures in LWR plants. Additional information on deterioration mechanisms and their potential effects on concrete materials are contained in Refs. 7-10.

#### DETECTION OF AGING OR ENVIRONMENTAL EFFECTS

Since the ability of a concrete component to meet its functional and performance requirements over an extended period of time is dependent on the durability of its constituents, techniques for the detection of concrete

Table 2. Predominant Environmental Stressors to Which Safety-Related Components in a LWR may be Subjected

| Structural subsystem               | Material components | Important material parameters <sup>a</sup> | Predominant environmental stressors <sup>b</sup> |
|------------------------------------|---------------------|--------------------------------------------|--------------------------------------------------|
| Prestressed concrete containment   | Concrete            | $f_c, E_c, \nu, CR$                        | D, L                                             |
|                                    | Rebars              | $f_y, E_s, \sigma_u, e$                    | C, L                                             |
|                                    | Prestressing        | $f_y, E_s, \sigma_u, R$                    | C, L                                             |
| Reinforced concrete containment    | Concrete            | $f_c, E_c, \nu$                            | D, L                                             |
|                                    | Rebars              | $f_y, E_s, \sigma_u, e$                    | C, L                                             |
| Containment base mat               | Concrete            | $f_c, E_c, \nu$                            | D, L, S                                          |
|                                    | Rebars              | $f_y, E_s, \sigma_u, e$                    | C, L                                             |
| Biological shield wall or building | Concrete            | $f_c, E_c, \nu$                            | T, I, L                                          |
|                                    | Rebars              | $f_y, E_s, \sigma_u, e$                    | T, I, L                                          |
|                                    | Prestressing        | $f_y, E_s, \sigma_u$                       | T, I, L                                          |
| Auxiliary buildings                | Concrete            | $f_c, E_c, \nu$                            | D, L                                             |
|                                    | Rebars              | $f_y, E_s, \sigma_u, e$                    | C, L                                             |

<sup>a</sup> $f_c$  = concrete compressive strength  
 $E$  = modulus of elasticity  
 $\nu$  = Poisson's ratio  
 $CR$  = concrete creep  
 $\sigma_u$  = ultimate strength  
 $e$  = elongation or ductility  
 $R$  = prestressing relaxation  
 $f_y$  = steel yield strength

<sup>b</sup> $T$  = temperature  
 $D$  = durability  
 $I$  = irradiation  
 $C$  = corrosion  
 $L$  = external, internal, or dead loads  
 $S$  = subgrade settlement

component degradation should address evaluation of the concrete, mild steel reinforcing, prestressing system, and anchorage embedments. Concrete cracking, voids and delaminations can be detected by visual inspections, non-destructive testing (ultrasonic and stress wave, acoustic impact, radiography, penetrating radar, thermal mapping), and core examination. In-situ concrete strength determinations are through either direct (core tests) or indirect techniques (surface hardness, rebound, penetration, pullout resistance, breakoff resistance, and ultrasonic pulse velocity). The primary distress to

which mild steel reinforcement could be subjected would be corrosive attack. Techniques available for corrosion monitoring and inspection of steel in concrete include visual, mechanical and ultrasonic tests, core sampling in conjunction with chemical and physical tests, potential and thermal mapping, and rate of corrosion probes. The condition and functional capability of unbonded posttensioning systems is assessed through selection of a random, representative sample of tendons; examination of the anchorage assembly hardware of the selected tendons, determination of the stress level in each sample tendon, examination of previously stressed wires or strands from one tendon of each type in the structure, and an analysis of a grease sample from each tendon in the surveillance. The present basis for conducting tendon inspections is presented in RG 1.35, "Inservice Inspections of UngROUTED Tendons in Prestressed Concrete Containments" and RG 1.35.1, "Determining Prestressing Forces for Inspection of Prestressed Concrete Containments." Failure of an embedment will generally occur as a result of either improper installation or deterioration of the concrete within which it is embedded. A combination of visual examinations and mechanical tests is used to evaluate the general condition of an embedment.

Table 3 summarizes primary and secondary nondestructive evaluation techniques for inspection of concrete components. Quantitative interpretation of the results obtained from many of these methods can be difficult, however, due to the requirement for correlation curves. Also, many of the methods only make surface determinations of concrete properties which can be quite different from internal properties, particularly where a component may be several meters thick. In addition, none of the techniques provide rate effect data which can be used for continued service considerations.

#### REMEDIAL MEASURES

Objectives of remedial work are to restore the component's structural integrity, to arrest the mechanism producing distress, and to ensure, as far as possible, that the cause of distress will not recur. Basic components of a program to meet these objectives include: diagnosis (damage evaluation), prognosis (can repair be made and is it economical), scheduling (priority assignments), method selection (depends on nature of distress, adaptability of proposed method, environment, and costs), preparation (function of extent and type of distress), and application.<sup>11</sup>

Typical types of distress that occur in LWR facilities include cracking, spalling or delamination, nonvisible voids, and fracturing or shattering. Although a wide variety of materials are available for the repair or maintenance of concrete exhibiting distress, they generally include one or more of the following materials: epoxy resins, shotcrete, preplaced aggregate concrete, epoxy ceramic foams, replacement mortar or concrete, wedge anchors and additional reinforcement, and miscellaneous sealant materials.<sup>12</sup> Selection of the technique for repair of a concrete structure depends to a large degree on

Table 3. Nondestructive Evaluation Methods for Inspection of Concrete Materials

| Material and characteristic | Available methods of detection                                                     |                                                         |
|-----------------------------|------------------------------------------------------------------------------------|---------------------------------------------------------|
|                             | Primary                                                                            | Secondary                                               |
| Concrete                    |                                                                                    |                                                         |
| General quality             | Ultrasonic pulse velocity<br>Rebound hammer<br>Penetrating probe                   | Ultrasonic pulse echo<br>Gamma radiography <sup>a</sup> |
| Cracking/voids              | Visual inspection<br>Ultrasonic pulse<br>Acoustic impact                           | Ultrasonic pulse echo<br>Gamma radiography <sup>a</sup> |
| Strength                    | Penetrating probe<br>Rebound hammer<br>Pullout methods                             | Breakoff methods<br>Surface hardness methods            |
| Mild steel reinforcing      |                                                                                    |                                                         |
| Location/size               | Pachometer<br>Gamma radiography <sup>a</sup>                                       | Ultrasonic pulse echo<br>Penetrating radar              |
| Corrosion                   | Visual inspection <sup>b</sup><br>Electrical potential measurements                | Rate of corrosion probes                                |
| Prestressing tendons        |                                                                                    |                                                         |
| Loads                       | Tendon liftoff tests                                                               | Load cells                                              |
| Corrosion                   | Visual inspections<br>Mechanical property tests<br>Tendon load vs elongation tests | Corrosion inhibitor analysis                            |
| Concrete embedments         | Visual inspections<br>Mechanical testing                                           |                                                         |

<sup>a</sup>Limited to concrete thickness  $\leq 450$  mm.

<sup>b</sup>Reflected through cracking and staining observed at concrete surface.

the size, depth, and area of repair required. Existing elements can also become inadequate due to either a change in performance requirements or occurrence of an overload condition. Under those conditions retrofitting may be required to reestablish serviceability. Retrofitting can be accomplished by either strengthening of existing elements, replacement, addition of new force-resisting elements, a combination of element strengthening and addition, or use of supplemental connecting devices.<sup>12</sup>

Reference 11 notes that a satisfactory repair meeting requirements for strength, durability, appearance and economy can be effected if the cause of the distress is eliminated, the area is prepared by removal of degraded materials, and the proper repair technique selected and correctly implemented. A cursory examination of the effectiveness of various techniques was conducted by reviewing the literature to identify examples where the performance of structural components was compared before and after repair. Pertinent examples identified included: (1) concrete-rebar bond;<sup>13</sup> (2) reinforced concrete beams, statically and cyclically loaded;<sup>14,15</sup> (3) concrete joints under static and dynamic loading;<sup>16,17</sup> (4) shear walls under fire exposure;<sup>18</sup> and (5) an earthquake-resistant structural wall.<sup>19</sup> Results of these studies indicate that remedial measures are capable of completely restoring a component's structural integrity, with many of the repaired components exhibiting equal or improved performance.

#### REMARKS CONCERNING CORRELATIONS BETWEEN DAMAGE ASSESSMENT AND CONTINUED SERVICE EVALUATIONS

When concrete structures have been fabricated with close attention to the factors related to the production of good concrete (material selection, production control, desirable properties, economy), the concrete will exhibit infinite durability; however, where there has been a breakdown in one of these factors or the component was subjected to an extreme environmental stressor, distress can occur. It has also been established that various techniques are available for identifying regions in structures subjected to deteriorating influences and that remedial measures exist for providing a satisfactory repair. Where the system breaks down, however, is that a damage methodology to provide a quantitative measure of the ability of a structure to meet potential future requirements does not presently exist. Three areas, however, that would provide significant input toward qualifying the ability of a LWR safety-related concrete component to meet its functional and performance requirements at some future time, based on its performance history or present status, can be addressed: (1) development of a representative material properties data base, (2) establishment and evaluation of an accelerated aging methodology for concrete materials, and (3) formulation of a methodology to provide a quantitative measure of structural reliability and residual life.

Under normal operating conditions, a high level of confidence can be placed in traditional material performance based on past experience. However, for concrete material systems used in LWR applications where operating conditions are

not necessarily considered normal because of potential elevated temperature and irradiation exposure over a protracted period of time, the confidence level will not be as high. This is not the result of obvious deteriorating influences operating on these structures, but rather from the lack of a historical material property data base that can be used to form the basis for life extension considerations. Three plants in the U.S. that are currently shut down (Dresden 1, Humbolt Bay and Shippingport), however, provide an opportunity for making major contributions to the material properties data base relative to aging effects. By obtaining concrete core samples from pertinent locations and conducting petrographic examinations and load-to-failure tests, an indication of the significance of aging can be obtained. Also, prestressing tendon inservice surveillance reports and containment integrated leak-rate test reports would provide significant information useful in trending material performance (concrete materials, prestressing materials, corrosion inhibitors, seals and gaskets, etc.).

Prediction of the service life of a building component or material is dependent on there being either sufficient available data on performance of the component or material under representative conditions for the period of interest, or accelerated testing methods can be used to develop the required data. The amount of long-term data on the performance of concrete material systems under conditions representative of an LWR environment are extremely limited. Also, the data which can be derived from plants which are shut down in all likelihood will be somewhat plant specific and probably not representative for either all safety-related concrete components or potential environmental stressors. Therefore, additional data must be developed. A possible approach to the development of supplemental data is to use accelerated aging techniques. It is envisaged that the required accelerated aging program would involve three major phases: (1) problem definition (material and component characterization, degradation factor identification and simulation, test performance requirement definition), (2) design and performance of predictive service life tests, and (3) mathematical model development. Results obtained from such a program will aid in describing and understanding the phenomena of potential deterioration with the passage of time, assist in determining the residual service life of materials and components in conjunction with actual degradation conditions, and help in establishing maintenance or remedial measure programs that will assist in either prolonging a component's service life or improving the probability of the components surviving an extreme event.

Assessment of functional and performance characteristics of concrete components is an important consideration in the extension of the operating life of nuclear facilities. Given the complex nature of the various environmental stressors that can exert deteriorating influences on the concrete components, a systems approach is probably best in addressing the evaluation of a structure for life extension considerations. Basic components of such an approach would encompass development of: (1) a classification scheme for structures,

elements, and deterioration causes and effects; (2) a methodology for conducting a quantitative assessment of the presence of active deteriorating influences; and (3) the structural reliability techniques to estimate the ability of a structure (component) to meet potential future requirements. Such an approach is shown schematically in Fig. 5.

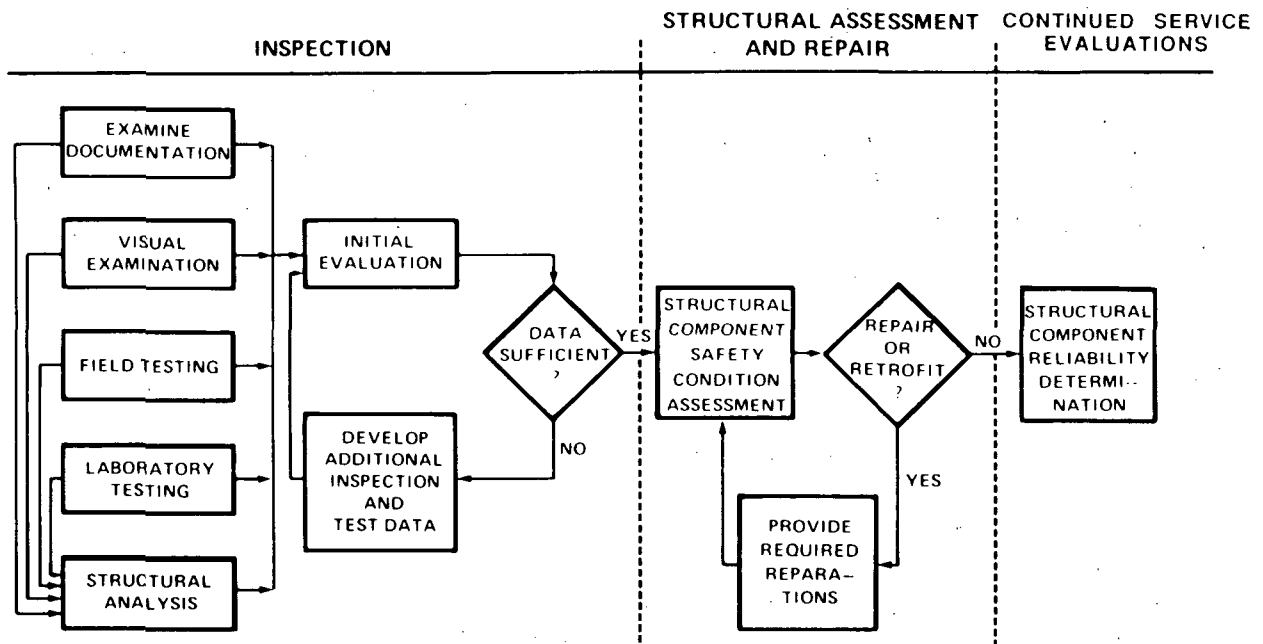


Fig. 5. Schematic of concrete component evaluation methodology.

## CONCLUSIONS AND RECOMMENDATIONS

### Conclusions

Based on the results of the NPAR investigation, the following conclusions can be derived:

1. The performance of concrete-based components in both general civil engineering and nuclear power applications has been exemplary. Distress that has occurred was generally due to construction or material errors.
2. Techniques for detecting effects of environmental stressors on concrete materials are sufficiently developed to provide qualitative data. However, quantitative interpretation can be complicated because of either (a) the requirement for development of correlation curves; (b) embedment (rebars, anchorages, etc.) effects on measured quantities such as time of ultrasonic wave transmission; or (c) accessibility. Also, a methodology

for application of this technology to provide required data for either structural reliability or continued service assessments needs development.

3. Remedial measures for repair of degraded concrete components are capable of completely restoring structural integrity when proper techniques and materials are used.
4. The durability of concrete constructions is affirmed by the presence of many structures that have been in existence for periods of time ranging from several decades to several millennia; however, well-documented data on concrete longevity that can be used as a basis for life extension considerations is almost nonexistent.
5. Primary effects that could lead to a loss of serviceability of concrete components in LWR plants include concrete cracking and loss of strength resulting from environmental stressors; however severity criteria for degradation of these components need to be established (e.g., statistically-based crack width tolerances and corrosion inhibitor impurity levels).
6. A damage methodology to provide a quantitative measure of the durability of a structure with respect to meeting potential future requirements such as a loss-of-coolant accident (LOCA) does not presently exist.

#### Recommendations

The following recommendations are made:

1. Existing facilities that have been shut down after an extended period of service should be used to obtain aging-related data for concrete materials (e.g., Shippingport, Dresden 1, and Humbolt Bay). Also, these facilities can be used to evaluate the applicability of various techniques (either existing or in the developmental stage) for detecting the effects of environmental stressors — primarily elevated temperature and irradiation — on the concrete materials. By comparing results from the non-destructive examination and tests with those obtained from core tests, considerable insight can be gained toward evaluating the ability of these tests to provide quantitative data useful for residual life assessments.
2. Accelerated aging techniques should be investigated as a method for supplementing the extremely limited data base on concrete aging. This technique would also have application to other materials that may exhibit aging effects in NPPs; e.g., seals and gaskets.
3. Available prestressing tendon inservice inspection records and data obtained during containment integrated leak-rate tests should be examined as potential sources of information for trending concrete component

behavior. Also, for plants that are likely candidates for continued service evaluations (e.g., plants with lengthy construction periods), consideration should be given to increased emphasis on inservice inspections to provide trending information that could potentially shorten the process required for continued service evaluations.

4. Criteria on durability factor significance need to be established (i.e., identification of the various deterioration phenomena acting on a particular structure and the assignment of a weighting factor to each of the phenomena based on its significance relative to continued service considerations).
5. A methodology needs to be developed to provide a quantitative measure of structural reliability, either now or at some future time. Such a methodology would use a systems approach and encompass: component classification; techniques for quantitative determination of presence, magnitude and rate effects of deteriorating influences; and structural reliability assessments. By using trending of environmental stressor data (concrete aging), the scheme would enable (a) an assessment of the ability (probability) of various safety-related concrete components to meet their design requirements (e.g., LOCA) later and (b) prediction of a component's residual life. For example, an estimation would then be made of the time when the influence of an environmental stressor would produce an unacceptable decrease in concrete strength. This could be a limiting value below that specified in the design as necessary to ensure that the structural component meets both normal operating and accident condition requirements.

#### IMPLEMENTATION OF NPAR PROGRAM RESULTS

Results of the NPAR Program were utilized to help formulate the USNRC Structural Aging Program (SAG). The overall objective of this program is to provide the USNRC with structural safety issues and acceptance criteria for use in NPP continued service evaluations. Potential Regulatory uses include: improved predictions of long-term material performance, establishment of limits on exposure to environmental stressors, and reduction in total reliance by licensing on inspection and surveillance. The damage inspection methodology to be developed will provide a quantitative measure of structural reliability, either at present, or at some future point in time. Furthermore, results of the SAG Program will provide an improved basis for the USNRC staff to permit continued operation of NPPs either near, at, or beyond their nominal 40-year design life.

Basic components of the SAG Program include three primary activities: (1) establishment of a material properties data base (MPDB), (2) assessment of structural component assessment and repair technology, and (3) development of a quantitative methodology for structural aging determinations. The MPDB will be in the form of an expandable handbook containing data obtained from

existing data bases, decommissioned plants, and accelerated aging tests. The data will provide a basis for trending the performance of concrete components under the influence of aging factors and/or environmental stressors; i.e., the MPDB would form the basis of an "expert system" of rules, frames or semantic nets to be developed under the third activity of the SAG Program. Under the structural component assessment and repair technology activity, recommended inservice inspection tests, test intervals and acceptance and rejection criteria will be provided as well as guidance on detection and potential techniques for mitigation of environmental stressors or aging factors. Also, recommendations will be provided on remedial actions according to type and extent of deterioration. Formulation of a quantitative methodology for structural aging determinations will include: development of algorithms for determination of aging effects on concrete material properties; development of modeling techniques to predict future performance of a concrete structure, given a certain state of damage resulting either from aging or extreme loading effects; and evaluation of the synergism of factors leading to aging (natural internal chemical, external stressor or environment, service wear and testing).

#### REFERENCES

1. L. R. Forest, Jr. and T. R. Deutsch, "Cost Savings from Extended-Life Nuclear Plants," Paper IAEA-SM-295/29, *International Symposium on Safety Aspects of the Aging and Maintenance of Nuclear Power Plants*, International Atomic Energy Agency, Vienna, Austria, June 29-July 3, 1987.
2. B. M. Morris and J. P. Vora, *Nuclear Plant Aging Research (NPAR) Program Plan*, NUREG-1144 (Rev. 1), Division of Engineering Technology, Office of Nuclear Regulatory Research, U.S. Nuclear Regulatory Commission, Washington, DC, July 1985.
3. D. J. Naus, "Appendix B. Concrete Material Systems in Nuclear Safety Related Structures - A Review of Factors Related to their Durability, Degradation Detection and Evaluation, and Remedial Measures for Areas of Distress," in *The Longevity of Nuclear Power Systems* by I. Spiewak and R. S. Livingston, EPRI NP-4208, Electric Power Research Institute, Palo Alto, CA, August 1985.
4. "Rules for Construction of Unfired Pressure Vessels," *ASME Boiler and Pressure Vessel Code*, Sect. VIII, American Society of Mechanical Engineers, New York, 1965.
5. J. Fraczek, "ACI Survey of Concrete Structure Errors," *J. Am. Concr. Inst.* 1(12), 14-20, December 1979.
6. R. Hauser, "Lessons Learned from European Failures," *J. Am. Concr. Inst.* 1(12), 21-25, December 1979.

7. D. J. Naus, *Concrete Component Aging and Its Significance Relative to Life Extension of Nuclear Power Plants*, NUREG/CR-4652, Martin Marietta Energy Systems, Inc., Oak Ridge National Laboratory, September 1986.
8. D. J. Naus, *A Review of the Effects of Elevated Temperature on Concrete Materials and Components with Particular Reference to the Modular High-Temperature Gas-Cooled Reactor (MHTGR)*, ORNL/LTR-88/2, Martin Marietta Energy Systems, Inc., Oak Ridge National Laboratory, March 1988.
9. B. L. Meyers and M. A. Daye, "PWR Containment Aging Under Service Environment," Vol. D, *Trans. of 9th Int'l. Conf. on Structural Mech. in Reactor Technology*, Lausanne, Switzerland, pp. 235-241, August 17-21, 1987.
10. C. J. Hookham, *Quantification of Degradation Damage in Light Water Reactor Concrete Containments*, Doc. No. INEL-12-6002, Multiple Dynamics Corp., Southfield, MI, March 1988 (Draft).
11. J. J. Waddell, "Basic Steps of a Concrete Repair Program," *Concr. Int.* 2(9), 30-33, September 1980.
12. J. Warner, "Methods for Repairing and Retrofitting (Strengthening) Existing Buildings," *Workshop on Earthquake-Resistant Reinforced Concrete Building Construction*, University of California, Berkeley, July 11-15, 1977.
13. H. W. Chung, "Epoxy Repair of Bond in Reinforced Concrete Members," pp. 799-82 in *Proc. J. Am. Concr. Inst.* 78(1), January-February 1981.
14. M. A. Mansur and K. C. G. Ong, "Epoxy-Repaired Beams," *Concr. Int.* 7(10), 46-50, October 1985.
15. P. C. Hewlett and J. G. D. Morgan, "Static and Cyclic Response of Reinforced Concrete Beams Repaired by Resin Injection," *Mag. Concr. Res.* 34(118), 5-17, March 1982.
16. H. W. Chung and L. M. Lui, "Epoxy-Repaired Concrete Joints," *Proc. J. Am. Concr. Inst.* 74(6), 264-67, June 1977.
17. H. W. Chung and L. M. Lui, "Epoxy-Repaired Concrete Joints Under Dynamic Loads," *Proc. J. Am. Concr. Inst.* 75(7), 313-16, July 1978.
18. J. M. Plecnik et al., "Epoxy-Repaired Concrete Walls Under Fire Exposure," *ASCE J. Str. Div.* 108(STP8), 1894-1908, August 1982.
19. A. E. Fiorato et al., "Behavior of Earthquake Resistant Structural Walls Before and After Repair," *J. Am. Concr. Inst.* 80(5), 403-13, September-October 1983.

APPLICATION OF SIGNATURE ANALYSIS FOR DETERMINING  
THE OPERATIONAL READINESS OF MOTOR-OPERATED  
VALVES UNDER BLOWDOWN TEST CONDITIONS\*

H. D. Haynes  
Oak Ridge National Laboratory  
Oak Ridge, Tennessee

ABSTRACT

In support of the NRC-funded Nuclear Plant Aging Research (NPAR) program, Oak Ridge National Laboratory (ORNL) has carried out a comprehensive aging assessment of Motor-Operated Valves (MOVs).

As part of this work, ORNL participated in the Gate Valve Flow Interruption Blowdown (GVFIB) tests carried out in Huntsville, Alabama. The GVFIB tests were intended primarily to determine the behavior of motor-operated gate valves under the temperature, pressure, and flow conditions expected to be experienced by isolation valves in Boiling Water Reactors (BWRs) during a high energy line break (blowdown) outside of containment. In addition, the tests provided an excellent opportunity to evaluate signature analysis methods for determining the operational readiness of the MOVs under those accident conditions.

ORNL acquired motor current and torque switch shaft angular position data on two test MOVs during various times of the GVFIB tests. The reduction in operating "margin" of both MOVs due to the presence of additional valve running loads imposed by high flow was clearly observed in motor current and torque switch angular position signatures. In addition, the effects of differential pressure, fluid temperature, and line voltage on MOV operations were observed and more clearly understood as a result of utilizing signature analysis techniques.

INTRODUCTION AND OBJECTIVES

Motor-operated valves (MOVs) are located in almost all nuclear power plant fluid systems. Their failures have resulted in significant maintenance

---

\*Research sponsored by the Office of Nuclear Regulatory Research, U.S. Nuclear Regulatory Commission under Interagency Agreement DOE 0551-0551-A1 with the U.S. Department of Energy under contract DE-AC05-84OR21400 with Martin Marietta Energy Systems, Inc.

"The submitted manuscript has been authored by a contractor of the U.S. Government under contract No. DE-AC05-84OR21400. Accordingly, the U.S. Government retains a nonexclusive, royalty-free license to publish or reproduce the published form of this contribution, or allow others to do so, for U.S. Government purposes."

efforts and, on occasion, have lead to the loss of safety system operational readiness. Consequently, in recent years MOVs have received considerable attention by the Nuclear Regulatory Commission (NRC) and the nuclear power industry. As a result, Oak Ridge National Laboratory (ORNL) has carried out a comprehensive aging assessment of MOVs in support of the Nuclear Plant Aging Research (NPAR) program which was established by the Office of Nuclear Regulatory Research (RES), primarily as a means to resolve technical safety issues related to the aging of electrical and mechanical components, systems, and structures used in commercial nuclear power plants.

A primary objective of the NPAR program is to identify and recommend methods of inspection, surveillance, and monitoring that would provide timely detection of service wear (aging) affecting important components and systems so that maintenance or replacement can be performed prior to loss of safety function(s). In that regard, ORNL research has focused on the evaluation of potentially useful signature analysis methods for determining the operational readiness of MOVs. This work provides technical information applicable to the resolution of Generic Issue II.E.6.1 (In Situ Testing of Valves) as well as IE Bulletins and Information Notices such as IEB 85-03 (Motor Operated Valve Common Mode Failures During Plant Transients Due to Improper Switch Settings).

In support of the NPAR programmatic objectives, ORNL participated in the Gate Valve Flow Interruption Blowdown (GVFIB) tests sponsored by the NRC/RES Mechanical Qualification Program and carried out under subcontract to INEL by WYLE Laboratories in Huntsville, Alabama. The results of the GVFIB tests are described in a paper presented by INEL at the 16th Water Reactor Safety Information Meeting (1). The GVFIB tests were intended primarily to determine the behavior of motor-operated gate valves under the temperature, pressure, and flow conditions expected to be experienced by isolation valves in Boiling Water Reactors (BWRs) during a high energy line break (blowdown) outside of containment. In addition, the tests provided an excellent opportunity to evaluate signature analysis methods for determining the operational readiness of the MOVs under those accident conditions.

## BACKGROUND

ORNL has, in the past, carried out research in order to identify the type and potential value of diagnostic information from many MOV measurable parameters. In the course of these investigations, it was discovered that the MOV's electric motor acted effectively as a transducer by directly converting variations in drive train mechanical loads into variations in motor current which were sensed remotely (at the motor control center) using a non-intrusive clamp-on current probe.

Further research led to the development of special signal conditioning electronics and motor-current signature analysis (MCSA) techniques which together provided a means of sensitively and selectively extracting motor-

current signal information from the power line to reveal MOV performance indicators on many levels including:

- Mean values of running current levels during "no load", pre-unseating, and "mid-stroke" portions of a valve stroke
- Variations in running current levels (both large and small) which are associated with changes in mechanical running loads during a valve stroke
- Initiation time, duration, and magnitude of motor-current transients which are characteristic of momentary motor operator and valve events including operator hammerblow, valve seating, valve unseating, valve backseating, and unusual transient events
- Worm gear tooth meshing indications on a tooth-by-tooth basis
- Overall current noise level which is generally indicative of smooth or rough operations
- Individual frequency spectral peaks associated with periodic current modulations resulting from periodic load variations within the MOV drive train.

Motor current spectra, which are comparable to vibration spectra, commonly include worm gear tooth meshing, stem nut rotation, motor shaft speed, and motor slip frequencies. Harmonic and sideband frequencies are often observed which provide indications of eccentricity and/or wear.

In addition to motor current, the monitoring method assessments carried out by ORNL illustrated that the angular position of the MOV torque switch shaft could be monitored and used as a meaningful diagnostic signal as well. Since the angular position of the torque switch shaft primarily reflects the motor operator torque output which is transferred as stem thrust via the operator's stem nut, a measure of the instantaneous angular position of the torque switch shaft during a valve stroke provides a relative measure of the instantaneous valve stem thrust.

## SYSTEM DESCRIPTIONS

The system utilized for the Gate Valve Flow Interruption Blowdown Test featured a large water tank which was pressurized by a nitrogen supply so that various system water pressure conditions could be established and regulated. Water was heated by means of an electric heater section and was circulated through the system by a high-pressure, high-temperature pump. A motor-operated valve was positioned in the system such that it could be actuated during times when the valve contained pressurized, heated water.

Two different motor-operated valves were tested in this system:

- Valve "A" - Anchor/Darling, 6-inch, 900 pound standard rated, flexwedge gate valve with a Limitorque SMB-2-40 motor operator
- Valve "B" - Velan, 6-inch, 900 pound standard rated, flexwedge gate valve with a Limitorque SMB-0-25 motor operator

Both MOVs utilized 460 VAC, 3 phase, 60 Hz electric motors. The motor operator used on valve "B" was sized in accordance with current practices, whereas the motor operator used by valve "A" was oversized, although its delivered torque was adjusted so that it did not damage the valve.

The system contained bleed valves which provided the means to reduce system pressure on both sides (upstream and downstream) of the test MOV. In this manner, differential pressure conditions were established across the MOV's obturator when the MOV was closed. The system also featured a fast acting, hydraulically operated valve which was positioned in the system downstream of the test MOV so that when actuated, the system's contained fluid was abruptly released externally resulting in a high flow (blowdown) condition through the MOV being tested. The test MOV was then actuated in the open-to-close direction during the blowdown in order to determine whether it could successfully close against the high energy event. System fluid pressure and temperature were varied for each blowdown. Several blowdowns were carried out on each MOV.

Before any blowdown tests were performed on a test MOV, a series of qualification tests and other pre-blowdown tests were carried out. The qualification tests included MOV actuations under various system fluid pressures, fluid temperatures, and motor line voltages. MOV actuations were carried out immediately prior to each full system blowdown at the same fluid pressure and temperature conditions as the blowdown but with no flow.

#### EQUIPMENT USED AND SIGNATURE ANALYSIS TECHNIQUES

ORNL acquired motor current and torque switch shaft angular position data for both test MOVs at various times throughout the GVFIB testing. The instrumentation used by ORNL is illustrated by Figure 1.

MOV torque switch shaft position was measured by an angular displacement transducer (ADT) which was installed on the torque switch of both MOVs in a manner which allowed the switch compartment to be closed during the MOV tests. The ADT utilized by ORNL was a variable capacitance device which provided a DC voltage output that varied linearly with the angular position of its shaft. The ADT provided high sensitivity (100 mv per degree of rotation), infinite resolution (analog output), and an insignificant load on the torque switch.

Motor-current monitoring was carried out using a clamp-on current transformer installed on a single motor lead at the MOV. Special signal conditioning electronics were used to transform raw current signals supplied by the current probe into two recordable signals: one optimized for time domain analyses and one optimized for analyses in the frequency domain.

Torque switch position and motor current signals were recorded in analog form by a high quality cassette data recorder. Analog signal recordings were

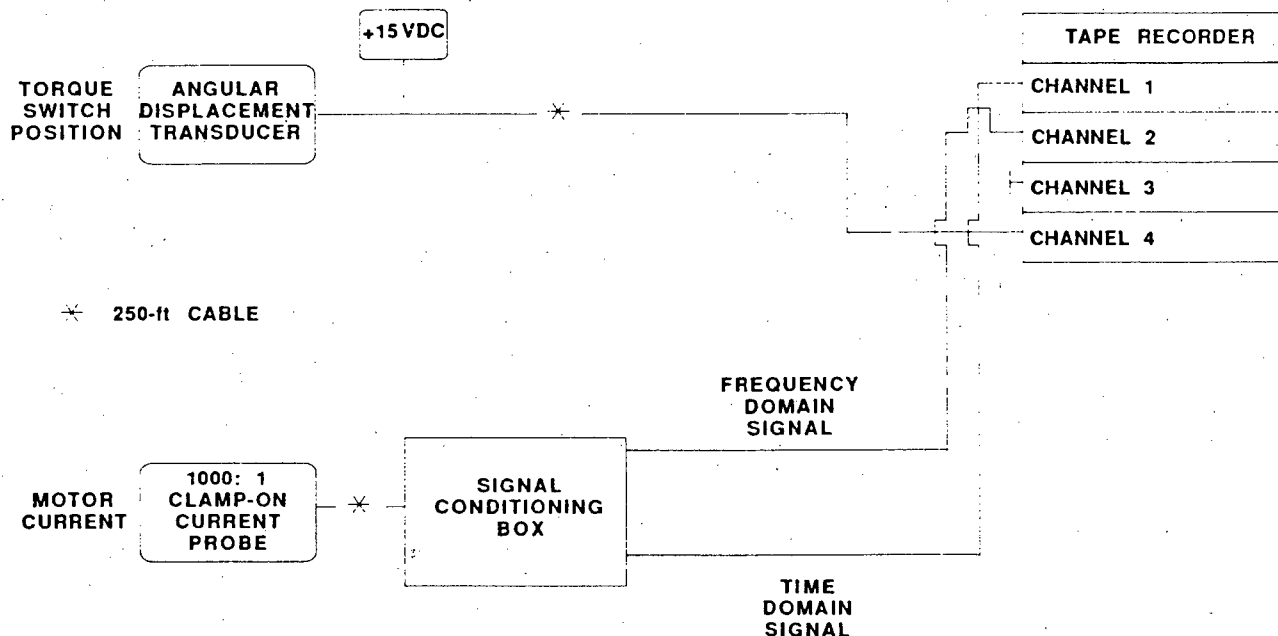


Fig. 1. GVFIB test instrumentation diagram.

made (rather than digital) so that time and frequency resolution of test data was not limited to an original digitization rate (as in direct digital recordings). Analog signal recordings were then post-digitized at whatever rate that was optimum for a particular analysis such as a MOV full-stroke waveform analysis using a relatively slow post-digitization rate or an analysis of seating and unseating transients where a higher post-digitization rate was desired.

In addition, time waveforms were produced after passing the recorded motor-current noise signals through a narrow frequency band filter. Using this selective waveform inspection method (SWIM), unique motor current signatures were developed which reflected the time dependent amplitude modulations of the worm gear tooth meshing frequency. These waveforms display worm gear meshing on a tooth by tooth basis and, when transferred to a polar coordinate system, provided a means to detect worm gear meshing symmetries and asymmetries.

Another novel MCSA technique used was a method for determining whether an observed motor current level change was a result of a change in mechanical load or from a deviation in motor voltage without having to actually measure the motor voltage. This was accomplished by recognizing that an induction motor's slip (speed) and current are related by the motor's characteristic curve and voltage. Different slip vs. current relationships can occur for a given motor only at different voltages. In other words, when a higher or lower voltage condition existed during the time when motor current data acquisitions were performed, the slip/current relationship provided one method for detecting and quantifying the actual voltage.

## TEST RESULTS - VALVE "A"

One of the initial observations made when analyzing motor-current signatures of valve "A" was that a general decrease in running current magnitudes occurred during the open-to-close stroke. This signature characteristic, along with the corresponding torque switch position signature, is shown in Figure 2. A drop in current of approximately 0.5 amps (5.75 to 5.25) was seen in this MOV actuation which was carried out prior to the first system blowdown test.

Motor current and torque switch angular position signatures were then acquired during the first system blowdown (1000 psig, 480 F) which occurred on 4/27/88. As shown in Figure 3, the previously observed decrease in motor running current was followed by a gradual increase in current as the valve was closed which reflected the additional running loads induced by the high velocity flow stream.

Near the end of the open-to-close stroke, a sudden increase in motor current and torque switch rotation was observed. This apparently reflected a momentary misalignment between valve contacting surfaces prior to the gate establishing full sliding contact with the seat. Once this sliding contact was made, valve running loads decreased abruptly which identified the point in the valve stroke when the flow was completely blocked by the gate. This occurred approximately 1.6 seconds from the complete "bottoming out" of the gate which initiated a sudden and significant rise in motor current and torque switch rotation which provided indications that the valve was fully seated.

Similar running load characteristics during the first blowdown valve closure were observed in the torque switch angular position signature, also

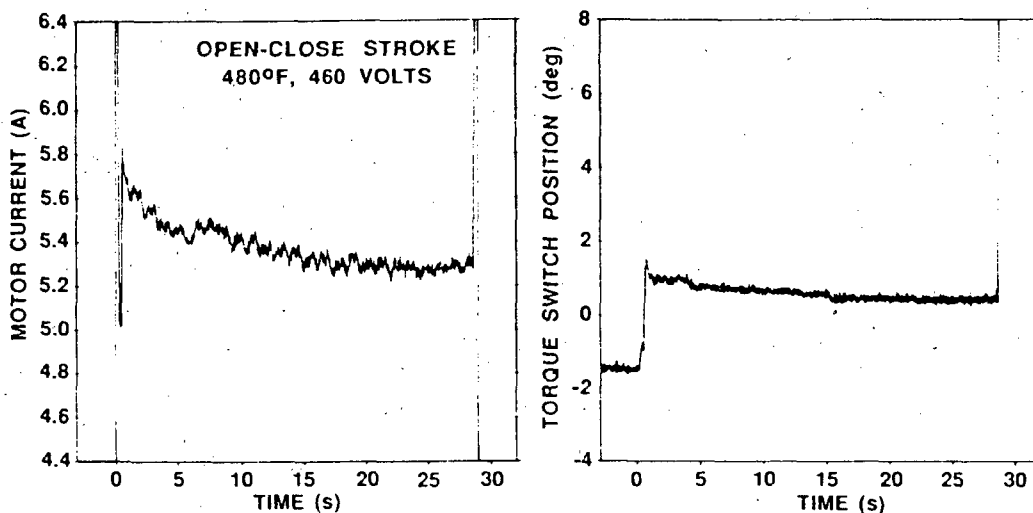


Fig. 2. Valve "A" - Typical signatures before blowdown (1000 psig, no flow).

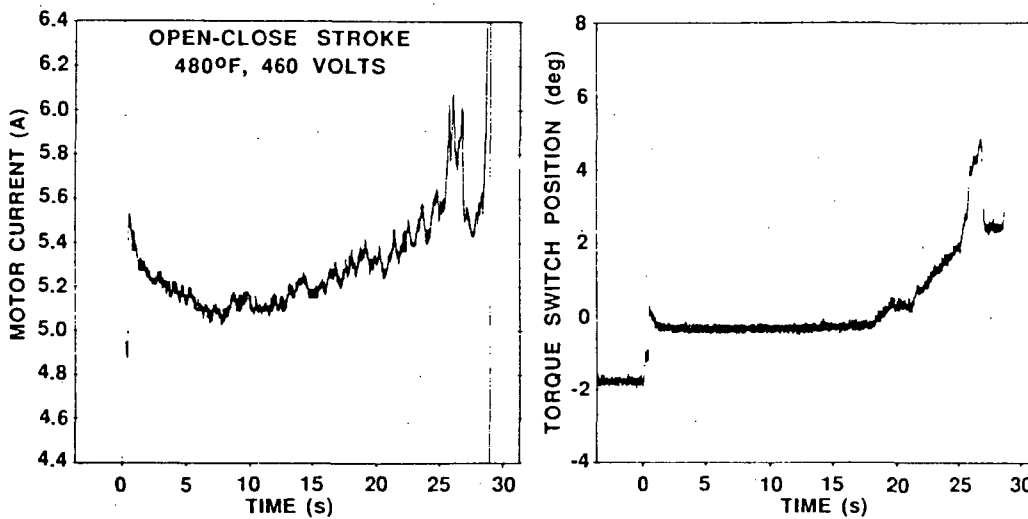


Fig. 3. Valve "A" - Signatures during first blowdown at 1000 psig (expanded vertical scale).

shown in Figure 3. One significant difference, however, should be noted. The torque switch position did not change during times when the valve running loads were below a level equivalent to 5.3 amps running current. This insensitivity to MOV running load variations below this point was apparently a reflection of springpack pre-load. A small difference (approximately 0.67 degrees) was also observed between the "no-load" (after motor starts but before running loads are observed) and pre-load torque switch positions. This difference may have resulted from a small clearance between the torque switch drive gear and rack assembly.

As large as the blowdown pressure and flow effects appeared in Figure 3, their relative insignificance to the successful operation of the MOV was clear when comparing their magnitude to the magnitude of the final valve seating load as shown in Figure 4. The running loads from the first system blowdown were then expressed as a fraction of the total range between "no-load" and torque switch trip load as follows:

| SIGNATURE     | MAXIMUM RUNNING LOAD DURING FIRST BLOWDOWN                                                    |
|---------------|-----------------------------------------------------------------------------------------------|
| Motor current | 24.8% of the difference between "no-load" current and the current at torque switch trip       |
| Torque switch | 23.7% of the difference between "no-load" position and the position at torque switch trip     |
| Torque switch | 18.1% of the difference between "no-load" position and the final position (including inertia) |

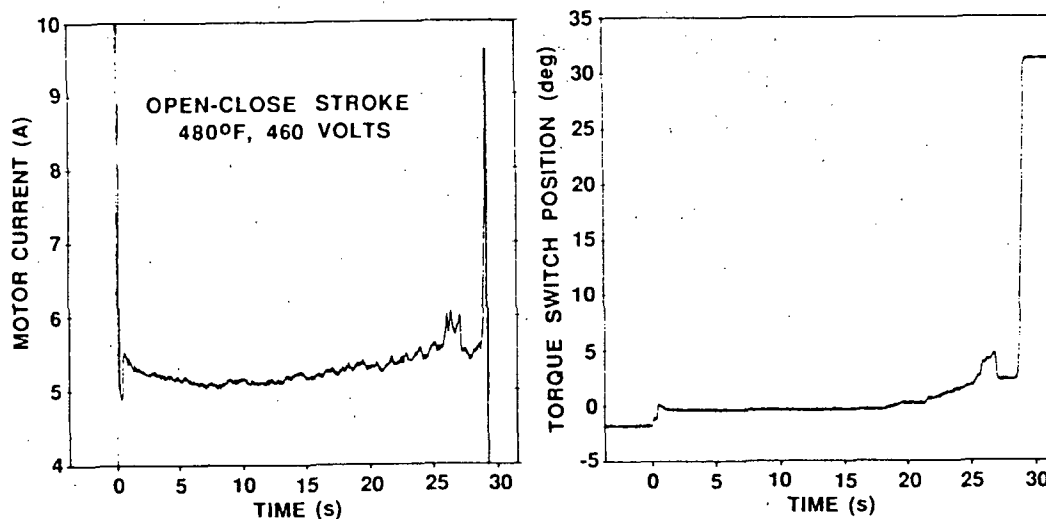


Fig. 4. Valve "A" - Signatures during first blowdown at 1000 psig (showing final values at torque switch trip).

Another way of visualizing the relative effects of blowdown pressure and flow on the closure of valve "A" was by cross-plotting the motor current and torque switch angular position magnitudes as shown in Figure 5. From this signature, the proximity of the running load magnitudes to the torque switch trip point is clearly seen as well as the additional inertial rotation of the torque switch after the motor tripped. The additional valve seating loads due to inertia were relatively large, as evidenced by the additional 32% in torque switch rotation after the motor shut off.

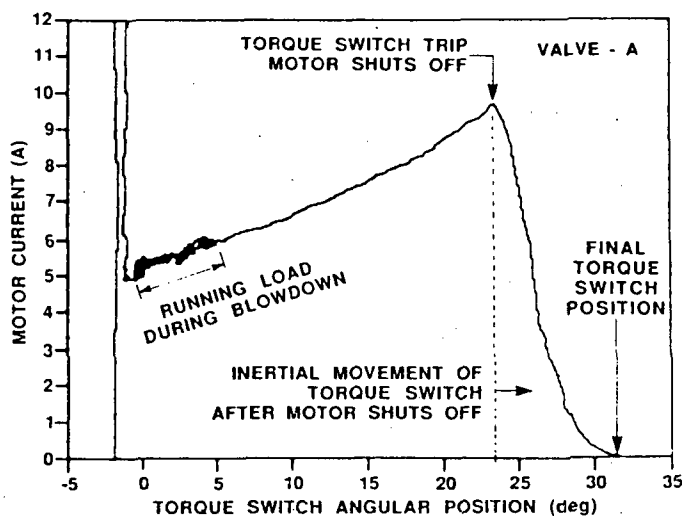


Fig. 5. Valve "A" - Motor current vs torque switch position during first blowdown.

In addition to the blowdown test, motor current data were acquired for several valve "A" unseatings during a variety of initial differential pressure, fluid temperature, and line voltage conditions. It should be noted that during these valve openings against initial differential pressure, no fluid flowed thru the MOV other than that which led to an equalization of upstream and downstream pressures once the flow path was opened.

Figure 6 illustrates the effect of differential pressure and fluid temperature on valve "A" unseating using MCSA. In each signature two major motor current peaks are shown. The first represents motor operator hammerblow, the second peak reflects gate unseating.

As expected, when opened under no differential pressure, the MOV motor current signature indicated that no additional significant loads were present after gate unseating. However, when opened against 1700 pounds per square inch differential (psid) of cold water, the valve unseating peak was followed immediately by a period of increased running load which primarily reflected the differential pressure-induced disk guide friction which persisted until the flow path was opened and the pressures upstream and downstream of the MOV were allowed to equalize. The time measured from initial disk unseating to the point when the running load began to suddenly drop was 1.6 seconds. This

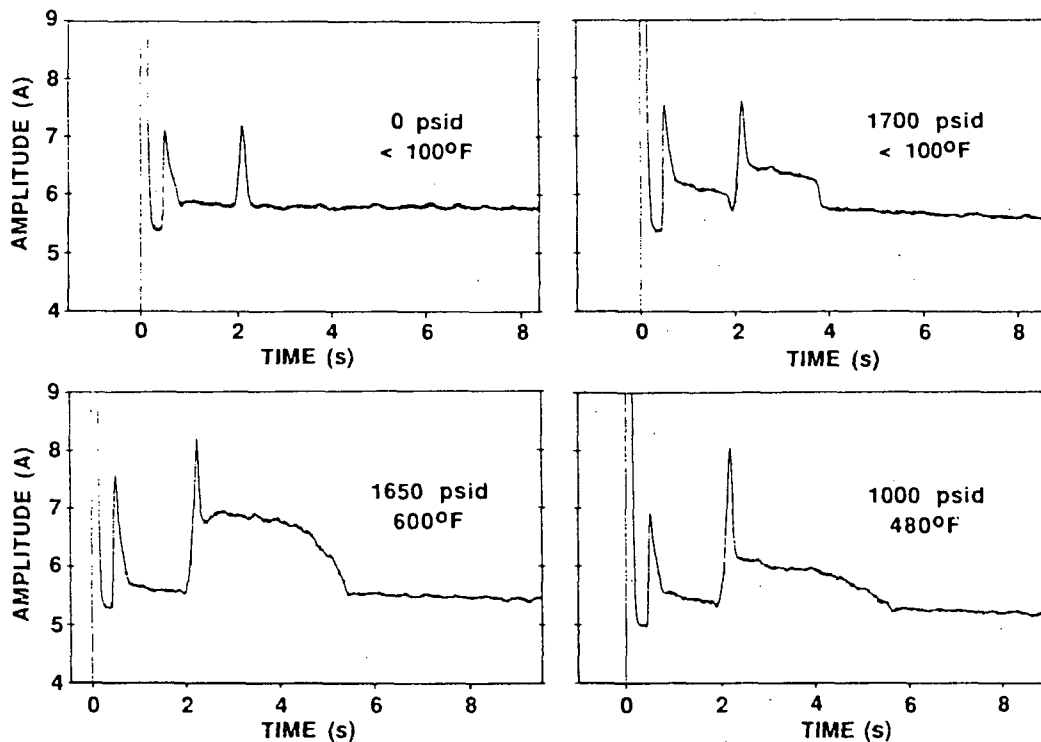


Fig. 6. Valve "A" - Effect of differential pressure and fluid temperature on gate valve unseating (460 volts).

was the same time differential that was measured between the flow cutoff point and the point of initial gate/seat contact during the blowdown test and therefore reflected the same stem/gate travel. Once the flow path was opened, the pressure rapidly equalized in approximately 0.1 seconds as shown by the sudden decrease in the motor current magnitude.

When opened against 1650 psid (600°F water), and 1000 psid (480°F water), the times required for complete pressure equalization increased to approximately 1.6 seconds and 1.8 seconds, respectively. These times were determined by measuring the time differential between the point when the flow path was first opened (1.6 seconds after the disk unseating transient) and the point when the motor running current first stabilized (indicating complete pressure equalization). The pressure equalization times were greater for the two hot water cases since the mass flow rate of the flashing two phase (steam and water) mixture was lower (through the same sized valve opening) and thus required more time for the transfer of the mass of water necessary for the pressures upstream and downstream of the gate to equalize.

As expected, motor voltage was seen to be very influential on motor current signature characteristics as well. The effect of reduced voltage on the unseating characteristics of valve "A" under 1650 psid (600°F water) initial conditions is illustrated by Figure 7. The observed distortion in the motor current signature features at 368 VAC (80% of rated voltage) resulted from a shift in the motor characteristic response curve, which is more completely illustrated by the following motor current test data.

Motor slip (determined from the motor current frequency spectrum) and average motor running current (from time waveform analyses) were cross-plotted for valve "A" actuations under various pressure, flow, temperature, and

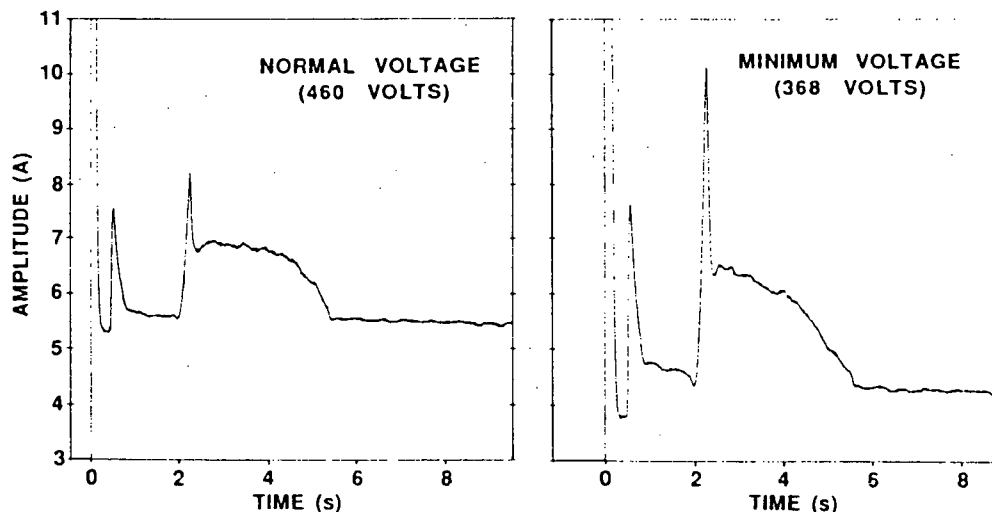


Fig. 7. Valve "A" - Effect of line voltage on gate valve unseating (1650 psid, 600°F).

voltage conditions. The slip/current relationship provided an indication of line voltage stability and was used in determining if a change in motor running current was a result of a change in running load or from a line voltage deviation. Figure 8 illustrates that in addition to major changes seen between 368 VAC (80%), 460 VAC (100%), and 510 VAC (111%) data sets, a relatively large amount of scatter was seen in the 460 VAC data. By a simple linear interpolation between the 460 VAC and 368 VAC data sets, a  $\pm 12$  VAC variance was estimated for the 460 VAC data ( $\pm 2.6\%$ ).

Further examinations of the 460 VAC slip/current data provided an indication that the apparent voltage variance was primarily due to data acquired on 4/27/88 (the day of the first blowdown). Figure 9 shows that with the exception of the 8 data points which represented MOV actuations on 4/27/88 before the first blowdown, the remaining data (25 points) were contained in a relatively narrow band which, using the above interpolation method, would account for an estimated voltage variation of only  $\pm 4$  VAC (or  $\pm 0.9\%$ ). Since ORNL did not monitor motor voltage during the GVFI tests, the apparent voltage variations at 460 VAC identified by MCSA could not be verified.

On 5/24/88, a partial stroking of valve "A" was carried out while the blowdown mechanism (hydraulic valve) was kept in the open position. Motor current and torque switch position signatures were acquired during a partial opening of the valve against blowdown flow which was immediately followed by a closure stroke. Figure 10 illustrates that, as expected, the flow-induced running loads were dependent on the position of the valve's obturator (gate) in the flow stream. In general, the greater the flow blockage was, the greater the flow-induced loads became (as evidenced by the motor current and torque switch angular position signatures).

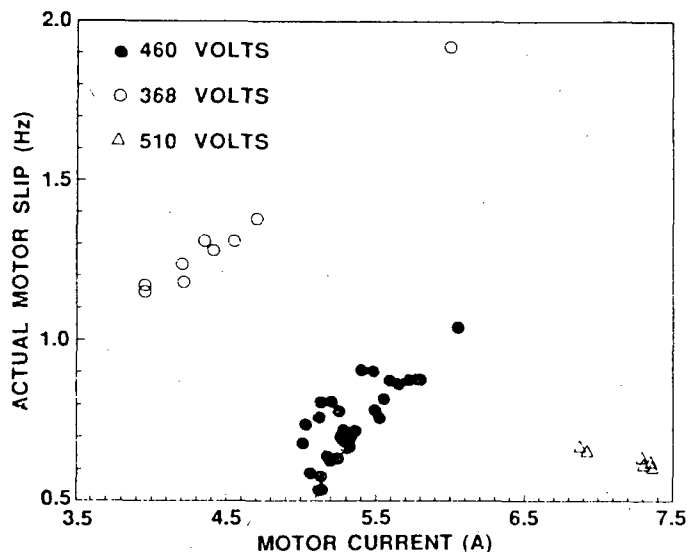


Fig. 8. Valve "A" - Motor characteristics from MCSA.

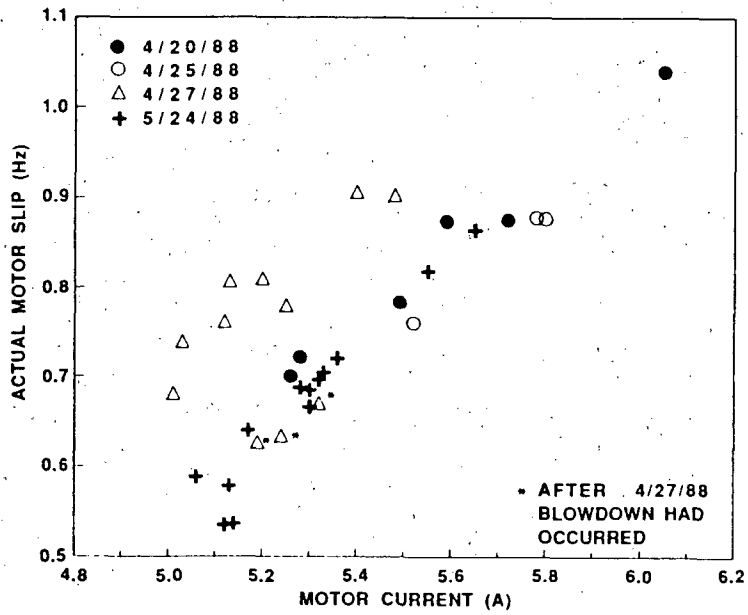


Fig. 9. Valve "A" - Motor characteristics at normal voltage (460 volts) from MCSA.

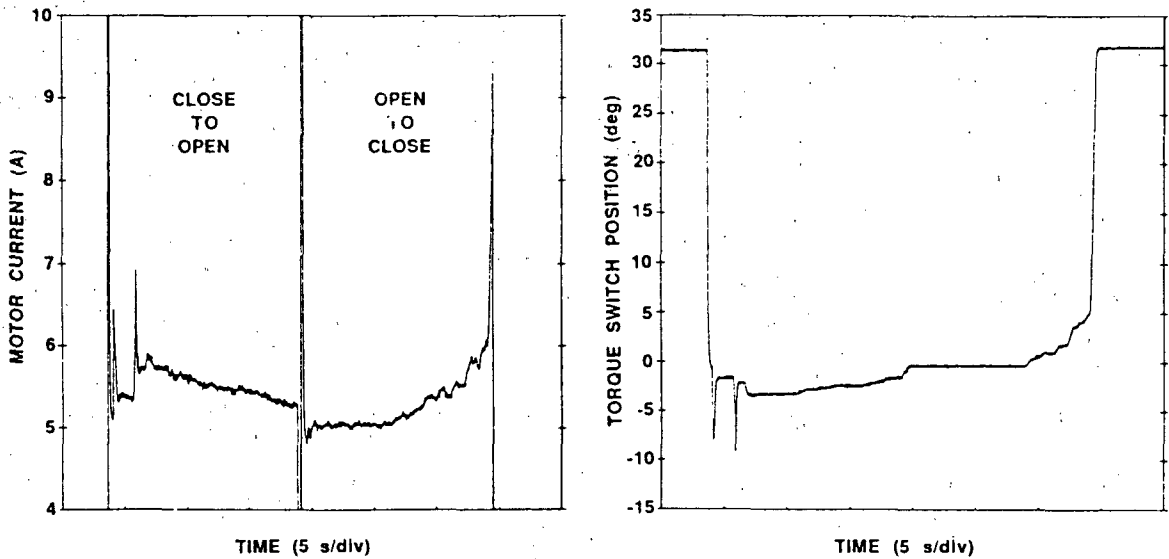


Fig. 10. Valve "A" - Partial opening and closing against blowdown flow (600 psig, 350°F, 460 volts).

#### TEST RESULTS - VALVE "B"

Motor current and torque switch angular position signatures were acquired on valve "B" during a system blowdown test which was carried out on 6/14/88 at

1000 psig and 530°F. The effects of blowdown flow-induced valve loads were expected to be more noticeable on valve "B" than on valve "A" primarily due to the size differences between their motor operators. Valve "B" used a smaller SMB-0 operator and thus was more limited in its output than the larger SMB-2 operator used by valve "A".

Figures 11 and 12 illustrate the effect of the system blowdown on the closure of valve "B" as seen via motor current and torque switch signatures, respectively. For comparison, signatures are also shown which were representative of an open-to-close stroke carried out prior to the blowdown at similar valve internal fluid pressure conditions but with no flow. An examination of these signatures indicated that the flow-induced valve running loads were so significant that they could have caused a torque switch trip prior to valve gate/seat contact if they had been a little larger.

Maximum running loads during blowdown therefore represented a large fraction of the operating range of valve "B" as shown below:

| SIGNATURE     | MAXIMUM RUNNING LOAD DURING BLOWDOWN                                                          |
|---------------|-----------------------------------------------------------------------------------------------|
| Motor current | 71.6% of the difference between "no-load" current and the current at torque switch trip       |
| Torque switch | 87.3% of the difference between "no-load" position and the position at torque switch trip     |
| Torque switch | 76.3% of the difference between "no-load" position and the final position (including inertia) |

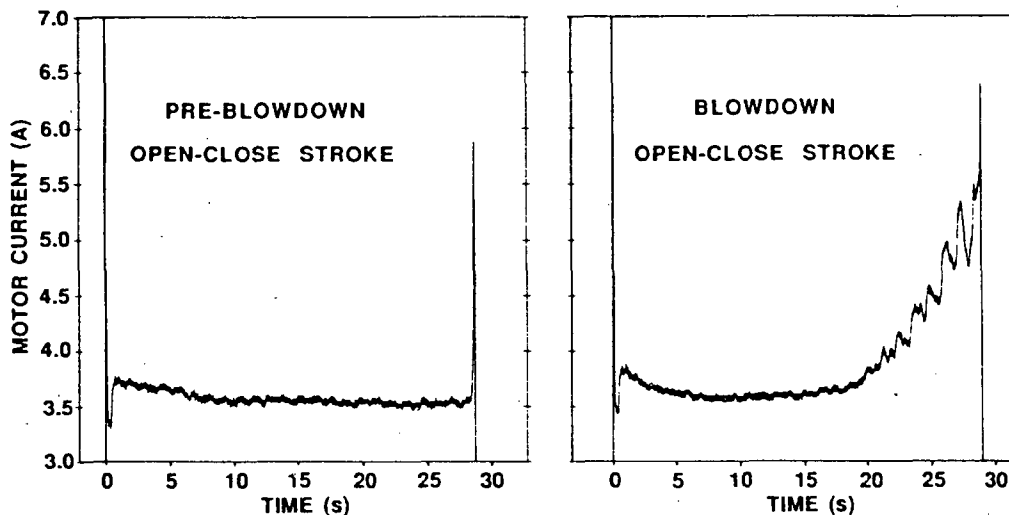


Fig. 11. Valve "B" - Effect of blowdown on motor current signature (1000 psig, 530°F, 460 volts).

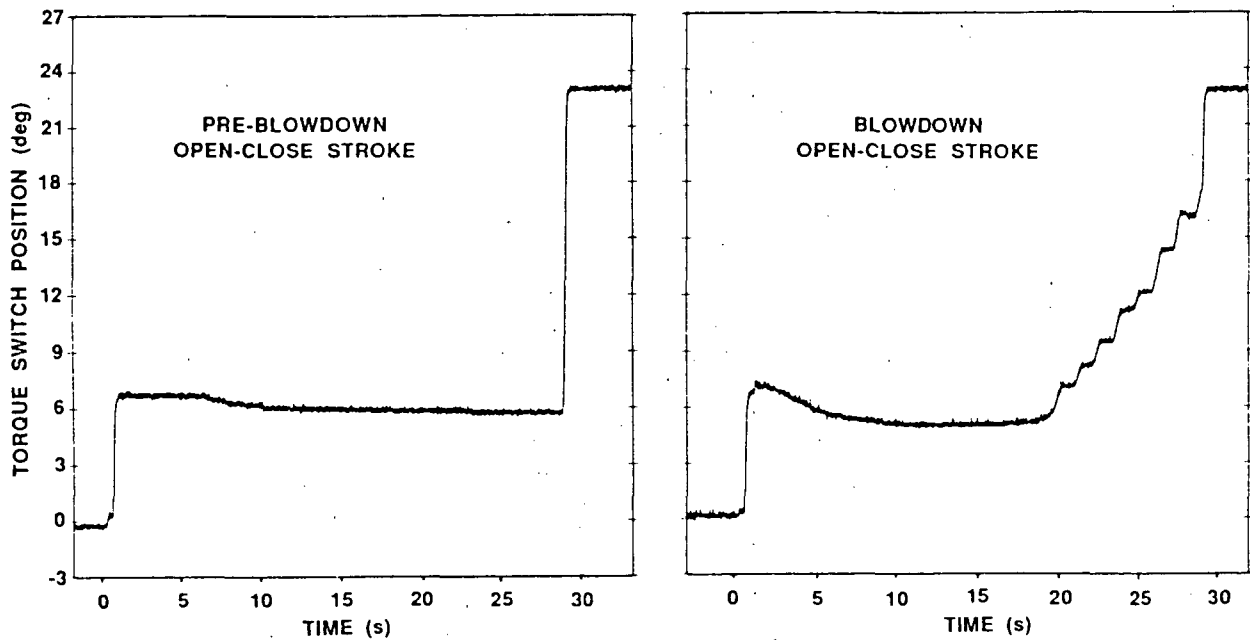


Fig. 12. Valve "B" - Effect of blowdown on torque switch position signature (1000 psig, 530°F, 460 volts).

Motor current and torque switch position magnitudes were cross-plotted as shown by Figure 13 and clearly illustrate the reduction in valve "B" operating margin due to the presence of flow-induced running loads. The close proximity of the maximum running load level to the torque switch trip point in the blowdown valve actuation indicated that after the valve gate contacted the seat, the torque switch rotated only a small amount (less than three degrees) before it tripped and shut off power to the motor. This small valve seating transient was also observed as a 0.8 amp motor current rise. For comparison, the torque switch and motor current signal rise during valve seating for the pre-blowdown (no-flow) actuation were approximately 11.9 degrees and 2.15 amps, respectively.

In a manner similar to that previously performed on valve "A", a partial stroking of valve "B" was carried out while the blowdown mechanism (hydraulic valve) was kept in the open position. The motor current and torque switch position signatures acquired during this operation are illustrated by Figure 14 and are similar in many respects to those shown in Figure 10 (partial stroking of valve "A" against blowdown flow); however, one major difference between the two signatures should be mentioned. The lack of an obvious valve unseating peak in Figure 14 reflected the lack of significant seating loads in the previous open-to-close stroke (see Figures 11, 12, and 13).

Once fluid was allowed to flow through the valve, an immediate increase in valve running loads were observed which subsequently decreased as the gate

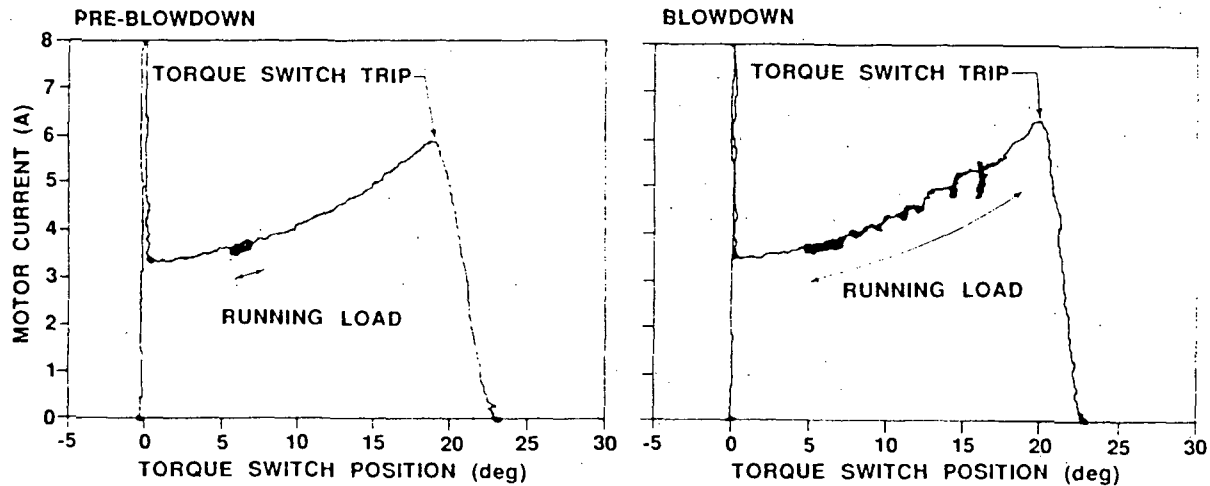


Fig. 13. Valve "B" - Motor current vs torque switch position before and during blowdown (1000 psig, 530°F).

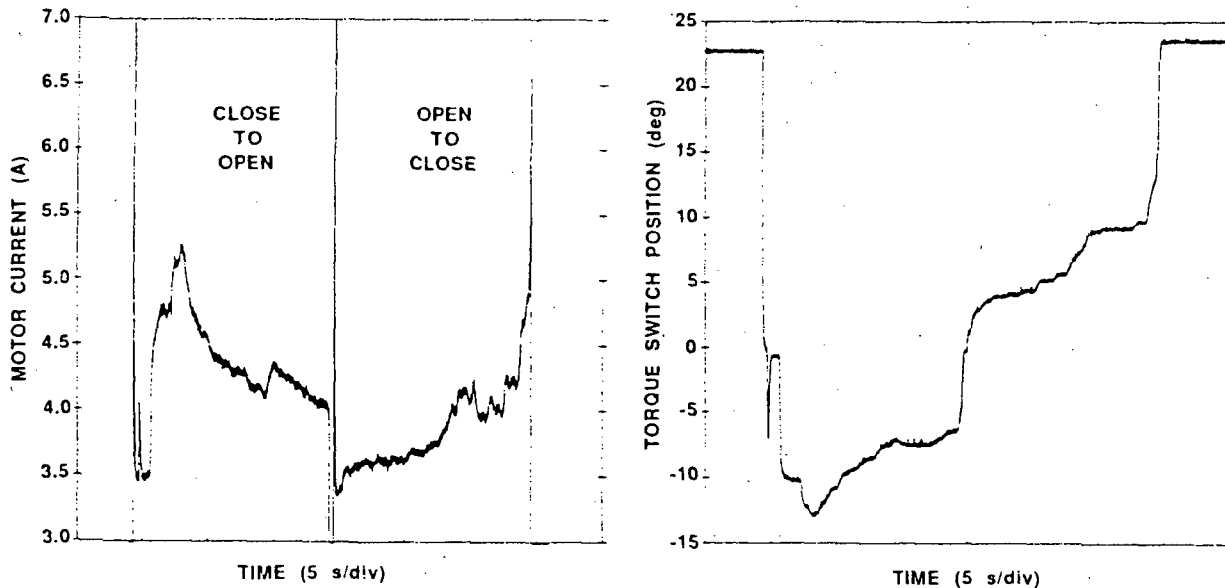


Fig. 14. Valve "B" - Partial opening and closing against blowdown flow (1000 psig, 350°F, 460 volts).

was pulled out of the flow path. As the valve "B" gate was once again lowered into the high velocity flow, the valve running loads increased until the valve seated. It should be noted that valve running loads at gate/seat contact were not as large during this valve closure as seen in the full closure against blowdown flow (see Figure 11) due to the reduction in system fluid pressure which occurred between these two tests. Consequently, valve seating (gate-to-

seat) loads were higher in this open-to-close stroke as evidenced by an increased motor current rise after gate/seat contact had been made.

Figures 15 and 16 are included in this paper primarily to illustrate additional MCSA techniques which, if utilized periodically, would be useful in identifying changes in internal operator characteristics and which may provide indicators of gear eccentricity and/or wear. Figure 15 shows a motor current noise signature obtained on valve "B" which includes spectral components at several known frequencies including motor speed and slip, worm gear rotation and worm gear tooth meshing. Amplitude modulations of the worm gear tooth meshing frequency, revealed using SWIM, are presented in Figure 16. The worm gear tooth meshing pattern shown in this figure provides indications that uneven worm gear tooth meshing loads were present at the time the motor current data were acquired, which may lead to uneven worm gear wear. No significant changes in motor current noise spectra or worm gear tooth meshing patterns were observed on either test MOV during the relatively short duration of the GVFI tests. This suggested that no significant degradation had occurred within the motor operators as part of this test.

In summary, the Gate Valve Flow Interruption Blowdown Test was an excellent opportunity for MOV diagnostic studies and more importantly, a means for

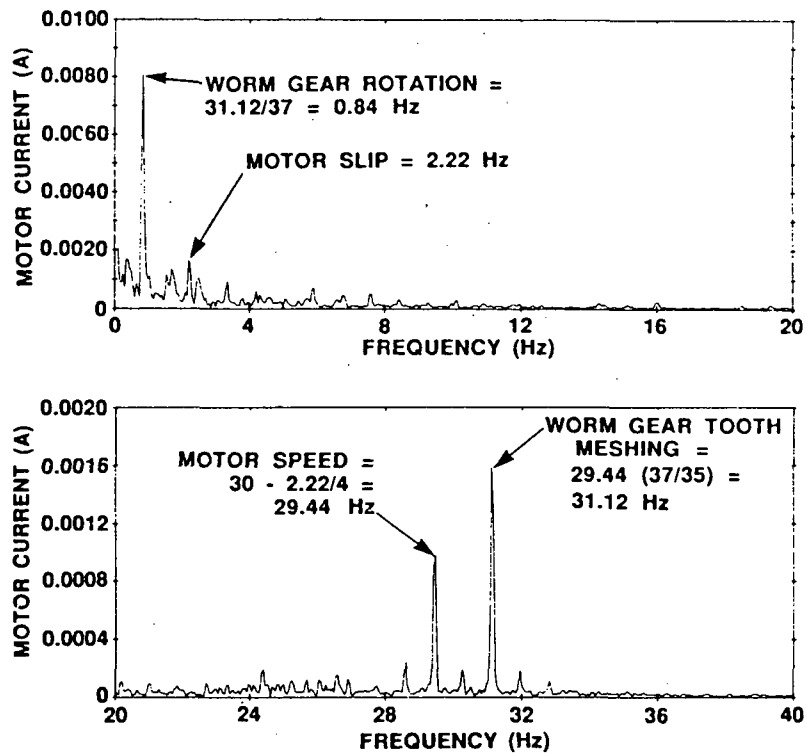


Fig. 15. Valve "B" - Typical motor current spectrum (open-close stroke, 1000 psig, 530°F, 460 volts).

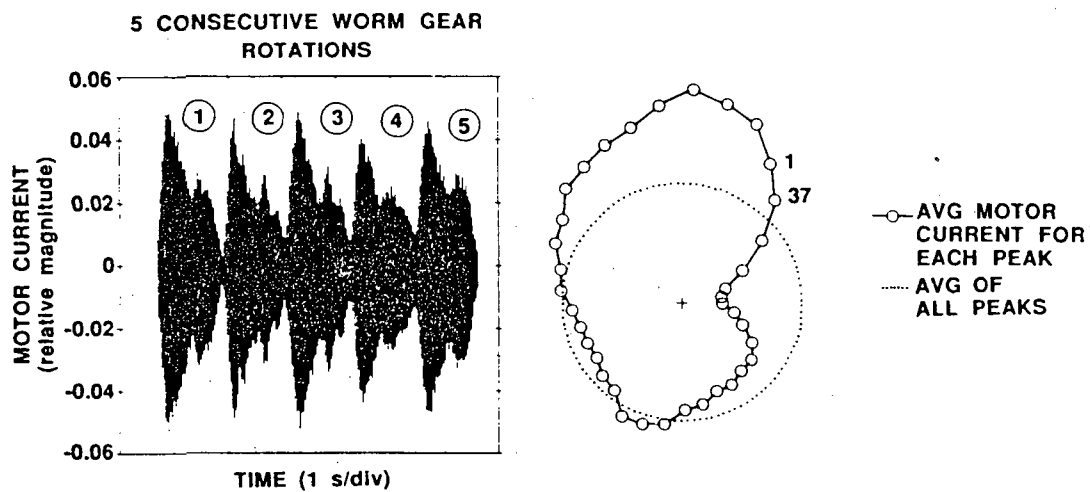


Fig. 16. Valve "B" - Typical worm gear tooth meshing pattern (open-close stroke, 1650 psig, 600°F).

determining the influences of high blowdown flow on the operation of BWR isolation valves. The reduction in operating "margin" of a motor-operated valve due to the presence of additional valve running loads imposed by high flow was clearly observed in motor current and torque switch angular position signatures. In addition, the effects of differential pressure, fluid temperature, and line voltage on MOV operations were observed and more clearly understood as a result of utilizing signature analysis techniques.

#### REFERENCE

1. K. G. DeWall, Idaho National Engineering Laboratory, "Results of Gate Valve Flow Interruption Blowdown Tests," presented at the 16th Water Reactor Safety Information Meeting, Gaithersburg, Maryland, October 24-27, 1988.



ASSESSMENT OF NONINTRUSIVE METHODS FOR MONITORING THE  
OPERATIONAL READINESS OF SOLENOID-OPERATED VALVES\*

"The submitted manuscript has been authored by a contractor of the U.S. Government under contract No. DE-AC05-84OR21400. Accordingly, the U.S. Government retains a nonexclusive, royalty-free license to publish or reproduce the published form of this contribution, or allow others to do so, for U.S. Government purposes."

Robert C. Kryter  
Oak Ridge National Laboratory†  
Building 3500  
P.O. Box 2008  
Oak Ridge, Tennessee 37831-6010

ABSTRACT

Solenoid-operated valves (SOVs) are being studied at Oak Ridge National Laboratory as part of the USNRC Nuclear Plant Aging Research (NPAR) Program. The primary objective of the study is to identify and recommend methods for inspection, surveillance, and maintenance of SOVs that can ensure their operational readiness-- that is, their ability to perform required safety functions under all anticipated operating conditions.

An earlier (Phase I) study described SOV failure modes and causes and identified measurable parameters that might be used to monitor the various degradations that lead to functional failure. The present (Phase II) study focuses on devising and then demonstrating the effectiveness of techniques and/or equipment with which to measure the previously identified performance parameters and thus detect and trend the progress of any degradation. Several nonintrusive techniques are currently under investigation. These include the monitoring of coil mean temperature by means of dc coil resistance, the monitoring of valve position by means of coil ac impedance, and the assurance of free plunger movement through measurement of current and voltage at the valve pickup and dropout points. Techniques slated for later investigation include the monitoring of coil hum or chattering, using either acoustic sensors or electrical noise indicators, and detecting the presence of shorted turns in the solenoid coil using interrupted-current test methods.

Recent experimental results which demonstrate the feasibility and practicality of the techniques being studied are presented.

---

\*Research sponsored by the U.S. Nuclear Regulatory Commission (USNRC), Office of Nuclear Regulatory Research, under DOE Interagency Agreement No. 0551-0551-A1, NRC FIN No. B0828.

†Operated by Martin Marietta Energy Systems, Inc., for the U.S. Department of Energy under Contract No. DE-AC05-84OR21400.

## PROBLEM BACKGROUND

Solenoid-operated valves (SOVs) are relatively simple devices with a long history of satisfactory operation in a variety of both nuclear and non-nuclear industrial applications. However, their application to nuclear plant safety systems requires an especially high degree of assurance that they are ready to perform at all times.

An earlier (Phase I) study<sup>1</sup> described SOV failure modes and their principal causes (Table 1). The study also identified measurable indicators of performance (Table 2), as well as nonquantitative testing and surveillance methods that might be used to detect the presence or monitor the progression of various degradations that may ultimately lead to functional failure of the valve. The findings and recommendations of this Phase I study are reinforced by similar conclusions reached by an IEEE task group composed of representatives from the utility, consulting, and manufacturing sectors of the nuclear power industry.<sup>2</sup>

Difficulties are encountered, however, in attempting to implement these ideas. The SOVs installed in present-day plants are uninstrumented, and the cost of backfitting them with instrumentation would, in most cases, be prohibitive. Also, many SOVs important to plant safety are inaccessible during plant operation. Moreover, many valves requiring assurance of operational readiness change state only rarely during normal plant operations (in some cases actuation is strictly prohibited), so little opportunity exists for measuring dynamic performance parameters. Accordingly, many utilities have elected to replace degradable components or subassemblies within SOVs that are embodied in safety-related systems on a periodic basis (i.e., preventive maintenance) rather than attempt to practice predictive maintenance using one or more of the approaches of Table 2. In the extreme, the entire SOV may be replaced as a precautionary measure at predetermined intervals based on lifetime expectations derived from environmental qualification tests, even though no obvious malperformance has been observed.

## MONITORING APPROACHES UNDER STUDY

Despite the recognized difficulties, the present (Phase II) studies are aimed at devising and then demonstrating the effectiveness of techniques and/or equipment with which to measure the performance parameters identified previously, so as to detect and trend the progress of any degradation that may eventually compromise the ability of a SOV to perform its intended function. In recognition of the cost effectiveness issue, initial attention has been focused on remotely applied, nonintrusive techniques, i.e., ones that do not require physical access to the SOV, the addition of sensors or signal wires, or even temporary removal of the valve from service. Once these nonintrusive techniques have been evaluated, we will study the technical merits of other monitoring methods that are less desirable from a standpoint of disruptiveness.

Table 1. Aging and malfunction of solenoid-operated valves--  
Phase I study findings

---

Proximate causes of SOV failure/malfunction

- Electrical failure (open- or short-circuited coil)
- Mechanical failure due to worn or degraded parts
- Mechanical binding due to the presence of foreign materials (build-up of dirt, paint, polymerized lubricant, oil)

Degradation sites

- Elastomeric components (core seat; seals)
- Solenoid coil (insulation)

Aging mechanisms

- Change in material properties with time, temperature, radiation, chemical attack
- Conductor burnout
- Insulation failure

Root causes of SOV failure/malfunction

- Excessive operating temperature
  - Chemical attack of elastomers by oil
  - High-voltage transients
- 

Table 2. Measurable performance parameters, testing and surveillance methods identified by Phase I study

---

Quantitative measures of performance

- Coil resistance
- Coil power consumption
- SOV temperature
- Valve actuation time
- Valve flow coefficient,  $C_v$
- Internal (through-valve) leakage rate
- Presence of hum or chattering

Nonquantitative indicators of performance

- Visual inspection
    - general appearance of exterior
    - accumulated moisture, burned paint, cracked or frayed wiring
  - Audible check
    - buzzing or rattling in energized state
  - Operational check
    - rapid, smooth change of state
    - best if performed at extremes of rated valve pressure range
  - Inspection of internal components
    - not recommended on a periodic basis
    - necessary to establish replacement intervals for limited-life components
-

## DESCRIPTION

Although a number of potentially workable nonintrusive performance monitoring techniques have been identified, the three studied initially in a laboratory environment as part of this continuing study are

- Inference of coil temperature via in-situ measurement of the coil's electrical dc resistance or ac impedance, combined with an experimentally established temperature coefficient of resistivity for the copper winding [(same principle as a resistance temperature detector (RTD))]
- Determination of the balance points between electrical (magnetic), spring (restoring), and friction forces within the SOV assembly by measuring electrical current (or voltage) at the SOV pickup and dropout points
- Indication of plunger position within the solenoid coil, as well as freedom of plunger movement, by means of SOV ac impedance changes associated with position-dependent magnetic flux coupling

The first technique addresses the issue of reduced coil life attributable to excessive SOV operating temperature. The principal merits of the cited approach include (a) the SOV coil serves as its own temperature sensor, (b) the true temperature of the critical part (the coil winding) is directly measured, (c) temperature readout can be provided at any location where the SOV lead wires can be accessed, no matter how remote from the valve, and (d) the SOV need not be disturbed (whether energized or de-energized) to infer its operating temperature.

The second technique addresses (a) the issue of mechanical failure due to worn, degraded, or improper parts or incorrect assembly of proper parts and (b) the issue of mechanical binding resulting directly from the presence of foreign materials or indirectly from chemical attack of elastomeric components. The principal merits of the technique are its ability to sense impending trouble both remotely and without need for add-on sensors or wiring. Its chief disadvantage is the need for application of a special ramped voltage profile during actuation of the SOV under test.

The third technique addresses mechanical issues similar to those of the second technique, but, as a method which establishes plunger position precisely, it should provide additional (or confirmatory) information regarding such problems as elastomeric seat degradation (and associated through-valve leakage), faulty valve assembly or the use of incorrect parts, or the presence of chips, dirt, and foreign objects. Depending upon the nature of the information to be obtained, the third technique can be implemented as a static measurement, a dynamic measurement performed during normal SOV actuation, or a dynamic measurement requiring application of a special ramped voltage profile.

## RESULTS

### Coil temperature inference

Figure 1 shows the results obtained when several SOVs, representing both ac and dc types and different manufacturers, were placed in a thermostatically controlled oven and their dc resistances measured at a number of elevated temperatures. In every case an extremely linear relationship (correlation coefficient  $>0.9997$ ) was obtained over the temperature range of interest ( $20^{\circ}$  to  $170^{\circ}\text{C}$ ). Note that the magnitude of the temperature coefficient of resistance is sufficiently large (0.3 to 0.4% per  $^{\circ}\text{C}$ ) to permit temperature inference to better than  $\pm 10^{\circ}\text{C}$  accuracy using resistance measurement equipment of only modest (3%) accuracy. Temperature measurement accuracy of this order is thought to be adequate for indicating coil temperatures that exceed good practice ceilings established by qualification tests or service life prediction curves. It is also important to realize that the trend of the indicated coil temperature over a time span of months may be as important to assessing SOV condition and operability as a knowledge of the coil's absolute temperature.

Figures 2 and 3 illustrate the practical application of this technique in which the SOV coil acts as its own RTD. In the first test (Fig. 2), a coil resistance of 798 ohms was established from applied electrical potential and current readings taken at ambient ( $24^{\circ}\text{C}$ ) when the SOV was first energized. Using this single calibration point, in conjunction with the empirically

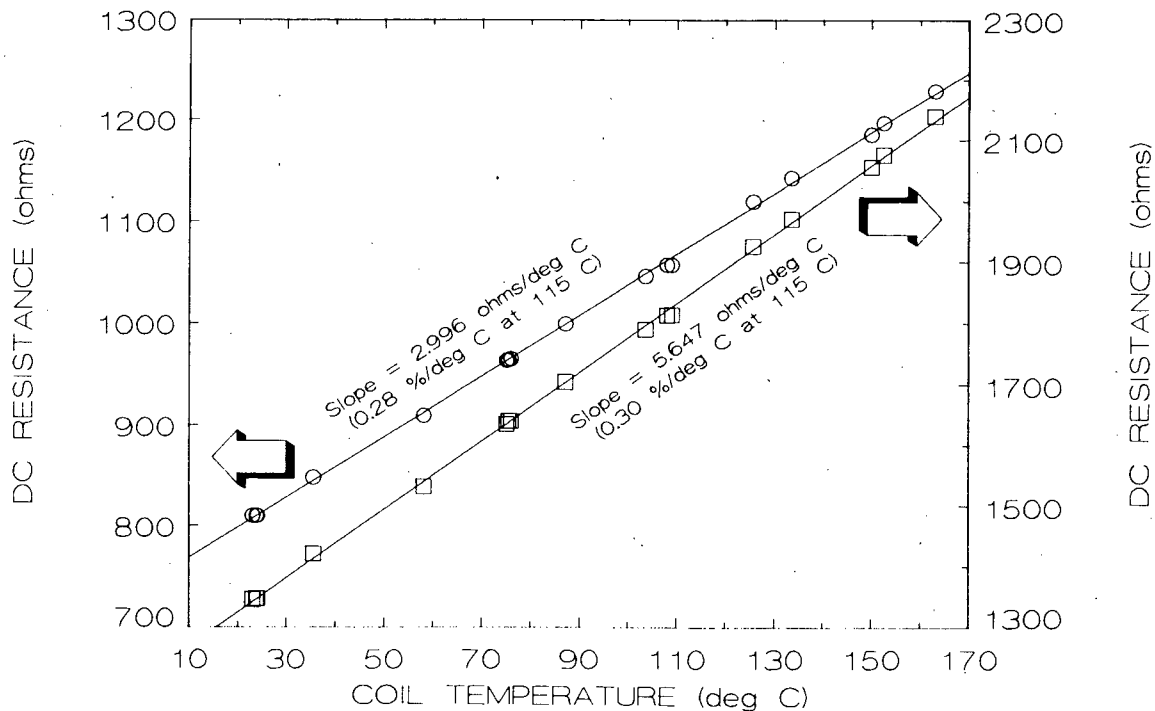


Fig. 1. Temperature dependence of coil dc resistance.

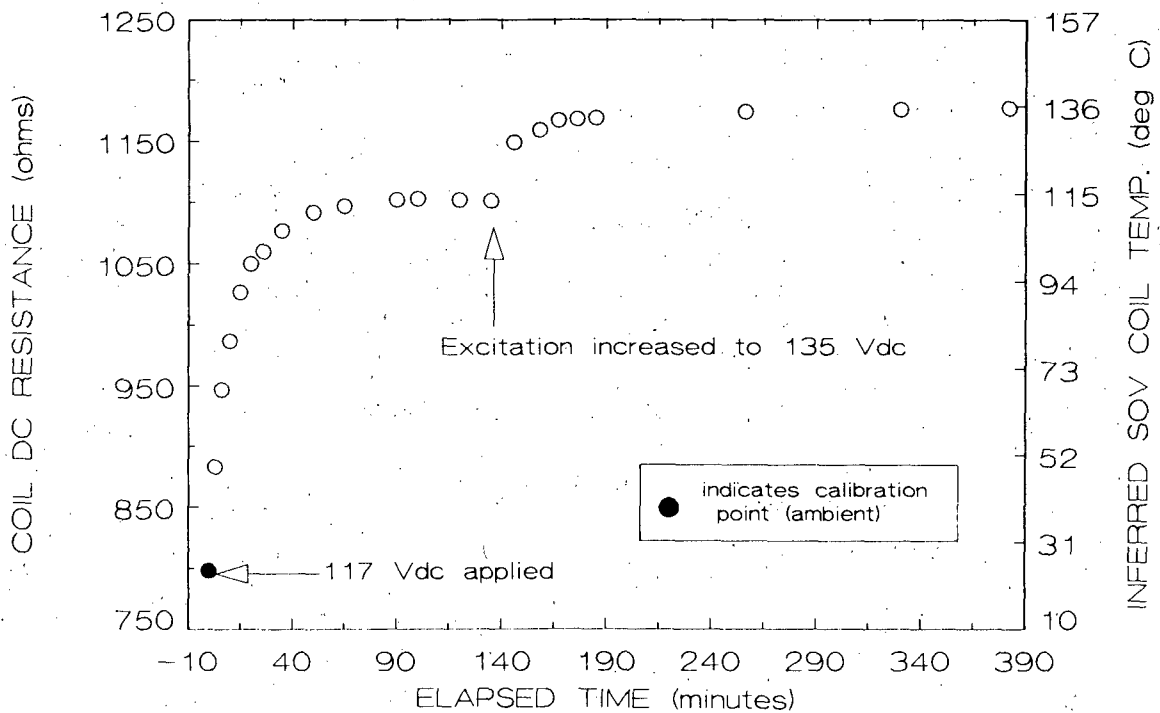


Fig. 2. Coil temperature increase resulting from continuous excitation at two different voltage levels.

determined slope of the resistance vs temperature relationship for this particular valve (3.41 ohms/°C), we can establish a temperature scale for the right-hand axis of the graph which exactly matches the directly measured resistance scale on the left-hand axis, and thereby we can track the changes in SOV coil temperature that accompany altered test conditions. The solenoid temperature is seen to rise to about 113°C during the first 90 minutes after application of 117 Vdc. At about 140 minutes into the test, the applied voltage was increased to 135 V (a typical value for station batteries on charge), causing the coil temperature to rise to 135°C. The following day (Fig. 3), the SOV was again brought to thermal equilibrium at about the same excitation voltage, but, owing to somewhat restricted air circulation around the SOV, a somewhat higher asymptotic temperature (139°C) was attained. At 95 minutes into the test, a fan was directed on the SOV, thereby increasing heat transfer and reducing the inner coil temperature to about 116°C. At a time of 145 minutes, power was removed from the valve, allowing its temperature to return to ambient rather rapidly. The final indicated temperature, based on coil resistance, was 23.4°C; this compares very well with the true temperature of 23.0°C (indicated in Fig. 3 by a square symbol) read from a mercury-in-glass thermometer placed in contact with the SOV.

#### Mechanical binding

Turning to the second (force balance) monitoring technique, Fig. 4 illustrates the current/voltage relationship obtained for an ac-powered SOV when the

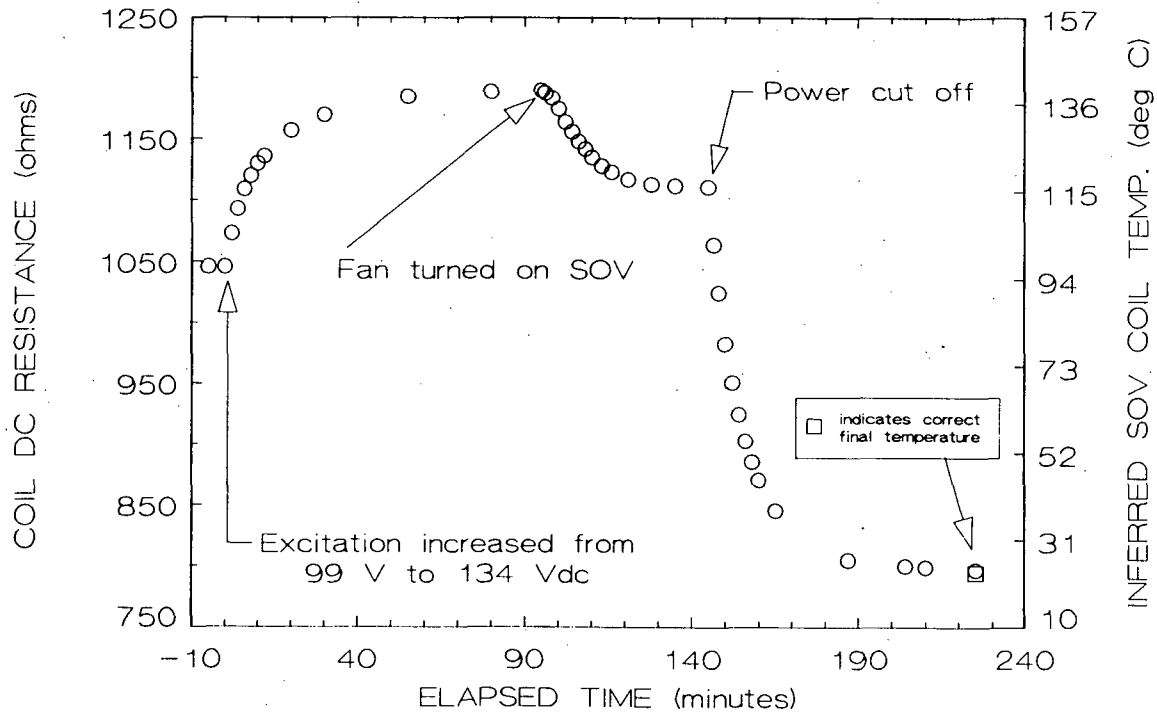


Fig. 3. Coil temperature decreases produced by forced convection cooling and de-energizing.

voltage was ramped up linearly over a time interval of about 50 s. Curve "A" was obtained with a clean, normally assembled valve, whereas curve "B" was obtained from a valve of identical construction except that the solenoid core (plunger) and the interior of its guide tube were liberally coated with shellac just prior to the test to simulate the mechanical binding reported in LERs caused by polymerized lubricants or unfiltered air supplies. The curves track each other extremely well in the low- and high-excitation regions representing static plunger positions (i.e., purely electrical properties), but differ markedly in the middle region of the graph where the valve actually changes state. The "normal" SOV is seen not only to change state at a lower level of excitation than its "gummy" counterpart, but also to exhibit some hesitancy to make the change of state (the valve was audibly buzzing at this time during the ramp-up) whereas the faulted SOV displays a smoother (damped) transition once sufficient magnetic force is present to overcome the resistance to movement produced by the sticky shellac. Figure 5, representing an excitation ramp in the decreasing rather than increasing direction, also shows a pronounced difference between the voltage/current transition points for the normal and abnormal SOVs. Although these early results appear promising, at this point in the study we have not performed a sufficient number of repeat tests to prove that trending the SOV pull-in and drop-out points provides a reliable, consistent indicator of SOV internal condition.

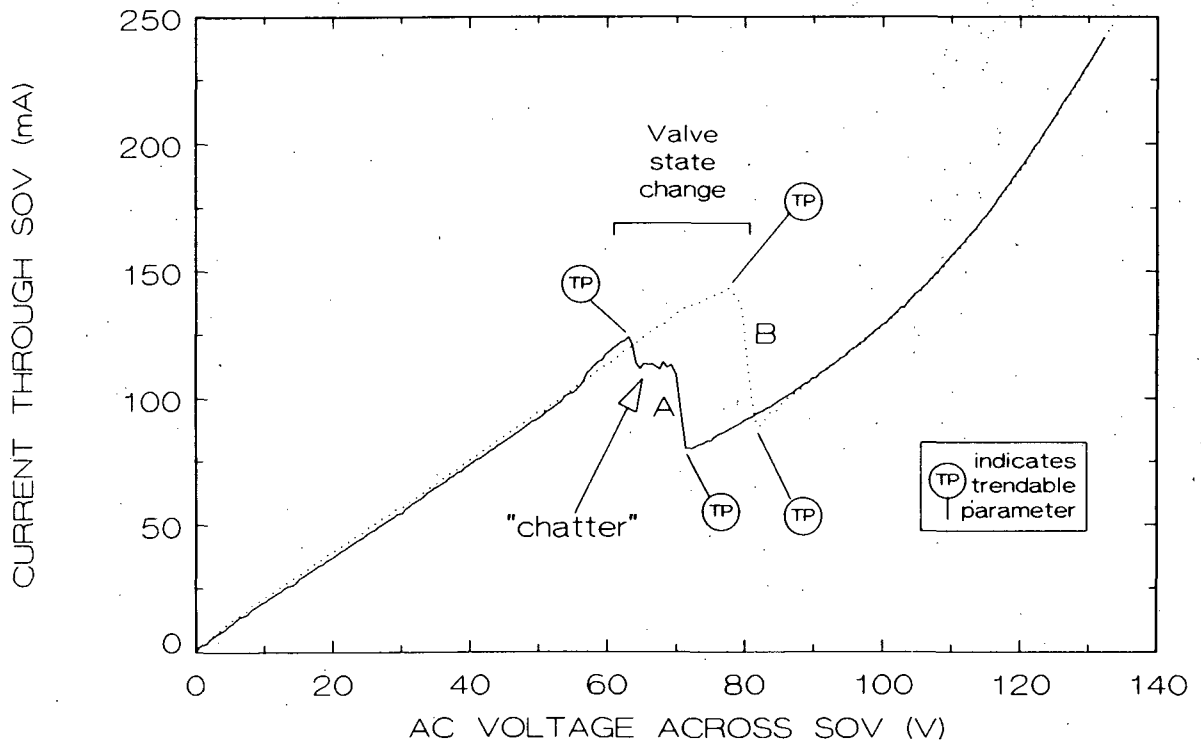


Fig. 4. Ac current/voltage characteristics obtained during excitation ramp-up. "A": clean, normally assembled SOV, "B": valve treated to produce mechanical binding.

#### Plunger position indication

Figure 6 illustrates the third electrically based performance-indicating technique studied thus far, the indication of absolute plunger position through measurement of ac impedance presented at the SOV electrical leads. SOV impedance (at 60 Hz) is seen to increase about 30% as mutual inductance builds in the current region 0 to 50 mA, then remains about constant until 130 mA is reached, at which point the plunger is abruptly drawn into the solenoid. This change of valve state produces nearly a doubling of the impedance, which then decreases fairly rapidly as excitation is increased, due to increased eddy currents and magnetic saturation of the core iron. This excitation-level-dependence of ac impedance unfortunately complicates considerably the relationship between measured impedance and coil temperature but can be turned to advantage in providing a very sensitive measure of plunger position within the coil (hence, position within the valve body). Measurements made with movement-restricting shims of various thicknesses have shown a typical impedance sensitivity figure of  $\delta Z/\delta d \approx 7$  ohms/mil of displacement (1.5% change in Z per mil) at the unenergized seat position, implying that an impedance measurement performed on an SOV at known

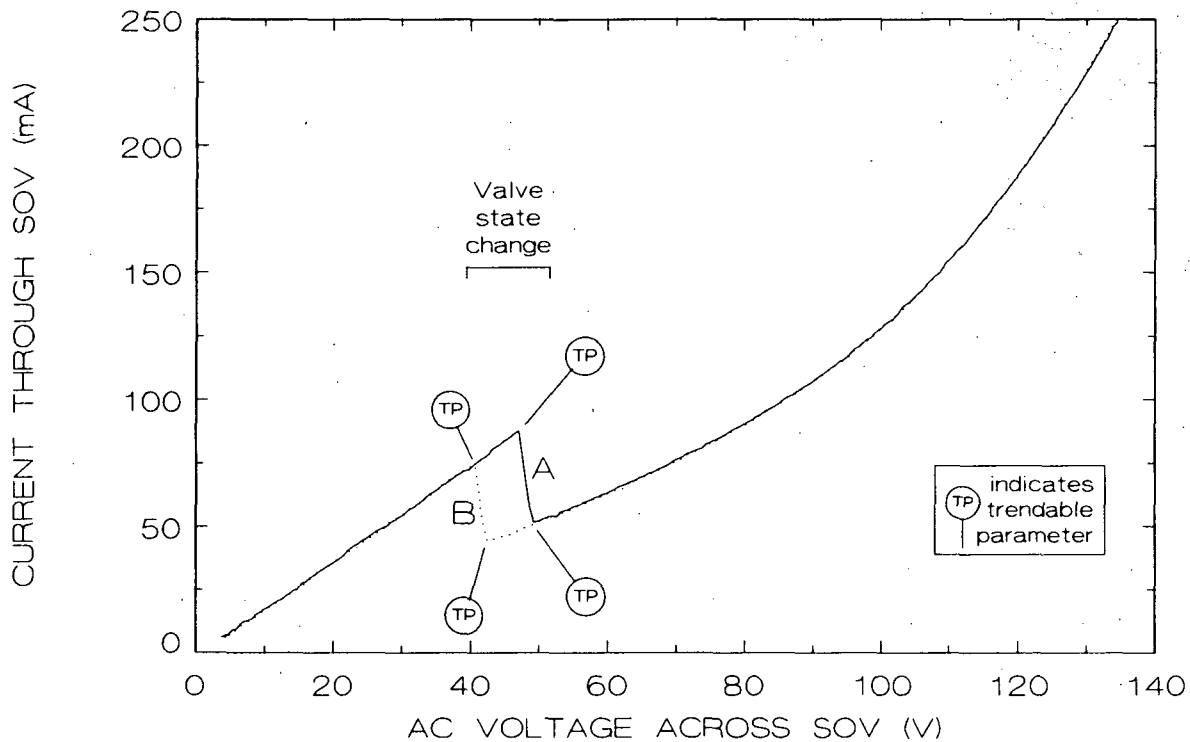


Fig. 5. Ac current/voltage characteristics obtained during excitation ramp-down. "A": clean, normally assembled SOV, "B": valve treated to produce mechanical binding.

temperature and excitation should provide indication of plunger displacements as small as a few thousandths of an inch. This technique may thus prove useful in detecting the presence of foreign objects within the valve, degraded seats, or other abnormalities leading to displacement of the plunger from its two normal resting points.

#### FUTURE WORK

A number of additional monitoring and diagnostic measurement techniques have been identified for study. These include:

- Sensing the presence of humming or chattering of the plunger assembly within ac-powered SOVs using either frequency analysis of the coil current signal or acoustic sensors placed in close proximity to the valve
- Analyzing the detailed time "signature" of the inrush current flow accompanying SOV actuation
- Detecting the presence of shorted turns in the SOV coil using interrupted-current testing principles

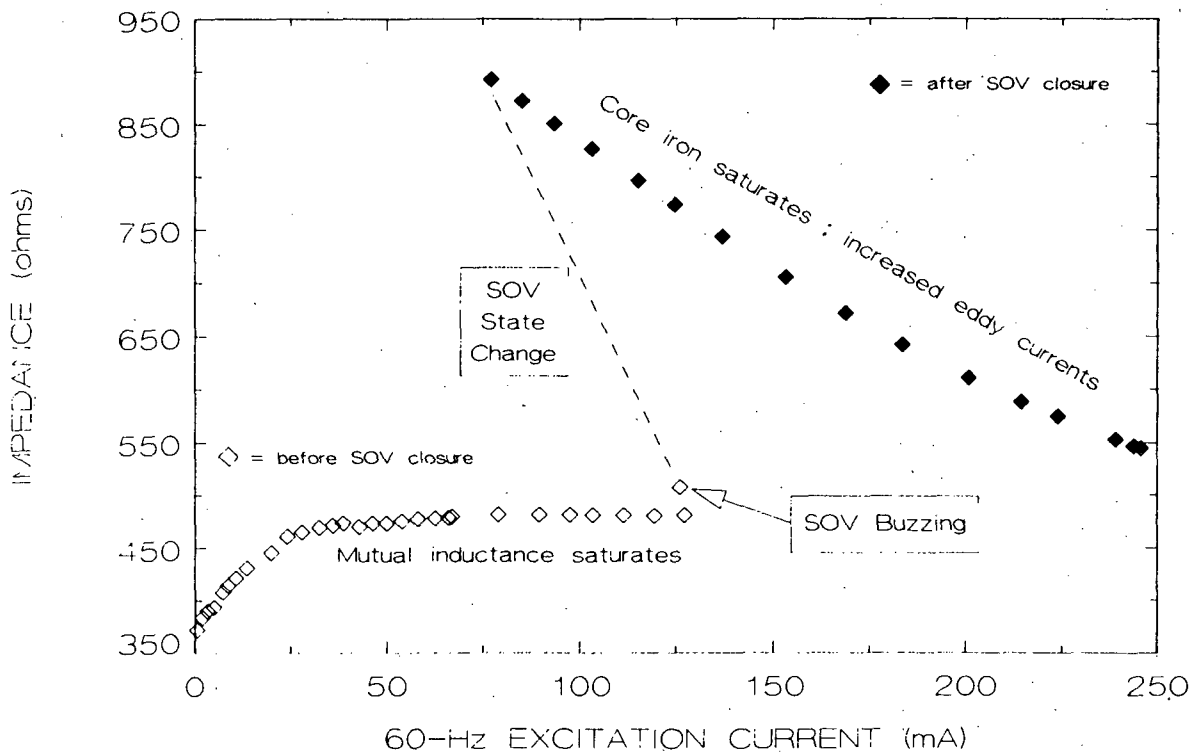


Fig. 6. Excitation current dependence of SOV impedance.

The first two techniques may be sensitive to worn or improper parts, valve misassembly, the presence of foreign materials, degraded elastomers, and misalignment of the solenoid core. The second technique (inrush current signature) has been studied by others<sup>3</sup> with somewhat inconclusive results; however, the data analysis employed focused almost exclusively on the frequency domain, and it is believed that time domain methods need further exploration before the merit of the technique can be determined. The third technique, which has apparently proved valuable to NASA,<sup>4</sup> should provide an early indication of SOV coils that have been damaged by high-voltage transients. It is well known that coils with turn-to-turn shorts soon self-destruct to an open-circuit condition due to the rapid rise of temperature caused by internal heating at the short-circuit locations.

#### INTERIM CONCLUSIONS

Results obtained during the first six work-months of this continuing study support the following conclusions:

- The trending of several measurable performance parameters shows promise for determining operational readiness of solenoid-operated valves

- Parameters are sensitive to historically important failure modes/causes
- Techniques are minimally disruptive to plant operations
- Parameters can be measured at a location remote from the SOV
- The SOV can often act as its own sensor, thereby eliminating the need for additional instrumentation
- Study of additional performance monitoring techniques is warranted
  - Seek sensitivity to failure modes/causes not covered by techniques investigated to date
  - Tradeoff between degree of invasiveness and information obtained needs to be established

Clearly, any SOV monitoring methods seriously proposed for implementation by nuclear plants will require further examination in order to ascertain their limitations and practicalities.

#### REFERENCES

1. V. P. Bacanskas, G. C. Roberts, and G. J. Toman, Aging and Service Wear of Solenoid-Operated Valves Used in Safety Systems of Nuclear Power Plants, Vol. 1: Operating Experience and Failure Identifications, NUREG/CR-4819, V.1 (ORNL/Sub/83-28915/4/V1), March 1987.
2. "Work-in-Progress Report: Evaluation of Maintenance and Related Practices for Solenoid Operated Valves in Nuclear Power Generating Stations," IEEE Power Engineering Society, Nuclear Power Engineering Committee, Subcommittee 3, Working Group 3.3, September 1988.
3. R. D. Meininger and T. J. Weir, Development of a Testing and Analysis Methodology to Determine the Functional Condition of Solenoid Operated Valves, NUREG/CR-5008, September 1987.
4. "Pulse Coil Tester," NASA Tech Briefs, MFS-29301, Technology Utilization Office, George C. Marshall Space Flight Center (undated).



## SIMILARITY PRINCIPLES FOR SEISMIC QUALIFICATION OF EQUIPMENT BY EXPERIENCE DATA

Daniel D. Kana and Daniel J. Pomerening

Engineering and Material Sciences Division, Southwest Research Institute,  
San Antonio, Texas, 78284, USA

### Abstract

A methodology is developed for seismic qualification of nuclear plant equipment by applying similarity principles to existing experience data. Experience data is that available from previous qualifications by analysis or testing, or from actual earthquake events. Similarity principles are defined in terms of excitation, equipment physical characteristics, and equipment response. Physical similarity is further defined in terms of a critical transfer function for response at a location on a primary structure, whose response can be assumed directly related to fragility of the item under elevated levels of excitation. Procedures are developed for combining experience data into composite specifications for qualification of equipment that can be shown to be physically similar to the reference equipment. Other procedures are developed for extending qualifications beyond the original specifications under certain conditions. Some examples for application and verification of the procedures are given for actual test data available from previous qualifications. The developments are intended to elaborate on the rather broad guidelines by the IEEE 344 Standards Committee for equipment qualification in new nuclear plants. The results also contribute to filling a gap that exists between the IEEE 344 methodology and that which was previously developed for equipment in existing plants by the Seismic Qualification Utilities Group.

### 1. Introduction

Since about 1971 and certainly since 1975, seismic qualification of equipment for use in nuclear power plants has generally been accomplished by means of analyses, tests, and/or combined test and analysis methods [1]. A large volume of qualification data has been generated from this effort. The current trend is to compile the available data from this experience, as well as that from nuclear and non-nuclear plants that have been subject to actual earthquake events, and develop a formal methodology for qualification based on such experience data. Obviously, a reduction in time schedules and costs required by the above conventional methods are sought. The general guidelines for development of experience data

methodology have already been formulated [2], and are based on the concept of qualification by similarity. However, more specific guidance is necessary for the approach to be practical and to avoid its potential misapplication. The purpose of this paper is to present a basis from which the similarity principals originate, more specific similarity methodology, and some practical examples of the use of that methodology in qualification by experience.

The general approach to qualification by similarity [2] includes development of an argument that qualification of a new equipment item follows a-priori because of appropriate similarities between certain data which describes the equipment and its intended environment, and that which already exists in an experience data base. Herein, similarity will be denoted by the symbol  $\approx$ , which also means "approximately equal to in a designated frequency bandwidth," for certain parameters of the problem. Appropriate similarities can be defined according to the dynamic characteristics of a) the seismic excitation, b) the physical system (equipment), c) certain dynamic responses of the system, or d) combinations of these characteristics. Details of the approach for a specific case, including the degree of similarity necessary, will depend on the nature of the equipment and the existing data. However, certain fundamental principals must be applied in any case.

The contents of this paper are condensed from Reference [3], which can be consulted for more examples of application and discussion of its relationship to other similar published work on qualification by use of experience data. General terminology follows that for Reference [2], except for some new terms defined herein.

## 2. Fragility basis for similarity

Herein, we postulate that the ultimate basis for similarity principles resides in the concept of fragility [4] as depicted by specific example for an electrical cabinet in Figure 1. The cabinet is excited in a given direction by an acceleration time history  $a_x(t)$ , whose response spectrum is  $R_x(f)$ . The interior panel of the cabinet contains several devices whose functions are safety-related to the operation of a nuclear plant. As the amplitude of the excitation is increased on each of several successive test runs, the primary structure response  $a_y(t)$  at the critical device location also increases via the critical transfer function  $H(f)$ . All of the safety-related devices continue to function properly through their functional mechanisms  $M_f(f)$ , as evidenced by the acceptance criteria function  $B_f$ . Eventually at some excitation level one of the devices (which is designated as the critical device) malfunctions. The excitation response spectrum  $R_x(f)$  for this excitation level is further designated as the fragility response spectrum  $R_f(f)$ . Note that the malfunction is not determined by a measure of  $M_f(f)$  per se, but simply by an observation of the related acceptance criteria function  $B_f$ , such as relay chatter or trip.

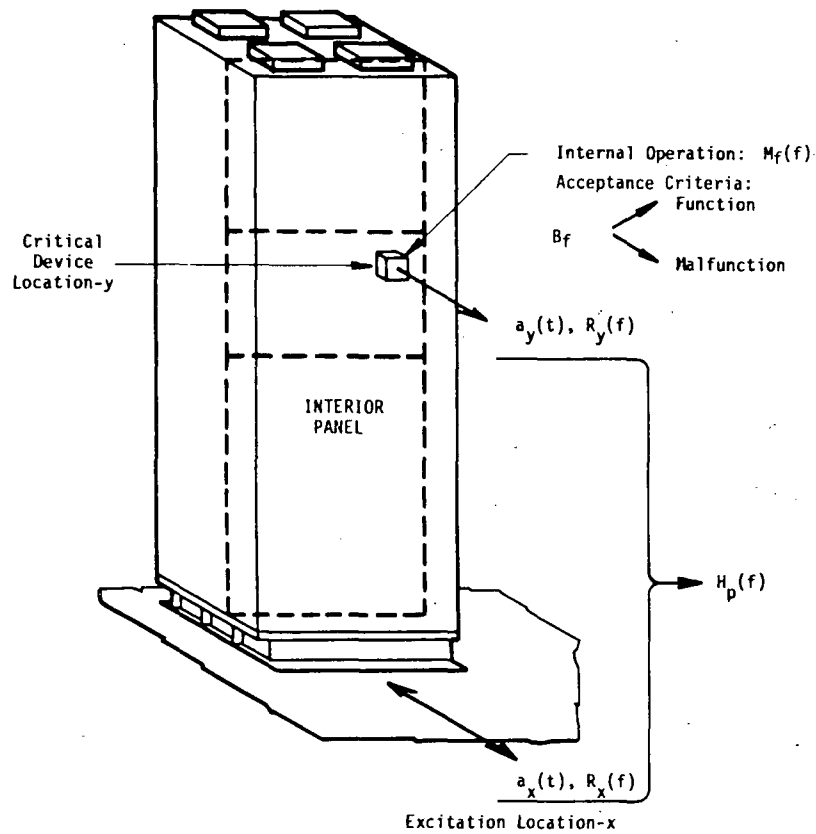
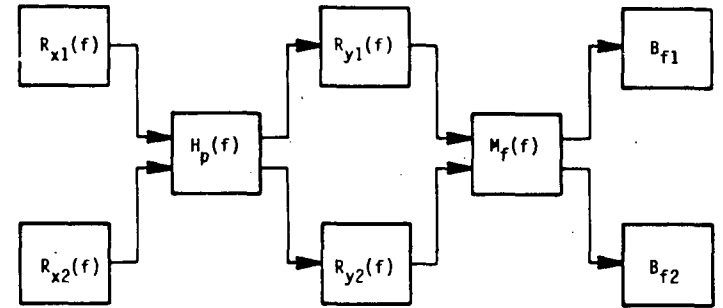


Figure 1. Specific example of equipment fragility



Given  $H_p(f)$  and acceptance function  $B_f$ ,

Excitational Equality:

If  $R_{x1}(f) = R_{x2}(f)$ ,

Then  $R_{y1}(f) = R_{y2}(f)$  and  $B_{f1} = B_{f2}$

so that

$$R_{F1}(f) \equiv R_{F2}(f) \text{ for all } f$$

Excitational Similarity:

If  $R_{x1}(\Delta f) \approx R_{x2}(\Delta f)$ ,

Then  $R_{y1}(\Delta f) \approx R_{y2}(\Delta f)$  and  $B_{f1} \approx B_{f2}$

so that

$$R_{F1}(\Delta f) \approx R_{F2}(\Delta f) \text{ for given } \Delta f,$$

which means "approximately equal response within a specified frequency range  $\Delta f$ ".

Figure 2. Definition of excitation similarity

Although response spectra are used for motion descriptions in Figure 1, power spectra can also be used. For example, if the critical transfer function  $H_p(f)$  is linear, one can write (see Refs. [5,6] for derivations):

$$a_y^* = 2\zeta_n |H_p(f_n)| R_x(f_n) \quad (2.1)$$

or 
$$G_y(f) = |H_p(f)|^2 G_x(f) \quad (2.2)$$

where  $| \cdot |$  denotes magnitude of the enclosed function. These two equations are expressed in forms that can be useful for both test and analysis purposes. At this point, they are used only generically to lend credence to the fragility concept displayed by the diagram in Figure 1. However, they are often used directly for analytical qualification or support of combined analytical and test qualifications.

It may be noted that Equation (2.1) is not a direct relationship for calculation of input and output response spectra, as Equation (2.2) is for power spectra, in conformance with Figure 1. In fact, no such simple direct relationship exists for response spectra. The relationship must be used 1) indirectly by a time history method, whereby a response spectrum  $R_y(f)$  is produced from a calculated response time history; or 2) indirectly whereby Equation (2.2) is used to calculate a response power spectrum  $G_y(f)$ , and this parameter is subsequently transformed to the response spectrum  $R_y(f)$ .

If the nature of the primary structure is nonlinear (which occurs to some degree in most equipment), Equations (2.1) and (2.2) do not apply directly, but are only approximations to the actual governing equations. Nevertheless, approximate linear evaluations are almost always used in analysis, since nonlinear approaches very quickly become impractical, except for special cases. Thus, quasi-linear developments which include evaluation of  $H_p(f)$  at a given response level may be appropriate when  $H_p(f)$  is a function of excitation amplitude. Furthermore, analytical expressions for  $R_y(f)$ ,  $M_f(f)$ , and  $B_f$  may be very complex and, in fact, are never determined explicitly. Also,  $M_f(f)$  represents a malfunction process that can be especially varied in the diversity of equipment used in nuclear plants. Usually, this process will apply to some critical device that is attached at an elevated position on the primary structure, as presented in Figure 1. However, it could also represent the stress level at some critical location in the primary structure itself. Some examples of how a critical process or device can malfunction are: exceeding threshold response for displacement, velocity, acceleration or stress; relay chatter or trip, etc. Thus,  $M_f(f)$  may be linear, nonlinear, or of logic form, which is difficult to write as a mathematical relationship. Nevertheless, the general concept depicted in Figure 1 is applicable in any case, and can be used in developing similarity principles without having to establish any mathematical relationships. In doing this, fragility is inherently

included by consideration of the function/malfunction of the equipment, rather than by development of exact fragility functions.

The use of the critical transfer function  $H_c(f)$  for the primary structure is inherent in all qualification scenarios by use of similarity principles to be used in this paper. In Figure 1, this transfer function has been defined relative to a base motion excitation, which typically may have been acquired from experimental resonance searches in previous qualifications. Herein, all applications and examples will be based on this type of transfer function, since it corresponds directly to excitation by earthquake ground or floor-level motion. However, it is apparent that the similarity procedures outlined in this paper can also be carried out by means of base-fixed transfer functions. This type of transfer function is typically measured by in-situ tests, or can readily be developed by analytical methods. Note that either type of transfer function can be used, but they cannot be mixed in the process of carrying out similarity arguments.

### 3. Types of similarity

A broad definition is given in Reference [2] for three types of similarity that are appropriate for use in equipment qualification. In this section, portions of these broad definitions will be paraphrased, and further developed into a correspondence with the general concept of equipment fragility defined in Figure 1. Each development will include, first, a definition of corresponding equality which, although it may be obvious, is the principle on which heretofore equipment qualification methodology is based. Then, follows a corresponding definition of similarity, so that the essential differences in equality and similarity can readily be established.

#### 3.1 Excitation similarity

##### 3.1.1 General definition

"Similarity of excitation constitutes likeness of parameters such as spectral characteristics, duration, directions of excitation axes, and location of measurement for the motions relative to the equipment mounting," [2]. Figure 2 provides an elaboration of this definition for application to a typical equipment qualification scenario, where a single equipment item with critical transfer function  $H_c(f)$  is alternately subjected to two different excitations corresponding to  $R_{x_1}(f)$  and  $R_{x_2}(f)$ . However, first consider this diagram as a representation of the current approach to qualification of a single equipment item not previously qualified, and then the similarity concept can be shown to be a direct extension of that approach. That is, in Figure 2, consider  $R_{x_1}(f)$  to be a RRS (Required Response Spectrum) that is prescribed for qualification of the item. If  $R_{x_2}$  is the TRS (Test Response Spectrum) for a test, then the current enveloping requirement is:

$$R_{x_2}(f) \geq R_{x_1}(f) \text{ for all } f.$$

The requirement is that not only excitational equality, but conservative similarity of excitation must exist at all frequencies.

Now consider a different practical situation in which the enveloping requirement will be relaxed somewhat. That is, given that a single equipment item has been qualified to excitation  $R_{x_1}(f)$ , what are the dynamic characteristics of excitation  $R_{x_2}(f)$  that must be similar to  $R_{x_1}(f)$  so that the item is also qualified to  $R_{x_2}(f)$ ? The intent behind the above quotation from Reference [2] becomes much clearer after referring to Figure 2, in which a more precise definition is based on the implied effects that the excitation has on the equipment. That is, the excitation causes some critical dynamic response via the equipment critical transfer function, and this response triggers some form of damage level in the equipment. However in contrast to the above described IEEE 344 requirements in which overall excitational equality is required, excitational similarity is defined whereby two spectra are required to be only approximately equal in certain discrete increments of the frequency range. Thus, a similar excitation is one which produces a similar damage level, even though the excitations are not identical at all frequencies. This can only occur if dynamic characteristics of the equipment also satisfy certain conditions. Therefore, the degree of similarity that must be shown in the excitation characteristics depends on what, if anything, can be predetermined about the equipment critical transfer function  $H_p(f)$  and the form of malfunction in the equipment in question. This leads to the definition of physical similarity, which is discussed hereafter. The implication is that two of the three types of similarity are necessary for qualification to be established when excitational identity is not present.

### 3.1.2 Waveform similarity

As defined in Figure 2, excitational similarity requires two spectra to be approximately equal within a designated bandwidth  $\Delta f$ , but not outside this band. However, it is intuitively apparent that differences of the spectra outside this band cannot be unlimited. This leads to the concept of waveform similarity, which assures that overall frequency bandwidth is sufficiently similar for two spectra, so that essential dynamic behavior of a system to which the excitation is applied is not changed dramatically outside the frequency band  $\Delta f$ . Therefore, waveform similarity may be assured providing that the ZPA/RMS (Zero Period Acceleration/Root Mean Square) ratio for the two excitations are nearly the same [6].

Since the ZPA/RMS ratio is not conveniently available from existing qualification data, it has been shown in Reference [7] that waveform similarity can be established approximately by comparing the maximum spectral acceleration to ZPA ratio ( $R_x^*(f)/ZPA$ ) for two response

spectra. This amplification factor varies with damping of the oscillator, and the bandwidth of the waveform. For example, at 5% damping, the amplification varies from 10.0 for a steady state sinewave, about 7.5 for a ten cycle per beat sinebeat, to about 2.6 for a random signal which matches a R.G. 1.60 spectrum. Therefore, waveform similarity of two spectra may be approximately assured when the maximum spectral amplification factors are nearly equal.

### 3.1.3 Excitation axes

The orientation of horizontal excitation is usually specified relative to principle geometric axes, i.e., front-to-back and side-to-side. The direction of excitation can have a significant bearing on the operation of various equipment. This direction of excitation has always been identified for qualifications in the past. Herein, it will be recognized throughout that subsequent use of data from such qualifications will include allowing for proper excitation orientation.

To summarize, when considering excitation similarity, the following specific items must be included:

- 1) Frequency distribution (response spectrum or PSD)
- 2) Peak amplitude
- 3)  $R_x^*(f)/ZPA$  factor
- 4) Time duration
- 5) Axes of orientation
- 6) Point of application

## 3.2 Physical similarity

### 3.2.1 General definition

"For a complete assembly, (physical) similarity may be demonstrated through comparison of make, model and serial numbers, and consideration of dynamic properties and construction. Since the end objective of qualification by the similarity method includes a consideration of the expected dynamic response, a rational approach can be used to establish similarity of dynamic structural properties by an investigation of physical parameters of equipment systems. This can be done by comparing the predominant resonant frequencies and mode shapes," [2].

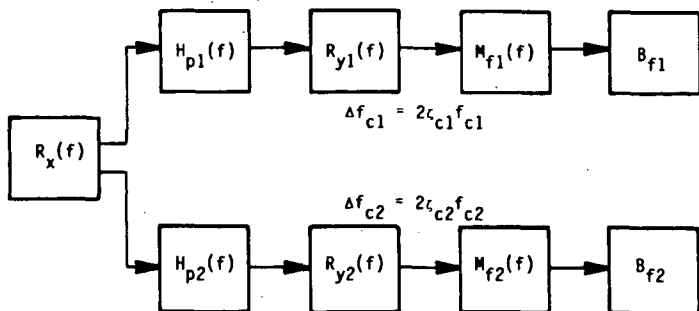
One explicit method to satisfy the above requirements includes development of transfer functions at locations important to the performance of the system. Therefore, herein, for the purpose of establishing physical similarity, the equipment will be characterized by a critical transfer function  $H_p(f)$ , which will be determined explicitly; and its acceptance function  $B_f$ , which will only be determined implicitly (i.e., by a pass/fail observation). This approach is consistent with previous qualification

procedures. The approach is shown conceptually in Figure 3, where two different equipment items are subject to the same excitation spectrum  $R_x(f)$ . The appropriate question becomes, how can the critical transfer functions for the two items best be established and compared, so that their common fragility response (and, therefore, physical similarity) can be established? The approach is outlined in the figure by first defining physical equality in terms of  $H(f)$  and  $B_f$ , and this leads to the further indicated definition of physical similarity. Therefore, the differences between the two can readily be distinguished. It may be noted that the definition of similarity indicated in Figure 3 could conceivably be satisfied even though the two equipment items were not similar functionally. That is, one might be an electrical cabinet and the other a valve. However, the most likely practical situation will be where both items are similar in general physical characteristics and function.

Figure 4 is useful to emphasize further how critical transfer functions can conveniently be used to compare directly the dynamic characteristics of different equipment, and to describe the "degree of physical similarity" in that equipment. In accordance with the concept shown in Figures 1 and 3, each equipment item is described by a primary structure critical transfer function  $H(f)$ . The dynamic response of the primary structure at the critical location is judged to be directly associated with the function/malfunction of the equipment. This transfer function may include a single dominant mode, as indicated for each item in Figure 4, or multiple modes. The critical bandwidth  $\Delta f_{c_i}$  for each item is a frequency band within which the dominant response occurs. (Obviously, the width of this band is determined by the damping in the equipment and any modal interaction present.) The composite bandwidth  $\Delta f_c$  is defined as the bandwidth between  $f_{c_i} - 1/2\Delta f_{c_i}$  and  $f_{c_j} + 1/2\Delta f_{c_j}$ , where  $f_{c_i}^{cc}$  is the lowest and  $f_{c_j}$  is the highest natural frequency present.

If two items had identical critical transfer functions, then they would satisfy physical equality (identity), as described in Figure 3. The amount of difference (i.e., bandwidth  $\Delta f_{c_i}$ , center frequency  $f_{c_j}$ , and magnitude  $H_i(f_{c_i})$ ) all determine the degree (i.e., large or small) of physical similarity present. Thus, large similarity denotes more nearly identical critical transfer functions for two items. Furthermore, it must be emphasized again that the critical transfer function  $H(f)$  is not just any dynamic response indicator, but in addition it must correspond to a critical location, whose response is directly associated with the function/malfunction of the equipment. Therefore, this description is totally sufficient, in that it includes all information necessary to describe the dynamic, functional, and fragility characteristics of the equipment, as required by Reference [2].

It may be noted that the indicated definition of physical similarity allows relaxation of the dynamic characteristics to where only approximate (but conservative) equality exists in certain discrete areas of the frequency range. The respective critical frequency  $f_{c_i}$  is one that



Given  $R_x(f)$ ,

Physical Equality:

If  $M_{f1}(f) = M_{f2}(f)$  and  $H_{p1}(f) = H_{p2}(f)$ ,

Then  $B_{f1} = B_{f2}$  and  $R_{y1}(f) = R_{y2}(f)$

$$\Delta f_{c1} = \Delta f_{c2}$$

so that

$$R_{F1}(f) \equiv R_{F2}(f) \text{ for all } f$$

Physical Similarity:

If  $M_{f1}(\Delta f) \approx M_{f2}(\Delta f)$  and  $H_{p1}(\Delta f) \approx H_{p2}(\Delta f)$

Then  $B_{f1} \approx B_{f2}$  and  $R_{y1}(\Delta f) \approx R_{y2}(\Delta f)$

$$\Delta f_{c1} \approx \Delta f_{c2}$$

with  $\Delta f_{c1}$  and  $\Delta f_{c2}$  both contained in  $\Delta f_{cc}$

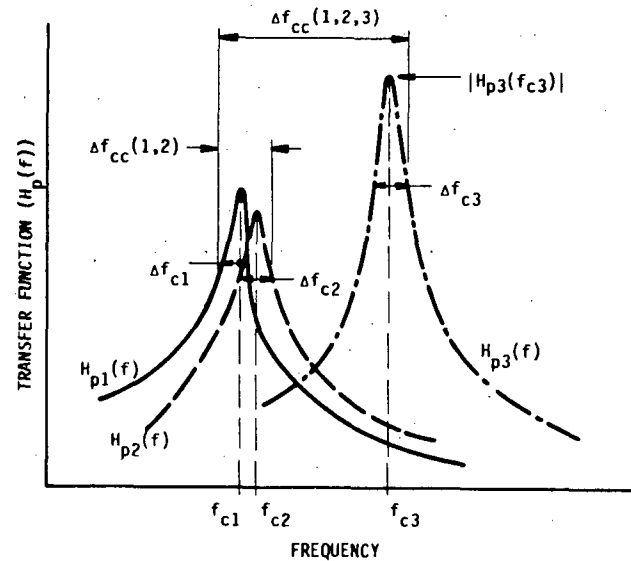
so that

$$R_{F1}(\Delta f_{cc}) \approx R_{F2}(\Delta f_{cc}) \text{ for given } \Delta f_{cc}$$

where

$$\Delta f_{cc} = \text{Preselected composite critical frequency bandwidth}$$

Figure 3. Definition of physical similarity



LARGE SIMILARITY: Items 1, 2

SMALL SIMILARITY: Items 1, 3  
Items 2, 3

$\Delta f_{ci}$  is bandwidth at half-power amplitude (i.e., 0.7 peak amplitude)

Figure 4. Degrees of physical similarity

would represent the minimum on a narrowband fragility function (or peak of  $H_p(f)$ ), and  $\Delta f_{ci}$  is taken as the frequency bandwidth of  $H_p(f)$  at the half-power response level. This selection of  $\Delta f_{ci}$  is relatively arbitrary, but is done to concentrate on a dominant bandwidth in which most of the response occurs. Use of the half-power bandwidth, as indicated in Figure 4, provides a simple relationship with the modal damping and critical frequency, or with the peak magnitude of  $H_p(f_{ci})$ , as will be indicated shortly. Note also that the composite critical bandwidth  $\Delta f_{cc}$  will be wider than  $\Delta f_{c1}$  and  $\Delta f_{c2}$ , as it must include them both, as indicated in Figure 4. Furthermore, only frequencies, bandwidths, and peak amplitudes of the critical transfer functions enter the essential part of the definition, as will be explained later. The degree of similarity, or extent of such commonality of approximation in frequency bands necessary to establish qualification in a given case also will depend on details of the excitation, as will be described later.

### 3.2.2 Procedure to establish physical similarity

In order to establish physical similarity between one equipment item (designated as Item 1) and another item (designated as Item 2), the following is one procedure that may be used:

- 1) Assume the most probable mode of malfunction for Item 1, and show by experience or deductive reasoning that this mode of failure is essentially alike that of Item 2.
- 2) Determine, by experience or deductive reasoning, a critical location on Item 1 whose dynamic response most probably affects the malfunction. Likewise, make this determination for Item 2.
- 3) Establish by test, analysis, or experience, a critical transfer function  $H_p(f)$  between the excitation point and the critical response point for both items. The degree of detail of this transfer function will vary considerably, depending on the method used and the accuracy of the data available. The most essential information is the critical frequency  $f_{ci}$ , the critical bandwidth  $\Delta f_{ci}$ , and the peak magnitude  $|H_{pi}(f_{ci})|$  for the critical transfer function. Note that:

$$\Delta f_{ci} = \Delta f \text{ at } 0.7 |H_{pi}(f_{ci})|$$

which can be obtained from an experimental plot, or

$$\Delta f_{ci} = 2\zeta_{ci} f_{ci}$$

which can be calculated if the modal damping  $\zeta_{ci}$  is available.

- 4) Verify that the critical transfer function peak magnitudes satisfy:

$$|H_{p1}(f_{c1})| \leq |H_{p2}(f_{c2})|$$

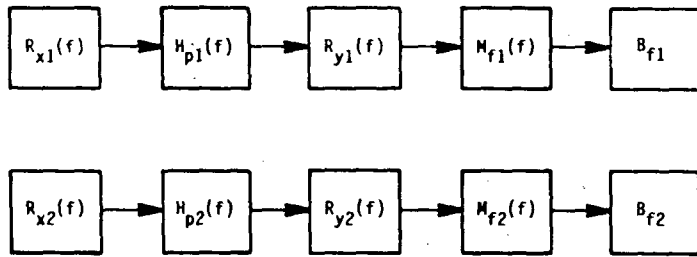
- 5) Within the assumptions of mode of failure and critical location, the two items can be defined to be physically similar in a bandwidth up to a composite critical bandwidth  $\Delta f_{cc}$ , where

$$\Delta f_{cc} = (f_{c1} - 1/2\Delta f_{c1}) \text{ to } (f_{c2} + 1/2\Delta f_{c2}). \quad (3.1)$$

The exact approach by which the above steps are performed will vary significantly depending on the kind of data available, and the nature of the two equipment items. Furthermore, the process must be repeated if more than one mode of failure is suspected to be present, unless all critical bandwidths  $\Delta f_{ci}$  are shown to be included in the composite bandwidth  $\Delta f_{cc}$ . Note also that the magnitudes of the critical transfer functions  $H_{pi}(f_i)$  are influenced both by equipment damping and modal participation factors. Thus, if the equipment is dynamically similar (i.e., stiffness, mass, boundary conditions), then similarity of modal participation is assured. Furthermore, if damping is approximately equal, then physical similarity is assured within a given  $\Delta f_{cc}$  simply by showing that the various  $f_{ci}$  fall within that band. The useful part of  $\Delta f_{cc}$  as defined above will depend on how the available excitation energy is distributed in the frequency band that corresponds to  $\Delta f_{cc}$  for the equipment in a given case, as will be shown later.

### 3.3 Dynamic response similarity

When used in combination, excitation and physical system similarity are probably sufficient to address most practical problems that will arise in equipment qualification. However, dynamic response similarity is a concept that may be used to extend the qualification by experience even further. "A physical system response can be described through the same quantities as excitation (e.g., duration, frequency content, amplitude, etc.) or through failure modes of the system." Figure 5 provides a more precise definition of dynamic response similarity. That is, given that similarity of response and malfunction behavior can be established, what further can be concluded about the similarity of the excitation and/or the physical system? The implication is that dynamic response similarity can be used in an inverse approach along with physical similarity to establish excitation similarity, or along with excitation similarity to establish physical similarity. This all follows from the interrelationship of the excitation, physical system, and response characteristics as depicted in Figure 1. The various detailed ways in which this interrelationship can be applied to solve practical problems is still very much under development. Some of these applications follow, herein.



Given two independent experiments,

Response Equality:

If  $R_{y1}(f) = R_{y2}(f)$  and  $B_{f1} = B_{f2}$

along with

Method: A)  $H_{p1}(f) = H_{p2}(f)$  or B)  $R_{x1}(f) = R_{x2}(f)$   
 and  $M_{f1}(f) = M_{f2}(f)$  then  $H_{p1}(f) = H_{p2}(f)$   
 then  $R_{x1}(f) = R_{x2}(f)$  and  $M_{f1}(f) = M_{f2}(f)$

so that

$R_{F1}(f) = R_{F2}(f)$  for all  $f$

Response Similarity

If  $R_{y1}(\Delta f) \approx R_{y2}(\Delta f)$  and  $B_{f1} \approx B_{f2}$

along with

Method: A)  $H_{p1}(\Delta f) \approx H_{p2}(\Delta f)$  or B)  $R_{x1}(\Delta f) \approx R_{x2}(\Delta f)$   
 and  $M_{f1}(\Delta f) \approx M_{f2}(\Delta f)$  then  $H_{p1}(\Delta f) \approx H_{p2}(\Delta f)$   
 then  $R_{x1}(\Delta f) \approx R_{x2}(\Delta f)$  and  $M_{f1}(\Delta f) \approx M_{f2}(\Delta f)$

with  $\Delta f_{c1}$  and  $\Delta f_{c2}$  both contained in  $\Delta f_{cc}$

so that

$R_{F1}(\Delta f_{cc}) \approx R_{F2}(\Delta f_{cc})$  for given  $\Delta f_{cc}$

where

$\Delta f_{cc}$  = Preselected composite critical frequency bandwidth

Figure 5. Definition of response similarity

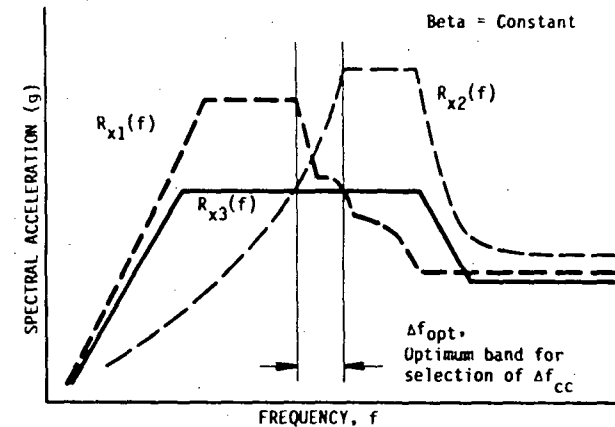


Figure 6. Development of composite response spectrum for physically identical equipment

#### 4. Similarity applications

There are many conceivable practical qualification scenarios to which the previously developed principles may be applied. Within this section, several typical hypothetical scenarios will be described, and details given for use of the principles for providing a solution to a typical problem. Examples which include data taken from actual qualifications will follow in Section 5.0.

##### 4.1 Composite spectra

Generation of composite spectra is one of the most fundamental requirements for equipment qualification by similarity. One typical objective may be to extend the qualification of a single previously-qualified item. Another typical objective may be to develop a generic data base for use in qualifying other equipment (candidate items) whose physical similarity can be established relative to previously-qualified equipment (reference items), whose available data are used to generate the composite spectrum. In accordance with Reference [2], a composite spectrum is defined to be formed within the envelope of several reference spectra (i.e., TRSs for several reference equipment items), and is likely to produce equal or less response than any one of the individual reference spectra. The procedure for generating the composite must include consideration of all equipment vibrational modes which are significant in determining its structural integrity and functional operability. This section contains several scenarios which include generation of a composite spectrum.

##### 4.1.1 Composite spectrum for physically identical equipment

For simplicity, a composite spectrum will first be developed for a case which involves only a single item of equipment. Generation of a composite spectrum will be described by the example shown in Figure 6. That is, given a single equipment item that has been qualified to  $R_{x_1}(f)$  and also to  $R_{x_2}(f)$ , demonstrate that it is also qualified to the composite spectrum  $R_{x_3}(f)$ . This requires the following steps:

- 1) Establish the critical transfer function  $H_p(f)$  for the item as performed in Paragraph 3.2.2. In this case, physical equality exists since only a single item is involved. The critical frequency range  $\Delta f_{cc}$  is taken as the bandwidth of  $H_p(f)$  at 0.7 times the peak value, or  $2\zeta_c f_{ci}$  (i.e.,  $\Delta f_{cc} = \Delta f_{cc}$ ).
- 2) Satisfy excitation similarity by confirming that  $R_{x_3}(f)$  is equal to or less than both  $R_{x_1}(f)$  and  $R_{x_2}(f)$  within  $\Delta f_{cc}$ . By this requirement, the approach is conservative within the critical bandwidth.

- 3) Confirm that the ZPA for  $R_{x_3}(f)$  is equal to or less than the largest ZPA present. By this requirement, the approach is conservative for rigid body response.
- 4) Satisfy waveform similarity by confirming that the ZPA/RMS ratio or the maximum spectral amplification factor for the composite spectrum is within the range of those for the individual constituent spectra.
- 5) If the absence of multimode interaction cannot be justified (i.e., when the constituent spectra represent sinewave, sinebeat, or other narrowband waveforms), the composite spectrum must be multiplied by 0.7 [8].

It should be noted that the complete determination of the critical bandwidth  $\Delta f_{cc}$  is accomplished in Step 1. However, the utility of the final process is greatly influenced by how the thereby determined  $\Delta f_{cc}$  matches with  $\Delta f_{opt}$ , the "optimum band for selection of  $\Delta f_{cc}$ ", as indicated in Figure 6. This has implications on how a database can optimally be developed from various response spectra that may be available from previous qualifications. Furthermore, if the individual constituent spectra  $R_{x_1}(f)$  and  $R_{x_2}(f)$  are based on relatively broadband waveforms, then use of the 0.7 factor is not warranted.

#### 4.1.2 Composite spectrum for physically similar equipment (direct method)

Consider now development of a composite spectrum  $R_{x_3}(f)$  for a case where one reference item has been qualified to  $R_{x_1}(f)$  and a second reference item has been qualified to  $R_{x_2}(f)$ , where the three spectra are as given in Figure 6. Physical similarity for the two reference items will be established by means of Paragraph 3.2.2, which involves direct consideration of equipment dynamic characteristics.

- 1) The critical transfer function  $H_{p_i}(f)$  for each item must be established by the 5-step physically similar process described in Paragraph 3.2.2. For illustration, assume that they correspond to  $H_{p_1}(f)$  and  $H_{p_2}(f)$ , respectively, in Figure 4. Establish the composite critical bandwidth  $\Delta f_{cc}$  by use of Equation (3.1), which results in the bandwidth  $\Delta f_{cc}(1,2)$  in Figure 4. Thus, physical similarity exists within  $\Delta f_{cc}(1,2)$ .
- 2) From this point, Steps 2-5 of Paragraph 4.1.1 for physically identical items are also required to generate the composite spectrum for this case.

Note that in view of Step 2 of Paragraph 4.1.1, knowledge about variation in the peak magnitudes on the transfer functions (i.e., Step 4 of

Paragraph 3.2.2) is not necessary for generating the composite spectrum. However, use of this step will be necessary for further use of the composite spectrum for qualifying other candidate similar equipment. Furthermore, the comments at the end of Paragraph 4.1.1 which relate to  $\Delta f_{\text{opt}}$  as the "optimum bandwidth for selection of  $\Delta f_{\text{cc}}$ " are again very pertinent.

#### 4.1.3 Composite spectrum for physically similar equipment (response method)

Again, consider the case where one equipment item has been qualified to  $R_{x1}(f)$  and a second equipment item has been qualified to  $R_{x2}(f)$ , where the two spectra are as given in Figure 6. No detailed resonance search data were acquired at elevated response locations on the primary structure during the original qualifications. However, elevated response spectra  $R_{y1}(f)$  and  $R_{y2}(f)$  were acquired, for it was anticipated that secondary devices might be exchanged on the primary structure at a later date. Generation of a composite response spectrum  $R_{x3}(f)$  is now desired. As before, generation of a composite spectrum requires demonstration of physical similarity and excitation similarity. However, in this case, physical similarity must be demonstrated indirectly via response similarity as described in Paragraph 3.3 and Method B) in Figure 5, because of the type of data available.

- 1) The respective elevated locations on the primary structures at which  $R_{y1}(f)$  and  $R_{y2}(f)$  were acquired are judged to be critical response locations. Therefore, the elevated spectra become critical response spectra in the dominant critical bandwidths which correspond to resonances of the equipment. It is also noted that, for these bands,

$$R_{y1}(\Delta f_{c1}) \approx R_{y2}(\Delta f_{c2})$$

where the  $\Delta f_{c_j}$  are selected at 0.7 times the amplified peak over the ZPA<sup>cj</sup> level of the spectrum.

- 2) Since both items functioned properly during their previous qualification, by definition:

$$B_{f1} \approx B_{f2}$$

for the given excitations  $R_{x1}(f)$  and  $R_{x2}(f)$ .

- 3) A critical bandwidth  $\Delta f_{\text{cc}}$  is selected so that:

$$R_{x1}(\Delta f_{\text{cc}}) \approx R_{x2}(\Delta f_{\text{cc}})$$

with both  $R_{x_1}(\Delta f_{cc})$  and  $R_{x_2}(\Delta f_{cc})$  greater than  $R_{x_3}(\Delta f_{cc})$ . Thus, excitation similarity is assured, and physical similarity follows within  $\Delta f_{cc}$  indirectly from Method B of Figure 5.

- 4) From this point, Steps 3-5 of Paragraph 4.1.1 are again required.

Note that again Step 4 of Paragraph 3.2.2 is not employed for generating the composite spectrum. However, that step is necessary for subsequent use of the composite spectrum for qualifying other candidate similar equipment. In all three examples (4.1.1, 4.1.2, and 4.1.3), the qualification data has been considered as a lower bound for the respective fragility response spectra. Furthermore, the latter two examples represent a procedure whereby a reference database for a similar set of equipment and its associated composite spectrum can be generated. In both cases, an optimum selection for the reference equipment and associated spectra will be possible, depending on the relationship of the  $\Delta f_{cc}$  developed from the critical transfer functions and the distribution of frequencies in the response spectra.

#### 4.2 Qualification by similarity

Assume that similarity for a group of existing reference equipment has been established according to Paragraph 3.2.2 and a composite spectrum based on test data for this equipment has been generated according to Paragraph 4.1.2 or 4.1.3. To qualify an additional candidate item for which no previous qualification has been performed, it must be shown that  $\Delta f_{c_i}$  for the candidate items falls within  $\Delta f_{cc}$  for the database items (and, therefore, within  $\Delta f_{opt}$  for the database excitation spectra). The procedure is as follows:

- 1) Establish physical similarity between the candidate item and at least one reference item according to Paragraph 3.2.2.
- 2) Note that Step 4 in Paragraph 3.2.2 is satisfied providing that the peak transfer function magnitude for the candidate item is less than or equal to that for at least one reference item in the data base, and the composite spectrum is relatively flat within  $\Delta f_{cc}$ . Magnitudes can be shown by measurements or by similarity of modal participation and damping. Furthermore, the critical bandwidth  $\Delta f_{c_i}$  for the candidate item must fall within the composite critical bandwidth  $\Delta f_{cc}$  for the group of reference equipment.
- 3) Qualification of the candidate item to the composite spectrum for the group of reference equipment is therefore accomplished.

## 5. Application to instrument panel qualification

Several applications which deal with actual equipment and data available from its qualification will now be discussed. The examples are based on generic groups of equipment whose functional (operational) characteristics are very similar.

Given that a selection of existing qualification data for instrument panels is available, it is desirable to organize the data into a form that can be used to qualify by experience various subsequent designs of instrument panels, and to develop appropriate justification for the process. This means that similarity of the equipment group must be established and a composite spectrum developed. Basically, the principles outlined in Paragraph 4.1.2 are to be applied. However, when various data is available, more must be said about optimum selection of the data on which the composite is to be based.

Physical data for three wall-mounted and one floor-mounted instrument panels are given in Table 1. Additional qualification data for these panels are given in the subsequent figures. All panels indicated are of similar design, in that they include very nearly the same instrumentation devices mounted on different primary structures. Furthermore, Panels 1-3 are wall-mounted, while Panel 4 is floor-mounted. Nevertheless, it is stipulated that the critical functioning of each item is governed by a device mounted at the respectively-indicated critical locations, whose transfer functions coincide with those given in the available data. Note that not much physical data is given in the tables. In fact, not much is needed, since the primary description necessary to establish similarity resides in the critical transfer functions.

### 5.1 Composite spectrum for wall-mounted panels

Generally, in developing a composite spectrum for use as a reference data base, it will be most advantageous to select two reference equipment items whose functional (operational) characteristics are quite similar, but whose critical transfer functions provide a relatively wide composite critical bandwidth  $\Delta f_{cc}$ . That is, the two items display relatively small similarity, such as Items 1 and 3 in Figure 4. At the same time, the two items should have been qualified to relatively high excitation levels. Furthermore, all individual spectra must be calculated at the same damping level for comparison purposes. It will be seen that this results in a relatively high level excitation composite which can be applied over a wide frequency range. Thus, the composite spectrum will be more generic in nature, and will be applicable to equipment having a wider range of dynamic characteristics. Therefore, the utility of the data base will be more extensive.

A composite spectrum is to be developed from the data for Panel 1, given in Figure 7, and that for Panel 2, given in Figure 8. The physical

**Table 1 Physical Data for Instrument Panels**

Panel 1

Description: Wall-mounted electric control panel with approximately 30 components. Critical device located on an internal swing-out panel.

Dimension: Enclosure: 36" (wide) x 16" (deep) x 48" (high)  
Swing-out panel: 36" (wide) x 20" (high)

Weight: 175 lb (Panel) + 75 lb (Components)

Response Location: Near critical device located in the center of an internal swing-out panel. Swing-out panel located in the upper panel.

Failure Mode: Relay chatter on critical device during and after seismic event for front-to-rear (X-axis) excitation.

Panel 2

Description: Wall-mounted electric control panel with approximately 20 components. Critical device located on an internal swing-out panel.

Dimension: Enclosure: 36" (wide) x 16" (deep) x 48" (high)  
Swing-out panel: 36" (wide) x 24" (high)

Weight: 180 lb (Panel) + 59 lb (Components)

Response Location: Same as above.

Failure Mode: Same as above.

Panel 3

Description: Wall-mounted electric control panel with approximately 35 components. Critical device located on an internal swing-out panel.

Dimension: Enclosure: 36" (wide) x 16" (deep) x 60" (high)  
Swing-out panel: 36" (wide) x 24" (high)

Weight: 220 lb (Panel) + 85 lb (Components)

Response Location: Same as above.

Failure Mode: Same as above.

Panel 4

Description: Floor-mounted electric control panel with approximately 105 components. Critical device located on an internal swing-out panel.

Dimension: Enclosure: 60" (wide) x 24" (deep) x 72" (high)  
Swing-out panel: 30" (wide) x 26" (high)

Weight: 1050 lb (Panel) + 260 lb (Components)

Response Location: Near critical device located in the center of an internal swing-out panel. Swing-out panel located in the top right of the enclosure.

Failure Mode: Same as above.

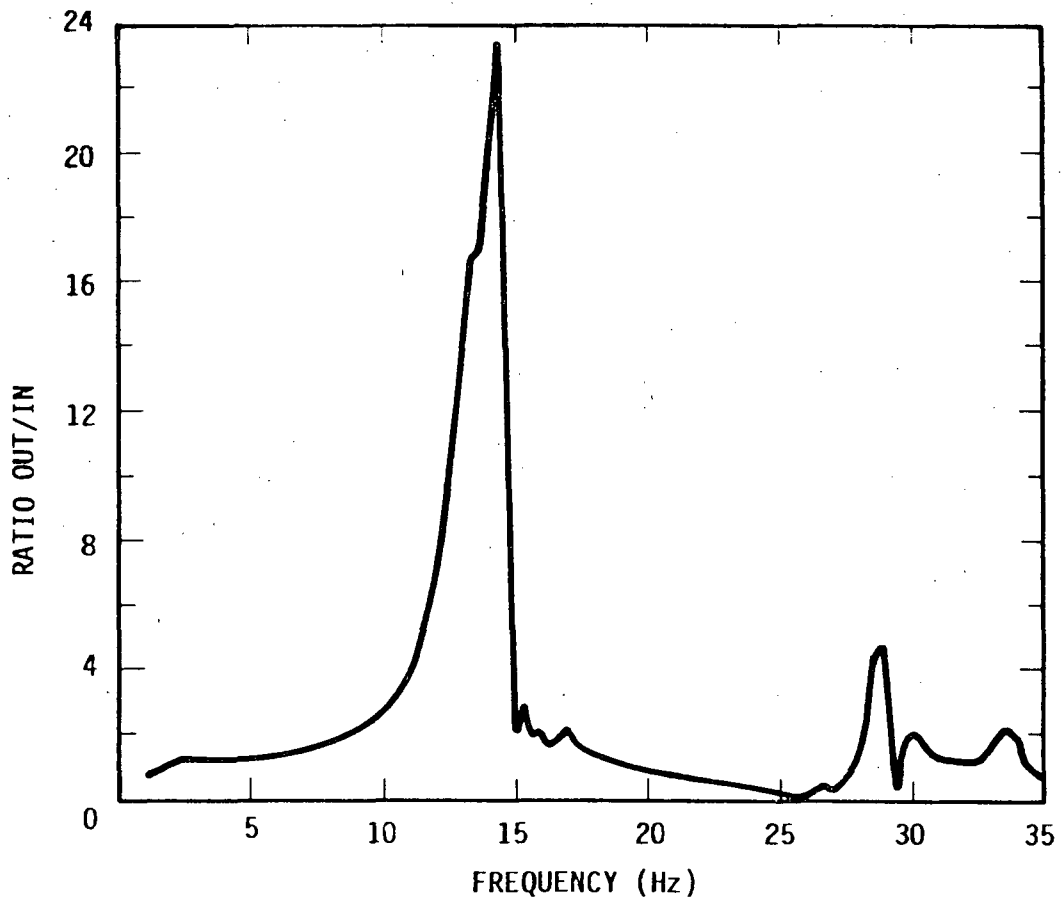


Figure 7a. Resonance search for Panel-1, X-axis, accelerometer on back of swing-out panel between Controllers, input 0.2 g peak, sweep 1.0 octaves/minute

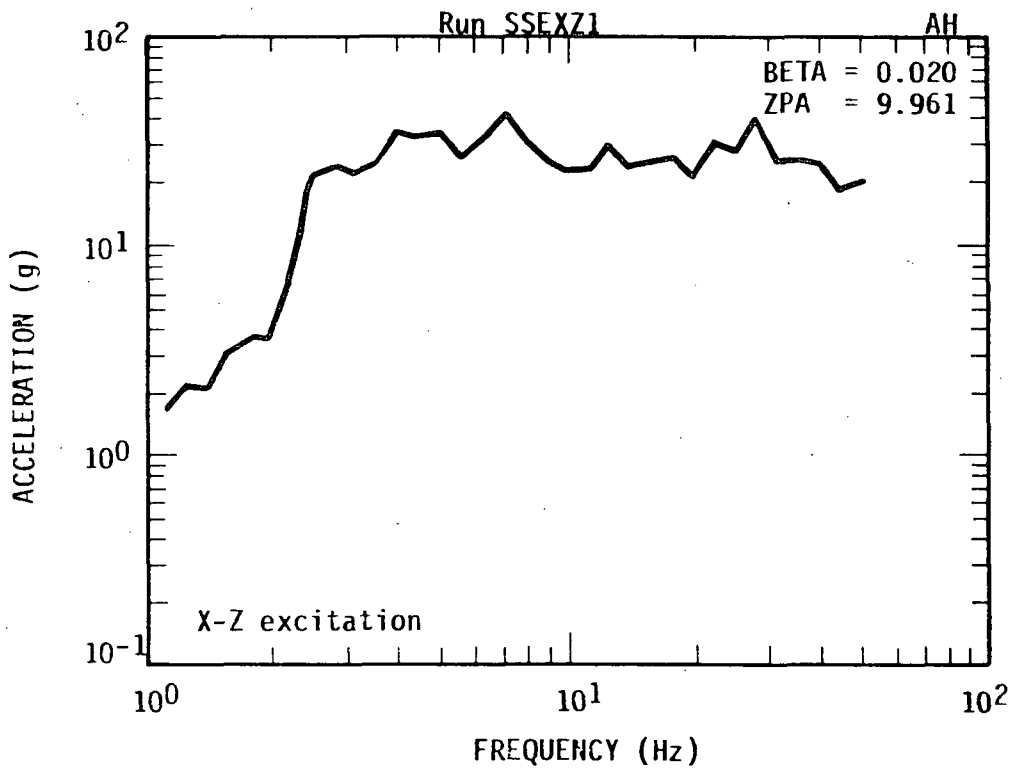


Figure 7b. TRS for qualification of Instrument Panel-1

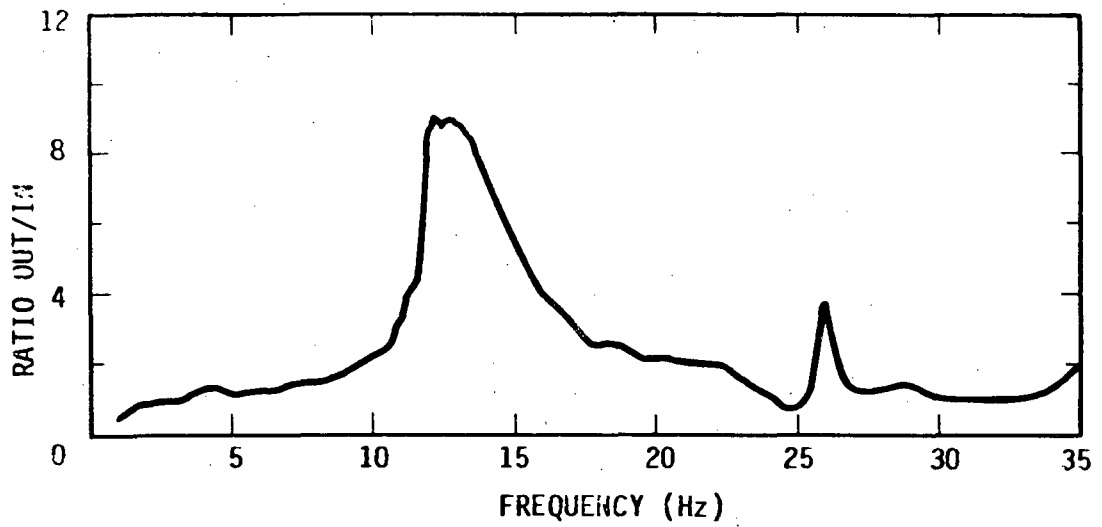


Figure 8a. Resonance search for Panel-2, X-axis, accelerometer located on front of the swing-out panel, input 0.2 g peak, sweep 0.5 octaves/minute

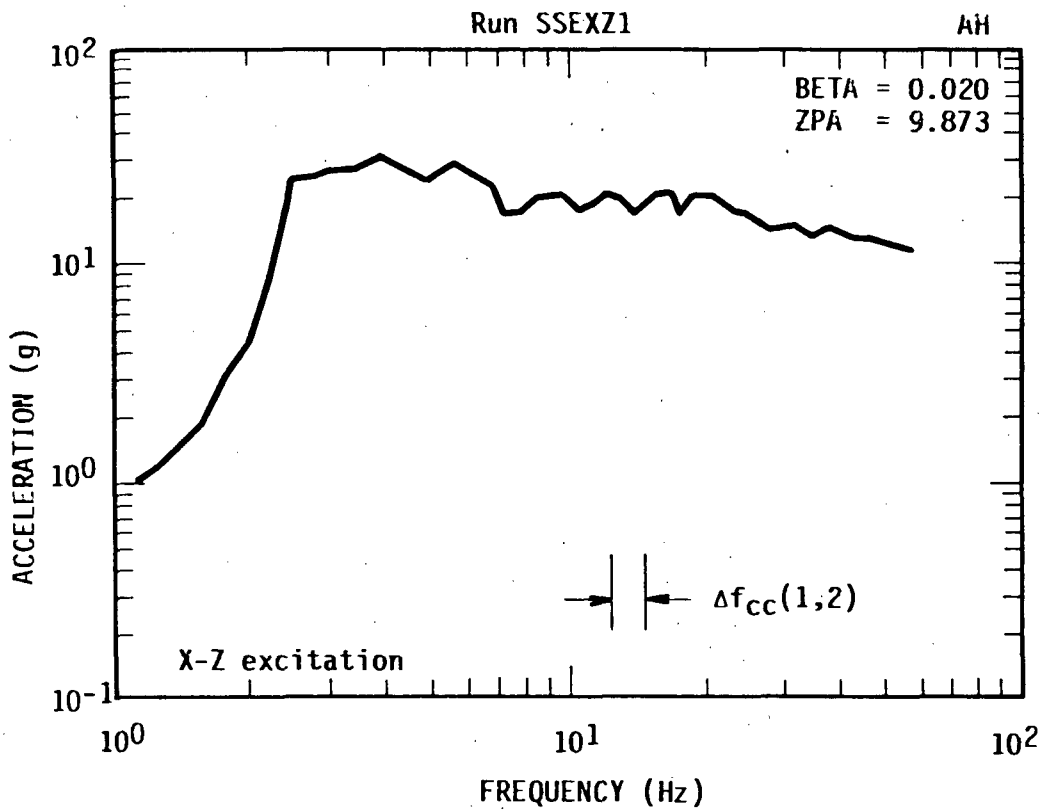


Figure 8b. TRS for qualification of Instrument Panel-2 and composite spectrum

similarity of these two panels is established by the procedures given in Paragraph 3.2.2. Thus, a critical bandwidth from about 13 to 14.5 Hz is identified. (A wider band could not be established from available data.) Although the original test spectra were developed at different values of damping, they are all transformed to  $\beta = 0.02$  by the following approximate relationship [9]:

$$R_{x1}(f)_2 = \sqrt{\beta_1/\beta_2} R_{x1}(f)_1$$

where  $R_{x1}(f)_2$  is an excitation response spectrum based on oscillator damping  $\beta_2$  and  $R_{x1}(f)_1$  is the same spectrum based on oscillator damping  $\beta_1$ . Thus, the somewhat lower overall spectrum in Figure 8b becomes a composite spectrum, and is associated with frequency bandwidth  $\Delta f_{cc}(1,2)$ . Note that a 0.7 modal interaction correction is not applied since both original spectra are relatively broadband.

In the present case,  $\beta = 0.02$  was used because most of the original spectra were calculated for this damping. However, eventually, when large volumes of data are handled for various types of equipment, a standardized value of  $\beta = 0.05$  may be desirable [9]. It may further be noted that having established the composite spectrum, any physically similar panel is now qualified to this spectrum.

## 5.2 Qualification upgrade for Panel 3

Now consider the qualification by experience for Panel 3, whose previous qualification data is given in Figure 9. By inspecting the critical transfer function of Figure 9a and the data of Table 1, it can be argued that Panel 3 is physically similar to the data base (i.e., Panels 1 and 2). Note that Panel 3 has previously been qualified to the relatively low spectrum given in Figure 9b. However, because of similarity, by experience, it can now be argued that it is also qualified to the much higher composite spectrum given in Figure 8b. In Reference [3], it is similarly shown that Panel 4 is also qualified to this composite spectrum, even though it is a floor-mounted system.

## 6. Discussion

The principles outlined herein should provide a significant step forward in extending the rather broad guidelines outlined in the revised IEEE 344 [2] and currently developing ASME Standard [10]. They also are useful for comparing with methods used by the Seismic Qualification Utilities Group (SQUG) for qualifying equipment in existing plants [9]. The former guidelines lack sufficient detail to be workable, while the latter methods are viewed by some to lack sufficient rigor for use in new plants. Thus, the methods herein are intended to show a path whereby a compromise between the two may be pursued. They are further intended to

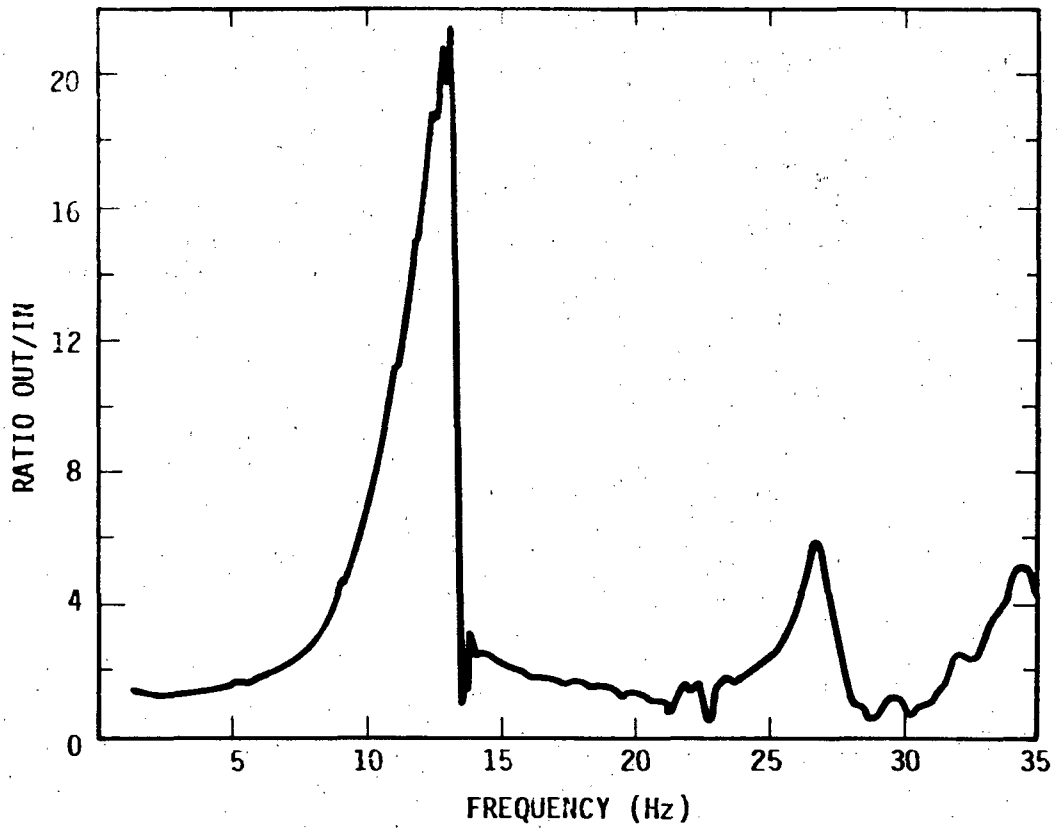


Figure 9a. Resonance search for Panel-3, X-axis, accelerometer on back of swing-out panel near Controller X-1.3, input 0.2 g peak, sweep 1.0 octaves/minute

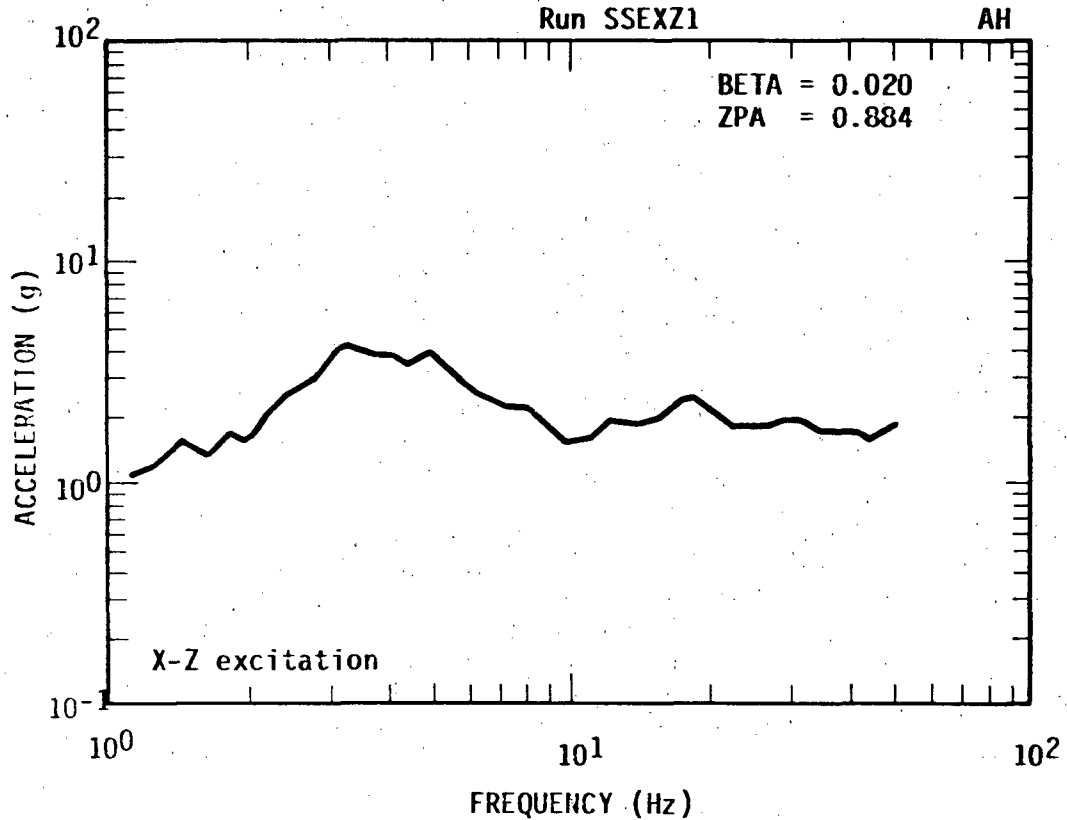


Figure 9b. TRS for qualification of Instrument Panel-3

provide detailed procedures for use by anyone who has available appropriate experience data.

It is apparent that the major difference between qualification by experience and more conventional methods lies in significantly greater use of what may be called "justifiable judgment". The methods developed herein are intended to be a basis for justification of judgments that typically will be made in lieu of detailed analyses or tests to carry out various qualification scenarios. There are several elements that form the essence of this basis. It is asserted that two of the three forms of similarity usually must be satisfied for a valid application. Furthermore, the two types of similarity must correspond within a critical frequency range in which the considered equipment is most susceptible to malfunction. Outside this bandwidth, the similarity requirements are much less stringent, but of course not unlimited. By using whatever means possible, the qualification engineer's job must be to predict what an equipment item's dynamic characteristics are, especially within the critical frequency band; and from that, show that the item's behavior would be essentially the same as other equipment in a database whose dynamic characteristics are similar. By concentrating on behavior only within the critical frequency band, much more freedom is allowed in the qualification.

A major concern lies in the detail to which physical similarity must be established. In effect, this means to what detail the critical transfer function must be established. Picking the critical location on a primary structure requires the assumption of the most likely form of malfunction. But even beyond this, what constitutes sufficient data for the transfer function at this location? It is our judgment that resonance search data of the type obtained from typical exploratory tests is quite adequate for this important step. If no such data is available, the transfer function must be estimated from comparisons of stiffness and mass properties (i.e., modal participation characteristics), and damping. From the examples given herein, it is obvious that the more generic the initial constituent response spectra, the broader the critical bandwidth  $\Delta f_{cc}$  can be made and, correspondingly, the less important is the accuracy of the estimate on the equipment critical transfer function. Conversely, the less generic (i.e., more site specific) the initial data, the narrower will be  $\Delta f_{cc}$ , and the more accurate the critical transfer function must be established. Thus, the most appropriate approach to a given qualification scenario will depend on the nature of the data and equipment characteristics which form the database.

The principles outlined herein rely heavily on the establishment of a critical transfer function (or equivalent modal properties) and its use to demonstrate physical similarity. Inherently, the use of low-input level transfer functions, such as typically measured during resonance search, are considered appropriate. However, should significant nonlinearity be suspected in a specific case, then additional measures could be implemented to develop quasi-linear transfer functions. One

approach would be to develop the data from fast Fourier transforms of the time histories of both excitation and response locations during the actual test events, if such data were available. However, in general, it is doubtful that any accuracy gained from such an approach would warrant the effort. In fact, virtually all known analytical qualification schemes are based on such linearity in any event.

## 7. Acknowledgments

The authors wish to express their sincere appreciation to several individuals who provided contributions to this program and to review of the final report. Mr. T. A. Fey helped develop the qualification experience data which demonstrated use of the methodology. Mr. V. J. Hernandez provided art work, and Mrs. D. A. Alexander typed the manuscript for the final report.

A special recognition is also given to Mr. G. L. Thinnis and the support of Idaho National Engineering Laboratories and the U.S. Nuclear Regulatory Commission.

## 8. References

1. "IEEE Recommended Practices for Seismic Qualification of Class 1E Equipment for Nuclear Power Generating Stations," Standard 344-1975, The Institute of Electrical and Electronics Engineers, Inc., New York, NY, January 31, 1975.
2. "Recommended Practices for Seismic Qualification of Class 1E Equipment for Nuclear Power Generating Stations," Standard 344-1987, The Institute of Electrical and Electronics Engineers," New York, NY, August 3, 1987.
3. Kana, D.D., and Pomerening, D.J., "Similarity Principles for Equipment Qualification by Experience," USNRC NUREG/CR-5012, EGG-2521, Idaho National Engineering Laboratories, July 1988.
4. Kana, D.D., and Pomerening, D.J., "A Method for Correlating Severity of Different Seismic Qualification Tests," ASME Journal Pressure Vessel Technology, Vol. 109, pp. 58-64, February 1987.
5. Kana, D.D., "Seismic Qualification Tests of Nuclear Plant Components - Damage Severity Factor Concept," Nuclear Engineering and Design, 59, pp. 155-170, 1986.
6. Bendat, J.S., and Piersol, A.G., Engineering Applications of Correlation and Spectral Analysis, John Wiley and Sons, New York, 1980.

7. Kana, D.D., and Pomerening, D.J., "Determination of Waveform Similarity from Seismic Response Spectra," (submitted for presentation at the 10th SMiRT Conference in Anaheim, CA, August 1989). Also Appendix A to Reference [3].
8. Kana, D.D., and Pomerening, D.J., "Determination of a Modal Interaction Correction for Narrowband Fragility Data," Paper No. JK/10, Proc. of 9th Structural Mechanics in Reactor Technology (SMiRT) Conference, Lausanne, Switzerland, August 1987 (NRC NUREG/CP-0088).
9. Merz, K.L., and Smith, C.B., "Generic Seismic Ruggedness of Power Plant Equipment," EPRI Report NP-5223, Electric Power Research Institute, Palo Alto, California, May 1987.
10. "Recommended Practices for Seismic Performance Qualification of Mechanical Equipment Used in Nuclear Power Plants With Particular Application to Pumps and Valves," ASME Draft Standard - Revision 5, American Society of Mechanical Engineers, New York, NY, September 1986.



## VALVE TESTING FOR UK PWR SAFETY APPLICATIONS

by  
S BRYANT  
P T GEORGE  
D R AIREY\*

Central Electricity Generating Board  
Sizewell 'B' Project Management Team  
United Kingdom

### SUMMARY

The Central Electricity Generating Board (CEGB) is currently building Sizewell 'B', the UK's first Civil PWR plant, and has mounted an extensive programme of valve testing in support of the licensing and operation of the plant. This paper deals with the testing of valves for safety applications on Sizewell 'B'.

The BRAVO test facility has been established at the CEGB's Marchwood Laboratories to permit the full scale type testing of the pressuriser relief system valves. Tests will be carried out to confirm the performance of the valves and to develop procedures for their in service testing. Tests have also been conducted at full secondary circuit conditions on candidate Main Steam Safety Valves in the Kraftwerk Union Test Facilities in W.Germany.

A further test programme has been established in which gate and globe valves are subjected to simulated high energy line break conditions to establish a methodology by which Sizewell valves may be qualified for this duty.

It is believed that the test programmes will result in increased availability, reduced maintenance and increased confidence in the safety of the plant.

### 1.0 BACKGROUND

Responsibility for the generation and supply of electricity in England and Wales rests with the Central Electricity Generating Board (CEGB) which operates a mixture of coal, oil and nuclear generating plant with a capacity of over 50 gigawatts.

The CEGB's nuclear power programme has to date been based upon gas cooled reactor technology, but in March 1987, following a 3 year Public Inquiry, the CEGB obtained government consent to build the UK's first civil PWR Plant, at Sizewell, 70 miles NE of London. The plant, scheduled for completion in 1994, is a Westinghouse 4 loop PWR based on the SNUPPS design. It is intended that the plant, called Sizewell 'B', will be the first of a programme of 4 replica PWR's to be completed in the UK by the end of the century.

In recognition of the novel demands of water reactor technology, the CEGB has considered it prudent to mount a number of development and testing programmes, to satisfy UK licensing authorities of the safety of the plant, to attempt to minimise plant maintenance requirements and to maximise availability.

\* CEGB Marchwood Engineering Laboratories, Southampton, England

Valves feature prominently in the component development and testing programmes carried out for Sizewell: A major programme of life cycle operability testing of candidate isolation valves, in which over 100 different designs of valve have been tested under primary circuit fluid conditions, is nearing completion and will be followed by valve testing in support of the elimination of cobalt from valve hardfacings. Extensive programmes have also been established for the operability testing of key primary and secondary circuit safety relief valves and the flow interruption testing of isolation valves. Preparations are now underway for the operability testing of control valves for high pressure drop applications.

The subject of this paper is the testing of valves for safety related applications on Sizewell 'B'.

## 2.0 TESTING STRATEGY

The strategy on which the valve testing programmes are based is one of full scale testing of key safety related valves with the following objectives:

- (i) To satisfy licensing concerns regarding operability and reliability of key safety related valves.
- (ii) To satisfy Sizewell 'B' system design requirements for valve performance data.
- (iii) To develop and validate in-service testing procedures.
- (iv) To make, where possible, a comparative assessment of the performance of different valve designs in support of the selection of suppliers for Sizewell 'B'.

## 3.0 PRESSURISER RELIEF SYSTEM VALVE TESTING

### 3.1 Background

Following a post TMI review of the SNUPPS Pressuriser Relief System (PRS) design, a substantially modified design has been adopted for Sizewell 'B'. The System now comprises three tandem pairs of Pilot Operated Safety Relief Valves (POSRVs) and two conventional safety valves.

Each Tandem pair of POSRV's comprises a relief valve and a downstream isolating valve, both of which are pilot operated valves which operate in response to system pressure or, at pressures below their hydraulic set points, via solenoid valves incorporated in the pilot system. The POSRV's constitute the first line of the PRS and are designed to cater for steam relief and for water discharge requirements such as Cold Overpressure Mitigation or Feed and Bleed.

The second line of the PRS comprises two spring loaded safety valves which have a higher pressure setpoint than the POSRV's and are required only during infrequent fault sequences and to provide diversity of pressure relief.

### 3.2 MEL BRAVO Facility Test Programme

To satisfy the Sizewell 'B' Pressuriser Relief System valve testing requirements, the CEGB has constructed a high flow rate test facility, at its Marchwood Engineering Laboratory. Called BRAVO - Blowdown Rig for the Assessment of Valve Operability, the facility is designed for the full-scale testing of Pressuriser Relief System valves (Ref 1). The BRAVO facility has the unique capability to reproduce primary circuit water chemistry as well as full system pressure, temperature and valve mass flowrates. In addition to its principal function - the testing of Pressuriser Relief System valves - the rig will be used for the full flow testing of other primary and auxiliary circuit valves, for example those requiring formal qualification for high energy flow interruption capability.

#### 3.2.1 Pressuriser POSRV Testing

The Sizewell 'B' POSRV has been selected for Sizewell 'B' on the basis of a major programme of development and testing carried out by Electricité de France (EdF). However, there are differences between EdF and CEGB in the approach to both licensing and operational issues and further confirmatory testwork is desirable in areas not covered by the EdF programme.

To this end, a full size Tandem pair of POSRVs is being subjected to a programme of testing under the full range of pressuriser pressure, temperature and flow conditions, to address the following issues:

- (i) The tests carried out by EdF indicate that the operating characteristics of the pressuriser POSRV are a function of system pressure and, to support the design of the Sizewell 'B' Cold Overpressure Mitigation System (COMS), tests have been carried out involving the discharge of cold water at pressures below 30 bar. The tests have yielded valuable information on valve operating time and discharge characteristics under Cold Shutdown conditions which is being used to specify appropriate pressure set points for use in the COMS design.
- (ii) As in EdF plants, the Sizewell POSRV will be fitted with an upstream water loop seal. The loop seal geometry is Sizewell specific and confirmatory tests will be carried out on a fully representative inlet pipework configuration to ensure that all test results can be directly applied to the Sizewell PRS design.
- (iii) The CEGB is required to satisfy the UK licensing authorities of the adequacy of procedures for the in-service testing of safety related valves. It is intended that the pressuriser POSRV will be tested in situ during the refuelling shutdown. The development of a suitable procedure for such testing will be carried out in the MEL BRAVO programme.

- (iv) The POSRV pilot system is designed to operate on demineralised water, but the unique water chemistry capability of the BRAVO facility will be utilised to confirm that no adverse effects arise from the inadvertent introduction of borated water.

### 3.2.2 Pressuriser Safety Valve Testing

A full-size spring loaded pressuriser safety valve will be subjected to a programme of testing at full PRS pressure, temperature and flow with the following objectives:

- (i) To ensure that the pressuriser safety valve meets the requirements of the Technical Specification in respect of blowdown and accumulation, tests will be carried out to confirm the relationship between these parameters and valve control ring settings.
- (ii) The CEGB is required to develop a suitable in-service testing procedure and tests will be conducted to assess the use of various forms of assist device for in-situ testing. The tests will attempt to optimise the testing procedure in respect of the installation of the assist device and will address any complications associated with the upstream water loop seal.
- (iii) The need for work to study the variation of discharge pipework loadings as a function of loop seal water temperature is being considered.

## 4.0 MAIN STEAM SAFETY VALVE TEST PROGRAMME

### 4.1 Background

The Sizewell 'B' Main Steam System comprises four main steam lines, each of which is provided with five conventional spring loaded Main Steam Safety Valves with staggered pressure setpoints.

In response to the licensing requirement to demonstrate safety valve operability both prior to and in service, a Test Programme was commissioned in which tests at full secondary system pressure, temperature and flow were conducted on a single MSSV from each of three potential Sizewell 'B' suppliers. The tests were carried out on the Siemens Kraftwerk Union Large Valve Test Facility at Karlstein, W.Germany, which is designed to reproduce PWR Main Steam system conditions for the full scale testing of large steam line valves.

Each valve was subjected to a representative lifetime of operations with the following objectives:

- (i) To confirm the operability of the valve and its compliance with the maximum and minimum discharge capacity required by the Technical Specification.

- (ii) To attempt to establish a correlation between blowdown, accumulation and valve settings and to assess the effect, on this correlation, of variations in valve set pressure and of potential production variations such as valve spring rate.
- (iii) To confirm the validity of the use of assist devices of various designs for set point checking and assessment of valve operability.

#### 4.2 Test Description

A test matrix was developed to provide a full parametric study of safety valve performance.

Initially the valves were subjected to a number of full pressure operations to compare their performance as supplied with that required by the Technical Specification. The valves were then tested through a range of guide and nozzle ring settings in an attempt to establish a correlation between accumulation, blowdown and the setting of each control ring. To confirm that this relationship was not significantly different for valves at different pressure settings, tests were carried out at two valve set pressures.

It was intended that the results from the tests should be applicable to all twenty MSSV's and it was therefore necessary to assess the effect of potential production variations on the established correlations. It was concluded that spring rate was likely to be the most significant variable. Tests were therefore repeated with a spring of different stiffness and the effect on the correlation investigated.

The effect of low pressure ramp rate and reduced steam quality on valve performance was also investigated.

Each valve was tested at reduced pressure, using various assist devices at intervals during the tests, the full pressure tests giving the opportunity to check the accuracy of the set pressure measurement obtained from the assist devices.

#### 4.3 Test Results

Each valve was subjected to about 30 full pressure operations and 20 reduced pressure 'assisted lifts'. All three valves remained operable throughout the programme, the only change in performance being an increase in seat leakage.

While the results did not in all cases indicate a strong correlation between valve settings and performance, an interdependence between accumulation and blowdown was demonstrated.

The relationship between setting and performance was shown to be influenced by the change of valve spring but large variations in pressure ramp rate did not significantly affect valve performance. The results gave confidence that valves could be selected for Sizewell 'B' which would meet the requirements of the technical specification given appropriate pre-service testing.

Assist devices were shown to give an acceptably accurate measurement of set pressure - no inaccuracy being discernable in the presence of the slight scatter normally associated with valve set pressure.

#### 4.4 Testing of Sizewell 'B' MSSV's

To confirm the compliance of the Sizewell 'B' Main Steam Safety valves with technical specification requirements, a valve identical to, and manufactured with, the valves supplied for Sizewell 'B' will be subjected to comprehensive tests at full pressure, temperature and flow prior to installation in the plant. As an alternative, the practicability of testing all 20 Sizewell MSSV's at full flow prior to installation is under consideration.

On the basis of the test results the CEGB now plans to carry out the in-service testing of the Sizewell 'B' MSSV's in situ by the use of an assist device at hot shutdown during refuelling outages.

### 5.0 HIGH ENERGY FLOW INTERRUPTION TESTING

#### 5.1 Background

Valves which may be required to isolate a High Energy Line Break are required to be qualified for the interruption of high energy flow by testing or a combination of testing and analysis. The testing requirements are based on a CEGB adaptation of ANSI B16.41 (Functional Qualification Requirements for Power Operated Active valve assemblies for Nuclear Power Plants) and its successor document ANSI QV4. It is recognised that this methodology is not well developed and a test programme is underway to obtain guidance on the performance of such tests and to assist in identifying facilities where tests can be carried out on the small number of Sizewell 'B' valves requiring flow interruption qualification.

#### 5.2 Test Programme and Results

The first flow interruption methodology test was carried out on a 3 ins motor operated parallel slide gate valve. The valve was subjected to two simulated pipebreaks under PWR primary circuit conditions and was successful in occluding the pipe bore and mitigating the high energy flow. However, the valve failed to achieve a full seal due to galling of the seat and disc.

The results indicate that, for this type of valve and application, the closing thrust requirement depends upon the adequacy of internal guidance. Unless parallel sliding contact is maintained between disc and seat, material removal is likely and the assumption of normal sliding friction factors in the calculation of closing thrust requirements will be invalid.

To ensure the adequacy of Sizewell 'B' valves for high energy flow interruption applications, further full scale tests will be carried out in the CEGB BRAVO facility and in alternative commercially available facilities on gate and globe valves. For example, the Sizewell Main Steam Isolating Valve will be qualified for Main Steam Line Break isolation by full scale testing on the Siemens Kraftwerk Union Large Valve Test Facility in W. Germany.

## 6.0 DISCUSSION AND CONCLUSIONS

The programmes outlined above arose largely from the need to satisfy licensing requirements, however, they have also established the CEGB as an informed buyer of plant for applications of which it had only limited previous experience.

The procurement of key valves for Sizewell 'B' is now based on a clearer understanding of their performance and limitations and Technical Specification requirements are known to be achievable. Aspects of valve design or manufacture which, on the basis of the test results, require particular attention have been identified and can now be addressed early enough to minimise Project cost and programme risks.

In conclusion therefore, the CEGB has recognised the importance of valve operability on PWR plants and has entered into a substantial valve testing commitment in support of Sizewell 'B' and future stations. It is believed that these benefits will include not only increased availability and reduced maintenance requirements, but also increased confidence in the safety of the plant.

## 7.0

### REFERENCES

1. Airey D.R., Richards D.J.W. and Bryant S., 'Valve Blowdown Test Facility for Testing High Flow Rate Safety/Relief and Block Valves.' ASME Conference Paper 87-PVP-7, San Diego, California, June 1987.



PIPING SUPPORT AND GATE VALVE BEHAVIOR DURING  
HIGH LEVEL HDR SIMULATED SEISMIC TESTS<sup>a</sup>

Robert Steele Jr.

Idaho National Engineering Laboratory  
EG&G Idaho, Inc.  
Idaho Falls, Idaho 83415

ABSTRACT

This paper describes a portion of the analysis and results to date from the SHAM<sup>D</sup> seismic research program, in which the USNRC/INEL<sup>C</sup> was a participant. The program was conducted by Kernforschungszentrum Karlsruhe (KfK) at the decommissioned Heissdampfreaktor (HDR) located near Frankfurt in the Federal Republic of Germany (FRG).

The research program included the study of the effects of increasing levels of seismic excitation on a full scale, in situ nuclear piping system containing a naturally aged U.S. 8-in. motor-operated gate valve. In all, 51 experiments were conducted with the piping supported by six different piping support systems, including a typical stiff U.S. piping support system made up of snubbers and rigid struts. Earthquake-like displacement histories were input to servohydraulic shakers attached directly to the piping system. Inputs to the piping system started with a magnitude of 0.6 g ZPA and were stepped up, using the same frequency content, to a maximum of 5 g ZPA. The resulting piping system response produced overload snubber failures and local piping strains of 0.9%.

The results of this testing will contribute to the technical basis used for support and development of equipment qualification standards and will help establish the seismic safety margins in piping and piping support system components.

---

a. Work sponsored by the United States Nuclear Regulatory Commission, Office of Nuclear Regulatory Research, Division of Engineering, Washington, D.C. 20555, under DOE Contract DE-AC07-76ID01570; Dr. G. H. Weidenhamer, USNRC Technical Monitor.

b. Servohydraulische Anregung Maschinetechnik.

c. United States Nuclear Regulatory Commission; Idaho National Engineering Laboratory.

## 1. INTRODUCTION

During the spring of 1988, the Idaho National Engineering Laboratory (INEL) and the Argonne National Laboratory (ANL), under sponsorship of the United States Nuclear Regulatory Commission (USNRC), participated, along with Kernforschungszentrum Karlsruhe (KfK), Kraftwerkunion (KWU), the Electrical Power Research Institute (EPRI), the Fraunhofer Institut für Betriebsfestigkeit (LBF) in Darmstadt, and the Central Electricity Generating Board of the United Kingdom (CEGB), in the KfK-designated SHAM (Servohydraulische Anregung Maschinetechnik) test series. This test program was conducted at the Heissdampfreaktor (HDR), a decommissioned experimental reactor facility located near Frankfurt in the Federal Republic of Germany.

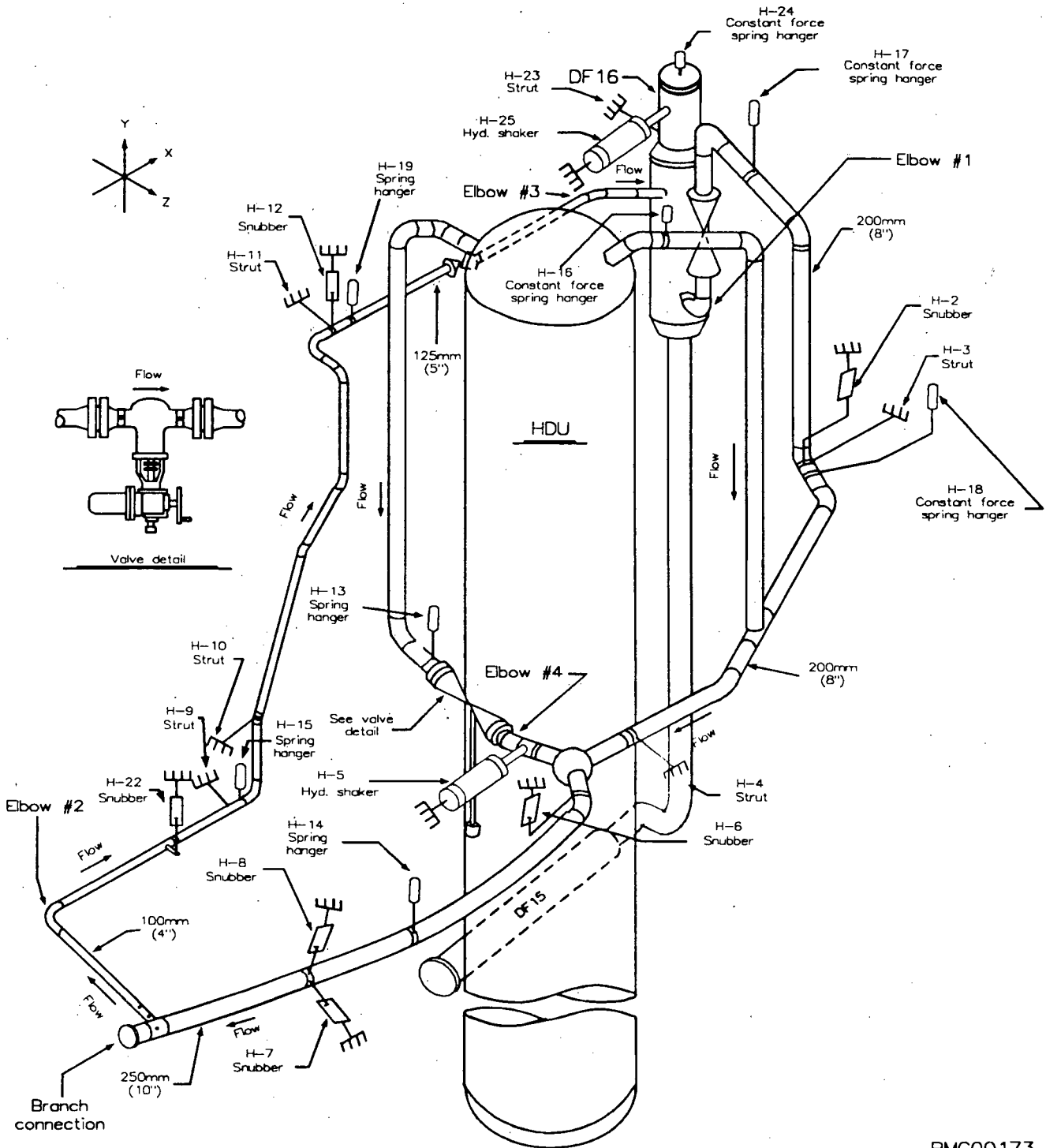
The SHAM experiments at the HDR consisted of the direct excitation of a piping system called the Versuchskreislauf (VKL) (Figure 1) through use of two large 40-ton servohydraulic shakers mounted to the HDR building and attached to the piping system. The input signal to the shakers was an earthquake-like displacement history. The shaker outputs were measured in multiples of the basic one SSE loading, which had a zero period acceleration (ZPA) of 0.6 g. Loads up to eight times the basic SSE were applied to the piping system.

Objectives of the INEL's participation in this multinational program were to:

1. Measure the effects of increasingly greater dynamic loadings on gate valve operability and determine, if possible, the loadings at which the valve would sustain structural damage.
2. Determine the safety margins and failure modes of nuclear grade snubbers, rigid supports, trunion attachments, and concrete anchors when subjected to dynamic excitation.
3. Determine the effects of individual support and multiple support failures on piping response in a simulated seismic event.
4. Provide data for comparing the performance of stiff, flexible, very flexible, and snubber replacement piping support systems.

Results of this series will contribute to the technical basis used for support and development of equipment qualification standards and will help establish the seismic safety margins in piping and piping support system components.

This paper presents a general overview of the SHAM test program and a specific review of the U.S. stiff support system response at 200, 600, and 800% SSE loadings.



BMG00173

Figure 1. The VKL with the U.S. rigid support system installed.

## 2. EXPERIMENTAL PROGRAM

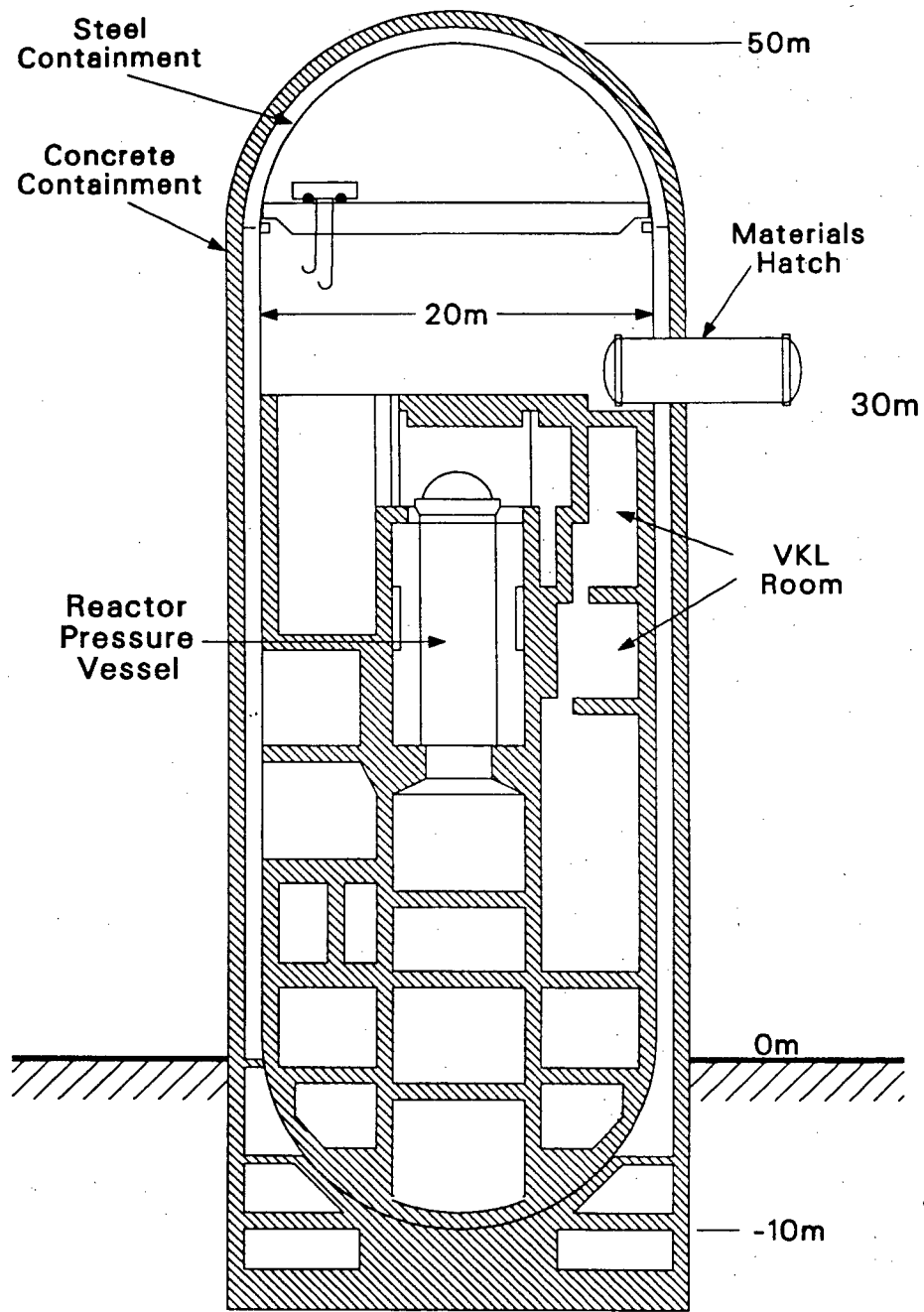
The VKL is constructed of stainless steel in four metric pipe sizes (equivalent to 10, 8, 5, and 4 in.), with the majority of the piping being 200 mm (8 in.). The system is located between the 18- and 24-m elevations in the HDR facility as shown in Figure 2. The system consists of two parallel flow loops connected to a large vessel called the Heissdampfumformer (HDU) and a manifold header (DF 16) as shown in Figure 1. The system is capable of operating under high temperature and high pressure; however, for the SHAM tests, the fluid remained pressurized [70 bar (1000 psig)] at ambient temperature to avoid the risk of damaging the sensitive instrumentation in the event of a test-induced line rupture. Seismic tests were conducted without fluid flow through the system; valve functional tests were conducted with flow through the valve.

The USNRC provided a valve from the decommissioned Shippingport Atomic Power Station for installation in the VKL. The valve was originally refurbished and functionally tested for a predecessor HDR seismic test program named SHAG. Due to problems with the motor operator during the SHAG tests, problems not related to seismic testing, the motor operator was refurbished for the SHAM tests. The refurbishment included installing a new motor, torque spring, and torque switch and subjecting the motor operator to dynamometer testing at the Limitorque Laboratory.

The piping system was also modified before SHAM testing began. A new branch connection was added, and the previously discussed servohydraulic shakers and a new piping support system were installed. The support system was typical of U.S. stiff seismic support systems made up of rigid supports and snubbers. The loads for each dynamic pipe support were calculated from seismic analyses based on 100% SSE excitation levels. The supports were then sized for each location using the support manufacturer's published ASME Code, Level C Allowables. The reason for the reduced conservatism in sizing the supports was so that support safety margins and failure modes could be determined in the lower level tests and the effects of multiple support failures could be investigated at the higher loadings. Table 1 lists the support type, the predicted One SSE design load, and the manufacturers' ASME Code Level C rated load. For the two hydraulic shakers, Table 1 defines output loads.

Over 260 instruments were installed on the VKL to measure the input and VKL response. Measurements included: acceleration, displacement, strain, and force on the piping system and supports; and acceleration, strain, stem position, current, voltage, pressure, differential pressure, and flow on the valve. For each experiment, KfK collected the data from the U.S. and KfK instruments and committed the data to permanent record. The recorded data will be shared with all participants.

In all, 51 tests were performed on six piping support configurations. The design and operation of the shakers was the responsibility of LBF; the



MGH1088-1

Figure 2. A simplified cross section of the HDR facility, showing the location of the VKL piping system room and the Reactor Pressure Vessel.

TABLE 1. U.S. SUPPORT CONFIGURATION AND DESIGN LOADS

| Support Number | Support Type | Design Load One SSE (kN) | Level C Rated Support Load (kN) |
|----------------|--------------|--------------------------|---------------------------------|
| H-2            | S            | 6.2                      | 9.34                            |
| H-3            | RS           | 3.8                      | 9.34                            |
| H-4            | RS           | 9.7                      | 110                             |
| H-5            | HS           | 15.2 <sup>a</sup>        | 390 <sup>b</sup>                |
| H-6            | S            | 4.2                      | 3.85                            |
| H-7            | S            | 3.5                      | 9.34                            |
| H-8            | S            | 1.9                      | 3.85                            |
| H-9            | RS           | 2.0                      | 3.85                            |
| H-10           | RS           | 1.3                      | 3.85                            |
| H-11           | RS           | 1.8                      | 3.85                            |
| H-12           | S            | 1.2                      | 2.3                             |
| H-22           | S            | 1.4                      | 2.3                             |
| H-23           | RS           | 18.8                     | 220                             |
| H-25           | HS           | 24.1 <sup>a</sup>        | 390 <sup>b</sup>                |

S = Snubber  
 RS = Rigid Strut  
 HS = Hydraulic Shaker

- a. Output force at One SSE.  
 b. Maximum rated output force.

other participants were responsible for the design of their respective piping support systems. These piping support systems were based on the INEL/ANL U.S. stiff pipe support system. Each participant removed one or more components from the U.S. stiff support system and in some cases, replaced them with components of their own. The result was generally a more flexible support system. The dead weight supports, and the rigid struts at locations H-4 and H-23, remained in place in all six systems. Table 2 lists the supports used in each of the six systems, and Table 3 provides the U.S. stiff system test matrix.

TABLE 2. SHAM PARTICIPANT SUPPORT CONFIGURATIONS

| <u>Support Number</u> | <u>KfK</u> | <u>KWU</u> | <u>U.S.</u> | <u>EPRI Bechtel</u> | <u>EPRI Cloud</u> | <u>CEGB</u> |
|-----------------------|------------|------------|-------------|---------------------|-------------------|-------------|
| H-2                   | --         | --         | S           | --                  | SS                | --          |
| H-3                   | --         | --         | RS          | RS                  | RS                | --          |
| H-4                   | RS         | RS         | RS          | RS                  | RS                | RS          |
| H-5                   | HS         | HS         | HS          | HS                  | HS                | HS          |
| H-6                   | --         | --         | S           | --                  | SS                | --          |
| H-7                   | --         | --         | S           | EA                  | SS                | RS          |
| H-8                   | --         | --         | S           | EA                  | SS                | RS          |
| H-9                   | --         | RS         | RS          | RS                  | RS                | RS          |
| H-10                  | --         | RS         | RS          | RS                  | RS                | --          |
| H-11                  | --         | RS         | RS          | RS                  | RS                | --          |
| H-12                  | --         | --         | S           | --                  | SS                | RS          |
| H-22                  | --         | --         | S           | EA                  | SS                | --          |
| H-23                  | RS         | RS         | RS          | RS                  | RS                | RS          |
| H-25                  | HS         | HS         | HS          | HS                  | HS                | HS          |

S = Snubber  
 RS = Rigid Strut  
 HS = Hydraulic Shaker  
 EA = Energy Absorber  
 SS = Seismic Stop

TABLE 3. U.S. STIFF PIPING SUPPORT SYSTEM TEST MATRIX

| <u>Test Number</u> | <u>Type of Load</u> | <u>Load Level</u> |
|--------------------|---------------------|-------------------|
| T41.302            | Random              | 0.3 g             |
| T41.301            | Random              | 0.3 g             |
| T41.310            | SSE                 | 100%              |
| T41.311            | SSE                 | 100%              |
| T41.312            | SSE                 | 100%              |
| T41.313            | SSE                 | 200%              |
| T41.314            | SSE                 | 300%              |
| T41.315            | SSE                 | 300%              |
| T41.811            | SSE                 | 200%              |
| T41.812            | SSE                 | 600%              |
| T41.813            | SSE                 | 800%              |

All participants except CEGB used multiples of the same earthquake-like displacement history. The 100% SSE input is shown in Figure 3 in the response spectra format. The spectrum is very representative of U.S. earthquake spectra in the frequencies associated with piping response. Each earthquake test was 15 s in duration with approximately 12 s of strong motion. Tests that imposed higher loadings used the same frequency content, but with a linear increase in the amplitude of the displacement history input to the shakers. CEGB used two other displacement histories in their lower level tests, one for the Sizewell B location and the other based on a generic All Sites spectrum. In their high level tests, they used a sine burst format. The CEGB inputs are very different from the ones used by the others. Comparison of the results will probably not be possible.

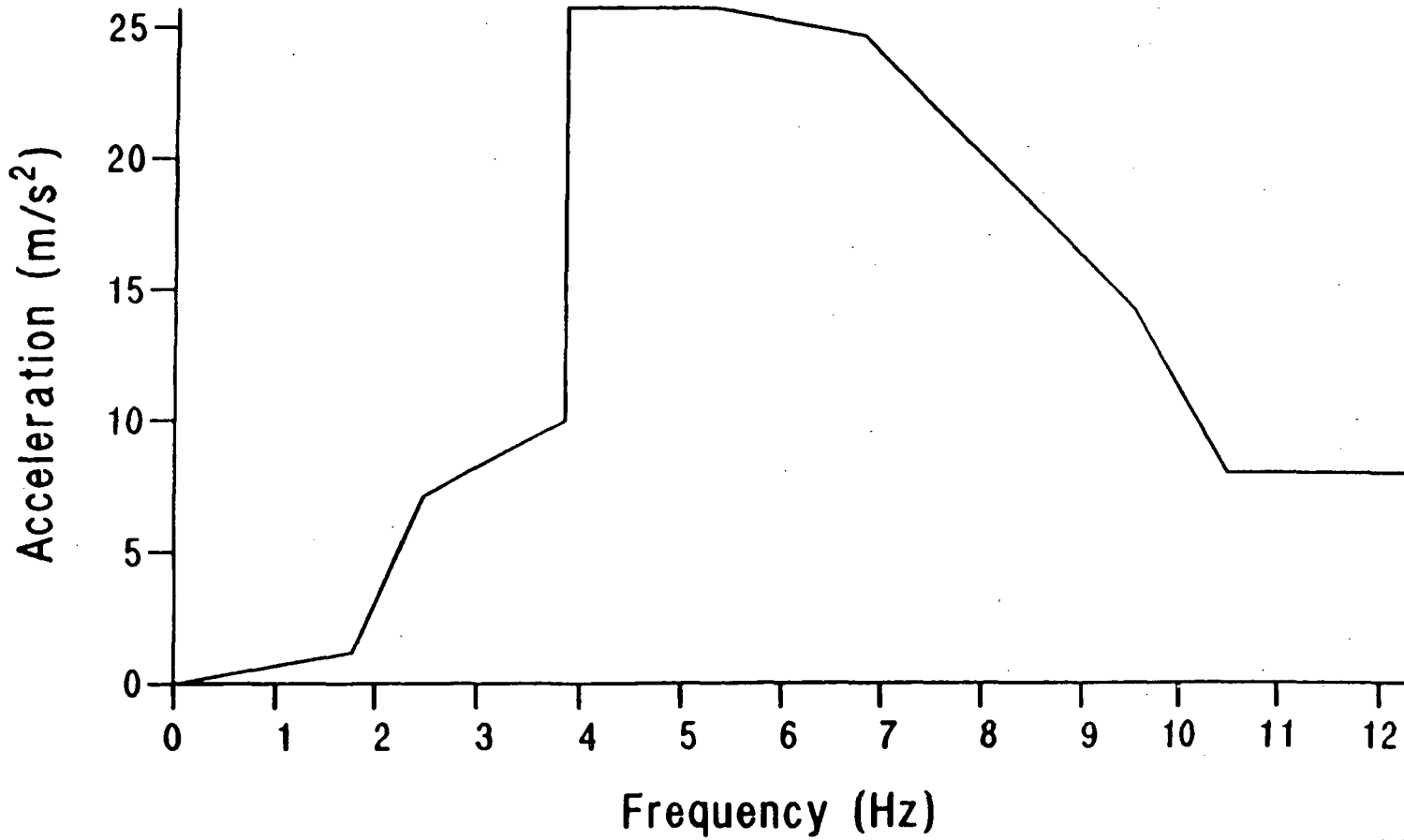
### 3. TEST RESULTS

Preliminary review of the quick-look data for all configurations and observations made during the test program indicate that measured data were acquired that will, after analyses, provide information for most of the program objectives. The one exception may be pipe failure modes. Strains in excess of 0.9% were experienced without visible physical damage.

Only the U.S. stiff piping support system components (snubbers, struts, and anchors) were sized to determine safety margins and failure modes. All other participants' support system components were sized for much higher loads; thus no support failures in these systems were anticipated, and none occurred. In the U.S. system, no rigid struts failures occurred with loadings up to eight times their published ASME Code Level B design loads. With one possible exception, snubber overload failures were obtained between three and seven times their published ASME Code Level B design loads. The one exception may be two samples of one size of snubber from Anchor/Darling that, according to preliminary data, may have failed below their published design load. A complete analysis of the failure is scheduled.

The U.S. 8-in. motor-operated gate valve experienced dynamic responses at the motor operator of approximately 11 g in the 800% SSE test without apparent damage or malfunction. Some limit switch chatter was observed; however, the limit switch did not stay open long enough during chatter to cause the motor controller circuit to interrupt current flow to the motor. Figure 4 is a valve motor current history during the 800% SSE test. The history shows that the valve operated smoothly.

Quick-look results from tests T41.811, 812, and 813 (the 200%, the 600%, and the 800% SSE tests) on the U.S. stiff piping support system are presented in the following paragraphs.



MGH01678

Figure 3. SHAM one SSE Response Spectrum peak broadened and smoothed in accordance with Reg. Guide 1.122 and utilizing PVRC damping.

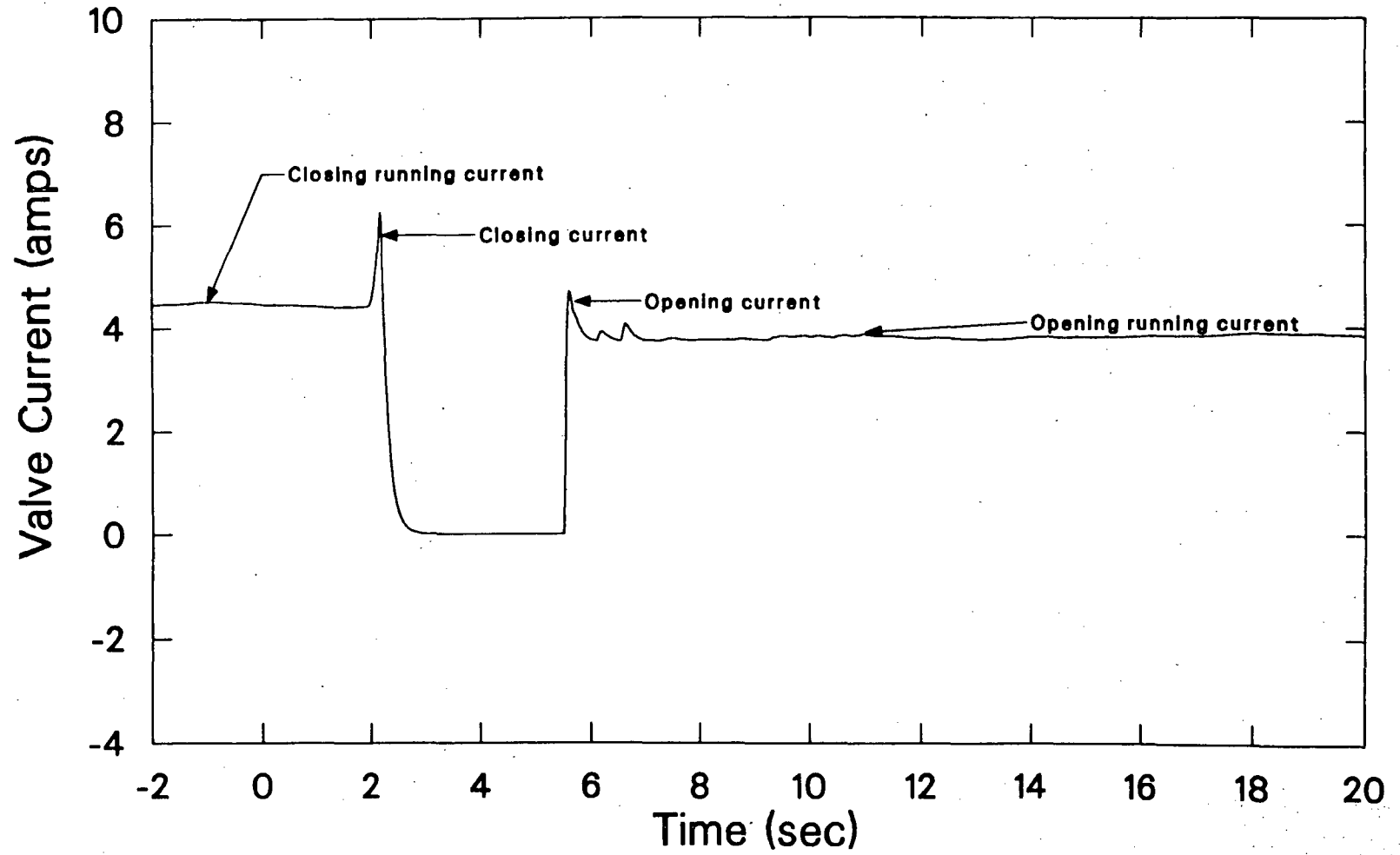


Figure 4. Valve current history during 800% SSE test.

### Repeat 200% SSE Test (T41.811)

Overload snubber failures in the earlier tests up to 300% SSE prevented a true characterization of the U.S. system exposed to the dynamic loading. We decided to repeat the 200% SSE test and to temporarily replace the smaller snubbers at locations H-8, -12 and -22. These snubbers did not have as much load safety margin as the larger snubbers at locations H-2, -6 and -7 (refer to Figure 1). The smaller mechanical snubbers were replaced with larger Pacific Scientific mechanical snubbers Size 1 (PSA-1), which were the same size as those installed at the other three locations. Review of the data from the 200% SSE tests show that the snubbers resisted loads up to 2.3 times their design loadings and allowed less than 0.03 in. of dead band travel (the distance a snubber travels from resisting the load in one direction to resisting in the other direction). The manufacturer specifies this distance shall be no more than 0.1 in. at design load and at frequencies above 3 Hz. In addition, the repeat 200% SSE test will provide stiff system performance, at significant loading, to which the other participants can compare the performance of their support systems.

### 600% SSE Test (T41.812)

The objectives of the 600 and 800% SSE tests were to study multiple support failures and possible damage to the piping system resulting from these failures. For the 600% SSE test, the smaller snubbers sized for the predicted loads at 100% SSE were reinstalled at locations H-8, -12, and -22. These snubbers were mechanical snubbers manufactured by Pacific Scientific and Anchor/Darling Industries. The snubbers at H-2, -6, and -7 locations were PSA-1s, also sized for the predicted loads at 100% SSE.

During the 600% SSE test, the snubbers at H-8, H-12 and H-22 failed on overload. Figures 5 and 6 are 4-s expanded histories from the full 15-s earthquake loading and are typical examples of snubber force and displacement histories showing the loads at which the snubbers failed and the resulting displacements allowed. Figure 5 shows the Anchor/Darling mechanical snubber size A/D-40 rated at 400 lb (Level B) failing after resisting an 8-kN loading just before the 2.5 s time mark. This 8-kN loading is equivalent to 1800/lb force; thus the snubber failed at 4.5 times its design load. This snubber did not resist any load after it failed. The displacement increased from 2 to 18 mm total travel.

Figure 6 shows the force and displacement histories for the Pacific Scientific snubber size 1/4 at the H-22 location. At approximately 7.5 s the snubber resisted a 7.5-kN loading; at this point the displacement increased. In the next loading cycle the displacement increased to 10 mm. Large displacements continued, but the snubber continued to resist motion, as shown in the force history. The Pacific Scientific size 1/4 snubber is rated for 350 lb (Level B); 7.5-kN is equal to 1690 lb. The snubber failed at 4.82 times its design load. Figure 1 shows that snubber locations H-8 and H-22 are both vertical locations and control the vertical response of

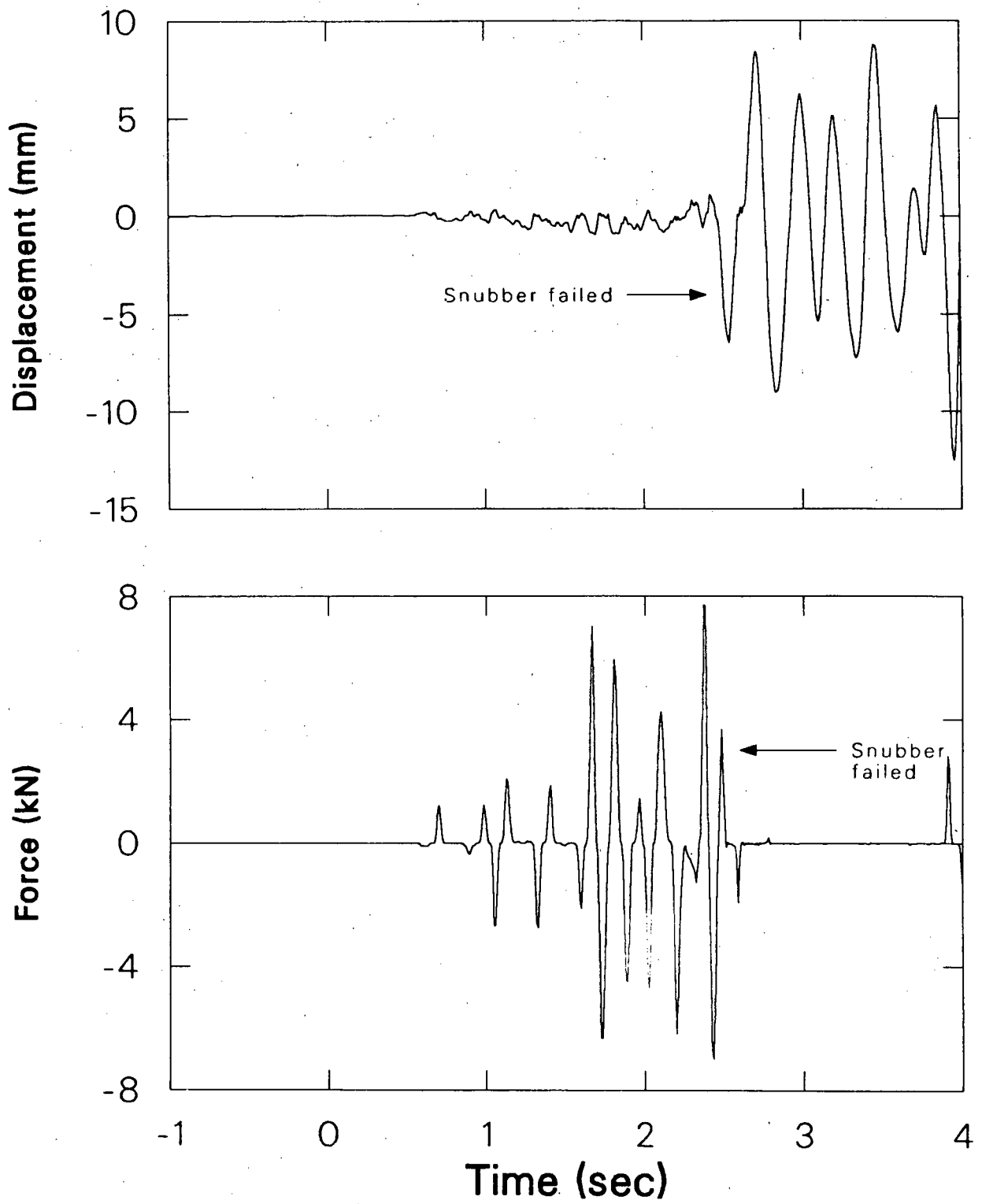


Figure 5. Force and displacement history comparison for the H-8 snubber location during 600% SSE test.

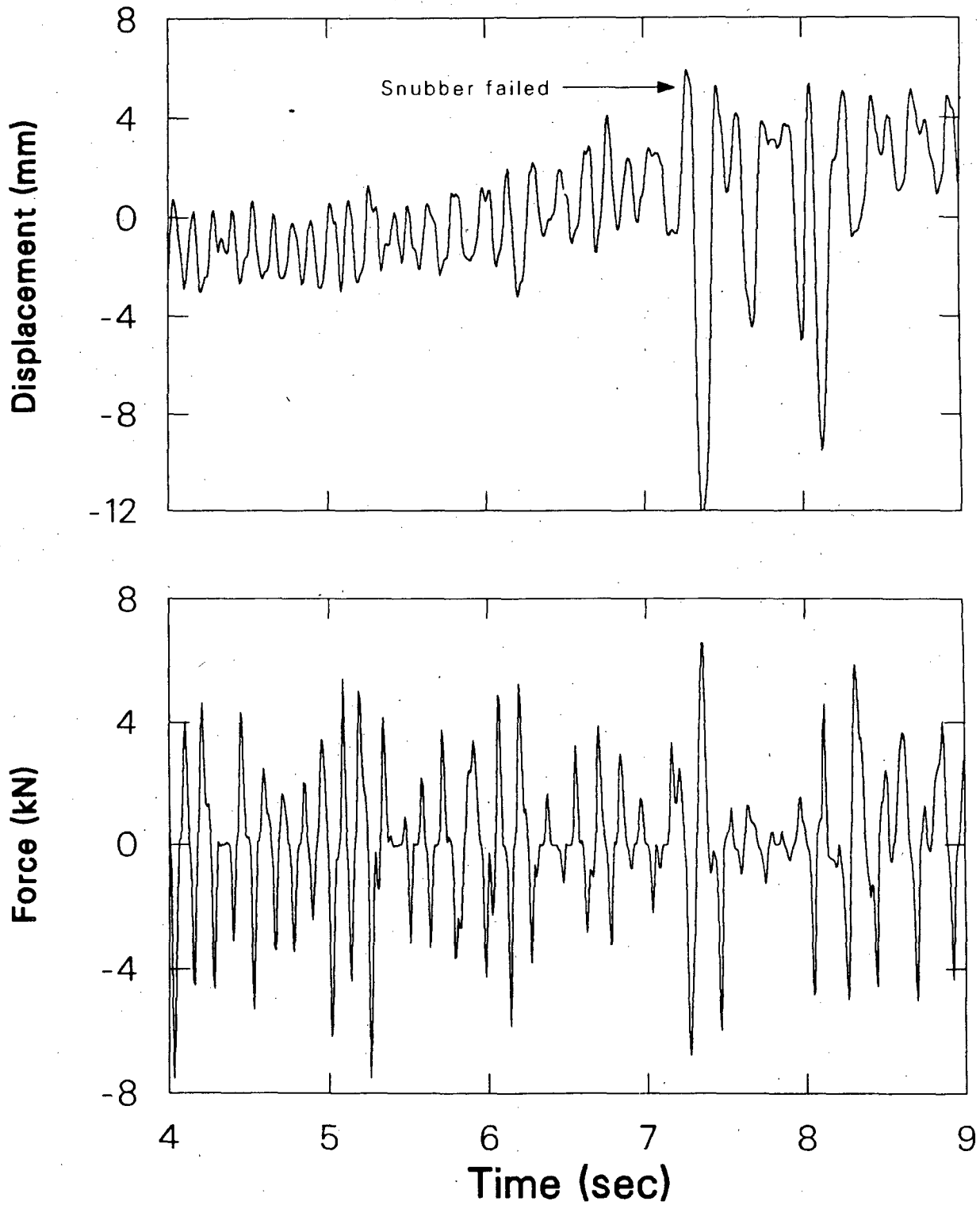


Figure 6. Force and displacement history comparison for the H-22 snubber location during 600% SSE test.

the 4-in. branch connection and the 4-in. loop. The strains on the branch connection and elbow 2 in the loop generally increase at 2.5 and 7 s. These are the respective times of the snubber failures.

The snubber at H-12 failed at 5 s in the transient after resisting loads up to 4.5 kN. This Anchor/Darling snubber size AD-40 was rated for 400 lb (Level B). The snubber failed at more than 2.53 times its design load. No physical damage was observed on the piping system and no permanent piping offsets were observed at the failed snubber locations.

#### 800% SSE Test (T41.813)

For the 800% SSE test, the snubbers that failed (at locations H-8, -12, and -22) during the 600% SSE test were not replaced. The snubber at H-22, which failed with resistance, was removed to simulate a failure without resistance. Figure 7 shows the shaker input displacement histories for the 800% SSE test. The peaks exceed 40 mm, and the peak forces input to the system at each shaker exceed 150 kN.

Figure 8 provides a 4-s excerpt from the force and displacement histories for the snubber at the H-7 location. The force history shows that the snubber resisted a 60-kN force at 5.7 s, approximately nine times its (Level B) design loading. The displacement history shows anomalous behavior at 6.5 s and by 7 s, the measured force drops to near zero with displacements greater than 16 mm. The peaks on the displacement history after 7 s are clipped because displacements were beyond the range of the instrument. The force history shows impacting after 8 s in both the positive and negative directions, which indicates the displacements were greater than 100 mm (the nominal travel for a PSA-1 snubber).

With the failure of the snubber at location H-7 in this test and of those at H-8 and -22 in the previous test, the loop from the snubber at H-6 (refer to Figure 1) to the strut at H-10 is supported only by two spring hangers (locations H-14 and H-15) and one strut (location H-9). Figures 9 and 10 are the complete 15 s displacement histories for the H-7 and -8 locations. The figures show that following the H-7 failure, the displacement also increased at the adjacent vertical H-8 location. Figures 11 and 12 are typical strain measurements from the branch connection and the elbow; they also show an increase in magnitude. The displacements and the strains also reflect a decrease in the response frequency, which is as one would expect, because after the final snubber failure, the piping system became more flexible in this area.

Figure 13 shows the force and displacement histories for H-6, a vertical snubber location. Both histories show the effect of the H-7 snubber failure. They also show the lower frequency response of the piping system. After the failure, this PSA-1 snubber resisted loads up to six times its Level B design load and maintained dead band travel within the manufacturer's specified tolerance.

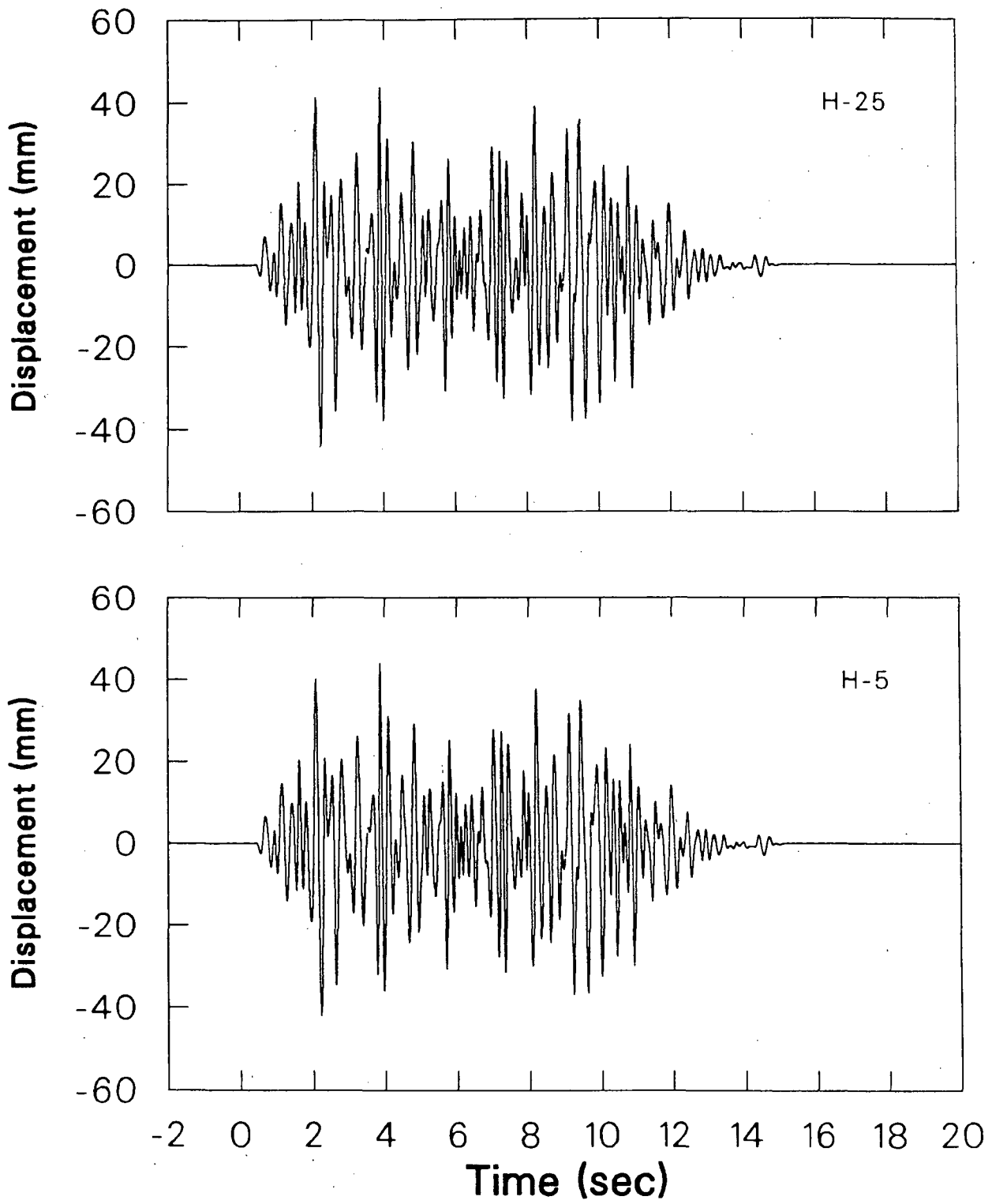


Figure 7. Servohydraulic shaker inputs exceed 40 mm in 800% SSE test.

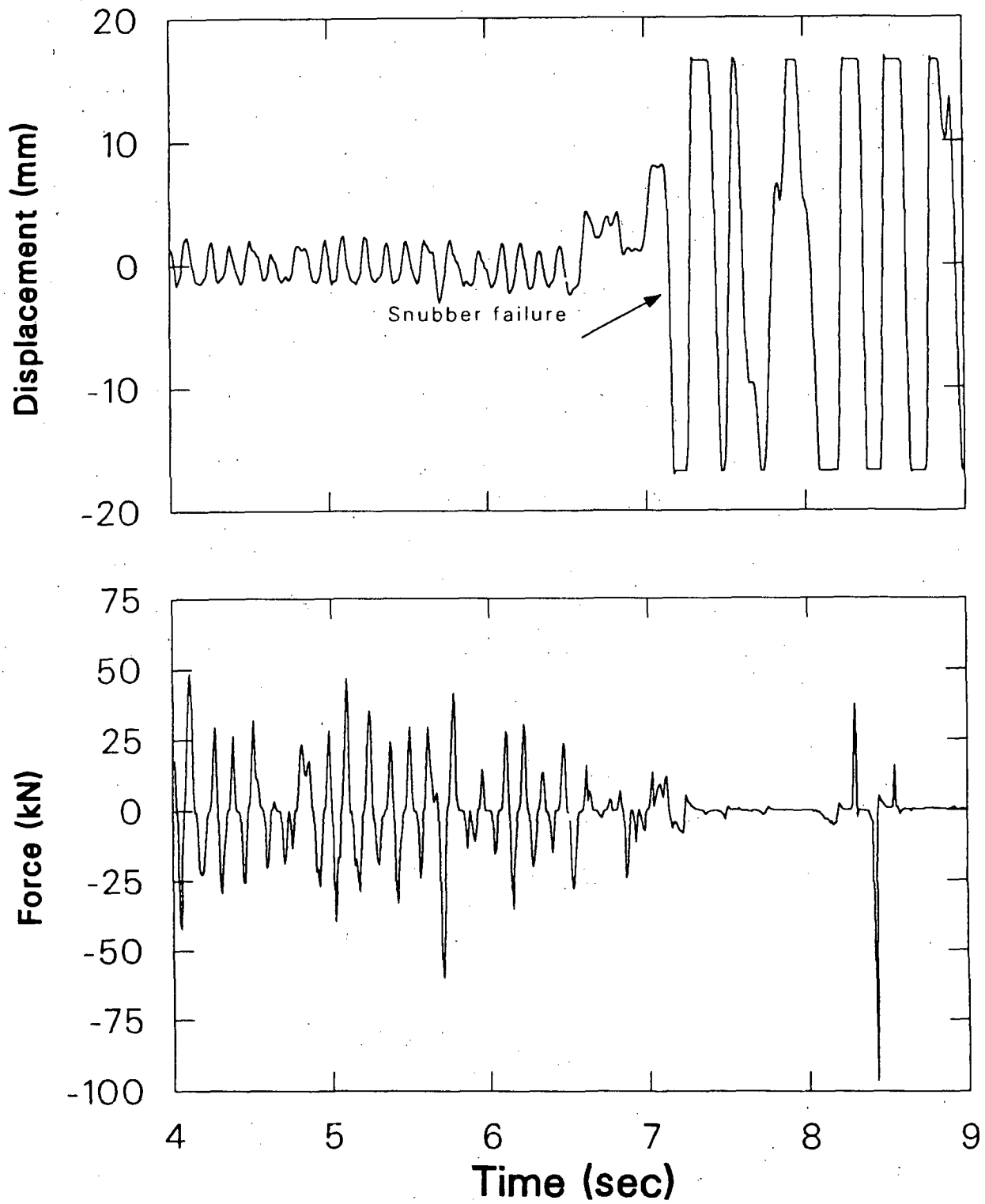


Figure 8. Force and displacement history comparison for the H-7 snubber location during 800% SSE test.

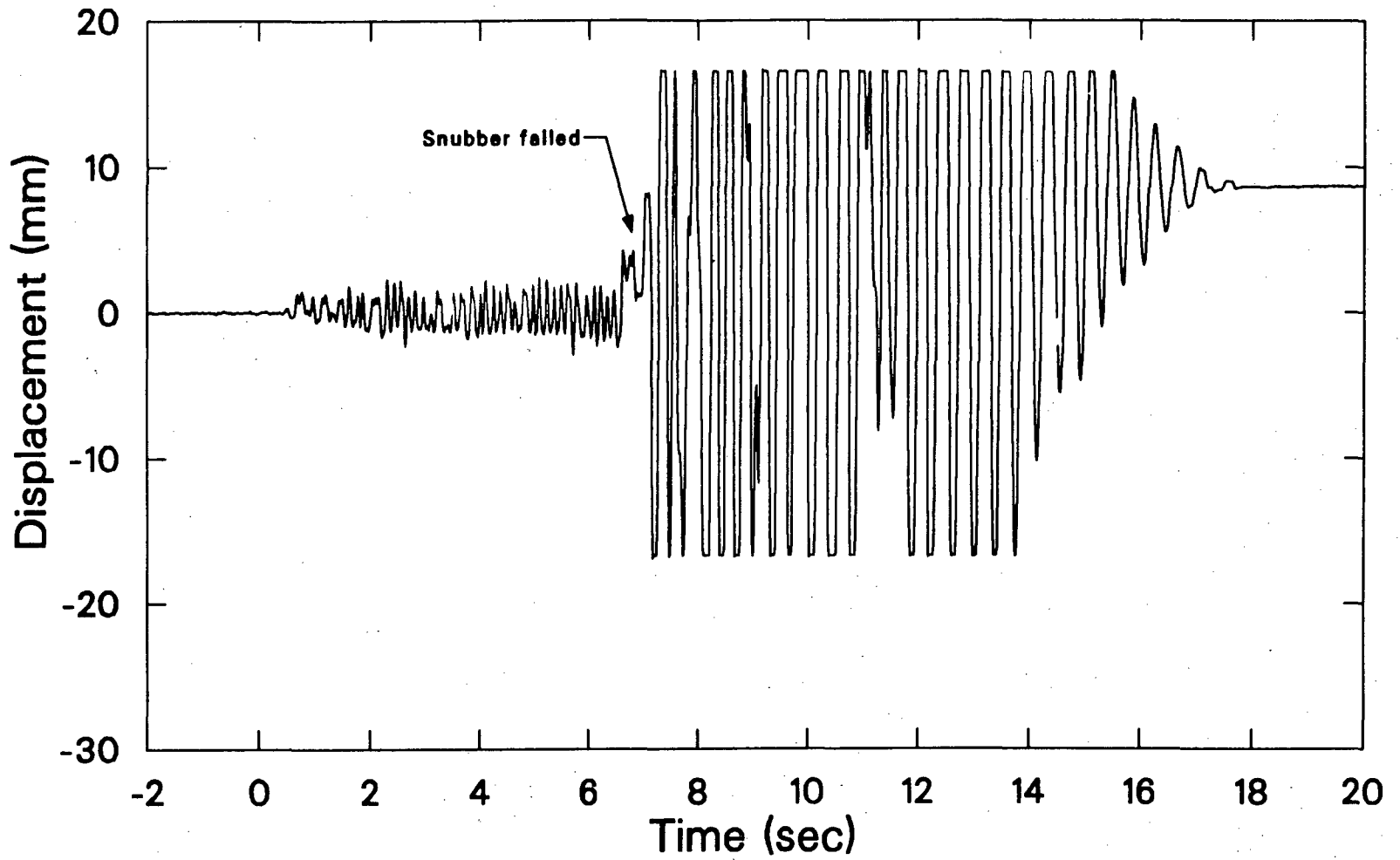


Figure 9. Complete displacement history for H-7 during 800% SSE test.

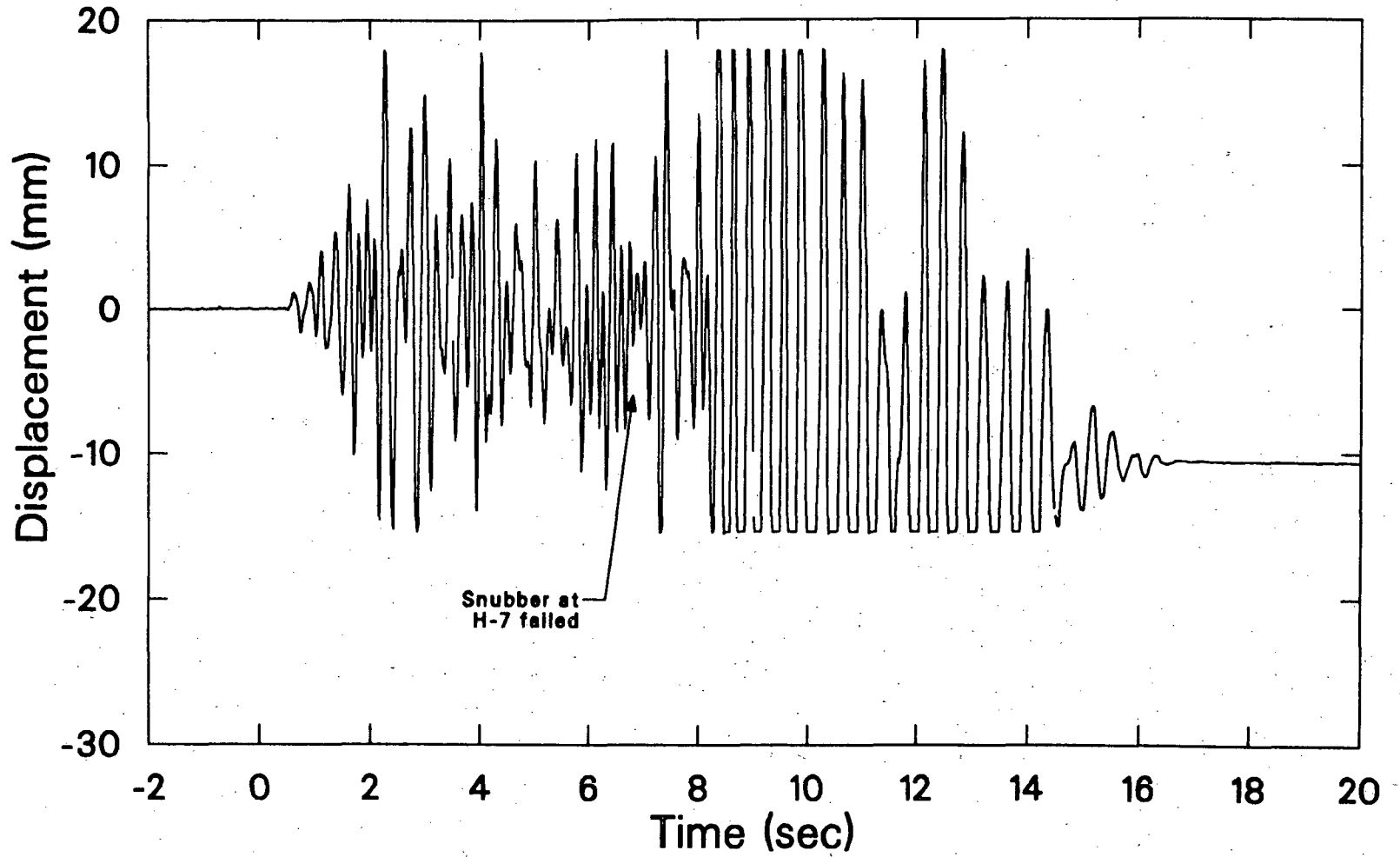


Figure 10. Complete displacement history for H-8 during 800% SSE test.

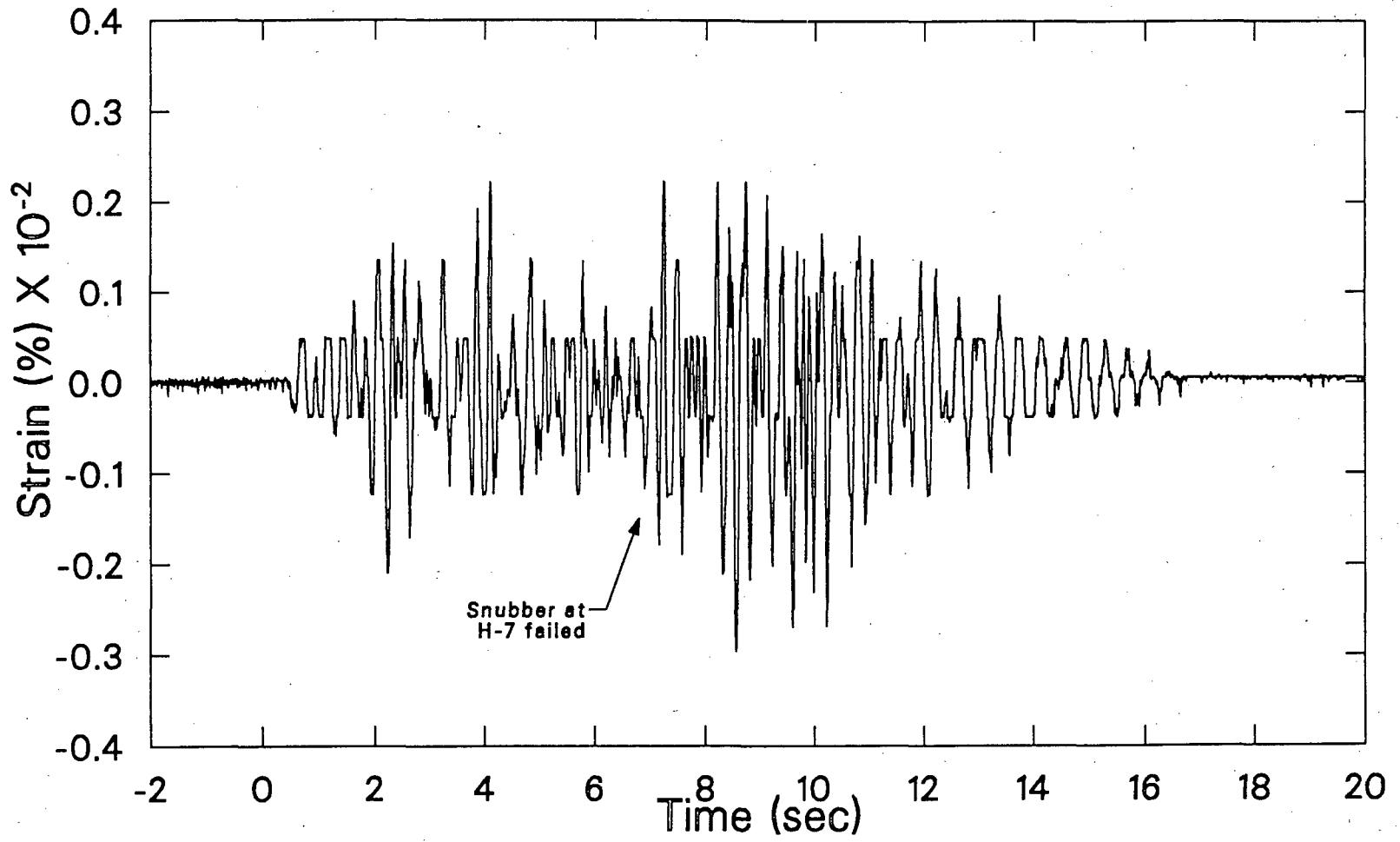


Figure 11. Strain history for the branch connection during 800% SSE test.

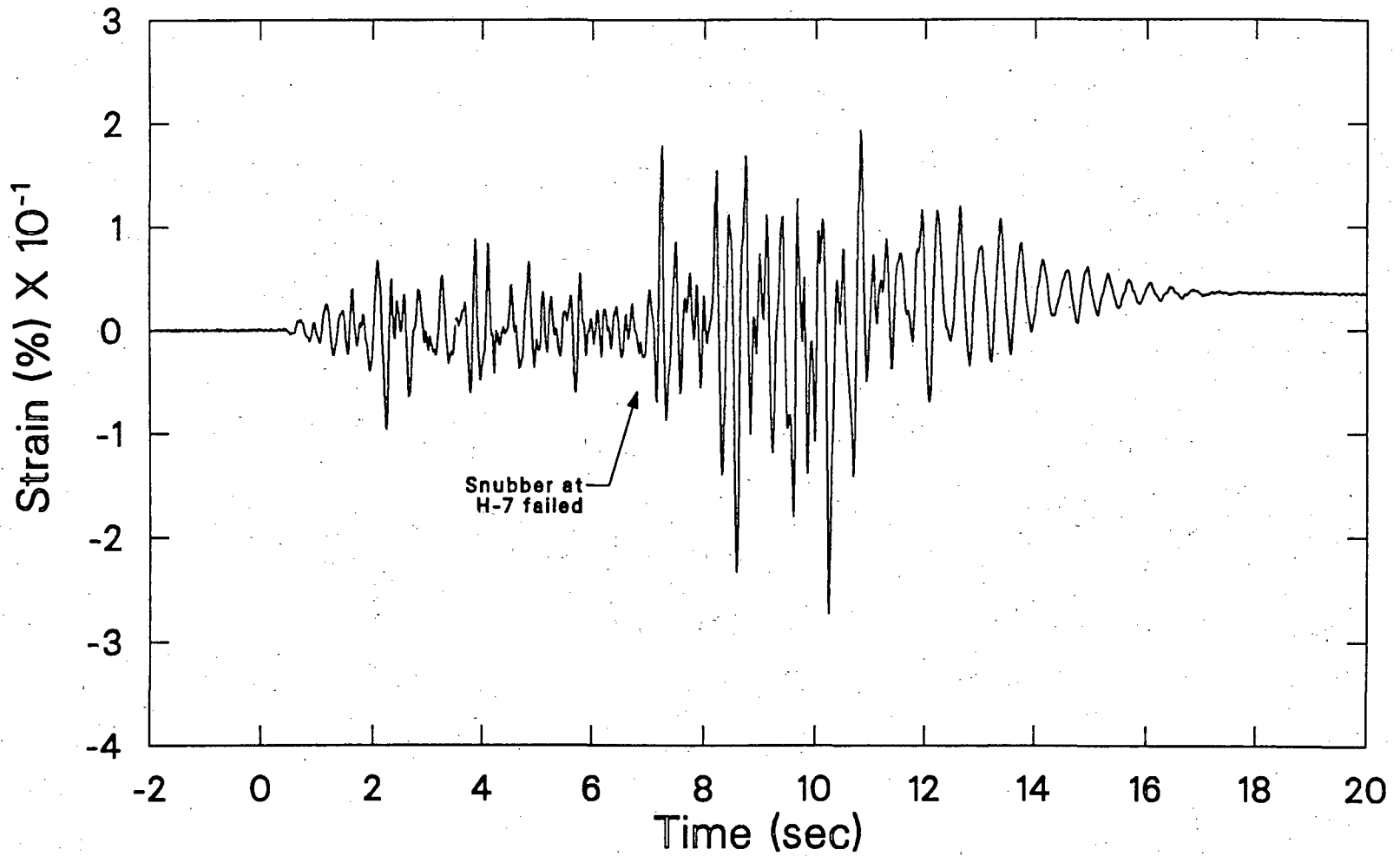


Figure 12. Strain history for the No. 2 elbow during 800% SSE test.

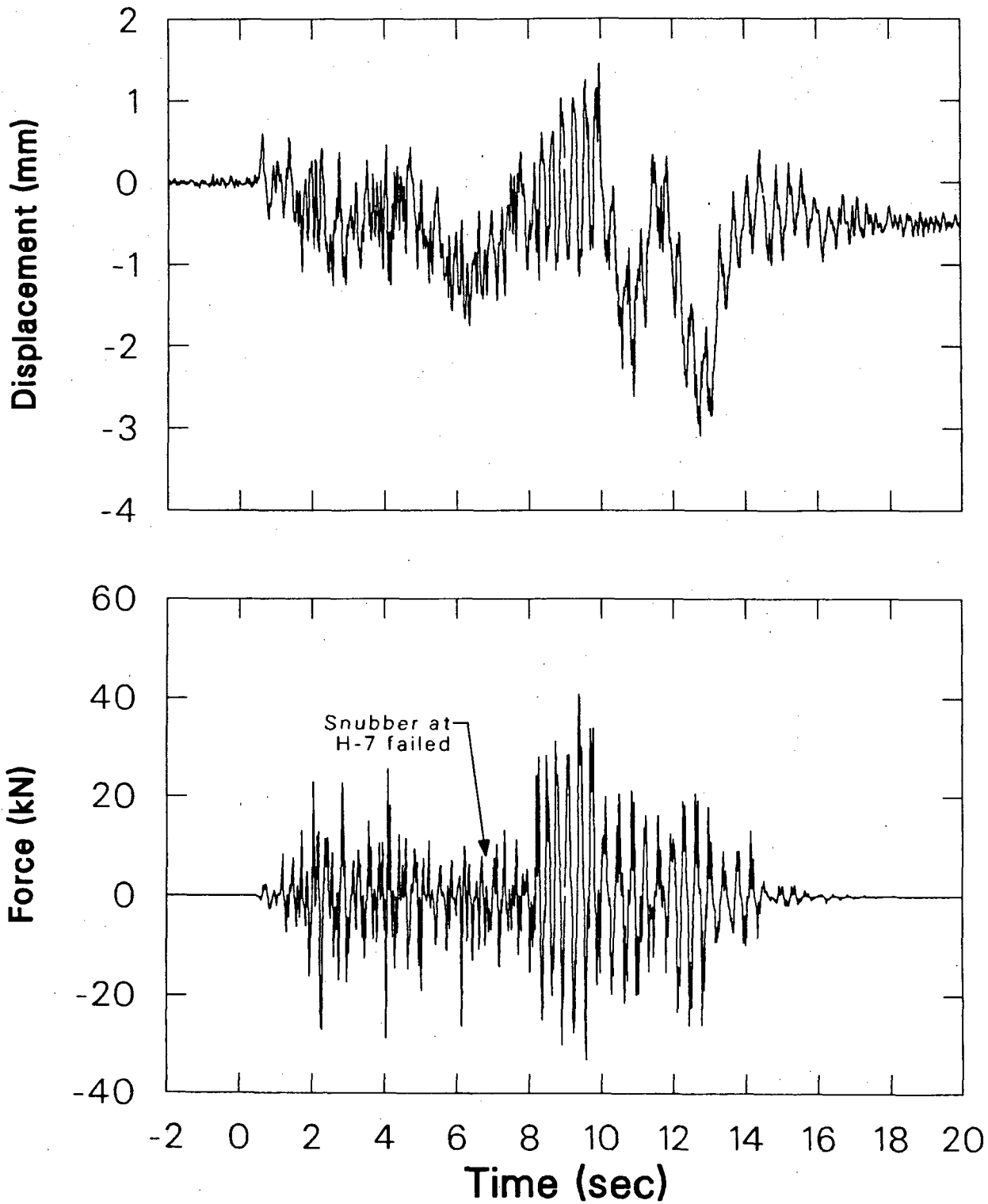


Figure 13. Force and displacement history comparison for the H-6 snubber location during 800% SSE test.

#### 4. CONCLUSIONS

The VKL was exposed to significant simulated seismic loadings. The U.S. stiff piping support system was designed and sized for a 100% SSE loading. Loadings in excess of 800% SSE were applied, resulting in significant piping system responses. The acceleration input to the valve body was in excess of 5 g, and the motor operator experienced responses of 11 g without structural or functional problems. The piping support components generally exceeded three times their design safety margins. The piping system sustained multiple adjacent support failures, with measured strains greater than yield, yet no significant damage occurred.

These preliminary results indicate that significant seismic loadings can be imposed on piping systems without creating a safety problem in modern nuclear plants.

# EARLY RESULTS OF GATE VALVE FLOW INTERRUPTION BLOWDOWN TESTS<sup>a</sup>

Kevin G. DeWall

Idaho National Engineering Laboratory  
EG&G Idaho, Inc.  
Idaho Falls, Idaho 83415

## ABSTRACT

The preliminary results of the USNRC/INEL<sup>b</sup> high-energy BWR line break flow interruption testing are presented. Two representative nuclear valve assemblies were cycled under design basis Reactor Water Cleanup pipe break conditions to provide input for the technical basis for resolving the Nuclear Regulatory Commission's Generic Issue 87. The effects of the blowdown hydraulic loadings on valve operability, especially valve closure stem forces, were studied. The blowdown tests showed that, given enough thrust, typical gate valves will close against the high flow resulting from a line break. The tests also showed that proper operator sizing depends on the correct identification of values for the sizing equation. Evidence exists that values used in the past may not be conservative for all valve applications. The tests showed that improper operator lock ring installation following test or maintenance can invalidate in-situ test results and prevent the valve from performing its design function.

## Introduction

As part of the Nuclear Regulatory Commission's (NRC) Equipment Operability research program, the Idaho National Engineering Laboratory (INEL) is performing research to provide input for the technical basis for resolving Generic Issue 87 (GI-87), "Failure of HPCI Steam Line Without Isolation." This INEL research program also provides information applicable to two additional regulatory items: (1) Generic Issue II.E.6.1, "In Situ Testing of Valves" and (2) IE Bulletin 85-03, "Motor Operated Valve Common Mode Failures During Plant Transients Due To Improper Switch Settings."

The objective of the INEL research program is to determine whether isolation valves in high-energy BWR piping systems will close against high flows in the event of a pipe break outside containment. GI-87 applies to those process lines that communicate with the primary system, pass through

---

a. Work supported by the U.S. Nuclear Regulatory Commission, Office of Nuclear Regulatory Research, under DOE Contract No. DE-AC07-76ID01570, under the direction of Dr. G. H. Weidenhamer, Technical Monitor.

b. United States Nuclear Regulatory Commission/Idaho National Engineering Laboratory.

containment, and contain normally open isolation valves. Three process lines meet these criteria: (1) the High Pressure Coolant Injection (HPCI) steam supply line, (2) the Reactor Core Isolation Cooling (RCIC) steam supply line, and (3) the Reactor Water Cleanup (RWCU) supply line. Of the three, an unisolated break in the RWCU supply line was determined to have the greatest safety impact. The design basis hot water blowdown testing was performed to provide information on valve operability questions associated with the RWCU environment (subcooled water flashing to steam). The majority of RWCU containment isolation valves are 6-inch, 900-pound, flexible-wedge gate valves with Limitorque electric motor operators.

### Background

The gate valve, Figure 1, is designed for use in a system where a positive shut-off is required with minimal pressure drop when the valve is open. It is ideally suited to those situations where isolation of one part of a system from another is required and control of the dynamic properties of the fluid (throttling) is unnecessary. With the disc (or gate) in the raised position, the run of the valve is free of any obstruction with approximately the same head loss as in the adjacent piping. When the disc is lowered into the seat, the upstream pressure forces it against the seat, creating a seal and isolating the downstream system from the fluid.

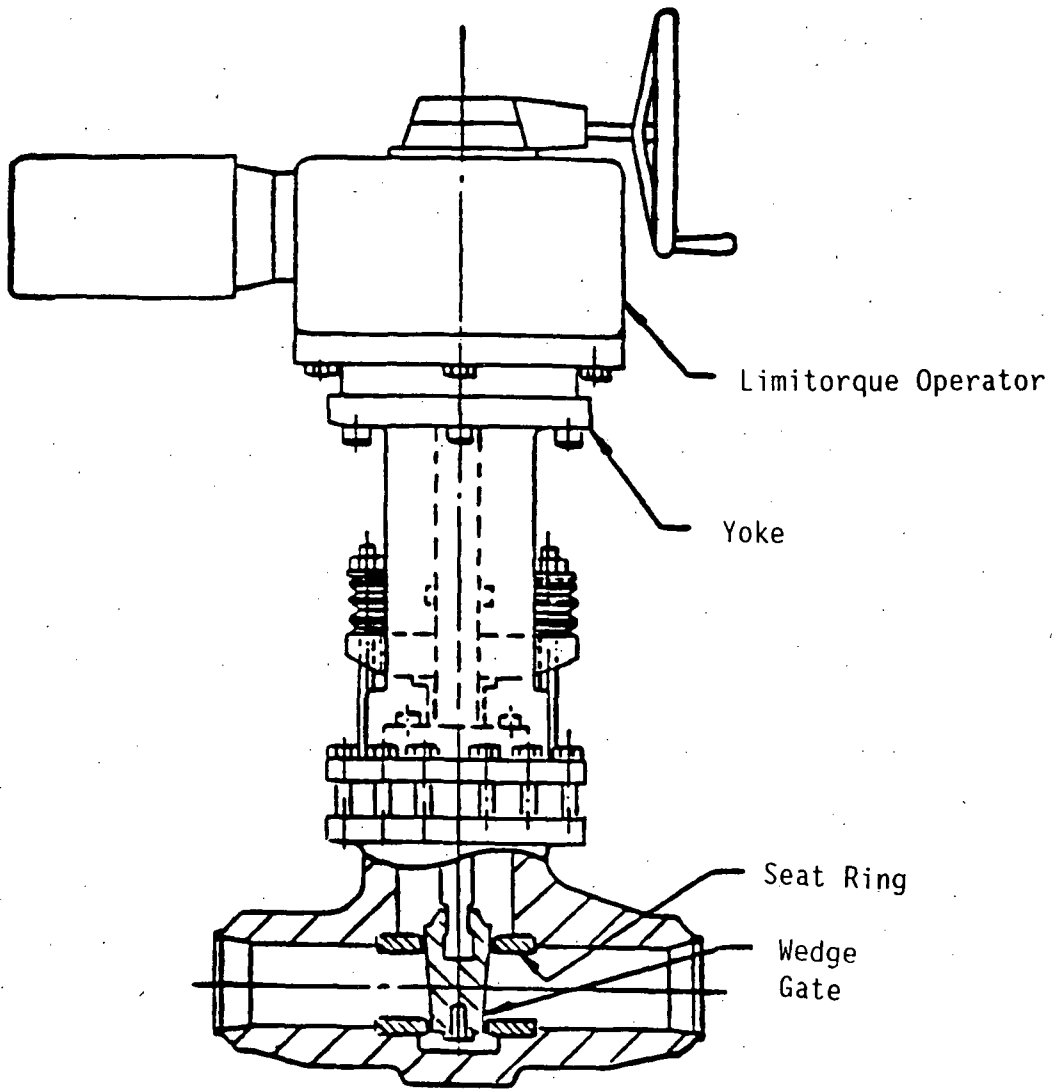
Most of the valve and operator manufacturers use the same equation to determine valve closure forces, with only minor variations in coefficients. In this equation, the required force to cycle the valve is equated to the sum of the disc drag load due to differential pressure, the stem rejection load (stem end pressure load), and the packing drag load, as detailed below.

$$F_t = \mu(A_d)(\Delta P) \pm A_s(P) + F_p \quad (1)$$

Where

|            |                                   |
|------------|-----------------------------------|
| $F_t$      | = Total stem force                |
| $\mu$      | = Disc friction factor            |
| $A_d$      | = Disc area                       |
| $\Delta P$ | = Differential pressure           |
| $A_s$      | = Stem cross-sectional area       |
| $P$        | = System pressure                 |
| $F_p$      | = Packing drag load (a constant). |

The disc load is determined by multiplying the exposed disc area by the differential pressure and a disc factor to account for seating surface and guide sliding friction. The disc factor normally used for wedge-type gate valves in Equation (1) is 0.3. The stem rejection load is found by taking the stem cross-sectional area and multiplying it by the system pressure. Note that in this equation the stem rejection load can be either positive or negative depending on whether the valve is closing or opening. This is because the stem rejection load is always in a direction out of the valve body; the stem rejection load resists valve closure and assists in valve opening. The service conditions used in the force equation are supplied by each individual plant.



(Closed Position)

Figure 1. Typical motor-operated gate valve.

## Test Design

In the blowdown test research program two full-scale, representative nuclear valve assemblies were cycled under design basis RWCU pipe break conditions. Both valves were modified to incorporate extended yokes (4 inches longer than normal) and stems cut in half and threaded to allow installation of the special stem force instrumentation. Flanges were attached to both sides of each valve for mating with the test system piping.

The first test specimen, Valve A, was a 6-inch, 900-pound standard rated, cast steel, flexible-wedge gate valve with a pressure seal bonnet and butt weld ends. The valve seats were hard faced with Stellite and seal welded to the valve body. The one-piece flexible wedge (disc) was also hard faced with Stellite on the seating faces, and the disc guides were carbon steel. The valve was manufactured for this test program by Anchor/Darling Valve Company using a nuclear-grade body casting, nuclear design and materials, without third-party inspections. The valve was powered by a Limatorque SMB-2-40 electric motor operator. The valve design was representative of valves installed in early nuclear power plants.

The second test specimen, Valve B, was a 6-inch, 900-pound standard rated, forged steel, flexible-wedge gate valve with a bolted bonnet and butt weld ends. The valve seats were hard faced with Stellite and seal welded to the valve body. The one-piece flexible wedge (disc) was also hard faced with Stellite on the seating faces. The valve was manufactured for this test program by Velan Incorporated using nuclear design and materials, without third-party inspections. The valve was powered by a Limatorque SMB-0-25 electric motor operator. Representing one of the newer valve assemblies delivered since 1970, the Valve B design incorporated hard-faced disc guide wear surfaces.

Both valves utilized 460 Vac, 3 phase, 60 Hz electric motor operators. To ensure valve closure and data collection at the anticipated greater-than-normal loadings, Valve A utilized a larger, greater-capacity motor operator than would normally be used. The motor operator used with Valve B was sized in accordance with current practices to represent a typical valve used in nuclear power plants today. With their differences in internal and friction bearing surface design, the two valve assemblies represented a large number of motor-operated valves used in nuclear plants today.

The test system used for the subcooled water blowdown testing featured a large water tank, heated and pressurized so that various system water conditions could be established and regulated, replicating actual BWR conditions. The water was propelled by high-pressure gaseous nitrogen. The water heating system consisted of a heating section and a high-pressure, high-temperature water pump. The heating section contained an electrical heater in an 8-inch pipe and heated the water as the pump recirculated water from the pressure vessel, through the test section and heating section, and back to the pressure vessel. The test section was a 6-inch pipe with the test specimen mounting flanges and appropriate fittings for obtaining temperature and pressure measurements. The system is shown schematically in Figure 2.

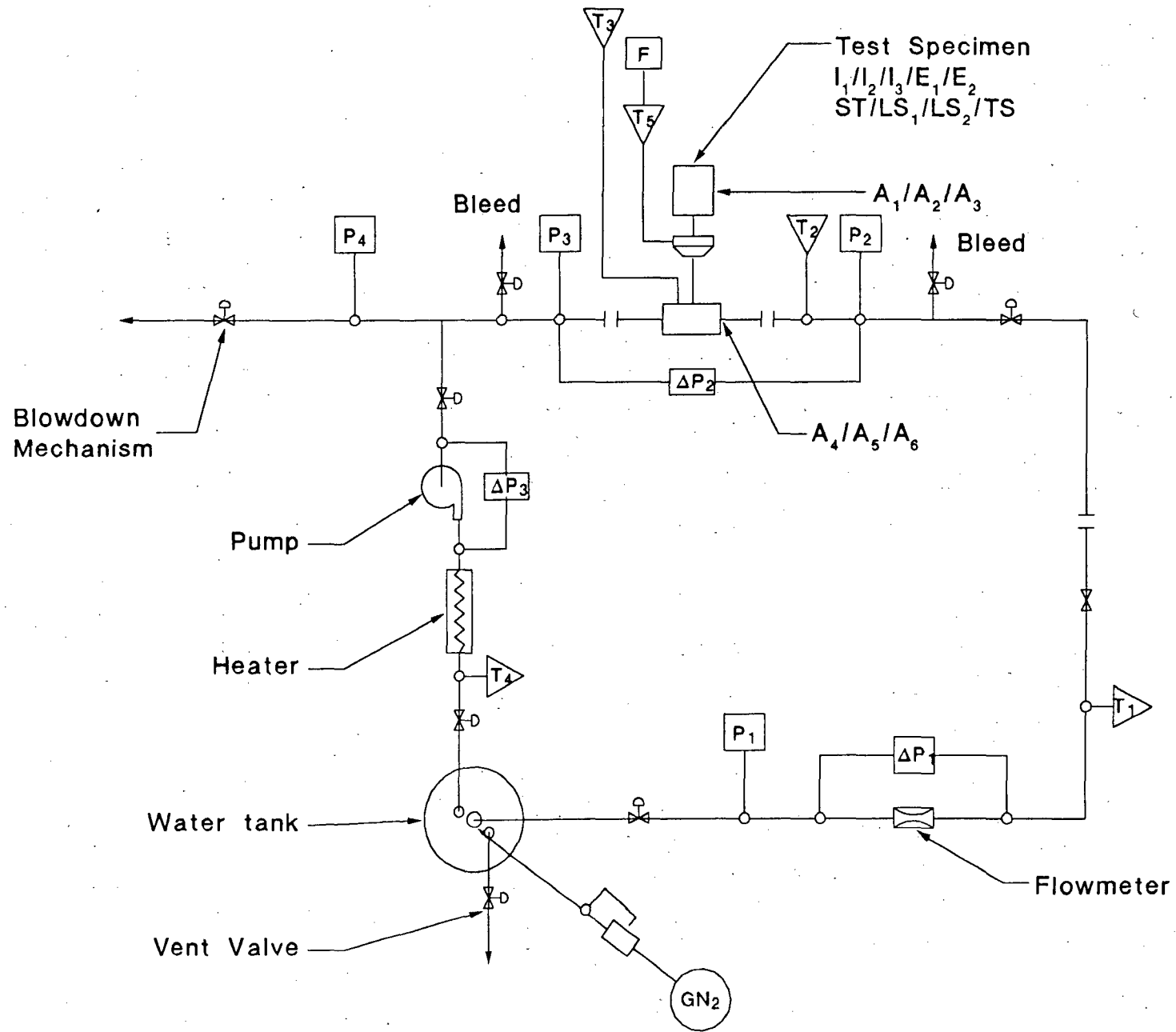


Figure 2. Test system schematic showing instrumentation locations.

BMG0017E

To accomplish the functional testing, the system contained bleed valves which provided the means to reduce system pressure on both sides (upstream and downstream) of the test specimen. In this manner, differential pressure conditions could be established across the test valve's disc. The test system also featured a fast-acting (approximately 300 msec opening stroke), hydraulically operated valve, positioned so that when the valve was actuated, the system's fluid was abruptly dumped to the atmosphere, resulting in high-flow (blowdown) conditions through the test specimen.

The test system was instrumented to monitor flow, pressure, and temperature at various locations, including test valve upstream and downstream positions. Motor operator electrical characteristics were also recorded. Valve stem force was monitored using a special high-temperature load cell installed between the two halves of the specially designed valve stems. The test parameters measured are listed in Table 1.

A secondary objective of the blowdown test program was to determine how normal utility in-situ valve testing, using available diagnostic equipment, could be used to provide assurance of a valve's ability to isolate pipe break flows. By measuring actual stem forces and associated motor operator parameters, in-situ plant testing plans may be developed using available diagnostic equipment; the values of the functions measured by this equipment are then extrapolated to actual stem forces. Several motor-operated valve (MOV) diagnostic system manufacturers supported this objective by participating in the testing as listed in Table 2 in chronological order. The manufacturer participation was not a competition but, rather, an attempt to determine what factors need to be considered to provide reasonable assurance of valve operability using each device.

While general observations are made in this paper concerning the use of this diagnostic equipment, in-depth analysis of the data taken and discussions of how the devices may best be utilized must await review of the digitized data, scheduled for early Fiscal Year-1989, as well as analysis coordination with the diagnostic equipment manufacturers.

### Test Procedure

Upon installation in the test system, each valve assembly was subjected to a typical ANSI B16.41<sup>1</sup> functional qualification test, including the valve leakage test (Annex A), cold cyclic test (Annex B), and hot cyclic test (Annex C). These tests were accomplished to provide a baseline characterization of valve assembly operation for comparison with the later testing. The valve leakage test established the mainseat valve leakage rate and the packing leakage rate of the test valves, while the cold cyclic test demonstrated the capability of the test valve assembly to open and close under adverse combinations of motive power and system pressure with the assembly at room temperature not exceeding 100°F. The hot cyclic test sequence was performed to demonstrate the capability of the test valve assemblies to open and close under adverse combinations of motive power and system pressure with the assembly at design temperature, in excess of 100°F. Annex G, flow isolation, was the subject of this test program and thus was not performed as part of the qualification series.

TABLE 1. TEST PARAMETERS MEASURED DURING BLOWDOWN TESTS

| Transducer | Measurement                    | FM Tape | Oscillo-<br>graph | Data<br>Logger | X-Y<br>Plotter |
|------------|--------------------------------|---------|-------------------|----------------|----------------|
| T1         | System Water Temp.             |         |                   | X              |                |
| T2         | Test Valve Inlet Water Temp.   |         |                   | X              |                |
| T3         | Test Valve Body Temp.          |         |                   | X              |                |
| T4         | Heating Section Water Temp.    |         |                   | X              |                |
| T5         | Load Cell Temp.                |         |                   | X              |                |
| P1         | System Water Press.            | X       | X                 | X              | X              |
| P2         | Test Valve Inlet Water Press.  | X       | X                 | X              |                |
| P3         | Test Valve Outlet Water Press. | X       | X                 | X              |                |
| P4         | Discharge Section Water Press. | X       | X                 | X              |                |
| ΔP1        | Test Valve Differential Press. | X       | X                 | X              |                |
| ΔP2        | Venturi Differential Press.    | X       | X                 | X              |                |
| ΔP3        | Pump Differential Press.       | X       |                   | X              |                |
| I1         | Actuator Current               | X       | X                 |                |                |
| I2         | Actuator Current               | X       |                   |                |                |
| I3         | Actuator Current               | X       |                   |                |                |
| E1         | Actuator Voltage               | X       | X                 |                |                |
| E2         | Actuator Voltage               | X       |                   |                |                |
| ST         | Valve Stroke - LVDT            | X       | X                 |                | X              |
| LS1        | Open Limit Switch              | X       | X                 |                |                |
| LS2        | Close Limit Switch *           |         |                   |                |                |
| TS         | Close Torque Switch            | X       | X                 |                |                |
| F          | Valve Stem Force               | X       | X                 | X              |                |
| A1         | Actuator Acceleration Y        | X       | X                 |                |                |
| A2         | Actuator Acceleration X        | X       |                   |                |                |
| A3         | Actuator Acceleration Z        | X       |                   |                |                |
| A4         | Valve Body Acceleration Y      | X       | X                 |                |                |
| A5         | Valve Body Acceleration X      | X       |                   |                |                |
| A6         | Valve Body Acceleration Z      | X       |                   |                |                |

\*Control room light indicator only.

TABLE 2. VALVE DIAGNOSTIC EQUIPMENT USED FOR SUBCOOLED BLOWDOWN TESTS

| <u>Valve</u> | <u>Test Series</u> | <u>Description</u>        | <u>Diagnostic Equipment</u> |
|--------------|--------------------|---------------------------|-----------------------------|
| A            | 1                  | Qualification Test        | MCSA                        |
| A            | 3                  | Blowdown, 1000psig, 480°F | MCSA                        |
| A            | 2                  | Blowdown, 1000psig, 530°F | None                        |
| A            | 4                  | Blowdown, 1000psig, 400°F | V-MODS                      |
| A            | 6                  | Blowdown, 1400psig, 530°F | V-MODS                      |
| A            | 5                  | Blowdown, 1400psig, 580°F | MOVATS                      |
| A            | 7                  | Blowdown, 1400psig, 450°F | MOVATS                      |
| A            | 9                  | Blowdown, 600psig, 430°F  | None                        |
| A            | 8                  | Blowdown, 600psig, 480°F  | None                        |
| A            | 10                 | Blowdown, 600psig, 350°F  | MAC, VOTES                  |
| A            | 11                 | Blowdown, 1000psig, 530°F | MCSA                        |
| B            | 1                  | Qualification Test        | MCSA                        |
| B            | 2                  | Blowdown, 1000psig, 530°F | MCSA, MOVATS                |
| B            | 3                  | Blowdown, 1400psig, 580°F | V-MODS                      |
| B            | 4                  | Blowdown, 600psig, 480°F  | MAC                         |
| B            | 5                  | Blowdown, 1000psig, 530°F | V-MODS                      |

MAC Limitorque Motor Actuator Characterizer  
MCSA ORNL Motor Current Signature Analysis  
MOVATS MOVATS, Inc. (MOV Analysis and Test System)  
V-MODS WYLE Labs. Valve Motor Operator Diagnostic System  
VOTES Liberty Technology Valve Operator Test & Evaluation System

Once baseline qualification testing of the test valve assemblies was completed, several test series were performed to address the questions of GI-87. Each test series included leakage tests, cyclic tests without flow, cyclic tests at normal system flow, and cyclic tests at full blowdown conditions. A wide range of design upstream pressures and temperatures was maintained throughout the valve closures, with blowdown flow limited only by flashing and choked flow at the test valve or piping exit. Each test series was structured to optimize the amount of useful data obtained. Required non-flow data were collected during the preparation period for full-scale flow and post full-scale flow.

Fourteen blowdown tests were accomplished, ten on Valve A and four on Valve B. All tests were performed to evaluate the engineering parameters required to calculate closure loads for a typical valve. In addition, the four tests with the Valve B and normally sized operator were performed to demonstrate expected in-service performance with the motive power closer to normal.

### Test Results and Interpretation

Valve A: A torque switch setting of 2.0 was selected for the motor operator so that the stem thrust capability was maximized without exceeding the valve and instrumentation capacity. (The torque switch was reset to 2.5 after test 10 to compensate for an observed torque-out anomaly, discussed later.) The valve closed satisfactorily for all tests; however, higher-than-predicted stem loads were observed during the blowdown flow isolation cycles.

Figure 3 is a reproduction of the stem force trace for the blowdown test with initial fluid conditions at 1000 psig and 530°F subcooled water. The figure shows the stem compression (negative values) increasing as the valve closes until it reaches a peak where the flow path is finally blocked and the valve disc is riding against the full seat ring. At this point the stem compression decreases sharply to a value representing the force required to slide the disc on the seat to the fully seated position. Then the force rises sharply through final seating and torque switch trip. The compressive force in the stem then continues to increase due to the time lag in the circuit dropout time and the momentum in the operator. The peak shown shortly before final seating of the valve is the force that must be overcome for successful closure. This peak is the flow isolation force referred to in comparisons and discussions throughout this paper.

Equation (1) was used to predict stem forces during closure at high flow. Following typical industry practices, the parameters chosen for use in the equation were conservatively chosen to be maximum design pressure (P & ΔP) and assumed worst-case packing drag force. The Valve A closure thrust was predicted using nominal valve size (6 in.) to calculate disc area, maximum upstream pressure for P & ΔP, a packing drag force of 1500 pounds, and a 0.3 disc factor. The calculation was repeated using a 0.5 disc factor following recent industry recommendations for gate valves in high-flow applications.

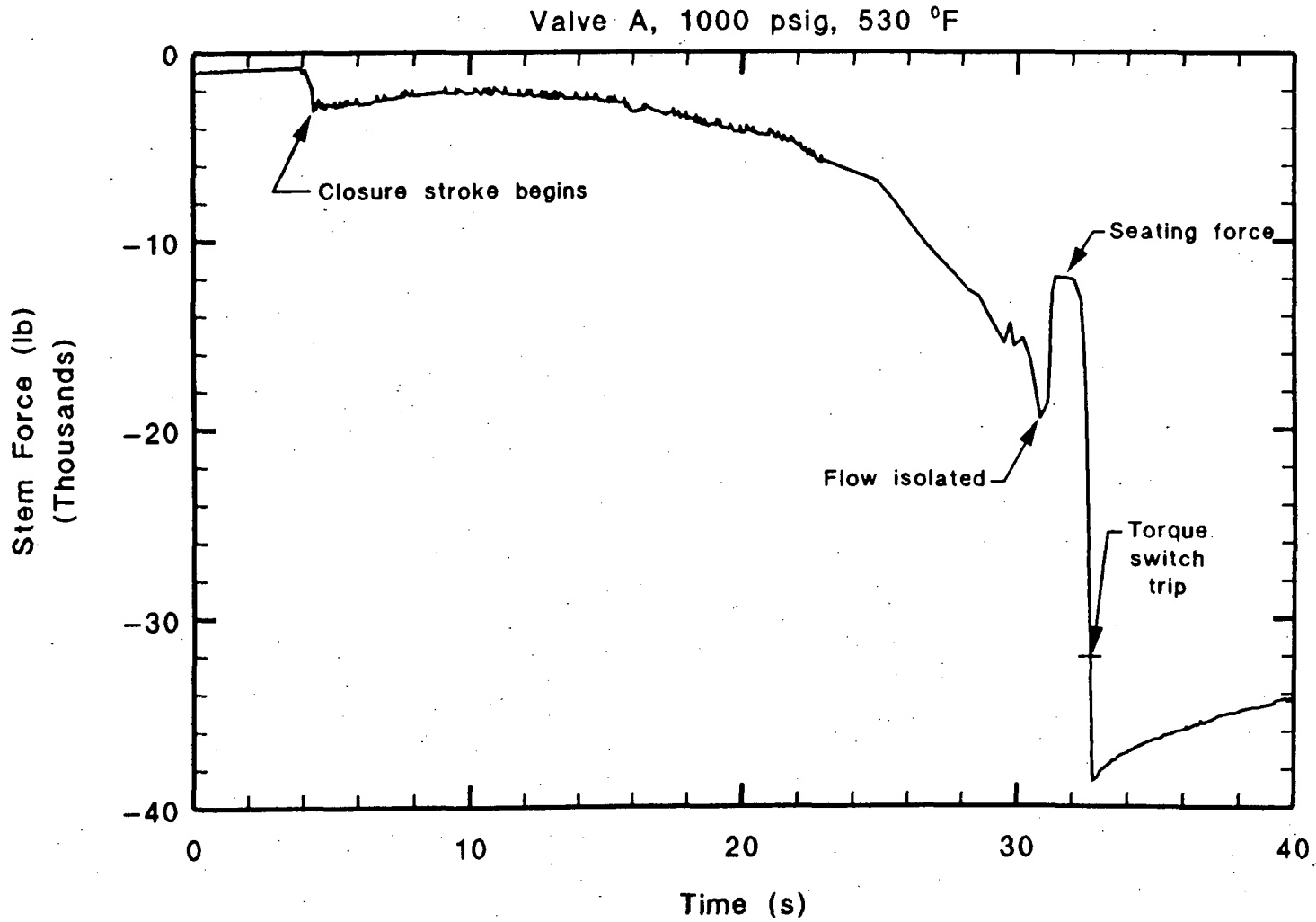


Figure 3. Load cell measurements show the effect of blowdown flows on valve closure stem loads.

Figure 4 shows a comparison between the predicted stem forces (using the above assumptions) using 0.3 and 0.5 disc factors and the actual stem forces measured during the blowdown isolation steps. For Valve A testing, both the pressures and temperatures were varied to change the degree of subcooling and thus degree of flashing occurring at the valve during closure. This figure shows that at the lower pressures the actual stem forces were closely predicted by the sizing calculation, as were the forces that were at higher pressures but greatly subcooled. The sizing calculations did not bound stem forces for the tests at higher pressures with water closer to saturation temperatures. A disc factor of about 0.57 would be necessary to reach the 19,400-pound stem force measured during the 1000 psig, 10°F subcooled water test.

In order to investigate how well Equation (1) models the actual behavior of the valve, the conservatism needs to be removed from the calculation. If the disc load is eliminated from Equation (1), such as would be the case without flow, what remains is a linear equation in slope-intercept form ( $y = mx + b$ ), namely:

$$F_t = -A_s(P) \pm F_p \quad (2)$$

Note that this equation has been written so that the stem rejection load is always negative (compression) while the packing load is either negative or positive depending on whether the valve is closing (compression) or opening (tension).

Figures 5 and 6 show the test data that are expected to apply to the above equation. The data plotted are the stem force measured at mid-stroke (running load) for tests at varying temperatures and pressures but without flow. The line fit through the data points has a slope equal to the stem cross-sectional area and provides an indication of the true packing load for each case. For Valve A, data show a packing load of 835 pounds for opening and 430 pounds for closing. Both values are well below the 1500 pounds used in the sizing equation, providing additional margin in the calculation. The difference between the two values can be partially accounted for by the weight of the disc and lower half of the stem. This difference also provides evidence that the packing load is affected by direction of travel, possibly caused by water carried with the shaft changing the lubrication of the packing/stem surfaces or by other phenomena associated with stem travel through packing.

Based on the packing load and stem rejection load characteristics determined from the running load evaluation, an evaluation of the total force equation [Equation (1)] was conducted. Here the conservatisms found in the application of the equation were eliminated by using measured parameters in the equation. Figure 7 contains the results of this calculation for the blowdown test shown in Figure 3 and compares it to the measured stem force. As might be expected, the calculated force bounds actual values during the first part of closure, when little of the disc area is exposed to the flow and differential pressure across the valve is small. As the disc drops further into the flow stream and differential pressure increases, the calculation ceases to bound measured values, where the actual flow isolation stem force exceeds those calculated.

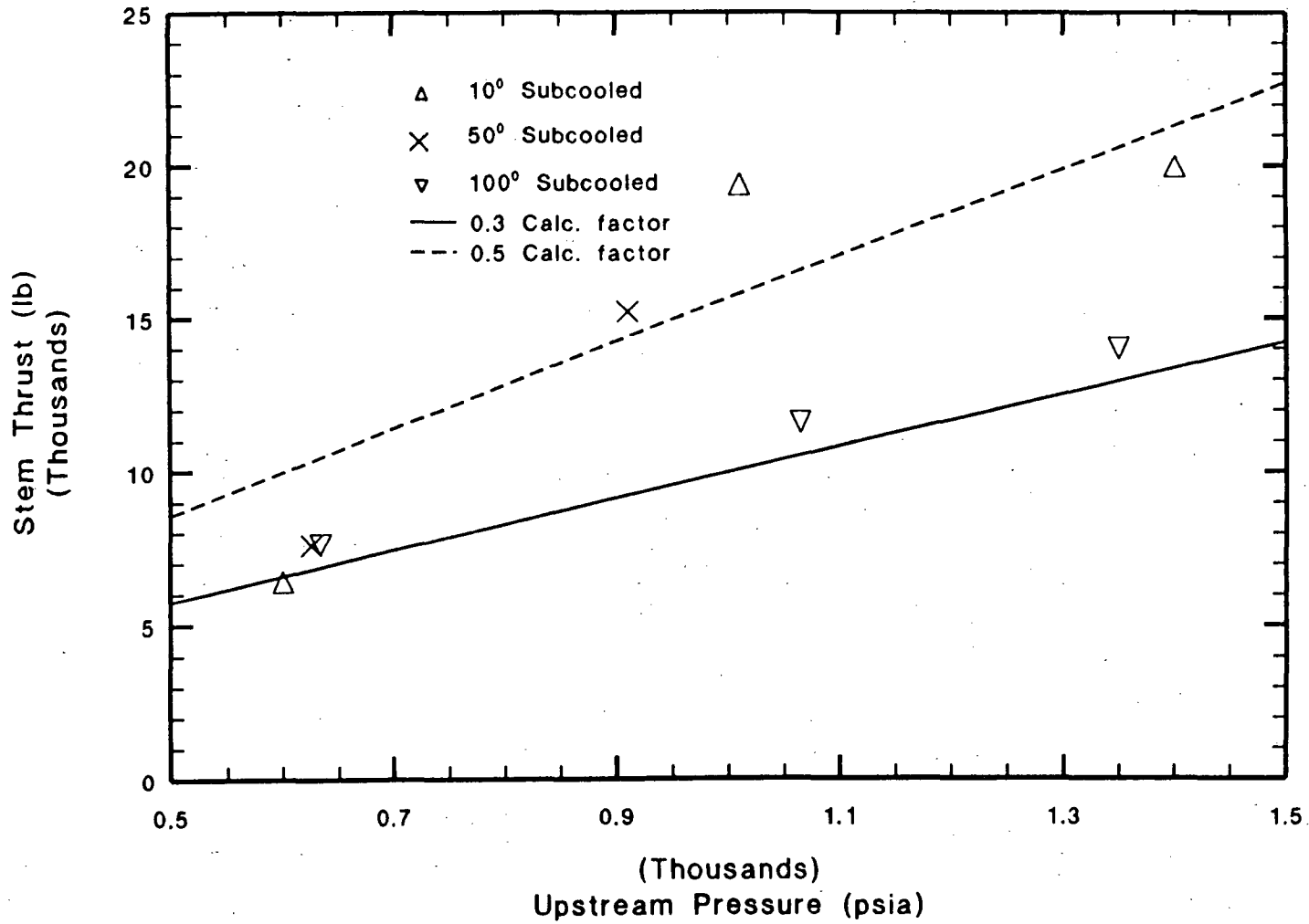


Figure 4. Valve A measured stem forces exceeded those calculated for tests at high pressure and slightly subcooled conditions.

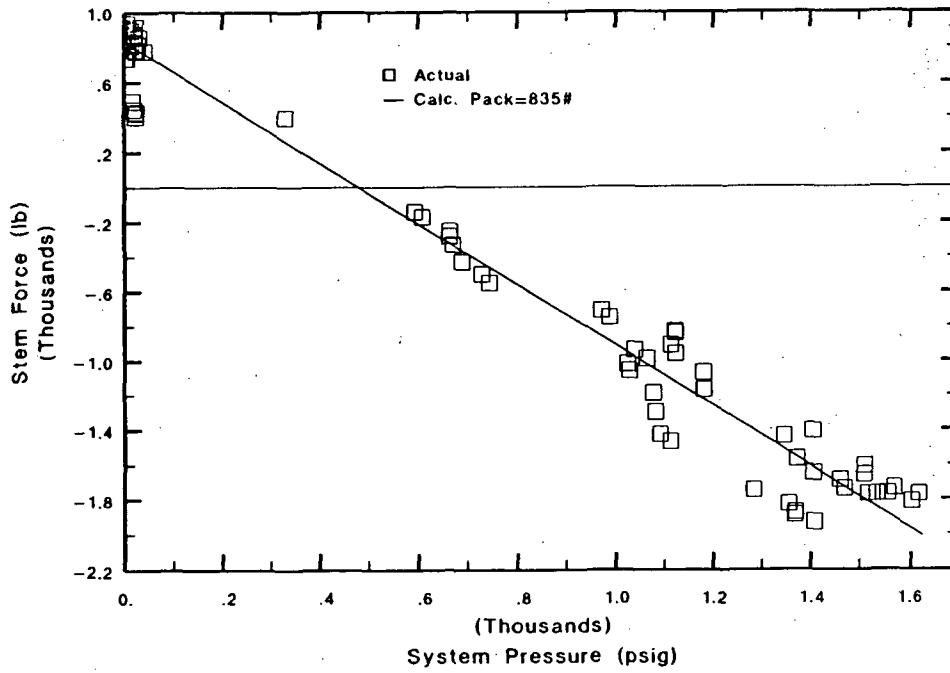


Figure 5. Linear curve fit using industry equation closely approximates Valve A running stem forces for opening without flow.

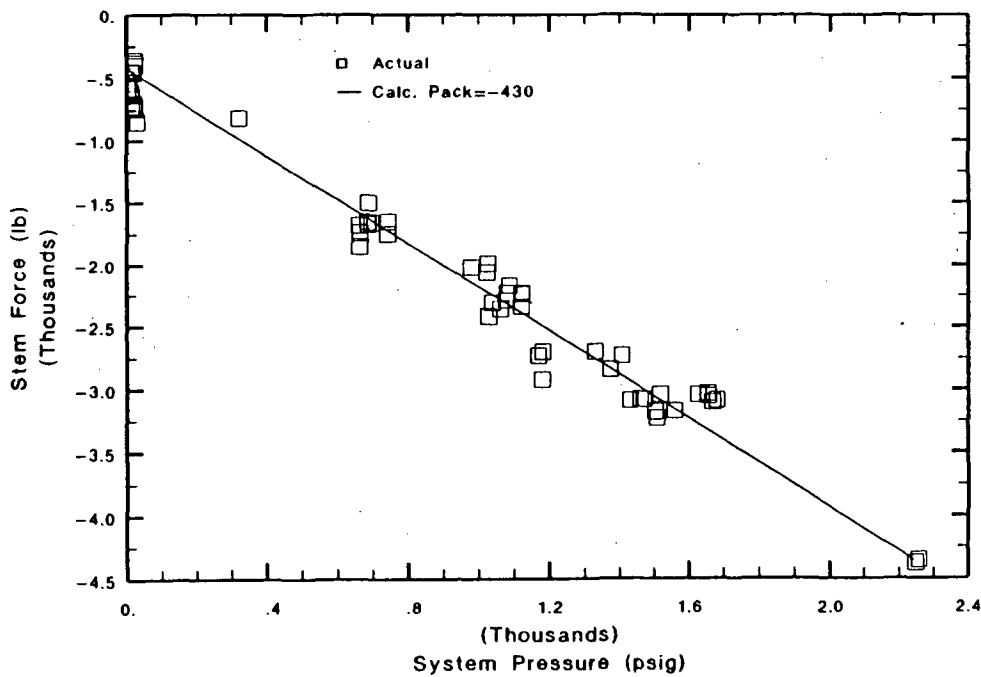
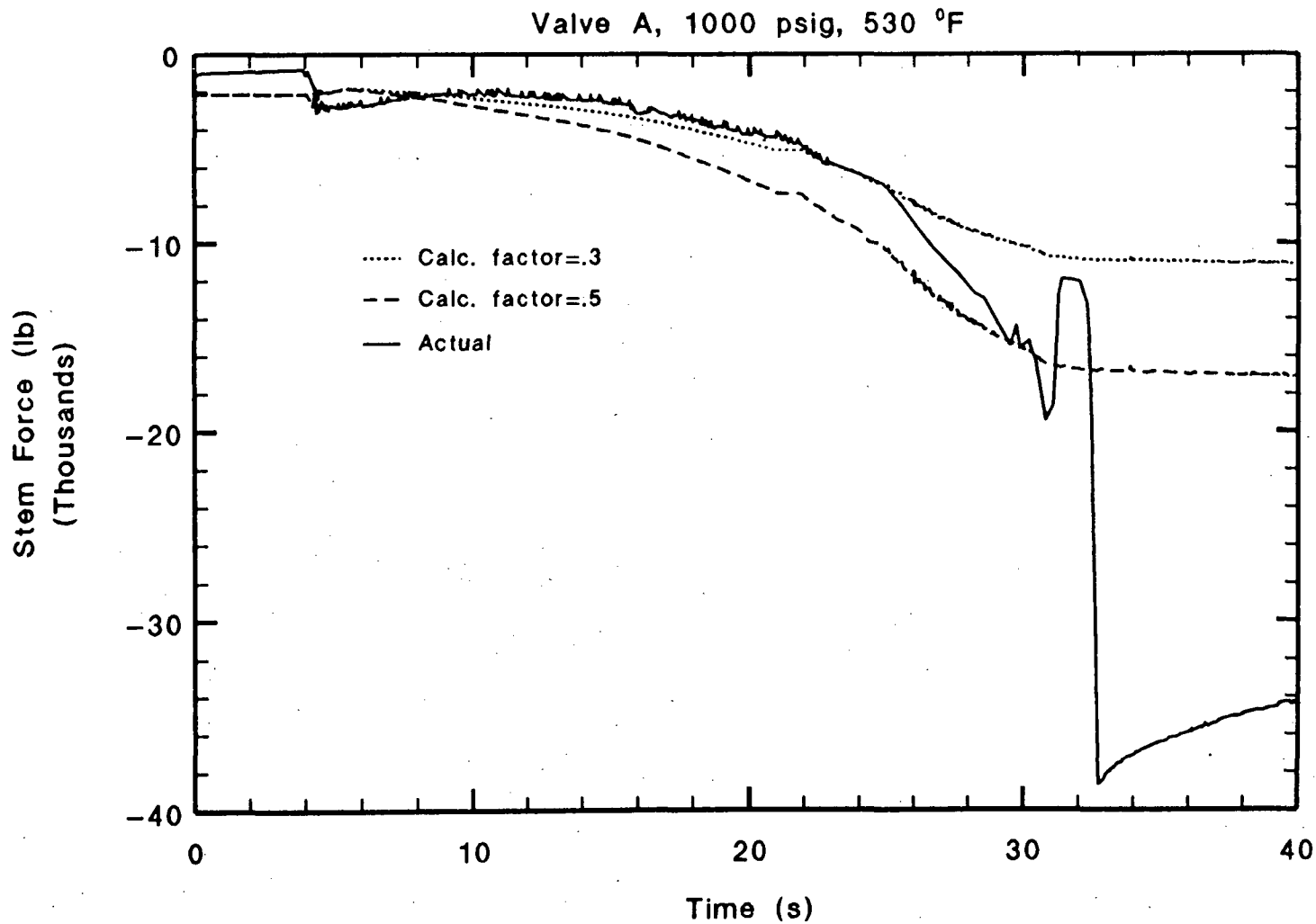


Figure 6. Linear curve fit using industry equation closely approximates Valve A running stem forces for closing without flow.



BMG00197

Figure 7. Calculations using 0.3 and 0.5 disc factors and removing typical conservatisms do not model test data for high-energy flow isolation.

The valve assembly was disassembled after testing to evaluate the condition of valve internals exposed to the high-flow testing. The disc (wedge) was removed and examined to determine how the blowdown forces had affected its condition. The disc was worn on the guides and sealing surfaces of the downstream face, indicating a cocking of the disc toward the downstream side. The upstream face was not damaged. An examination of the assembled position of the disc valve body revealed large clearances of about 1/4 inch between the disc and disc guide rails mounted to the valve body. This clearance plus the wear on the disc guides and guide rails allowed the disc to cock downstream far enough to come in contact with the seat ring during the last half of the closure stroke. This contact explains the wear pattern found on the disc face, and may also be the cause of the high closure forces noted just prior to flow isolation during the higher-energy blowdown tests (see Figure 3).

Judging by the wear patterns observed, it is unlikely that the valve could have produced a tight seal using the downstream face alone. A tight seal on the downstream face would have been required to isolate flow if the valve torqued out prior to full travel but with the disc on the seat. The valve, however, maintained a tight seal throughout testing, indicating a tight seal on the upstream face of the disc--a benefit of using an oversized operator with a higher-than-necessary torque switch setting.

Valve B: A torque switch setting of 1.75 was selected for the Valve B assembly to provide the needed closure thrust for the given test conditions. This setting, however, resulted in delivered stem thrust (as determined by the stem-mounted load cell) that was below the calculated magnitude. The torque switch setting was therefore raised to 2.0 prior to the first system blowdown test.

The valve performed satisfactorily during the testing except for the 1400 psig test, where the operator torqued out before the disc reached the fully closed position (1/4 inch travel remaining). Even during this test, however, the valve had closed far enough to produce a tight seal, with no leakage observed.

In accordance with manufacturer procedures, the valve thrust was predicted using actual orifice area for disc area, upstream pressure for  $P$  &  $\Delta P$ , a disc factor of 0.3, and a packing drag force of 5000 pounds (the maximum expected for this packing configuration). Based on the initial results of the Valve A tests, all of the blowdown tests with Valve B were conducted at near-saturation temperatures for the various pressures. Figure 8 shows a comparison between the test measurements and the thrust calculations for the Valve B tests. The estimated stem forces, shown as the solid line, provide reasonable predictions of actual forces for lower-pressure cases. Maximum flow isolation forces could not be measured for the 1400 psig test because the torque switch tripped prior to full closure. Figure 8 therefore shows the extrapolated stem force at 1300 psig (pressure at flow isolation) based on actual stem force characteristics prior to torque switch trip for two closure cycles. Here, as with Valve A, predicted stem forces are not conservative at higher pressures.

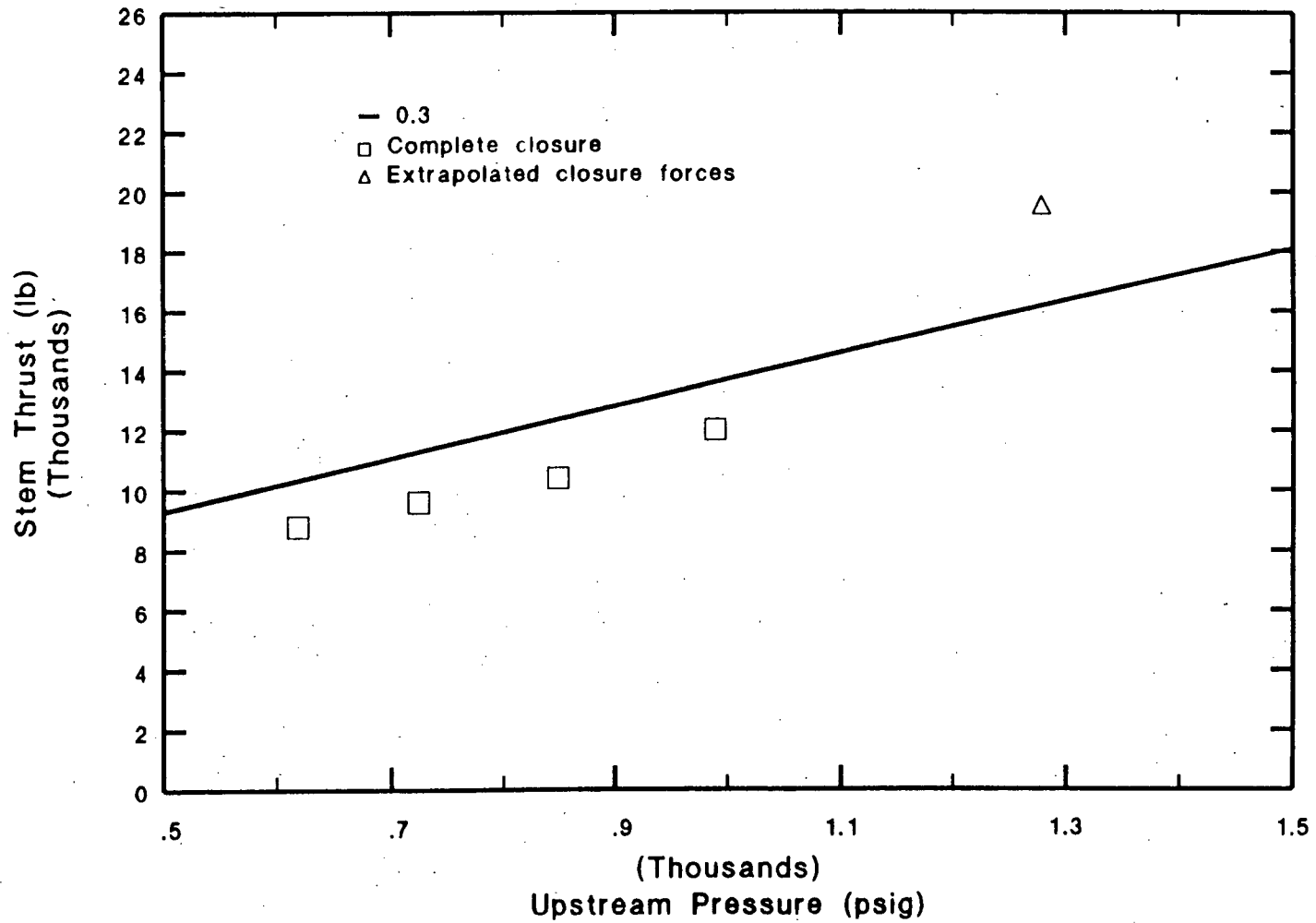


Figure 8. Valve B extrapolated stem forces exceeded those calculated for tests at high pressure and slightly subcooled conditions.

Figures 9 and 10 show the Valve B test data that are expected to apply to Equation (2). Here again, the data plotted are the stem forces measured at mid-stroke for tests at varying temperatures and pressures but without flow. The line fit through the data points has a slope equal to the stem cross-sectional area and provides an indication of the true packing load for both the opening and closing strokes. The increase in packing forces over those found for Valve A is believed to result from the different packing design and greater stem diameter of this valve.

The line fit through the data points for this valve shows a packing load of 1610 pounds opening and 1632 pounds closing. The force calculation for this case included a 5000-pound packing load, again providing conservatism. The difference between the opening and closing values is less than expected, given the weight of the disc and lower stem half (over 50 pounds). This may indicate a directional relationship for packing load, believed to be a characteristic of the packing type used and its orientation.

Based on the packing load and stem rejection load characteristics determined from the running load evaluation, an evaluation of the total force equation was conducted. Here again the conservatisms found in the application of the equation were eliminated by using measured parameters in the equation. For the Valve B assembly, stem force calculations under-predicted actual measurements. Figure 11 shows the maximum stem forces for closure during the blowdown testing at 1400 psig and 580°F. As with the previous valve, the calculated force bounds actual values during most of the closure cycle. As the valve isolates flow and differential pressure approaches full system pressure, the stem force exceeds that calculated.

No wear patterns were noted on the Valve B disc after testing. The inspection of the valve internals noted tight clearances in the disc guide/guide rail interface and machined, hard-faced disc guide surfaces.

Operator Torque Switch Trip Anomaly: During the blowdown testing of Valve A, there were three incidences of anomalous operator torque switch trip behavior. It is believed these incidences occurred in conjunction with installation and removal of the MOV diagnostic test equipment. The valve stem forces associated with torque switch trip were normal in the numerous tests performed with diagnostic devices installed. The anomaly appeared in the form of abnormally low valve torque-out stem forces during the tests immediately after removal of two types of diagnostic equipment. The investigation that followed the discovery of the low stem forces showed that incorrect installation of the motor operator spring pack lock ring was the problem. The removal of the diagnostic test equipment and the subsequent incorrect installation of the lock ring invalidated the findings of the diagnostic test. A recent problem investigation at Brunswick (LER 87-023-01)<sup>2</sup> has identified a similar lock ring installation problem and illustrates the potential for invalidated diagnostic testing elsewhere.

The point at which the torque switch contacts open is dependent only on the setting of the torque switch, rate of the torque spring, and spring pack

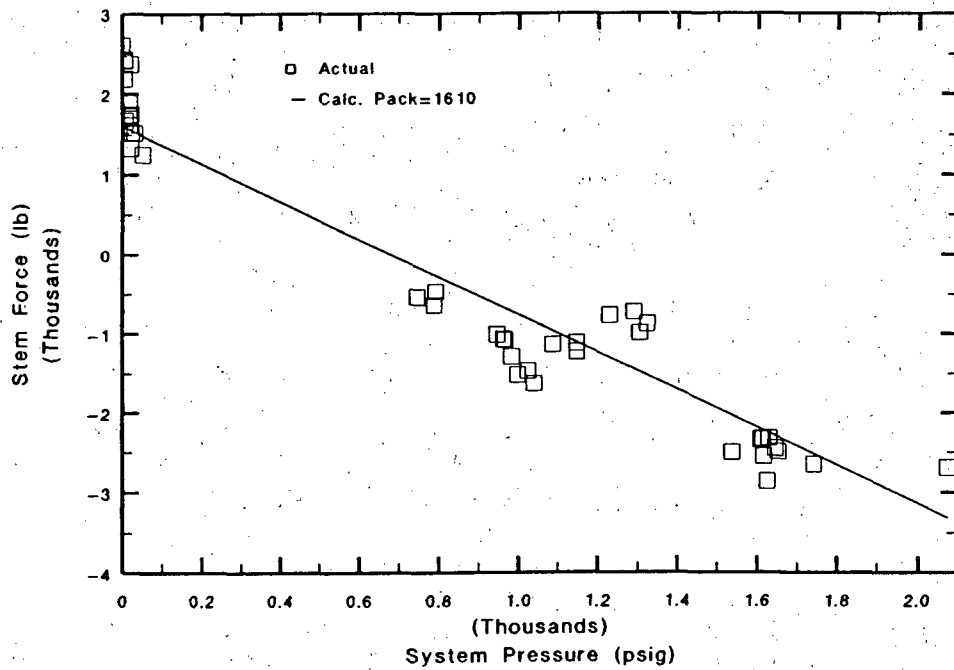


Figure 9. Linear curve fit using industry equation closely approximates Valve B running stem forces for opening without flow.

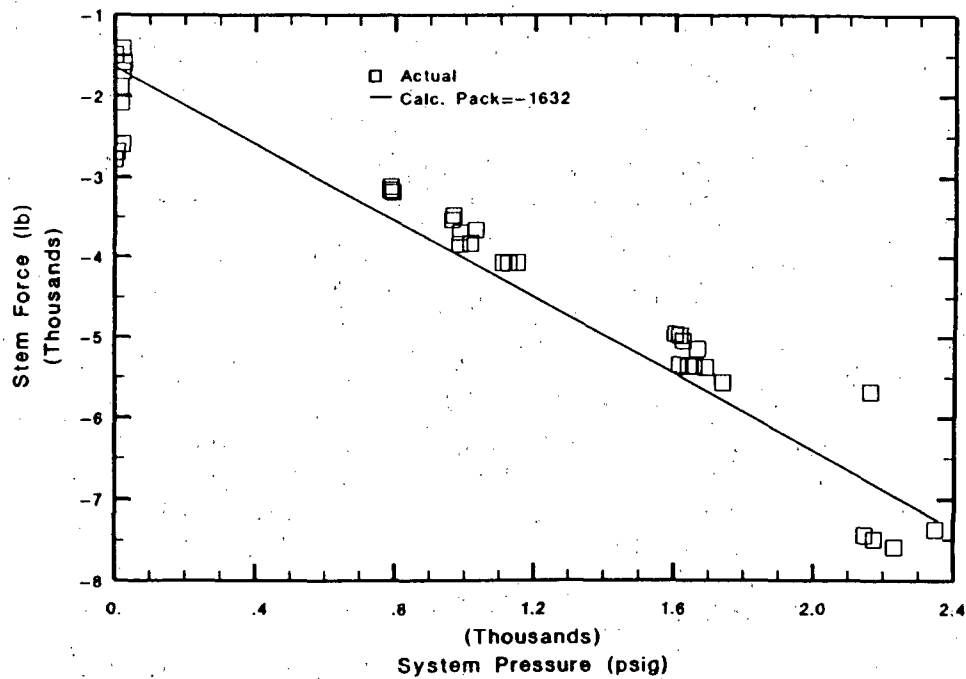


Figure 10. Linear curve fit using industry equation closely approximates Valve B running stem forces for closing without flow.

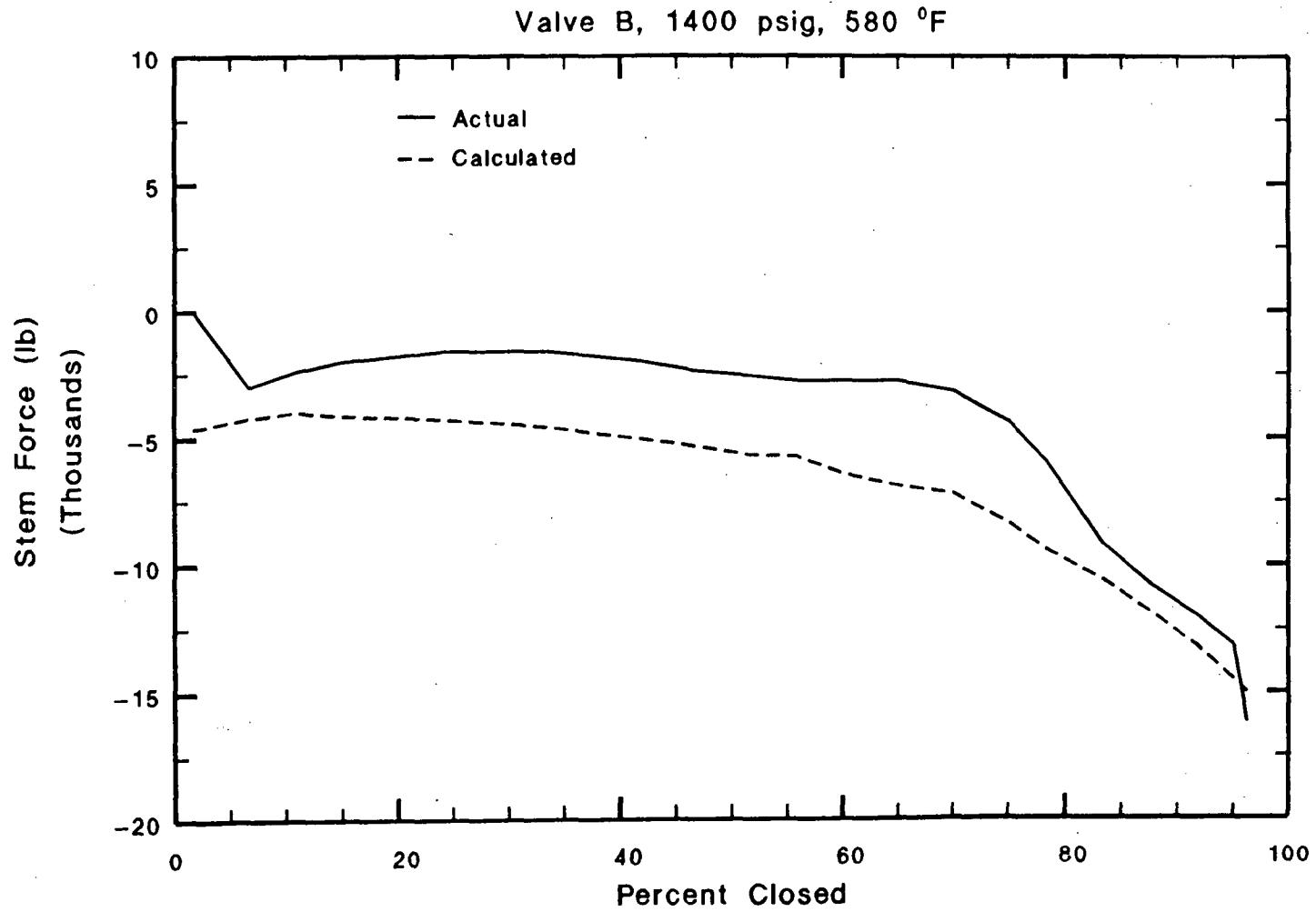


Figure 11. Calculations using 0.3 disc factor and removing typical conservatisms do not model final flow isolation forces.

preload and gap. No matter what causes the stem force to increase, whether flow loads, valve reaching full stroke, or even an obstacle in the disc path, the switch will always open when the torque spring compresses to the predetermined point. The force at torque switch trip was used to trace the function of the operator from one test to another through various diagnostic equipment installations and removals. Figure 12 shows the average stem compression at torque switch trip for each of the 11 tests performed on Valve A, arranged in chronological order. The force measurements were made using the INEL load cell installed as an integral part of the valve stem.

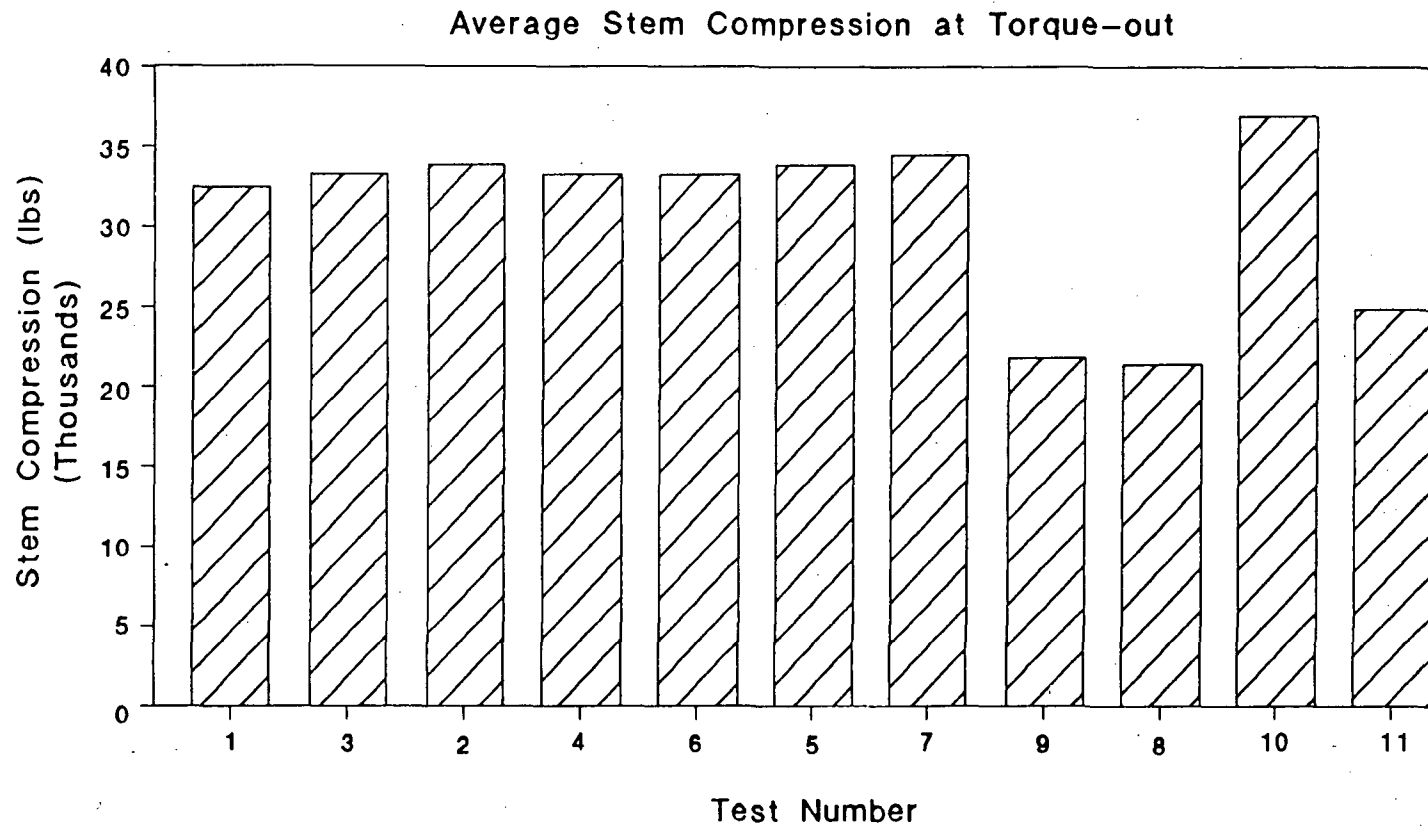
During tests 1 through 7 the valve operator functioned consistently, with a stem compression at torque switch trip of approximately 33,000 pounds. Tests 9 and 8, accomplished without operator diagnostic monitoring, showed consistent torque-out forces, but at a significantly reduced level. Here a drop of approximately 10,000 pounds appeared in the torque-out stem compression.

Two different sets of valve operator diagnostic equipment were installed to monitor test 10, and the valve stem torque-out compression returned to about the same level as tests 1 through 7 (re-lubrication of the valve stem threads increased loads slightly). The diagnostic equipment was removed after test 10, and the results of test 11 show a similar reduction in force, even after the torque switch setting was increased from 2.0 to 2.5.

After the completion of testing for Valve A, the Limitorque motor operator was removed and partially disassembled by Limitorque representatives with INEL personnel attending. The spring pack cover was removed and the internal configuration inspected. The lock ring that retains the torque spring and its locking set screw appeared to be properly installed. The set screw was removed and a special tool was used to attempt to further tighten the lock ring. The ring was tightened almost one full turn before it reached its proper position.

Limitorque design records were used to correlate the loosening of the lock ring to torque switch setting and torque-out thrust. One full turn of the lock ring is equivalent to 19 degrees rotation of the torque switch. One full torque switch setting is about 21 degrees. This loosening of the lock ring had the effect of backing off the torque switch from 2.0 (the actual setting) to 1.1 (the equivalent setting). From the torque spring curve the loss of thrust was estimated at 10,600 pounds, very close to the discrepancy in the measured data.

Improper positioning of the lock ring sometime after test 7 but before the next test would explain the reduction in stem force after test 7. How it happened is not completely understood. None of the diagnostic devices installed prior to test 9 require the removal or adjustment of the torque spring lock ring; in fact, several of the devices are designed to diagnose spring pack gap, the result of improper lock ring installation. Review of the data taken by the various diagnostic devices shows no indication of spring pack gap. Also, none of the devices are designed such that their installation would correct for this problem, with the exception of the Limitorque motor actuator characterizer (MAC) device.



BMG00179

Figure 12. Below-normal stem forces were observed for three test series with Valve A.

Installation of the MAC device requires the removal of the torque spring lock ring to facilitate the installation of its spring pack load cell device. According to the Limitorque technician, the position of the lock ring was marked prior to removal and the number of turns during removal was noted. The load cell device was installed and tightened to the proper position to provide the design spring preload. After testing, the load cell was removed and the lock ring installed the appropriate number of turns to the previously marked position. We believe this explains the similar reduction in stem force before and after test 10.

A correlated event was determined from a review of the Brunswick LER. In this case, the HPCI steam line isolation valve (a GI-87 valve) had successfully undergone several diagnostic tests using the MAC system. Later, the valve motor failed on opening for an unrelated reason. During the subsequent motor operator check, greatly reduced torque-out forces were observed. Investigating personnel discovered that a burr on the threads of the spring pack housing cover had prevented the lock ring from being fully installed after diagnostic testing and had caused the lower-than-expected torque readings.

Both instances of improper lock ring positioning could have been easily diagnosed. A simple measurement of the lock ring position can be compared with both the position of torque spring transducer during testing and the manufacturer design position in order to validate post-test valve operation. Apparently this procedure was not completed for the above-described tests.

### Conclusions

The design basis hot water blowdown testing has shown that, given enough thrust, typical gate valves will close against the high flow resulting from a line break. Proper operator sizing depends on correct identification of the values for the sizing equation. Evidence exists that values used in the past may not be conservative for all valve applications. The following items need to be considered during sizing of gate valve operators.

1. Gate valve internal and friction-bearing surface design can have a significant effect on the operator force requirements for pipe break flow isolation.
2. The degree of subcooling at the valve inlet can greatly influence valve closure forces. Valve operator force requirements increase as inlet fluid conditions approach saturation temperatures.
3. Industry trends toward using 100 percent system pressure for all pressure terms in the sizing calculation are justified for high-flow applications.

Improper operator lock ring installation following test or maintenance can invalidate in-situ test results and render the valve unable to perform its design function. This is important in light of the present trend by

utilities to perform diagnostic testing of safety-related valve assemblies to answer regulatory concerns such as IE Bulletin 85-03. A final quality check following diagnostic testing and maintenance must be made to ensure correct lock ring installation.

#### References

1. ANSI B16.41, Functional Qualification Requirements for Power Operated Active Valve Assemblies for Nuclear Power Plants, 1983.
2. Brunswick Steam Electric Plant Unit 1, Inoperability of High Pressure Injection (HPCI) System (E41) Due to Failure of HPCI Turbine Steam Inlet Isolation Valve E41-F001, LER 87-023-01, June 27, 1988.



# Environmentally Assisted Cracking in Light Water Reactors

W. J. Shack, T. F. Kassner, P. S. Maiya, J. Y. Park, and W. E. Ruther

Materials and Components Technology Division  
Argonne National Laboratory  
Argonne, Illinois 60439

## Abstract

Research during the past year focused on (1) stress corrosion cracking (SCC) of austenitic stainless steels (SS), (2) fatigue of Type 316NG SS, and (3) SCC of ferritic steels used in reactor piping, pressure vessels, and steam generators. Stress corrosion cracking studies on austenitic SS explored the critical strains required for crack initiation, the effects of crevice conditions on SCC susceptibility, heat-to-heat variations in SCC susceptibility of Type 316NG and modified Type 347 SS, the effect of heat treatment on the susceptibility of Type 347 SS, threshold stress intensity values for crack growth in Type 316NG SS, and the effects of cuprous ion and several organic salts on the SCC of sensitized Type 304 SS. Crevice conditions were observed to strongly promote SCC. Significant heat-to-heat variations were observed in SCC susceptibility of Types 316NG and 347 SS. No correlation was found between SCC behavior and minor variations in chemical composition. A significant effect of heat treatment was observed in Type 347 SS. A heat that was extremely resistant to SCC after heat treatment at 650°C for 24 h was susceptible to transgranular stress corrosion cracking (TGSCC) in the solution-annealed condition. Although there was no sensitization in either condition, the presence or absence of precipitates and differences in precipitate morphology appear to influence the SCC behavior. In fracture-mechanics crack-growth-rate tests on Type 316NG SS, steady-state crack growth under high R loading was observed only at stress intensity values greater than  $\sim 22 \text{ MPa}\cdot\text{m}^{1/2}$ . Cuprous ion additions were shown to be very deleterious at and above  $\sim 1 \text{ ppm}$  at 289°C; however, below  $\sim 200^\circ\text{C}$ , SCC occurred at much lower concentrations ( $\sim 0.03 \text{ ppm}$ ). SCC susceptibility tests were performed at 289°C in water containing ethylenediamine-tetraacetate (EDTA) salts at low concentrations. Transgranular SCC was observed but the crack growth rates were very low, primarily because these substances reduce the dissolved oxygen concentration in the water. None of these impurities appears to be deleterious. In-air fatigue data on Type 316NG SS at  $\sim 22$ ,  $\sim 288$ , and  $320^\circ\text{C}$  were in good agreement with the ASME mean data curve for fairly short lives corresponding to plastic strain ranges of greater than 0.5%, but fell below the mean data curve at longer lives. A small ( $\sim 20\%$ ) but consistent decrease in fatigue life was evident when the test temperature was increased from room temperature to temperatures more typical of operating reactors. Constant-extension-rate tests on a variety of ferritic steels used in piping, pressure vessels, and steam generators showed a strong correlation between the sulfur content and sulfide distribution of the steels and susceptibility to SCC.

The submitted manuscript has been authored by a contractor of the U. S. Government under contract No. W-31-109-ENG-38. Accordingly, the U. S. Government retains a nonexclusive, royalty-free license to publish or reproduce the published form of this contribution, or allow others to do so, for U. S. Government purposes.

## 1 Introduction

---

Piping in light-water-reactor (LWR) power systems has been affected by several types of environmental degradation. Intergranular stress corrosion cracking (IGSCC) of austenitic stainless steel (SS) piping in boiling-water reactors (BWRs) has required research, inspection, and mitigation programs that will ultimately cost several billion dollars. As extended lifetimes are envisaged, other potential environmental degradation problems such as corrosion fatigue must be considered. During this year the program has been primarily directed at the problems associated with SCC of austenitic SSs, although work has also been performed on SCC of ferritic steels and fatigue of Type 316NG SS.

## 2 Summary of Research Progress

---

### 2.1 Stress Corrosion Cracking of Austenitic Stainless Steels

#### Critical Strain for Initiation of Stress Corrosion Cracking

Most investigations of the SCC susceptibility of BWR piping materials involve fracture-mechanics and constant-extension-rate (CERT) tests. These tests are primarily measures of crack propagation rather than crack initiation. Although crack initiation, the precursor to crack growth, is of critical importance, it is difficult to define and study experimentally. The present studies have focused on the determination of the strains required to produce measurable cracks in CERT tests.

Interrupted CERT tests have been used in previous studies to estimate the strains required to initiate cracks [1, 2]. However, the procedures required that initiation be defined by either large, easily observed cracks or extensive examination of specimens by scanning electron microscopy (SEM). A modified CERT specimen geometry was developed in which the strain in the specimen was localized, and hence, the region in which crack initiation was likely to occur was greatly reduced in size. A small-diameter (1.0 mm) through-hole was drilled in the center of the gage length (Fig. 1). The tests were interrupted at relatively low plastic strains and then the specimens were cross sectioned by electrical discharge machining (EDM), as shown in Fig. 2, so that the entire region of crack initiation could be examined relatively easily by SEM at magnifications of 1000X or more. This approach provided a convenient technique for identifying crack initiation, i.e., detecting cracks less than 10–20  $\mu\text{m}$  in length.

Since strains are not directly measured in CERT tests, the tests were either interrupted at a predetermined time, which corresponded to the desired nominal strain for the strain rate imposed on the specimen, or at a predetermined stress that was calculated from the desired nominal strain through the stress-strain law. Preliminary experiments indicated that it was more reliable to interrupt the test at the predetermined stress than at the predetermined time. The actual nominal plastic strain was determined *a posteriori* by measuring the change in length between two marks placed at the ends of the gage section. The local strain ( $\epsilon_{loc}$ ) was then determined by multiplying the nominal strain ( $\epsilon_{nom}$ ) by a strain concentration factor. Both elastic-plastic finite-element calculations [3] and Neuber's rule [4] suggest that the strain concentration factor is  $\approx 8$ , and this value was used in the analysis of the results.

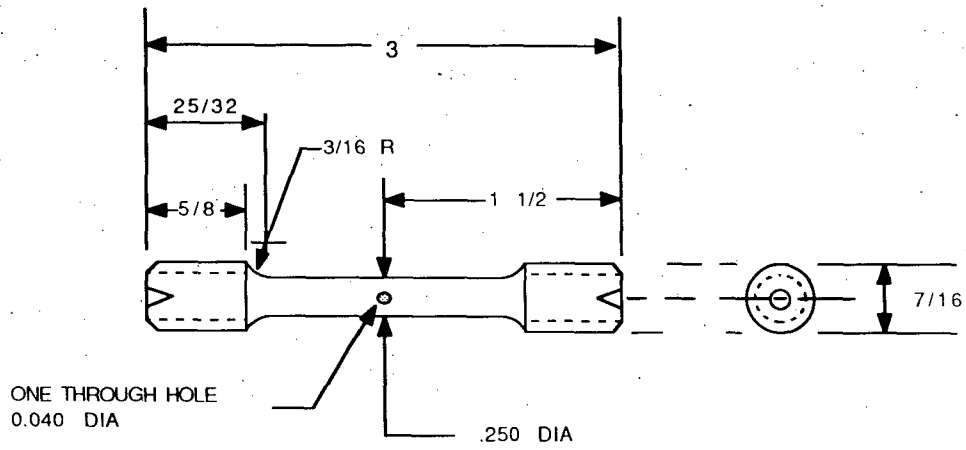


Figure 1. Geometry of CERT Specimen Used for Crack Initiation Studies. Dimensions in inches.

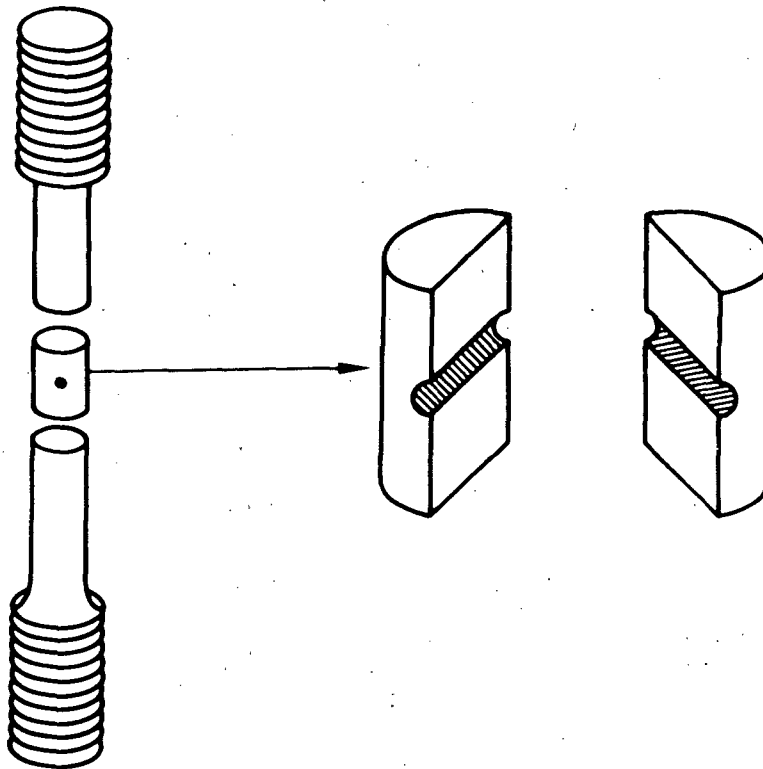


Figure 2. Cross-Sectioning Scheme for CERT Specimen Shown in Fig. 1.

The plastic strains required to initiate cracks in a simulated BWR environment were determined for a Type 316NG SS (Ht P91576) and two heats of Type 304 SS (Hts 53319 and 30956). The composition of these materials is given in Table 1. The heat treatments for the different stainless steels, the degree of sensitization determined by the electrochemical-potentiokinetic-reativation (EPR) technique, and the CERT test parameters and results are summarized in Table 2. The heat treatments did not sensitize Type 316NG SS. Scanning electron microscopy (SEM) photographs of the regions of strain concentration are shown in Figs. 3-5. Crack initiation occurs at local strains of approximately 2.0%, 3.0%, and 4.0% for Types 304 (sensitized), 316NG, and 304 (solution annealed) SS, respectively. Initiation of SCC occurs at relatively low plastic strains for all the materials, although Type 316NG and solution-annealed Type 304 SS tend to be slightly more resistant. The Type 316NG and solution-annealed Type 304 SS exhibited transgranular stress corrosion cracking (TGSCC); the sensitized material exhibited intergranular SCC (IGSCC).

Table 1. Chemical Composition (wt.%) of Test Alloys

| Element | 316NG<br>(P91576) <sup>a</sup> | 304<br>(53319) | 304<br>(30956) | 316NG<br>(467958) | 316NG<br>(NDE-28) |
|---------|--------------------------------|----------------|----------------|-------------------|-------------------|
| C       | 0.015                          | 0.06           | 0.06           | 0.02              | 0.014             |
| Mn      | 1.63                           | 1.69           | 1.54           | 1.53              | 1.77              |
| P       | 0.02                           | 0.024          | 0.019          | 0.023             | 0.02              |
| S       | 0.01                           | 0.013          | 0.007          | 0.008             | 0.002             |
| Si      | 0.42                           | 0.59           | 0.48           | 0.65              | 0.52              |
| Ni      | 10.95                          | 8.88           | 8.0            | 12.60             | 13.58             |
| Cr      | 16.42                          | 18.33          | 18.99          | 17.29             | 17.79             |
| Mo      | 2.14                           | 0.14           | 0.44           | 2.51              | 2.59              |
| Cu      | -                              | 0.06           | 0.19           | 0.16              | 0.11              |
| N       | 0.068                          | 0.029          | 0.1            | 0.0682            | 0.11              |
| B       | 0.002                          | 0.0005         | -              | 0.002             | 0.0006            |
| Fe      | Balance                        | Balance        | Balance        | Balance           | Balance           |

<sup>a</sup>Heat or identification numbers are indicated in parentheses.

The effect of dissolved-oxygen level and the corresponding changes in electrochemical potential (ECP) on crack initiation was also studied. Tests were performed on solution-annealed Type 304 SS in water containing 0.005-0.25 ppm dissolved oxygen and 0.1 ppm sulfate, with corresponding ECPs ranging from 100 to -560 mV (SHE). Figure 6 shows the cracking observed in solution-annealed Type 304 SS at several different combinations of ECP and local plastic strain. Even at potentials below -400 mV (SHE), SCC occurred at strains of ~4%, i.e., about the same level as in the tests at ~100 mV (SHE).

#### Effect of Crevices on Stress Corrosion Cracking Susceptibility

A specimen geometry similar to that used for the initiation studies was used to study the effects of crevices on SCC. In this case, two holes, which penetrated only halfway through the specimen, were drilled in the gage length, and Type 304 SS pins (0.84 mm in dia) were inserted in the holes. A schematic representation of the specimen is shown in Fig. 7. The tests were continued to failure, and the fracture always occurred at one of the drilled holes. The fracture surface was examined by SEM to determine the length of the largest crack and whether the failure occurred by SCC. Average crack growth rates were estimated from the measurements of maximum crack length.

Table 2. Crack Initiation Observations on Types 316NG and 304 SS in Interrupted CERT Tests after Various Strains at 289°C.  $\dot{\epsilon} = 2 \times 10^{-7} \text{ s}^{-1}$ . Environment: 0.25 ppm O<sub>2</sub> + 0.1 ppm SO<sub>4</sub>

| Material                                                | Specimen Number <sup>a</sup> | EPR, C/cm <sup>2</sup> | ECP, <sup>b</sup> mV(SHE) | $\sigma_{nom}$ , MPa | $\epsilon_{nom}$ , % | $\epsilon_{loc}$ , <sup>c</sup> % | SCC <sup>d</sup> |
|---------------------------------------------------------|------------------------------|------------------------|---------------------------|----------------------|----------------------|-----------------------------------|------------------|
| <i>Type 316NG SS, 1050°C/0.5h + 650°C/24h</i>           |                              |                        |                           |                      |                      |                                   |                  |
| 316NG                                                   | PM9-54                       | 0                      | 78                        | 229                  | 6.04                 | 48.3                              | Yes              |
| 316NG                                                   | PM9-58                       | 0                      | 111                       | 147                  | 1.43                 | 11.4                              | Yes              |
| 316NG                                                   | PM9-59                       | 0                      | 27                        | 144                  | 1.36                 | 10.9                              | Yes              |
| 316NG                                                   | PM9-52                       | 0                      | 24                        | 125                  | 0.59                 | 4.7                               | Yes              |
| 316NG                                                   | PM9-53                       | 0                      | 12                        | 124                  | 0.38                 | 3.0                               | Yes              |
| 316NG                                                   | PM9-50                       | 0                      | 45                        | 107                  | 0.22                 | 1.8                               | No               |
| <i>Type 304 SS, 1050°C/0.5h</i>                         |                              |                        |                           |                      |                      |                                   |                  |
| 304                                                     | 5-57                         | 0                      | 94                        | 244                  | 5.79                 | 46.3                              | Yes              |
| 304                                                     | 5-85                         | 0                      | 31                        | 171                  | 1.60                 | 12.8                              | Yes              |
| 304                                                     | 5-82                         | 0                      | 109                       | 144                  | 1.00                 | 8.0                               | Yes              |
| 304                                                     | 315                          | 0                      | 49                        | 118                  | 0.57                 | 4.6                               | Yes              |
| 304                                                     | 5-83                         | 0                      | 62                        | 102                  | 0.38                 | 3.0                               | No               |
| <i>Type 304 SS, 1050°C/0.5h + 600°C/24h<sup>e</sup></i> |                              |                        |                           |                      |                      |                                   |                  |
| 304                                                     | 5-34                         | 24                     | 94                        | 225                  | 5.80                 | 46.3                              | Yes              |
| 304                                                     | 5-71                         | 24                     | 70                        | 144                  | 1.40                 | 11.2                              | Yes              |
| 304                                                     | 311                          | 2                      | 120                       | 128                  | 0.29                 | 2.3                               | Yes              |
| 304                                                     | 5-70                         | 24                     | 83                        | 102                  | 0.19                 | 1.5                               | No               |

<sup>a</sup> PM9-XX: HT P91576  
 5-XX: HT 53319  
 3-XX: HT 30956

<sup>b</sup> Electrochemical potential.

<sup>c</sup> Based on an estimated strain concentration factor of 8.

<sup>d</sup> Stress corrosion crack initiation detected at 1000X magnification.

<sup>e</sup> Except Specimen 311, 1050°C/0.5h + 700°C/0.25h + 500°C/24h.

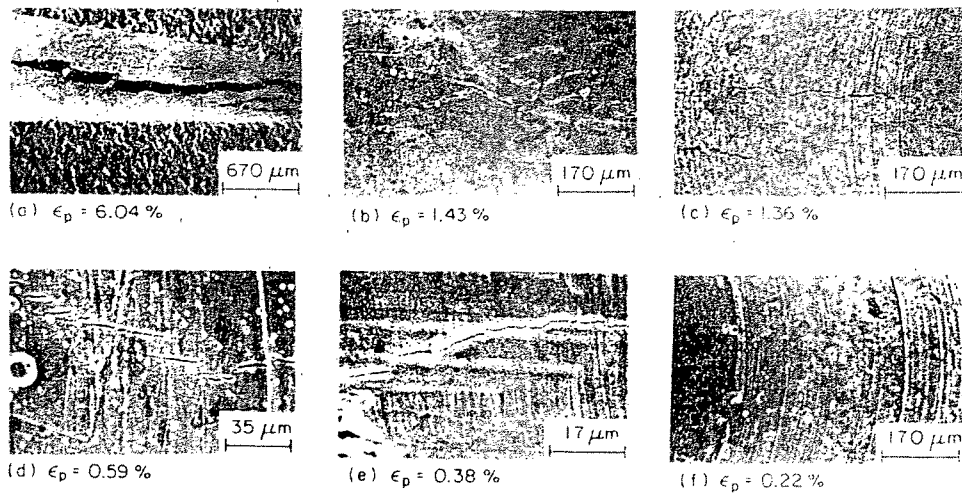


Figure 3. SEM Photomicrographs of the Hole Regions of CERT Specimens of Type 316NG SS Subjected to Crack Initiation Tests. Nominal plastic strains in the specimen are indicated; localized strain in the hole region is higher by a factor of ~8.

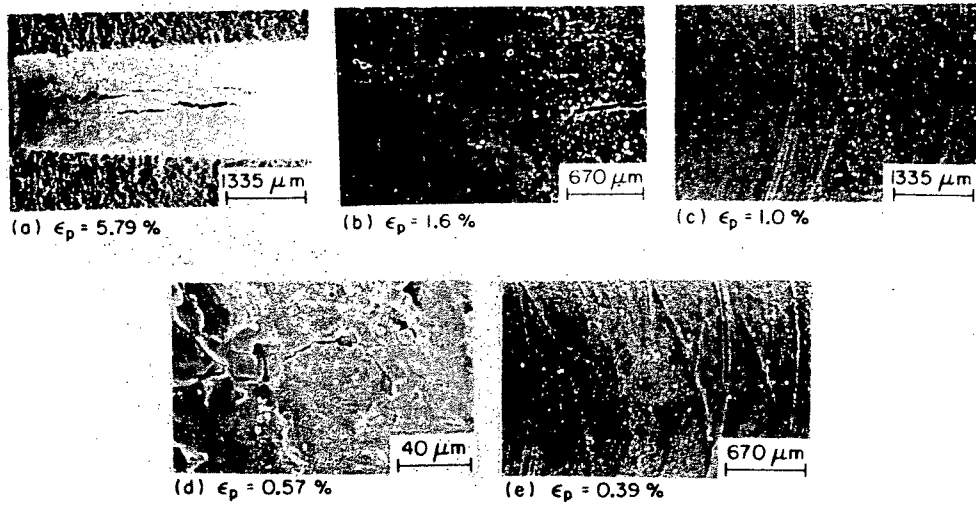


Figure 4. SEM Photomicrographs of the Hole Regions of CERT Specimens of solution-annealed Type 304 SS Subjected to Crack Initiation Tests. Nominal plastic strains in the specimen are indicated; localized strain in the hole region is higher by a factor of ~8.

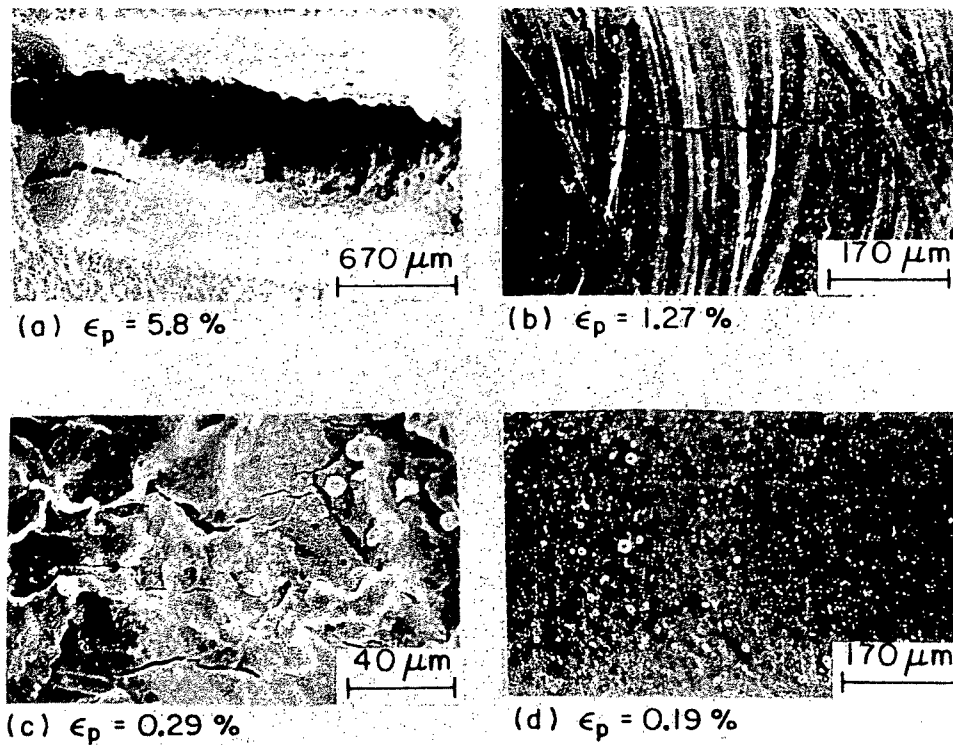


Figure 5. SEM Photomicrographs of the Hole Regions of CERT Specimens of sensitized Type 304 SS Subjected to Crack Initiation Tests. Nominal plastic strains in the specimen are indicated; localized strain in the hole region is higher by a factor of ~8.

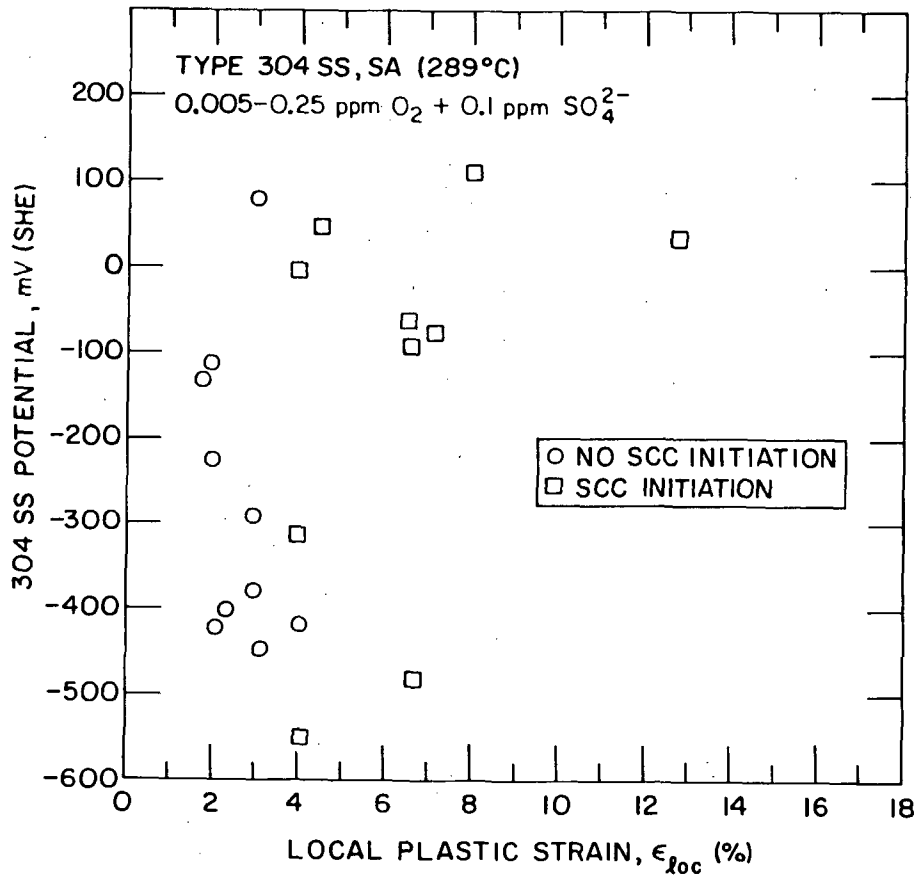


Figure 6. Effect of Open-Circuit ECP on Crack Initiation in Solution-Annealed Type 304 SS.

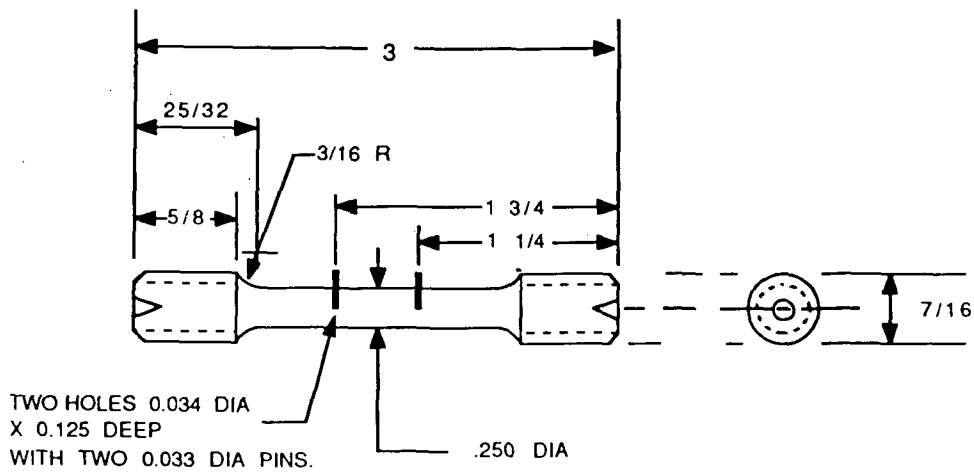


Figure 7. Geometry of CERT Specimen Used in Crevice SCC Studies, with SS Pins Inserted in Two Holes Drilled Half Through. Dimensions in inches.

Two heats of Types 316NG SS (Hts P91576 and 467958) and one heat of Type 304 SS (Ht 53319) were studied. Type 304 SS was tested in both the sensitized and nonsensitized conditions. The heat treatments were similar to those used for the crack initiation studies (see Table 2) and produced no measurable sensitization in the Type 316NG SS. The results of the tests on the crevice specimens are summarized in Table 3 along with corresponding results obtained from standard, smooth CERT specimens without the drilled holes.

Types 316NG and 304 SS are very sensitive to SCC under crevice conditions. SEM photomicrographs of the fracture surfaces and the corresponding cross sections through the other hole in the specimens of Type 316NG SS (Ht P91576) are shown in Fig. 8. Comparison tests were performed with and without the pins. Without the pins (Fig. 8a), the specimens failed in a completely ductile fashion in high-purity water. Standard CERT specimens from this heat also failed in a completely ductile manner in high-purity water. With the pins in place, SCC occurred both in high-purity water (Fig. 8b) and in sulfate environments (Fig. 8c). The presence of sulfate increased the average crack growth rate by nearly a factor of 4 (see Table 3, lines 3 and 5). Under non-crevice conditions, Ht 467958 of Type 316NG SS was resistant to TGSCC not only in high-purity water containing 0.2 ppm dissolved oxygen, but also in impurity environments, even at very slow strain rates (Table 4). However, under crevice conditions, even Ht 467958 exhibited TGSCC, as is illustrated in Fig. 9.

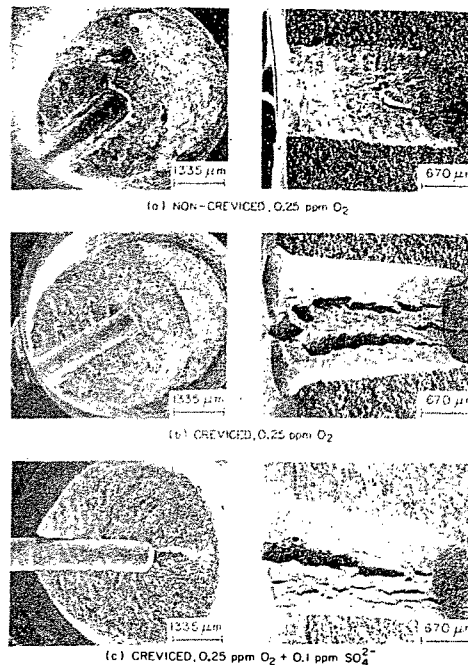


Figure 8. SEM Photomicrographs of the Hole Regions and of Type 316NG SS Specimens (Ht P91486) with and without Crevices, Tested in 289°C Water at a Strain Rate of  $2 \times 10^{-7} \text{ s}^{-1}$ . In each case, the photomicrograph on the left side shows the fracture surface at one hole and the photomicrograph on the right shows the cross section of the other hole in the specimen.

Table 3. CERT Test Results Obtained under Noncrevice and Crevice Conditions.  $\dot{\epsilon} = 2 \times 10^{-7} \text{ s}^{-1}$ ;  $T = 289^\circ\text{C}$

| Material <sup>a</sup> | Heat No. | Condition           | Environment, ppm                                        | $t_f$ , h | $\sigma_{max}$ , MPa | $\epsilon_t$ , % | $\epsilon_u$ , % | $\Delta A/A_0$ , % | Failure Mode | $\dot{a}_{av}$ , $\text{m} \cdot \text{s}^{-1}$ | ECP, mV(SHE) |
|-----------------------|----------|---------------------|---------------------------------------------------------|-----------|----------------------|------------------|------------------|--------------------|--------------|-------------------------------------------------|--------------|
| 316NG                 | P91576   | Smooth, Noncrevice  | 0.25 O <sub>2</sub>                                     | 492.6     | 460                  | 35.5             | 30.5             | 68                 | Ductile      | 0                                               | 15           |
| 316NG                 | P91576   | Hole, Noncrevice    | 0.28 O <sub>2</sub>                                     | 382.5     | 410                  | 27.5             | 23.4             | 44                 | Ductile      | 0                                               | -12          |
| 316NG                 | P91576   | Hole + Pin, Crevice | 0.24 O <sub>2</sub>                                     | 266.5     | 533                  | 19.2             | 16.3             | 53                 | TGSCC        | $6.84 \times 10^{-10}$                          | -17          |
| 316NG                 | P91576   | Smooth, Noncrevice  | 0.25 O <sub>2</sub> + 0.1 SO <sub>4</sub> <sup>2-</sup> | 474.0     | 461                  | 34.1             | 29.8             | 44                 | TGSCC        | $7.35 \times 10^{-10}$                          | 2            |
| 316NG                 | P91576   | Hole + Pin, Crevice | 0.25 O <sub>2</sub> + 0.1 SO <sub>4</sub> <sup>2-</sup> | 202.5     | 314                  | 14.6             | 12.9             | 43                 | TGSCC        | $3.06 \times 10^{-9}$                           | 21           |
| 316NG                 | 467958   | Smooth, Noncrevice  | 0.25 O <sub>2</sub>                                     | 638.0     | 510                  | 45.9             | 40.3             | 74                 | Ductile      | 0                                               | 25           |
| 316NG                 | 467958   | Hole + Pin, Crevice | 0.25 O <sub>2</sub>                                     | 240.8     | 384                  | 17.3             | 13.4             | 55                 | TGSCC        | $1.20 \times 10^{-9}$                           | 34           |
| 304 <sup>b</sup>      | 53319    | Smooth, Noncrevice  | 0.25 O <sub>2</sub>                                     | 600.0     | 500                  | 43.2             | 36.0             | 69                 | Ductile      | 0                                               | 15           |
| 304 <sup>c</sup>      | 53319    | Hole + Pin, Crevice | 0.26 O <sub>2</sub>                                     | 200.0     | 324                  | 14.4             | 11.7             | 49                 | TGSCC        | $1.39 \times 10^{-9}$                           | 51           |
| 304 <sup>c</sup>      | 53319    | Smooth, Noncrevice  | 0.25 O <sub>2</sub>                                     | 260.7     | 415                  | 18.8             | 16.5             | 31                 | IGSCC        | $2.18 \times 10^{-9}$                           | 38           |
| 304 <sup>c</sup>      | 53319    | Hole + Pin, Crevice | 0.25 O <sub>2</sub>                                     | 193.7     | 330                  | 13.9             | 12.2             | 45                 | IGSCC        | $3.04 \times 10^{-9}$                           | 12           |

<sup>a</sup>All 316NG specimens were solution-annealed for 0.5 h at 1050°C and heat-treated for 24 h at 650°C.

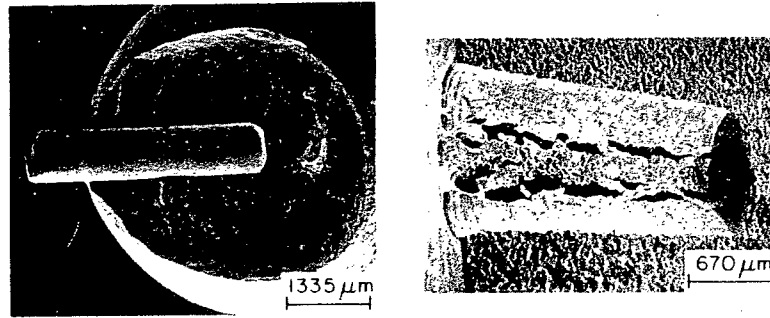
<sup>b</sup>Solution annealed for 0.5 h at 1050°C.

<sup>c</sup>Solution annealed for 0.5 h at 1050°C and sensitized for 24 h at 600°C, resulting in an EPR value of 24 C/cm<sup>2</sup>.

Table 4. Effects of Environment and Strain Rate on the SCC Susceptibility of Type 316NG SS (Ht 467958) at 289°C

| Test No.         | Oxygen, ppm | Sulfate, ppm | Chloride, ppm | Conductivity, $\mu\text{S}/\text{cm}$ | $\dot{\epsilon}$ , $\text{s}^{-1}$ | $t_f$ , h | $\epsilon_f$ , % | $\epsilon_u$ , % | $\Delta A/A_0$ , % | $\sigma_{max}$ , MPa | Failure Mode |
|------------------|-------------|--------------|---------------|---------------------------------------|------------------------------------|-----------|------------------|------------------|--------------------|----------------------|--------------|
| 189              | 0.2         | -            | -             | <0.1                                  | $1 \times 10^{-7}$                 | 1276.2    | 45.9             | 40.3             | 74                 | 485                  | Ductile      |
| 303              | 0.2         | 0.1          | -             | 0.9                                   | $1 \times 10^{-5}$                 | 10.7      | 38.4             | 32.8             | 75                 | 466                  | Ductile      |
| 158              | 0.2         | 0.1          | -             | 0.9                                   | $2 \times 10^{-6}$                 | 62.5      | 45.0             | 38.7             | 74                 | 485                  | Ductile      |
| 192              | 0.2         | 0.1          | -             | 0.9                                   | $4 \times 10^{-7}$                 | 291.4     | 42.0             | 32.0             | 75                 | 491                  | Ductile      |
| 193              | 0.2         | 0.1          | -             | 0.9                                   | $2 \times 10^{-7}$                 | 577.3     | 41.6             | 34.4             | 74                 | 501                  | Ductile      |
| 146              | 8           | 0.1          | -             | 0.9                                   | $1 \times 10^{-6}$                 | 129.7     | 46.7             | 39.3             | 75                 | 494                  | Ductile      |
| 138 <sup>a</sup> | 8           | -            | 0.5           | 5.7                                   | $2 \times 10^{-6}$                 | 53.0      | 38.2             | 36.4             | 71                 | 495                  | Ductile      |
| 137              | 8           | -            | 0.5           | 5.7                                   | $2 \times 10^{-6}$                 | 63.0      | 45.4             | 37.1             | 73                 | 499                  | Ductile      |

<sup>a</sup>This specimen was tested after a heat treatment of 1050°C/0.5 h.



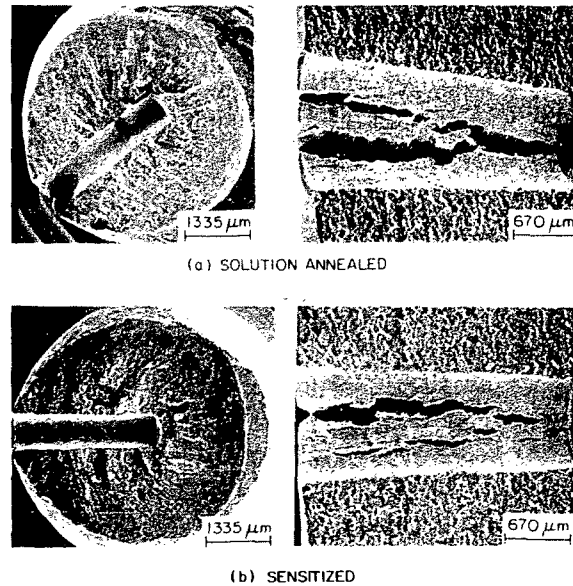
CREVICED SCC IN TYPE 316NG SS (HT 467958)  
 1050°C / 1/2 h + 650°C/24 h  
 $\dot{\epsilon} = 2 \times 10^{-7} \text{ s}^{-1}$   
 0.25 ppm O<sub>2</sub>

Figure 9. SEM Photomicrograph of the Hole Region of a Type 316NG SS Specimen (Ht 467958) with a Crevice.

Similarly, smooth specimens of solution-annealed Type 304 SS exhibited ductile failure, but the same material cracked transgranularly under crevice conditions (Fig. 10a) with an average crack growth rate of  $1.39 \times 10^{-9} \text{ m}\cdot\text{s}^{-1}$  (Table 3). Unlike the solution-annealed Type 304 SS, sensitized Type 304 SS failed by IGSCC even under non-crevice conditions in high-purity water, but the presence of an artificial crevice (Fig. 10b) slightly aggravated IGSCC, as indicated by the enhanced crack growth rates (see last two lines of Table 3).

The test results clearly demonstrate that SCC can occur under crevice conditions in environments where no SCC was observed under non-crevice conditions. Since the electrochemical conditions at the tip of a stress corrosion crack may be similar to those in a crevice of the same composition, these results may explain why some fracture-mechanics tests show crack propagation for materials and environmental conditions under which no cracking was observed in CERT tests on a smooth specimen [4].

Crevice bent-beam SCC tests were performed on two heats of Type 316NG SS (Ht P91576 plate and Ht NDE-28 pipe) in high-purity water with 0.2–0.3 ppm dissolved oxygen at 289°C. The plate specimens were shot peened to three different levels, representing different degrees of surface cold work. Some of the specimens were furnace heat treated for 24 h at 500 or 600°C after the shot peening. The specimens from the pipe were fabricated from the inside diameter near the weld heat-affected zone. The specimens and specimen holders were designed to provide a 0 to 0.25-mm crevice and 15% total strain. The specimens were tested for ~5000 h. Transgranular cracking was observed in one specimen from Ht P91576. Intergranular and transgranular cracking was observed in one specimen from Ht NDE-28. In this case the crack actually propagated through the thickness of the specimen. It is possible that this particular crack may have initiated from a weld defect. Additional tests are planned to better assess the actual potential for cracking induced by cold work.



CREVICED SCC IN TYPE 304 SS (289°C)  
 $\dot{\epsilon} = 2 \times 10^{-7} \text{ s}^{-1}$   
 0.25 ppm  $\text{O}_2$

Figure 10. SEM Photomicrograph of the Hole Region of Sensitized and Solution-annealed Type 304 SS Specimens with a Crevice.

#### Heat-To-Heat Variations in Susceptibility of Types 316NG and 347 SS to Stress Corrosion Cracking

CERT results for Type 316NG SS revealed significant heat-to-heat variations in susceptibility to SCC. Typical results are shown in Table 5. Susceptibility to TGSCC in chloride solutions depends on the concentration of Ni, Si, Be, and Cu [5,6]. However, no simple correlation was found between resistance to crack growth and minor variations in chemical composition among these heats. The heats were also analyzed to determine whether the origin of heat-to-heat variations can be attributed to the presence of trace elements such as P, S, Cu, V, Ti, and Pb. Again, no correlation between cracking susceptibility and the concentration of residual elements was found.

CERT tests have also been performed on five different heats of Type 347 SS. The results are summarized in Table 6. Except for Ht 316642, all the heats of material were susceptible to TGSCC. However, susceptibility was observed only at strain rates  $< 5 \times 10^{-7} \text{ s}^{-1}$ , which is lower than that generally required to induce TGSCC in Type 316NG SS in similar environments. The strain rate at or below which SCC occurs is the (upper bound) critical strain rate. Above this critical strain rate, purely mechanical failure dominates. In terms of this measure of resistance to SCC, Type 347 SS is somewhat superior to Type 316NG SS.

Table 5. Heat-to-Heat Variations in SCC Susceptibility of Type 316NG SS<sup>a,b</sup>

| Heat No. | t <sub>f</sub> ,<br>h | ε <sub>f</sub> ,<br>% | σ <sub>max</sub> ,<br>MPa | Avg. Crack Growth Rate<br>m·s <sup>-1</sup> |
|----------|-----------------------|-----------------------|---------------------------|---------------------------------------------|
| P91756   | 474.0                 | 34.1                  | 461                       | 7.35 x 10 <sup>-10</sup>                    |
| 467958   | 577.0                 | 41.6                  | 501                       | 0                                           |
| 08056    | 641.0                 | 46.0                  | 390                       | 4.38 x 10 <sup>-10</sup>                    |
| 59076    | 398.1                 | 28.7                  | 487                       | 3.83 x 10 <sup>-10</sup>                    |
| NDE-28   | 653.0                 | 47.0                  | 470                       | 1.28 x 10 <sup>-9</sup>                     |
| D440104  | 712.0                 | 51.0                  | 464                       | 3.49 x 10 <sup>-10</sup>                    |
| D472701  | 647.0                 | 46.6                  | 455                       | 2.97 x 10 <sup>-10</sup>                    |
| D442604  | 669.0                 | 48.2                  | 463                       | 0                                           |
| D450905  | 664.0                 | 47.8                  | 468                       | 7.41 x 10 <sup>-11</sup>                    |

<sup>a</sup> All specimens were heat treated at 1050°C/0.5 h + 650°C/24 h.

<sup>b</sup> Tests were conducted in water containing 0.25 ppm dissolved oxygen with 0.1 ppm sulfate at 289°C and a strain rate of 2 x 10<sup>-7</sup> s<sup>-1</sup>.

Table 6. Heat-to-Heat Variations in SCC Susceptibility of Type 347 SS

| Test No. | Heat No. | ε̇,<br>s <sup>-1</sup> | t <sub>f</sub> ,<br>h | σ <sub>max</sub> ,<br>MPa | Failure | ā <sub>av</sub> ,<br>m·s <sup>-1</sup> | SS Potential,<br>mV(SHE) |
|----------|----------|------------------------|-----------------------|---------------------------|---------|----------------------------------------|--------------------------|
| 263      | 174100   | 1 x 10 <sup>-6</sup>   | 65.5                  | 432                       | Ductile | 0                                      | 21                       |
| 274      | 174100   | 5 x 10 <sup>-7</sup>   | 114.5                 | 417                       | TGSCC   | 1.63 x 10 <sup>-9</sup>                | 94                       |
| 272      | 174100   | 2 x 10 <sup>-7</sup>   | 301.5                 | 448                       | TGSCC   | 1.10 x 10 <sup>-9</sup>                | -8                       |
| 275      | 174100   | 1 x 10 <sup>-7</sup>   | 574.5                 | 451                       | TGSCC   | 7.58 x 10 <sup>-10</sup>               | 55                       |
| 301      | 170162   | 1 x 10 <sup>-6</sup>   | 55.7                  | 427                       | Ductile | 0                                      | 84                       |
| 305      | 170162   | 5 x 10 <sup>-7</sup>   | 114.1                 | 430                       | Ductile | 0                                      | 91                       |
| 310      | 170162   | 2 x 10 <sup>-7</sup>   | 250.5                 | 471                       | TGSCC   | 5.50 x 10 <sup>-10</sup>               | 22                       |
| 349      | 869962   | 1 x 10 <sup>-6</sup>   | 94.5                  | 460                       | Ductile | 0                                      | 22                       |
| 350      | 869962   | 5 x 10 <sup>-7</sup>   | 182.8                 | 466                       | TGSCC   | 3.80 x 10 <sup>-10</sup>               | 34                       |
| 348      | 869962   | 2 x 10 <sup>-7</sup>   | 442.0                 | 472                       | TGSCC   | 2.97 x 10 <sup>-10</sup>               | 80                       |
| 364      | 316642   | 1 x 10 <sup>-6</sup>   | 100.0                 | 438                       | Ductile | 0                                      | -1                       |
| 365      | 316642   | 5 x 10 <sup>-7</sup>   | 198.0                 | 444                       | Ductile | 0                                      | 3                        |
| 367      | 316642   | 2 x 10 <sup>-7</sup>   | 487.0                 | 443                       | Ductile | 0                                      | -87                      |
| 382      | LPN      | 1 x 10 <sup>-6</sup>   | 93.8                  | 452                       | Ductile | 0                                      | 86                       |
| 380      | LPN      | 5 x 10 <sup>-7</sup>   | 174.8                 | 459                       | TGSCC   | 1.22 x 10 <sup>-9</sup>                | 90                       |
| 377      | LPN      | 2 x 10 <sup>-7</sup>   | 530.5                 | 460                       | TGSCC   | 9.83 x 10 <sup>-10</sup>               | -54                      |

<sup>a</sup> The tests were performed in water with 0.25 ppm dissolved oxygen and 0.1 sulfate at 289°C.

## Effect of Heat Treatment on Susceptibility of Type 347 SS to Stress Corrosion Cracking

Table 7 summarizes results on both base metal and weldment specimens from Ht 316642 of Type 347 SS. The base metal specimens, which are designated as K2-..., are extremely resistant to SCC after heat treatment at 1050°C/0.5 h followed by 650°C/24 h. The weldment specimens, which are designated as K2W-..., were tested both in the as-welded condition and after a subsequent 500°C/24-h heat treatment. No cracking was observed in the weld specimens at strain rates of either  $1 \times 10^{-6}$  or  $5 \times 10^{-7} \text{ s}^{-1}$ , although the strains-to-failure are lower by approximately 50% for the weldments, as expected. However, at a strain rate of  $2 \times 10^{-7} \text{ s}^{-1}$ , cracking occurred in a weld specimen but not in the base metal specimen tested at this strain rate. The crack was located in the base metal relatively far from the weld. Additional tests were performed on material from Ht 316642 in the solution-annealed condition. These results also are given in Table 7. The material, which was extremely resistant to TGSCC in the aged condition, is susceptible to TGSCC in the solution-annealed condition as well as the as-welded state. The results suggest that heat treatment and thermomechanical history have a significant effect on the susceptibility of Type 347 SS to TGSCC.

To better understand the possible effects of heat treatment on susceptibility to SCC, the precipitate size and morphology of specimens from three heats of Type 347 SS (Ht 174100, 170162 and 869962) were examined by SEM. All the heat-treated specimens contain precipitates (Fig. 11) that were Nb-rich, as determined by energy-dispersive x-ray analysis. The precipitates are less than a micron in diameter. The crack growth rates appear to decrease with an increase in precipitate size. The increased resistance to crack growth with an increase in precipitate size is consistent with the idea that precipitates offer resistance to slip and hence can retard the film rupture process that is generally involved in the crack growth process.

### Fracture-Mechanics Crack-Growth-Rate Tests

Fracture-mechanics crack-growth-rate tests have been performed on two 0.7T compact-tension specimens, one of CF3M cast SS (Specimen CTC24-2) and the other of Type 316NG SS (Ht D440104, Specimen 104-2). The ferrite level of the cast material was 5%, as determined by magnetic permeability measurements. The specimens were fatigue precracked in high-temperature water with 0.2-0.3 ppm oxygen and 0.1 ppm sulfate at 289°C under a cyclic load with  $R = 0.25$ . Crack growth tests were then performed with a cyclic load with  $R = 0.95$  (sawtooth wave shape, 12-s rise and 1-s fall time). Crack lengths were measured by dc electric potential and by compliance measurement techniques. Measurements by the two techniques were in good agreement. The crack lengths as a function of time for the two specimens are shown in Figs. 12 and 13 for Type 316NG and CF3M SS, respectively. Because the fatigue crack growth rate was higher in the cast specimen during precracking, the initial stress intensity factor  $K$  under the  $R = 0.95$  loading was  $\sim 21 \text{ MPa}\cdot\text{m}^{1/2}$  ( $19 \text{ Ksi}\cdot\text{in}^{1/2}$ ) in the Type 316NG SS specimen and  $\sim 22 \text{ MPa}\cdot\text{m}^{1/2}$  ( $20 \text{ Ksi}\cdot\text{in}^{1/2}$ ) in the CF3M SS specimen. As is shown in Fig. 12, for  $K < \sim 22 \text{ MPa}\cdot\text{m}^{1/2}$  ( $20 \text{ Ksi}\cdot\text{in}^{1/2}$ ), sustained crack growth did not occur in the Type 316NG SS specimen. The bursts of transient crack growth shown in the figure are associated with the compliance measurements. To make the compliance measurement, the usual load history must be interrupted by  $\sim 10$  cycles of relatively low  $R$  loading ( $R = 0.4$ ). Apparently this change in loading history is sufficient to initiate crack growth, which however, is not sustained. For  $K > \sim 20 \text{ Ksi}\cdot\text{in}^{1/2}$  ( $22 \text{ MPa}\cdot\text{m}^{1/2}$ ), steady-state crack growth was achieved under  $R = 0.95$

Table 7. Effect of Heat Treatment on SCC Susceptibility of Type 347 SS<sup>a</sup>

| Test No.                                               | Specimen No.       | $\dot{\epsilon}$ ,<br>s <sup>-1</sup> | t <sub>f</sub> ,<br>h | $\epsilon_f$ ,<br>% | $\epsilon_{L1}$ ,<br>% | $\sigma_{max}$ ,<br>MPa | $\Delta A/A_0$ ,<br>% | SS Potential,<br>mV(SHE) | $\dot{a}_{av}$ ,<br>m·s <sup>-1</sup> |
|--------------------------------------------------------|--------------------|---------------------------------------|-----------------------|---------------------|------------------------|-------------------------|-----------------------|--------------------------|---------------------------------------|
| Heat treatment: 1050°C/0.5 h + 650°C/24 h (air cooled) |                    |                                       |                       |                     |                        |                         |                       |                          |                                       |
| 364                                                    | K2-1 <sup>b</sup>  | 1 x 10 <sup>-6</sup>                  | 100                   | 36.0                | 28.8                   | 438                     | 59                    | -1                       | 0                                     |
| 365                                                    | K2-2               | 5 x 10 <sup>-7</sup>                  | 198                   | 35.6                | 30.1                   | 444                     | 63                    | 3                        | 0                                     |
| 367                                                    | K2-3               | 2 x 10 <sup>-7</sup>                  | 487                   | 35.1                | 28.8                   | 443                     | 55                    | -87                      | 0                                     |
| Heat treatment: 1050°C/0.5 h + 600°C/24 h              |                    |                                       |                       |                     |                        |                         |                       |                          |                                       |
| 408                                                    | K2-7               | 2 x 10 <sup>-7</sup>                  | 320.0                 | 23.0                | 20.4                   | 435                     | 16                    | 119                      | 1.37 x 10 <sup>-9</sup>               |
| Heat treatment: 1050°C/0.5 h (water quenched)          |                    |                                       |                       |                     |                        |                         |                       |                          |                                       |
| 399                                                    | K2-6               | 2 x 10 <sup>-7</sup>                  | 478.5                 | 34.5                | 32.0                   | 444                     | 45                    | 45                       | 1.27 x 10 <sup>-9</sup>               |
| 398                                                    | K2-5               | 1 x 10 <sup>-7</sup>                  | 923.0                 | 33.2                | 30.5                   | 446                     | 22                    | 83                       | 9.30 x 10 <sup>-10</sup>              |
| Heat treatment: As welded + 500°C/24 h                 |                    |                                       |                       |                     |                        |                         |                       |                          |                                       |
| 387                                                    | K2W-2 <sup>c</sup> | 1 x 10 <sup>-6</sup>                  | 50.5                  | 18.2                | 11.5                   | 445                     | 54                    | 88                       | 0                                     |
| 385                                                    | K2W-1              | 5 x 10 <sup>-7</sup>                  | 126.9                 | 22.8                | 17.3                   | 455                     | 54                    | 100                      | 0                                     |
| 389                                                    | K2W-3              | 2 x 10 <sup>-7</sup>                  | 184.0                 | 13.2                | 10.4                   | 455                     | 46                    | 68                       | 2.26 x 10 <sup>-9</sup>               |
| 396                                                    | K2W-4              | 2 x 10 <sup>-7</sup>                  | 210.0                 | 15.1                | 13.2                   | 454                     | 21                    | 29                       | 1.92 x 10 <sup>-9</sup>               |
| (e) Heat treatment: As welded                          |                    |                                       |                       |                     |                        |                         |                       |                          |                                       |
| 397                                                    | K2W-5              | 2 x 10 <sup>-7</sup>                  | 307.0                 | 22.1                | 19.1                   | 456                     | 39                    | 110                      | 1.72 x 10 <sup>-9</sup>               |

<sup>a</sup>All tests were performed in water containing 0.25 ppm dissolved oxygen with 0.1 ppm sulfate at 289°C.

<sup>b</sup>Specimens numbered K2-X: base metal.

<sup>c</sup>Specimens numbered K2W-X: weldment.

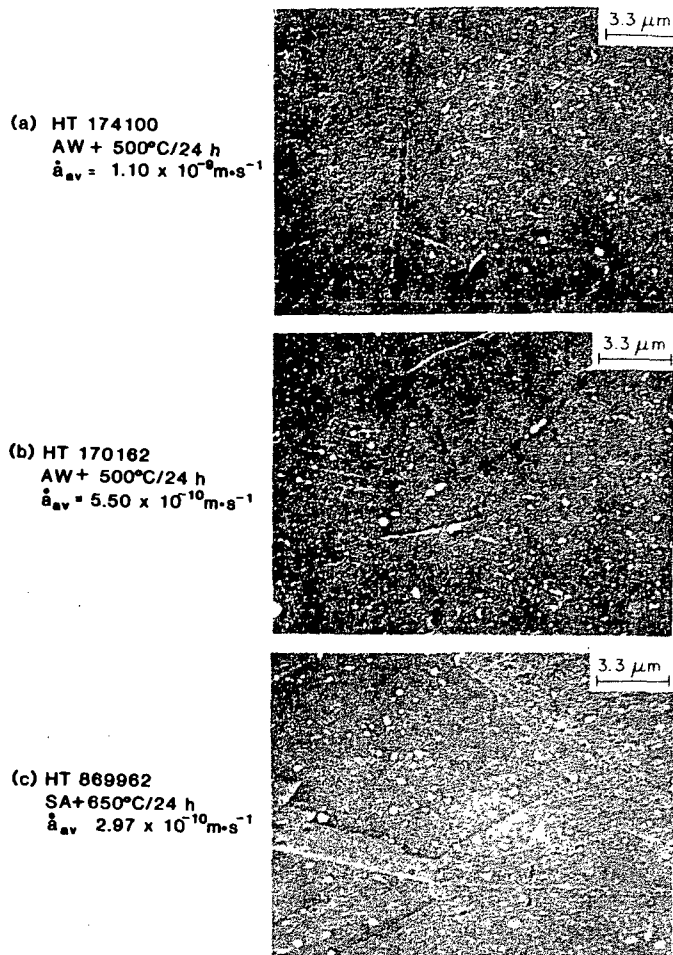


Figure 11. Precipitate Distributions in Type 347 SS and Corresponding Crack Growth Rates.

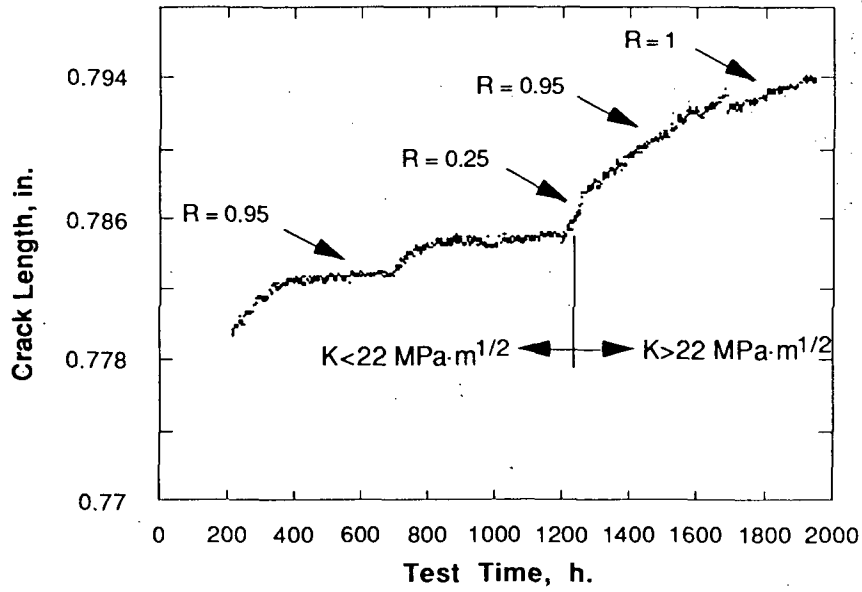


Figure 12. Crack Growth in a Type 316NG SS Specimen under  $R = 0.95$  ( $0.25$  and  $1.0$ ) Loading in Water with  $\sim 0.25$  ppm Dissolved Oxygen and  $0.1$  ppm  $\text{SO}_4^-$ .

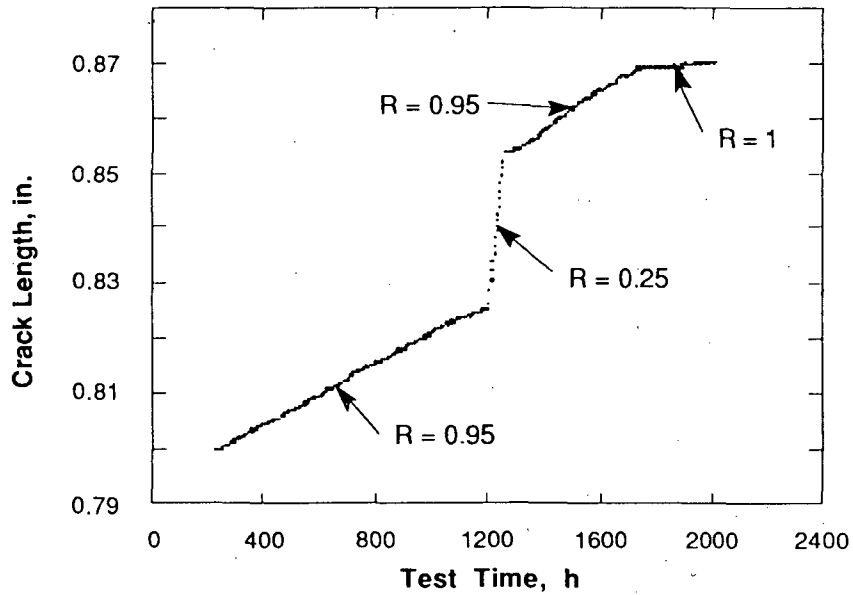


Figure 13. Crack Growth in a CF3M SS Specimen under  $R = 0.95$  ( $0.25$  and  $1.0$ ) Loading in Water with  $\sim 0.25$  ppm Dissolved Oxygen and  $0.1$  ppm  $\text{SO}_4^-$ .

loading. Although compliance measurements were still made, no transient behavior was observed, presumably because the steady-state rate under these conditions was relatively high. This suggests that  $\sim 22 \text{ MPa}\cdot\text{m}^{1/2}$  ( $20 \text{ Ksi}\cdot\text{in}^{1/2}$ ) represents a threshold stress intensity for growth of SCC in this material under this loading condition. The stress intensity of the cast specimen was always  $\geq 20 \text{ Ksi}\cdot\text{in}^{1/2}$  ( $22 \text{ MPa}\cdot\text{m}^{1/2}$ ) because of the longer precrack produced by the initial fatigue loading. In this case steady-state crack growth occurred under the  $R = 0.95$  loading, but there was a significant decrease in the crack growth rate under constant load,  $R = 1$ . The effect is related to environmental crack growth and is not simply due to a change in mechanical fatigue crack growth; under hydrogen water chemistry conditions, no measurable crack growth has been observed under  $R = 0.95$  loading.

#### Effects of Cuprous Ion and Ethylene-diamine-tetraacetate Salts on Stress Corrosion Cracking

In plants with admiralty brass, aluminum brass, or copper-nickel condenser tubes and/or feedwater heaters, copper is one of the metallic impurities present in reactor coolant water. Previous work indicated that the minimum concentration of  $\text{Cu}^{2+}$  required for severe IGSCC of sensitized Type 304 SS decreased from  $\sim 1.0 \text{ ppm}$  at  $289^\circ\text{C}$  to  $\sim 0.1 \text{ ppm}$  at  $150^\circ\text{C}$ . These concentrations are higher than those typically encountered in the reactor coolant water in BWRs and in secondary system water of recirculating or once-through steam generators in PWRs. However, since the thermodynamic stability regime of  $\text{Cu}^+$  increases relative to that of  $\text{Cu}^{2+}$  as the temperature of the water increases,  $\text{Cu}^+$  and  $\text{Cu}^0$  are the most likely copper species to be present at the potential-pH conditions in BWR and PWRs, and tests were performed to determine the minimum concentration of  $\text{Cu}^+$  needed to promote SCC of sensitized Type 304 SS.

The feedwater chemistries, ECP values, and test results are summarized in Table 8. As in the case of  $\text{CuCl}_2$ , the time-to-failure of the specimens exhibits an abrupt change over a narrow  $\text{Cu}^+$  concentration range, as is shown in Fig. 14, and the fracture mode changes from predominantly ductile fracture to IGSCC. The dependence of the crack growth rate on  $\text{Cu}^+$  concentration is shown in Fig. 15. For the most part, the data lie along a line of slope  $\sim 1$ , which is consistent with the hypothesis that the cathodic-reduction partial process is  $\text{Cu}^+ + \text{e}^- = \text{Cu}^0$  and the heuristic result that the crack growth rate is proportional to  $1/|\text{e}^-|$  when the process is controlled by the rate of cathodic reduction [7, 8]. Previous tests on  $\text{Cu}^{2+}$  indicated that the crack growth rate increased as the  $1/2$  power of the  $\text{Cu}^{2+}$  concentration, which is consistent with the reduction of  $\text{Cu}^{2+}$  to  $\text{Cu}^0$ , which consumes two electrons [9].

The temperature dependence of the crack growth rate of the steel in low-oxygen water ( $< 5 \text{ ppb}$ ) containing  $\sim 1\text{--}2 \text{ ppm}$   $\text{Cu}^+$  is shown in Fig. 16. The broad maximum in the crack growth rate between  $\sim 170$  and  $250^\circ\text{C}$  and the decrease in IGSCC susceptibility at both lower and higher temperatures is similar to the behavior observed in water containing  $0.2 \text{ ppm}$  dissolved oxygen with and without sulfate additions [10, 11]. The crack growth rate of the steel at  $\sim 200^\circ\text{C}$  in water with  $\sim 1\text{--}2 \text{ ppm}$   $\text{Cu}^+$  is higher by factors of 10 and 3 than it is in high-purity water with  $0.2 \text{ ppm}$  dissolved oxygen and in similarly oxygenated water with  $1 \text{ ppm}$  sulfate, respectively.

The effect of pH on SCC behavior in  $\text{Cu}^+$  solutions was also investigated. Hydrochloric acid and  $\text{NH}_4\text{OH}$  additions were used to obtain  $\text{pH}_{25^\circ\text{C}}$  values ranging from 3.6 to 8.7. Tests were also conducted in solutions containing only HCl for comparison with the results in solutions containing  $\text{Cu}^+$ . At a  $\text{pH}_{25^\circ\text{C}}$  of  $\sim 4.7$  (e.g.,  $\sim 1.0 \text{ ppm}$  HCl), the crack growth rates in water containing  $0.1$  and  $1.0 \text{ ppm}$   $\text{Cu}^+$  are larger by factors of  $\sim 7$  and  $45$ , respectively.

Table 8. Influence of Temperature on the SCC Susceptibility of Sensitized Type 304 SS Specimens<sup>a</sup> in Water Containing CuCl at a Low (<5 ppb) Dissolved-Oxygen Concentration

| Test No. | Temp., °C | Feedwater Chemistry  |                            |                  |                      |            | CERT Parameters |                     |                          |             | Potential                                       |                      |
|----------|-----------|----------------------|----------------------------|------------------|----------------------|------------|-----------------|---------------------|--------------------------|-------------|-------------------------------------------------|----------------------|
|          |           | Cation Concentration |                            | Anion Conc., ppm | Cond. at 25°C, µS/cm | pH at 25°C | Failure Time, h | Maximum Stress, MPa | Total Elong., in Area, % | Reduction % | SCC Growth Rate, <sup>c</sup> m·s <sup>-1</sup> | Type 304 SS, mV(SHE) |
|          |           | Influent, ppm        | Effluent, <sup>b</sup> ppm |                  |                      |            |                 |                     |                          |             |                                                 |                      |
| 237      | 135       | 2.0                  | 1.53                       | 1.10             | 7.60                 | 5.90       | 67              | 406                 | 24                       | 45          | 8.2 x 10 <sup>-9</sup>                          | 264                  |
| 228      | 150       | 0.1                  | 0.09                       | 0.06             | 0.68                 | 6.20       | 154             | 520                 | 55                       | 81          | -                                               | 229                  |
| 220      | 150       | 0.3                  | 0.22                       | 0.17             | 1.41                 | 6.14       | 150             | 534                 | 54                       | 81          | -                                               | 208                  |
| 229      | 150       | 0.8                  | 0.66                       | 0.45             | 3.30                 | 6.07       | 66              | 432                 | 24                       | 47          | 9.6 x 10 <sup>-9</sup>                          | 305                  |
| 232      | 150       | 2.0                  | 1.23                       | 1.10             | 7.60                 | 6.26       | 77              | 420                 | 28                       | 34          | 8.9 x 10 <sup>-9</sup>                          | 278                  |
| 243      | 170       | 0.02                 | 0.02                       | 0.01             | 0.36                 | 6.29       | 146             | 504                 | 53                       | 81          | -                                               | 38                   |
| 238      | 170       | 0.05                 | 0.05                       | 0.03             | 0.46                 | 6.18       | 89              | 440                 | 32                       | 45          | 7.2 x 10 <sup>-9</sup>                          | 141                  |
| 234      | 170       | 2.0                  | 1.05                       | 1.10             | 7.50                 | 5.98       | 36              | 310                 | 13                       | 21          | 3.2 x 10 <sup>-8</sup>                          | 301                  |
| 231      | 200       | 0.02                 | 0.06                       | 0.01             | 0.44                 | 6.31       | 81              | 430                 | 30                       | 45          | 5.2 x 10 <sup>-9</sup>                          | 130                  |
| 227      | 200       | 0.05                 | 0.05                       | 0.03             | 0.49                 | 6.22       | 91              | 483                 | 33                       | 41          | 3.4 x 10 <sup>-9</sup>                          | 53                   |
| 212      | 200       | 0.1                  | 0.15                       | 0.06             | 0.66                 | 6.60       | 63 <sup>c</sup> | 504                 | 52                       | 76          | -                                               | 83                   |
| 223      | 200       | 0.1                  | 0.07                       | 0.06             | 0.63                 | 6.25       | 89              | 476                 | 32                       | 41          | 4.3 x 10 <sup>-9</sup>                          | 116                  |
| 219      | 200       | 0.3                  | 0.38                       | 0.17             | 1.43                 | 6.26       | 85              | 447                 | 31                       | 54          | 8.1 x 10 <sup>-9</sup>                          | 22                   |
| 213      | 200       | 0.5                  | 0.55                       | 0.28             | 2.30                 | 5.97       | 95              | 476                 | 34                       | 60          | 5.4 x 10 <sup>-9</sup>                          | 116                  |
| 230      | 200       | 0.5                  | 0.42                       | 0.28             | 2.10                 | 6.08       | 39              | 297                 | 14                       | 31          | 2.6 x 10 <sup>-8</sup>                          | 219                  |
| 214      | 200       | 0.8                  | 0.76                       | 0.45             | 3.60                 | 6.00       | 47              | 298                 | 17                       | 20          | 2.8 x 10 <sup>-8</sup>                          | 193                  |
| 211      | 200       | 1.0                  | 0.94                       | 0.55             | 4.40                 | 5.92       | 25              | 254                 | 9                        | 18          | 5.2 x 10 <sup>-8</sup>                          | 220                  |
| 226      | 200       | 2.0                  | 0.90                       | 1.10             | 7.70                 | 5.94       | 24              | 245                 | 9                        | 16          | 5.1 x 10 <sup>-8</sup>                          | 246                  |
| 233      | 250       | 2.0                  | 0.78                       | 1.10             | 7.50                 | 6.31       | 33              | 256                 | 12                       | 10          | 3.5 x 10 <sup>-8</sup>                          | 87                   |
| 215      | 289       | 0.8                  | 0.52                       | 0.45             | 3.50                 | 5.87       | 147             | 534                 | 53                       | 58          | 1.1 x 10 <sup>-9</sup>                          | -403                 |
| 216      | 289       | 2.0                  | 0.73                       | 1.10             | 7.90                 | 5.86       | 152             | 529                 | 55                       | 65          | 1.1 x 10 <sup>-9</sup>                          | -381                 |
| 217      | 289       | 5.0                  | 1.46                       | 2.75             | 20.0                 | 5.98       | 139             | 527                 | 50                       | 41          | 6.0 x 10 <sup>-9</sup>                          | -296                 |
| 218      | 289       | 10.0                 | 3.65                       | 5.50             | 38.0                 | 6.23       | 28              | 249                 | 10                       | 11          | 4.7 x 10 <sup>-8</sup>                          | -246                 |

<sup>a</sup>Lightly sensitized (EPR = 2 C/cm<sup>2</sup>) specimens (Heat No. 30956) were exposed to the environments for ~20 h before being strained at a rate of 1 x 10<sup>-6</sup> s<sup>-1</sup>.

<sup>b</sup>Copper concentration of the effluent water was determined by inductively-coupled-plasma (ICP) spectrophotometry analyses.

<sup>c</sup>SCC growth rates are based on measurement of the depth of the longest crack in an enlarged micrograph of the fracture surface and the time period from the onset of yield to the point of maximum load on the tensile curve.

<sup>c</sup>Strain rate was 2.3 x 10<sup>-6</sup> s<sup>-1</sup>.

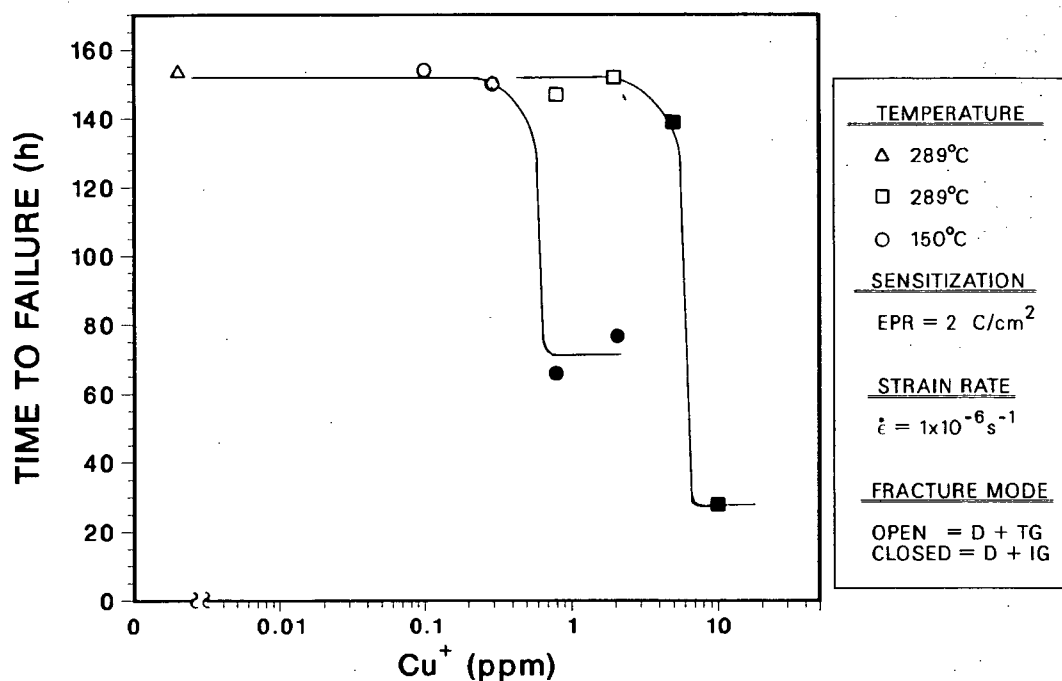


Figure 14. Dependence of the Time to Failure of Lightly Sensitized ( $EPR = 2 C/cm^2$ ) Type 304 SS Specimens on Cuprous Ion Concentration in CERT Experiments at 150 and 289°C.

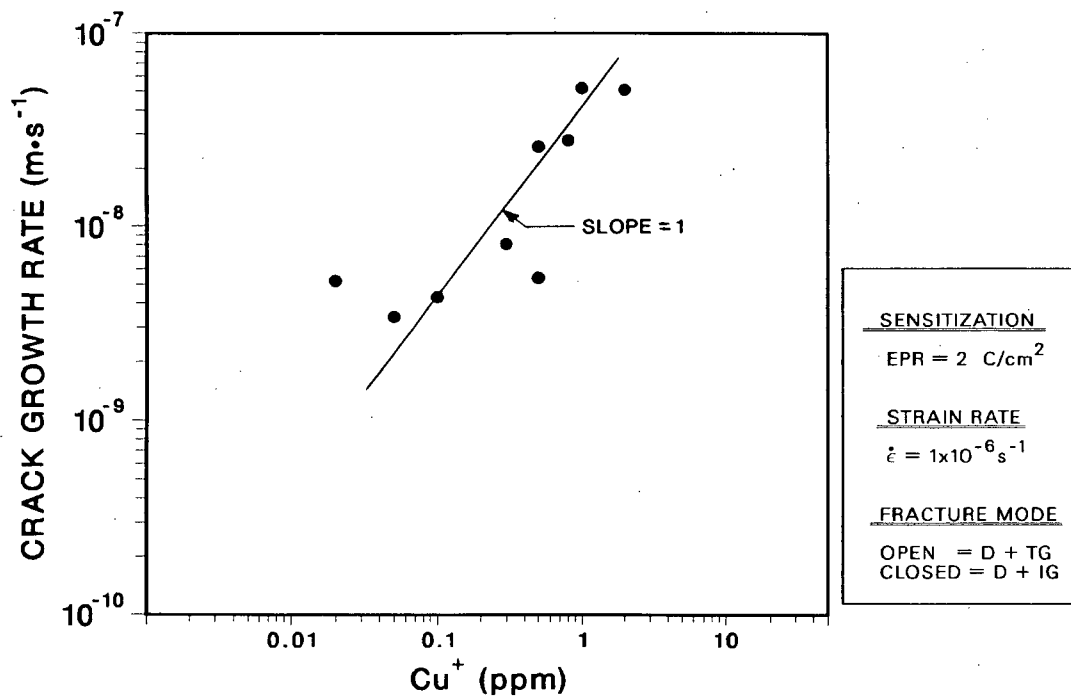


Figure 15. Dependence of the Crack Growth Rate of Lightly Sensitized ( $EPR = 2 C/cm^2$ ) Type 304 SS Specimens on Cuprous Ion Concentration in CERT Experiments at 200°C.

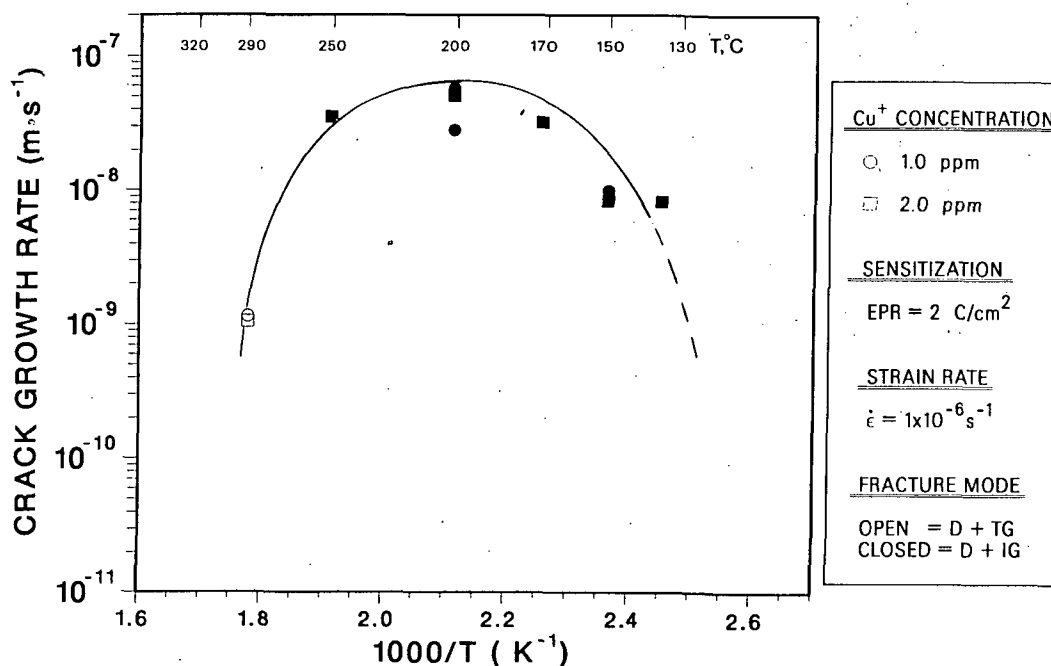


Figure 16. Effect of Temperature on the Crack Growth Rate of Lightly Sensitized ( $EPR = 2 \text{ C/cm}^2$ ) Type 304 SS in Low-Oxygen (<5 ppb) Feedwater Containing ~1–2 ppm Cuprous Ion as CuCl.

compared to those in solutions without  $\text{Cu}^+$ . In a basic solution containing 0.1 ppm  $\text{Cu}^+$  and  $\text{NH}_4\text{OH}$  ( $\text{pH}_{25^\circ\text{C}} = 8.7$ ), the effluent copper concentration was lower by a factor of 10 than in the feedwater and no SCC occurred.

These results and similar results, obtained in water containing  $\text{Cu}^{2+}$  and reported previously [11], demonstrate that cuprous and cupric ions at concentrations  $>0.1 \text{ ppm}$  in high-temperature, low-oxygen water strongly promote IGSCC of sensitized stainless steel. These species undergo cathodic reduction on the surface of the steel, which couples with anodic dissolution at the crack tip and leads to rapid advance of the stress corrosion crack. Since the crack growth rates are, in general, higher by a factor of 10 at a given strain rate and temperature than for other species at similar concentrations (e.g., dissolved oxygen or various oxyanions), it appears that the kinetics of the cathodic reduction process for the cuprous ions are faster than those associated with the other species.

As part of the investigation of the effects of organic contaminants on the SCC of sensitized Type 304 SS in oxygenated water, CERT tests were performed in water containing 0.2 ppm dissolved oxygen and four EDTA salts at an anion concentration of 1 ppm. Although some transgranular cracking was observed, the crack growth rates, which are given in Table 9, are very low compared to those observed in high-purity oxygenated water [13]. Since the dissolved-oxygen concentrations in the effluent were  $<5 \text{ ppb}$  and the ECP values of the steel and the platinum and copper electrodes were also quite negative [ $-510$  to  $-680 \text{ mV(SHE)}$ ], these substances apparently react with dissolved oxygen and thereby decrease susceptibility to IGSCC. This contrasts with the behavior observed with for carboxylic (acetic, formic, lactic, and oxalic) and short-chain aliphatic (propionic and butyric) acids, which also decreased the crack growth rates significantly, but did not

Table 9. Influence of Several EDTA Salts<sup>a</sup> in Feedwater with 0.2 ppm Dissolved Oxygen<sup>b</sup> on the SCC Susceptibility of Sensitized (EPR = 2 C/cm<sup>2</sup>) Type 304 SS Specimens<sup>c</sup> in 289°C Water

| Test No. | Feedwater Chemistry  |                  |                      |            | CERT Parameters |                     |                 |                      |                                                 | Potential <sup>b</sup> |
|----------|----------------------|------------------|----------------------|------------|-----------------|---------------------|-----------------|----------------------|-------------------------------------------------|------------------------|
|          | Species <sup>a</sup> | Anion Conc., ppm | Cond. at 25°C, µS/cm | pH at 25°C | Failure Time, h | Maximum Stress, MPa | Total Elong., % | Reduction in Area, % | SCC Growth Rate, <sup>d</sup> m·s <sup>-1</sup> | Type 304 SS mv(SHE)    |
| A162     | 4Na-EDTA             | 1.0              | 1.71                 | 7.55       | 239             | 522                 | 45              | 48                   | 1.6 x 10 <sup>-9</sup>                          | -682                   |
| A164     | Hydroxy-EDTA         | 1.0              | 1.95                 | 5.41       | 243             | 526                 | 46              | 44                   | 1.6 x 10 <sup>-9</sup>                          | -612                   |
| A165     | Cu,2Na-EDTA          | 1.0              | 0.91                 | 6.17       | 277             | 534                 | 52              | 57                   | 3.1 x 10 <sup>-10</sup>                         | -518                   |
| A163     | Fe,Na-EDTA           | 1.0              | 0.62                 | 6.16       | 295             | 532                 | 55              | 74                   | 3.1 x 10 <sup>-10</sup>                         | -586                   |

<sup>a</sup>Ethylenediaminetetraacetate (EDTA) salts in the experiments were as follows: 4Na·EDTA·3H<sub>2</sub>O; N-(2-Hydroxyethyl)-EDTA acid; Cu,2Na·EDTA·2H<sub>2</sub>O; and Fe,Na·EDTA·2H<sub>2</sub>O.

<sup>b</sup>Effluent dissolved-oxygen concentration determined by Chemetrics analyses was <5 ppb.

<sup>c</sup>Lightly sensitized (EPR = 2 C/cm<sup>2</sup>) specimens (Heat No. 30956) were exposed to the environments for ~20 h before being strained at a rate of 5.2 x 10<sup>-7</sup> s<sup>-1</sup>.

<sup>d</sup>SCC growth rates are based on measurement of the depth of the longest crack in an enlarged micrograph of the fracture surface and the time period from the onset of yield to the point of maximum load on the tensile curve.

decrease dissolved oxygen or ECP values [13]. Fracture-mechanics crack-growth-rate tests are in progress to confirm the relatively innocuous (or even potentially beneficial) effects of several of these organic acids. Initial results indicate that the addition of 1 ppm of propionic acid to the feedwater decreased the crack growth rate of a sensitized Type 304 SS specimen by an order of magnitude compared to that observed in high-purity water; however, the crack growth rate of a Type 316NG SS specimen was unaffected by the change.

## 2.2 Fatigue of Type 316NG SS

In LWR primary piping, low-cycle fatigue is potentially a significant degradation mechanism which must be considered to justify extended operation of the plants [14]. Current fatigue design is based on the ASME Section III fatigue design curves, which do not explicitly consider environmental effects. Instead, the design curves are obtained by introducing a factor of 2 on the strain range, or 20 on the cycles from the mean life curve, whichever is more conservative. It has been shown that the effect of the standard BWR environment on the fatigue life of A106-GrB, and A333-Gr6 steels can completely erode the "2 or 20" margin in the Code design curve [15]. Tests on Types 304 and 304L SS in the Dresden I reactor [16] showed that the BWR environment had a significant effect both on sensitized materials and on as-received materials, at least under some loading conditions, even in relatively high plastic strain ranges. It is possible that environmental degradation would be even more significant at lower strain ranges. Although the current data for Type 316NG SS [17] are above the ASME Section III design curve, it appears that the environment eliminates a substantial portion of the safety margins built into the Code. The objective of the current work is to provide additional information on the effects of operating temperature and environment on the fatigue behavior of Type 316NG SS.

Specimens were fabricated from a Type 316NG SS 22-in.-diam pipe, manufactured by Sumitomo, with no additional heat treatment. Baseline in-air tests were performed under strain control with a triangular wave form and a strain rate of  $5 \times 10^{-3} \text{ s}^{-1}$  with the same specimen design and loading systems that were to be used for the tests in the environment. The results of the in-air tests are summarized in Table 10. Figure 17 compares these results with the design curve for austenitic stainless steels in ASME Section III and the ASME mean data curve. The lives at 320 and 288°C are somewhat shorter (22-35%) than those observed at room temperature, but the differences are not large. The relatively small difference in temperature between the 320°C and the 288°C tests has little effect on fatigue life in air. However, in an aqueous environment, somewhat larger differences may be observed. In stress corrosion tests on sensitized Type 304 SS, susceptibility to cracking can decrease quite markedly as the temperature increases over this range.

The results are in good agreement with the mean data curve for fairly short lives corresponding to plastic strain ranges of greater than 0.5%, but they fall below the mean data curve at longer lives. However, this does not necessarily indicate that the fatigue strength of the Type 316NG SS is less than that of Type 304 SS. The mean data curve is based almost entirely on tests with lives of less than  $10^5$  cycles [18]; the portion of the curve for lower linear stress amplitudes was obtained by extrapolation. The results for Type 316NG SS are close to the actual data for Type 304 SS. The departure from the mean data curve occurs only for the portion of the curve that is extrapolated beyond the range of the supporting data.

Table 10. Cycles to Failure as a Function of Strain Range for Strain-Controlled Fatigue Tests on Type 316NG SS

| Test Number | Strain Range % | Cycles to Failure |
|-------------|----------------|-------------------|
| 25°C        |                |                   |
| 1390        | 0.75           | 25,736            |
| 1391        | 1.0            | 13,561            |
| 1392        | 0.5            | 60,741            |
| 1393        | 0.4            | 127,386           |
| 1394        | 1.5            | 4,649             |
| 1395        | 0.35           | 183,979           |
| 1396        | 0.75           | 30,000            |
| 1397        | 0.30           | 347,991           |
| 1398        | 0.27           | -666,000          |
| 1399        | 0.25           | <sup>a</sup>      |
| 1400        | 0.25           | -1,775,000        |
| 320°C       |                |                   |
| 1404        | 0.5            | 47,011            |
| 1405        | 0.75           | 20,425            |
| 1406        | 0.4            | 82,691            |
| 288°C       |                |                   |
| 1407        | 0.4            | 82,691            |
| 1408        | 0.75           | 21,548            |
| 1409        | 0.5            | 54,144            |

<sup>a</sup>The test failed at -1,900,000 due to an equipment malfunction.

### 2.3 Stress Corrosion Cracking of Ferritic Steels

CERT tests were continued on specimens fabricated from several ferritic steels (A333, A106, A155, A516, and A533B). The tests were performed in oxygenated water at 289°C with and without 0.01 and 0.1 ppm sulfate (as H<sub>2</sub>SO<sub>4</sub>) at strain rates of 1.0 x 10<sup>-6</sup> and 2.5 x 10<sup>-7</sup> s<sup>-1</sup>. The dissolved-oxygen concentrations were ~0.2-0.3 ppm.

The results of the tests are summarized in Table 11. Except for one specimen of A533B (Ht A5401 Specimen W7-3), all materials showed transgranular cracking on the fracture surfaces. The average crack growth rates varied widely (1 x 10<sup>-10</sup> to 3 x 10<sup>-8</sup> m·s<sup>-1</sup>), even for same heat of material. The addition of 0.1 ppm sulfate did not seem to have an appreciable effect on crack growth rates in these materials. Presumably, crack tip impurity levels from the inclusions overwhelm the contributions from the bulk water chemistry.

As expected from related work on the fatigue crack growth of ferritic steels in reactor environments [19, 20], there appears to be a strong correlation between the sulfur content of the steel (particularly the presence of sulfide inclusions) and susceptibility to SCC. Figure 18 shows TGSCC on the fracture surface of Specimen 30C-1 (A106B Ht DP2-30). Figure 19 shows ductile fracture of Specimen W7-3 (A533B, Ht No. A5401). Micrographs of the cross section of Specimens 30C-1 and W7-3, are shown in Figs. 20 and 21, respectively. There are far fewer inclusions in the less susceptible A533B steel than in the more susceptible

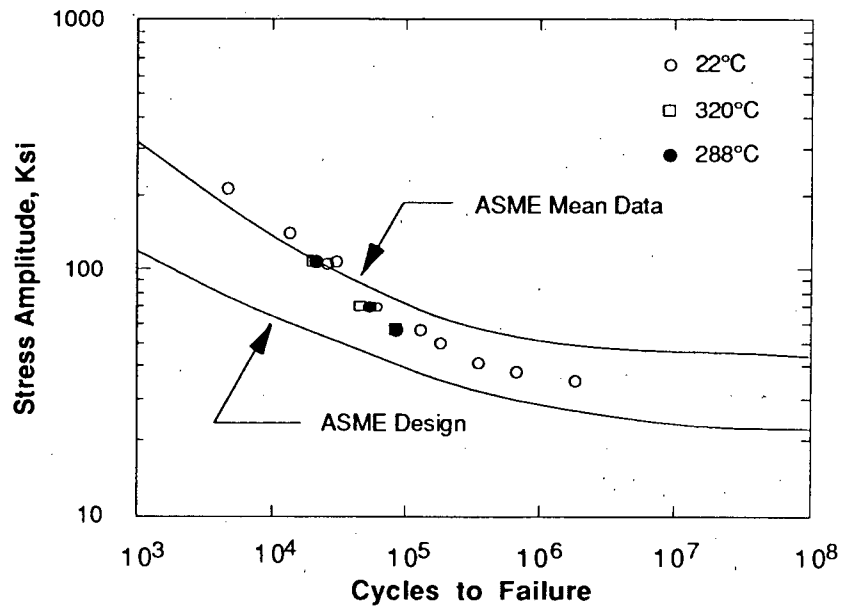


Figure 17. Comparison of Current Results on Fatigue of Type 316NG SS in Air with the ASME Section III Design and Mean Data Curves.

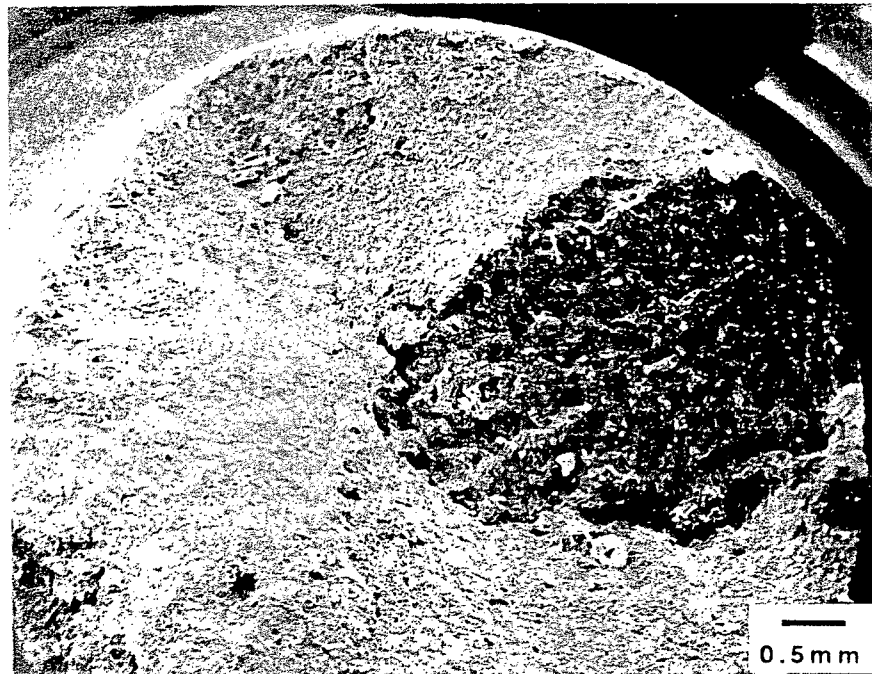


Figure 18. Transgranular Cracking on the Fracture Surface of A106B Ferritic Steel.

Table 11. Results of CERT Tests for Ferritic Steels in Oxygenated Water at 289°C

| Material Heat No.                                         | Specimen ID | Strain Rate, $s^{-1}$ | Max. Load MPa | $T_f$ , h | RA, % | Elong, % | Crack Growth $ms^{-1}$ | ECP, mV(SHE) |
|-----------------------------------------------------------|-------------|-----------------------|---------------|-----------|-------|----------|------------------------|--------------|
| <i>High-Purity Water with 0.2-0.3 ppm Oxygen</i>          |             |                       |               |           |       |          |                        |              |
| A533B<br>A5401                                            | W7-2        | $1 \times 10^{-6}$    | 657           | 63.7      | 72.5  | 22.0     | $1.4 \times 10^{-10}$  | -40          |
| A533B<br>XE5-M                                            | 5M-2        | "                     | 614           | 55.6      | 71.7  | 23.5     | $6.4 \times 10^{-9}$   | +40          |
| A516 GR70<br>DP2-F34                                      | 34-2A       | "                     | 507           | 95.9      | 78.8  | 40.4     | $1.5 \times 10^{-10}$  | -40          |
| A155-CK70<br>DP2-F26                                      | 26-2        | "                     | 527           | 82.6      | 49.8  | 28.3     | $1.2 \times 10^{-9}$   | 0            |
| A106B<br>DP2-F29                                          | 29B-2       | "                     | 570           | 75.2      | 57.6  | 28.5     | $1.4 \times 10^{-10}$  | -            |
| A106B<br>DP2-F30                                          | 30C-3       | "                     | 640           | 76.7      | 29.8  | 28.4     | $4.6 \times 10^{-9}$   | -20          |
| "                                                         | 30C-1       | "                     | 626           | 47.4      | 16.5  | 17.6     | $3 \times 10^{-8}$     | +50          |
| "                                                         | 30C-2       | $2.5 \times 10^{-7}$  | 632           | 291.7     | 39.3  | 29.2     | $3 \times 10^{-9}$     | -20          |
| <i>High-Purity Water with 0.5 ppm Oxygen</i>              |             |                       |               |           |       |          |                        |              |
| A106B<br>DP2-F30                                          | 30C-4       | $1 \times 10^{-6}$    | 627           | 68.0      | 15.5  | 27.4     | $2.8 \times 10^{-9}$   | +110         |
| <i>Water with 0.01 ppm Sulfate and 0.2-0.3 ppm Oxygen</i> |             |                       |               |           |       |          |                        |              |
| A106B<br>DP2-F29                                          | 29B-6       | $1 \times 10^{-6}$    | 554           | 81.3      | 42.0  | 28.4     | -                      | -75          |
| A106B<br>DP2-F30                                          | 30C-6       | "                     | 619           | 70.5      | 46.3  | 22.5     | $4.2 \times 10^{-9}$   | -110         |
| <i>Water with 0.1 ppm Sulfate and 0.2-0.3 ppm Oxygen</i>  |             |                       |               |           |       |          |                        |              |
| A106 B<br>DP2-F29                                         | 29B-5       | $1 \times 10^{-6}$    | 472           | 68.7      | 41.6  | 34.5     | $3.9 \times 10^{-9}$   | - 170        |
| "                                                         | 29B-7       | "                     | 554           | 60.9      | 29.9  | 21.9     | $5.9 \times 10^{-9}$   | -            |
| A106 B<br>DP2-F30                                         | 30C-7       | "                     | 624           | 66.8      | 63.2  | 25.8     | $6.2 \times 10^{-9}$   | -            |
| "                                                         | 30C-8       | "                     | 620           | 71.1      | 39.1  | 24.8     | $7.2 \times 10^{-9}$   | - 188        |
| A533 B<br>A5401                                           | W7-3        | "                     | 646           | 61.2      | 85.9  | 25.8     | Ductile                | - 68         |
| A533 B<br>XE5-M                                           | 5M-3        | "                     | 593           | 43.5      | 42.3  | 20.9     | $1.0 \times 10^{-8}$   | - 70         |
| A155-CK70<br>DP2-F26                                      | 26-3        | "                     | 514           | 64.4      | 38.8  | 26.4     | $6.0 \times 10^{-9}$   | - 63         |

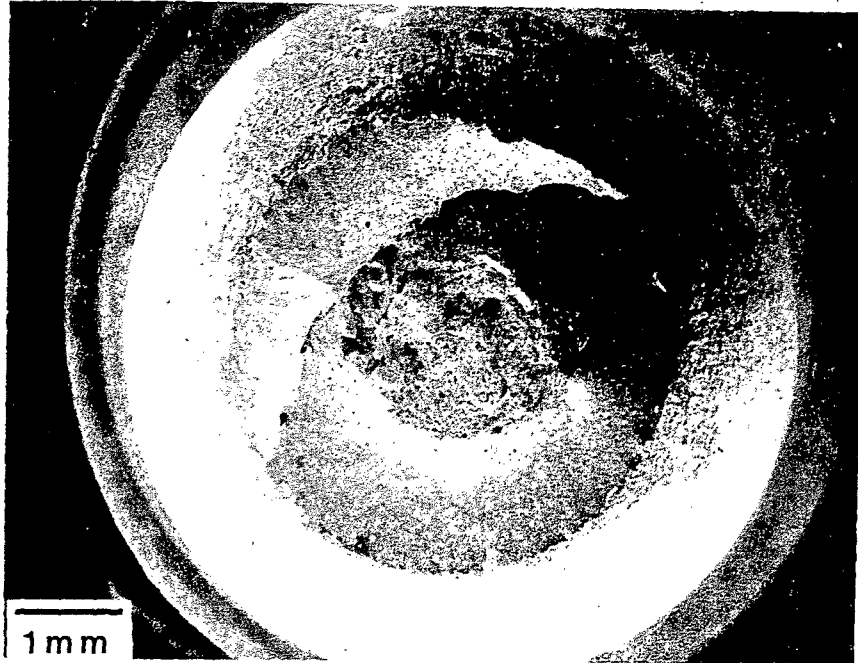


Figure 19. Fracture Surface of A533B Ferritic Steel Showing Only Ductile Failure.

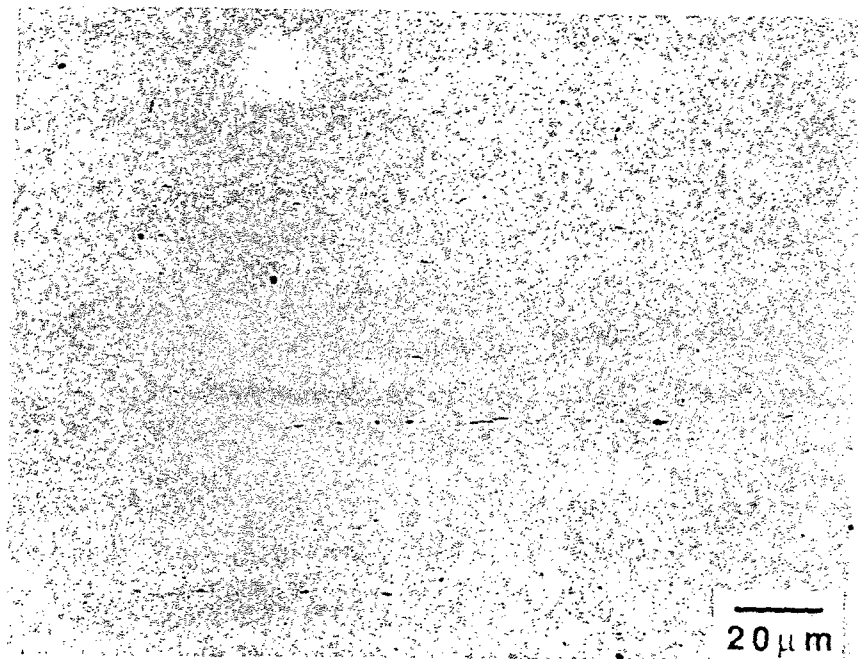


Figure 20. Longitudinal Cross Section of A106B Ferritic Steel (Heat No. DP2-F30, Specimen 30C-1) Showing Distribution of Inclusions.

  
200 μm

Figure 21. Longitudinal Cross Section of A533B Ferritic Steel (Heat No. A5401, Specimen W7-3) Showing Distribution of Inclusions.

### 3 References

---

1. P. L. Andresen, "Crack Initiation in CERT Tests on Type 304 Stainless Steel in Pure Water," *Corrosion Houston* **28**(1), pp. 153-58 (1982).
2. P. S. Maiya, "Prediction of Environmental and Strain-Rate Effects on the Stress Corrosion Cracking of Austenitic Stainless Steels," *J. Pressure Vessel Technol.*, **109**, pp. 116-123 (1987).
3. Bipin Pai, Purdue University at Calumet, Hammond, IN, to be published.
4. W. E. Ruther, W. K. Soppet, and T. F. Kassner, in *Environmentally Assisted Cracking in Light Water Reactors: Semiannual Report, April-September 1985*, NUREG/CR-4667 Vol.1, ANL-86-31, pp. 27-54 (June 1986).
5. A. J. Sedriks, *Corrosion of Stainless Steels*, John Wiley & Sons, New York 1979, pp. 145-150.
6. J. Hochmann and J. Bourrat, "Stress Corrosion in Austenitic Stainless Steel," *Mem. Sci. Rev. Met.*, **60**, 551-563 (1963).
7. W. E. Ruther, W. K. Soppet, and T. F. Kassner, in *Light-Water-Reactor Safety Research Programs: Quarterly Progress Report, January-March 1985*, NUREG/CR-4490 Vol. I, ANL-85-75 Vol. I, pp. 25-42 (March 1986).

8. W. E. Ruther, W. K. Soppet, and T. F. Kassner, in *Environmentally Assisted Cracking in Light Water Reactors: Semiannual Report, April-September 1985*, NUREG/CR-4667 Vol. I, ANL-86-31, pp. 27-41 (June 1986).
9. W. E. Ruther, W. K. Soppet, and T. F. Kassner, in *Environmentally Assisted Cracking in Light Water Reactors: Semiannual Report, October 1986-March 1987*, NUREG/CR-4667 Vol. IV, ANL-87-41, pp. 35-47 (December 1987).
10. W. E. Ruther, W. K. Soppet, and T. F. Kassner, in *Light-Water-Reactor Safety Materials Engineering Research Programs: Quarterly Progress Report, January-March 1984*, NUREG/CR-3998 Vol. I, ANL-84-60, pp. 38-49 (September 1984).
11. W. E. Ruther, W. K. Soppet, and T. F. Kassner, "Effect of Temperature and Ionic Impurities at Very Low Concentrations on Stress Corrosion Cracking of Type 304 Stainless Steel," *Corrosion/85*, Paper No. 102, Boston, MA, March 1985.
13. W. E. Ruther, W. K. Soppet, and T. F. Kassner, in *Environmentally Assisted Cracking in Light Water Reactors: Semiannual Report, October 1986-March 1987*, NUREG/CR-4667 Vol. IV, ANL-87-41, pp. 47-53 (December 1987).
14. V. N. Shah and P. E. MacDonald, *Residual Life Assessment of Major Light Water Reactor Components-Overview Vol. 1*, NUREG/CR-4731 EGG-2469 Vol. 1 (June 1987).
15. H. S. Mehta, S. Ranganath, and D. Weinstein, *Application of Environmental Fatigue Stress Rules to Carbon Steel Reactor Piping*, EPRI NP-4644M, Vols. 1 and 2 (July 1986).
16. D. A. Hale, S. A. Wilson, E. Kiss, A. J. Gianuzzi, *Low Cycle Fatigue Evaluation of Primary Piping Materials in a BWR Environment*, GEAP-20244 (September 1977).
17. J. Alexander et al., *Alternative Alloys for BWR Pipe Applications*, EPRI NP-2671-LD, pp. 5-43 to 5-55 (October 1982).
18. *Criteria of the ASME Boiler and Pressure Vessel Code for Design by Analysis in Sections III and VIII, Division 2*, American Society of Mechanical Engineers, New York 1969.
19. P. M. Scott, A. E. Truswell, and S. G. Bruce, "Corrosion Fatigue of Pressure Vessel Steels in PWR Environment-Influence of Steel Sulfur Content," *Corrosion Houston* **40**, 350-357 (1984).
20. J. H. Bulloch, "The Effect of Sulfide Distribution and Morphology on Environmentally Assisted Cracking Behavior of Ferritic Reactor Pressure Vessel Materials," in *Proceedings of the Third International Symposium on Environmental Degradation of Materials in Nuclear Power Systems-Water Reactors*, G. J. Theus and J. R. Weeks, eds., American Nuclear Society, LaGrange Park, IL, 1988.

INITIAL ASSESSMENT OF THE PROCESSES AND SIGNIFICANCE  
OF THERMAL AGING IN CAST STAINLESS STEELS\*

O. K. Chopra and H. M. Chung

Materials and Components Technology Division  
Argonne National Laboratory  
Argonne, Illinois 60439

Abstract

Charpy-impact and J-R curve data for thermally aged cast stainless steel are presented. The effects of material variables on the embrittlement of cast materials are evaluated. The chemical composition and ferrite morphology have a strong effect on the kinetics and extent of embrittlement. The procedure and correlations for predicting the impact strength and fracture toughness of cast components during reactor service are described.

1. Introduction

A program is being conducted to investigate the significance of low-temperature embrittlement of cast duplex stainless steels under LWR operating conditions and to evaluate possible remedies to the embrittlement problem for existing and future plants. The scope of the investigation includes the following goals: (1) characterize and correlate the microstructure of in-service reactor components and laboratory-aged material with loss of fracture toughness in order to establish the mechanism of aging and validate the simulation of in-reactor degradation by accelerated aging, (2) establish the effects of key compositional and metallurgical variables on the kinetics and extent of embrittlement, and (3) obtain fracture toughness data on long-term-aged materials to predict the degree of toughness loss suffered by cast stainless steel components during normal and extended service life of reactors.

Microstructural and mechanical properties data are being obtained on 19 experimental heats (static-cast keel blocks) and six commercial heats (centrifugally cast pipes and a static-cast pump impeller and pump casing ring) as well as reactor-aged material of CF-3, CF-8, and CF-8M grades of cast stainless steel. Six of the experimental heats are also in the form of 76-mm-thick slabs. The reactor-aged material is from the recirculating cover plate assembly of the KRB reactor, which was in service for ~12 yrs (~8 yr at service temperature of 284°C). Fractured impact test bars from five heats of aged cast stainless steel were obtained from Georg Fischer Co. (GF), Switzerland, for microstructural characterization. The materials are from a previous study of long-term aging behavior of cast stainless steel.<sup>1</sup> The data on chemical composition, ferrite content, hardness, ferrite morphology, and grain structure of the experimental and commercial heats have been reported earlier.<sup>2-6</sup> The chemical composition, hardness, and ferrite content and distribution of some of the cast materials are given in Table 1. Specimen

---

\*RSR FIN Budget No. A2243; RSR Contact: J. Muscara.

TABLE I. Product Form, Chemical Analysis, Hardness, and Ferrite Morphology of Various Heats of Cast Stainless Steel

| Heat | Grade | Product Form     | Size (mm)         | Composition (wt %) |       |      |       |       |       |      | Hardness<br>R <sub>B</sub> | Ferrite Content (%) |       | Ferrite Intercept<br>(μm) |
|------|-------|------------------|-------------------|--------------------|-------|------|-------|-------|-------|------|----------------------------|---------------------|-------|---------------------------|
|      |       |                  |                   | C                  | N     | Mn   | Si    | Ni    | Cr    | Mo   |                            | Calc.               | Meas. |                           |
| 59   | CF-8  | Keel B.          | 180 x 120 x 30-90 | 0.062              | 0.045 | 0.60 | 1.08  | 9.34  | 20.33 | 0.32 | 83.2                       | 8.8                 | 13.5  | 75                        |
| 61   | CF-8  |                  |                   | 0.054              | 0.080 | 0.65 | 1.01  | 8.86  | 20.65 | 0.32 | 85.2                       | 10.0                | 13.1  | 82                        |
| 60   | CF-8  |                  |                   | 0.064              | 0.058 | 0.67 | 0.95  | 8.34  | 21.05 | 0.31 | 86.7                       | 15.1                | 21.1  | 63                        |
| 47   | CF-3  |                  |                   | 0.018              | 0.028 | 0.60 | 1.06  | 10.63 | 19.81 | 0.59 | 79.6                       | 8.4                 | 16.3  | 68                        |
| 52   | CF-3  |                  |                   | 0.009              | 0.052 | 0.57 | 0.92  | 9.40  | 19.49 | 0.35 | 81.6                       | 10.3                | 13.5  | 69                        |
| 51   | CF-3  |                  |                   | 0.010              | 0.058 | 0.63 | 0.86  | 9.06  | 20.13 | 0.32 | 83.8                       | 14.2                | 18.0  | 52                        |
| 63   | CF-8M |                  |                   | 0.055              | 0.031 | 0.61 | 0.58  | 11.85 | 19.37 | 2.57 | 81.5                       | 6.4                 | 10.4  | 81                        |
| 65   | CF-8M |                  |                   | 0.049              | 0.064 | 0.50 | 0.48  | 9.63  | 20.78 | 2.57 | 89.9                       | 20.9                | 23.4  | 43                        |
| 64   | CF-8M | 0.038            | 0.038             | 0.60               | 0.63  | 9.40 | 20.76 | 2.46  | 89.7  | 28.9 | 28.4                       | 35                  |       |                           |
| P1   | CF-8  | Pipe             | 890 OD 63 wall    | 0.036              | 0.056 | 0.59 | 1.12  | 8.10  | 20.49 | 0.04 | 84.9                       | 17.7                | 24.1  | 90                        |
| P2   | CF-3  | Pipe             | 930 OD 73 wall    | 0.019              | 0.040 | 0.74 | 0.94  | 9.38  | 20.20 | 0.16 | 83.8                       | 12.4                | 15.6  | 69                        |
| I    | CF-3  | Impeller         | 930 OD 73 wall    | 0.019              | 0.032 | 0.47 | 0.83  | 8.65  | 20.14 | 0.45 | 81.0                       | 20.9                | 17.1  | 65                        |
| P4   | CF-8M | Pipe             | 580 OD 32 wall    | 0.040              | 0.151 | 1.07 | 1.02  | 10.00 | 19.64 | 2.05 | 83.1                       | 5.9                 | 10.4  | 182                       |
| 68   | CF-8  | Slab             | 610 x 610 x 76    | 0.060              | 0.062 | 0.62 | 1.03  | 8.04  | 20.53 | 0.28 | 84.6                       | 14.8                | 23.4  | 87                        |
| 69   | CF-3  | Slab             | 610 x 610 x 76    | 0.021              | 0.027 | 0.62 | 1.10  | 8.54  | 20.14 | 0.31 | 83.7                       | 21.4                | 23.6  | 35                        |
| 74   | CF-8M | Slab             | 610 x 610 x 76    | 0.064              | 0.048 | 0.54 | 0.73  | 9.03  | 19.11 | 2.51 | 85.8                       | 15.5                | 18.4  | 90                        |
| 75   | CF-8M | Slab             | 610 x 610 x 76    | 0.063              | 0.056 | 0.47 | 0.61  | 8.88  | 20.76 | 2.30 | 89.5                       | 23.7                | 27.8  | 73                        |
| KRB  | CF-8  | Pump Cover Plate |                   | 0.062              | 0.038 | 0.31 | 1.17  | 8.03  | 21.99 | 0.17 | -                          | 27.7                | -     | -                         |

blanks for Charpy-impact, tensile, and J-R curve tests are being aged at 290, 320, 350, 400, and 450°C for times up to 50,000 h. This paper presents an analysis of the mechanical property data for several heats of cast stainless steel aged for up to 30,000 h.

## 2. Charpy-Impact Tests

Impact tests were conducted on standard Charpy V-notch specimens machined from the aged and unaged materials according to ASTM specification E 23. A Dynatup Model 8000A drop-weight impact machine with an instrumented tup and data readout system was used for the tests. The data for room temperature impact energy were analyzed to determine the kinetics and extent of embrittlement. The Charpy-impact energy, KCV, is expressed as

$$KCV = K_m + \beta \{1 - \tanh [(P - \theta)/\alpha]\} , \quad (1)$$

where P is the aging parameter,  $K_m$  is the minimum impact energy reached after long-term aging,  $\beta$  is half the maximum decrease in impact energy (i.e., half the difference between initial and minimum impact energy),  $\theta$  is the log of the time to achieve  $\beta$  reduction in impact energy, and  $\alpha$  is a shape factor representing the time between the start and end of the decrease in impact energy. The time, t, at different aging temperatures is expressed by the Arrhenius relationship

$$t = 10^P \exp \left[ \frac{Q}{R} \left( \frac{1}{T} - \frac{1}{673} \right) \right] , \quad (2)$$

where Q is the activation energy, R the gas constant, and T the absolute temperature. The aging parameter, P, represents the degree of aging reached after  $10^P$  h at 400°C.

The values of the constants in Eqs. (1) and (2) for various heats of cast stainless steel are given in Table II and the best fit curves for some of the heats are shown in Figs. 1-3. The Charpy-impact data are plotted as a function of the aging parameter in Figs. 4-6. The actual time and temperature of aging are shown on five separate axes below the figures. The service time, in years, at the hot-leg temperature of LWRs is shown at the top of the figure.

The effect of aging temperature and time on the shifts in upper-shelf energy (USE) and transition temperature of the three grades of cast material are shown in Figs. 7 and 8. The impact energy data were analyzed with the hyperbolic tangent function given by

$$KCV = K_0 + B \{1 + \tanh [(T-C)/D]\} , \quad (3)$$

where  $K_0$  is the lower-shelf energy, T is the test temperature, B is half the distance between upper- and lower-shelf energy, C is the mid-shelf transition temperature in °C, and D is the half width of the transition region. The values of B, C, and D change with aging time whereas  $K_0$  is assumed to be unaffected by aging. The best-fit curves for the different heats and aging conditions are shown in Figs. 7 and 8 and the values of the constants are given in Table III.

TABLE II. Values of the Constants Representing the Kinetics of Embrittlement for Cast Stainless Steel

| Heat | Constants                  |                              |          |          | Activation Energy (kcal/mole) |
|------|----------------------------|------------------------------|----------|----------|-------------------------------|
|      | $K_m$ (J/cm <sup>2</sup> ) | $\beta$ (J/cm <sup>2</sup> ) | $\theta$ | $\alpha$ |                               |
| 47   | 163.6                      | 38.5                         | 2.89     | 1.11     | 21.90                         |
| 51   | 153.0                      | 31.0                         | 3.06     | 0.58     | 44.06                         |
| 56   | 100.4                      | 51.3                         | 4.22     | 1.05     | 56.05                         |
| 59   | 91.2                       | 63.5                         | 3.26     | 1.55     | 46.94                         |
| 60   | 64.7                       | 63.9                         | 2.82     | 0.63     | 47.51                         |
| 63   | 140.2                      | 58.4                         | 2.43     | 0.92     | 24.30                         |
| 64   | 53.3                       | 73.9                         | 2.47     | 0.66     | 34.06                         |
| 65   | 54.3                       | 78.9                         | 2.84     | 1.07     | 36.39                         |
| 66   | 94.9                       | 74.9                         | 2.72     | 1.73     | 30.23                         |

The results indicate that thermal aging decreases the impact energy and shifts the ductile-to-brittle transition curves to higher temperatures. However, different heats exhibit different degrees of embrittlement. In general, the low-carbon CF-3 grades of cast materials are the most resistant, and the molybdenum-containing CF-8M grades are least resistant to embrittlement. For all grades of cast materials, the extent of embrittlement increases with an increase in ferrite content. The significant results are summarized below.

(a) High-carbon CF-8 stainless steels exhibit low lower-shelf energy and high mid-shelf transition temperature relative to the low-carbon CF-3 steels. The lower impact energy for CF-8 steels is attributed to  $M_{23}C_6$  carbides which form at the ferrite/austenite phase boundaries during production heat treatment of the casting. The presence of large carbides weakens the phase boundaries, and the fracture mode in the lower-shelf or transition regime is predominantly phase boundary separation and cleavage of the ferrite.<sup>7,8</sup> In contrast, the CF-3 steels show a dimpled ductile failure at all test temperatures.

(b) The mid-shelf transition temperature of unaged CF-8M steels is lower than that of unaged CF-8 steels. The difference is due to the absence of phase boundary carbides in the as-cast material. Fracture by phase boundary separation is observed in only a few heats of CF-8M steel, depending on whether or not the material contained phase boundary carbides.

(c) Additional precipitation of phase boundary carbides and/or growth of existing carbides occurs in the high-carbon steels during aging at 450 or 400°C.<sup>8</sup> The fracture mode of Charpy-impact specimens aged at 450°C and tested at low temperatures, i.e., below the transition temperature, was predominantly phase boundary separation. Although phase boundary carbides are not present in the as-cast CF-8M material, they form during aging.

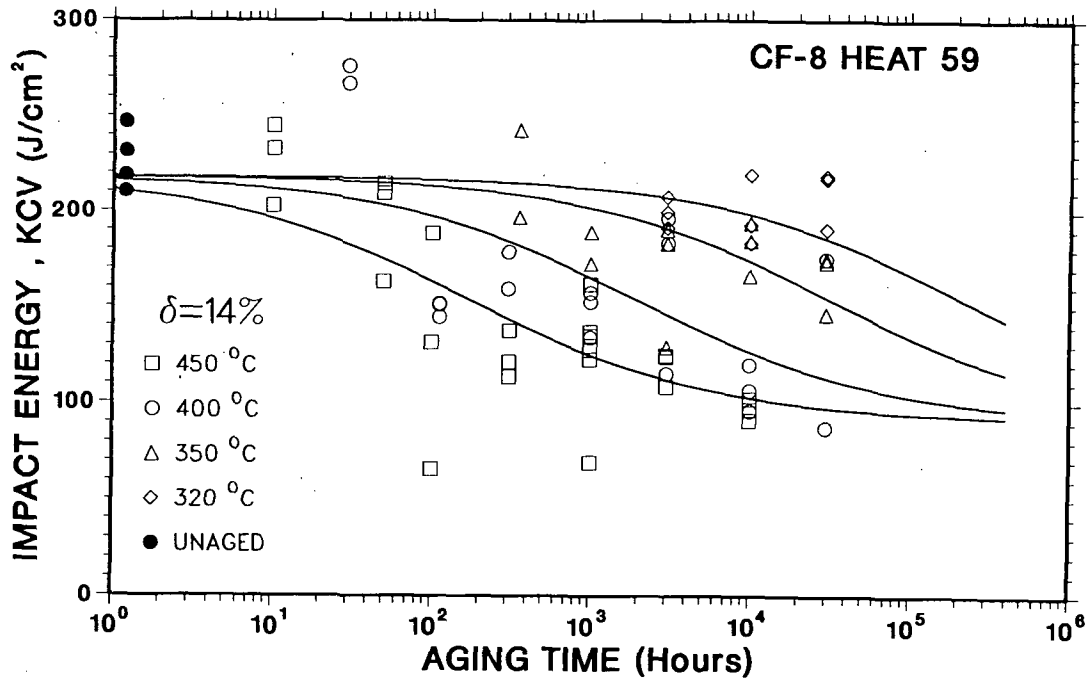
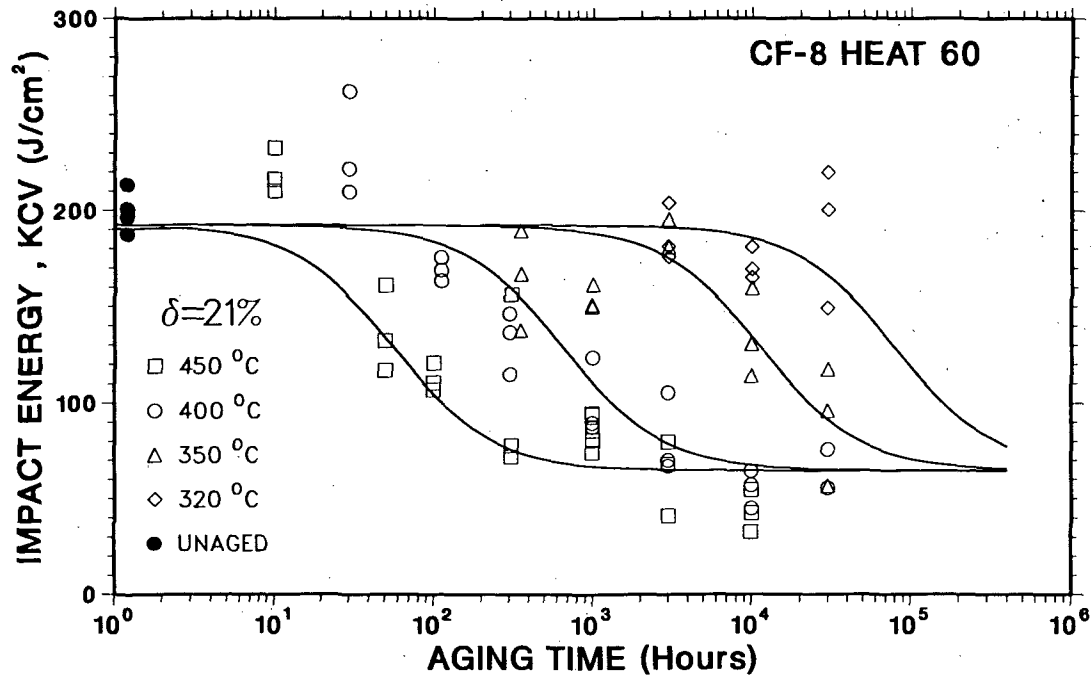


Fig. 1. Effect of Aging Time and Temperature on the Room Temperature Impact Energy of CF-8 Cast Stainless Steel.

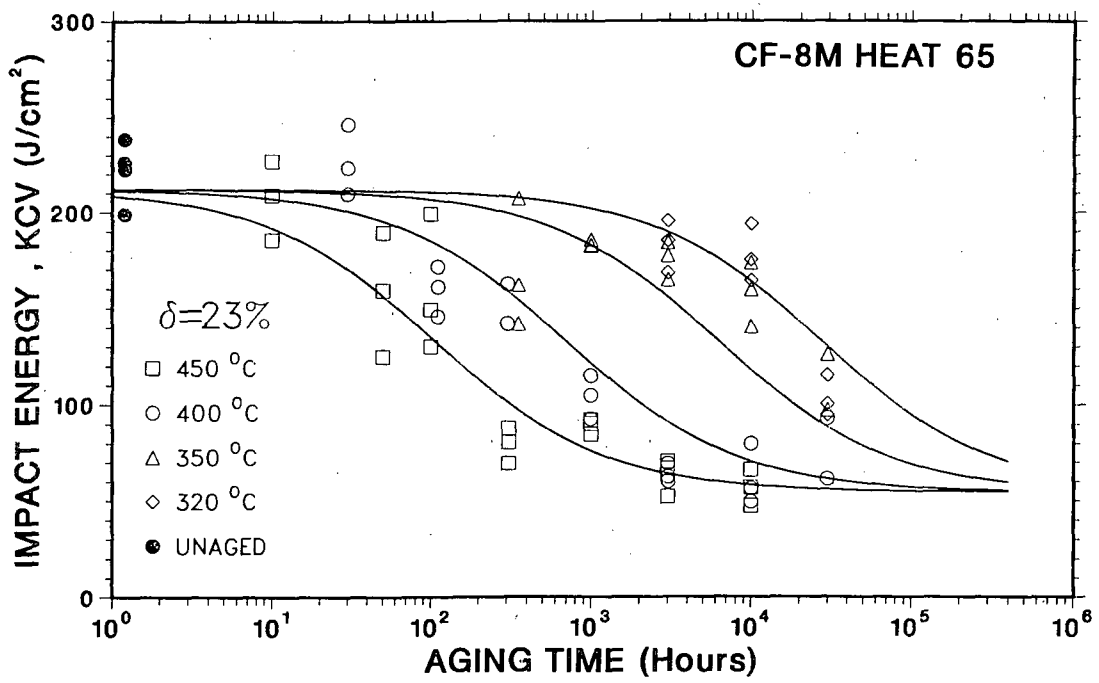
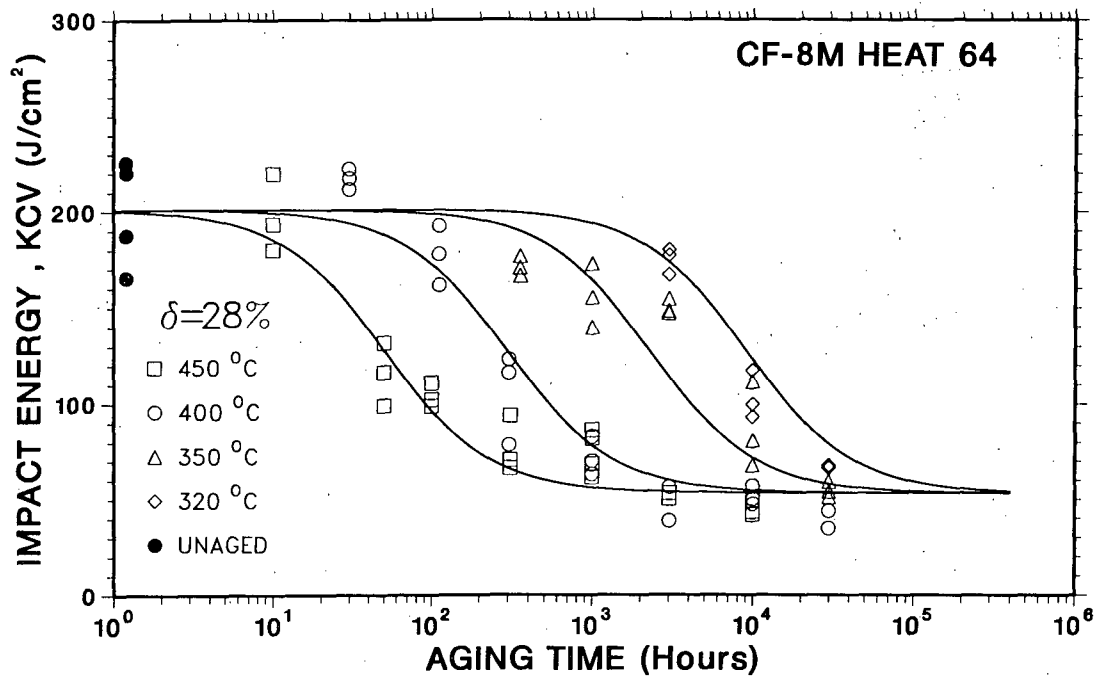


Fig. 2. Effect of Aging Time and Temperature on the Room Temperature Impact Energy of CF-8M Cast Stainless Steel.

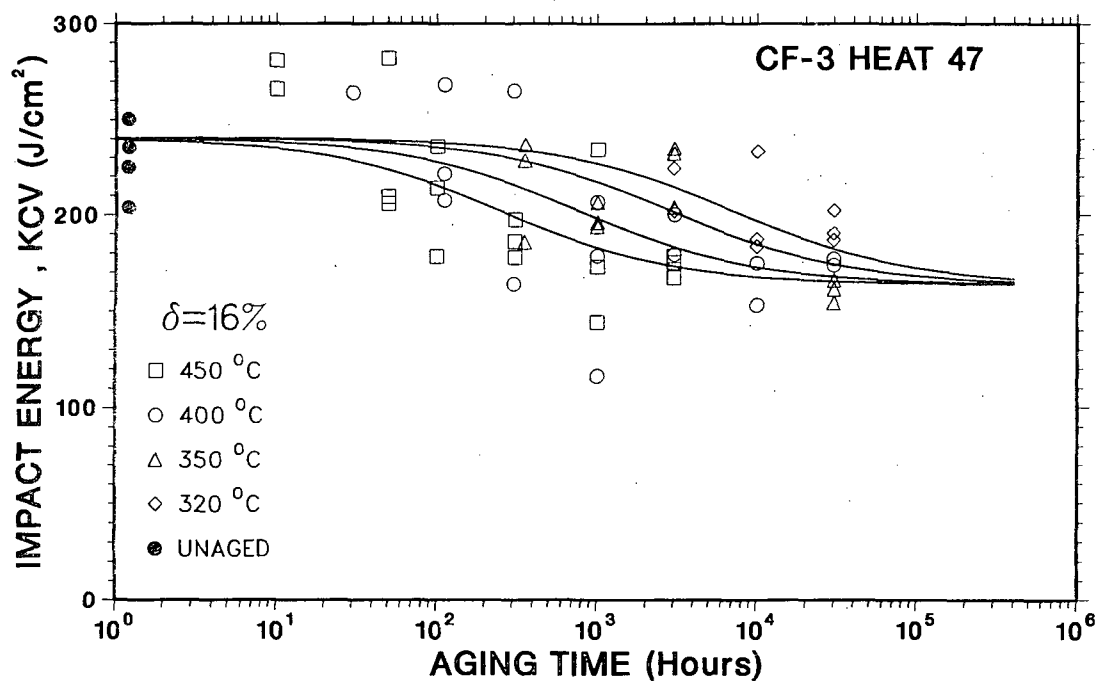
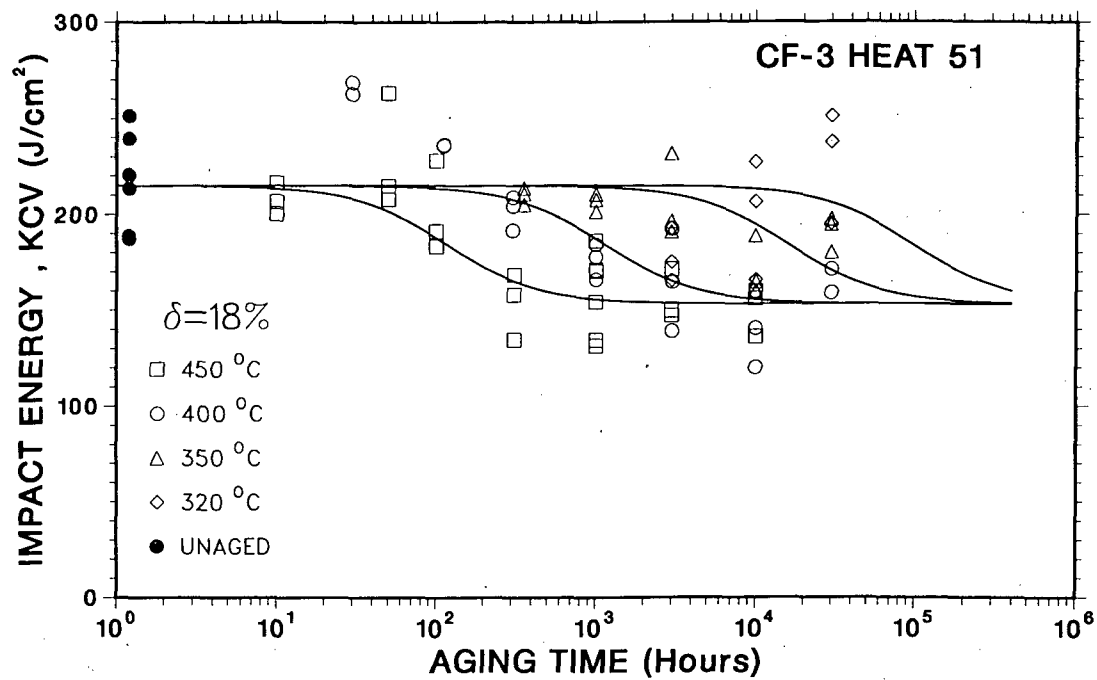


Fig. 3. Effect of Aging Time and Temperature on the Room Temperature Impact Energy of CF-3 Cas Stainless Steel.

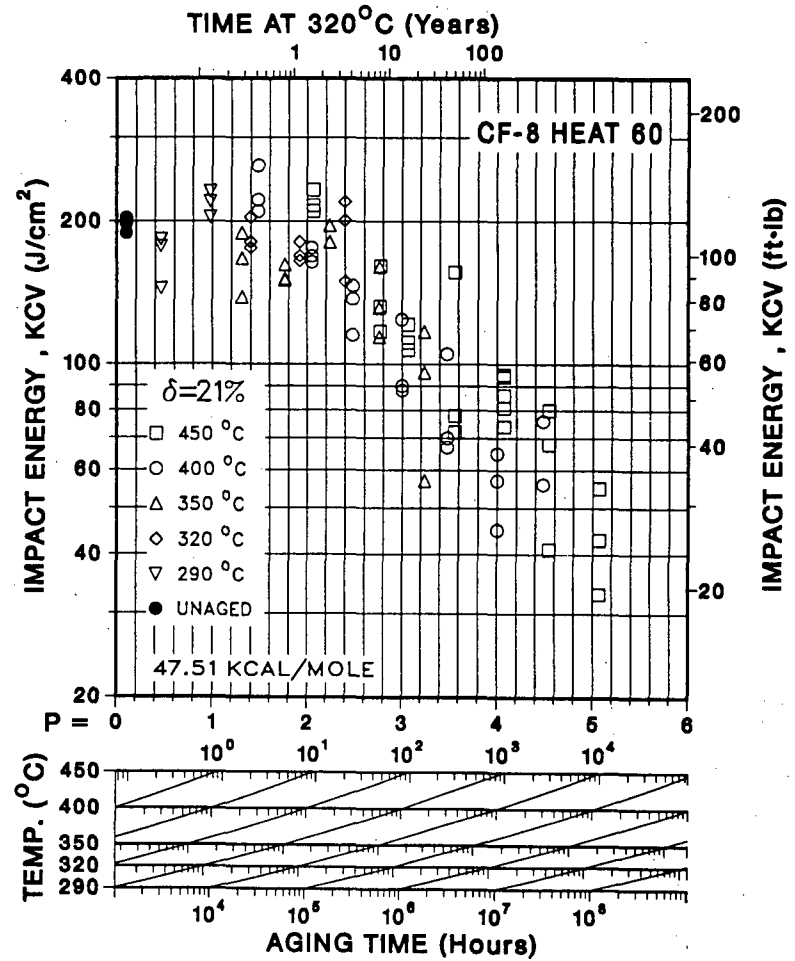
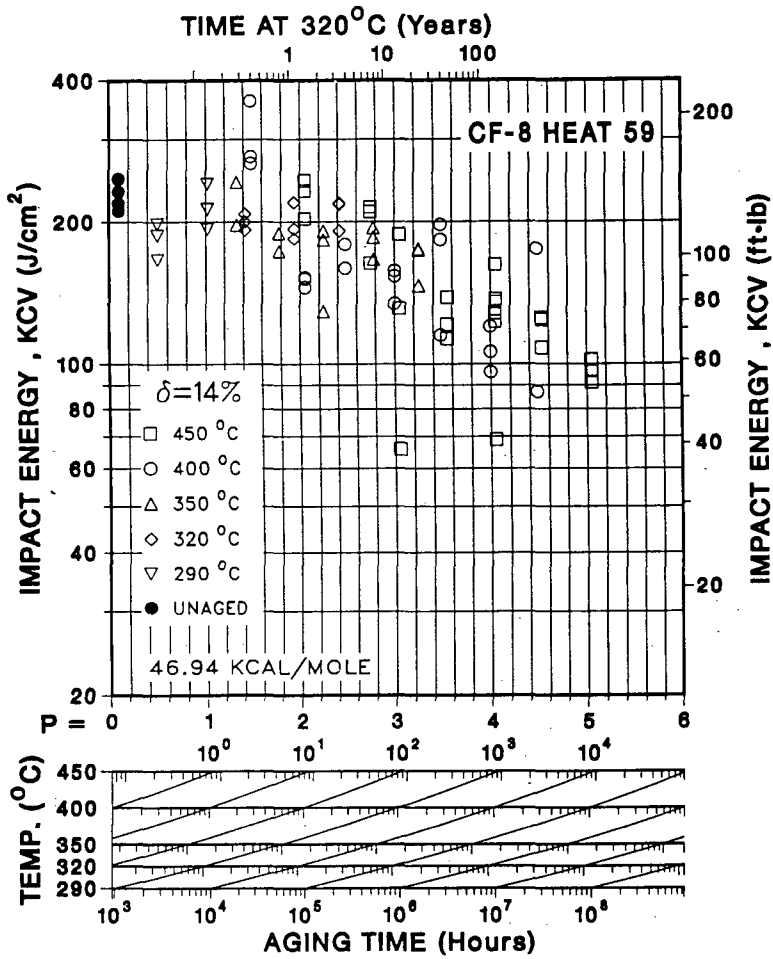


Fig. 4. Influence of Thermal Aging on the Room Temperature Impact Energy of CF-8 Cast Stainless Steel.

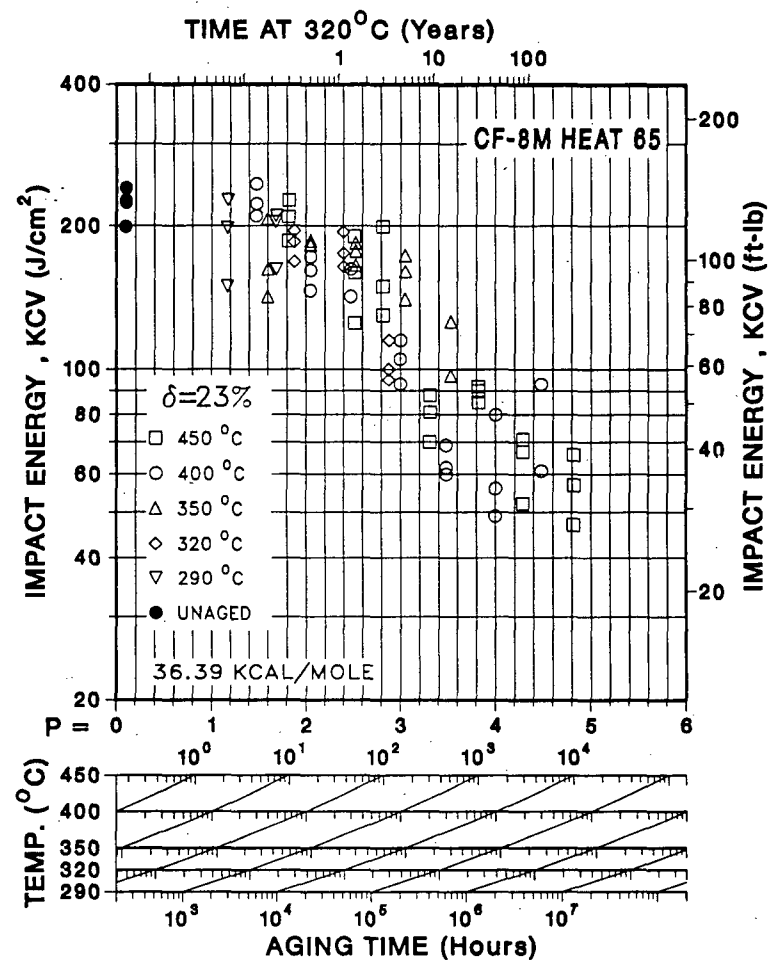
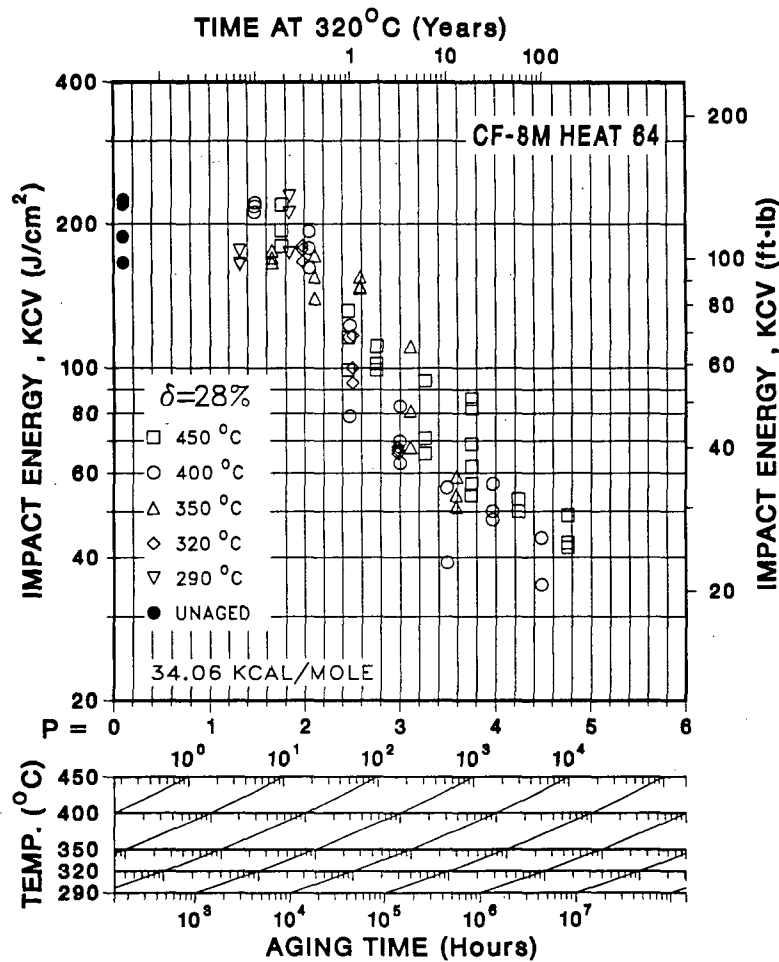


Fig. 5. Influence of Thermal Aging on the Room Temperature Impact Energy of CF-8M Cast Stainless Steel.

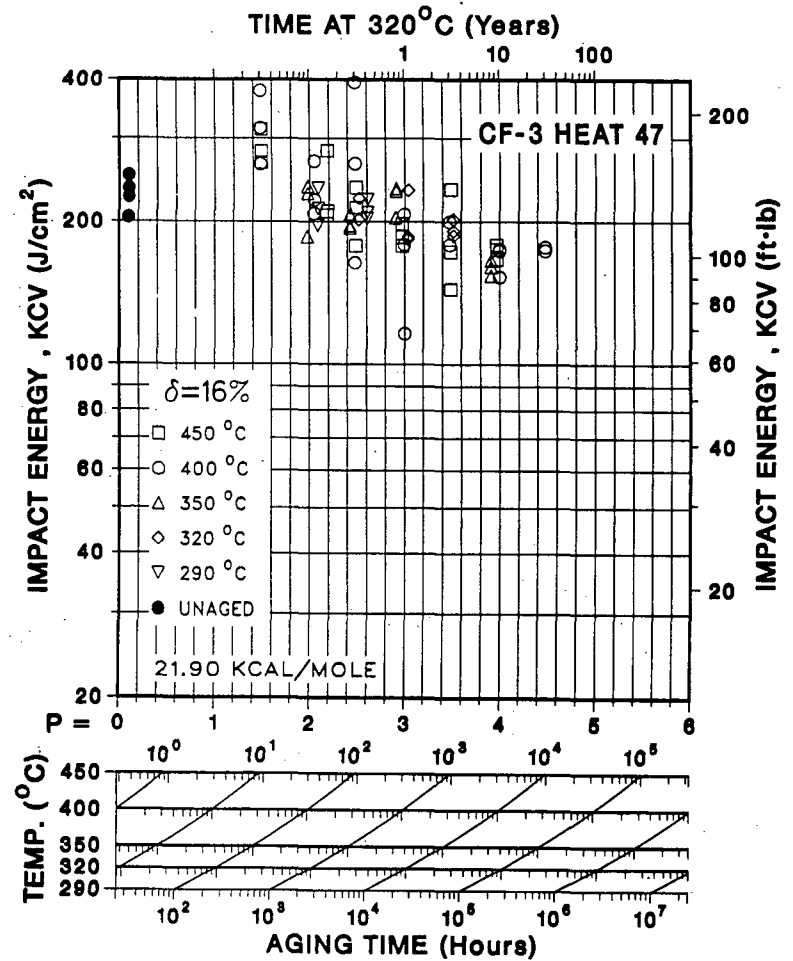
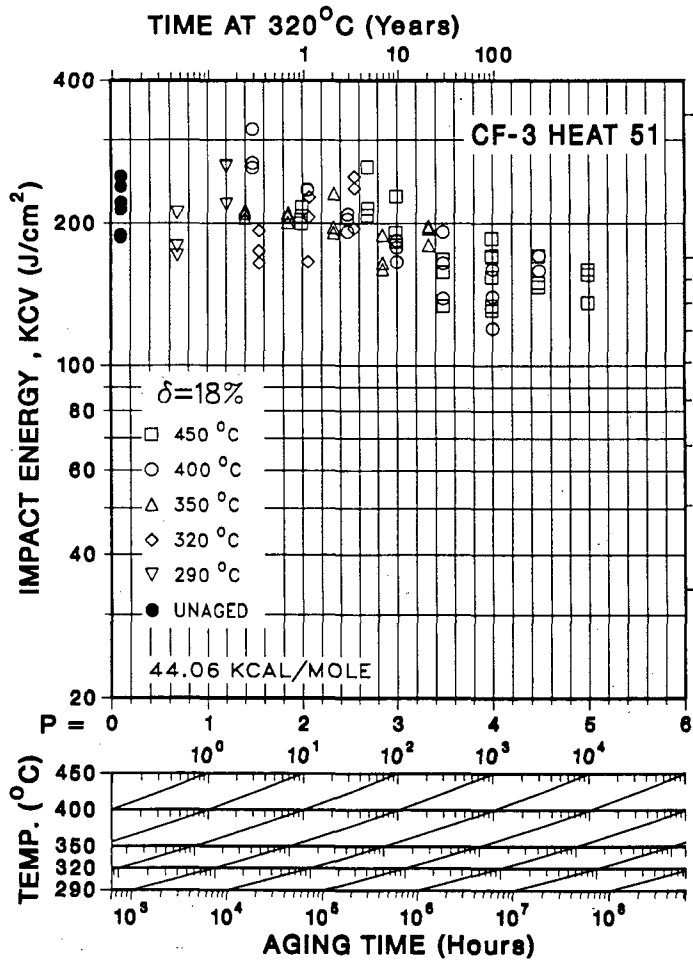


Fig. 6. Influence of Thermal Aging on the Room Temperature Impact Energy of CF-3 Cast Stainless Steel.

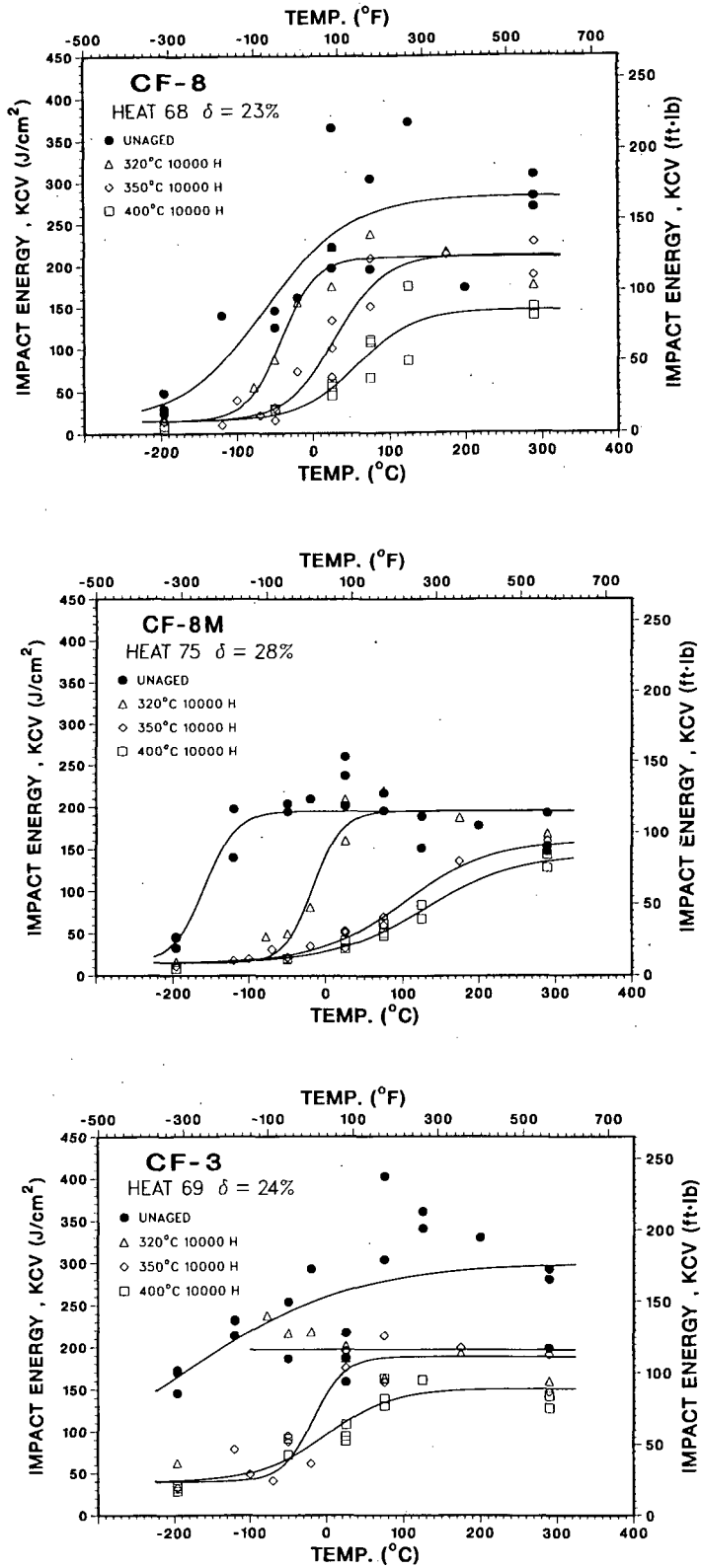


Fig. 7. Effect of Aging Temperature on the Ductile-to-Brittle Transition Curves for CF-8, CF-8M, and CF-3 Grades of Cast Stainless Steel.

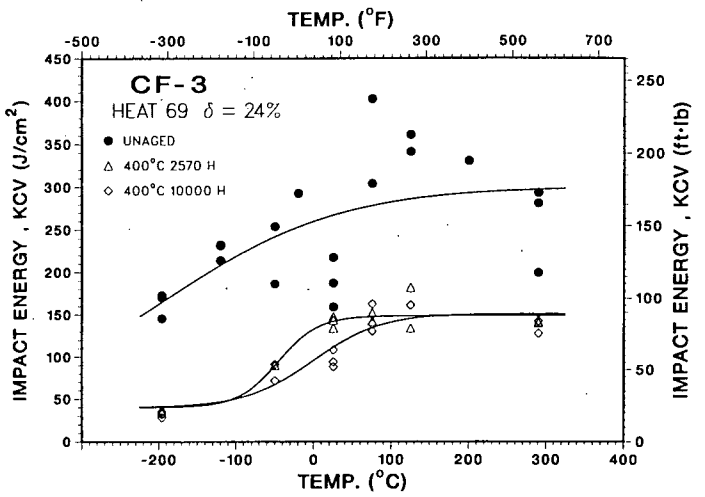
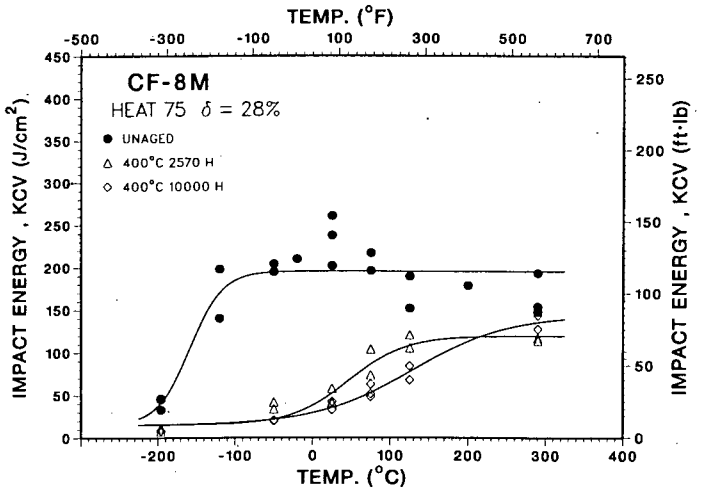
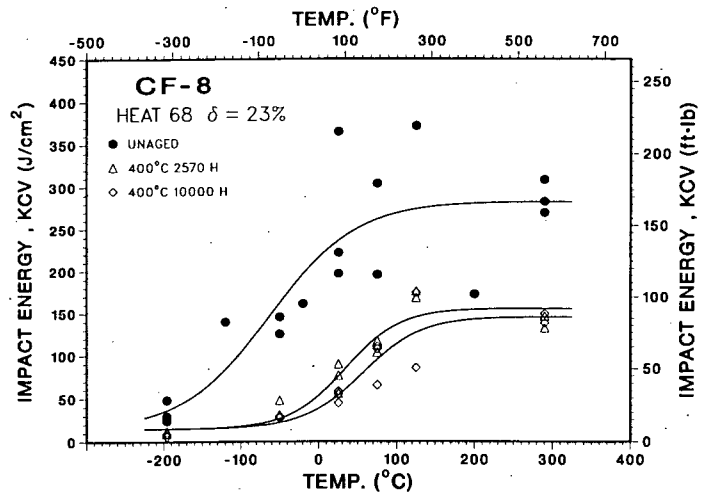


Fig. 8. Effect of Aging Time on the Ductile-to-Brittle Transition Curves for CF-8, CF-8M, and CF-3 Grades of Cast Stainless Steel.

TABLE III. Values of the Constants in Eq. (3) for Ductile-to-Brittle Transition Curve for Cast Stainless Steels

| Heat | Aging Condition |          | Constants                     |                           |           |           |
|------|-----------------|----------|-------------------------------|---------------------------|-----------|-----------|
|      | Temp. (°C)      | Time (h) | $K_0$<br>(J/cm <sup>2</sup> ) | B<br>(J/cm <sup>2</sup> ) | C<br>(°C) | D<br>(°C) |
| 69   | Unaged          | -        | 40                            | 130.34                    | -186.74   | 222.03    |
|      | 320             | 10,000   |                               | 78.56                     | -191.22   | 5.33      |
|      | 350             | 10,000   |                               | 74.32                     | -17.43    | 41.07     |
|      | 400             | 2,570    |                               | 54.29                     | -45.79    | 51.20     |
|      | 400             | 10,000   |                               | 55.53                     | -1.05     | 87.47     |
|      | 450             | 2,570    |                               | 48.49                     | -107.84   | 104.34    |
| I    | Unaged          | -        | 50                            | 62.71                     | -328.09   | 182.38    |
|      | 350             | 9,980    |                               | 48.96                     | -117.63   | 7.58      |
|      | 400             | 9,980    |                               | 47.04                     | -78.09    | 84.96     |
| 68   | Unaged          | -        | 15                            | 133.94                    | -61.47    | 110.48    |
|      | 320             | 10,000   |                               | 97.36                     | -40.89    | 45.97     |
|      | 350             | 10,000   |                               | 98.30                     | 29.64     | 64.12     |
|      | 400             | 2,570    |                               | 70.38                     | 34.65     | 70.83     |
|      | 400             | 10,000   |                               | 65.46                     | 57.54     | 75.62     |
|      | 450             | 2,570    |                               | 51.49                     | 34.28     | 41.04     |
| 74   | Unaged          | -        | 15                            | 89.54                     | -177.55   | 119.54    |
|      | 320             | 10,000   |                               | 91.07                     | -94.95    | 65.49     |
|      | 350             | 10,000   |                               | 71.40                     | -39.79    | 77.57     |
|      | 400             | 2,570    |                               | 61.55                     | -37.18    | 49.59     |
|      | 400             | 10,000   |                               | 65.58                     | 19.20     | 123.65    |
|      | 450             | 2,570    |                               | 39.19                     | -46.99    | 63.52     |
| 75   | Unaged          | -        | 15                            | 90.22                     | -158.27   | 42.33     |
|      | 320             | 10,000   |                               | 90.36                     | -16.13    | 37.90     |
|      | 350             | 10,000   |                               | 72.63                     | 102.56    | 113.50    |
|      | 400             | 2,570    |                               | 52.29                     | 47.19     | 73.84     |
|      | 400             | 10,000   |                               | 64.64                     | 129.44    | 123.04    |
|      | 450             | 2,570    |                               | 33.46                     | 16.80     | 93.04     |
| KRB  | 284             | 68,000   | 8                             | 119.70                    | 36.81     | 83.22     |
|      | Reannealed      |          |                               | 161.89                    | -16.54    | 87.20     |

(d) Phase boundary carbides have a strong influence on the transition temperature, but have little or no effect on USE, e.g., transition curves for heats 68 and 69 in Fig. 7. The presence of carbides at the phase boundaries leads to phase boundary separation and/or initiation of cleavage of the ferrite at low temperatures, while ductile fracture at high temperatures, by void formation and growth, is not influenced by the phase boundary carbides.

(e) The results suggest a "saturation effect" for USE after aging. For example, the values of USE decrease significantly after aging for 2600 h at 400°C and do not change for longer aging times, Fig. 8. This behavior is observed for all grades of material.

(f) Thermal aging leads to a decrease in the ferrite content of all grades of cast stainless steel, Fig. 9; particularly after aging at 450°C. The decrease in ferrite content is significantly greater for CF-8M steels than for the other grades. Microstructural studies<sup>9,10</sup> indicate that aging of cast stainless steels at temperatures below 500°C leads to the formation of chromium-rich  $\alpha'$  phase, nickel- and silicon-rich G phase, and  $\gamma_2$  austenite in the ferrite and  $M_{23}C_6$  carbides at the phase boundaries. The ferrite phase typically contains ~26% Cr and 5% Ni. The formation of  $\alpha'$  or carbides depletes the matrix of chromium, which leads to the transformation of ferrite to austenite. The larger decrease in the ferrite content for CF-8M steels and during 450°C aging may be attributed to the formation and/or growth of phase boundary carbides. The migration of phase boundaries is often observed in aged CF-8M steels.

(g) Charpy-impact data for CF-3 and some CF-8M steels indicate an inversion in impact energy at temperatures in the transition region, i.e., the impact energy of samples aged at 450°C is higher than that of samples aged for equivalent times at 400 or 350°C. For example, the mid-shelf transition temperature (constant C in Table III) for heats 69 and 75, aged for 2570 h at 450°C, is lower than that after aging at 400°C for the same time. Furthermore, the room temperature impact energies of heats 52, 47, 51, and P2, aged for 10,000 h at 450°C, were 10 to 15% higher than after aging for 10,000 h at 400°C. This behavior was observed for cast materials which contain no phase boundary carbides and have a very low mid-shelf transition temperature in the unaged condition, i.e., for most of the low-carbon CF-3 grades and some CF-8M grades of cast stainless steel.

(h) The kinetics of embrittlement vary significantly for the various heats of cast stainless steel; the activation energies range between 20 and 56 kcal/mole. The activation energy is lower for the molybdenum-containing CF-8M steels or for steels with higher nickel content. The values obtained for activation energy in the present study are significantly higher than those observed in the GF study,<sup>1</sup> e.g., activation energies between 17 and 25 kcal/mole.

(i) The shape of the impact energy vs aging time curves also varies considerably for the various heats, e.g., shape factor  $\alpha$  varies between ~0.6 and 1.7.

These results indicate that the kinetics and extent of embrittlement are controlled by several mechanisms that depend on material parameters and aging temperature. Data obtained at 450°C aging are not representative of reactor operating conditions; materials aged at 450°C show significant precipitation and growth of phase boundary carbides and a large decrease in ferrite content of the material. Consequently, extrapolation of the 450°C data to predict the extent of embrittlement at reactor temperatures may not be valid.

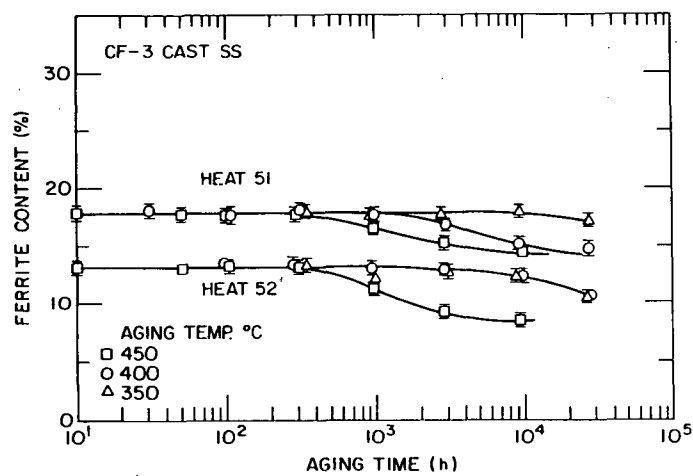
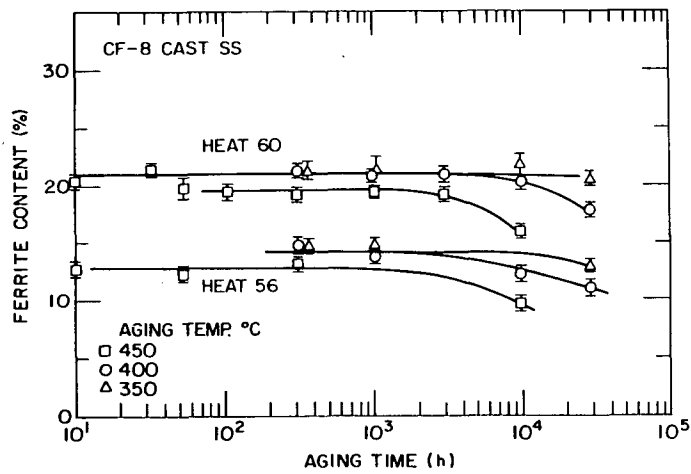
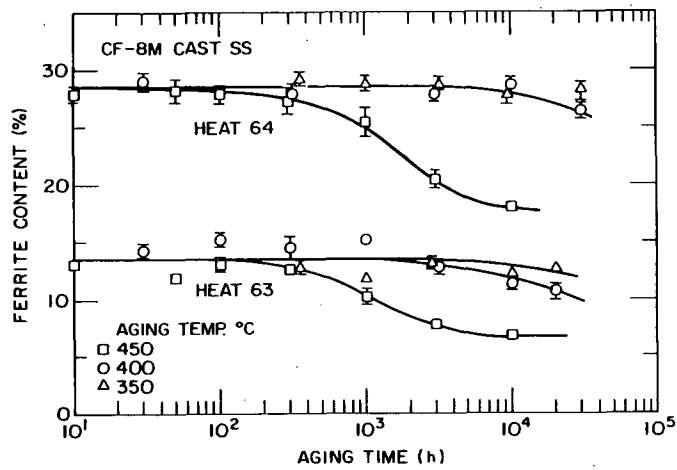


Fig. 9. Decrease in Ferrite Content of Thermally Aged CF-8M, CF-8, and CF-3 Cast Stainless Steel.

The results also indicate that the published correlations for estimating the kinetics of embrittlement are not accurate. The activation energy for the process of embrittlement is currently described as a function of the chemical composition of the cast material,<sup>11</sup> and is given by the equation

$$Q(\text{kcal/mole}) = -43.64 + 4.76(\% \text{ Si}) + 2.65(\% \text{ Cr}) + 3.44(\% \text{ Mo}). \quad (3)$$

The activation energy from Eq. (3) ranges between 15 and 25 kcal/mole for the various grades of cast stainless steels. These values are significantly lower than those observed in the present study. Consequently, the predictions based on Eq. (3) will be conservative for most heats of cast stainless steel. For example, extrapolation of a 40 yr reactor lifetime at 320°C, based on an activation energy of 20 or 45 kcal/mole, is equivalent to 47,000 or 3700 h at 400°C, respectively. Figures 5 and 6 show that for the CF-8 and CF-3 steels, the minimum impact energy is not reached during the reactor lifetime. However, Eq. (3) may be nonconservative for some heats of cast stainless steel since it does not include the effects of other elements, such as nickel, carbon, and nitrogen, on the kinetics of embrittlement.

### 3. Kinetics of Embrittlement

The kinetics data from FRA,<sup>11</sup> GF,<sup>1</sup> and the present study were analyzed to develop a correlation between the activation energy for embrittlement and the chemical composition of the cast material. Initially, all major elements and carbon and nitrogen were included in the correlation. Elements with poor coefficients of correlation were then excluded. The analyses yielded two separate correlations: one for the Argonne and FRA data, given by

$$Q(\text{kcal/mole}) = 21.64 + 2.30 \text{ Cr} - 1.94 \text{ Ni} - 1.8 \text{ Mo} \\ + 4.92 \text{ Si} - 29.40 \text{ Mn} + 75.93 \text{ N} \quad (4)$$

and the other for the GF data, given by

$$Q(\text{kcal/mole}) = -15.93 + 1.65 \text{ Cr} - 1.30 \text{ Ni} + 1.93 \text{ Mo} \\ + 4.10 \text{ Si} + 10.54 \text{ Mn} + 71.00 \text{ N}. \quad (5)$$

The observed and predicted activation energies for the two data sets are plotted in Fig. 10. The coefficients for chromium, nickel, silicon, and nitrogen show the same behavior in the two correlations, however, the constants and the coefficients for molybdenum and manganese have opposite sign.

Equation (4) represents a wide range of material composition and was used to predict the activation energy for embrittlement of two heats of cast material not used in obtaining the correlation. The impact energies for the heats are plotted as a function of the aging parameter in Fig. 11. The data obtained for different aging temperatures follow a single curve. The results indicate that for both heats, the minimum values of impact energy will be reached within the reactor lifetime of 40 yr.

The different effects of constituent elements in the two correlations are not clearly understood. In binary Fe-Cr alloys, an increase in chromium content is known to decrease the time for  $\alpha'$  formation.<sup>12</sup> Nitrogen also enhances chromium clustering.<sup>13,14</sup> The positive sign of the coefficients for

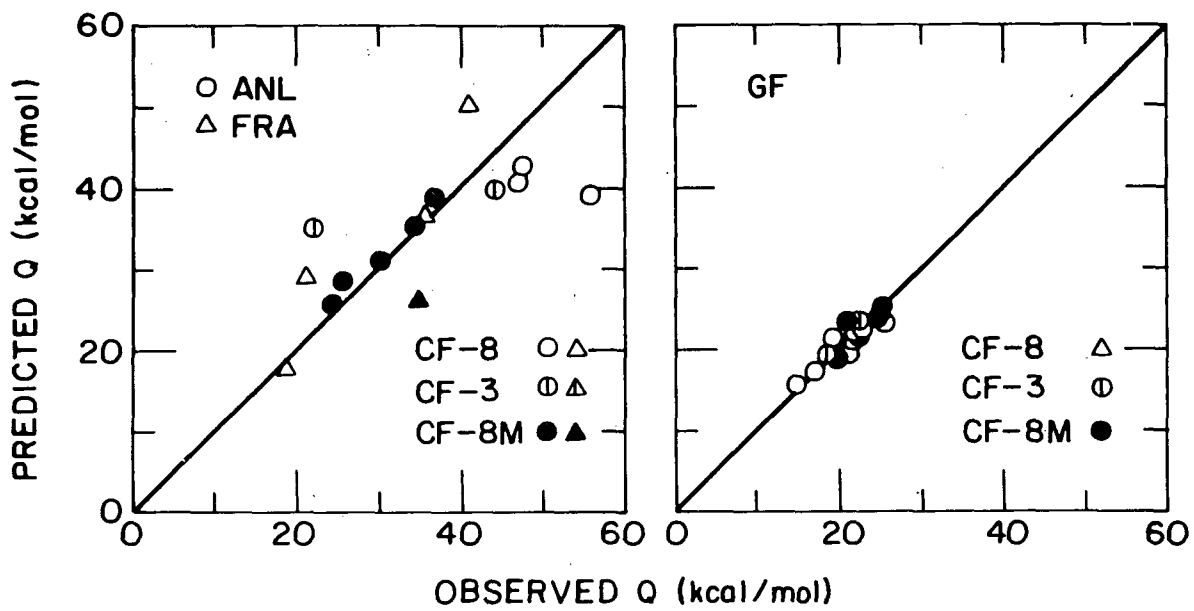


Fig. 10. Observed and Predicted Activation Energy for Low-Temperature Embrittlement of Cast Stainless Steel. ANL: Argonne National Laboratory, FRA: Framatome (Ref. 11), and GF: Georg Fischer Co. (Ref. 1).

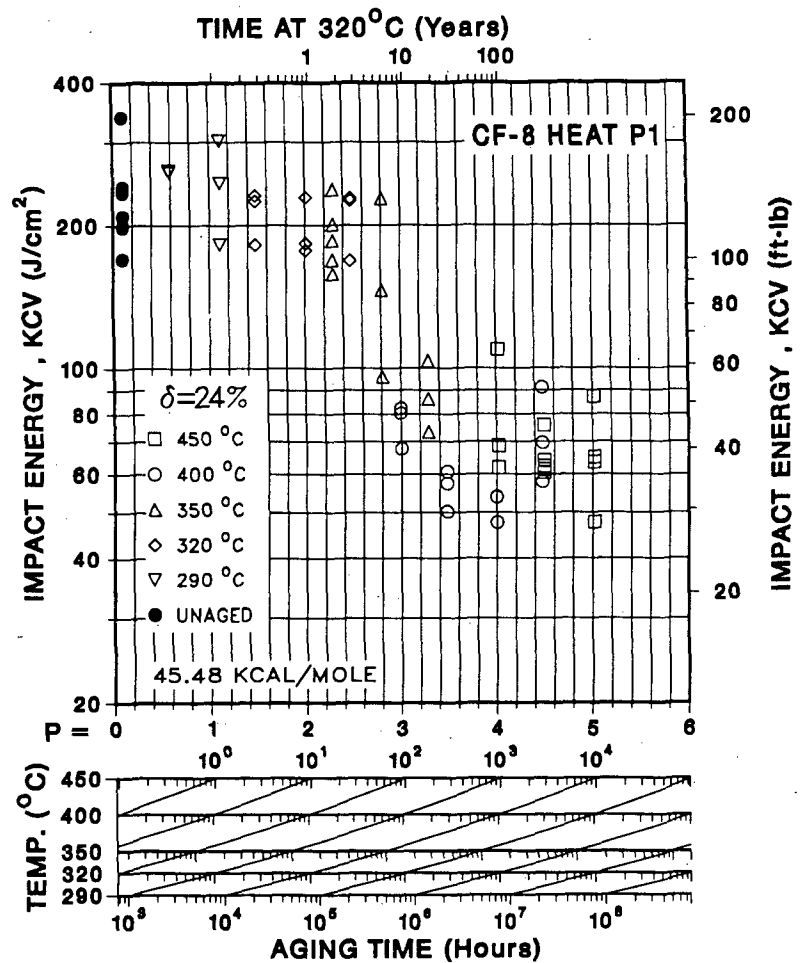
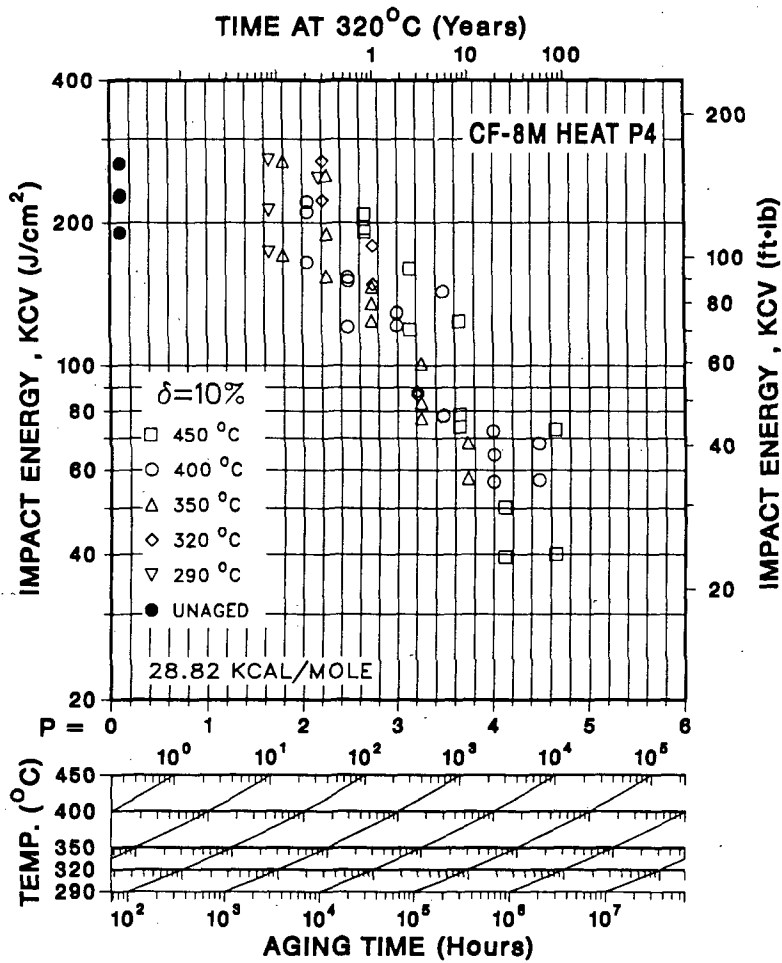


Fig. 11. Impact Energy vs Aging Parameter Curves Based on Calculated Activation Energy for CF-8M and CF-8 Cast Stainless Steel.

chromium and nitrogen indicates that such effects are greater at high temperatures. These elements also influence the precipitation of carbides, nitrides, or carbonitrides. Precipitation of carbides or nitrides occurs primarily at 450 or 400°C and is extremely slow at lower temperatures. Consequently, the formation of phase boundary carbides would increase the activation energy for embrittlement.

The influence of other elements, most likely, is on the precipitation of G phase, a multicomponent phase consisting of nickel, silicon, chromium, molybdenum, iron, and some manganese and carbon. Microstructural studies<sup>9,10</sup> indicate that G-phase precipitation decreases the activation energy for embrittlement. However, the effect of constituent elements on G-phase precipitation is not known. Limited data<sup>15,16</sup> suggest that the composition of G phase may change with aging temperature. For example, the G phase observed in two similar heats of CF-8M steels aged at 400 and 450°C consisted of ~25% nickel and ~14% molybdenum, but the silicon and chromium contents were 14 and 25% at 450°C and 28 and 12% at 400°C. The effect of material composition on G-phase precipitation must be established to better understand and develop a single correlation for the kinetics of embrittlement.

#### 4. Extent of Embrittlement

The Charpy-impact data were analyzed to obtain a correlation between the extent of embrittlement (i.e., minimum impact energy,  $K_m$ , achieved after long-term aging) and material variables. The minimum impact energy is plotted in Fig. 12 as a function of a material parameter consisting of the measured ferrite content ( $\delta_m$  in %); chromium, molybdenum, silicon, carbon, and nitrogen content (in %) of the steel; and the mean ferrite spacing ( $\bar{\lambda}$  in  $\mu\text{m}$ ). The results for all heats for which the material variables were known are shown in the figure. The data show a good correlation with the material parameter. The results indicate that the impact energy will be less than 50 J/cm<sup>2</sup> (~30 ft·lb) for those cast stainless steels for which the material parameter is greater than ~60.

For cast stainless steels containing >10% ferrite, the mean ferrite spacing is in the range of 40 to 200  $\mu\text{m}$ ; Cr + Mo + Si concentration is ~22% for CF-8 or CF-3 and ~24% for CF-8M; and nitrogen content is typically 0.04%. Thus, for cast materials with 0.06% C and 100  $\mu\text{m}$  ferrite spacing, the impact energy will be below 50 J/cm<sup>2</sup> when the ferrite content is above 20%. Cast materials with 10 or 15% ferrite can also reach very low impact strength when the ferrite spacing or the nitrogen content is high.

For all cast stainless steels in service, the variables in the material parameter are readily available. The composition is known, ferrite content can be calculated from the composition or measured with a ferrite scope, and the ferrite spacing can be determined by a surface replica technique. Thus, Fig. 12 can be used to estimate the extent of embrittlement for any cast stainless steel component.

#### 5. J-R Curves

The results of the J-R curve tests<sup>17</sup> indicate that thermal aging decreases  $J_{IC}$  and the tearing modulus of cast stainless steel at room temperature as well as at 290°C. The reduction in toughness is greater for

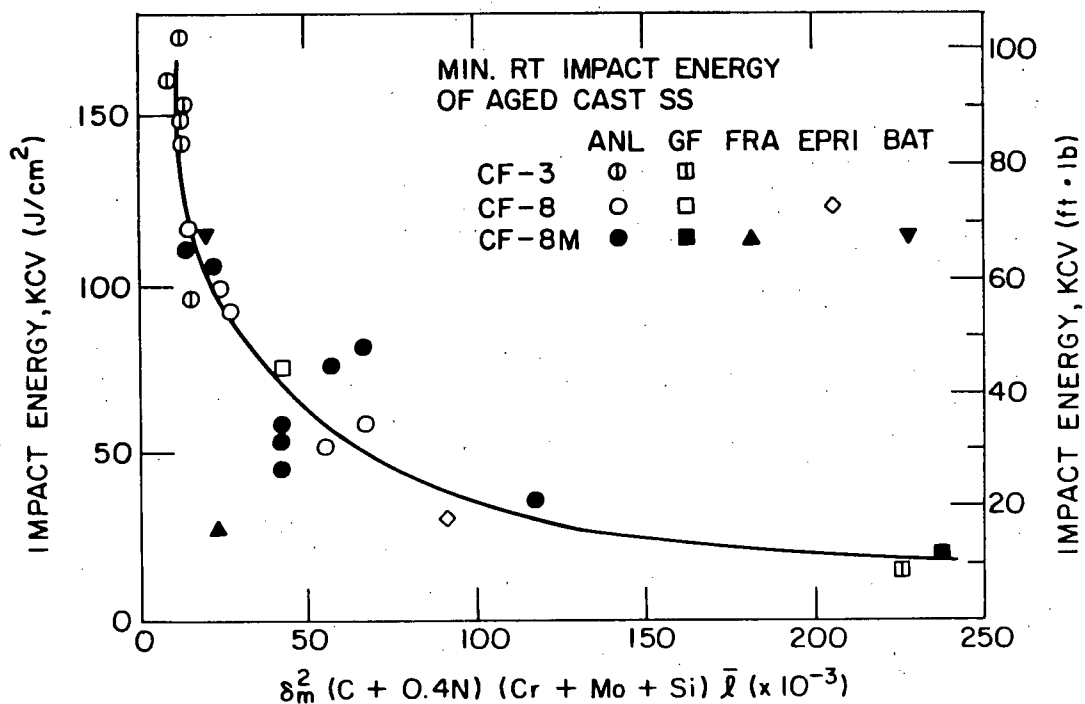


Fig. 12. Correlation between Minimum Room Temperature Impact Energy and Material Parameter for Aged Cast Stainless Steel. EPRI: Electric Power Research Institute (Ref. 17), BAT: Battelle Columbus Division.

materials aged at 400 or 450°C than for those aged at 350°C for similar lengths of time. The fracture toughness of the high-carbon CF-8 steels is lower than for the low-carbon CF-3 steels. After aging for 9980 h at 400°C, the  $J_{IC}$  value for heat P1 (CF-8 grade) at room temperature decreased from 2171 to 254 kJ/m<sup>2</sup>, and the tearing modulus decreased from 546 to 200.

The fracture toughness results are consistent with the Charpy-impact data, i.e., unaged and aged materials that show low impact strength also exhibit lower fracture toughness. The  $J_{IC}$  values and Charpy V-notch impact energies obtained at room temperature and at 290°C are plotted in Fig. 13. Results from the studies at Westinghouse (WH),<sup>19</sup> Electric Power Research Institute (EPRI),<sup>18</sup> and Framatome (FRA)<sup>11</sup> are also shown. The dashed lines represent the lower-bound values. Thermal aging decreases the  $J_{IC}$  values, and the relative reductions in  $J_{IC}$  are similar to the relative decreases in impact energy. Figure 12 shows that the minimum impact energy can be as low as 20 J/cm<sup>2</sup> for some heats of cast stainless steel. The corresponding  $J_{IC}$  value from the lower band curve in Fig. 13a would be ~40 kJ/m<sup>2</sup>. Thus, the correlations in Figs. 12 and 13 can be used to predict the minimum  $J_{IC}$  values for any heat of cast stainless steel aged for a long time.

The tearing modulus also decreases with thermal aging. The tearing modulus and  $J_{IC}$  value for various heats and aging conditions are shown in Fig. 14. At both test temperatures, the tearing modulus decreases with a

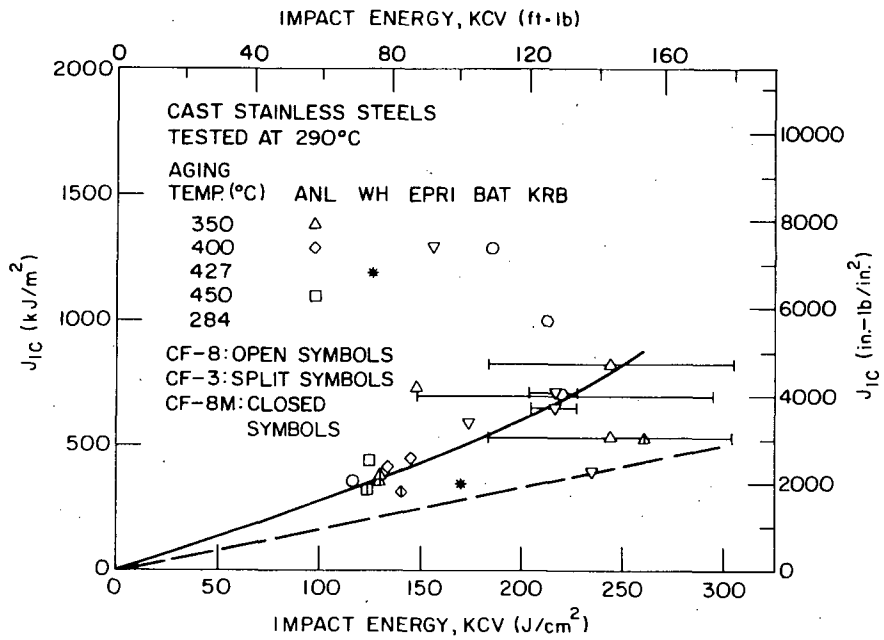
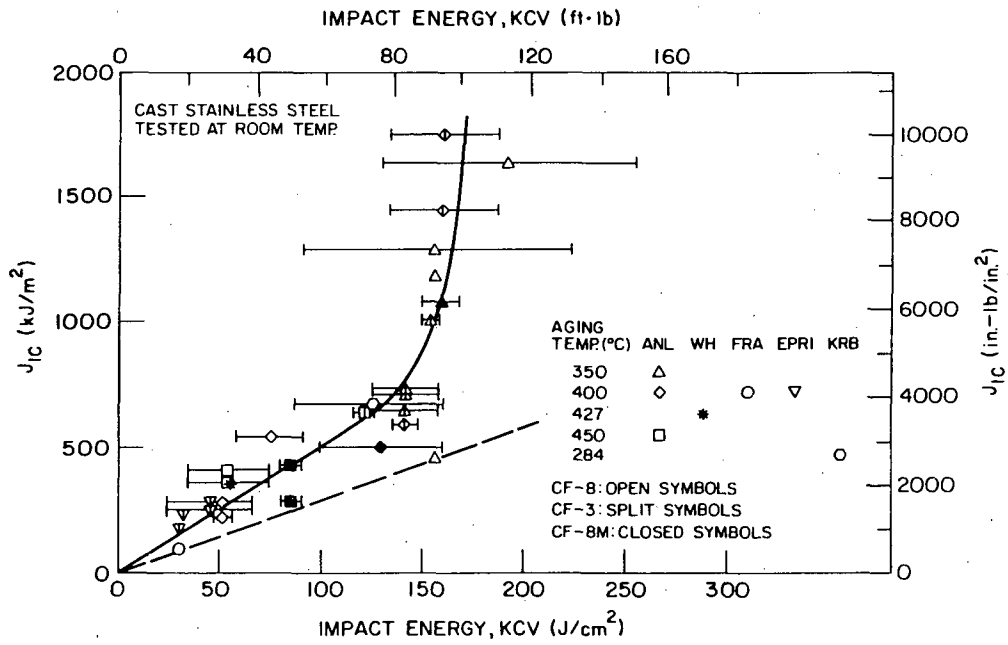


Fig. 13. Correlation between  $J_{IC}$  and Impact Energy for Aged Cast Stainless Steel Tested at Room Temperature and at 290°C. WH: Westinghouse (Ref. 19).

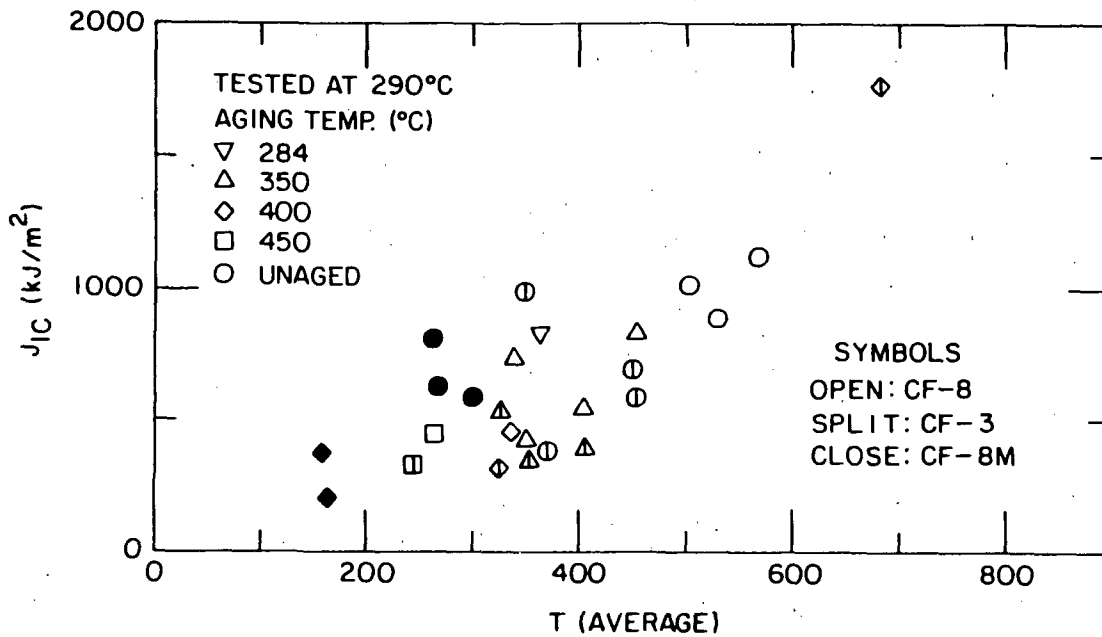
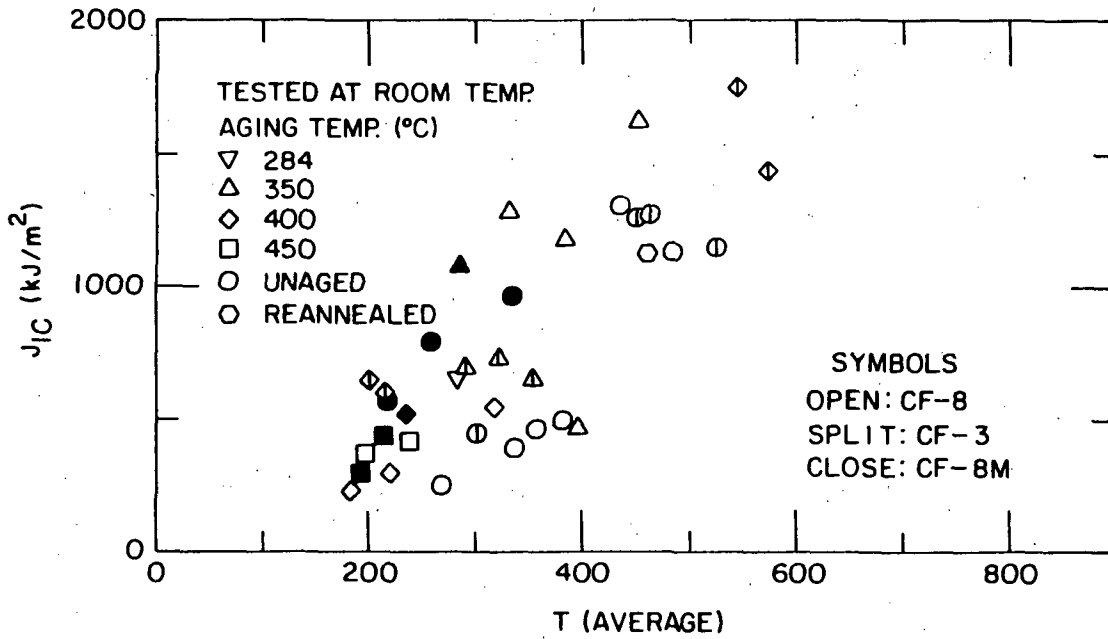


Fig. 14. Correlation between  $J_{IC}$  and Tearing Modulus for Cast Stainless Steel Tested at Room Temperature and 290°C.

decrease in  $J_{IC}$ . Fracture toughness data for other aging conditions as well as other heats are being obtained to better establish the correlation between  $J_{IC}$ , tearing modulus, and Charpy-impact energy.

#### 6. Preliminary Assessment of Embrittlement under LWR Conditions

The embrittlement of any cast stainless steel component during reactor service can be estimated from Fig. 12 and Eqs. (1), (2), and (4). The material information needed for the assessment is the chemical composition, ferrite content and spacing, and initial impact strength of the cast material. When the material parameter is known, the minimum room temperature impact energy,  $K_m$ , is determined from Fig. 12. The constant  $\beta$  is obtained from the difference between the initial and minimum values of impact energy, and the activation energy,  $Q$ , is determined from Eq. (4). The average values of the constants  $\theta$  and  $\alpha$  in Eq. (1) are 2.8 and 1.0, respectively. The decrease in impact energy during service at reactor temperature is determined from Eqs. (1) and (2).

Examples of the predicted embrittlement behavior of heats susceptible to embrittlement (A and C) and typical heats (B and D) of CF-8M and CF-8 cast stainless steel are shown in Fig. 15. The theoretical chemical composition and the ferrite content and spacing of the heats are given in Table IV. All compositions are within ASTM specifications. The compositions of heats A and C are selected to give high ferrite content and fast kinetics of embrittlement i.e., low activation energy. The mean ferrite spacing for most cast stainless steels with >10% ferrite varies between 40 and 200  $\mu\text{m}$ . A large value of the ferrite spacing is selected for heats A and C to get a conservative estimate of the extent of embrittlement.

The results show that the impact energy of heats A and C will decrease to below 40  $\text{J}/\text{cm}^2$  (~20 ft·lb) after 4 or 5 yr of service at 320°C. Heats B and D, with lower ferrite content (15%), exhibit much less embrittlement, i.e., the impact energy will not decrease below 90  $\text{J}/\text{cm}^2$  even after long-time service. The kinetics of embrittlement are also slower for these heats; the activation energy is >40 kcal/mole, compared to 18 kcal/mole for heats A and C. The results also show that the minimum impact energy is the important factor in estimating the embrittlement behavior. Slow kinetics of embrittlement, i.e., high activation energy, delay the decrease in impact strength, but the material reaches the lowest value of impact strength near the end of reactor lifetime. This behavior is seen for heat E which has the same material parameters as heat C, but the activation energy was arbitrarily assumed to be 45 kcal/mole rather than the calculated value of 18 kcal/mole to illustrate the effect of slower kinetics. Even with very slow kinetics, the impact energy decreases to ~40  $\text{J}/\text{cm}^2$  after 40 yr of service.

The decrease in fracture toughness, i.e., values of  $J_{IC}$  and tearing modulus, during reactor service can be estimated from the room temperature impact energy and Figs. 13 and 14. For example, an impact energy of 25  $\text{J}/\text{cm}^2$  corresponds to a lower bound value of 70  $\text{kJ}/\text{m}^2$  for  $J_{IC}$ . The tearing modulus can be estimated from Fig. 14; however, the correlations between  $J_{IC}$  and tearing modulus are not well established at present.

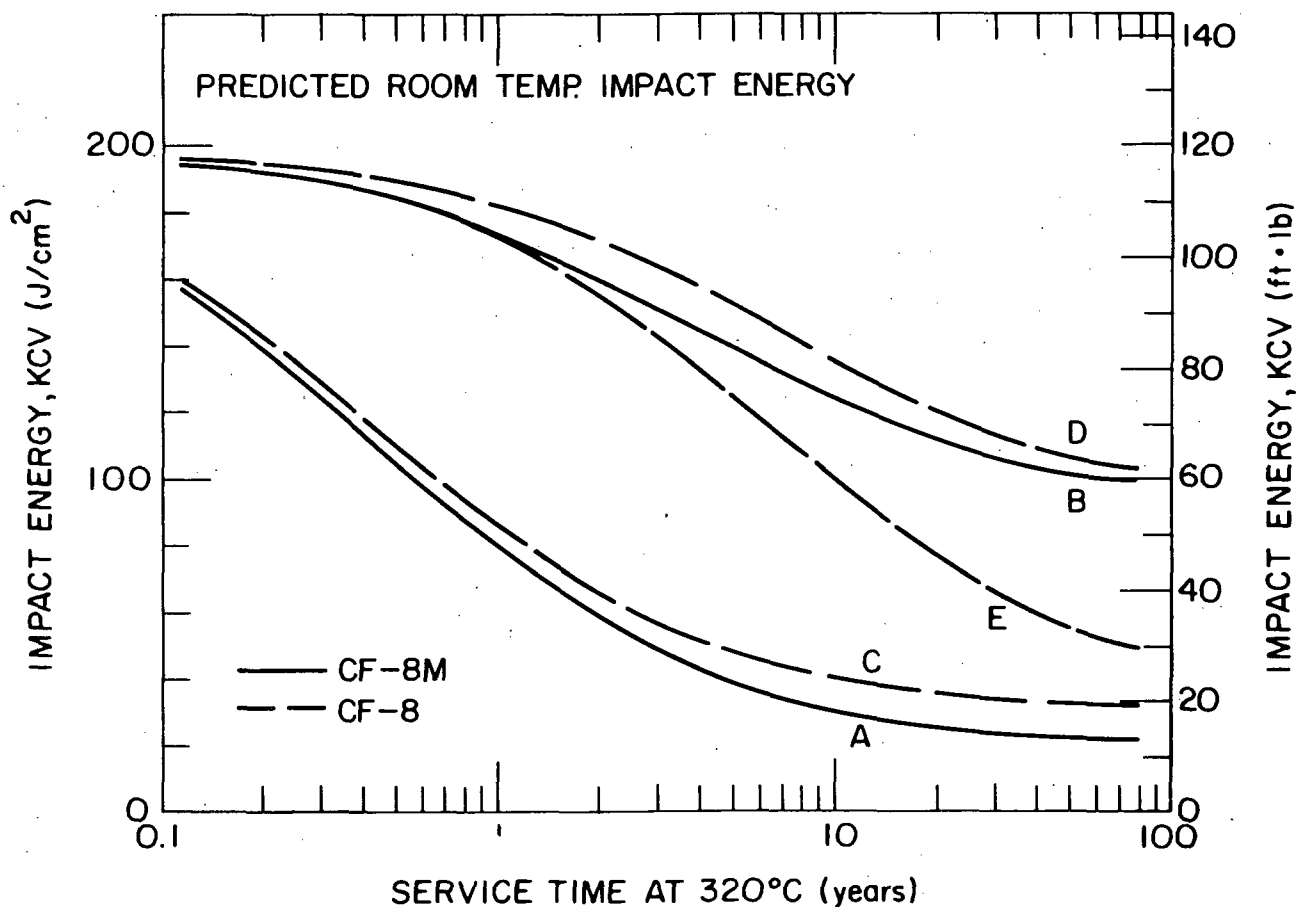


Fig. 15. Predicted Embrittlement Behavior of CF-8M and CF-8 Cast Stainless Steel.

#### 7. Recovery Anneal

The low-temperature embrittlement of cast stainless steel can be reversed by annealing at 550°C for 1 h and water quenching.<sup>8</sup> The ductile-to-brittle transition curves for the KRB pump cover plate material, after reactor service and after reannealing for ~1 h at 550°C, are shown in Fig. 16. The results show that the USE of the material increases from 247 to 330 J/cm<sup>2</sup> after reannealing and the mid-shelf transition temperature decreases from 37 to -16°C. Microstructural characterization of the reactor-aged material showed  $\alpha'$  and G phases in the ferrite matrix and large carbides at the phase boundaries.<sup>9,10</sup> The  $\alpha'$  phase is unstable at 550°C and thus dissolves after annealing. The reannealed material showed no  $\alpha'$ ; however, the size and distribution of the G phase were essentially the same as in the reactor-aged material.<sup>9,10</sup> These results indicate that the primary mechanism for embrittlement is the formation of  $\alpha'$  phase.

The annealed material was aged at 320, 350, and 400°C to investigate the reembrittling behavior. The results are shown in Fig. 17. The material reembrittles in a relatively short time. For example, aging for 100 h at

TABLE IV. Theoretical Chemical Composition and Ferrite Morphology of Cast Stainless Steel used for Predicting the Extent of Embrittlement under LWR Conditions

| Heat | Grade | Composition (wt %) |      |     |     |      |      |     | Ferrite                     |                                | Q <sup>c</sup><br>(kcal/mole) | K <sup>d</sup><br>(J/cm <sup>2</sup> ) |
|------|-------|--------------------|------|-----|-----|------|------|-----|-----------------------------|--------------------------------|-------------------------------|----------------------------------------|
|      |       | C                  | N    | Mn  | Si  | Ni   | Cr   | Mo  | Content <sup>a</sup><br>(%) | Intercept <sup>b</sup><br>(μm) |                               |                                        |
| A    | CF-8M | 0.05               | 0.02 | 1.2 | 1.2 | 10.0 | 21.0 | 2.6 | 28                          | 180                            | 18                            | 20                                     |
| B    | CF-8M | 0.05               | 0.05 | 0.5 | 1.0 | 9.0  | 19.5 | 2.0 | 15                          | 80                             | 40                            | 90                                     |
| C    | CF-8  | 0.04               | 0.02 | 1.3 | 0.5 | 8.4  | 21.0 | 0.4 | 24                          | 200                            | 18                            | 30                                     |
| D    | CF-8  | 0.05               | 0.05 | 0.5 | 1.0 | 8.5  | 20.5 | 0.4 | 15                          | 80                             | 45                            | 90                                     |
| E    | CF-8  | 0.04               | 0.02 | 1.3 | 0.5 | 8.4  | 21.0 | 0.4 | 24                          | 200                            | 45                            | 30                                     |

<sup>a</sup>Calculated from chemical composition with Hull's equivalent factor.

<sup>b</sup>Assumed values.

<sup>c</sup>Calculated from Eq. (4), value for heat E was arbitrarily assumed.

<sup>d</sup>Determined from Fig. 12.

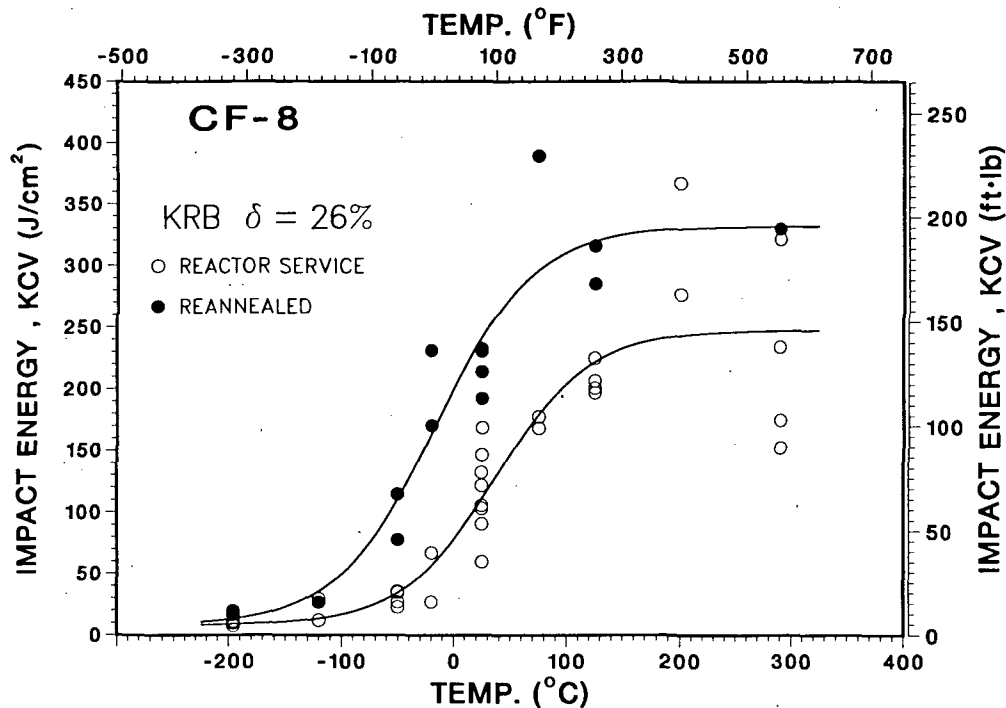


Fig. 16. Effect of Reannealing on the Ductile-to-Brittle Transition Curve for the KRB Pump Cover Plate Material.

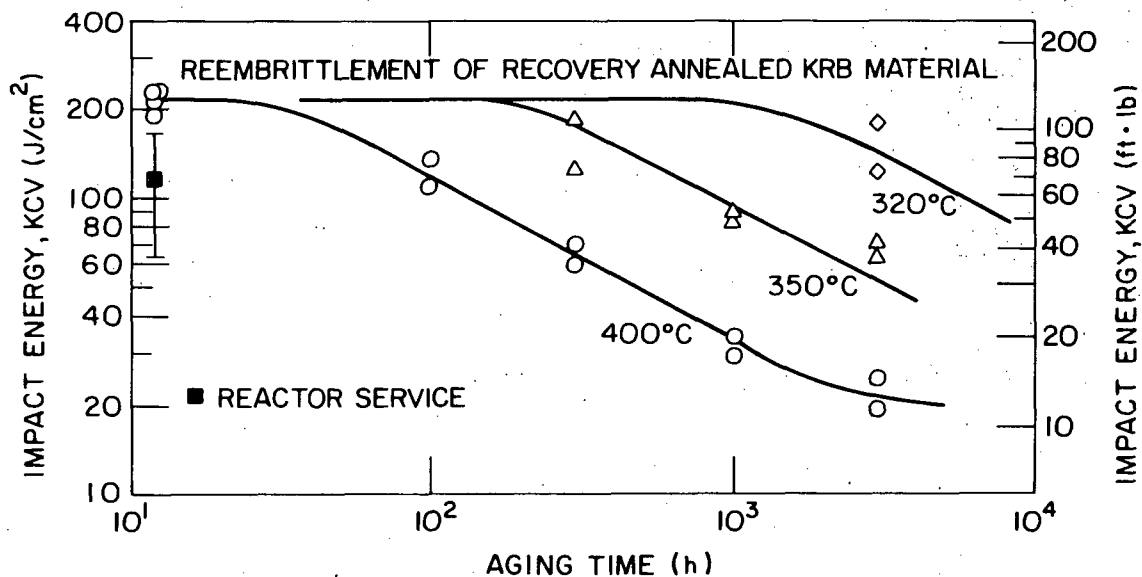


Fig. 17. Reembrittlement Behavior of Recovery Annealed KRB Pump Cover Plate Material.

400°C or 3000 h at 320°C decreased the impact energy to the value observed after reactor service. After 3000 h of aging at 400°C, the impact energy decreased to  $\sim 20$  J/cm<sup>2</sup>, a value close to the lower-shelf energy for the material.

It is not clear at present whether this behavior is typical of all reannealed cast stainless steels or is unique to this material. Recovery annealed material from other heats and grades of cast stainless steel are being aged to better establish the reembrittlement behavior.

## 8. Conclusions

Charpy-impact and J-R curve data for thermally aged cast stainless steel are presented. The effects of material variables on the embrittlement of cast materials are evaluated. The results show that the material composition and the ferrite content and spacing are important parameters in controlling the kinetics and extent of embrittlement. The ferrite morphology has a strong effect on the extent of embrittlement while the material composition influences the kinetics of embrittlement. The results indicate that the kinetics of embrittlement can vary significantly with the composition of the cast material.

Mechanical property results from the present study and data from other investigations were analyzed to develop the procedure and correlations for predicting the kinetics and extent of embrittlement, under reactor operating conditions, from the material parameters. The method and examples of estimating the room temperature impact strength and fracture toughness of cast components during reactor service are described. Correlations for predicting the toughness loss at reactor temperatures are also being developed. Mechanical tests are in progress on long-term laboratory-aged material and reactor-aged material to validate and/or modify the correlations.

## 9. Acknowledgments

This work was supported by the Office of Nuclear Regulatory Research, U. S. Nuclear Regulatory Commission. The authors are grateful to A. Sather, C. Ensel, and W. K. Soppet for conducting the mechanical tests and to G. M. Dragel for experimental contributions.

## References

1. A. Trautwein and W. Gysel, "Influence of Long Time Aging of CF-8 and CF-8M Cast Steel at Temperatures Between 300 and 500°C on the Impact Toughness and the Structure Properties," Spectrum, Technische Mitteilungen aus dem+GF+Konzern, No. 5, May 1981; Stainless Steel Castings, V. G. Behal and A. S. Melilli, eds., ASTM STP 756, Philadelphia, p. 165 (1982).
2. O. K. Chopra and H. M. Chung, Long-Term Embrittlement of Cast Duplex Stainless Steels in LWR Systems: Annual Report, October 1983-September 1984, NUREG/CR-4204, ANL-85-20 (March 1985); Nucl. Eng. Des., 89, 305 (1985).
3. O. K. Chopra and H. M. Chung, Long-Term Embrittlement of Cast Duplex Stainless Steels in LWR Systems: Annual Report, October 1984-September 1985, NUREG/CR-4503, ANL-86-3 (January 1986).
4. O. K. Chopra and H. M. Chung, Long-Term Embrittlement of Cast Duplex Stainless Steels in LWR Systems: Semiannual Report, October 1985-March 1986, NUREG/CR-4744 Vol. I, No. 1, ANL-86-54 (September 1986).
5. O. K. Chopra and G. Ayrault, in Materials Science and Technology Division Light-Water-Reactor Safety Research Program: Quarterly Progress Report, October-December 1983, NUREG/CR-3689 Vol. IV, ANL-83-85 Vol. IV, pp. 129-151 (August 1984).
6. O. K. Chopra and H. M. Chung, in Materials Science and Technology Division Light-Water-Reactor Safety Materials Engineering Research Programs: Quarterly Progress Report, January-March 1984, NUREG/CR-3998 Vol. I, ANL-84-60 Vol. I, p. 52 (September 1984).
7. O. K. Chopra and H. M. Chung, in Environmental Degradation of Materials in Nuclear Power Systems-Water Reactors, G. J. Theus and J. R. Weeks, eds., The Metallurgical Society, Warrendale, p. 737 (1988).
8. O. K. Chopra and H. M. Chung, in Properties of Stainless Steels in Elevated Temperature Service, M. Prager, ed., MPC-Vol. 26/PVP-Vol. 132, ASME, New York, p. 79 (1988).
9. H. M. Chung and O. K. Chopra, in Properties of Stainless Steels in Elevated Temperature Service, M. Prager, ed., MPC-Vol. 26/PVP-Vol. 132, ASME, New York, p. 17 (1988).

10. H. M. Chung and O. K. Chopra, in Proc. Second Intl. Symp. on Environmental Degradation of Materials in Nuclear Power Systems-Water Reactors, September 9-12, 1985, Monterey, CA, American Nuclear Society, LaGrange Park, IL, pp. 287-292 (1986).
11. G. Slama, P. Petrequin, and T. Magep, "Effect of Aging on Mechanical Properties of Austenitic Stainless Steel Castings and Welds," presented at SMIRT Post-Conference Seminar 6, Assuring Structural Integrity of Steel Reactor Pressure Boundary Components, August 29-30, 1983, Monterey CA.
12. P. J. Grobner, Metall. Trans. 4, 251 (1973).
13. R. Langneborg, ASM Trans. Q. 60, 67 (1967).
14. A. Hendry, Z. F. Mazur, and K. H. Jack, Met. Sci. 13, 482 (1979).
15. M. K. Miller, J. Bentley, S. S. Brenner, and J. A. Spitznagel, in Proc. 43rd Annual Meeting Electron Microscopy Society of America, G. W. Bailey, ed., San Francisco Press, p. 328 (1985).
16. M. Vrinat, R. Cozar, and Y. Meyzaud, Scr. Metall. 20, 1101 (1986).
17. A. L. Hiser, Tensile and J-R Curve Characterization of Thermally Aged Cast Stainless Steels, NUREG/CR-5024, MEA-2229 (September 1988).
18. P. McConnell and J. W. Sheckherd, Fracture Toughness Characterization of Thermally Embrittled Cast Duplex Stainless Steel, EPRI Report NP-5439 (March 1987).
19. E. I. Landerman and W. H. Bamford, in Ductility and Toughness Considerations in Elevated Temperature Service, MPC-8, ASME, New York, p. 99 (1988).

## Shippingport Aging Studies—Results and Plans

W. J. Shack, O. K. Chopra, and H. M. Chung

Materials and Components Technology Division  
Argonne National Laboratory  
Argonne, Illinois 60439

S. T. Rosinski

Sandia National Laboratory  
Albuquerque, New Mexico 87185

### Abstract

This paper describes the materials obtained from the primary- and secondary- coolant systems and the neutron shield tank of the Shippingport reactor and the initial work done to characterize the materials. The samples from the primary- and secondary-coolant systems include primary coolant system valves, sections of a coolant pipe, a main steam pipe, a feedwater pipe, an instrument pipe, a purification pipe, and a fuel pool pipe; and two cast pump volutes. Eleven samples, approximately 6 in. in diameter were obtained from the inner wall of the shield tank along with the corresponding samples from the very slightly irradiated outer wall. Test plans and initial Charpy-impact test data for the shield tank material are presented. Although large uncertainties exist at present, the preliminary results suggest that the changes in transition temperature are not as severe as might be expected on the basis of the changes observed in HFIR. However, the actual value of the transition temperature is high, and the toughness at service temperature is low, even when compared with the HFIR data. The chemical composition, hardness, and the amount and distribution of ferrite for the cast materials obtained from Shippingport are described. All materials are CF-8-grade cast stainless steel. Examination of specimens from the valves by transmission electron microscopy (TEM) showed very finely scaled mottle images (~1-2 nm) in the ferrite, which are known to be characteristic of  $\alpha'$  prime formation by spinodal decomposition. G phase was also observed in the ferrite. These observations are consistent with studies on laboratory-aged materials.

## 1 Introduction

---

The objective of this program is to develop an understanding of the metallurgical phenomena that may occur in nuclear reactor structural materials as a consequence of extended service at operating temperatures within and outside of the radiation environment and to assess the impact of these phenomena on structural integrity.

Although many aging phenomena such as the embrittlement of cast stainless steel, low-temperature sensitization of austenitic stainless steels, and radiation embrittlement of pressure vessel steels have been studied in the laboratory, most of the studies have been based on simulation of actual reactor conditions. The Shippingport reactor offers a unique opportunity to validate and benchmark the laboratory studies, and thereby, provide a sound basis for evaluating the integrity of structural components near the end of the projected life of a plant. Additional work will be undertaken to identify possible new mechanisms of

The submitted manuscript has been authored by a contractor of the U. S. Government under contract No. W-31-109-ENG-38. Accordingly, the U. S. Government retains a nonexclusive, royalty-free license to publish or reproduce the published form of this contribution, or allow others to do so, for U. S. Government purposes.

component degradation. As the opportunity arises, additional materials will be procured from other reactors, and the extent of degradation in these materials will be evaluated and compared with results from the Shippingport components.

## 2 Summary of Technical Progress

### 2.1 Primary and Secondary-Coolant System Materials

Samples of all materials from the primary- and secondary-coolant systems at Shippingport that were likely to have undergone metallurgical changes during aging have been obtained. They include primary coolant system valves, sections of a coolant pipe, a main steam pipe, a feedwater pipe, an instrument pipe, a purification pipe, and a fuel pool pipe; and two cast pump volutes. One volute had never seen service; the other was in use over the entire life of the plant. The components and materials obtained from the primary- and secondary-coolant systems are listed in Table 1.

In most cases the valve-to-pipe weldments were obtained with the valves. The actual time at temperature for the cast components was ~13 years at ~281°C (538°F) for the hot-leg components and ~264°C (507°F) for the cold-leg components. The components were at a hot stand-by condition >204°C (400°F) for an additional time of ~2 years.

The chemical composition, hardness, and the amount and distribution of ferrite for the check valves and the spare pump volute are given in Table 2. All materials are CF-8-grade cast stainless steel. The hardness of the materials increases with an increase in ferrite content. For some of the materials an effect of orientation was observed; the hardness and ferrite content of the axial cross sections was higher than that of the circumferential cross sections.

Table 1. Primary- and Secondary-Coolant System Materials Obtained from the Shippingport Reactor

| <u>Cast Stainless Steel</u>                   |                  |
|-----------------------------------------------|------------------|
| Hot-Leg Valves                                | Loops A, B, C    |
| Cold-Leg Valves                               | Loops A, B, C    |
| Check Valves                                  | Loops A, B, C, D |
| Pump Volutes                                  | Loop A, spare    |
| <u>Miscellaneous Materials</u>                |                  |
| Primary coolant piping and weldment (wrought) |                  |
| Feedwater pipe                                |                  |
| Main steam pipe                               |                  |

Table 2. Chemical Composition and Ferrite Content of Cast Components

| ANL Designation  | Valve ID | Loop | Composition, <sup>1</sup> wt% |       |      |      |       |       |       |       |      | Ferrite, % |       | R <sub>B</sub> | l, μm |
|------------------|----------|------|-------------------------------|-------|------|------|-------|-------|-------|-------|------|------------|-------|----------------|-------|
|                  |          |      | C                             | N     | Si   | Mn   | P     | S     | Ni    | Cr    | Mo   | Calc.      | Meas. |                |       |
| CA7 <sup>2</sup> | 05-H7-1  | A    | 0.058                         | 0.041 | 1.43 | 1.09 | 0.018 | 0.009 | 8.72  | 20.22 | 0.01 | 10.9       | 10.0  | 78.6±1.5       | 148   |
| CA4              | 05-H7-1  | A    | 0.056                         | 0.041 | 1.45 | 1.10 | 0.018 | 0.009 | 8.84  | 20.26 | 0.01 | 10.8       | 10.9  | 79.8±2.3       | 157   |
| CB7              | 05-H7-2  | B    | 0.052                         | 0.053 | 1.36 | 1.07 | 0.018 | 0.011 | 8.85  | 19.12 | 0.02 | 5.9        | 3.2   | 75.0±2.8       | 296   |
| CC4              | 05-H7-3  | C    | 0.056                         | 0.067 | 1.42 | 1.11 | 0.018 | 0.012 | 9.64  | 20.12 | 0.01 | 5.3        | 6.0   | 77.0±2.1       | 211   |
| MA1              | 05-H6-2  | A    | 0.052                         | 0.049 | 0.22 | 0.72 | 0.038 | 0.012 | 10.51 | 20.75 | 0.24 | 5.2        | 9.5   | 76.9±3.0       | 217   |
| MA9              | 05-H6-2  | A    | 0.052                         | 0.051 | 0.24 | 0.72 | 0.041 | 0.011 | 10.54 | 20.81 | 0.24 | 5.2        | 10.0  | 77.6±1.7       | 245   |
| MB2              | 05-H6-4  | B    | 0.042                         | 0.073 | 0.51 | 0.73 | 0.042 | 0.017 | 10.77 | 19.74 | 0.19 | 2.6        | 1.9   | 74.2±2.7       | 620   |
| VR               | Volute   | —    | 0.046                         | 0.049 | 1.14 | 0.50 | 0.027 | 0.017 | 9.56  | 20.79 | 0.04 | 9.8        | 16.2  | 82.9±1.7       | 181   |

<sup>1</sup>Duplicate analyses illustrate variability observed in different regions of the valve body.

<sup>2</sup>In the Argonne designation, the first letter indicates the type of valve (C, check valve; M, manually operated hot-leg stop valve); the second letter indicates the loop, and the number is a number designating the segment from the component from which the sample was taken.

<sup>3</sup>Mean ferrite spacing.

All the valve materials have a radially oriented columnar grain structure. Typical examples of the grain structure for the check valves and manual isolation valves are shown in Figs. 1 and 2, respectively. Figure 1 also shows the weld between the valve and piping. All the valves also contained repair welds; an example is shown in Fig. 2. The pump volute has a mixed grain structure, i.e., columnar and equiaxed, Fig. 3.

The ferrite morphology of the different materials is shown in Figs. 4 and 5. The materials contain lacy ferrite with a mean ferrite spacing,  $l$ , in the range of 150 to 300  $\mu\text{m}$ . The check valve materials show that a significant amount of ferrite has been transformed into austenite. Most of the ferrite/austenite phase boundaries have migrated. The original phase boundaries are decorated with carbides, which most likely have formed during the production heat treatment of the material (Fig. 6a). The new phase boundaries are also decorated with carbides. Transformed islands of austenite are also seen within the ferrite regions.

Recent investigations suggest that embrittlement of the ferrite phase in cast duplex stainless steel may occur after 10 to 20 years at reactor operating temperatures. Such embrittlement could influence the mechanical response and integrity of pressure boundary components [1-3]. Laboratory studies have identified a number of metallurgical processes that produce embrittlement in accelerated (higher temperature) aging tests. These processes include: (1) spinodal decomposition involving segregation of Fe, Cr, and Ni; (2) nucleation and growth of the  $\alpha'$  phase out of the spinodal structure; (3) precipitation of Ni- and Si-rich G phase; (4) growth of small spherical  $\text{M}_{23}\text{C}_6$  carbides; and (5) precipitation of  $\gamma_2$  austenite within the ferrite [3]. The primary embrittling process appears to be the spinodal decomposition, with carbide precipitation on austenite-ferrite boundaries as the secondary embrittling process. The components from Shippingport are being examined to determine if corresponding changes can be observed in reactor-aged materials.

Examination of specimens from the valves by transmission electron microscopy (TEM) showed very finely scaled mottle images ( $\sim 1-2$  nm) in the ferrite, which are known to be characteristic of  $\alpha'$  prime formation by spinodal decomposition. Atom probe field ion microscopy is needed to provide conclusive evidence of spinodal decomposition. G phase was also observed in the ferrite. The G-phase precipitates are  $\sim 5-15$  nm in diameter, with a particle density of  $\sim 10^{21}/\text{m}^3$ . These observations are consistent with studies on low-temperature ( $\sim 300^\circ\text{C}$ ), laboratory-aged materials. An unexpected microstructural feature, a new phase that precipitated on slip bands and stacking faults, was observed (Fig. 6b) in the austenite phase. It has been tentatively identified as  $\sigma$  phase, which precipitated on stacking faults in the austenite. Microhardness measurements, made directly on the ferrite and austenite, are summarized in Table 3.

Tensile and Charpy V-notch impact specimens have been fabricated from materials containing  $>6\%$  ferrite, but the tests have not yet been performed. The microhardness levels observed in the ferrite are consistent with those observed in aged cast stainless steels that have shown significant loss of toughness. Because of the relatively low ferrite levels in the Shippingport components, the actual loss of toughness is expected to be relatively modest. However, the microstructural changes in the ferrite are consistent with a much larger toughness decrease in materials with higher ferrite levels and more continuous distributions.

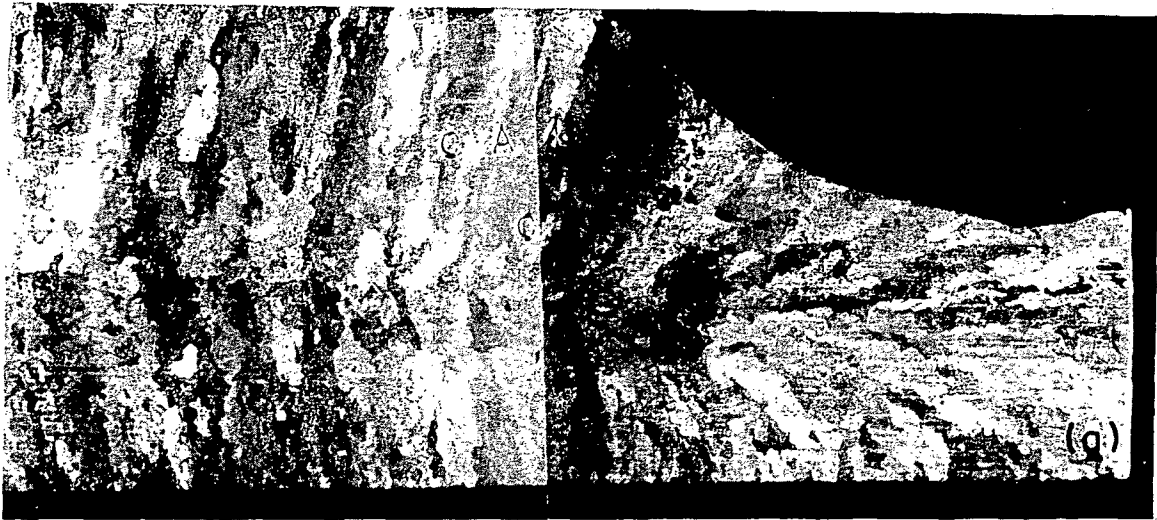


Figure 1. Microstructure along an Axial Section of the Loop A Check Valve. (a) Valve body and (b) weld.



*Figure 2. Microstructure along an Axial Section of the Loop B Manual Isolation Valve. A repair weld is also seen on the outer diameter of the valve.*



*Figure 3. Microstructure along an Axial Section of the Spare Volute.*

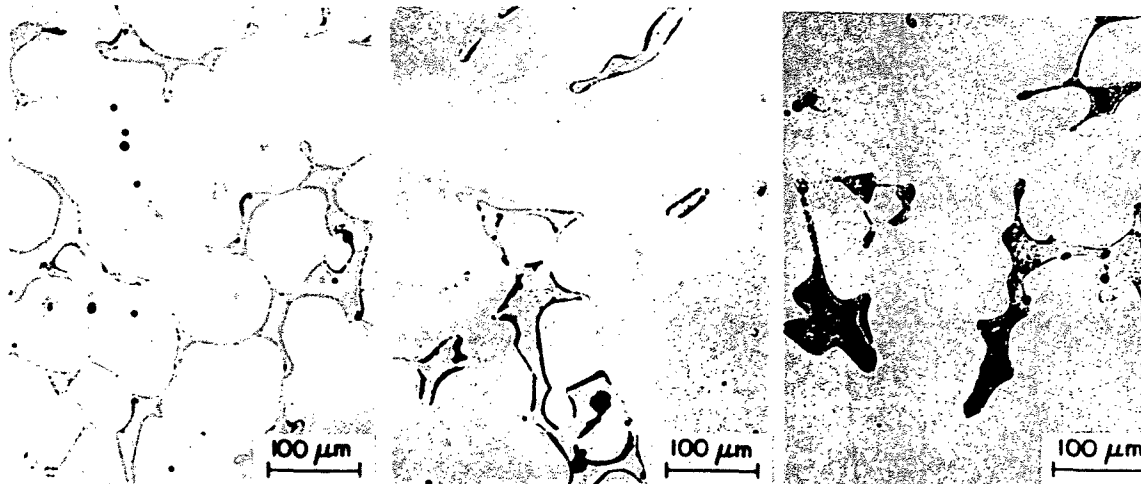


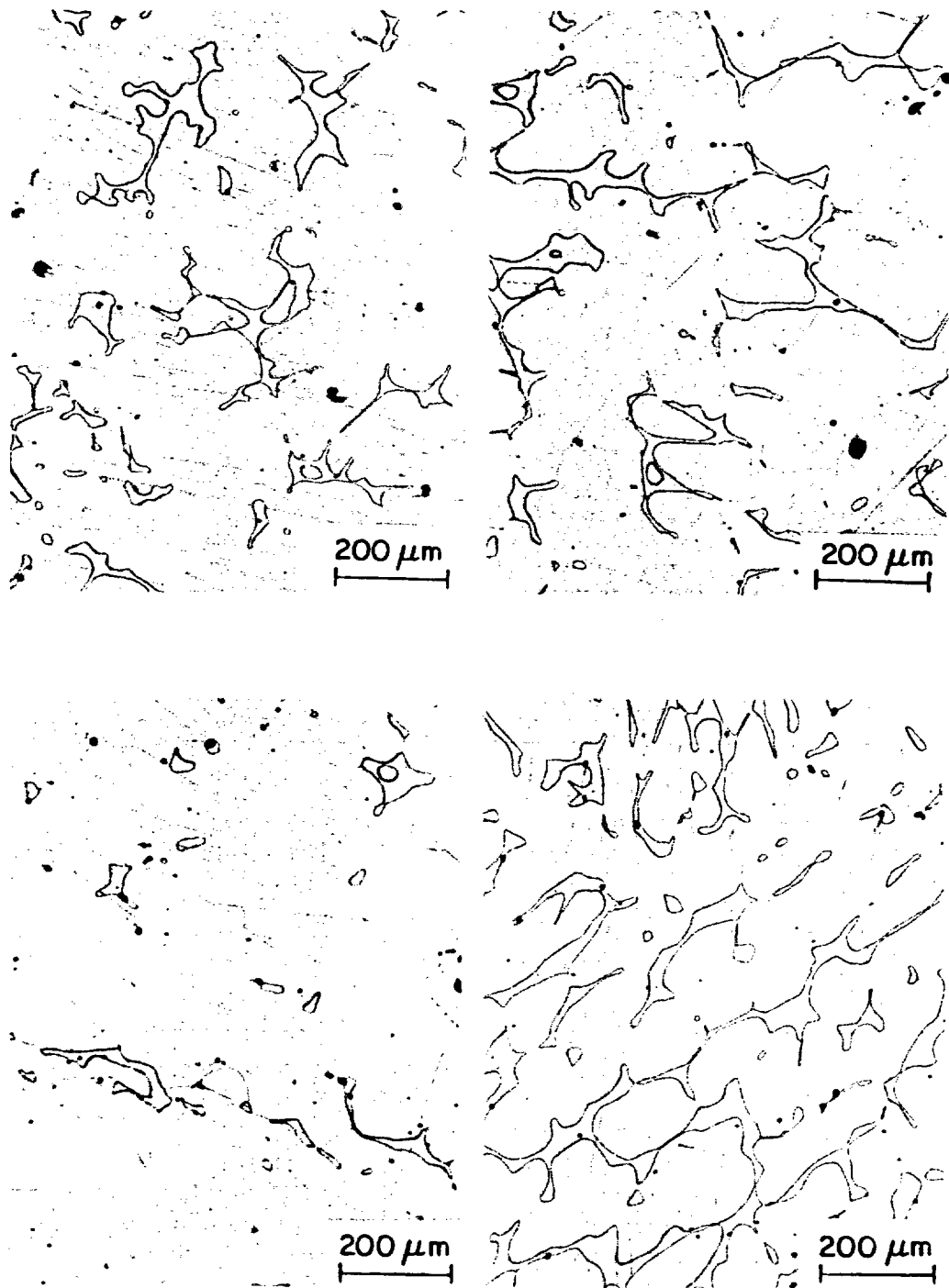
Figure 4. Ferrite Morphology of Cast Materials from (a) Loop A, (b) Loop B, and (c) Loop C Cold-Leg Check Valves.

Table 3. Microhardness Measurements on Aged Components from Shippingport

| ANL Designation | Valve ID | Loop | Ferrite Vickers Hardness | Austenite Vickers Hardness |
|-----------------|----------|------|--------------------------|----------------------------|
| CA7             | 05-H7-1  | A    | 243                      | 165                        |
| CA4             | 05-H7-1  | A    | 252                      | 167                        |
| CB7             | 05-H7-2  | B    | 230                      | 142                        |
| CC4             | 05-H7-3  | C    | 234                      | 159                        |
| MA1             | 05-H6-2  | A    | -                        | -                          |
| MA9             | 05-H6-2  | A    | 310                      | 176                        |
| MB2             | 05-H6-4  | B    | 286                      | 178                        |
| VR              | Volute   | -    | 260                      | 199                        |

## 2.2 Neutron Shield Tank Material

The embrittlement suffered by the HFIR vessel at Oak Ridge National Laboratory has raised the issue of whether low-temperature, low-flux irradiation can produce an unexpectedly high degree of embrittlement of reactor support structures. To help resolve this question, samples were obtained from the neutron shield tank of the Shippingport reactor. This sampling effort was sponsored jointly by the NRC and the DOE Plant Life Extension Program (PLEX) at Sandia National Laboratory. The actual sampling was performed by Pacific Northwest Laboratory under subcontract to Argonne and Sandia. The samples are approximately 6 in. in diameter and were obtained from the inner wall of the shield tank along with the corresponding samples from the very slightly irradiated outer wall. The locations of the samples from the outer and inner shell of the shield tank are shown in Figs. 7 and 8. The material from the Shippingport neutron shield tank is an A212 Gr-B steel



**Figure 5.** Ferrite Morphology of Cast Materials from loop A (a) and (b) loop B (c), and loop C (d) Hot-Leg Manual Isolation Valves.

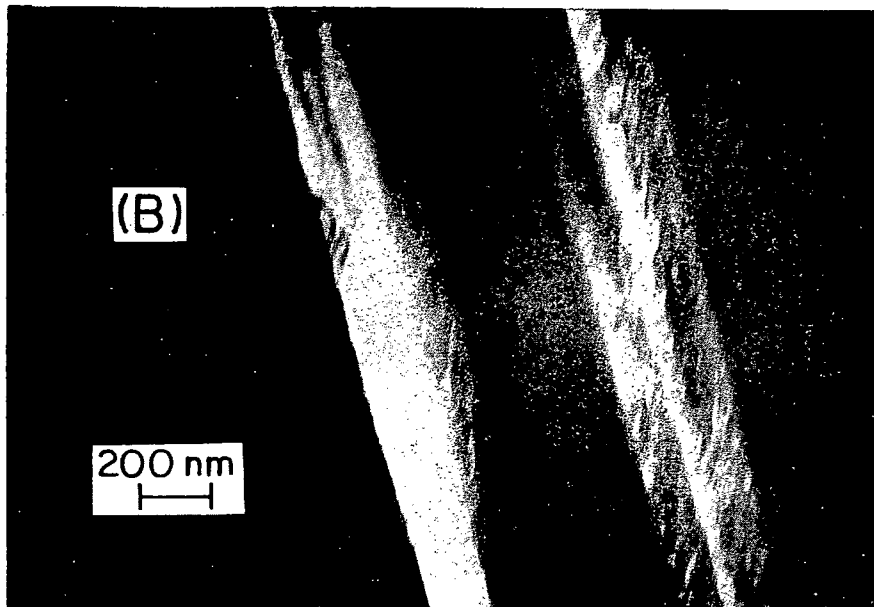
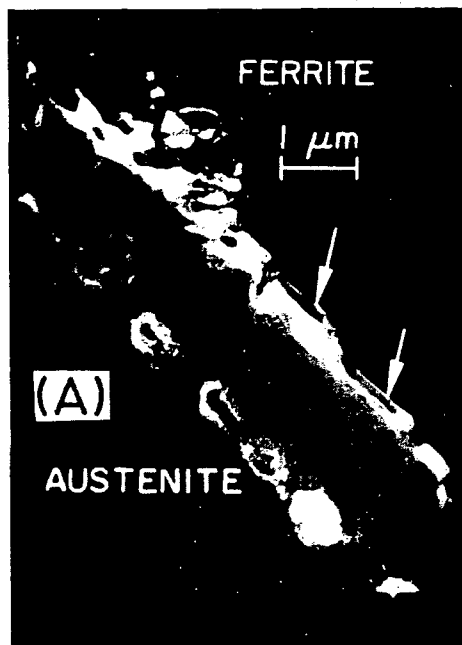


Figure 6. (a) Morphologies of  $M_{23}C_6$  Carbides on the Austenite-Ferrite Boundaries; (b) Sigma Phase Formed on Slip Bands in Austenite of Cold-Leg Check Valves.



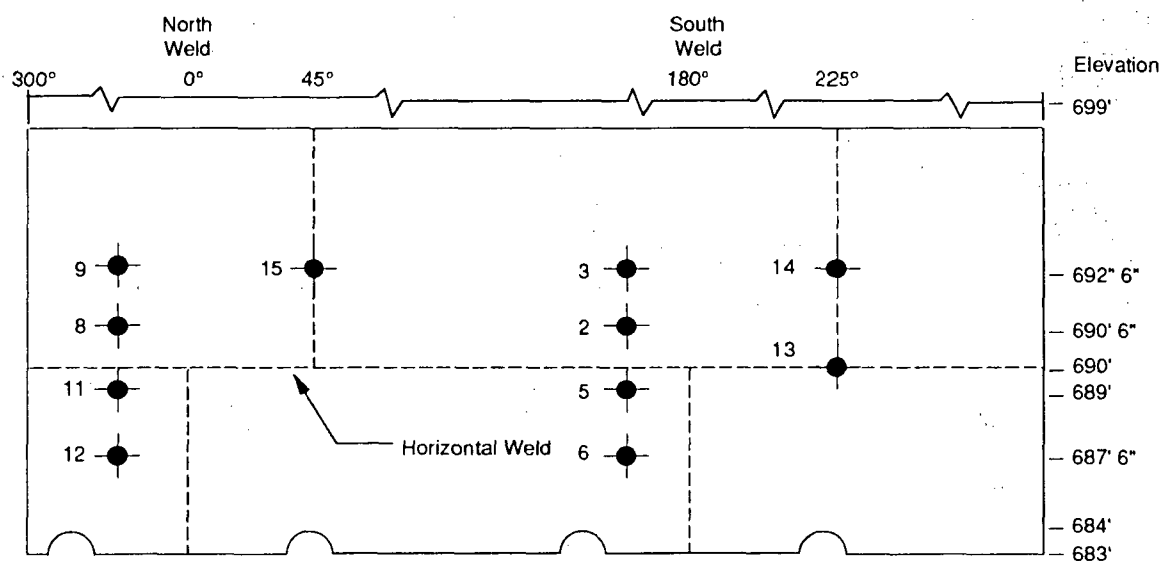
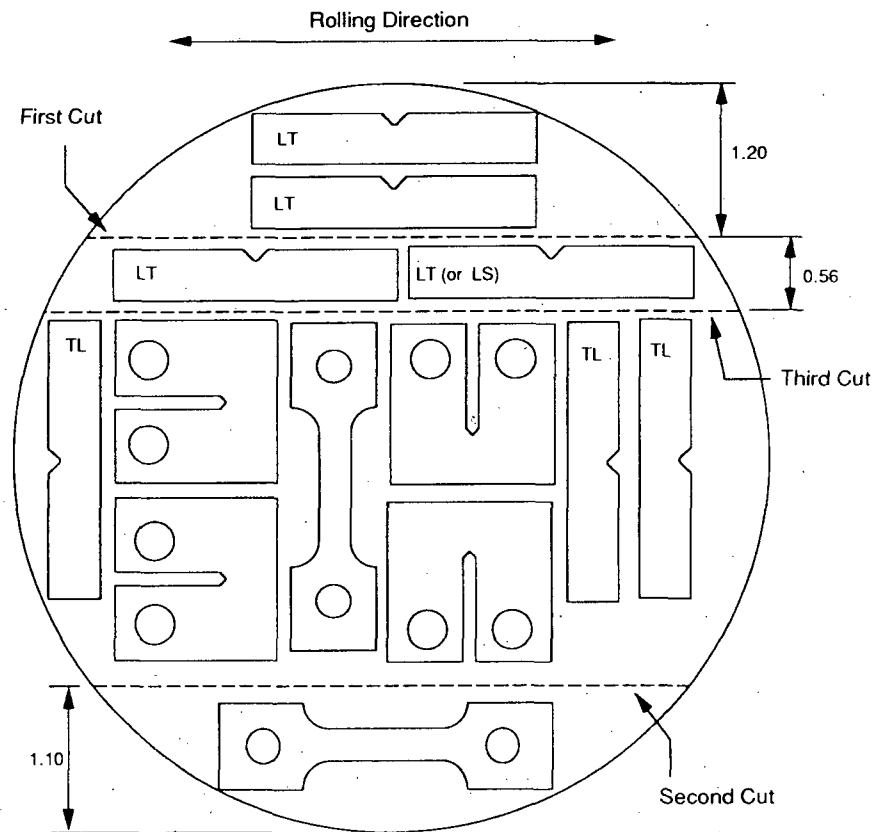


Figure 8. Sample Locations on the Inner Shell of the Shippingport Shield Tank.

Table 4. Typical Composition of A212 Gr-B Plate from the Neutron Shield Tank

| Element        | Level (wt.%) |
|----------------|--------------|
| C              | 0.23         |
| Mn             | 0.78         |
| P              | 0.02         |
| S              | 0.03         |
| Si             | 0.20         |
| Cu             | 0.05         |
| Ni             | 0.04         |
| Cr             | 0.04         |
| O              | 0.01         |
| N              | 0.004        |
| Ta             | 0.03         |
| Mo, Ca, Ti, Al | <0.01        |
| B, Se, Sn      | <0.01        |
| V, Zn, Zr      | <0.005       |

the toughness of the material. The increases in the NDT temperature obtained from the HFIR surveillance specimens and corresponding changes in A212 Gr-B steel irradiated in a high flux research reactor are shown in Fig. 11 [4]. The current data from the shield tank permits only rough estimates of the changes in transition temperature under irradiation, and there is considerable uncertainty in the actual irradiation conditions. Estimates of the change in transition temperature based on the limited testing to date, are shown in Fig. 10 for comparison with the data from the HFIR reactor. Although large uncertainties exist at present, these preliminary results suggest that the changes in transition temperature are not as severe as might be expected on the basis of the changes observed in HFIR. However, the actual value of the transition temperature is high, and the toughness at service temperature is low, even when compared with the HFIR data.



Note: Diagram based on an assumed diameter of 5.75 in.  
All Dimensions in inches.

Figure 9. Cutting Diagram for Base Metal Samples from the Inner Shell of the Neutron Shield Tank.

### 3 Future Plans

An attempt is being made to organize a cooperative effort to obtain samples from the Shippingport pressure vessel. Expressions of interest in the endeavor have been obtained from DOE, EPRI, the B&W Owners Group, Yankee Atomic, Electricité de France, and Bettis Atomic Power Laboratory. Although the materials and operating conditions of the Shippingport reactor are not exactly prototypical of modern PWRs, valuable information can be obtained on several important issues such as the throughwall variation of toughness, comparisons among different types of specimens (CT, Charpy, EPRI miniature specimen designs) used in surveillance studies, and activation and radioactive product studies for decommissioning. The actual sampling operation would be performed after shipment of the pressure vessel to the Hanford site in Washington, which is currently scheduled for the second quarter of FY 1989.

Characterization and mechanical testing of the material from the neutron shield tank is the highest priority task during FY 1989. Activation analyses are currently in progress to try to get a better understanding of the actual irradiation conditions. Microstructural analyses will be performed to determine the actual mechanisms of embrittlement.

Table 5 Charpy Toughness Values of Samples from the Inner and Outer Halves of the Shield Tank Inner and Outer Shells

| Sample Number/Shell | Location/Plate | Temperature |     | C <sub>v</sub> Inner Half |        | C <sub>v</sub> Outer Half |        |
|---------------------|----------------|-------------|-----|---------------------------|--------|---------------------------|--------|
|                     |                | °C          | °F  | joules/cm <sup>2</sup>    | ft. lb | joules/cm <sup>2</sup>    | ft. lb |
| 9/I                 | Top North      | 25          | 77  | 8.1                       | 4.7    | 11.3                      | 6.52   |
| 9/I                 | "              | 55          | 131 | 39.0                      | 22.5   | 48.5                      | 28.1   |
| 8/I                 | "              | 25          | 77  | 10.3                      | 6.0    | 12.8                      | 7.4    |
| 8/I                 | "              | 55          | 131 | 43.5                      | 24.9   | 53.5                      | 31     |
| 3/I                 | Top South      | 25          | 77  | 10.9                      | 6.3    | 14.5                      | 8.1    |
| 3/I                 | "              | 55          | 131 | 45.5                      | 26.1   | 61.0                      | 35.3   |
| 2/I                 | "              | 25          | 77  | 13.5                      | 7.8    | 11.6                      | 6.7    |
| 2/I                 | "              | 55          | 131 | 52.8                      | 30.6   | 68.6                      | 39.7   |
| 9/O                 | Top            | 25          | 77  | 43.2                      | 25.0   | 46.4                      | 26.9   |
| 9/O                 | "              | 55          | 131 | 85.7                      | 49.5   | 87.7                      | 50.8   |
| 3/O                 | "              | 25          | 77  | 35.1                      | 20.3   | 48.0                      | 27.8   |
| 3/O                 | "              | 55          | 131 | 94.8                      | 54.9   | 98.3                      | 56.9   |
| 2/O                 | "              | 25          | 77  | 29.4                      | 17.0   | 48.0                      | 27.8   |
| 2/O                 | "              | 55          | 131 | 114.3                     | 66.2   | 92.0                      | 53.3   |
| 6/O                 | Bottom         | 25          | 77  | 24.0                      | 13.9   | 42.5                      | 24.6   |
| 6/O                 | "              | 55          | 131 | 89.1                      | 51.6   | 93.1                      | 53.9   |
| 12/O                | "              | 25          | 77  | —                         | —      | 49.4                      | 28.6   |
| 12/O                | "              | 55          | 131 | 84.0                      | 48.6   | 96.5                      | 55.9   |

Table 6. Estimated Fluence Levels for the Inner Shell of the Shield Tank

| Sample | Fluence<br>(neutrons/cm <sup>2</sup> , > 1MeV) | Flux<br>(neutrons/cm <sup>2</sup> . s, > 1MeV) |
|--------|------------------------------------------------|------------------------------------------------|
| 9      | 8 x 10 <sup>17</sup>                           | 4 x 10 <sup>9</sup>                            |
| 3      | 8 x 10 <sup>17</sup>                           | 4 x 10 <sup>9</sup>                            |
| 2      | 5 x 10 <sup>17</sup>                           | 3 x 10 <sup>9</sup>                            |
| 8      | 5 x 10 <sup>17</sup>                           | 3 x 10 <sup>9</sup>                            |

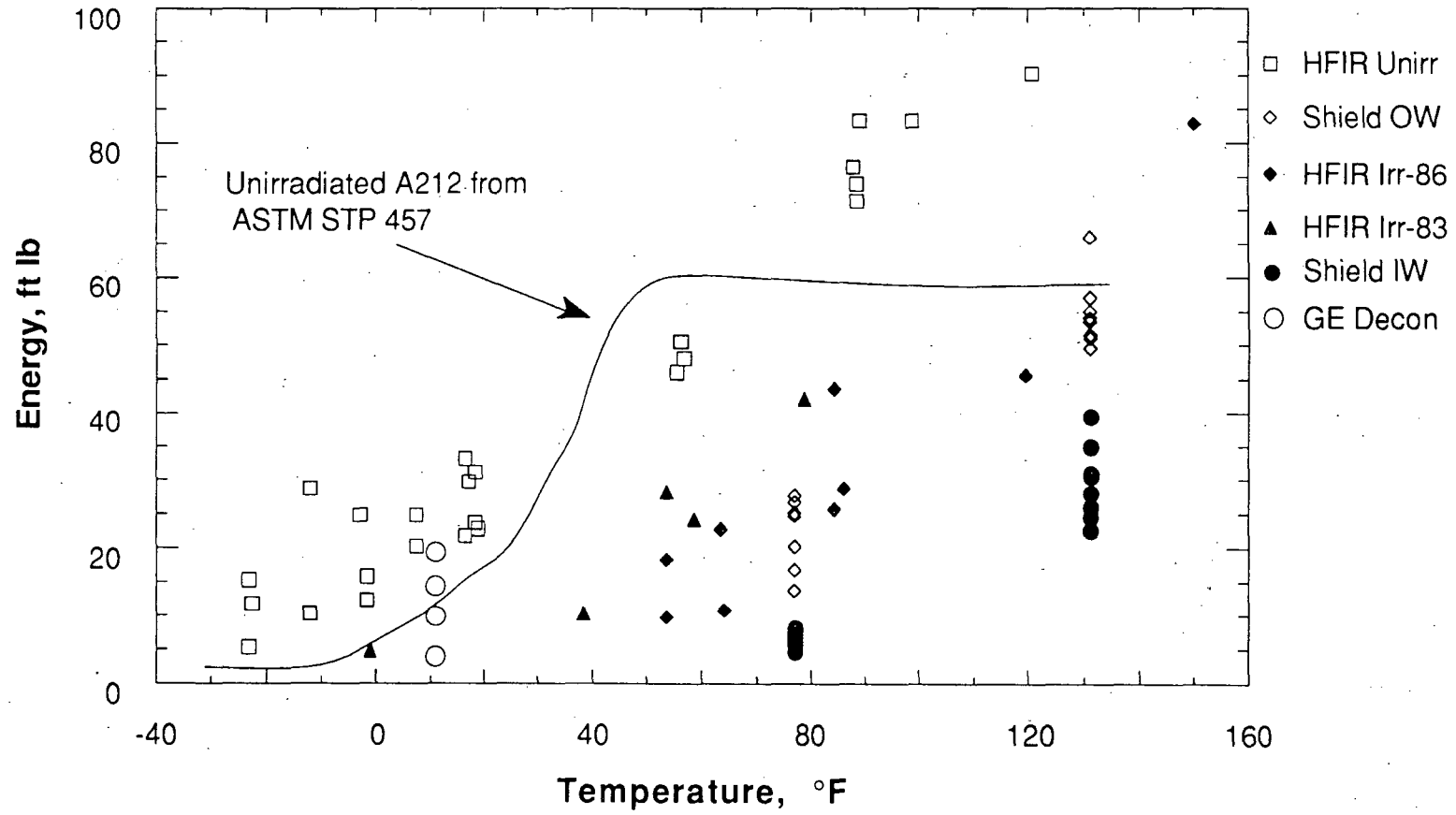


Figure 10. Comparison of Charpy Test Data from the Neutron Shield Tank with Data from Irradiated and Unirradiated HFIR and an Unirradiated A212 Gr-B Steel.

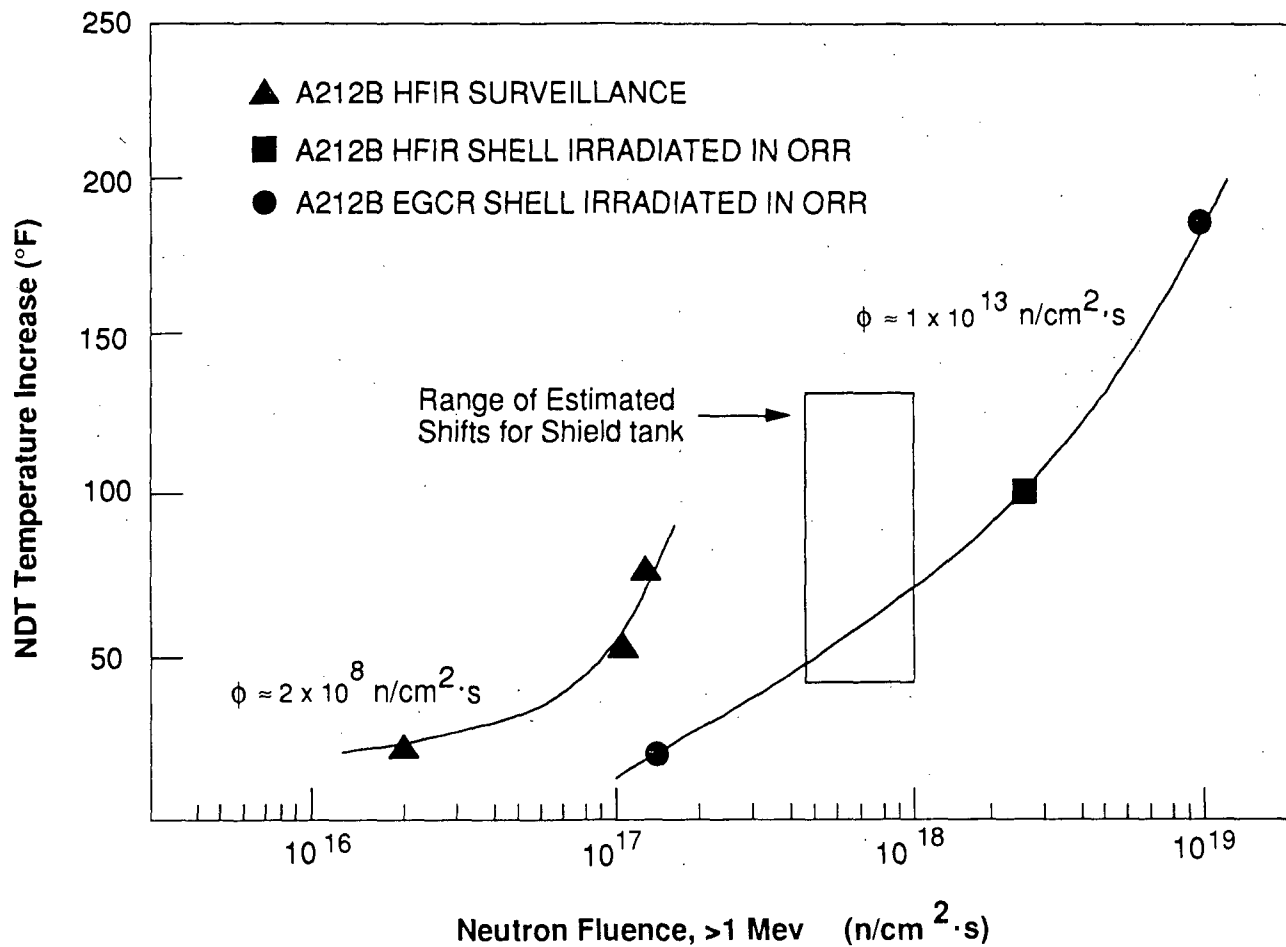


Figure 11. Comparison of Estimated Transition Temperature Shifts for the Shippingport Neutron Shield Tank with HFIR A212 Gr-B Surveillance Data and High Flux Test Reactor Irradiations of the HFIR A212 Gr-B and Another Heat of A212 Gr-B.

Mechanical testing of the cast stainless steel materials will be performed to determine whether the losses in toughness are consistent with those predicted by correlations developed from the laboratory database. Stress corrosion and corrosion fatigue tests will be performed to investigate relative susceptibility to environmentally assisted cracking. Selected materials will be thermally aged further at temperatures between 290 and 400°C in the laboratory to obtain additional information and to identify possible artifacts introduced during laboratory studies. Thermal aging will also be carried out on material which has been annealed for 1 h at 550°C to recover toughness.

#### **4 References**

---

1. G. Slama, P. Petrequin, S. H. Masson, and T. Mager, "Effect of Aging on Mechanical Properties of Austenitic Stainless Steel Castings and Welds," *SMIRT Post Conference Seminar 6, Assuring Structural Integrity of Steel Reactor Pressure Boundary Components*, August 29-30, 1983, Monterey, CA.
2. O. K. Chopra and H. M. Chung, "Effect of Low-Temperature Aging on the Mechanical Properties of Cast Stainless Steels," in *Properties of Stainless Steels in Elevated Temperature Service — MPC-Vol. 26/PVP-Vol. 132*, M. Prager, Ed., American Society of Mechanical Engineers, New York, 1988.
3. H. M. Chung and O. K. Chopra, "TEM, APFIM, and SANS Examination of Aged Duplex Stainless Steel Components from Some Decommissioned Reactors," American Nuclear Society Annual Meeting, June 12-16, 1988, San Diego, CA.
4. R. D. Cheverton, J. G. Merkle, R. K. Nanstad, Eds, *Evaluation of HFIR Pressure Vessel Integrity Considering Radiation Embrittlement*, ORNL/TM-10444, Oak Ridge National Laboratory, August 1988.
5. M. S. Wechsler, R. G. Berggren, N. E. Hinkle, and W. J. Stelzman, "Radiation Hardening and Embrittlement in a Reactor Pressure Vessel Steel," in *Irradiation Effects in Structural Alloys for Thermal and Fast Reactors*, ASTM Special Technical Publication 457, American Society for Testing and Materials, New York, 1968.
6. S. Iskander, ORNL. Private Communication. September 1988.

#### **Acknowledgments**

The authors would like to thank J. Schreiber, DOE Project Manager of the Shippingport Decommissioning Project, whose cooperation and support of the recovery of materials from the Shippingport reactor was invaluable. The cooperation of the staff of the decommissioning contractor, the General Electric Company, especially Mr. R. Pratt, has also been critical to the success of the sampling operations at Shippingport. R. Allen and his colleagues at Pacific Northwest Laboratory developed and tested the system used to obtain the shield tank samples and successfully performed the sampling operation.

|                                                                                                                                                                                                                                                                                                                                                                                                                                                                                                                                                                                                                                                                                                                                                                                                                                                                                                  |                                                                                                                                                                                                                                                                                 |                                                                                           |       |      |          |      |
|--------------------------------------------------------------------------------------------------------------------------------------------------------------------------------------------------------------------------------------------------------------------------------------------------------------------------------------------------------------------------------------------------------------------------------------------------------------------------------------------------------------------------------------------------------------------------------------------------------------------------------------------------------------------------------------------------------------------------------------------------------------------------------------------------------------------------------------------------------------------------------------------------|---------------------------------------------------------------------------------------------------------------------------------------------------------------------------------------------------------------------------------------------------------------------------------|-------------------------------------------------------------------------------------------|-------|------|----------|------|
| NRC FORM 335<br>(8-87)<br>NRCM 1102,<br>3201, 3202<br>SEE INSTRUCTIONS ON THE REVERSE                                                                                                                                                                                                                                                                                                                                                                                                                                                                                                                                                                                                                                                                                                                                                                                                            | U.S. NUCLEAR REGULATORY COMMISSION<br><b>BIBLIOGRAPHIC DATA SHEET</b>                                                                                                                                                                                                           | 1. REPORT NUMBER (Assigned by PPMB: DPS, add Vol. No., if any)<br>NUREG/CP-0097<br>Vol. 3 |       |      |          |      |
| 2. TITLE AND SUBTITLE<br>Proceedings of the Sixteenth Water Reactor Safety Information Meeting                                                                                                                                                                                                                                                                                                                                                                                                                                                                                                                                                                                                                                                                                                                                                                                                   | 3. LEAVE BLANK                                                                                                                                                                                                                                                                  |                                                                                           |       |      |          |      |
| 5. AUTHOR(S)<br>Compiled by Allen J. Weiss, BNL                                                                                                                                                                                                                                                                                                                                                                                                                                                                                                                                                                                                                                                                                                                                                                                                                                                  | 4. DATE REPORT COMPLETED<br><table border="1" style="width: 100%;"> <tr> <td style="text-align: center;">MONTH</td> <td style="text-align: center;">YEAR</td> </tr> <tr> <td style="text-align: center;">February</td> <td style="text-align: center;">1989</td> </tr> </table> |                                                                                           | MONTH | YEAR | February | 1989 |
| MONTH                                                                                                                                                                                                                                                                                                                                                                                                                                                                                                                                                                                                                                                                                                                                                                                                                                                                                            | YEAR                                                                                                                                                                                                                                                                            |                                                                                           |       |      |          |      |
| February                                                                                                                                                                                                                                                                                                                                                                                                                                                                                                                                                                                                                                                                                                                                                                                                                                                                                         | 1989                                                                                                                                                                                                                                                                            |                                                                                           |       |      |          |      |
| 7. PERFORMING ORGANIZATION NAME AND MAILING ADDRESS (Include Zip Code)<br>Office of Nuclear Regulatory Research<br>U. S. Nuclear Regulatory Commission<br>Washington, D. C. 20555                                                                                                                                                                                                                                                                                                                                                                                                                                                                                                                                                                                                                                                                                                                | 6. DATE REPORT ISSUED<br><table border="1" style="width: 100%;"> <tr> <td style="text-align: center;">MONTH</td> <td style="text-align: center;">YEAR</td> </tr> <tr> <td style="text-align: center;">March</td> <td style="text-align: center;">1989</td> </tr> </table>       |                                                                                           | MONTH | YEAR | March    | 1989 |
| MONTH                                                                                                                                                                                                                                                                                                                                                                                                                                                                                                                                                                                                                                                                                                                                                                                                                                                                                            | YEAR                                                                                                                                                                                                                                                                            |                                                                                           |       |      |          |      |
| March                                                                                                                                                                                                                                                                                                                                                                                                                                                                                                                                                                                                                                                                                                                                                                                                                                                                                            | 1989                                                                                                                                                                                                                                                                            |                                                                                           |       |      |          |      |
| 10. SPONSORING ORGANIZATION NAME AND MAILING ADDRESS (Include Zip Code)<br>Same as Item 7 above                                                                                                                                                                                                                                                                                                                                                                                                                                                                                                                                                                                                                                                                                                                                                                                                  | 8. PROJECT/TASK/WORK UNIT NUMBER<br><br>9. FIN OR GRANT NUMBER<br>A-3282                                                                                                                                                                                                        |                                                                                           |       |      |          |      |
| 12. SUPPLEMENTARY NOTES<br>Proceedings prepared by Brookhaven National Laboratory                                                                                                                                                                                                                                                                                                                                                                                                                                                                                                                                                                                                                                                                                                                                                                                                                | 11a. TYPE OF REPORT<br>Proceedings of conference on safety research<br><hr/> b. PERIOD COVERED (Inclusive Dates)<br>October 24-27, 1988                                                                                                                                         |                                                                                           |       |      |          |      |
| 13. ABSTRACT (200 words or less)<br><br><p style="text-align: center;">           This five-volume report contains 141 papers out of the 175 that were presented at the Sixteenth Water Reactor Safety Information Meeting held at the National Institute of Standards and Technology, Gaithersburg, Maryland, during the week of October 24-27, 1988. The papers are printed in the order of their presentation in each session and describe progress and results of programs in nuclear safety research conducted in this country and abroad. Foreign participation in the meeting included twenty different papers presented by researchers from Germany, Italy, Japan, Sweden, Switzerland, Taiwan and the United Kingdom. The titles of the papers and the names of the authors have been updated and may differ from those that appeared in the final program of the meeting.         </p> |                                                                                                                                                                                                                                                                                 |                                                                                           |       |      |          |      |
| 14. DOCUMENT ANALYSIS - KEYWORDS/DESCRIPTORS<br>reactor safety research<br>nuclear safety research<br>decontamination and decommissioning<br><br>b. IDENTIFIERS/OPEN-ENDED TERMS                                                                                                                                                                                                                                                                                                                                                                                                                                                                                                                                                                                                                                                                                                                 | 15. AVAILABILITY STATEMENT<br>Unlimited<br><hr/> 16. SECURITY CLASSIFICATION<br>(This page)<br>Unclassified<br>(This report)<br>Unclassified<br><hr/> 17. NUMBER OF PAGES<br><hr/> 18. PRICE                                                                                    |                                                                                           |       |      |          |      |